

APPLIED
SCIENTIFIC RESEARCH
B. ELECTROPHYSICS, ACOUSTICS, OPTICS,
MATHEMATICAL METHODS

Governing Board:

Prof. ir. J. J. BROEZE, Delft.
Prof. dr H. B. DORGELO, Eindhoven.
Prof. dr H. W. JULIUS, The Hague.
Dr G. H. REMAN, Amsterdam.
Prof. ir J. T. THIJSSSE, Delft.
Prof. dr ir A. VAN WIJNGAARDEN, Amsterdam

Editorial Board:

Prof. dr R. KRONIG, Delft (General Editor).
Prof. dr ir C. B. BIEZENO, Delft.
Prof. dr L. J. F. BROER, Delft.
Dr W. DE GROOT, Eindhoven.
Prof. dr H. A. LAUWERIER, Amsterdam.

National Editors:

Prof. dr G. BORELIUS, Stockholm, for Sweden.
Prof. dr A. VAN ITTERBEEK, Louvain, for Belgium.
Prof. J. RYBNER, Copenhagen, for Denmark.
Prof. dr M. J. O. STRUTT, Zürich, for Switzerland.
Prof. dr S. WESTIN, Trondheim, for Norway.

Articles should be sent to *the Secretary*, ir H. G. DE WINTER, Laboratorium voor Technische Physica, Mijnbouwplein 11, Delft.

APPLIED SCIENTIFIC RESEARCH

ELECTROPHYSICS, ACOUSTICS, OPTICS,
MATHEMATICAL METHODS

Reports published under the auspices of

*The Central National Organization for Applied Scientific
Research in the Netherlands (T.N.O.)*

*The Netherlands Physical Society,
Section for Applied Physics*

*The Royal Institute of Engineers of the Netherlands,
Section for Technical Scientific Research*

The Mathematical Centre, Amsterdam

*

VOLUME B VIII



THE HAGUE
MARTINUS NIJHOFF
1960

*Copyright 1960 by Martinus Nijhoff, The Hague, Netherlands
All rights reserved, including the right to translate or to
reproduce this book or parts thereof in any form*

PRINTED IN THE NETHERLANDS

INDEX OF AUTHORS AND PAPERS

	Page
BOESCHOTEN, F., W. VAN EGMOND and H. M. J. KINDERDIJK, Measurements on the permeability of hydrogen from H_2 and H_2O through steel, stainless steel and aluminium	378
BROER, L. J. F. and L. VAN WIJNGAARDEN, On the motion of a charged particle in an almost homogeneous magnetic field	159
BROER, L. P. F., L. A. PELETIER and L. VAN WIJNGAARDEN, A mechanical Hall effect — <i>Letter to the Editor</i>	259
BRUYNNOOGHE, W. M., see VERHAEGHE, J. L.	
CHEN TO TAI, Wave propagation in an inhomogenous transversely magnetized rectangular waveguide	141
DRAKE, D. G., Rayleigh's problem in magnetohydrodynamics for a non-perfect conductor	467
DIJKERMAN, H. A., C. HUISZON and A. DYMANUS, A power stabilizer for frequency modulated microwave oscillators	1
DYMANUS, A., see DIJKERMAN, H. A.	
ECKMAN, P. K. and E. M. WILLIAMS, Plasma dynamics in an arc formed by low-voltage sparkover of a liquid dielectric	299
EGMOND, W. VAN, see BOESCHOTEN, F.	
FRANKENA, H. J., Transient phenomena associated with Sommerfeld's horizontal dipole problem	357
FRANKENA, H. J., see HOOP, A. T. DE.	
GEMANT, A., Infrared spectra of ion-producing species in hydrocarbons	149
GOODRICH, R. F., see SIEGEL, K. M.	
GORTER, C. J., see KLERK, D. DE.	
HANSEN, E. B., The diffraction of a plane wave through two or more slits in a plane screen	73
HANSEN, E. B., On the influence of shape and variations in conductivity of the sample on four-point measurements	93
HOMANN, J., see YOUNG, F.	

	Page
HOOP, A. T. DE, A reciprocity theorem for the electromagnetic field scattered by an obstacle	135
HOOP, A. T. DE, A modification of Cagniard's method for solving seismic pulse problems	349
HOOP, A. T. DE and H. J. FRANKENA, Radiation of pulses generated by a vertical electric dipole above a plane non-conducting earth	369
HUISZON, C., see DIJKERMAN, H. A.	
ITTERBEEK, A. VAN, W. PEELAERS and F. STEFFENS, Susceptibility measurements of Nb between room temperature and liquid helium temperatures	177
ITTERBEEK, A. VAN, W. PEELAERS and F. STEFFENS, The magnetic susceptibility of Ag-Mn and Cu-Mn solid solutions between 1.2°K and 368°K	337
JACKSON, H. L. W., see POWER, G.	
KINDERDIJK, H. M. J., see BOESCHOTEN, F.	
KISER, R. W., Characteristic parameters of gas-tube proportional counters I	183
KISER, R. W., see STORRS, C. D.	
KLERK, D. DE and C. J. GORTER, A criterion for the efficiency of iron core electromagnets	265
LAUWERIER, H. A., The surface charge of a semi-infinite cylinder due to an axial point charge	277
LEVINE, H., A corner effect in plane diffusion theory	105
MITTRA, R., On the solution of an eigenvalue equation of the Wiener-Hopf type in finite and infinite ranges	201
PEELAERS, W., see ITTERBEEK, A. VAN.	
PELETIER, W., see BROER, L. J. F.	
POWER, G., Extremum methods for certain electrical problems involving homogeneous anisotropic material	84
POWER, G. and H. L. W. JACKSON, Sphere and circle theorems involving surface discontinuities of potential	254
POWER, G. and H. L. W. JACKSON, Use of Stokes' stream function for discontinuities of potential at a spherical boundary	463
ROBBRECHT, G. G., see VERHAEGHE, J. L.	
ROWLANDS, G., The method of images and the solution of certain partial differential equations	62

	Page
SAERMARK, K., Acoustic forces and torques on a system of strips	13
SAERMARK, K., Transmission coefficient for a system of parallel slits in a thin plane screen	29
SENIOR, T. B. A., Diffraction by an imperfectly conducting half-plane at oblique incidence	35
SENIOR, T. B. A., Impedance boundary conditions for imperfectly conducting surfaces	418
SENIOR, T. B. A., Impedance boundary conditions for statistically rough surfaces.	437
SIEGEL, K. M., R. F. GOODRICH and V. H. WESTON, Comments on far field scattering from bodies of revolution	8
SODHA, M. S., Heating of an ionized gas sheath by microwaves	208
STEFFENS, F., see IITERBEEK, A. VAN.	
STORRS, C. D. and R. W. KISER, Characteristic parameters of Geiger-Müller counter gases I	387
VERHAEGHE, J. L., G. G. ROBBRECHT and W. M. BRUYNNOOGHE, On the specific heat of Mn-Zn and Ni-Zn ferrite between 20°C and 350°C	128
WAIT, J. R., Propagation of electromagnetic pulses in a homogeneous conducting earth	213
WAIT, J. R., The electromagnetic fields of a dipole in the presence of a thin plasma sheet	397
WESTON, V. H., see SIEGEL, K. M.	
WILLIAMS, E. M., see ECKMAN, P. K.	
WIJN, H. W. DE, A harmonic generator and detector for the short millimeter wave region	261
WIJNGAARDEN, L. VAN, see BROER, L. J. F.	
YOUNG, F. and J. HOMANN, Characteristics of ridge waveguides	321
YUTZE CHOW, Scattering of electromagnetic waves by coaxial ferrite cylinders of different tensor permeabilities	290

A POWER STABILIZER FOR FREQUENCY MODULATED MICROWAVE OSCILLATORS

by H. A. DIJKERMAN, C. HUISZON and A. DYMANUS

Physical Laboratory, University of Utrecht, Netherlands

Summary

A description is presented of a microwave power stabilizer with short time-constant. By means of this stabilizer a frequency-modulated microwave signal of constant amplitude is obtained. Possible applications in measurements on microwave components and in the field of microwave spectroscopy are mentioned.

§ 1. *Introduction.* In many applications the microwave klystron oscillator is frequency-modulated by applying a modulating voltage to the repeller. With this type of frequency modulation the outgoing wave is, however, also amplitude-modulated on account of the curvature of the klystron mode. This amplitude-modulation can be eliminated by inserting a power stabilizer in the microwave line between the klystron and the load. To our present knowledge three power stabilizers have been described in the literature ¹⁾²⁾³⁾. All of them have a rather long time-constant (~ 0.1 s) and are thus useful only at low modulation frequencies.

In this paper a power stabilizer is described with a short time-constant ($\sim 10^{-4}$ s) which provides a frequency-modulated microwave signal of constant amplitude if the rate of frequency-modulation is less than 10 kHz. The essential feature of the stabilizer is the use of a Faraday modulator of special design. The present stabilizer has been developed especially for use in the 1.25 cm wavelength region, but it can readily be adapted for other wavelengths too.

§ 2. *Design considerations.* A simplified diagram of the stabilizer is shown in fig. 1. A fraction R of the power P_2 leaving the ferrite modulator is detected by a crystal rectifier. The resulting DC-

output voltage V_c is compared with a reference voltage V_0 in a mixing circuit. The voltage difference $V_d = V_c - V_0$ after amplification in a broadband DC-amplifier controls the current i through the modulator coil and hence the power transmission of the modulator.

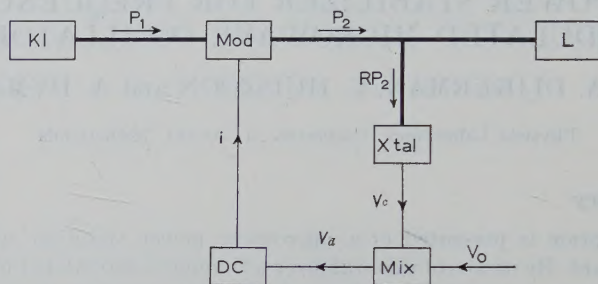


Fig. 1. Simplified diagram of a power stabilizer.

Kl = klystron oscillator;

Mod = modulator, containing the ferrite rod;

L = load;

X-tal = crystal detector;

Mix = mixing circuit;

DC = d.c. amplifier;

P_1, P_2 = input- and output power of the modulator, respectively;

RP_2 = fraction of the power P_2 in the feedback loop.

V_c = crystal output voltage;

V_0 = reference voltage;

V_d = voltage difference $V_c - V_0$;

i = current through modulator coil.

It can readily be shown that the power stabilization factor S , defined as

$$S = \frac{\Delta P_2'}{\Delta P_2''}, \quad (1)$$

is given by

$$S = 1 - \frac{\Delta P_2}{\Delta i} \frac{\Delta i}{\Delta V_c} \frac{\Delta V_c}{\Delta P_2} = 1 + mkARP_2. \quad (2)$$

In (1) and (2) $\Delta P_2'$ and $\Delta P_2''$ are variations of the power P_2 for a given variation ΔP_1 of the klystron power P_1 without and with stabilization, respectively; $m = -(1/P_2)(\Delta P_2/\Delta i)$ the control sensitivity of the modulator; $k = (1/R)(\Delta V_c/\Delta P_2)$ the voltage

sensitivity of the crystal detector; and $A = \Delta i_i \Delta V_d$ the so-called "transconductance" of the amplifier. In the case that the last stage of the amplifier is a cathode follower with the modulator coil in the cathode lead, A is approximately equal to Gg_m , where G is the gain of the amplifier and g_m the transconductance of the cathode follower tube.

In order to obtain a high stabilization factor the product $mkARP_2$ must be made as large as possible. The klystron output power P_1 and hence the maximum value of P_2 generally increase with increasing wavelength. Since the crystal sensitivity k is roughly independent of the power level, a higher stabilization factor can be obtained at longer wavelengths. The fraction R is determined by the desired useful output power. The control sensitivity of the modulator depends on composition and dimensions of the ferrite rod, on the diameter of the circular guide housing the latter, as well as on the number of turns of the modulator coil; it is proportional to the length of the rod and increases rapidly with increasing ratio of rod and guide diameters. However, to avoid ellipticity of the resulting wave⁴) and conversion of the circular TE_{11} mode into modes which are not attenuated by the absorbing vanes (see § 3), this ratio should generally not exceed ~ 0.25 .

The choice of the coil providing the magnetizing field is determined by the desired response time of the stabilizer. For a given response time τ the resonance frequency of the coil should be much higher than τ^{-1} . Otherwise, unavoidable phase shifts in the neighbourhood of the resonance frequency cause regeneration of the stabilizer. Hence a rather low-turn coil should be used at the sacrifice of the m -value.

For a short response time the amplifier should possess a large bandwidth, while for a large stabilization factor a high gain and a low output impedance are desired. The ultimate value of A is set by the stability requirements.

In the 1.25 cm band the following values seem a reasonable estimate: $P_2 = 10^{-3}$ W, $R = 1/2$, $k = 500$ V/W, $m = 100$ /A, and $A = 10$ A/V ($G = 2000$, $g_m = 5 \times 10^{-3}$ A/V). Thus at this wavelength a stabilization factor of about 250 seems feasible.

§ 3. Description of the stabilizer.

1. The modulator. A longitudinal cross-section of the ferrite

modulator is shown in fig. 2. The two transition sections TS_1 and TS_2 transform the rectangular TE_{01} mode into the circular TE_{11} mode and vice versa, respectively. The midsection of the circular waveguide contains a ferrite rod kept in the axis by styrofoam. The absorbing vane V_2 placed behind the ferrite rod absorbs tangential components of the rotated microwave electric field vector \mathbf{E} . The vane V_1 is inserted to eliminate multiple rotated waves within the modulator. The midsection of the circular guide was made of a perspex tube coated on the inside with aluminium foil about $7\ \mu$ thick in order to reduce losses due to eddy currents at high modulation frequencies.

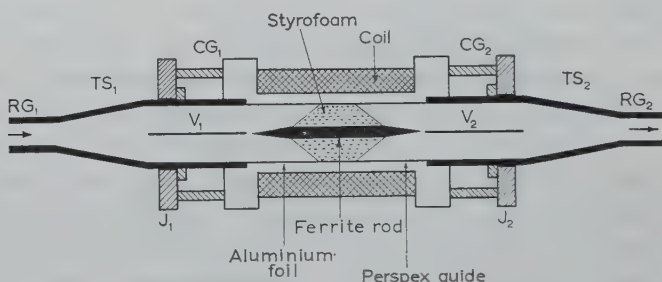


Fig. 2. Longitudinal cross-section of the modulator.
 RG_1, RG_2 = rectangular input and output guide;
 TS_1, TS_2 = transition sections;
 CG_1, CG_2 = circular guide sections;
 V_1, V_2 = absorbing vanes;
 J_1, J_2 = joints.

The length of the ferrite rod (Ferroxcube 4A, Philips) was about 8 cm, the diameter about 0.3 cm. The rod, the vanes, and the styrofoam supports were tapered at the ends to reduce reflections.

The control sensitivity of the present modulator was about 90/A.

2. The DC-amplifier. The DC-amplifier (gain ~ 4800), a symmetric two-stage difference amplifier, was of conventional design. The reference voltage V_0 , and the crystal output voltage V_e were applied independently to the grids of the two tubes of the first difference stage. The last stage of the amplifier was a double cathode follower shown diagrammatically in fig. 3. The variable resistor R_1 was used to adjust the transconductance of the amplifier, and hence the stabilization factor. Usually, the value of R_1 was close to zero. An additional battery B provided a direct

current (~ 5 mA, adjustable with R_3) to adjust the working point in the transmission-current characteristics of the modulator. The resistor R_2 was used to damp the resonance of the modulator coil and so to shorten the time constant of the stabilizer by reducing the total phase shift in the feed-back loop.

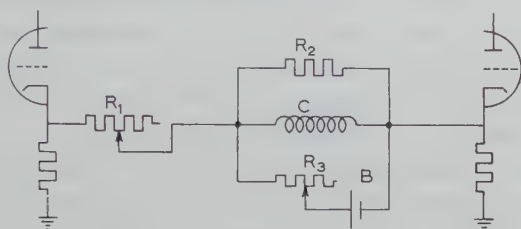


Fig. 3. Last stage of d.c. amplifier.
B = battery, C = modulator coil.

§ 4. *Performance.* The performance of the stabilizer is illustrated in figs. 4a and 4b, taken from an oscilloscope connected to a crystal detector terminating the useful power line. The well known mode of the klystron (2 K 33, Raytheon) obtained by applying a sawtooth voltage to the repeller and by switching off the stabilizer is reproduced in fig. 4a. The repetition rate of the sawtooth voltage was

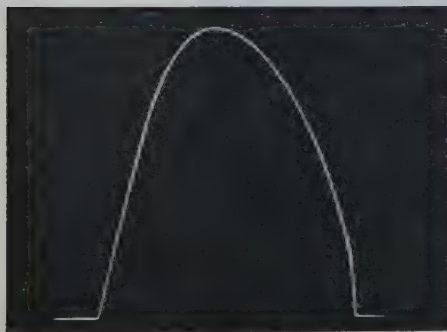


Fig. 4a. Klystron mode.

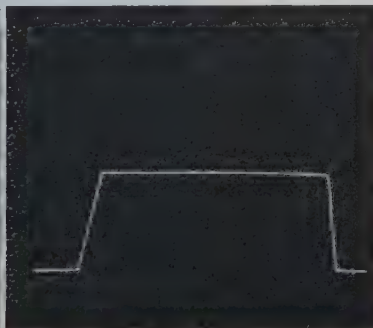


Fig. 4b. Stabilized klystron mode.

about 100 Hz. In fig. 4b the same mode is shown with the stabilizer on. The power variation throughout the flat portion of the mode is less than 1 percent. The level of the transmitted power can be adjusted by varying the reference voltage.

If the repetition rate of the sawtooth voltage was increased to about 1 kHz, an overshoot appeared on the leading edge of the mode. At repetition rates far above 1 kHz this overshoot became quite strong and was followed by a damped oscillation which covered a considerable fraction of the flat portion. The main cause of these phenomena was the rather low (~ 20 kHz) resonance frequency of the modulator coil. This resonance frequency can easily be increased to, say, 100 kHz. In the present applications the repetition rates did not exceed 500 Hz.

The time constant of the stabilizer was about 10^{-4} s. The stabilization factor, about 250 at $P_2 = 10^{-3}$ W, was limited mainly by the resonance frequency of the coil and by the low gain of the DC-amplifier. The coil resonance also set a limit to the time constant.

§ 5. *Applications.* The present stabilizer can be useful in applications in which a frequency-modulated microwave signal of constant amplitude is desired, e.g. in dynamic measurements of the Q -factor of cavities, in broadband tuning of components and circuits and in investigations of the transmission properties of microwave systems. An example of the latter application is shown in fig. 5.

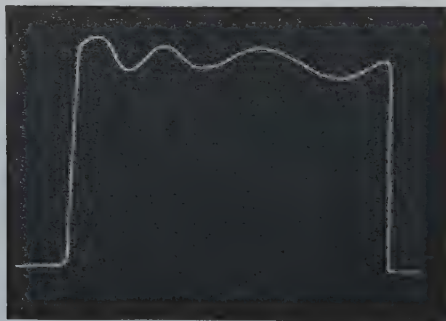


Fig. 5. Stabilized mode behind a Stark-cell.

Here the stabilized klystron mode detected behind an X-band Stark-waveguide cell used in microwave spectroscopy is reproduced. As a result of reflections in the cell the power transmitted by the cell is a function of frequency. If the mode is provided with a frequency scale (e.g. with the aid of frequency markers), the pattern of fig. 5 can be analyzed. It is thus possible to locate the reflecting points and to measure their reflection coefficients.

Acknowledgements. This investigation is part of the research program of the "Stichting voor Fundamenteel Onderzoek der Materie" and was made possible by financial support from the "Nederlandse Organisatie voor Zuiver Wetenschappelijk Onderzoek".

We are greatly indebted to Drs R. Braams and A. Noordergraaf for their careful reading of the manuscript.

Received 5th January, 1959.

REFERENCES

- 1) Munsen, J. K., Rev. Sci. Instrum. **21** (1950) 622.
- 2) Engen, G. F., I.R.E. Trans. on Microwave Theory and Techniques, MTT-6 (1958) 202.
- 3) Fray, S. J. and M. F. Kimmitt, J. Sci. Instrum. **33** (1956) 363.
- 4) Melchor, J. L., W. P. Ayres, and P. Vartanian, J. Appl Phys. **27** (1956) 72.

COMMENTS ON FAR FIELD SCATTERING FROM BODIES OF REVOLUTION

by K. M. SIEGEL, R. F. GOODRICH and V. H. WESTON

The Radiation Laboratory Department of Electrical Engineering The University of
Michigan Ann Arbor, Michigan, U.S.A.

Summary

A previous paper ¹⁾ on the subject, although 35 pages in length, omitted a good many physical explanations and mathematical details. As a result this paper discusses Rayleigh and resonance scattering for a cone. Two minus sign errors are corrected in the cone's cross section obtained by the local wedge field approximation.

§ 1. *Comments and answers on Rayleigh and resonant scattering region.* The Rayleigh approximation presented for the nose-on axially symmetric radar cross-sections for perfectly conducting bodies of revolution depended only on the volume and length-to-width ratio. A question received was; "Does this imply that the author expects the nose-on and base-on cross sections in the Rayleigh region for a finite cone to be approximately equal?". The answer is "Yes". It is expected that the base-on cross-section dominates the nose-on result in the optics region and this ratio approaches 1 as resonance is approached from the small wavelength side. Experimental verification of the ratio tending towards 1 as resonance is approached has been obtained by Olte and Silver ²⁾. Hiatt and Olte ³⁾ have measured cones nose-on and base-on in the Rayleigh region and the agreement is within $\frac{1}{2}$ db.

In ¹⁾ it was stated that for thin cones the resonance cross-section would agree with that of the ring of radius equal to the cone base radius. For fat cones no comment was made, it being realized that the limit of a fat cone is a disc, and the disc maximum then could be used to approximate the location of the maximum of the fat cone. The author then felt the location of the cone's major maximum

would be between that of a ring and that of a disc of the same radii as the cone base, as the cone angle was increased. Keys and Primich ⁴⁾, commenting on ¹⁾, present several experimental verifications including the fact that the second and third maximum agree with those of a ring. They show that the first maximum even for 8° cones still lies much closer to the disc than the ring. The rapidity of the first maximum's location shifting towards that of a disc was not known before results of experiments were presented by Keys and Primich ⁴⁾. Ref. ⁴⁾ purported to exhibit that an 8° cone gave Rayleigh results significantly different from those predicted in ¹⁾. Analysis ⁵⁾ showed that these measurements were not in the Rayleigh region for that cone and that experiments ⁵⁾ in the Rayleigh region do agree with the predictions of ¹⁾.

§ 2. *Comments and answers on optical scattering region.* In ¹⁾, by the Kirchhoff approximation, equation (3-19) was obtained:

$$H^s = \frac{i e^{-ik(r+2z_0)}}{2kr} \hat{i}_y \tan^2 \alpha \left(\frac{1}{2} + ikz_0 - \frac{1}{2} e^{2ikz_0} \right), \quad (3-19)$$

where H^s is the nose-on field at short wavelengths and scattered from a finite cone of half-angle α and of length z_0 . For thin cones $kz_0 \gg 1$ only the middle term in the bracket at the right was kept. However, analysis of equation (3-19) shows that for fat cones $kz_0 \ll 1$ as the disc is approached ($\alpha \rightarrow \frac{1}{2}\pi$) all three terms must be kept. The $\tan^2 \alpha$ times the expression in the bracket becomes indeterminate. Evaluation of the indeterminate form yields the proper disc result. It was not made clear that the intended approximation to be used for the cone at small wavelengths was that obtained by the local wedge field analysis for thin cones and the results obtained from equation (3-19) for fat cones. The exact point of matching was not discussed by the author.

§ 3. J. B. Keller has pointed out a minus sign error in the cone field derivation from wedge theory, namely that the \hat{p} in equation (3-30) should be $-\hat{p}$. To make the correction, however, we will interchange A and B. This causes many changes which are listed below.

(3-30): interchange A and B

(3-33): interchange A and B

(3-37): interchange *)

$$1 - \cos\left(\frac{\pi^2}{2\pi - \gamma}\right) \text{ with } \cos\left(\frac{2\pi\theta}{2\pi - \gamma}\right) + \cos\left(\frac{\pi^2}{2\pi - \gamma}\right).$$

(3-38): replace

$$1 - \cos\left(\frac{\pi^2}{2\pi - \gamma}\right) \text{ by } \cos\left(\frac{2\pi\theta}{2\pi - \gamma}\right) + \cos\left(\frac{\pi^2}{2\pi - \gamma}\right).$$

(3-39): replace the right-hand side by

$$\frac{4\pi^3 a^2}{(2\pi - \gamma)^2} \frac{\sin^2\left(\frac{\pi^2}{2\pi - \gamma}\right)}{\left[\cos\left(\frac{\pi^2}{2\pi - \gamma}\right) - \cos\left(\frac{3\pi^2}{2\pi - \gamma}\right)\right]^2}.$$

Omit equations (3-40) and (3-41).

(3-42): should be written

$$\sigma = \frac{\pi^3 a^2}{(3\pi/2 + \alpha)^2} \operatorname{cosec}^2\left(\frac{4\pi^2}{3\pi + 2\alpha}\right).$$

(3-43): should be written

$$\frac{\sigma}{\pi a^2} = \frac{4\pi^2}{(2\pi - \gamma)^2} \frac{\sin^2\left(\frac{\pi^2}{2\pi - \gamma}\right)}{\left[\cos\left(\frac{\pi^2}{2\pi - \gamma}\right) - \cos\left(\frac{2\pi^2}{2\pi - \gamma}\right)\right]^2}.$$

(3-44): should be written

$$\frac{\sigma}{\pi a^2} = \frac{4\pi^2}{(\pi + \alpha)^2} \frac{\sin^2\left(\frac{\pi^2}{\pi + \alpha}\right)}{\left[\cos\left(\frac{\pi^2}{\pi + \alpha}\right) - \cos\left(\frac{2\pi^2}{\pi + \alpha}\right)\right]^2}.$$

Substitute for line 2, page 317, the following: The wedge solution need be restricted to cases when the ring singularity is dominant. As an example, for the cone with $ka \gg 1$, this obtains for α such that $kz_0 \gg 1$.

Substitute for fig. 3.10 the figure below.

Delete fig. 3.16.

Substitute in line 4, page 318, (3-43) by (3-38).

*) θ = angle of incidence measured from the bisector of the exterior wedge angle.

The curves below (fig. 3.10) are quite deceptive and they need some discussion. First, the Y_1 curve is the important one. The purpose of the Y_2 curve was to show how poor the Kirchhoff answer is for scattering from the base. The above curves are only valid for thin cones. For fat cones, as discussed above, the Kirchhoff treatment is quite good, going into the correct answer for the disc, remembering that all three terms in equation (3-19) must be used. One term,

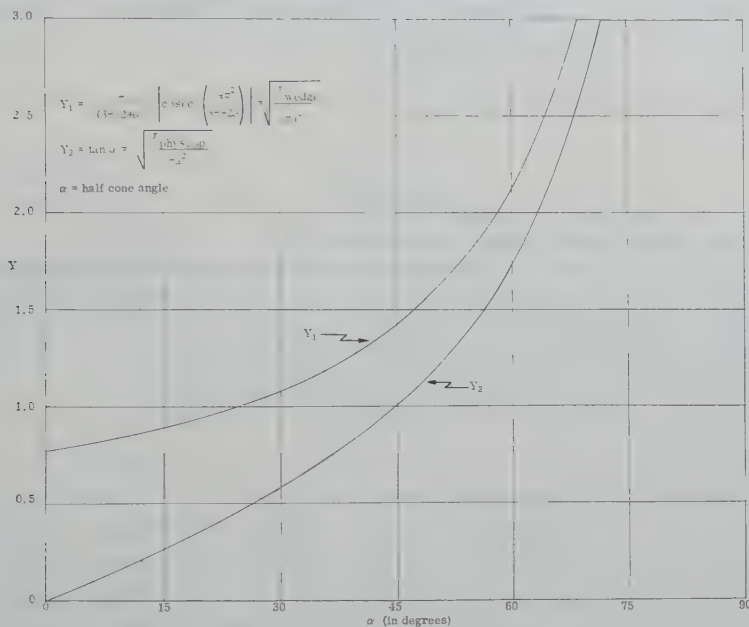


Fig. 3.10. Nose-on finite cross-sections as computed by physical optics and circular wedge approximations.

namely, the base term alone, increased without limit. Thus, we know that tip scattering must play an important role at any fixed wavelength as the cone approaches a disc. This then suggests how we can correct the cone formula using wedge theory so that it can apply to both fat and thin cones. For those who, having used the results presented before the signs were corrected, might be overly disturbed by the different forms of the corrected results the following may be mentioned: The percentage error in using the old results for Y_1 instead of the new ones is for half cone angles $\alpha = 0$: 1.3 percent, $\alpha = 10^\circ$: 1.5 percent, $\alpha = 20^\circ$: 6.2 percent, and $\alpha = 30^\circ$: 16 percent.

The errors in the squares of Y are 2.6 percent, 3.0 percent, 12.8 percent, and 34.6 percent. This points out why the error was never noticed by experimenters. Since the other terms in the asymptotic expansion are such as to lessen the increase in cross-section as the angle increases, the true discrepancy between the formulae is in fact less than the percentages given above which are maxima. The geometric theory of diffraction predicts that the corrected formula is the leading term of the asymptotic expansions at small wavelengths and for thin cones.

Received 22nd April, 1959.

REFERENCES

- 1) Siegel, K. M., Appl. Sci. Res. B **7** (1959) 293.
- 2) Olte, A. and S. Silver, New Results on Back Scattering from Cones and Spheroids. To be published in a special issue of Transactions of the PGAP, IRE, covering the URSI-Toronto Symposium, June 1959.
- 3) Hiatt, R. E. and A. Olte, Radar Cross-Section Measurements on Cones in the Rayleigh Region. To be submitted to the Can. J. Phys.
- 4) Keys, J. E. and R. I. Primich, Can. J. Phys. **37**, No. 4 (1959) 521.
- 5) Brysk, H., R. E. Hiatt, V. H. Weston and K. M. Siegel, Can. J. Phys. **37**, No. 5 (1959) 675.

ACOUSTIC FORCES AND TORQUES ON A SYSTEM OF STRIPS

by K. SÆRMARK

Physics Department, Technical University of Denmark, Copenhagen, Denmark

Summary

In continuation of an earlier paper, we report some calculations of the forces and torques on a system of strips. Numerical calculations are presented for the case of two coplanar strips with the parameter-value $kb = 1$ and an arbitrary angle of incidence. Further, simple and yet rather accurate expressions for the forces and torques are derived. These relate the forces and torques of the present problem to those acting on a single strip, present alone in an unlimited radiation field.

§ 1. *Introduction.* In a recent paper ¹⁾, in the following quoted as I, we considered the two-dimensional scattering of an incoming, plane, monochromatic wave by a general system of strips, the boundary conditions being that the normal gradient of the wave function should be zero on the strips. By means of Babinet's principle, numerical calculations of the transmission coefficient for a system of two parallel slits in an infinite, perfectly conducting, thin screen were performed. In these calculations the incoming wave was considered as an electromagnetic wave with the electric field vector polarised along the slit-axes. In the present paper we will regard the incoming plane wave as an acoustical wave and calculate the forces and torques on the system and its separate parts. We make the usual assumption that all effects of viscosity, vortex and turbulence formation etc. may be neglected. To what extent this is a valid assumption is, of course, an open question. We further assume that we may treat the strips as absolutely rigid so that the boundary conditions used in I may also be used here. For details of the notation we refer to I.

§ 2. *Expressions for the scattered wave.* In this paragraph we summarize the general expressions for the scattering problem. The velocity potential ψ_i of the incoming, plane, monochromatic wave will be given by

$$\psi_i = e^{ik(x\cos v + y\sin v)} \quad (k = 2\pi/\lambda), \quad (1)$$

the wave-vector \mathbf{k} making an arbitrary angle v with the x -axis. In (1) and in the following equations we have omitted the time factor $\exp(-i\omega t)$. The scattered wave ψ_s satisfies Sommerfeld's radiation condition at infinity:

$$\psi_s(r \rightarrow \infty) = f(\vartheta; v) \frac{e^{ikr}}{\sqrt{r}}, \quad (2)$$

and the total velocity potential

$$\psi = \psi_i + \psi_s \quad (3)$$

satisfies the boundary condition

$$\text{grad}_n \psi = 0 \quad (4)$$

on the strips. Finally ψ satisfies the wave-equation

$$\Delta\psi + k^2\psi = 0. \quad (5)$$

The scattering object may in general be a system of a finite number of parallel, non-overlapping strips (I, § 2). However, in order to avoid a cumbersome notation, we will here restrict ourselves to the consideration of a system of only two parallel strips, A and B, of equal width $2b$ in a non-overlapping but otherwise arbitrary position. The geometry of the problem is as shown in fig. 1. Generalization to systems including more than two strips will be obvious.

As in I, we assume that the scattered wave ψ_s may be written in the form

$$\begin{aligned} \psi_s &= \psi_A + \psi_B, \\ \psi_A &= \sqrt{8\pi} \sum_m A_m' \text{So}_m(s, \alpha) \text{Ho}_m(s, \mu), \\ \psi_B &= \sqrt{8\pi} \sum_m B_m' \text{So}_m(s, \beta) \text{Ho}_m(s, \rho). \end{aligned} \quad (6)$$

Here the parameter s is defined by $s = (kb)^2$, while (α, μ) and (β, ρ) are elliptical cylinder coordinates defined by means of the strips A and B respectively; i.e. the distance between the focal

points in each coordinate system is $2b$, and the coordinate lines $\alpha = 0$ and $\beta = 0$ coincide with the x - and x' -axis (see fig. 1). The functions $\text{So}_m(s, \alpha)$ and $\text{Ho}_m(s, \mu)$ are, respectively, the periodic, odd Mathieu-functions and the associated, Hankel-like Mathieu-functions. Finally, $A_{m'}$ and $B_{m'}$ are expansion coefficients to be determined by the equations given in I, i.e. I eqs (17).

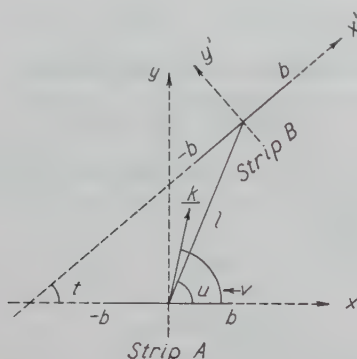


Fig. 1. The geometry of the scattering obstacle.

§ 3. *General expressions for the forces on A and B.* In this paragraph we want to derive an expression for the forces, per unit length of the axes, on the strips A and B. It is well-known²⁻⁴⁾ that the mean radiation force per unit length on a single strip, present alone in an unlimited radiation field, is related to the total scattering cross-section Q by the equation

$$\bar{K} = \frac{1}{2} k^2 Q \sin v. \quad (7)$$

Here the bar indicates a mean value over a whole number of periods. The angle v is the angle between the wave vector and the plane of the strip. By means of the cross-section theorem⁶⁾ this expression may be written in the form

$$\bar{K} = -k^2 \sqrt{\frac{2\pi}{k}} \sin v \cdot \text{Re}[e^{i\pi/4} f(v; v)] \quad (8)$$

with $f(v; v)$ defined by (2).

In order to calculate the mean radiation force on a single strip, e.g. strip A, in the presence of a second strip, e.g. strip B, it is

necessary to evaluate the integral (cf. 7))

$$\bar{K}_A = \int_{-b}^{+b} [\bar{\Delta p}(y = -0) - \bar{\Delta p}(y = +0)] dx. \quad (9)$$

Here $\bar{\Delta p}$ is the mean pressure which, omitting the density of the surrounding medium, is

$$\bar{\Delta p} = \frac{1}{4} [k^2 \psi^* \psi - \text{grad } \psi^* \cdot \text{grad } \psi]. \quad (10)$$

From (3) and (6) the total velocity potential is

$$\psi = \psi_i + \psi_A + \psi_B.$$

Here we may assume ψ_B to be expressed in terms of the coordinates x, y . The integrand in (9) may then be written in the form

$$\begin{aligned} \bar{\Delta p}(y = -0) - \bar{\Delta p}(y = +0) = \\ = \frac{1}{2} \text{Re} \left[k^2 \psi_i^* \delta(\psi_A) - \frac{\partial}{\partial x} \psi_i^* \frac{\partial}{\partial x} \delta(\psi_A) \right] + \\ + \frac{1}{2} \text{Re} \left[k^2 \psi_B^* \delta(\psi_A) - \frac{\partial}{\partial x} \psi_B^* \frac{\partial}{\partial x} \delta(\psi_A) \right] \end{aligned} \quad (11)$$

with

$$\delta(\psi_A) = \psi_A(y = -0) - \psi_A(y = +0).$$

Introducing this expression into the integral (9), the force \bar{K}_A will be given by a sum of two terms \bar{K}_A' and \bar{K}_A'' . By using the fact that $\delta(\psi_A)$ is zero at the strip edges, the first of these may readily be shown to be

$$\bar{K}_A' = \frac{k^2}{2} \text{Re} \left[\sin^2 v \int_{-b}^{+b} e^{-ikx \cos v} \delta(\psi_A) dx \right], \quad (12)$$

while the second term becomes

$$\bar{K}_A'' = \frac{1}{2} \text{Re} \int_{-b}^{+b} \left[k^2 \psi_B^* \delta(\psi_A) - \frac{\partial}{\partial x} \psi_B^* \frac{\partial}{\partial x} \delta(\psi_A) \right] dx. \quad (13)$$

The force \bar{K}_A' may by means of Greens-function methods, analogous to those used by Levine⁵⁾ and Keller³⁾ in deriving (8), be

expressed as

$$\bar{K}_A' = -k^2 \sin v \operatorname{Re} \left[\sqrt{\frac{2\pi}{k}} e^{i\pi/4} f_A(v; v) \right], \quad (14)$$

where $f_A(\vartheta; v)$ is defined by

$$\psi_A(r \rightarrow \infty) = f_A(\vartheta; v) \frac{e^{ikr}}{\sqrt{r}}.$$

Here r, ϑ are polar coordinates with the origin at $x = y = 0$.

The force \bar{K}_A'' is more cumbersome, however. By a partial integration, again using the fact that $\delta(\psi_A)$ is zero at the strip edges, (13) may be rewritten as

$$\begin{aligned} \bar{K}_A'' &= \frac{1}{2} \operatorname{Re} \int_{-b}^{-b} \left[k^2 \psi_B^* + \frac{\partial^2}{\partial x^2} \psi_B^* \right] \delta(\psi_A) dx = \\ &= -\frac{1}{2} \operatorname{Re} \int_{-b}^{+b} \left[\frac{\partial^2}{\partial y^2} \psi_B^* \right]_{y=0} \delta(\psi_A) dy. \end{aligned} \quad (16)$$

Further simplification of \bar{K}_A'' seems impossible unless the distance l between the two strip axes is large enough to allow one to employ the asymptotic form of ψ_B . However, one may readily see, e.g. from (13), that only that part of ψ_B which is *even* in y will contribute to \bar{K}_A'' . This implies that \bar{K}_A'' vanishes in the case that the two strips lie in the same plane because ψ_B then will be an odd function of y . The mean radiation force \bar{K}_A will in this case accordingly be given by (14).

For the radiation force \bar{K}_B on strip B in the presence of strip A one may in the same way write $\bar{K}_B = \bar{K}_B' + \bar{K}_B''$, with \bar{K}_B' and \bar{K}_B'' given by expressions analogous to (14) and (16). However, as the numerical calculations given in a later section will be restricted to the case of two coplanar strips, we quote only \bar{K}_B corresponding to the values $t = u = 0$ of the angles t and u shown in fig. 1:

$$\begin{aligned} \bar{K}_B = \bar{K}_B' &= -k^2 \sin v \operatorname{Re} \left[e^{-ikl \cos v} \sqrt{\frac{2\pi}{k}} e^{i\pi/4} f_B(v; v) \right], \quad (17) \\ (t = u = 0) \end{aligned}$$

where $f_B(\vartheta'; v)$ is defined by

$$\psi_B(r' \rightarrow \infty) = f_B(\vartheta'; v) \frac{e^{ikr'}}{\sqrt{r'}}. \quad (18)$$

Here r', ϑ' are polar coordinates with the origin at $x' = y' = 0$.

It may be noted that \bar{K}_A'' and \bar{K}_B'' may be regarded as small corrections to \bar{K}_A' and \bar{K}_B' for increasing values of l , especially if t and u are \sim zero. After the radiation forces \bar{K}_A and \bar{K}_B have been calculated in the general case, one may of course find the radiation force acting on the total system by the usual rules of vector addition.

§ 4. *General expressions for the torques on A and B.* The mean torques \bar{H}_A and \bar{H}_B acting on strips A and B, respectively, may analogously be expressed as a sum of two terms. By definition the torque \bar{H}_A with respect to the axis of strip A is given by

$$\bar{H}_A = \int_{-b}^{+b} [\bar{\Delta p}(y = -0) - \bar{\Delta p}(y = +0)] x dx. \quad (19)$$

Introducing (11) in (19), one gets from the first bracket in (11) the term

$$\bar{H}_A' = -k \operatorname{Im} \left[e^{i\pi/4} \sqrt{\frac{2\pi}{k}} \left(\frac{\partial}{\partial \vartheta} f_A(\vartheta; v) \right)_{\vartheta=v} \right]. \quad (20)$$

Here we have again used a procedure similar to the one used by Levine⁵⁾ and Keller³⁾. The second term in (11) gives rise to the following term in \bar{H}_A :

$$\bar{H}_A'' = \frac{1}{2} \operatorname{Re} \int_{-b}^{+b} \left[k^2 \psi_B^* \delta(\psi_A) - \frac{\partial}{\partial x} \psi_B^* \frac{\partial}{\partial x} \delta(\psi_A) \right] x dx. \quad (21)$$

This expression for \bar{H}_A'' will, as was the case for \bar{K}_A'' , vanish if the two strips are coplanar, but otherwise (21) is not readily simplified. Finally

$$\bar{H}_A = \bar{H}_A' + \bar{H}_A''. \quad (22)$$

For the torque \bar{H}_B' with respect to the axis of strip B one gets similar expressions. However, for the reasons mentioned earlier

we give only the expression valid in the case of coplanar strips, viz.

$$\bar{H}_B = \bar{H}_{B'} = -k \operatorname{Im} \left[e^{-ikl \cos v} \sqrt{\frac{2\pi}{k}} e^{i\pi/4} \left(\frac{\partial}{\partial \vartheta'} f_B(\vartheta'; v) \right)_{\vartheta'=v} \right]. \quad (23)$$

Here the angles t and u of fig. 1 are again both zero.

After the torques \bar{H}_A and \bar{H}_B have been calculated in the general case, one may, by means of \bar{K}_A and \bar{K}_B together with the geometry of the scattering object, also find the torque on the total system with respect to an arbitrary axis.

§ 5. *Numerical calculations.* Using the expressions derived in the preceding paragraphs, we have carried out some numerical calculations for the same geometrical arrangement of the strips as in I, i.e. two parallel strips lying in the same plane. The distance l between the strip axes may assume the values $l > 2b$; the case $l = 2b$ corresponds to a single strip of total width $4b$. The angles t and u shown in fig. 1 are now zero, while the x - y coordinate system will be placed with the origin midway between the two strip axes. The coefficients $A_{m'}$ and $B_{m'}$ occurring in the expression (6) for ψ_A and ψ_B are accordingly to be replaced by $A_m = e^{-\frac{1}{2}ikl \cos v} A_{m'}$ and $B_m = e^{+\frac{1}{2}ikl \cos v} B_{m'}$. A_m and B_m are to be determined by I, eqs (20).

All quantities calculated in this paragraph are per unit length in the direction of the strip axes.

a. The forces on A and B. As mentioned in § 3, the forces \bar{K}_A and \bar{K}_B reduce to $\bar{K}_{A'}$ and $\bar{K}_{B'}$ when the strips lie in the same plane. Accordingly, we get by means of (6) and the expression for the asymptotic behaviour of $\operatorname{Ho}_m(s, \mu)$, see e.g. I, the following explicit formula for the amplitude $f_A(\vartheta; v)$:

$$f_A(\vartheta; v) = \sqrt{\frac{8\pi}{k}} e^{-i(\pi/4)} \sum_{m=1}^{\infty} (-i)^m \operatorname{So}_m(s, \vartheta) A_m e^{\frac{1}{2}ikl \cos \vartheta}. \quad (24)$$

It then follows from (14) that \bar{K}_A is given by

$$\bar{K}_A = -k^2 \sin v \frac{4\pi}{k} \sum_{m=1}^{\infty} \operatorname{So}_m(s, v) \operatorname{Re} [(-i)^m A_m e^{\frac{1}{2}ikl \cos v}]. \quad (25)$$

Analogously we find for \bar{K}_B

$$\bar{K}_B = -k^2 \sin v \frac{4\pi}{k} \sum_{m=1}^{\infty} \operatorname{So}_m(s, v) \operatorname{Re} [(-i)^m B_m e^{-\frac{1}{2}ikl \cos v}]. \quad (26)$$

Here the coefficients A_m and B_m are, as mentioned before, to be determined by eqs (20) of I.

We make the following change in notation. Hitherto we have used the expression (1) for the incoming, plane wave ψ_i , whereas we now assume that ψ_i has the amplitude u_m/k ; i.e. the amplitude of the particle velocity in the incoming, plane wave is u_m . With the introduction of the mean density of the medium the factor in front of the summation signs in (25) and (26) then becomes

$$-\frac{4\pi\rho_0 u_m^2}{k} \sin v = -\frac{8\pi\rho_0 \overline{u_0^2}}{k} \sin v, \quad (27)$$

where $\overline{u_0^2}$ is the mean square of the particle velocity in the incoming wave.

The following numerical calculations have been carried out. For fixed values of the parameters $s = (kb)^2$ and kl , viz. $s = 1$ and $kl = 3$, we have calculated the dependence of the forces \bar{K}_A and \bar{K}_B on the angle v . The calculations have been based upon the expressions given above, breaking the series off, however, after the term $m = 3$. The coefficients A_m and B_m were found by solving the corresponding system of equations given by I eqs (20). For all angles the term $m = 3$ yields a relative contribution of the order of 10^{-3} . The results are shown in fig. 2, where we also have plotted the angular variation of the mean radiation force \bar{K} on a *single* strip of width $2b$, corresponding to the limiting case $l \rightarrow \infty$. In accordance with the results given in I, the latter curve is approximately equal to the mean value of the curves for \bar{K}_A and \bar{K}_B .

One notes the large difference in the magnitudes of \bar{K}_A and \bar{K}_B . Over most of the range \bar{K}_B is almost equal to twice the value of \bar{K}_A . However, this picture will change radically for values of l immediately above $2b$, i.e. in the present case for values of kl just beyond 2. This may be seen from fig. 3a and b where for $v = \frac{1}{4}\pi$ and $s = 1$ we have plotted \bar{K}_A and \bar{K}_B as functions of kl .

The last-mentioned calculations have been carried out for the values $kl = 2.1, 2.5, 3, 4, 5$ and, as above, we have included the terms $m \leq 3$. However, in view of the accuracy of the approximate expression (see I, eq. (38) and I, fig. 5) for the transmission coefficient of the complementary electromagnetic diffraction problem, it may reasonably be expected that similar, rather accurate ex-

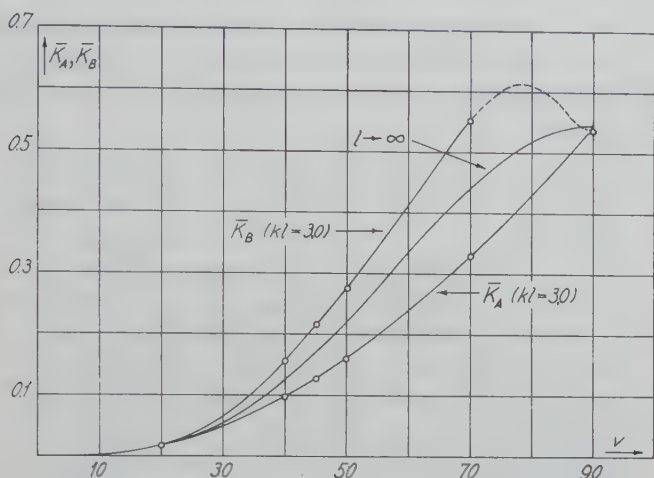


Fig. 2. The forces \bar{K}_A and \bar{K}_B , in units of $4\rho_0 u_0^2 b$, as functions of the angle v . The values of the parameters are: $kb = 1$ and $kl = 3$. Also shown is the limiting case $l \rightarrow \infty$ corresponding to a single strip.

pressions may be deduced for \bar{K}_A and \bar{K}_B . Proceeding as in I, we find here the following approximations for \bar{K}_A and \bar{K}_B .

$$\bar{K}_{A,B} = \bar{K}_1[1 - \sigma_{A,B}],$$

$$\sigma_{A,B} = \frac{\kappa_1 \cos[kl(1 \pm \cos v)] - \kappa_2 \sin[kl(1 \pm \cos v)]}{(kl)^{3/2}}, \quad (28)$$

the upper and lower sign in $\sigma_{A,B}$ corresponding to A and B respectively. Here \bar{K}_1 is the first approximation to the force on a single strip, of total width $2b$, present alone in the radiation field, see e.g. 4), and κ_1, κ_2 are given by I, eq. (39).

In fig. 3a, b the broken curves show the result of using (28) in the calculation of \bar{K}_A and \bar{K}_B . Both quantities are measured in units of $4\rho_0 u_0^2 b$. All of the above-mentioned, more accurately calculated values of \bar{K}_A and \bar{K}_B (except the ones for $kl = 2.1$) lie close to the broken curves. We consider it safe to regard the solid curves, also shown in fig. 3a and b, as an adequate representation of the forces \bar{K}_A and \bar{K}_B as functions of kl (for $s = 1$ and $v = \frac{1}{4}\pi$). One notes that even for small values of l , although larger, of course, than $2b$, the force \bar{K}_B does not become negative as one would perhaps expect. Further, it may be noticed that the oscillations of the curve for \bar{K}_A are much more pronounced than

the oscillations of the curve for \bar{K}_B . It follows from the occurrence of the argument $kl(1 - \cos v)$ in σ_B in (28) that this difference in the behaviour of the two curves will become even more marked for still smaller values of the angle v .

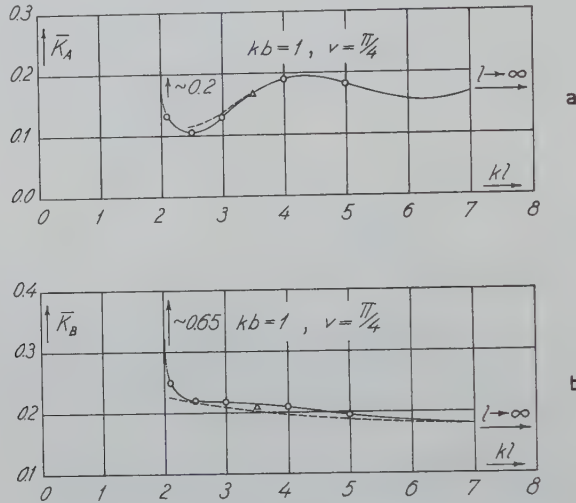


Fig. 3. The forces \bar{K}_A and \bar{K}_B , in units of $4\rho_0\bar{u}_0^2b$, as functions of kl , for $v = \frac{1}{4}\pi$ and $kb = 1$. The points shown by circles have been calculated including the terms $m \leq 3$ in (6), while the point at $kl = 3.5$ has been calculated including the terms $m \leq 2$. The broken curves show the result of using (28) in the calculation of \bar{K}_A and \bar{K}_B .

Finally we remark that the values which \bar{K}_A and \bar{K}_B assume in the limiting case $l = 2b$, where the strips touch each other, may be found by means of the expression for the wave scattered by a single strip of total width $4b$. We have *roughly* estimated the values of the two forces in this case and shown these in fig. 3 *a* and *b*.

b. The torques on A and B. In the case of two coplanar strips the torques \bar{H}_A and \bar{H}_B reduce to \bar{H}_A' and \bar{H}_B' as mentioned in § 4. By means of (20) and (24) we therefore get the following expression for the torque \bar{H}_A acting on strip A (note that the torques are calculated with respect to the corresponding strip axis):

$$\bar{H}_A = - \frac{8\pi\rho_0\bar{u}_0^2}{k^2} \sum_m \text{So}_m'(s, v) \text{Im}[(-i)^m A_m e^{ikl\cos v}]. \quad (29)$$

In a similarly way, we find for the torque acting on strip B

$$\bar{H}_B = - \frac{8\pi\rho_0 \bar{u}_0^2}{k^2} \sum_m \text{So}_m'(s, v) \text{Im}[(-i)^m B_m e^{-\frac{1}{2}ikl\cos v}]. \quad (30)$$

Here the coefficients A_m and B_m are again found as the solution of eqs. (20) of I.

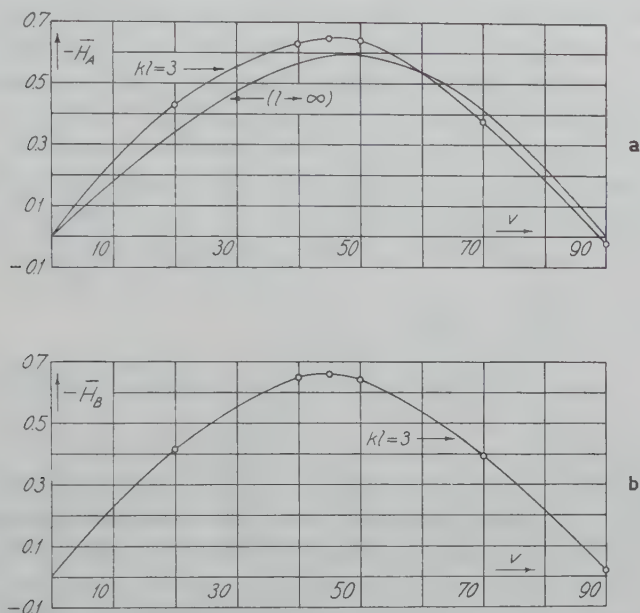


Fig. 4. The torques \bar{H}_A and \bar{H}_B , in units of $\pi\rho_0\bar{u}_0^2b^2$, as functions of the angle v . The values of the parameters are $kb = 1$ and $kl = 3$. Also shown is the limiting case $l \rightarrow \infty$ corresponding to a single strip.

Using these expressions, we have in fig. 4a and b plotted the dependence of the torques \bar{H}_A and \bar{H}_B , in units of $\pi\rho_0\bar{u}_0^2b^2$, on the angle v . The values of the other parameters in the calculations are $s = (kb)^2 = 1$ and $kl = 3$. All values are calculated as discussed above with inclusion of the terms $m \leq 3$. Also shown in this figure is the angular variation of the torques corresponding to the limiting case $l \rightarrow \infty$. Apart from a change in the numerical magnitude, the curves are quite similar to each other. On the other hand, it will be seen from fig. 5a and b that this change in the

numerical magnitude may become *very large* for values of l immediately above $2b$. One might, of course, by means of the expression for the wave scattered by a single strip of width $4b$, calculate the curves corresponding to the limiting case $l = 2b$. However, we have not attempted to do so since the calculations are very tedious.

The rapid variation of \bar{H}_A and \bar{H}_B with kl is more clearly shown in fig. 5a and b. Here we have plotted \bar{H}_A and \bar{H}_B , in units of $\pi\rho_0 u_0^2 b^2$, as functions of kl , for $s = 1$ and $v = \frac{1}{4}\pi$. The calculations have for $kl = 2.1, 2.5, 3, 4, 5$ again been based on the expressions (29) and (30) together with I, eq. (20) including the terms $m \leq 3$. This again represents a good approximation to \bar{H}_A and \bar{H}_B .

It is possible to derive approximate expressions for the torques \bar{H}_A and \bar{H}_B in much the same way as for the forces \bar{K}_A and \bar{K}_B . We proceed again as in I and find the following results:

$$\bar{H}_{A,B} = \bar{H}_1[1 + \nu_{A,B}],$$

$$\nu_{A,B} = \frac{1}{f_{0,1}} \frac{\kappa_2 \cos [kl(1 \pm \cos v)] + \kappa_1 \sin [kl(1 \pm \cos v)]}{(kl)^{3/2}}, \quad (31)$$

where the upper sign applies for ν_A and the lower one for ν_B . The quantities κ_1, κ_2 are defined in I eq. (39) while the definition of $f_{0,1}$ may be found in I, § 3. Finally \bar{H}_1 is the first approximation to the torque on a *single* strip of total width $2b$, see e.g. 4). In fig. 5a and b, the broken curves show the values of \bar{H}_A and \bar{H}_B (for $s = 1$ and $v = \frac{1}{4}\pi$) calculated by means of (31). It will be seen that the expressions (31) do represent a rather good approximation to \bar{H}_A and \bar{H}_B as soon as l is somewhat larger than $2b$. Further one notes that, as was also the case for the forces \bar{K}_A and \bar{K}_B , the curve giving \bar{H}_B oscillates *much* less than the corresponding curve for \bar{H}_A .

As shown in fig. 4a and b, \bar{H}_A and \bar{H}_B are different from zero in the case of normal incidence of the plane wave. For a *single* strip, present alone in the radiation field, the torque will, by reasons of symmetry, vanish in this case. When the two strips are present together in the radiation field, however, the symmetry of the problem only requires that the torque on the *total* system with respect to the z -axis vanishes, i.e. $\bar{H}_A(v = \frac{1}{2}\pi) = -\bar{H}_B(v = \frac{1}{2}\pi)$.

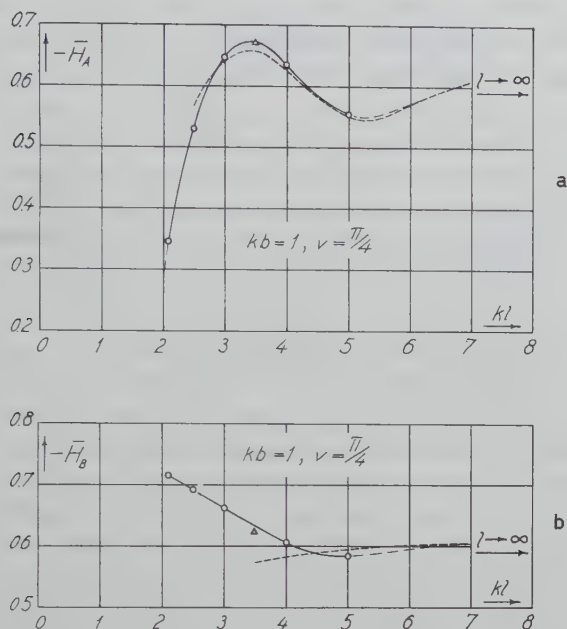


Fig. 5. The torques \bar{H}_A and \bar{H}_B , in units of $\pi\rho_0\overline{u_0^2}b^2$, as functions of kl for $v = \frac{1}{4}\pi$ and $kb = 1$. The points shown by circles have been calculated including the terms $m \leq 3$ in (6), while the point at $kl = 3.5$ has been calculated including the terms $m \leq 2$. The broken curves show the result of using (31) in the calculation of \bar{H}_A and \bar{H}_B .

From (29) we get for normal incidence

$$\bar{H}_A(v = \frac{1}{2}\pi) = -\frac{8\pi\rho_0\overline{u_0^2}}{k^2} \sum_{p=1}^{\infty} (-1)^p \text{So}_{2p}'(s, \frac{1}{2}\pi) \text{Im } A_{2p}, \quad (32)$$

because $\text{So}'_{2p+1}(s, \frac{1}{2}\pi) = 0$. One may thus, rather easily, calculate $\bar{H}_A(v = \frac{1}{2}\pi)$ as function of kl . The results of such a calculation are given in fig. 6. It will be seen that only when the strips are very close together the torque will be appreciably different from zero. Further one notes that, as a consequence of the oscillatory approach to zero for increasing values of kl , the torque may become *negative* although of course of a small numerical magnitude.

Finally, we have calculated the torque \bar{H}_A as a function of kb for a fixed ratio of $l/b = 5$ and $v = \frac{1}{4}\pi$. Here it suffices to use only the term $m = 1$ in (29) and I. eq. (20) in order to get a sufficiently

good approximation. The results are shown in fig. 7. Apart from minor deviations this curve essentially coincides with the corresponding one for a single strip.

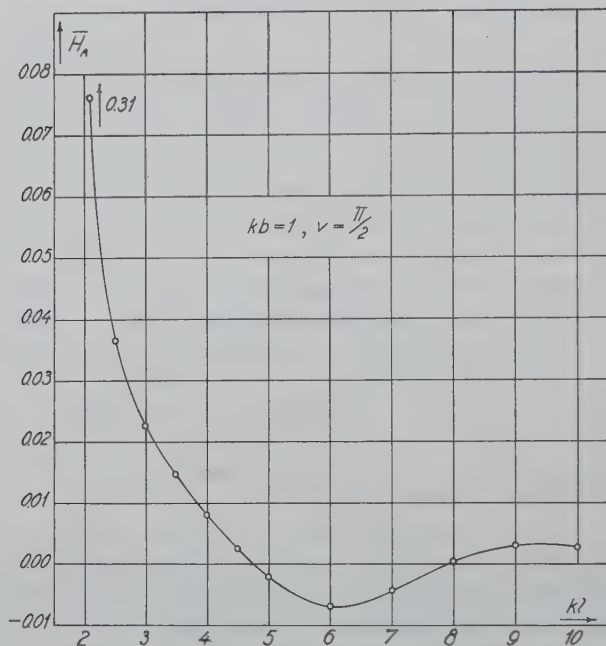


Fig. 6. The torque \bar{H}_A for normal incidence of the plane wave as a function of kl for $kb = 1$. The unit used is $\pi\rho_0\mu_0^2b^2$.

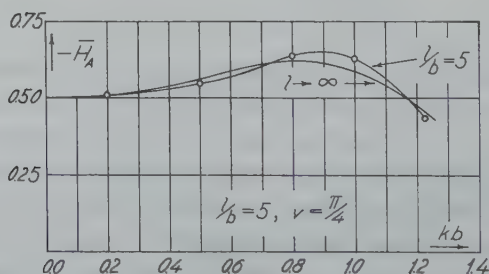


Fig. 7. The torque \bar{H}_A for $v = \frac{1}{4}\pi$ and $l/b = 5$ as a function of kb . The unit used is $\pi\rho_0\mu_0^2b^2$. Also shown is the limiting case $l \rightarrow \infty$ corresponding to a single strip.

§ 6. *Conclusion.* We admit that the foregoing calculations may in no way be considered exhaustive. For instance, we have essentially used only one value for the ratio between half the strip width and the wavelength, i.e. $kb = 1$, although it would have been desirable to have extended the calculations to other values of kb . Analogously, it would have been of interest to perform more calculations for values of l immediately above the limiting value $l = 2b$. However, in view of the following considerations we have refrained from doing so.

First of all, it is our opinion that the results of the present paper together with those of I give, for wavelengths in the region $kb \lesssim 2$, a rather clear picture of the diffraction of a plane wave by a system of two strips lying in the same plane. When the distance between the two innermost strip edges is *very* small, the interaction between the two strips will naturally be very strong. However, this interaction will diminish *rapidly* with increasing distance between the strips. This is reflected, for instance, in the very steep decay of the forces and torques on the strips as shown in figs 3*a* and *b*; 5*a* and *b* and in fig. 6. If one considers the complementary electromagnetic diffraction problem, the same feature is shown by the transmission coefficient (see I). After the rapid decay the two strips behave essentially like two independent strips. This over-all behaviour is, furthermore, qualitatively independent of the angle of incidence of the plane wave. To round off the picture somewhat, we remark that in the region following the rapid decay that strip which is reached first by the wave-fronts of the incoming plane wave will, in a certain sense, be most strongly influenced by the presence of the other strip. We conclude this from the more pronounced oscillations of the force and torque on this strip, e.g. strip A, compared to those on the other strip, e.g. strip B.

Secondly, and more important, if one is interested in the diffraction problem not just as a mathematical question of solving the wave equation (5) with due regard to the boundary conditions, but as a description of an actual physical process, one is forced to investigate whether the basic assumptions underlying the calculations are valid. Thus it is necessary to investigate in detail whether it is allowable to neglect all effects of the viscosity of the medium surrounding the strips. This may eventually be allowable

when the strips are far apart from each other. When the strips are close together, however, the influence of viscosity, boundary-layer effects etc., is most likely very great. Thus, in the region where the present diffraction problem shows an interesting behaviour, the comparatively simple model represented by (4) and (5) is likely to be a bad approximation to the actual physical process. It is therefore hardly profitable to carry out more calculations of the type presented here. On the other hand, it may be pointed out that a comparison of experimental results with the calculations given here might give some information on the role played by viscosity in diffraction problems.

Acknowledgement. It is a pleasure to thank Professor H. Højgaard Jensen and Mr. V. Frank, M.Sc. for many discussions and for reading of the manuscript.

Received 8th April, 1959.

REFERENCES

- 1) Særmark, K., Appl. Sci. Res. B7 (1959).
- 2) Levine, H. and J. Schwinger, Phys. Rev. **87** (1952) 224.
- 3) Keller, J. B., Res. Rep. No. EM-104, New York Univ. 1957; P. J. Westervelt: J. Acoust. Soc. Amer. **29** (1957) 26.
- 4) Højgaard Jensen, H. and K. Særmark: Acoustica **8** (1958) 79.
- 5) Levine, H., Proc. Camb. Phil. Soc. **53** (1957) 234.
- 6) Bouwkamp, C. J., Rep. Progr. Phys. **17** (1954) 35.
- 7) Olsen, H., W. Romberg and H. Wergeland: J. Acoust. Soc. Amer. **30** (1958) 69.

TRANSMISSION COEFFICIENT FOR A SYSTEM
OF PARALLEL SLITS IN A THIN, PLANE SCREEN

by K. SÆRMARK

Physics Department, Technical University of Denmark, Copenhagen, Denmark

Summary

Some numerical results for the transmission coefficient of a system of parallel slits in a thin, plane and perfectly conducting screen are given. The electric field vector is polarised along the slit axes.

§ 1. *Introduction.* In a previous paper ¹⁾ we considered the scattering of an incoming plane wave ψ_i by a system of two infinitely long, thin, parallel strips. The boundary condition, satisfied by the total wave function $\psi = \psi_i + \psi_s$, was that the normal gradient of ψ should be zero on the surface of the two strips. Further, numerical calculations were performed for the special case of two coplanar strips. By means of Babinet's principle, these calculations were utilised to find the transmission coefficient of the complementary diffraction problem, i.e. the diffraction of a plane, electromagnetic wave by a thin, plane, perfectly conducting screen containing two parallel slits congruent with the above mentioned strips. The electric field vector is polarised along the slit axes.

In this note we give some additional numerical results obtained by including more than two strips in the calculations. The procedure followed will be the same as in ¹⁾, and we refer to that paper for a more detailed explanation.

The results obtained in this note are compared with calculations of the transmission coefficient for an infinite grating. This problem has been treated in several papers among which we may mention those of Miles ²⁾ and of Baldwin and Heins ³⁾. In both of these papers the problem of an infinite plane grating is treated by means of integral equation methods applicable only for normal incidence of the plane wave. This is not the case for the method used in this note;

however, numerical calculations will be performed only for normal incidence.

§ 2. *General expressions.* We consider $2N$ strips, situated in the x - z plane, symmetrically arranged with respect to $x = 0$ and with their axes parallel to the z -axis. The strips are of equal width $2b$ and the distance between two consecutive strip axes is l . The wave vector \mathbf{k} of the incoming plane wave lies in the x - y plane and may, in general, make an arbitrary angle v with the x -axis. As usual, the wave function is required to satisfy Helmholtz's wave equation and Sommerfeld's radiation condition at infinity. The boundary condition to be satisfied at the surface of the strips is

$$\text{grad}_{\mathbf{n}}(\psi_i + \psi_s) = 0. \quad (1)$$

As in ¹⁾, we now assume that the scattered wave ψ_s may be written as a sum of scattered waves, one for each strip:

$$\psi_s = \sum_{j=1}^{2N} \varphi_j, \quad (2)$$

and that each of the functions φ_j may be expanded in the following way:

$$\varphi_j = \sqrt{8\pi} \sum_{q=1}^{\infty} A_{j,q} \text{So}_q(s, \alpha_j) \text{Ho}_q(s, \mu_j). \quad (3)$$

Here α_j, μ_j are elliptical cylinder coordinates defined by the j -th strip, while $\text{So}_q(s, \alpha_j)$ and $\text{Ho}_q(s, \mu_j)$ are the periodic odd Mathieu-functions and the associated Hankel-like Mathieu-functions, respectively. The parameter s is defined by $s = (kb)^2$ and the expansion coefficients $A_{j,q}$ are to be determined so that the boundary condition (1) is satisfied. As shown in ¹⁾ it is possible, by means of an addition theorem for Mathieu-functions ⁴⁾, together with the fact that the incoming plane wave ψ_i may be expanded in terms of the various elliptical cylinder coordinates involved, to satisfy the boundary condition (1) by solving an infinite system of linear equations for the coefficients $A_{j,q}$. This procedure will, of course, become extremely complicated for more than two strips. For small values of s ($\lesssim 4-5$), however, it is natural to attempt to simplify the equations by retaining only the first term in the expansion (3); the calculations of the scattering cross-section for two strips show, see ¹⁾, that this

is a good approximation as soon as the strip axes are separated by a distance l somewhat greater than $2b$.

We therefore approximate φ_j by

$$\varphi_j = \sqrt{8\pi} A_j \text{So}_1(s, \alpha_j) \text{Ho}_1(s, \mu_j). \quad (4)$$

As mentioned earlier, numerical calculations will be performed only for normal incidence of the plane wave, i.e.

$$\psi_i = e^{iky}. \quad (5)$$

(In this and in the foregoing expressions we have suppressed the time factor $\exp(-i\omega t)$.) It then follows from the symmetry of the scattered wave around $x = 0$ and from the symmetry properties of the Mathieu-functions that the coefficients A_j will be equal in pairs: $A_1 = A_{2N}$; $A_2 = A_{2N-1}$; etc. Accordingly the number of coefficients to be determined is in this case reduced by a factor 2.

With the approximations given above we may now write down N equations in the unknown coefficients A_1, \dots, A_N . Without giving the details of the derivation (cf.¹), we will give the equations obtained in the case of eight strips:

$$\begin{aligned} A_1[1 + \gamma(7kl)] + A_2[\gamma(kl) + \gamma(6kl)] + A_3[\gamma(2kl) + \gamma(5kl)] + \\ + A_4[\gamma(3kl) + \gamma(4kl)] = -a, \\ A_1[\gamma(kl) + \gamma(6kl)] + A_2[1 + \gamma(5kl)] + A_3[\gamma(kl) + \gamma(4kl)] + \\ + A_4[\gamma(2kl) + \gamma(3kl)] = -a, \quad (6) \\ A_1[\gamma(2kl) + \gamma(5kl)] + A_2[\gamma(kl) + \gamma(4kl)] + A_3[1 + \gamma(3kl)] + \\ + A_4[\gamma(kl) + \gamma(2kl)] = -a, \\ A_1[\gamma(3kl) + \gamma(4kl)] + A_2[\gamma(2kl) + \gamma(3kl)] + A_3[\gamma(kl) + \gamma(2kl)] + \\ + A_4[1 + \gamma(kl)] = -a, \end{aligned}$$

where $a = \text{Ko}_1(1 + if_{0,1})^{-1}$ and $\gamma(nkl) = \gamma_{-1,-1}(nkl)$ are defined as in ¹, eqs. (8) and (18).

When this system of equations has been solved, one may, by means of (4) and (2), find the scattered wave ψ_s . If r and ϑ are the usual polar coordinates, one finds for large values of r the well-known expression for the asymptotic behavior of ψ_s :

$$\psi_s(r \rightarrow \infty) = f(\vartheta) \frac{e^{ikr}}{\sqrt{r}}. \quad (7)$$

The quantity which we want to calculate is the transmission

coefficient for the complementary problem, i.e. we now replace the strips by a congruent system of slits in a thin, infinite, perfectly conducting plane. Interpreting the incoming wave as an electromagnetic wave with the electric field vector polarised along the slit axes, it follows from Babinet's principle that the scattered wave ψ_s' for this problem may be found from the above mentioned ψ_s by the relation

$$\psi_s' = -\psi_s, \quad (8)$$

valid in the region $y > 0$. The transmission coefficient may then be found by the definition

$$T_{2N} \equiv \frac{1}{4Nb} \int_0^\pi |f(\vartheta)|^2 d\vartheta = -\frac{1}{4Nb} \sqrt{\frac{2\pi}{k}} \operatorname{Re} \left[e^{i(\pi/4)} f\left(v = \frac{\pi}{2}\right) \right] \quad (9)$$

(see 1)).

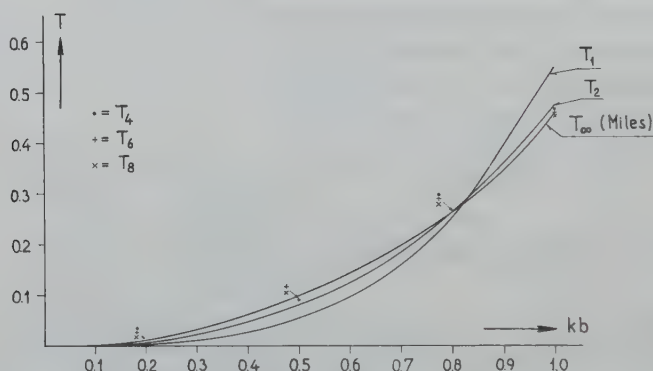


Fig. 1. The transmission coefficient T for systems of 1, 2, 4, 6 and 8 parallel slits in an infinite screen as function of kb . The distance between the slit axes is $l = 4b$. The incoming plane wave has its electric field vector polarised along the slit axes and is normally incident on the screen. Also shown is the transmission coefficient for an infinite grating as calculated by Miles²⁾.

§ 3. *Numerical results.* The formalism sketched in the preceding section has been applied to the following numerical calculations. For normal incidence and the fixed ratio $l/b = 4$ the transmission coefficients T_2 and T_4 have been calculated as functions of kb for wavelengths in the region $kb \leq 2$, while T_6 and T_8 have been calculated for wavelengths in the region $kb \leq 1$. The results of these calculations are shown in fig. 1 and fig. 2. Here we have also

plotted the transmission coefficient for a single slit and for the corresponding infinite grating as calculated by Miles³⁾.

From the curves shown one notes the rather remarkable fact, and this is actually the reason for publishing this note, that for *all* wavelengths, except a small range around the resonance value $\lambda = l$, the transmission coefficient for a system of but four slits is

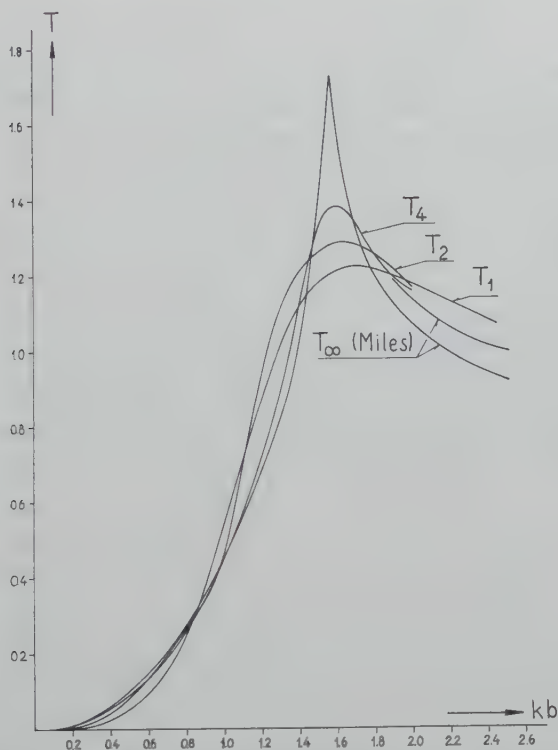


Fig. 2. The transmission coefficient for a system of 1, 2 and 4 parallel slits in an infinite screen as function of kb . The distance between the slit axes is $l = 4b$. The incoming plane wave has its electric field vector polarised along the slit axes and is normally incident on the screen. Also shown is the transmission coefficient for an infinite grating as calculated by Miles²⁾. For $kb = 2.0$ also T_6 and T_8 have been calculated. The results are practically identical with T_4 .

nearly identical with the transmission coefficient for an infinite grating. In fact, for $kb \lesssim 1$ even T_2 is practically identical with T_{∞} . This behaviour of the transmission coefficient for an increasing

number of slits is *not* found if the incoming plane wave is polarized with the electric field vector *perpendicular* to the *slit* axes. E. B. Hansen ⁵⁾ has treated the latter case by means of methods analogous to those used by Bouwkamp ⁶⁾ in the wavelength-region $kb \lesssim 0.6$ and finds that the approach to an infinite grating in this case is much slower than the one found in the polarisation case treated in this note.

Note added in proof. In ref. ¹⁾ there is a misprint in eq. (A7). The factor in front of the summation sign should be $i^{(m-q)}$ and *not* $i^{(q-m)}$. The related eq. (A4) of ref. ¹⁾ is correct.

Received 15th May, 1959

REFERENCES

- 1) Særmark, K., Appl. Sci. Res. B **7** (1959) 417.
- 2) Miles, J. W., Quart. Appl. Math. VII (1949) 45.
- 3) Baldwin, G. L. and A. E. Heins, Mathematica Scandinavica **2** (1954) 103.
- 4) Særmark, K., to be published in Z. angew. Math. Phys., July 1959.
- 5) Hansen, E. B., Thesis Technical University of Denmark, 1958 (unpublished).
- 6) Bouwkamp, C. J., NY Univ. Math. Res. Rep. No EM-50, 1953.

DIFFRACTION BY AN IMPERFECTLY CONDUCTING
HALF-PLANE AT OBLIQUE INCIDENCE

by T. B. A. SENIOR

The University of Michigan, Ann Arbor, Michigan, U.S.A.

Summary

The exact solution is obtained for the problem of a plane wave incident at an oblique angle on a half-plane of large but finite conductivity. The usual approximate boundary conditions are applied and lead to coupled Wiener-Hopf integral equations from which to determine the currents excited on the surface of the sheet. The resulting expressions for the field components are found to be entirely different from those which would have been obtained by applying the technique used for the derivation of three-dimensional solutions in the case of perfectly conducting structures, and, indeed, not one component is given to the required accuracy by this technique.

§ 1. *Introduction.* In this paper attention will be confined to diffracting structures which are two-dimensional in the sense of being composed of cylinders of arbitrary cross-section whose generators are all parallel to the z -axis of some coordinate system.

If a structure of this type is perfectly conducting, it is possible to deduce the solution for a three-dimensional incident field from the solution for a two-dimensional field, and, in particular, the solution for a plane wave at oblique incidence can be obtained from that in which the plane wave is normal to the z -axis. The method is based upon the fact that any solution of the two-dimensional wave equation gives rise to a solution of the three-dimensional equation on replacing the propagation constant k by $k \cos \beta$ and multiplying by $\exp(-ikz \sin \beta)$. If the particular solution considered represents the solution for the electromagnetic problem in which the incident field is a two-dimensional plane wave, and if it is modified in the above way and then taken to be the z -component of an electric or magnetic Hertz vector whose other components are zero, a solution of the three-dimensional problem is produced. The corresponding incident field has either H_z or E_z zero (depending

on whether the two-dimensional field was E or H polarized), and the two fundamental fields so generated can be combined to give the solution for any incident field. The method has been described in detail by Clemmow¹⁾ and was used by Senior²⁾ to determine the field of a dipole in the presence of a half-plane.

When the structure is not perfectly conducting, the method is no longer applicable and the question then is whether an analogous technique can be developed to treat such cases. To attempt an answer to this, an obvious approach is to tackle a particular problem in the hope that its solution may indicate a general transformation, and apart from the problem of a circular cylinder (for which the solution is almost trivial) one of the most simple is that of a plane wave incident at an oblique angle on a half-plane of large but finite conductivity. The present paper is devoted entirely to a consideration of this problem.

The crux of the analysis is the determination of coupled integral equations for the electric and magnetic current distributions excited on the surface of the half-plane. These are of the Wiener-Hopf type and can be solved to give expressions for the currents in terms of the "split" functions which characterized the solution for normal incidence³⁾. The field components are then given as integrals over the currents, and some ramifications of the results are examined.

§ 2. *The integral equations.* Consider a thin semi-infinite sheet of large but finite conductivity occupying the half-plane $y = 0$, $x > 0$ of a rectangular Cartesian coordinate system (x, y, z) . A plane wave is incident in a direction making an angle α with the positive x axis and an angle $\pi/2 - \beta$ with the z axis; $\beta = 0$ then corresponds to incidence in the plane perpendicular to the diffracting edge.

The actual form of the incident field matters little as regards the analysis, but in order to simplify the comparison of the results with those for a perfectly conducting sheet the field is taken to be a quasi three-dimensional plane wave which is E -polarized and whose components are given by

$$\mathbf{E}^i = (-\cos \alpha \sin \beta \cos \beta, -\sin \alpha \sin \beta \cos \beta, \cos^2 \beta) \exp[-ik(x \cos \alpha \cos \beta + y \sin \alpha \cos \beta + z \sin \beta)], \quad (1)$$

$$\mathbf{H}^i = (-Y \sin \alpha \cos \beta, Y \cos \alpha \cos \beta, 0) \exp[-ik(x \cos \alpha \cos \beta + y \sin \alpha \cos \beta + z \sin \beta)], \quad (2)$$

where $Y = 1/Z$ is the intrinsic admittance of free space and a time factor $e^{-i\omega t}$ is suppressed. The above field is that which is obtained by modifying a two-dimensional E -polarized plane wave in the manner described in the previous paragraph.

If η is the reciprocal of the complex refractive index of the material comprising the sheet, the boundary conditions to be applied can be written as

$$\mathbf{E} - (\mathbf{n} \cdot \mathbf{E}) \mathbf{n} = \eta Z \mathbf{n} \times \mathbf{H}, \quad (3)$$

where \mathbf{n} is a unit vector normal, drawn outwards from the sheet. On the upper surface \mathbf{n} is in the positive y direction, and (3) then gives

$$E_x = \eta Z H_z, \quad E_z = -\eta Z H_x.$$

Similarly, on the lower surface

$$E_x = -\eta Z H_z, \quad E_z = \eta Z H_x.$$

As a consequence of these conditions, the tangential components of both the electric and the magnetic vectors will be discontinuous on crossing the sheet, and it is convenient to regard these discontinuities as due to the presence of electric and magnetic currents in the sheet. We therefore write

$$\begin{aligned} E_z \Big|_{y=+0}^{y=-0} &= I_1(x', z'), & H_x \Big|_{y=+0}^{y=-0} &= I_2(x', z'), \\ E_x \Big|_{y=+0}^{y=-0} &= I_3(x', z'), & E_z \Big|_{y=+0}^{y=-0} &= I_4(x', z'), \end{aligned}$$

where I_2 and I_4 are the electric currents and I_1 and I_3 are the magnetic ones. I_1 and I_4 are perpendicular to the diffracting edge whilst I_2 and I_3 are parallel, and when the field is normally incident ($\beta = 0$) I_3 and I_4 are identically zero.

The electric field at a point (x, y, z) can be expressed as a surface integral in the form

$$\mathbf{E}(x, y, z) = \frac{1}{4\pi} \int_S [ikZ(\mathbf{n} \times \mathbf{H}) - (\mathbf{n} \times \mathbf{E}) \times \nabla - (\mathbf{n} \cdot \mathbf{E}) \nabla] \frac{e^{ik\rho}}{\rho} dS, \quad (4)$$

(see for example ⁴) p. 467) where \mathbf{n} is a unit vector normal drawn into the volume contained by the surface S . The differentiation is with respect to the coordinates of the observation point and ρ is the distance to a variable point (x', y', z') on S .

The surface S is made up of two sheets which envelop the diffracting structure, together with a cylinder of infinitely large radius centered on the z -axis and meeting the two sheets at $x = \infty$. The integration over the cylindrical portion is easily shown to produce the incident field, and accordingly (4) can be written

$$\mathbf{E}(x, y, z) = \mathbf{E}^i(x, y, z) + \frac{1}{4\pi} \int_0^\infty \int_{-\infty}^\infty [ikZ(\mathbf{n} \times \mathbf{H}) - (\mathbf{n} \times \mathbf{E}) \times \nabla - (\mathbf{n} \cdot \mathbf{E}) \nabla] \frac{e^{ik\rho}}{\rho} \bigg|_{y=-0}^{y=+0} dx' dz'. \quad (5)$$

On the upper surface of the half-plane

$$\mathbf{n} \times \mathbf{H} = (H_z, 0, -H_x),$$

from which we obtain

$$\mathbf{n} \times \mathbf{H} \bigg|_{y=-0}^{y=+0} = (I_4, 0, -I_2).$$

Similarly,

$$(\mathbf{n} \times \mathbf{E}) \times \nabla \frac{e^{ik\rho}}{\rho} \bigg|_{y=-0}^{y=+0} = \left(I_3 \frac{\partial}{\partial y}, -I_3 \frac{\partial}{\partial x} - I_1 \frac{\partial}{\partial z}, I_1 \frac{\partial}{\partial y} \right) \frac{e^{ik\rho}}{\rho}$$

and

$$(\mathbf{n} \cdot \mathbf{E}) \nabla \frac{e^{ik\rho}}{\rho} \bigg|_{y=-0}^{y=+0} = i \frac{Z}{k} \left(\frac{\partial I_2}{\partial z'} - \frac{\partial I_4}{\partial x'} \right) \left(\frac{\partial}{\partial x}, \frac{\partial}{\partial y}, \frac{\partial}{\partial z} \right) \frac{e^{ik\rho}}{\rho},$$

and if these are inserted into (5), the equation becomes

$$\begin{aligned} \mathbf{E}(x, y, z) = & \mathbf{E}^i(x, y, z) + \frac{1}{4\pi} \int_0^\infty \int_{-\infty}^\infty \left[ikZ(I_4, 0, -I_2) - \left(I_3 \frac{\partial}{\partial y}, -I_3 \frac{\partial}{\partial x} - I_1 \frac{\partial}{\partial z}, I_1 \frac{\partial}{\partial y} \right) \right. \\ & \left. - i \frac{Z}{k} \left(\frac{\partial I_2}{\partial z'} - \frac{\partial I_4}{\partial x'} \right) \left(\frac{\partial}{\partial x}, \frac{\partial}{\partial y}, \frac{\partial}{\partial z} \right) \right] \frac{e^{ik\rho}}{\rho} dx' dz'. \quad (6) \end{aligned}$$

At normal incidence the fields and currents are independent of z' (and hence z), and, in addition, there is no current I_4 ; the terms in the third group of the above integrand then disappear.

An assumption is now made concerning the dependence of the field upon the coordinate z . The diffracting structure itself is two-

dimensional, and since all the components of the incident field involve z only through a factor $\exp(-ikz \sin \beta)$, it seems reasonable to assume that this dependence will also apply to the total field. A consequence of this is that

$$I_p(x', z') = e^{-ikz' \sin \beta} I_p(x')$$

for $p = 1, 2, 3, 4$, which makes it a trivial matter to carry out the integration with respect to z' in equation (6).

To evaluate the z' integral it is sufficient to consider

$$\int_{-\infty}^{\infty} e^{-ikz' \sin \beta} \frac{e^{ikp}}{\rho} dz' = e^{-ikz \sin \beta} \int_{-\infty}^{\infty} e^{-ik(z' - z) \sin \beta} \frac{e^{ikp}}{\rho} dz',$$

where, of course, $\rho = \sqrt{(x' - x)^2 + y^2 + (z' - z)^2}$, and if we put $z' - z = Q \sinh \gamma$ with $Q = \sqrt{(x' - x)^2 + y^2}$ the integral becomes

$$\begin{aligned} e^{-ikz \sin \beta} \int_{-\infty}^{\infty} e^{ikQ(\cosh \gamma - \sin \beta \sinh \gamma)} d\gamma &= \\ &= e^{-ikz \sin \beta} \int_{-\infty}^{\infty} e^{ikQ \cos \beta \cosh(\gamma + \tanh^{-1} \sin \beta)} d\gamma = \pi i e^{-ikz \sin \beta} H_0^{(1)}(kQ \cos \beta). \end{aligned}$$

The nature of this result shows that the assumption about the z -dependence is self-consistent and allows us to suppress the coordinate z throughout the subsequent analysis. Equation (6) can then be written as

$$\begin{aligned} \mathbf{E}(x, y) = \mathbf{E}^i(x, y) - \frac{1}{4} \int_0^{\infty} \left[kZ(I_4, 0, -I_2) + \right. \\ \left. + i \left(I_3 \frac{\partial}{\partial y}, -I_3 \frac{\partial}{\partial x} + ik \sin \beta I_1, I_1 \frac{\partial}{\partial y} \right) + \right. \\ \left. + \frac{Z}{k} \left(ik \sin \beta I_2 + \frac{\partial I_4}{\partial x'} \right) \left(\frac{\partial}{\partial x}, \frac{\partial}{\partial y}, -ik \sin \beta \right) \right] H_0^{(1)}(kQ \cos \beta) dx'. \quad (7) \end{aligned}$$

The above integrand involves $\partial I_4 / \partial x'$, and if I_4 were zero at the edge of the half-plane, integration by parts would enable the derivative to be replaced by $I_4 (\partial / \partial x)$. It is known that in the case of an H -polarized plane wave at normal incidence the magnetic current perpendicular to the edge vanishes at the edge³), and for simplicity it will be assumed that the same is true at oblique

incidence. If this behaviour is not postulated at the outset, the solution of the integral equations becomes more complicated, although the analysis can still be carried through. The details are given in the Appendix, and from these results it follows that $I_4(0)$ must be identically zero.

Equation (7) now gives rise to three scalar equations for the currents:

$$E_x(x, y) - E_x^i(x, y) = -\frac{1}{4} \int_0^\infty \left[kZI_4 \left(1 + \frac{1}{k^2} \frac{\partial^2}{\partial x^2} \right) + iI_3 \frac{\partial}{\partial y} + iZ \sin \beta I_2 \frac{\partial}{\partial x} \right] H_0^{(1)}(kQ \cos \beta) dx', \quad (8)$$

$$E_y(x, y) - E_y^i(x, y) = \frac{1}{4} \int_0^\infty \left(iI_3 \frac{\partial}{\partial x} + k \sin \beta I_1 - iZ \sin \beta I_2 \frac{\partial}{\partial y} - \frac{Z}{k} I_4 \frac{\partial^2}{\partial x \partial y} \right) H_0^{(1)}(kQ \cos \beta) dx', \quad (9)$$

$$E_z(x, y) - E_z^i(x, y) = \frac{1}{4} \int_0^\infty \left(kZ \cos^2 \beta I_2 - iI_1 \frac{\partial}{\partial y} + iZ \sin \beta I_4 \frac{\partial}{\partial x} \right) H_0^{(1)}(kQ \cos \beta) dx'. \quad (10)$$

Integral equations for I_2 and I_4 can be obtained from these by letting the field point approach the half-plane successively from above and from below. By taking the limits of equations (8) and (10) as $y \rightarrow \pm 0$ and using the fact that

$$(\lim_{y \rightarrow +0} + \lim_{y \rightarrow -0}) \int_0^\infty I_p(x') \frac{\partial}{\partial y} H_0^{(1)}(kQ \cos \beta) dx' = 0,$$

we have

$$\begin{aligned} E_x(x, +0) + E_x(x, -0) - 2E_x^i(x, 0) &= \\ &= -\frac{1}{2} \int_0^\infty \left[kZI_4 \left(1 + \frac{1}{k^2} \frac{\partial^2}{\partial x^2} \right) + iZ \sin \beta I_2 \frac{\partial}{\partial x} \right] H_0^{(1)}(k|x' - x| \cos \beta) dx', \\ E_z(x, +0) + E_z(x, -0) - 2E_z^i(x, 0) &= \\ &= \frac{1}{2} \int_0^\infty \left(kZ \cos^2 \beta I_2 + iZ \sin \beta I_4 \frac{\partial}{\partial x} \right) H_0^{(1)}(k|x' - x| \cos \beta) dx', \end{aligned}$$

and since

$$E_x(x, +0) + E_x(x, -0) = \eta Z I_4,$$

$$E_z(x, +0) + E_z(x, -0) = -\eta Z I_2,$$

it follows that

$$\begin{aligned} \eta I_4(x) + 2Y \cos \alpha \sin \beta \cos \beta \exp[-i k x \cos \alpha \cos \beta] = \\ = -\frac{1}{2} \int_0^\infty \left[k I_4 \left(1 + \frac{1}{k^2} \frac{\partial^2}{\partial x^2} \right) + i \sin \beta I_2 \frac{\partial}{\partial x} \right] H_0^{(1)}(k |x' - x| \cos \beta) dx' \quad (11) \end{aligned}$$

$$\begin{aligned} \eta I_2(x) + 2Y \cos^2 \beta \exp[-i k x \cos \alpha \cos \beta] = \\ = -\frac{1}{2} \int_0^\infty \left(k \cos^2 \beta I_2 + i \sin \beta I_4 \frac{\partial}{\partial x} \right) H_0^{(1)}(k |x' - x| \cos \beta) dx', \quad (12) \end{aligned}$$

which are coupled Wiener-Hopf equations for the determination of the electric currents I_2 and I_4 .

To obtain the integral equations for I_1 and I_3 either of two procedures can be followed. The first of these has its origin in the observation that the currents I_2 and I_4 whose equations have already been found are both electric currents, and the starting point for the derivation of (11) and (12) was the expression of the electric field at a point (x, y, z) in terms of a surface integral over the currents. Consequently, it is to be expected that if the magnetic field were written as a surface integral analogous to that in (4), the same analysis as the above would lead to equations for I_1 and I_3 .

The second method is equivalent to this, but avoids the necessity of going back to the expression of the magnetic field as a surface integral over the field components. If (8) and (10) are differentiated with respect to y before the field point is allowed to approach the surface of the sheet, (9) can then be used to determine H_x and H_z .

If this second method is adopted, the fact that

$$H_x = i \frac{Y}{k} \left(\frac{\partial E_y}{\partial z} - \frac{\partial E_z}{\partial y} \right)$$

and

$$H_z = i \frac{Y}{k} \left(\frac{\partial E_x}{\partial y} - \frac{\partial E_y}{\partial x} \right)$$

gives, by suitable differentiation of (8), (9) and (10),

$$H_x(x, y) - H_x^i(x, y) = \frac{1}{4} \int_0^\infty \left[kY I_1 \left(1 + \frac{1}{k^2} \frac{\partial^2}{\partial x^2} \right) - iI_2 \frac{\partial}{\partial y} + iY \sin \beta I_3 \frac{\partial}{\partial x} \right] H_0^{(1)}(kQ \cos \beta) dx', \quad (13)$$

$$H_z(x, y) - H_z^i(x, y) = \frac{1}{4} \int_0^\infty \left(kY \cos^2 \beta I_3 - iI_4 \frac{\partial}{\partial y} - iY \sin \beta I_1 \frac{\partial}{\partial x} \right) H_0^{(1)}(kQ \cos \beta) dx'. \quad (14)$$

Comparison with the equations for E_x and E_z reveals the expected symmetry between the electric and magnetic fields and currents. Indeed, (13) and (14) correspond to (8) and (10) under the transformation

$$\begin{aligned} \mathbf{E} &\rightarrow \mathbf{H}, & Z\mathbf{H} &\rightarrow -Y\mathbf{E}, \\ I_1 &\rightarrow I_4, & ZI_2 &\rightarrow -YI_3, \\ I_3 &\rightarrow I_2, & ZI_4 &\rightarrow -YI_1, \end{aligned}$$

and this duality enables us to write down immediately the integral equations for I_1 and I_3 by reference to the equations for I_2 and I_4 . The results obtained in this manner are identical to those which would have been found if the first of the above methods had been employed, and are

$$\begin{aligned} \frac{1}{\eta} I_1(x) - 2 \sin \alpha \cos \beta \exp [-ikx \cos \alpha \cos \beta] = \\ = -\frac{1}{2} \int_0^\infty \left[kI_1 \left(1 + \frac{1}{k^2} \frac{\partial^2}{\partial x^2} \right) + i \sin \beta I_3 \frac{\partial}{\partial x} \right] H_0^{(1)}(k|x' - x| \cos \beta) dx', \quad (15) \end{aligned}$$

$$\frac{1}{\eta} I_3(x) = -\frac{1}{2} \int_0^\infty \left(k \cos^2 \beta I_3 + i \sin \beta I_1 \frac{\partial}{\partial x} \right) H_0^{(1)}(k|x' - x| \cos \beta) dx' \quad (16)$$

(c.f. (11) and (12)). To complete the duality between the electric and magnetic quantities, it will be observed that the additional trans-

formation $\eta \rightarrow 1/\eta$ is required. The absence of the inhomogeneous term in (16) is caused by the fact that H_z^i is zero.

§ 3. *The solution of the equations.* In view of the similarity between the equations for I_1 , I_2 , I_3 and I_4 it is sufficient to restrict the analysis to just one of the coupled pairs. Let us therefore consider (11) and (12) and attempt to cast them into forms suitable for solution by the Wiener-Hopf method.

Take first equation (11). This holds only for $x > 0$, but if a function $\phi_4(x)$ is introduced such that $\phi_4(x)$ is zero for $x > 0$ and is equal to the right hand side of (11) for $x < 0$, the equation can be written as

$$\eta I_4(x) + \phi_4(x) + 2Y \cos \alpha \sin \beta \cos \beta \psi(x) = \\ = -\frac{1}{2} \int_{-\infty}^{\infty} \left[k I_4 \left(1 + \frac{1}{k^2} \frac{\partial^2}{\partial x^2} \right) + i \sin \beta I_2 \frac{\partial}{\partial x} \right] H_0^{(1)}(k|x' - x| \cos \beta) dx', \quad (17)$$

where I_2 and I_4 are defined to be zero for $x < 0$ and

$$\psi(x) = \begin{cases} \exp[-ikx \cos \alpha \cos \beta] & \text{for } x > 0, \\ 0 & \text{for } x < 0. \end{cases}$$

In this form the equation is valid for all x .

The application of a Fourier transform to (17) can be justified by a study of the growth orders of the functions $\psi(x)$, $I_2(x)$, $I_4(x)$ and $\phi_4(x)$ for large $|x|$. The Fourier transform of, for example, $\psi(x)$ is

$$\bar{\psi}(\zeta) = \frac{1}{\sqrt{2\pi}} \int_{-\infty}^{\infty} e^{-i\zeta x} \psi(x) dx,$$

and from the definition of $\psi(x)$ it is immediately obvious that $\bar{\psi}(\zeta)$ is regular in a lower half-plane of the transform variable ζ . For the currents $I_p(x)$, $p = 1, 2, 3, 4$, the assumption that

$$I_p(x) \sim \exp[-ikx \cos \alpha \cos \beta]$$

as $x \rightarrow \infty$ implies that the transforms $\bar{I}_p(\zeta)$ are regular in the same region, and, finally, by using the asymptotic expansion for the Hankel function when x is large and negative we have that $\bar{\phi}_p(\zeta)$ is regular in an upper half-plane. All these regions of regularity

overlap, and within the common strip it is permissible to apply a Fourier transform to (17).

By inserting the Fourier integral representation of the Hankel function, the right hand side of equation (17) becomes

$$-\frac{1}{2\pi} \int_{-\infty}^{\infty} \left[k I_4(x') \left(1 + \frac{1}{k^2} \frac{\partial^2}{\partial x'^2} \right) + i \sin \beta I_2(x') \frac{\partial}{\partial x} \right] \int_C \frac{e^{i\zeta(x-x')}}{\sqrt{k^2 \cos^2 \beta - \zeta^2}} d\zeta dx',$$

which can be written alternatively as

$$-\frac{1}{\sqrt{2\pi}} \int_C \left(\frac{1}{k} (k^2 - \zeta^2) \bar{I}_4(\zeta) - \zeta \sin \beta \bar{I}_2(\zeta) \right) \frac{e^{i\zeta x}}{\Gamma} d\zeta,$$

where $\Gamma = \sqrt{k^2 \cos^2 \beta - \zeta^2}$ and C is a straight line path from $-\infty$ to ∞ lying within the strip of regularity of the integrand. Application of a Fourier transform now gives

$$\begin{aligned} -\bar{\phi}_4(\zeta) = & \sqrt{\frac{2}{\pi}} \frac{Y \cos \alpha \sin \beta \cos \beta}{i(\zeta + k \cos \alpha \cos \beta)} + \\ & + \left(\eta + \frac{k^2 - \zeta^2}{k\Gamma} \right) \bar{I}_4(\zeta) - \frac{\zeta \sin \beta}{\Gamma} \bar{I}_2(\zeta) \quad (18) \end{aligned}$$

and similarly, from (12),

$$\begin{aligned} -\bar{\phi}_2(\zeta) = & \sqrt{\frac{2}{\pi}} \frac{Y \cos^2 \beta}{i(\zeta + k \cos \alpha \cos \beta)} - \frac{\zeta \sin \beta}{\Gamma} \bar{I}_4(\zeta) + \\ & + \left(\eta + \frac{k \cos^2 \beta}{\Gamma} \right) \bar{I}_2(\zeta) \quad (19) \end{aligned}$$

These are sufficient to specify $\bar{I}_2(\zeta)$ and $\bar{I}_4(\zeta)$.

The obvious way in which to attempt the solution is to eliminate $\bar{I}_2(\zeta)$ and $\bar{I}_4(\zeta)$ in turn and thereby to obtain equations for each current separately. Unfortunately, however, the resulting equations are not capable of being treated by the Wiener-Hopf technique. An essential feature of the technique is the separation of the terms into two groups having overlapping regions of regularity, and in the process of eliminating a current it is necessary to multiply one or other of the functions $\bar{\phi}_2(\zeta)$ or $\bar{\phi}_4(\zeta)$ by a quantity which destroys its regularity in the upper half-plane. A consequence of this is that

coupled equations of the above type are, in general, not capable of being solved, and it is only by virtue of a particular symmetry existing between (18) and (19) that $\bar{I}_2(\zeta)$ and $\bar{I}_4(\zeta)$ can be determined.

The clue to the method of solution came from an attempt to guess a relationship between the currents. If it is assumed that

$$\bar{I}_2(\zeta) = f(\zeta) \bar{I}_4(\zeta),$$

then $f(\zeta)$ must be such as to reduce (18) and (19) to essentially the same equation. Since both $\bar{I}_2(\zeta)$ and $\bar{I}_4(\zeta)$ are regular in a lower half-plane, $f(\zeta)$ must also be regular in this region, and from the way in which η enters into the factors multiplying the currents it is clear that $f(\zeta)$ must be chosen to satisfy

$$(k^2 - \zeta^2) f - k\zeta \sin \beta = (k^2 \cos^2 \beta - k\zeta f \sin \beta) f.$$

The resulting values of $f(\zeta)$ are

$$\frac{\zeta}{k \sin \beta} \quad \text{and} \quad -\frac{k \sin \beta}{\zeta},$$

but neither of these is sufficient to bring into agreement the remaining terms in (18) and (19).

The failure of the method is not very surprising since it presupposes an extremely close connection between the currents. On the other hand, the method does reveal a simple relation between the coefficients of $\bar{I}_2(\zeta)$ and $\bar{I}_4(\zeta)$ in (18) and (19), and suggests that a profitable approach would be to use the values for $f(\zeta)$ to derive equations for certain linear combinations of the currents.

If (18) and (19) are multiplied by $k \sin \beta$ and ζ respectively and then subtracted, we obtain

$$\begin{aligned} & [\zeta \bar{I}_2(\zeta) - k \sin \beta \bar{I}_4(\zeta)] \left(\eta + \frac{k}{\Gamma} \right) + \\ & + \sqrt{\frac{2}{\pi}} \frac{Y (\zeta \cos \beta - k \cos \alpha \sin^2 \beta) \cos \beta}{i(\zeta + k \cos \alpha \cos \beta)} = k \sin \beta \bar{\phi}_4(\zeta) - \zeta \bar{\phi}_2(\zeta), \quad (20) \end{aligned}$$

and since the manipulation has not affected the regions of regularity, this is an equation for $\zeta \bar{I}_2(\zeta) - k \sin \beta \bar{I}_4(\zeta)$ which can be solved by the Wiener-Hopf technique. For this purpose, let

$$\eta \cos \beta + \frac{k \cos \beta}{\Gamma} = \frac{K_-(\zeta)}{K_+(\zeta)},$$

where $K_+(\zeta)$ and $K_-(\zeta)$ are regular in the upper and lower half-planes respectively. Bearing in mind the definition of Γ , it is apparent that $K_+(\zeta)$ and $K_-(\zeta)$ differ from the "split" functions given by Senior³) only in having k replaced by $k \cos \beta$, and accordingly their analytical expressions can be obtained from that paper.

If (20) is multiplied through by $\cos \beta K_+(\zeta)$, it can be written as

$$\begin{aligned} & [\zeta \bar{I}_2(\zeta) - k \sin \beta \bar{I}_4(\zeta)] K_-(\zeta) - \sqrt{\frac{2}{\pi}} Y k \cos \alpha \cos^2 \beta \frac{K_+(-k \cos \alpha \cos \beta)}{i(\zeta + k \cos \alpha \cos \beta)} \\ &= -\sqrt{\frac{2}{\pi}} Y \cos^2 \beta \frac{(\zeta \cos \beta - k \cos \alpha \sin^2 \beta) K_+(\zeta) + k \cos \alpha K_+(-k \cos \alpha \cos \beta)}{i(\zeta + k \cos \alpha \cos \beta)} \\ & \quad + [k \sin \beta \bar{\phi}_4(\zeta) - \zeta \bar{\phi}_2(\zeta)] \cos \beta K_+(\zeta). \end{aligned}$$

The left hand side is regular in a lower half-plane, whilst the right hand side is regular in an upper half-plane, and, moreover, these two regions have a common strip. It follows that each side must be equal to a function which is regular throughout the whole ζ plane, and its growth order as $|\zeta| \rightarrow \infty$ then shows it to be at most a constant. Hence

$$\begin{aligned} & \zeta \bar{I}_2(\zeta) - k \sin \beta \bar{I}_4(\zeta) = \\ &= -i \sqrt{\frac{2}{\pi}} Y k \cos \alpha \cos^2 \beta \frac{K_+(-k \cos \alpha \cos \beta)}{(\zeta + k \cos \alpha \cos \beta) K_-(\zeta)} + \frac{A'}{K_-(\zeta)}, \quad (21) \end{aligned}$$

where A' is independent of ζ .

To determine $\bar{I}_2(\zeta)$ and $\bar{I}_4(\zeta)$ individually, another linear combination is considered which introduces the second value of $f(\zeta)$. Multiplying (18) by ζ , (19) by $k \sin \beta$ and then adding, we have

$$\begin{aligned} & [k \sin \beta \bar{I}_2(\zeta) + \zeta \bar{I}_4(\zeta)] \left(\eta + \frac{\Gamma}{k} \right) + \\ & + \sqrt{\frac{2}{\pi}} Y \sin \beta \cos \beta \frac{k \cos \beta + \zeta \cos \alpha}{i(\zeta + k \cos \alpha \cos \beta)} = -\zeta \bar{\phi}_4(\zeta) - k \sin \beta \bar{\phi}_2(\zeta), \quad (22) \end{aligned}$$

which is an equation of the Wiener-Hopf type for $k \sin \beta \bar{I}_2(\zeta) + \zeta \bar{I}_4(\zeta)$. The factor multiplying these currents can be written

$$\frac{\eta \Gamma}{k \cos \beta} \left(\frac{\cos \beta}{\eta} + \frac{k \cos \beta}{\Gamma} \right) = \frac{\eta \Gamma}{k \cos \beta} \frac{L_-(\zeta)}{L_+(\zeta)},$$

where $L_+(\zeta)$ and $L_-(\zeta)$ are regular in an upper and a lower half-plane respectively, and since $L_+(\zeta)$ and $L_-(\zeta)$ differ from $K_+(\zeta)$ and $K_-(\zeta)$ only in having $\eta \cos \beta$ replaced by $(\cos \beta)/\eta$, their expressions can also be deduced from the formulae given by Senior³).

If (22) is multiplied through by

$$\frac{k \cos \beta}{\eta} \frac{L_+(\zeta)}{\sqrt{k \cos \beta + \zeta}},$$

its terms can be rearranged to give

$$\begin{aligned} & [k \sin \beta \bar{I}_2(\zeta) + \zeta \bar{I}_4(\zeta)] \sqrt{k \cos \beta - \zeta} L_-(\zeta) + \\ & + \sqrt{\frac{2}{\pi}} Y \frac{k^2}{\eta} \frac{\sin^2 \alpha \sin \beta \cos^3 \beta}{i(\zeta + k \cos \alpha \cos \beta)} \frac{L_+(-k \cos \alpha \cos \beta)}{\sqrt{k \cos \beta (1 - \cos \alpha)}} = \\ & = -\sqrt{\frac{2}{\pi}} Y \frac{k}{\eta} \frac{\sin \beta \cos^2 \beta}{i(\zeta + k \cos \alpha \cos \beta)} \left[(k \cos \beta + \zeta \cos \alpha) \frac{L_+(\zeta)}{\sqrt{k \cos \beta + \zeta}} - \right. \\ & \quad \left. - k \sin^2 \alpha \cos \beta \frac{L_+(-k \cos \alpha \cos \beta)}{\sqrt{k \cos \beta (1 - \cos \alpha)}} \right] - \\ & \quad - [\zeta \bar{\phi}_4(\zeta) + k \sin \beta \bar{\phi}_2(\zeta)] - \frac{k \cos \beta}{\eta} \frac{L_+(\zeta)}{\sqrt{k \cos \beta + \zeta}}, \quad (23) \end{aligned}$$

and by the same argument as before each side of this equation must be equal to a function regular throughout the whole ζ -plane. Using the fact that for large $|\zeta|$, $L_+(\zeta)$ and $L_-(\zeta)$ are $O(1)$, the right hand side of (23) then shows that the analytic function is at most a constant and hence

$$\begin{aligned} & k \sin \beta \bar{I}_2(\zeta) + \zeta \bar{I}_4(\zeta) = \\ & = i \sqrt{\frac{2}{\pi}} Y \frac{k^2}{\eta} \frac{\sin^2 \alpha \sin \beta \cos^3 \beta}{\zeta + k \cos \alpha \cos \beta} \frac{L_+(-k \cos \alpha \cos \beta)}{\sqrt{k \cos \beta (1 - \cos \alpha)} (k \cos \beta - \zeta) L_-(\zeta)} + \\ & \quad + \frac{B'}{\sqrt{k \cos \beta - \zeta} L_-(\zeta)}, \quad (24) \end{aligned}$$

where B' is independent of ζ .

Expressions for $\bar{I}_2(\zeta)$ and $\bar{I}_4(\zeta)$ can be obtained from (21) and (24) by eliminating each current in turn. The resulting formulae can be

simplified to some extent by defining new constants A and B such that

$$A' = i \sqrt{\frac{2}{\pi}} Y \cos \beta [A + K_+ (-k \cos \alpha \cos \beta)],$$

$$B' = i \sqrt{\frac{2}{\pi}} \frac{Y}{\eta} \sin^2 \alpha \sin \beta \cos^2 \beta \sqrt{\frac{k \cos \beta}{1 - \cos \alpha}} B,$$

and this leads to the equations

$$\begin{aligned} (\zeta^2 + k^2 \sin^2 \beta) \bar{I}_2(\zeta) = & \\ & i \sqrt{\frac{2}{\pi}} Y \zeta \cos \beta \frac{\zeta K_+ (-k \cos \alpha \cos \beta) + A(\zeta + k \cos \alpha \cos \beta)}{(\zeta + k \cos \alpha \cos \beta) K_-(\zeta)} + \\ & + i \sqrt{\frac{2}{\pi}} Y \frac{k}{\eta} \sin^2 \alpha \sin^2 \beta \cos^2 \beta \cdot \\ & \cdot \sqrt{\frac{k \cos \beta}{(1 - \cos \alpha)(k \cos \beta - \zeta)}} \frac{k L_+ (-k \cos \alpha \cos \beta) + B(\zeta + k \cos \alpha \cos \beta)}{(\zeta + k \cos \alpha \cos \beta) L_-(\zeta)} \quad (25) \end{aligned}$$

$$\begin{aligned} (\zeta^2 + k^2 \sin^2 \beta) \bar{I}_4(\zeta) = & \\ & -i \sqrt{\frac{2}{\pi}} Y k \sin \beta \cos \beta \frac{\zeta K_+ (-k \cos \alpha \cos \beta) + A(\zeta + k \cos \alpha \cos \beta)}{(\zeta + k \cos \alpha \cos \beta) K_-(\zeta)} + \\ & + i \sqrt{\frac{2}{\pi}} Y \frac{\zeta}{\eta} \sin^2 \alpha \sin \beta \cos^2 \beta \cdot \\ & \cdot \sqrt{\frac{k \cos \beta}{(1 - \cos \alpha)(k \cos \beta - \zeta)}} \frac{k L_+ (-k \cos \alpha \cos \beta) + B(\zeta + k \cos \alpha \cos \beta)}{(\zeta + k \cos \alpha \cos \beta) L_-(\zeta)}. \quad (26) \end{aligned}$$

As they stand, the above equations do not have the required regularity in that the expressions for $\bar{I}_2(\zeta)$ and $\bar{I}_4(\zeta)$ have poles at the points $\zeta = \pm i k \sin \beta$ which lie in the region where the transforms must be free of singularities. If the poles are eliminated, however, two conditions are obtained, and these serve to specify A and B uniquely.

The equations for $\bar{I}_2(\zeta)$ and $\bar{I}_4(\zeta)$ each give rise to the same conditions for A and B , and it is therefore sufficient to consider only (26). For $\bar{I}_4(\zeta)$ to be regular at $\zeta = i k \sin \beta$, the right hand side of (26) must be zero at this point in order to balance the correspond-

ing factor on the left, and the condition for this is

$$\begin{aligned}
 A = & i e^{i\beta} \frac{1}{\eta} \sin^2 \alpha \sin \beta \cos \beta . \\
 & \cdot \sqrt{\frac{\cos \beta}{1 - \cos \alpha}} \frac{K_{-}(ik \sin \beta)}{L_{-}(ik \sin \beta)} B - i \sin \beta \frac{K_{+}(-k \cos \alpha \cos \beta)}{\cos \alpha \cos \beta + i \sin \beta} + \\
 & + i e^{i\beta} \frac{1}{\eta} \sin^2 \alpha \sin \beta \cos \beta . \\
 & \cdot \sqrt{\frac{\cos \beta}{1 - \cos \alpha}} \frac{L_{+}(-k \cos \alpha \cos \beta)}{\cos \alpha \cos \beta + i \sin \beta} \frac{K_{-}(ik \sin \beta)}{L_{-}(ik \sin \beta)} . \quad (27)
 \end{aligned}$$

Similar analysis applied to the point $\zeta = -ik \sin \beta$ gives

$$\begin{aligned}
 A = & -i e^{-i\beta} \frac{1}{\eta} \sin^2 \alpha \sin \beta \cos \beta . \\
 & \cdot \sqrt{\frac{\cos \beta}{1 - \cos \alpha}} \frac{K_{-}(-ik \sin \beta)}{L_{-}(-ik \sin \beta)} B + i \sin \beta \frac{K_{+}(-k \cos \alpha \cos \beta)}{\cos \alpha \cos \beta - i \sin \beta} - \\
 & - i e^{-i\beta} \frac{1}{\eta} \sin^2 \alpha \sin \beta \cos \beta . \\
 & \cdot \sqrt{\frac{\cos \beta}{1 - \cos \alpha}} \frac{L_{+}(-k \cos \alpha \cos \beta)}{\cos \alpha \cos \beta - i \sin \beta} \frac{K_{-}(-ik \sin \beta)}{L_{-}(-ik \sin \beta)} , \quad (28)
 \end{aligned}$$

and from (27) and (28) it is a simple matter to determine A and B . The values obtained are

$$\begin{aligned}
 A = & \frac{\sin \beta}{(\cos^2 \alpha \cos^2 \beta + \sin^2 \beta) P(\beta)} . \\
 & \cdot \left\{ [i \cos \alpha \cos \beta Q(\beta) - \sin \beta P(\beta)] K_{+}(-k \cos \alpha \cos \beta) + \right. \\
 & \left. + 2 \sin^2 \alpha \sin \beta \cos \beta \sqrt{\frac{\cos \beta}{1 - \cos \alpha}} L_{+}(-k \cos \alpha \cos \beta) \right\} , \quad (29)
 \end{aligned}$$

$$\begin{aligned}
 B = & \frac{1}{(\cos^2 \alpha \cos^2 \beta + \sin^2 \beta) P(\beta)} . \\
 & \cdot \left\{ [i \sin \beta Q(\beta) - \cos \alpha \cos \beta P(\beta)] L_{+}(-k \cos \alpha \cos \beta) + \right. \\
 & \left. + 2\eta \frac{\cos \alpha}{\sin^2 \alpha} \sqrt{\frac{1 - \cos \alpha}{\cos \beta}} K_{+}(-k \cos \alpha \cos \beta) \right\} , \quad (30)
 \end{aligned}$$

where

$$P(\beta), Q(\beta) = e^{\pm i\beta} \frac{K_-(ik \sin \beta)}{L_-(ik \sin \beta)} \pm e^{-\pm i\beta} \frac{K_-(-ik \sin \beta)}{L_-(-ik \sin \beta)}. \quad (31)$$

If the expressions for $\bar{I}_2(\zeta)$ and $\bar{I}_4(\zeta)$ are now examined, several facts are immediately apparent. Since all the split functions are $O(1)$ for large $|\zeta|$, $\eta \neq 0$, it follows that

$$\bar{I}_2(\zeta) = O(|\zeta|^{-1}), \quad \bar{I}_4(\zeta) = O(|\zeta|^{-3/2}),$$

and hence

$$I_2(x) \sim \text{constant}, \quad I_4(x) \sim x^{\frac{1}{2}}$$

as $x \rightarrow 0$. This shows that the electric current perpendicular to the edge is zero for $x = 0$ (in accordance with our previous assumption), whilst the electric current parallel to the edge is finite there. The same behaviour is found *) in the case of normal incidence ($\beta = 0$), and it will be noted that a consequence of the finite conductivity is the removal of the current singularity at the edge.

When $\beta = 0$, equation (29) gives $A = 0$, and (25) and (26) then reduce to

$$\bar{I}_2(\zeta) = i \sqrt{\frac{2}{\pi}} Y \frac{K_+(-k \cos \alpha)}{(\zeta + k \cos \alpha) K_-(\zeta)}$$

and

$$\bar{I}_4(\zeta) = 0,$$

which agree with the known solution for normal incidence. The only other case of interest is that in which $\eta = 0$, but this is most conveniently considered in the next section.

It is now time to turn our attention to the magnetic currents $\bar{I}_1(\zeta)$ and $\bar{I}_3(\zeta)$. These have to be determined from the integral equations (15) and (16), which are similar to the equations (11) and (12) already discussed. Although the correspondence is not complete because of the lack of symmetry in the incident electric and magnetic fields, it is sufficiently close for us to omit the details of the solution. By the same method as was used for equations (11) and (12) it is

*) In ⁹ it is incorrectly stated that $K_+(\zeta)$, etc. are $O(|\zeta|^{-\frac{1}{2}})$ for large $|\zeta|$. This does not affect the derivation of the solution given therein, but does invalidate the statements about the behaviour of the currents for small x .

found that

$$\begin{aligned}
 (\zeta^2 + k^2 \sin^2 \beta) \bar{I}_1(\zeta) = & \\
 = -i \sqrt{\frac{2}{\pi}} k \sin \alpha \sin^2 \beta \cos^2 \beta & \frac{k L_+(-k \cos \alpha \cos \beta) + C(\zeta + k \cos \alpha \cos \beta)}{(\zeta + k \cos \alpha \cos \beta) L_-(\zeta)} - \\
 - i \sqrt{\frac{2}{\pi}} \eta \zeta \sin \alpha \cos \beta & \sqrt{\frac{k \cos \beta}{(1 - \cos \alpha)(k \cos \beta - \zeta)}} \cdot \\
 \cdot \frac{\zeta K_+(-k \cos \alpha \cos \beta) + D(\zeta + k \cos \alpha \cos \beta)}{(\zeta + k \cos \alpha \cos \beta) K_-(\zeta)}, & \quad (32)
 \end{aligned}$$

$$\begin{aligned}
 (\zeta^2 + k^2 \sin^2 \beta) \bar{I}_3(\zeta) = & \\
 = i \sqrt{\frac{2}{\pi}} \zeta \sin \alpha \sin \beta \cos^2 \beta & \frac{k L_+(-k \cos \alpha \cos \beta) + C(\zeta + k \cos \alpha \cos \beta)}{(\zeta + k \cos \alpha \cos \beta) L_-(\zeta)} - \\
 - i \sqrt{\frac{2}{\pi}} \eta k \sin \alpha \sin \beta \cos \beta & \sqrt{\frac{k \cos \beta}{(1 - \cos \alpha)(k \cos \beta - \zeta)}} \cdot \\
 \cdot \frac{\zeta K_+(-k \cos \alpha \cos \beta) + D(\zeta + k \cos \alpha \cos \beta)}{(\zeta + k \cos \alpha \cos \beta) K_-(\zeta)}, & \quad (33)
 \end{aligned}$$

(c.f. (25) and (26)), where the constants C and D have the values

$$\begin{aligned}
 C = & \frac{1}{(\cos^2 \alpha \cos^2 \beta + \sin^2 \beta) P'(\beta)} \cdot \\
 \cdot \left\{ [i \sin \beta Q'(\beta) - \cos \alpha \cos \beta P'(\beta)] L_+(-k \cos \alpha \cos \beta) + \right. & \\
 \left. + 2\eta \cos \alpha \sqrt{\frac{\cos \beta}{1 - \cos \alpha}} K_+(-k \cos \alpha \cos \beta) \right\}, & \quad (34)
 \end{aligned}$$

$$\begin{aligned}
 D = & \frac{\sin \beta \sqrt{(\cos \beta / 1 - \cos \alpha)}}{(\cos^2 \alpha \cos^2 \beta + \sin^2 \beta) P'(\beta)} \cdot \\
 \cdot \left\{ [i \cos \alpha \cos \beta Q'(\beta) - \sin \beta P'(\beta)] K_+(-k \cos \alpha \cos \beta) + \right. & \\
 \left. + 2 \sin \beta \cos \beta \sqrt{\frac{1 - \cos \alpha}{\cos \beta}} L_+(-k \cos \alpha \cos \beta) \right\} & \quad (35)
 \end{aligned}$$

with

$$P'(\beta), Q'(\beta) = e^{-i\beta} \frac{K_-(ik \sin \beta)}{L_-(ik \sin \beta)} \pm e^{i\beta} \frac{K_-(-ik \sin \beta)}{L_-(-ik \sin \beta)}. \quad (36)$$

The remarks made about the electric currents $\bar{I}_2(\zeta)$ and $\bar{I}_4(\zeta)$ apply also to the magnetic currents $\bar{I}_3(\zeta)$ and $\bar{I}_1(\zeta)$.

§ 4. *The field components.* Since the electric and magnetic fields can be written in terms of the transforms $\bar{I}_p(\zeta)$ alone, explicit determination of the currents $I_p(x)$ is unnecessary. From (8), (9) and (10) we have, by inserting the Fourier representation of the Hankel function and restoring the z -dependence,

$$E_x = E_x^i - \frac{1}{4} \sqrt{\frac{2}{\pi}} \int_C \left[\frac{Z}{k} \frac{k^2 - \zeta^2}{\Gamma} \bar{I}_4(\zeta) - \zeta \frac{\sin \beta}{\Gamma} \bar{I}_2(\zeta) - \bar{I}_3(\zeta) \frac{y}{|y|} \right] \phi \, d\zeta, \quad (37)$$

$$E_y = E_y^i - \frac{1}{4} \sqrt{\frac{2}{\pi}} \int_C \left\{ \frac{\zeta}{\Gamma} \bar{I}_3(\zeta) - \frac{k \sin \beta}{\Gamma} \bar{I}_1(\zeta) - Z \left[\sin \beta \bar{I}_2(\zeta) + \frac{\zeta}{k} \bar{I}_4(\zeta) \right] \frac{y}{|y|} \right\} \phi \, d\zeta, \quad (38)$$

$$E_z = E_z^i + \frac{1}{4} \sqrt{\frac{2}{\pi}} \int_C \left[Z \frac{k \cos^2 \beta}{\Gamma} \bar{I}_2(\zeta) - Z \frac{\zeta \sin \beta}{\Gamma} \bar{I}_4(\zeta) + \bar{I}_1(\zeta) \frac{y}{|y|} \right] \phi \, d\zeta, \quad (39)$$

with $\phi = \exp(i\zeta x + i|y|\Gamma - ikz \sin \beta)$

and if these are expressed in the form

$$\mathbf{E} = \mathbf{E}^i + \frac{1}{2\pi i} \int_C \frac{\mathbf{E}(\zeta)}{\zeta^2 + k^2 \sin^2 \beta} \frac{\cos \beta}{\zeta + k \cos \alpha \cos \beta} \phi \, d\zeta, \quad (40)$$

the components of $\mathbf{E}(\zeta)$ are

$$\begin{aligned} E_x(\zeta) = & \frac{1}{\eta} \frac{\zeta}{k} \sin \alpha \sin \beta \cos \beta \sqrt{k \cos \beta (1 + \cos \alpha) (k \cos \beta + \zeta)} \cdot \\ & \cdot \frac{kL_+(-k \cos \alpha \cos \beta) + B(\zeta + k \cos \alpha \cos \beta)}{L_-(\zeta)} \\ & - \frac{k^2}{\sqrt{k^2 \cos^2 \beta - \zeta^2}} \sin \beta \frac{\zeta K_+(-k \cos \alpha \cos \beta) + A(\zeta + k \cos \alpha \cos \beta)}{K_-(\zeta)} \\ & - \frac{y}{|y|} \zeta \sin \alpha \sin \beta \cos \beta \frac{kL_+(-k \cos \alpha \cos \beta) + C(\zeta + k \cos \alpha \cos \beta)}{L_-(\zeta)} \\ & + \eta \frac{y}{|y|} k \sin \beta \cdot \\ & \cdot \sqrt{\frac{k \cos \beta (1 + \cos \alpha)}{k \cos \beta - \zeta}} \frac{\zeta K_+(-k \cos \alpha \cos \beta) + D(\zeta + k \cos \alpha \cos \beta)}{K_-(\zeta)}, \quad (41) \end{aligned}$$

$$E_y(\zeta) = \frac{\zeta^2 + k^2 \sin^2 \beta}{\sqrt{k^2 \cos^2 \beta - \zeta^2}} \sin \alpha \sin \beta \cos \beta \frac{1}{L_-(\zeta)} \cdot \{kL_+(-k \cos \alpha \cos \beta) + C(\zeta + k \cos \alpha \cos \beta) - \frac{1}{\eta} \frac{y}{|y|} \sqrt{\frac{\cos \beta(1 + \cos \alpha)(k \cos \beta + \zeta)}{k}} \cdot [kK_+(-k \cos \alpha \cos \beta) + B(\zeta + k \cos \alpha \cos \beta)]\}, \quad (42)$$

$$E_z(\zeta) = -\frac{1}{\eta} \sin \alpha \sin^2 \beta \cos \beta \sqrt{k \cos \beta(1 + \cos \alpha)(k \cos \beta - \zeta)} \cdot \frac{kL_+(-k \cos \alpha \cos \beta) + B(\zeta + k \cos \alpha \cos \beta)}{L_-(\zeta)} - \frac{k\zeta}{\sqrt{k^2 \cos^2 \beta - \zeta^2}} \frac{\zeta K_+(-k \cos \alpha \cos \beta) + A(\zeta + k \cos \alpha \cos \beta)}{K_-(\zeta)} + \frac{y}{|y|} k \sin \alpha \sin^2 \beta \cos \beta \frac{kL_+(-k \cos \alpha \cos \beta) + C(\zeta + k \cos \alpha \cos \beta)}{L_-(\zeta)} + \eta \frac{y}{|y|} \zeta \sqrt{\frac{k \cos \beta(1 + \cos \alpha)}{k \cos \beta - \zeta}} \cdot \frac{\zeta K_+(-k \cos \alpha \cos \beta) + D(\zeta + k \cos \alpha \cos \beta)}{K_-(\zeta)}. \quad (43)$$

The corresponding equations for the magnetic field can be deduced from (37), (38) and (39) by using the duality referred to in § 2, and if we similarly write

$$\mathbf{H} = \mathbf{H}^i + \frac{1}{2\pi i} \int_C \frac{\mathbf{H}(\zeta)}{\zeta^2 + k^2 \sin^2 \beta} \frac{\cos \beta}{\zeta + k \cos \alpha \cos \beta} \phi \, d\zeta, \quad (44)$$

(c.f. (40)), it can be shown that

$$H_x(\zeta) = \eta \frac{\zeta}{k} \sqrt{k \cos \beta(1 + \cos \alpha)(k \cos \beta + \zeta)} \cdot \frac{\zeta K_+(-k \cos \alpha \cos \beta) + D(\zeta + k \cos \alpha \cos \beta)}{K_-(\zeta)} + \frac{k^2}{\sqrt{k^2 \cos^2 \beta - \zeta^2}} \sin \alpha \sin^2 \beta \cos \beta \cdot \frac{kL_+(-k \cos \alpha \cos \beta) + C(\zeta + k \cos \alpha \cos \beta)}{L_-(\zeta)}$$

$$\begin{aligned}
 & - \frac{y}{|y|} \zeta \frac{\zeta K_+(-k \cos \alpha \cos \beta) + A(\zeta + k \cos \alpha \cos \beta)}{K_-(\zeta)} - \\
 & - \frac{1}{\eta} \frac{y}{|y|} k \sin \alpha \sin^2 \beta \cos \beta \sqrt{\frac{k \cos \beta (1 + \cos \alpha)}{k \cos \beta - \zeta}} \cdot \\
 & \cdot \frac{k L_+(-k \cos \alpha \cos \beta) + B(\zeta + k \cos \alpha \cos \beta)}{L_-(\zeta)}, \quad (45)
 \end{aligned}$$

$$\begin{aligned}
 H_y(\zeta) &= \frac{\zeta^2 + k^2 \sin^2 \beta}{\sqrt{k^2 \cos^2 \beta - \zeta^2}} \frac{1}{K_-(\zeta)} \cdot \\
 & \cdot \left\{ K_+(-k \cos \alpha \cos \beta) + A(\zeta + k \cos \alpha \cos \beta) - \right. \\
 & - \eta \frac{y}{|y|} \sqrt{\frac{\cos \beta (1 + \cos \alpha)(k \cos \beta + \zeta)}{k}} \cdot \\
 & \cdot [\zeta K_+(-k \cos \alpha \cos \beta) + D(\zeta + k \cos \alpha \cos \beta)] \left. \right\}, \quad (46)
 \end{aligned}$$

$$\begin{aligned}
 H_z(\zeta) &= -\eta \sin \beta \sqrt{k \cos \beta (1 + \cos \alpha)(k \cos \beta + \zeta)} \cdot \\
 & \cdot \frac{\zeta K_+(-k \cos \alpha \cos \beta) + D(\zeta + k \cos \alpha \cos \beta)}{K_-(\zeta)} + \\
 & + \frac{k \zeta}{\sqrt{k^2 \cos^2 \beta - \zeta^2}} \sin \alpha \sin \beta \cos \beta \cdot \\
 & \cdot \frac{k L_+(-k \cos \alpha \cos \beta) + C(\zeta + k \cos \alpha \cos \beta)}{L_-(\zeta)} + \\
 & + \frac{y}{|y|} k \sin \beta \frac{\zeta K_+(-k \cos \alpha \cos \beta) + A(\zeta + k \cos \alpha \cos \beta)}{K_-(\zeta)} + \\
 & - \frac{1}{\eta} \frac{y}{|y|} \zeta \sin \alpha \sin \beta \cos \beta \sqrt{\frac{k \cos \beta (1 + \cos \alpha)}{k \cos \beta - \zeta}} \cdot \\
 & \cdot \frac{k L_+(-k \cos \alpha \cos \beta) + B(\zeta + k \cos \alpha \cos \beta)}{L_-(\zeta)}. \quad (47)
 \end{aligned}$$

An exact evaluation of the integrals in (40) and (44) would appear to be impossible, but for most purposes approximate values are sufficient, and these can be obtained by the method of steepest descents. The present paper, however, is more concerned with the formulae themselves; and of particular interest is the extent to

which they differ from the ones predicted by the technique described in § 1. If the technique were valid for imperfect conductivity, the field components would be given by

$$\mathbf{E} = \left(-\frac{i \sin \beta}{k} \frac{\partial U}{\partial x}, -\frac{i \sin \beta}{k} \frac{\partial U}{\partial y}, U \cos^2 \beta \right),$$

$$\mathbf{H} = \frac{iY}{k} \left(-\frac{\partial U}{\partial y}, \frac{\partial U}{\partial x}, 0 \right),$$

where U is the modified two-dimensional solution, and hence

$$\mathbf{E} = \mathbf{E}^i - \frac{1}{2\pi i} \int_C \frac{\mathbf{R}}{\sqrt{k^2 \cos^2 \beta - \zeta^2}} \frac{\cos \beta}{\zeta + k \cos \alpha \cos \beta} \phi \, d\zeta, \quad (48)$$

$$\mathbf{H} = \mathbf{H}^i - \frac{1}{2\pi i} \int_C \frac{\mathbf{S}}{\sqrt{k^2 \cos^2 \beta - \zeta^2}} \frac{\cos \beta}{\zeta + k \cos \alpha \cos \beta} \phi \, d\zeta, \quad (49)$$

with

$$\begin{aligned} \mathbf{R} = & \left(\zeta \sin \beta, \Gamma \frac{y}{|y|} \sin \beta, k \cos^2 \beta \right) \frac{K_+(-k \cos \alpha \cos \beta)}{K_-(\zeta)} \\ & \cdot \left[1 - \eta \frac{y}{|y|} \sqrt{\frac{(1 + \cos \alpha)(k \cos \beta + \zeta)}{k \cos \beta}} \right], \\ \mathbf{S} = & \left(\Gamma \frac{y}{|y|}, -\zeta, 0 \right) \frac{K_+(-k \cos \alpha \cos \beta)}{K_-(\zeta)} \\ & \cdot \left[1 - \eta \frac{y}{|y|} \sqrt{\frac{(1 + \cos \alpha)(k \cos \beta + \zeta)}{k \cos \beta}} \right]. \end{aligned}$$

It is immediately obvious that this differs from the true field, and with many of the components the discrepancy is at least $O(\eta)$. On the other hand, the boundary conditions themselves only reproduce the physical conditions to $O(\eta)$, and if this accuracy were achieved by even two of the components found by the above technique, they might be sufficient to describe that portion of the true solution to which a physical interpretation can be attached. To determine whether such components exist, it is necessary to expand $\mathbf{E}(\zeta)$ and $\mathbf{H}(\zeta)$ as series in ζ .

Using the expressions for the split functions³⁾, we have

$$K_+(\zeta) = \sqrt{\frac{k \cos \beta + \zeta}{k \cos \beta}} \left[1 - \frac{\eta}{\pi k} \sqrt{k^2 \cos^2 \beta - \zeta^2} \cdot \right. \\ \left. \cdot \left(\frac{\pi}{2} - \sin^{-1} \frac{\zeta}{k \cos \beta} \right) + \frac{\eta \zeta}{\pi k} \left(\ln \frac{\eta \cos \beta}{2} - 1 \right) + O(\eta^2 \ln \eta) \right], \quad (50)$$

$$L_+(\zeta) = \sqrt{\frac{\eta}{\cos \beta}} \left[1 - \frac{\eta k}{\pi \sqrt{k^2 \cos^2 \beta - \zeta^2}} \cdot \right. \\ \left. \cdot \left(\frac{\pi}{2} - \sin^{-1} \frac{\zeta}{k \cos \beta} \right) + O(\eta^2) \right], \quad (51)$$

where the expansions have been carried out under the assumption that ζ is finite. Substitution into the equations for A , B , C and D gives

$$A = \frac{\eta}{\pi} \frac{\sin^2 \beta}{\cos \beta} \left[\sqrt{1 - \cos \alpha} \left(\ln \frac{\eta \cos \beta}{2} - 1 \right) - \right. \\ \left. - \sqrt{1 + \cos \alpha} (\pi - \alpha) + O(\eta \ln \eta) \right], \\ B = - \sqrt{\frac{\eta}{\cos \beta}} \frac{1}{(1 + \cos \alpha) \cos \beta} \cdot \\ \cdot \left[1 + \frac{\eta}{\pi \cos \beta} \left(\ln \frac{\eta \cos \beta}{2} - 1 \right) - \frac{\eta}{\pi} (\pi - \alpha) \frac{1 + \cos \alpha}{\sin \alpha \cos \beta} + O(\eta^2 \ln \eta) \right], \\ C = - \frac{\eta}{\pi} \sqrt{\frac{\eta}{\cos \beta}} \left[\ln \frac{\eta \cos \beta}{2} - 1 - (\pi - \alpha) \cot \alpha + O(\eta \ln \eta) \right], \\ D = - \frac{\eta}{\pi} \frac{(\pi - \alpha) \sin^2 \beta}{\sin \alpha \sqrt{\cos \beta}} [1 + O(\eta \ln \eta)],$$

and it is now a simple matter to compare the two sets of field components.

From a study of (40) and (44) it is seen that because of the factor $(\zeta^2 + k^2 \sin^2 \beta)$ in the integrands, the components H_z and E_y are the only ones for which the technique is likely to succeed. The former is identically zero according to (49), but from (44) the true field has a component

$$\begin{aligned}
H_z = \eta \sin \beta (\zeta^2 + k^2 \sin^2 \beta) & \left\{ \frac{\zeta \sin \alpha}{\sqrt{k^2 \cos^2 \beta - \zeta^2}} + \frac{1}{\pi} \frac{y}{|y|} \cdot \right. \\
& \cdot \sqrt{\frac{1 - \cos \alpha}{k \cos \beta (k \cos \beta - \zeta)}} \left[(\zeta + k \cos \alpha \cos \beta) \left(\ln \frac{\eta \cos \beta}{2} - 1 \right) - \right. \\
& - k (\pi - \alpha) \cos \alpha \cos \beta \sqrt{\frac{1 + \cos \alpha}{1 - \cos \alpha}} + \\
& \left. \left. + \zeta \left(\frac{\pi}{2} + \sin^{-1} \frac{\zeta}{k \cos \beta} \right) \sqrt{\frac{k \cos \beta - \zeta}{k \cos \beta + \zeta}} \right] + O(\eta \ln \eta) \right\},
\end{aligned}$$

which is of order $\eta \ln \eta$. For the component E_y a similar analysis shows that the value predicted by the technique is again in error by terms $O(\eta \ln \eta)$ and, in fact, this is the same with all the field components. In consequence, the technique which is so useful for treating perfectly conducting bodies fails completely when the surfaces are imperfectly conducting.

The above discussion is based upon a comparison of the expansions for $\mathbf{E}(\zeta)$ and $\mathbf{H}(\zeta)$ with those for

$$\frac{\zeta^2 + k^2 \sin^2 \beta}{\sqrt{k^2 \cos^2 \beta - \zeta^2}} \mathbf{R} \quad \text{and} \quad \frac{\zeta^2 + k^2 \sin^2 \beta}{\sqrt{k^2 \cos^2 \beta - \zeta^2}} \mathbf{S},$$

and the implication is that discrepancies are automatically reflected in the corresponding expansions for the fields. Since the proof is not quite straightforward, a few words of explanation are in order.

The expansions for the split functions were derived under the assumption that ζ is finite, and this restriction applies to all the subsequent formulae. In (40) and (44), however, the variable of integration ζ takes values from $-\infty$ to ∞ , and if the expansions for $\mathbf{E}(\zeta)$ and $\mathbf{H}(\zeta)$ are merely integrated term by term, the expressions which are obtained are incorrect.

The difficulty can be overcome by using the method of steepest descents to approximate the integrals in (40) and (44). Almost the entire non-exponential portions of the integrands can then be removed at the saddle point $\zeta = \zeta_0$, and included in this are the functions $\mathbf{E}(\zeta)$ and $\mathbf{H}(\zeta)$. Since ζ_0 is, of course, finite, $\mathbf{E}(\zeta)$ and $\mathbf{H}(\zeta)$ can now be expanded as before, and the individual terms generate corresponding terms in the expansions for \mathbf{E} and \mathbf{H} . A direct con-

sequence of this is that all the field components contain terms in $\eta \ln \eta$ in addition to those involving powers of η alone.

§ 5. *Conclusions.* In this paper the solution has been obtained for the problem of a plane wave incident at an oblique angle on a metallic half-plane. The analysis requires the solution of coupled Wiener-Hopf integral equations for the Fourier transforms of the four current distributions, and the resulting expressions for the fields are exact, subject only to the (physical) approximation implied by the impedance-type boundary conditions. The solution has applications to the coastal refraction of radio waves, but this topic is reserved for future consideration.

It has been shown that the technique commonly employed to determine oblique incidence solutions for perfectly conducting bodies cannot be used when the conductivity is finite, and, indeed, all the field components produced in this way are in error by terms $O(\eta \ln \eta)$. It would be extremely valuable if a technique could be developed for treating finite conductivity, but unfortunately the analysis has not suggested one. From the solution given in this paper it is clear that such a method would have to call upon the normal incidence results for both polarizations, with η replaced by $\eta \cos \beta$ in one case and by $\eta \sec \beta$ in the other. However, the presence of the factor $\zeta^2 + k^2 \sin^2 \beta$ in the expressions for all but two components and, in addition, the occurrence of the complicated constants A , B , C and D , make the existence of a technique very unlikely.

Acknowledgement. This research was sponsored by the Rome Air Development Center of the U.S. Air Force under contract AF-30 (602)- 1853.

APPENDIX

Proof that $I_4(0) = 0$. If it is not assumed at the outset that $I_4(0)$ is zero, the equations from which to determine $\bar{I}_2(\zeta)$ and $\bar{I}_4(\zeta)$ are

$$\begin{aligned}
 -\bar{\phi}_4(\zeta) = & \sqrt{\frac{2}{\pi}} \frac{Y \cos \alpha \sin \beta \cos \beta}{i(\zeta + k \cos \alpha \cos \beta)} - \frac{i\zeta}{k\sqrt{2\pi}} \frac{I_4(0)}{\Gamma} + \\
 & + \left(\eta + \frac{k^2 - \zeta^2}{k\Gamma} \right) \bar{I}_4(\zeta) - \frac{\zeta \sin \beta}{\Gamma} \bar{I}_2(\zeta), \quad (\text{A } 1)
 \end{aligned}$$

$$\begin{aligned}
 -\bar{\phi}_2(\zeta) = & \sqrt{\frac{2}{\pi}} \frac{Y \cos^2 \beta}{i(\zeta + k \cos \alpha \cos \beta)} - \\
 & - \frac{i \sin \beta}{\sqrt{2\pi}} \frac{I_4(0)}{\Gamma} - \frac{\zeta \sin \beta}{\Gamma} \bar{I}_4(\zeta) + \left(\eta + \frac{k \cos^2 \beta}{\Gamma} \right) \bar{I}_2(\zeta), \quad (\text{A } 2)
 \end{aligned}$$

which differ from (18) and (19) only by the single terms involving $I_4(0)$.

As in § 3, the first step is to derive new integral equations for those linear combinations of $\bar{I}_2(\zeta)$ and $\bar{I}_4(\zeta)$ which are suggested by the functions $f(\zeta)$. If (A 1) and (A 2) are multiplied by $k \sin \beta$ and ζ respectively and then subtracted, a Wiener-Hopf integral equation for $\zeta \bar{I}_2(\zeta) - k \sin \beta \bar{I}_4(\zeta)$ is obtained. What is more, this process has also served to eliminate $I_4(0)$, and consequently the solution is identical to that given in equation (21).

The second equation for a linear combination of $\bar{I}_2(\zeta)$ and $\bar{I}_4(\zeta)$ is found by multiplying (A 1) by ζ and (A 2) by $k \sin \beta$. On adding the resulting equations, we have

$$\begin{aligned}
 [k \sin \beta \bar{I}_2(\zeta) + \zeta \bar{I}_4(\zeta)] & \left(\eta + \frac{\Gamma}{k} \right) - \frac{i I_4(0)}{k \sqrt{2\pi}} \frac{\zeta^2 + k^2 \sin^2 \beta}{\Gamma} + \\
 & + \sqrt{\frac{2}{\pi}} Y \sin \beta \cos \beta \frac{k \cos \beta + \zeta \cos \alpha}{i(\zeta + k \cos \alpha \cos \beta)} = -\zeta \bar{\phi}_4(\zeta) - k \sin \beta \bar{\phi}_2(\zeta),
 \end{aligned}$$

which can be written alternatively as

$$\begin{aligned}
 & \left\{ [k \sin \beta \bar{I}_2(\zeta) + \zeta \bar{I}_4(\zeta)] (k \cos \beta + \zeta) - \right. \\
 & \quad \left. - \frac{i I_4(0)}{\sqrt{2\pi}} \frac{\zeta^2 + k^2 \sin^2 \beta}{k \cos \beta - \zeta} \right\} \sqrt{k \cos \beta - \zeta} L_-(\zeta) + \\
 & \quad + \frac{i I_4(0)}{\sqrt{2\pi}} \sqrt{\frac{k \cos \beta}{2}} \frac{\zeta^2 + k^2 \sin^2 \beta}{k \cos \beta - \zeta} L_+(k \cos \beta) + \\
 & \quad + \sqrt{\frac{2}{\pi}} Y \frac{k^2}{\eta} (k \cos \beta + \zeta) \frac{\sin^2 \alpha \sin \beta \cos^3 \beta}{i(\zeta + k \cos \alpha \cos \beta)} \frac{L_+(-k \cos \alpha \cos \beta)}{\sqrt{k \cos \beta (1 - \cos \alpha)}} \\
 & = - \sqrt{\frac{2}{\pi}} Y \frac{k}{\eta} (k \cos \beta + \zeta) \frac{\sin \beta \cos^2 \beta}{i(\zeta + k \cos \alpha \cos \beta)} \cdot \\
 & \quad \cdot \left[(k \cos \beta + \zeta \cos \alpha) \frac{L_+(\zeta)}{k \cos \beta + \zeta} - k \sin^2 \alpha \cos \beta \frac{L_+(-k \cos \alpha \cos \beta)}{\sqrt{k \cos \beta (1 - \cos \alpha)}} \right]
 \end{aligned}$$

$$-\frac{iI_4(0)}{\sqrt{2\pi}} k \cos \beta \frac{\zeta^2 + k^2 \sin^2 \beta}{k \cos \beta - \zeta} \left[\frac{L_+(\zeta)}{\sqrt{k \cos \beta + \zeta}} - \frac{L_+(k \cos \beta)}{\sqrt{2k \cos \beta}} \right] -$$

$$- [\zeta \bar{\phi}_4(\zeta) + k \sin \beta \bar{\phi}_2(\zeta)] \frac{k \cos \beta}{\eta} \sqrt{k \cos \beta + \zeta} L_+(\zeta).$$

This is now in the form required for a Wiener-Hopf split. The left hand side is regular in a lower half-plane, whilst the right hand side is regular in an upper half-plane, and since the two regions overlap, each side must be equal to a function regular throughout the whole ζ plane. The growth orders of the two sides as $|\zeta| \rightarrow \infty$ then specify the function as $B'' + C'' \zeta$, where B'' and C'' are independent of ζ , and hence

$$k \sin \beta \bar{I}_2(\zeta) + \zeta \bar{I}_4(\zeta) =$$

$$= i \sqrt{\frac{2}{\pi}} Y \frac{k^2 \sin^2 \alpha \sin \beta \cos^3 \beta}{\eta \zeta + k \cos \alpha \cos \beta} \frac{L_+(-k \cos \alpha \cos \beta)}{\sqrt{k \cos \beta (1 - \cos \alpha)} (k \cos \beta - \zeta)} L_-(\zeta)$$

$$- \frac{iI_4(0)}{\sqrt{2\pi}} \frac{\zeta^2 + k^2 \sin^2 \beta}{k^2 \cos^2 \beta - \zeta^2} \left[\sqrt{\frac{k \cos \beta}{2(k \cos \beta - \zeta)}} \frac{L_+(k \cos \beta)}{L_-(\zeta)} - 1 \right] +$$

$$+ \frac{B'' + C'' \zeta}{(k \cos \beta + \zeta) \sqrt{k \cos \beta - \zeta} L_-(\zeta)}. \quad (\text{A } 3)$$

From (21) and (A 3), $I_2(\zeta)$ can be eliminated to give an expression for $\bar{I}_4(\zeta)$ alone. The equation obtained in this manner is

$$(\zeta^2 + k^2 \sin^2 \beta) \bar{I}_4(\zeta) =$$

$$= i \sqrt{\frac{2}{\pi}} Y k^2 \cos \alpha \sin \beta \cos^2 \beta \frac{K_+(-k \cos \alpha \cos \beta)}{(\zeta + k \cos \alpha \cos \beta) K_-(\zeta)}$$

$$+ i \sqrt{\frac{2}{\pi}} Y \frac{k \zeta}{\eta} \sin^2 \alpha \sin \beta \cos^2 \beta.$$

$$+ \sqrt{\frac{k \cos \beta}{(1 - \cos \alpha)(k \cos \beta - \zeta)}} \frac{L_+(-k \cos \alpha \cos \beta)}{(\zeta + k \cos \alpha \cos \beta) L_-(\zeta)} -$$

$$- \frac{iI_4(0)}{\sqrt{2\pi}} \zeta \frac{\zeta^2 + k^2 \sin^2 \beta}{k^2 \cos^2 \beta - \zeta^2} \left[\sqrt{\frac{k \cos \beta}{2(k \cos \beta - \zeta)}} \frac{L_+(k \cos \beta)}{L_-(\zeta)} - 1 \right]$$

$$+ \frac{(B'' + C'' \zeta) \zeta}{(k \cos \beta + \zeta) \sqrt{k \cos \beta - \zeta} L_-(\zeta)} - \frac{A' k \sin \beta}{K_-(\zeta)},$$

from which it is seen that $\bar{I}_4(\zeta) = O(|\zeta|^{-3/2})$. The Fourier transform relationship now gives

$$I_4(x) \sim x^{1/2} \text{ as } x \rightarrow 0,$$

and accordingly the electric current perpendicular to the edge is zero there.

Received 27th February, 1959

REFERENCES

- 1) Clemmow, P. C., Proc. Roy. Soc. **205** (1951) 286.
- 2) Senior, T. B. A., Quart. J. Mech. Appl. Math. **6** (1953) 101.
- 3) Senior, T. B. A., Proc. Roy. Soc. **213** (1952) 436.
- 4) Stratton, J. A., Electromagnetic Theory, McGraw-Hill, New York, 1941.

THE METHOD OF IMAGES AND THE SOLUTION OF CERTAIN PARTIAL DIFFERENTIAL EQUATIONS

by G. ROWLANDS *)

Atomic Energy Research Establishment, Harwell, England

Summary

A series solution of certain partial differential equations is obtained by a generalisation of a method well known in the field of electrostatics, the so-called method of images. Over certain ranges of the variables these series solutions are more rapidly convergent than the usual solution in terms of orthogonal functions. In general these two types of solutions are to be taken as complementary.

§ 1. *Introduction.* In many distinct fields of physics, the solution of certain problems reduces to that of finding solutions of certain well known differential equations subject to appropriate initial and boundary conditions. (The present investigation arose out of a mathematical study of certain problems associated with heterogeneous reactor calculations). The solutions appropriate to simple shaped boundaries can usually be obtained in the form of an infinite series of orthogonal functions, but the convergence of such series is usually very slow except over rather special ranges of the variables. However, much more rapidly convergent series may sometimes be obtained by a method which is essentially a generalisation of a method which is well known in the field of electrostatics, the so-called method of images. In certain cases it is found that by considering the first few terms only, or what is equivalent, the nearest images, solutions correct to of order 1% can be obtained.

The nature of the method of images is to replace the boundary conditions by a set of fictitious source terms so that the solution of the original equation satisfying the appropriate boundary

*) Harwell Junior Research Fellow.

conditions reduces to that of finding solutions of the equation appropriate to a set of sources but with no boundary conditions. In the case of linear differential equations, the process of obtaining the final solution divides into three distinct steps.

1) Solving the differential equation appropriate to a point source in an infinite medium, but with no boundary conditions except that of good behaviour at infinity,

2) Finding the set of image source, and

3) Summing the solution of 1) over the set of images obtained by step 2).

For certain rather simple geometric shapes, the set of images may be obtained by inspection, but in general some more powerful method is necessary and an analytic method is developed below. The main advantage of the method proposed here is that the solution of step 1) is usually relatively simple, and since the final solution may be obtained with sufficient accuracy as the sum of a small number of such solutions, the final solution is also relatively simple.

§ 2. *General method.* In this section we shall consider solutions of the following equation

$$(\nabla^2 + B^2) \phi(\mathbf{r}) = S(\mathbf{r}), \quad (2.1)$$

subject to the condition $\phi(\mathbf{r}) = 0$ on some specified boundary. $S(\mathbf{r})$ is the real source distribution and is assumed zero outside the specified boundary. B^2 is a constant.

The quantities $\phi(\mathbf{r})$ and $S(\mathbf{r})$ are defined inside the boundary over which $\phi(\mathbf{r}) = 0$. We now define a function $\phi_\infty(\mathbf{r})$ which inside this region coincides with $\phi(\mathbf{r})$ and, similarly, a function $S_\infty(\mathbf{r})$ which coincides with $S(\mathbf{r})$ inside this region. Further we assume that

$$(\nabla^2 + B^2) \phi_\infty(\mathbf{r}) = S_\infty(\mathbf{r}), \quad (2.2)$$

so that inside the specified region (2.1) is automatically satisfied. We do not impose any boundary condition on $\phi_\infty(\mathbf{r})$, but $S_\infty(\mathbf{r})$ must be such as to make $\phi_\infty(\mathbf{r}) = 0$ on the specified boundary. In this way we have replaced the boundary condition by a set of fictitious sources $S_\infty(\mathbf{r})$. For certain rather simple geometries the form of $S_\infty(\mathbf{r})$ may be obtained by inspection and then (2.2) may be solved.

However in general this is not so and we now proceed to the general case.

The functions $\phi_\infty(\mathbf{r})$ and $S_\infty(\mathbf{r})$ are defined over all space, although they may be discontinuous, and we may solve (2.2) by taking a complex Fourier transform of (2.2) to obtain

$$\tilde{\phi}_\infty(\mathbf{w}) = \tilde{S}(\mathbf{w})/(B^2 - w^2), \quad (2.3)$$

where

$$\tilde{\phi}_\infty(\mathbf{w}) = \int_{-\infty}^{+\infty} \phi_\infty(\mathbf{r}) e^{i\mathbf{w} \cdot \mathbf{r}} d\mathbf{r}, \quad (2.4)$$

and likewise for $\tilde{S}_\infty(\mathbf{w})$. Inverting the transform we find

$$\phi_\infty(\mathbf{r}) = \frac{1}{(2\pi)^n} \int_{-\infty}^{+\infty} \frac{\tilde{S}_\infty(\mathbf{w}) e^{-i\mathbf{w} \cdot \mathbf{r}} d\mathbf{w}}{B^2 - w^2}, \quad (2.5)$$

where n is the number of components of the vectors \mathbf{r} and \mathbf{w} .

We now consider the set of functions $\Psi_m(\mathbf{r})$ which satisfy

$$(\nabla^2 + w_m^2) \Psi_m(\mathbf{r}) = 0 \quad (2.6)$$

and are also zero over the specified boundary. These functions we assume are orthogonal and hence satisfy

$$\int_V \Psi_n^\dagger(\mathbf{r}) \Psi_m(\mathbf{r}) d\mathbf{r} = \delta_{n,m}, \quad (2.7)$$

where the integral is over the volume enclosed by the specified boundary, $\delta_{n,m}$ is the Kronecker delta function and the superfix \dagger denotes the adjoint function. We expand the function $\Psi_m(\mathbf{r})$ in a Fourier series, and since these functions obey (2.6), we have

$$\Psi_m(\mathbf{r}) = \frac{1}{(2\pi)^n} \int_{-\infty}^{+\infty} A(\mathbf{w}) \delta(w^2 - w_m^2) e^{-i\mathbf{w} \cdot \mathbf{r}} d\mathbf{w}, \quad (2.8)$$

where δ is the Dirac delta function. Further, since the $\Psi_m(\mathbf{r})$ form a complete orthogonal set, we may write

$$S_\infty(\mathbf{r}) = \sum_m C_m \Psi_m(\mathbf{r}). \quad (2.9)$$

Combining (2.5), (2.8) and (2.9) we obtain

$$\phi_\infty(\mathbf{r}) = \frac{1}{(2\pi)^{2n}} \sum_m C_m \int_{-\infty}^{+\infty} \int_{-\infty}^{+\infty} \int_{-\infty}^{+\infty} \frac{A(\mathbf{w}') \delta(w'^2 - w_m^2)}{B^2 - w^2} \cdot e^{+i(-\mathbf{w}' \cdot \mathbf{r}' + \mathbf{w} \cdot \mathbf{r}' - \mathbf{w} \cdot \mathbf{r})} d\mathbf{r}' d\mathbf{w}' d\mathbf{w}, \quad (2.10)$$

and using the result

$$\int_{-\infty}^{+\infty} e^{i\mathbf{w} \cdot \mathbf{r}} d\mathbf{r} = \delta(\mathbf{w}) (2\pi)^n \quad (2.11)$$

we find

$$\begin{aligned} \phi_{\infty}(\mathbf{r}) &= \frac{1}{(2\pi)^n} \sum_m C_m \int_{-\infty}^{+\infty} \frac{A(\mathbf{w}') \delta(w'^2 - w_m^2)}{B^2 - w'^2} e^{-i\mathbf{w}' \cdot \mathbf{r}} d\mathbf{w}' \\ &= \sum_m \frac{C_m \Psi(\mathbf{r})}{B^2 - w_m^2}. \end{aligned} \quad (2.12)$$

We have from (2.7) and (2.9) that

$$C_m = \int_{\Gamma} \Psi_m^{\dagger}(\mathbf{r}) S_{\infty}(\mathbf{r}) d\mathbf{r}, \quad (2.13)$$

and hence

$$\phi_{\infty}(\mathbf{r}) = \sum_m \frac{\left(\int \Psi_m^{\dagger}(\mathbf{r}') S_{\infty}(\mathbf{r}') d\mathbf{r}' \right) \Psi_m(\mathbf{r})}{B^2 - w_m^2}. \quad (2.14)$$

Now the function $\phi_{\infty}(\mathbf{r})$ as defined by (2.14) is zero on the required boundary, satisfies an equation of the form (2.1) inside this boundary, and hence for values of \mathbf{r} which denote points inside this region we may replace $\phi_{\infty}(\mathbf{r})$ by $\phi(\mathbf{r})$. Further, the volume integral in (2.14) is over the volume enclosed by the specified boundary and by definition $S_{\infty}(\mathbf{r})$ equals $S(\mathbf{r})$ in this region. Thus we may write finally as the general solution of (2.1):

$$\phi(\mathbf{r}) = \sum_m \frac{\left[\int \Psi_m^{\dagger}(\mathbf{r}') S(\mathbf{r}') d\mathbf{r}' \right] \Psi_m(\mathbf{r})}{B^2 - w_m^2}. \quad (2.15)$$

This result could have been obtained directly from the well-known properties of the Green's functions, since these functions are defined such that they satisfy

$$(\nabla^2 + B^2) G(\mathbf{r}, \mathbf{r}') = \delta(\mathbf{r} - \mathbf{r}') \quad (2.16)$$

and are zero over the specified boundary, in which case we may write

$$\phi(\mathbf{r}) = \int_{\Gamma} G(\mathbf{r}, \mathbf{r}') S(\mathbf{r}') d\mathbf{r}'. \quad (2.17)$$

However, the above analysis has been carried out since we may now obtain an explicit form for the system of images. Combinin

(2.9) and (2.13) and remembering that over the volume of integration in (2.13) $S_\infty(\mathbf{r}) = S(\mathbf{r})$, we find

$$S_\infty(\mathbf{r}) = \sum_m \left[\int_v S(\mathbf{r}') \Psi_m^\dagger(\mathbf{r}') d\mathbf{r}' \right] \Psi_m(\mathbf{r}). \quad (2.18)$$

Thus knowing the real source distribution $S(\mathbf{r})$ and the set of orthogonal functions $\Psi_m(\mathbf{r})$ we can obtain an expression for $S_\infty(\mathbf{r})$. Further, as seen from (2.17), if we can obtain the system of images for a delta-function source, that is a solution of (2.16), then in virtue of (2.17) we may obtain the general solution of (2.1). The image source appropriate to such a source is readily obtainable from (2.18) and is given by

$$S_{\infty,\delta}(\mathbf{r}, \mathbf{r}_0) = \sum \Psi_m^\dagger(\mathbf{r}_0) \Psi_m(\mathbf{r}). \quad (2.19)$$

Having obtained the general form for $S_\infty(\mathbf{r})$ we may now return to the general solution as given by (2.5). Using the convolution theorem this may be written in the form

$$\phi_\infty(\mathbf{r}) = \int_{-\infty}^{+\infty} S_\infty(\mathbf{r}') G(\mathbf{r} - \mathbf{r}') d\mathbf{r}', \quad (2.20)$$

where

$$G(\mathbf{r}) = \frac{1}{(2\pi)^n} \int_{-\infty}^{+\infty} \frac{e^{-i\mathbf{w} \cdot \mathbf{r}} d\mathbf{w}}{B^2 - w^2}. \quad (2.21)$$

Further, if we restrict \mathbf{r} to be inside the specified region, we have

$$\phi(\mathbf{r}) = \int_{+\infty}^{-\infty} S_\infty(\mathbf{r}') G(\mathbf{r} - \mathbf{r}') d\mathbf{r}', \quad (2.22)$$

and this automatically satisfies (2.1) and the boundary conditions, the latter because of the form of $S_\infty(\mathbf{r})$. The above equation is exact, but the nature of the method of image approximation is to consider the contribution from the nearest images only. It is usually found, due to rapid fall of $G(\mathbf{r})$ with \mathbf{r} , that only a few images need be considered.

In the case of Laplace's equation, $\nabla^2 \phi(\mathbf{r}) = 0$, the results obtained above with $B^2 = 0$ are appropriate. However, it will be noted that B^2 does not enter the expression for $S_\infty(\mathbf{r})$ (cf. (2.18)), and hence the set of images appropriate to (2.1) is the same as for the equivalent electrostatic problem.

The form of solution given by (2.16) is that obtained by the well-

known method of expansion in terms of orthogonal functions, and for certain ranges of the variables is rapidly convergent. However, it is usually found that this range does not include values of the variables of practical interest (see for example Jain¹). On the other hand, the solution as given by (2.23) usually converges in the region of practical interest. In general these two different types of solutions should be taken as complementary.

Other boundary conditions. We have imposed on the solution $\phi(\mathbf{r})$ of (2.1) that it be zero over the specified boundary, but equally we could demand a condition of the form $\text{grad } \phi(\mathbf{r}) = 0$ over this boundary. This condition can be taken account of in the above method by simply defining the function $\Psi_m(\mathbf{r})$ to be a solution of (2.6), but now being such that $\text{grad } \Psi_m(\mathbf{r}) = 0$ on the boundary. In a similar manner we may impose the condition $\text{grad } \phi(\mathbf{r})/\phi(\mathbf{r}) = \text{constant}$ over the boundary. The only restriction on the type of boundary condition that may be considered is that the functions $\Psi_m(\mathbf{r})$, which satisfy equations (2.6) and (2.7) and also satisfy the imposed boundary condition, must exist.

§ 3. *Other differential equations.* In § 2 we have shown how an equation of the form given by (2.1) can be solved by the method of images. In this section we consider a few examples of other differential equations which can be transformed into the form (2.1) and solutions obtained as above. The first which we shall consider is the well known diffusion equation or age equation which may be written in the form

$$\nabla^2 \phi(\mathbf{r}, t) - \frac{\partial \phi(\mathbf{r}, t)}{\partial t} = 0, \quad (3.1)$$

with $\phi(\mathbf{r}, t) = 0$ on a specified boundary and $\phi(\mathbf{r}, 0)$ some known function. Subjecting the above to a Laplace Transform we find

$$\nabla^2 \bar{\phi}(\mathbf{r}, \eta) - \eta \bar{\phi}(\mathbf{r}, \eta) = \phi(\mathbf{r}, 0), \quad (3.2)$$

where

$$\bar{\phi}(\mathbf{r}, \eta) = \int_0^\infty \phi(\mathbf{r}, t) e^{-\eta t} dt. \quad (3.3)$$

This is now of the form (2.1) with $B^2 = -\eta$ and $S(\mathbf{r}) = \phi(\mathbf{r}, 0)$. From (2.20) and (2.21) we may write the general solution

$$\bar{\phi}(\mathbf{r}, \eta) = -\frac{1}{(2\pi)^n} \int_{-\infty}^{+\infty} \int_{-\infty}^{+\infty} \frac{\phi_{\infty}(\mathbf{r}', 0)}{w^2 + \eta} e^{-i\mathbf{w} \cdot (\mathbf{r} - \mathbf{r}')} d\mathbf{r}' d\mathbf{w}. \quad (3.4)$$

Inverting the transform (3.3) we find

$$\phi(\mathbf{r}, t) = -\frac{1}{(2\pi)^n} \int_{-\infty}^{+\infty} \int_{-\infty}^{+\infty} \phi_{\infty}(\mathbf{r}', 0) e^{-w^2 t} e^{-i\mathbf{w} \cdot (\mathbf{r} - \mathbf{r}')} d\mathbf{r}' d\mathbf{w}. \quad (3.5)$$

This is of the form (2.22) with

$$G(\mathbf{r}) = G_1(\mathbf{r}, t) = -\frac{1}{(2\pi)^n} \int_{-\infty}^{+\infty} e^{-w^2 t} e^{-i\mathbf{w} \cdot \mathbf{r}} d\mathbf{w}.$$

Thus a knowledge of the system of images appropriate to the boundary conditions and $\phi(\mathbf{r}, 0)$ will enable a solution of (3.1) to be obtained.

A further equation which is of some importance is given by

$$\nabla^2 \phi(\mathbf{r}, t) - \frac{\partial \phi(\mathbf{r}, t)}{\partial t} = C(\mathbf{r}), \quad (3.6)$$

where $C(\mathbf{r})$ is some external source, assumed constant in time. The transformed equation is given by

$$(\nabla^2 - \eta) \bar{\phi}(\mathbf{r}, \eta) = C(\mathbf{r})/\eta. \quad (3.7)$$

This is still of the form given by (2.1), and a solution may be obtained by the methods given in § 2. We find

$$\phi(\mathbf{r}, t) = -\frac{1}{(2\pi)^n} \int_{-\infty}^{+\infty} \int_{-\infty}^{+\infty} C_{\infty}(\mathbf{r}') \frac{(1 - e^{-w^2 t})}{w^2} e^{-i\mathbf{w} \cdot (\mathbf{r} - \mathbf{r}')} d\mathbf{w} d\mathbf{r}', \quad (3.8)$$

which is also of the form (2.22) with

$$G(\mathbf{r}) = G_2(\mathbf{r}, t) = -\frac{1}{(2\pi)^n} \int_{-\infty}^{+\infty} \frac{(1 - e^{-w^2 t})}{w^2} e^{-i\mathbf{w} \cdot \mathbf{r}} d\mathbf{w}. \quad (3.9)$$

Consider the equation of the form

$$(\nabla^2 - \alpha) \phi(\mathbf{r}, t) = \frac{\partial \phi(\mathbf{r}, t)}{\partial t}, \quad (3.10)$$

with the usual boundary conditions. A solution of the form (2.22) is readily obtained by the method outlined above with

$$\begin{aligned} G(\mathbf{r}) = G_3(\mathbf{r}, t) &= -\frac{1}{(2\pi)^n} \int_{-\infty}^{+\infty} e^{-i\mathbf{w} \cdot \mathbf{r}} e^{-(w^2 + \alpha)t} d\mathbf{w} \quad (3.11) \\ &= e^{\alpha t} G_1(\mathbf{r}, t). \end{aligned} \quad (3.12)$$

This last result is also readily obtainable direct from the differential equation.

§ 4. *Example.* In this section we illustrate the general method as given above by considering a problem treated by Jain¹⁾. He considers the solution of an equation of the form (3.1) appropriate to slab geometry and shows that for the case of practical interest the solution is approximately equal to the superposition of solutions appropriate to semi-infinite media. We show below that the approximate solution obtained by Jain is equivalent to considering the nearest images only.

In plane geometry, (3.1) takes the form

$$\frac{\partial^2 \phi(x, t)}{\partial x^2} - \frac{\partial \phi(x, t)}{\partial t} = 0, \quad (4.1)$$

and the general solution (3.5) the form

$$\phi(x, t) = -\frac{1}{2\tau} \int_{-\infty}^{+\infty} \int_{-\infty}^{+\infty} \phi_{\infty}(x', 0) e^{-w^2 t} e^{-i w(x-x')} dw dx'. \quad (4.2)$$

The first case we consider is that of an semi-infinite medium with $\phi(x, 0)$ equal to a constant C_i in the medium and zero outside. The quantity $\phi(x, t)$ is zero on the surface of the medium, namely at $x = 0$, and the image system can be obtained by inspection:

$$\begin{aligned} \phi_{\infty}(x, 0) &= +C_i, \quad 0 < x < \infty, \\ &= -C_i, \quad -\infty < x < 0, \end{aligned} \quad (4.3)$$

but we will give an analytic derivation to illustrate the general procedure.

We first must obtain the functions $\Psi_m(x, t)$ which in this case satisfy

$$\frac{\partial^2 \Psi_m(x, t)}{\partial x^2} + w_m^2 \Psi_m(x, t) = 0 \quad (4.4)$$

and $\Psi_m(0, t) = 0$ for all t , and we find

$$\Psi_m(x, t) = \left[\lim_{L \rightarrow \infty} \sqrt{\frac{2}{L}} \sin\left(\frac{m\pi x}{L}\right) \right] g(t), \quad (4.5)$$

satisfy (4.4) and are orthogonal if we suitably define the integration procedure at infinity, the limiting process being carried out after the integration over x . $g(t)$ is any function of time and $m = 1, 2, 3$ etc.

From (2.18) we obtain

$$\phi_\infty(x, 0) = \frac{C_i}{\pi} \int_{-\infty}^{+\infty} \frac{\sin(wx)}{w} dw. \quad (4.6)$$

We immediately see that $\phi_\infty(x, 0) = -\phi_\infty(-x, 0)$ and, for positive x , $\phi_\infty(x, 0) = C_i$.

This form for the image system then agrees with that obtained by inspection and given by (4.3) above. The general solution (4.2) may now be written in the form

$$\begin{aligned} \phi(x, t) &= -\frac{C_i}{2\pi} \int_{-\infty}^{+\infty} e^{-w^2 t} dw \left[\int_0^\infty e^{-iw(x-x')} dx' - \int_{-\infty}^0 e^{-iw(x-x')} dx' \right], \\ &= C_i \operatorname{erf}(x/\sqrt{4t}), \end{aligned} \quad (4.7)$$

where

$$\operatorname{erf}(x) = \frac{2}{\sqrt{\pi}} \int_0^x e^{-y^2} dy.$$

Jain defines the fractional loss in concentration v , in our notation, by the equation

$$v = 1 - \phi(x, t)/C_i,$$

which from the above gives

$$v = \operatorname{erfc}(x/\sqrt{4t}), \quad (4.8)$$

which agrees with Jain's equation (4).

We now consider the finite slab in which case $\phi(x, 0) = C_i$ for $0 < x < L$ and zero elsewhere. The appropriate solutions of (4.4) are

$$\Psi_m(x, t) = \sqrt{\frac{2}{L}} \sin\left(\frac{m\pi x}{L}\right) g(t) \quad (4.9)$$

with

$$w_m^2 = m^2 \pi^2 / L^2 \quad (4.10)$$

and $m = 1, 2, 3$, etc.

The system of images is obtained from (2.18) and we find

$$\phi_\infty(x, 0) = \frac{2C_i}{L} \sum_m \frac{(1 - \cos m\pi) \sin(m\pi x/L)}{m\pi/L}. \quad (4.11)$$

Again the analytic expression for the system of images is easily shown to be the same as that obtained by inspection. Using this result, the final expression for $\phi(x, t)$ may be written in the form

$$\begin{aligned} \frac{\phi(x, t)}{C_i} = & \operatorname{erf}(x') + \operatorname{erf}(l - x') - \operatorname{erf}(l + x') + \\ & + \frac{2}{\sqrt{\pi}} \sum_{m=2}^{\infty} (-1)^m \int_{ml-x'}^{ml+x'} e^{-y^2} dy, \end{aligned} \quad (4.12)$$

where $x' = x \sqrt{4t}$ and $l = L \sqrt{4t}$, each term corresponding to the contribution from the various image sources. Introducing the quantity v as defined by (4.8) we have

$$v = \operatorname{erfc}(x') + \operatorname{erfc}(l - x') - \operatorname{erfc}(l + x') - \frac{2}{\sqrt{\pi}} \sum_{m=2}^{\infty} (-1)^m \int_{ml-x'}^{ml+x'} e^{-y^2} dy. \quad (4.13)$$

Denoting with a suffix s the value for a semi-infinite medium we see that for $l + x'$ sufficiently large, such that $\operatorname{erfc}(l + x') \rightarrow 0$, we may write

$$v \approx v_s(x') + v_s(l - x'). \quad (4.13)$$

This is the result obtained by Jain and is equivalent to considering the nearest image only. By symmetry $v(x') = v(l - x')$, and hence we need only consider the above for $x' \leq l/2$, and a rough criterion for the applicability of (4.13) is that

$$v \gg \operatorname{erfc}(3l/2). \quad (4.14)$$

To this same approximation

$$\phi(x, t) = \phi_s(x', t) + \phi_s(l - x', t) - 1. \quad (4.15)$$

The higher approximations to $\phi(x, t)$ and v are easily obtained from the exact expressions (4.12) and (4.13), but in most cases of practical

interest, as shown by Jain, the approximations (4.13) and (4.15) are sufficient.

Although in the above we have only considered the special case of slab geometry, other geometries can be considered by use of the general method given in § 3.

Received 27th April, 1959.

REFERENCES

- 1) Jain, S. C., Proc. Roy. Soc. A **243** (1957) 359.

THE DIFFRACTION OF A PLANE WAVE THROUGH TWO OR MORE SLITS IN A PLANE SCREEN

ERIK B. HANSEN

Institute of Electromagnetic Theory of the Royal Technical University of Denmark
Copenhagen, Denmark *)

Summary

The diffraction of a plane acoustic wave through two or more parallel slits in a plane screen is investigated by means of integral equation technique. Numerical calculations of the transmission coefficient are carried out in some simple cases.

§ 1. *Introduction.* Among the mathematical methods which have been used in the theoretical study of diffraction phenomena those founded on the formulation of integral equations seem to be very promising. As an example of problems which have been treated in this way the transmission of a plane wave through an infinite plane grating may be mentioned. This problem has been considered among others by Miles¹⁾ who calculated the transmission coefficient of an infinite grating as a function of the width of the slits and the separation between them. The diffraction of a plane wave through a single slit in an infinite screen of vanishing thickness forms another example which has been treated by means of the integral equation technique. Incidentally, this problem is one of those relatively few which are manageable by the separation method in its usual form; indeed, this approach has been used by Strutt²⁾, by Morse and Rubenstein³⁾ and by Skavlem⁴⁾, while integral equation methods have been applied by Sommerfeld⁵⁾, by Groschwitz and Hönl⁶⁾ and by Bouwkamp⁷⁾.

The geometrical arrangements mentioned above may be considered as limiting cases of a finite grating, i.e. a finite number of parallel slits in an infinite screen of vanishing thickness. As the

*) Present address: The Haldor Topsøe Research Laboratory, Hellerup, Denmark.

method used by Miles is profoundly connected with the spatial periodicity of the field which results when a plane wave falls perpendicularly on an infinite regular grating, this method is not applicable when finite gratings are considered. On the other hand, the method applied by Bouwkamp is easily generalized to the case of several slits. Unfortunately, the labour involved in the solution of the integral equation increases seriously when the number of slits is increased. Therefore, in the present note only the case of two slits of equal width is treated in some detail while the case of more than two slits is considered more briefly. As in most of the papers mentioned above (the only exception being the one by Morse and Rubenstein) only perpendicular incidence is considered. However, the present method may also be applied in the case of oblique incidence, but with a further increase of labour.

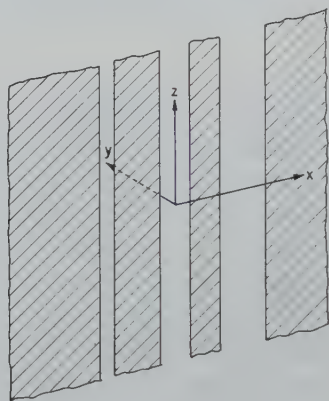


Fig. 1. A system of slits in an infinite screen.

§ 2. *Formulation of the integral equation.* In what follows a system of N slits cut in a perfectly rigid screen of vanishing thickness is considered. The screen is thought to be hit by a plane sound wave propagated in the positive direction of the y -axis of the coordinate system shown in fig. 1. The velocity potential of the incoming wave is taken to be

$$u^i(\mathbf{r}) = e^{ik_y y}. \quad (1)$$

In (1) and throughout the time factor $\exp(-i\omega t)$ is omitted. If u denotes the velocity potential of the total field surrounding the

screen, the boundary condition on the perfectly rigid screen is

$$\partial u / \partial y = 0. \quad (2)$$

Application of Green's theorem to the two half-spaces $y \lesseqgtr 0$ together with the fulfillment of the requirement of a continuous fit of the velocity potential through the apertures leads to the following integral equation for the y -component $v_y(\mathbf{r}) = \partial u / \partial y$ of the particle velocity in the apertures:

$$2i = \int_{\text{all slits}} H_0^{(1)}(k|x - x'|) v_y(x', 0, 0) dx', \quad (3)$$

where $H_0^{(1)}(z)$ is the Hankel function of first kind, order zero. This equation should be satisfied for every x lying in one of the apertures.

When the system of slits is symmetrical about the z -axis, the same will be true for the total field as long as only perpendicular incidence is considered. Thus, when the number of slits $N = 2N'$ for the sake of definiteness is taken to be even and all of equal width $2b$ and with a constant distance $2a$ between neighbouring slits, (3) may be written

$$2i = \sum_{n=1}^{n=N'} \int_{(2n-1)a-b}^{(2n-1)a+b} [H_0^{(1)}(k|x + x'|) + H_0^{(1)}(k|x - x'|)] v_y(x', 0, 0) dx'. \quad (4)$$

Obviously, it is sufficient to consider only values of x lying in one of the intervals of integration. By means of the substitutions

$$x = (2m - 1)a - b \cos \varphi, \quad x' = (2n - 1)a - b \cos \varphi' \quad (5)$$

(4) is rewritten in the following form, which is suitable for the subsequent solution of the equation:

$$2i = \sum_{n=1}^{n=N'} \int_0^\pi K_{n,m}(\varphi, \varphi') f_n(\varphi') d\varphi', \quad 1 \leq m \leq N'; \quad 0 \leq \varphi \leq \pi,$$

$$\begin{aligned} K_{n,m}(\varphi, \varphi') = & H_0^{(1)}[k(2(m+n-1)a - b(\cos \varphi + \cos \varphi'))] + H_0^{(1)}[k(2(m-n)a \\ & - b(\cos \varphi - \cos \varphi'))], \\ f_n(\varphi') = & v_y(x', 0, 0) b \sin \varphi'; \quad (2n-1)a - b \leq x' \leq (2n-1)a + b. \end{aligned} \quad (6)$$

§ 3. *Solution of the integral equation in the case of two slits.* For $2N' = 2$ equation (6) is expressed by

$$2i = \int_0^\pi \{H_0^{(1)}[2ka - kb(\cos \varphi + \cos \varphi')] + H_0^{(1)}[kb|\cos \varphi - \cos \varphi'|]\} f(\varphi') d\varphi'. \quad (7)$$

In order to solve this equation the same method is used as that applied by Bouwkamp⁷⁾ for the case of a single slit; thus the kernel of (7) as well as the unknown function $f(\varphi')$ are expanded in series of a complete system of functions. This procedure leads to an infinite system of linear equations, from which the expansion coefficients of $f(\varphi')$ may be found.

The first term of the kernel is most conveniently expanded by means of the addition theorem for Hankel functions. When the Bessel functions occurring in this expansion in turn are expanded about $kb = 0$, a power series in $\cos \varphi$ and $\cos \varphi'$, which eventually is transformed into a Fourier series, results. Similarly the second term is expanded in a Fourier series by means of the expansion about the origin of the Hankel functions together with the formula

$$\ln (2 |\cos \varphi - \cos \varphi'|) = -2 \sum_{p=1}^{\infty} \frac{\cos p\varphi \cos p\varphi'}{p}. \quad (8)$$

As is well known, the particle velocity near an edge of a rigid screen of vanishing thickness behaves like $d^{-\frac{1}{2}}$, d being the distance from the edge; therefore the function $f(\varphi')$ is finite in the closed interval $0 \leq \varphi' \leq \pi$ and may thus be expanded in a Fourier series too. In this way the following infinite system of linear equations is derived:

$$\frac{4i}{\pi} \delta_{0,r} = \sum_{s=0}^{\infty} (1 + \delta_{0,s}) F_{r,s} C_s, \quad (9)$$

where $r = 0, 1, 2, \dots$, $F_{r,s}$ and C_s are the coefficients in the Fourier expansion of the kernel in (7) and of the function $f(\varphi')$ respectively and $\delta_{r,s}$ is Kronecker's delta.

The explicit expressions for the Fourier coefficients $F_{r,s}$ are rather complicated and shall not be given here. They turn out to depend on ka through $H_0^{(1)}(2ka)$, $H_1^{(1)}(2ka)$ and $(ka)^{-n}$ ($n > 0$), while the dependence on kb is through $(kb)^n$ ($n > 0$) and $\ln kb$; the coefficients C_s depend on ka and kb in a similar way. A closer examination of the Fourier coefficients shows that when kb tends to zero, the coefficient $F_{r,s}$ decreases faster than $(kb)^{r+s}$ when $r+s$ is odd, while $F_{r,s}$ decreases faster than $(kb)^{|r-s|}$ when $r+s$ is even. Application of well-known theorems concerning systems of linear equations leads to the conclusion that the coefficients C_s may be written

$$C_s = \sum_{p=0}^{\infty} C_s^{(s+2p)} \left(\frac{kb}{2} \right)^{s+2p}, \quad (10)$$

where $C_s^{(s+2p)}$ tends to zero together with kb . Therefore all those coefficients $C_s^{(s+2p)}$ for which $s + 2p \leq M - 1$ may be found by substitution of (9) by the first M equations of this system.

The procedure described above has been carried out for $M = 5$, and the following expressions for $C_0^{(0)}$, $C_0^{(2)}$ and $C_0^{(4)}$ were found:

$$\begin{aligned} C_0^{(0)} &= \frac{1}{A}, \\ C_0^{(2)} &= \frac{1}{A} + \frac{1}{A^2} \left[B + \frac{(\pi H_1)^2}{2} \right], \\ C_0^{(4)} &= -\frac{1}{4} + \frac{1}{2A} \left[\frac{3}{8} + (\pi H_1)^2 - B \right] \\ &+ \frac{1}{2A^2} \left\{ B \left[-\frac{B}{2} + \frac{1}{2} + \left(\frac{3}{2ka} - i\pi H_1 \right)^2 \right] + \frac{1}{4} - \frac{3(\pi H_1)^2}{4} + \right. \\ &\left. + i\pi H_0 \left[(\pi H_1)^2 - \frac{9}{16} \right] \right\} + \frac{1}{A^3} \left[B + \frac{(\pi H_1)^2}{2} \right]^2, \end{aligned} \quad (11)$$

where

$$\begin{aligned} A &= \ln \frac{kb}{4} + \gamma - i \frac{\pi}{2} (1 + H_0^{(1)}(2ka)); \\ B &= i \frac{\pi}{2} \left[\frac{1}{ka} H_1^{(1)}(2ka) - H_0^{(1)}(2ka) \right] \end{aligned}$$

$H_1 = H_1^{(1)}(2ka)$, $H_0 = H_0^{(1)}(2ka)$, $\gamma = 0.57722 \dots$ (Eulers constant).

These expressions may be checked by letting a tend to infinity in which case they become consistent with the corresponding expressions derived by Bouwkamp ⁷⁾ for a single slit.

§ 4. *Calculation of the transmission coefficient.* The transmission coefficient defined as the power transmitted through the aperture measured in units of its value for vanishing wavelength turns out to be

$$t_2 = \frac{1}{2kb} \operatorname{Im} \int_{a-b}^{a+b} v_y dx = \frac{\pi}{2kb} \operatorname{Im} C_0. \quad (12)$$

When the two first terms of the series (10) for C_0 are inserted in

(12), this expression becomes

$$t_2 = -\frac{\pi}{2kb} \frac{A_I}{|A|^2} \left\{ 1 + \left[1 - \frac{B_I + D_I}{A_I} + \right. \right. \\ \left. \left. + 2 \frac{A_I(B_I + D_I) + A_R(B_R + D_R)}{|A|^2} \right] \left(\frac{kb}{2} \right)^2 \right\} \quad (13)$$

where A_R , A_I , B_R and B_I denote the real and the imaginary parts respectively of the two quantities A and B given in (11) while D_R and D_I are the real and imaginary parts respectively of $D = \frac{1}{2}[H_1^{(1)}(2ka)]^2$. When a tends to infinity, (13) tends to Bouwkamp's⁷⁾ expression for the single slit

$$t_1 = \frac{\pi^2}{4kb} \frac{1 + (\frac{1}{2}kb)^2}{(\ln \frac{1}{4}kb + \gamma)^2 + (\frac{1}{2}\pi)^2} \quad (14)$$

as it should do. The same expression with $2b$ substituted for b should result when $a = b$, that is when the two slits join together forming a single slit of double width. However, when a is set equal to b in (13), and the Hankel functions occurring in this expression are substituted by the first terms of their expansions near zero, the following expression is found:

$$t_2(a = b) = \frac{\pi^2}{8kb} \frac{1}{(\ln \frac{1}{2}kb + \gamma)^2 + (\frac{1}{2}\pi)^2} \cdot \\ \left\{ 1 + \left[1 + \frac{3}{2} \frac{(\ln \frac{1}{2}kb + \gamma)(\ln 2 - \frac{3}{4})}{(\ln \frac{1}{2}kb + \gamma)^2 + (\frac{1}{2}\pi)^2} \right] (kb)^2 \right\}. \quad (15)$$

Comparison between (15) and the formula derived from (14) shows a small discrepancy in the second term. As the series expression for C_0 is not a power series, it might be expected that this discrepancy could be removed or deferred to a later term in the series if more terms were taken into account. In order to investigate this possibility the limiting expression for $\text{Im } C_0^{(4)}$ for a tending towards b was derived; it turned out that when $C_0^{(4)}$ is taken into account, the factor to the second term in the square bracket in (15) is numerically reduced from $(3/2)(\ln 2 - 3/4) = -0.085279$ to -0.008578 . This result makes one apt to conclude that the discrepancy might be further reduced if more terms were taken into account. However, the serious increase in labour connected with the calculation of further terms has prevented the author from investigating this point.

§ 5. *Connection with the variational method.* It is interesting to note that application of a variational procedure may lead to a system of linear equations essentially identical with (9). This fact is by no means surprising as $f(\varphi)$ in the two cases is expanded in the same complete system of functions. As is easily seen by reference to (7) and (12), the following stationary expression for t_2 is valid:

$$t_2 = \frac{1}{kb} \operatorname{Re} \frac{\int_0^\pi f(\varphi) d\varphi)^2}{\int_0^\pi \int_0^\pi f(\varphi) K(\varphi, \varphi') f(\varphi') d\varphi d\varphi'}, \quad (16)$$

where $K(\varphi, \varphi')$ is the kernel of (7). Insertion of the Fourier series for $f(\varphi)$ and $K(\varphi, \varphi')$ in (16) and application of the stationary property of this expression yields a system of linear equations identical with (9) except for the fact that the number of unknown coefficients C_s exceeds the number of equations derived in this way by one; this difference is caused by the fact that (16) is homogeneous to the zero'th order in $f(\varphi)$ so that t_2 may be found from (16) for $f(\varphi)$ being uncertain by an arbitrary factor.

§ 6. *Calculation of the transmission coefficient in the case of more than two slits.* As already mentioned the labour involved in the calculation of the field quantities increases considerably when the number of slits is increased. Therefore, in the case of more than two slits the investigation has been limited to the determination of the zero-order coefficients of the expansions corresponding to (10), i.e. v_y in the apertures has been approximated by the functions

$$v_y \sim \frac{D_n}{\sqrt{b_n^2 - (x - x_n)^2}}, \quad (17)$$

where D_n is a constant, x_n is the abscissa of the centre of the n 'th slit and b_n is the half-width of the slit.

For systems consisting of $2N'$ slits of equal width $2b$ and equally spaced with the distance $2a$ between the centre lines of neighbouring slits, functions of the type (17) may be inserted in (6) where $K_{n,m}$, in harmony with the approximation introduced by (17), is replaced by the first term of the expansion near $kb = 0$. In this way a system of N' equations determining the N' constants D_n results. From these

equations the first term of the transmission coefficient

$$t_{2N'} = \frac{\pi}{2N'kb} \operatorname{Im} \sum_{n=1}^{N'} D_n \quad (18)$$

may be found.

This procedure has been carried out for systems of four or six slits. The resulting expressions are rather complicated and will not be given here. It should only be mentioned that, when checked by letting a become equal to b and with the same approximations as described in § 4, they take on the same form as (14) with kb replaced by $4kb$ and $6kb$ respectively, but with the slight discrepancy that γ is increased from a value equal to Eulers constant (0.57722...) by an amount of 0.0133.. in the case of four slits and 0.0144.. in the case of six slits.

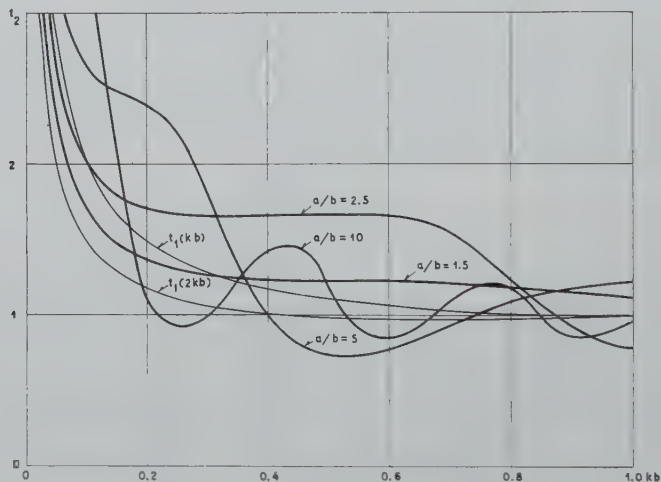


Fig. 2. The transmission coefficient t_2 for two slits of equal width as a function of $kb = 2\pi b/\lambda$. Width of the slits: $2b$; distance between the centre lines of the slits: $2a$.

§ 7. *Numerical results and discussion.* The transmission coefficient t_2 for two slits of equal width $2b$ separated by the distance $2a$ has been calculated from (12) for the four ratios $a/b = 1.5, 2.5, 5$, and 10 as a function of kb and for $kb = 0.1, 0.2$, and 0.5 as a function of ka . In all cases C_0 in (12) was approximated by $C_0^{(0)} + C_0^{(2)}(\frac{1}{2}kb)^2$, where $C_0^{(0)}$ and $C_0^{(2)}$ are given by (11).

The results are shown in fig. 2 and fig. 3. The most striking feature of t_2 as seen from these curves is probably that t_2 for $a/b \neq 1$ and ∞ by no means can be said to have some "intermediate" value between its values in these two limiting cases. The discrepancy in fig. 3 for $a = b$ is discussed in § 4.

In fig. 4 the transmission coefficients for systems of one, two, four, or six slits and for an infinite grating are shown as a function of kb when $a/b = 2.5$. The transmission coefficient for an infinite

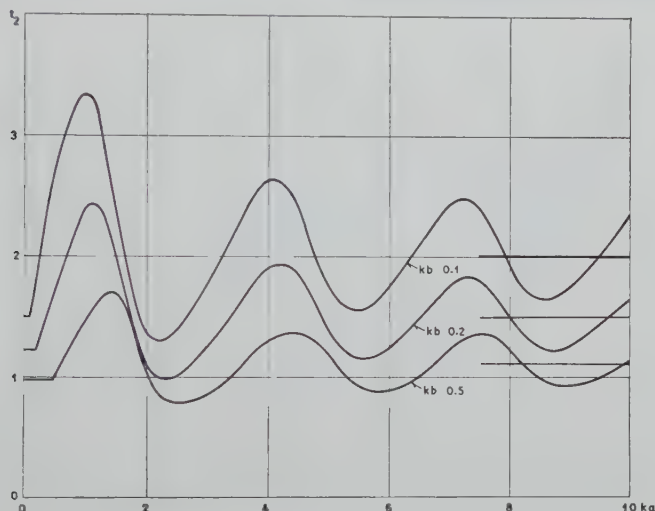


Fig. 3. The transmission coefficient t_2 for two slits of equal width as a function of $ka = 2\pi a/\lambda$. The notation is the same as in fig. 2. The horizontal lines to the left of the curves denote the limiting values of t_2 for $a = b$ and for $a \rightarrow \infty$ respectively.

grating is calculated from formula (86) of the aforementioned paper by Miles¹). This formula reads in our notation

$$t_{\infty} = \frac{a}{b} \frac{1}{1 + K^2(kb)^2};$$

$$K = \frac{1}{\varphi} \left\{ \ln(\sin \varphi) - \frac{[(1 - (kb/2\varphi)^2)^{-\frac{1}{2}} - 1] \cos^4 \varphi}{1 + [(1 - (kb/2\varphi)^2)^{-\frac{1}{2}} - 1] \sin^4 \varphi} \right\}; \quad \varphi = \frac{\pi b}{2a}. \quad (19)$$

As expected, the transmission coefficient for a finite grating tends mainly to that of an infinite grating when the number of slits is increased. However, for very small values of kb this is not the case,

as t_N (N finite) tends to infinity when kb tends to zero. It may be seen directly from the integral equation that this behaviour will occur when the wave length becomes large compared with the horizontal extension of the system of slits. This explains the fact that the discrepancy of t_N from t_∞ occurs for still smaller values of kb when N is increased. One is thus led to the conclusion that high values of the transmission coefficient will occur whenever finite gratings are considered and that they only fail to occur in the case of the fictitious infinite grating.

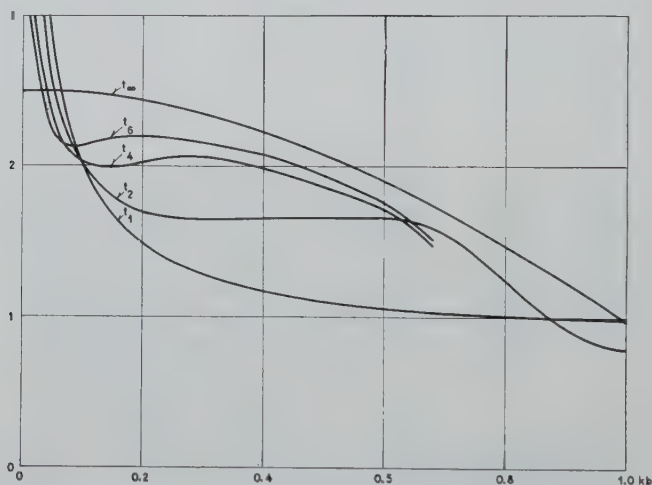


Fig. 4. The transmission coefficient t_N for a system of N slits of equal width $2b$ and with a constant distance $2a$ between the centre lines of neighbouring slits as a function of $kb = 2\pi b/\lambda$.

Acknowledgements. The work described in the present note was carried out in partial fulfillment of the requirements for the licentiate degree at the Royal Technical University of Denmark. The author was at this time associated with the Institute of Electromagnetic Theory at this University. He wishes to express his most cordial thanks to professor H. Lottrup Knudsen, Head of the Institute, for his never failing help and encouragement during the author's appointment at the institute. The author also wishes to express his thanks to professor Anker Engelund, President of the University, for a grant which made this appointment possible.

Received 30th May, 1959.

REFERENCES

- 1) Miles, J. W., Quart. Appl. Math. **7** (1949) 45.
- 2) Strutt, M. J. O., Z. Phys. **69** (1931) 597.
- 3) Morse, P. M. and P. J. Rubenstein, Phys. Rev. **54** (1938) 895.
- 4) Skavlem, S., Arch. Mat. Naturvidensk. **51** (1951) 61.
- 5) Sommerfeld, A., Vorlesungen über theoretische Physik. Vol. 4, Wiesbaden 1950, p. 294.
- 6) Groschwitz, E. and H. Hönl, Z. Phys. **131** (1952) 305.
- 7) Bouwkamp, C. J., Diffraction Theory, N.Y. Univ. Math. Research Rep. No. EM-50. 67, 1953.

EXTREMUM METHODS FOR CERTAIN ELECTRICAL PROBLEMS INVOLVING HOMOGENEOUS ANISOTROPIC MATERIAL

by G. POWER

Department of Mathematics, The University, Nottingham, England.

Summary

Methods are suggested for quickly estimating the value of an important unknown occurring in certain types of electrical problems which involve homogeneous anisotropic material, by bracketing it between upper and lower bounds. These bounds can be obtained by using arbitrarily-chosen admissible functions, or they can be made to depend, in an elementary manner, on the geometry of the system concerned.

§ 1. *Introduction.* Electrical and magnetic problems frequently arise in which a full analysis would be out of the question or uneconomical in time and labour. In such cases an approximate value of an important unknown quantity can be quickly obtained by bracketing it between upper and lower bounds. One way is to make these bounds correspond to arbitrarily-chosen admissible functions, and in this manner the error can be held to within pre-assigned limits. Often a close approximation to the actual value can be obtained from comparatively simple admissible functions. This method has already been exploited with considerable success in many branches of applied science and a great deal of literature is available ¹⁾. Other bounds can be made to depend in an elementary way on the geometry of the system concerned, and these can give quite respectable results under certain circumstances. It seems therefore to be worthwhile obtaining some bounds that can be used in an electrical or magnetic context, even though they may be mentioned elsewhere. Some of the approaches used here were developed from lectures given by Dr. E. E. Jones at the University of Nottingham.

The group of problems we will be mainly concerned with are those that involve homogeneous anisotropic dielectric material and in which we bound a generalized dirichlet integral. For convenience we will restrict our attention to certain simple capacitance and resistance considerations (more complicated problems can be treated in a somewhat similar way), and the bounds that are obtained will be quite easy to manipulate, at least in the first instance in order to find a rough estimate. However, it may be rather tedious in some cases to find close bounds.

Consider a condenser formed by two conducting surfaces S_i , S_0 , with S_i lying entirely inside S_0 , the volume V between the surfaces being filled with homogeneous anisotropic dielectric. Rectangular axes Ox , Oy , Oz are taken to coincide with the electrical axes of the dielectric. We also assume that there is no volume distribution of charge in V and no singularities, so that the potential ϕ satisfies the differential equation

$$\nabla_1^2 \phi = 0, \quad (1)$$

where

$$\nabla_1 \equiv \mathbf{i}\sqrt{k_1} \frac{\partial}{\partial x} + \mathbf{j}\sqrt{k_2} \frac{\partial}{\partial y} + \mathbf{k}\sqrt{k_3} \frac{\partial}{\partial z} \quad (2)$$

with the usual notation, k_1 , k_2 , k_3 being known positive constants.

If ϕ_i , ϕ_0 are the potentials of S_i , S_0 respectively, then the capacitance of the condenser is given by

$$C = \frac{1}{4\pi(\phi_i - \phi_0)} \int_{S_i} \frac{\partial \phi}{\partial n_1} dS, \quad (3)$$

where

$$\frac{\partial}{\partial n_1} \equiv lk_1 \frac{\partial}{\partial x} + mk_2 \frac{\partial}{\partial y} + nk_3 \frac{\partial}{\partial z},$$

(l , m , n) being direction -cosines of the surface normal. Since

$$\int_{S_i + S_0} \frac{\partial \phi}{\partial n_1} dS = \int_V \nabla_1^2 \phi dv = 0$$

and

$$\int_{S_i + S_0} \phi \frac{\partial \phi}{\partial n_1} dS = \phi_i \int_{S_i} \frac{\partial \phi}{\partial n_1} dS + \phi_0 \int_{S_0} \frac{\partial \phi}{\partial n_1} dS,$$

we obtain immediately from (3)

$$C = I(\phi)/4\pi(\phi_i - \phi_0)^2, \quad (4)$$

where $I(\phi)$ is a generalized form of the dirichlet integral given by

$$I(\phi) \equiv \int_{S_i + S_0} \phi \frac{\partial \phi}{\partial n_1} dS = \int_V (\nabla_1 \phi)^2 dv. \quad (5)$$

For a single conductor in an infinite medium we set $\phi_0 = 0$ and let S_0 tend to infinity.

Again, if S_i is an internal electrode and current flows from S_i to S_0 , an external electrode, through homogeneous anisotropic conducting material, then the resistance R is easily shown to be of the form

$$1/R = I(\phi)/(\phi_i - \phi_0)^2, \quad (6)$$

where k_1, k_2, k_3 are now conductivities.

In the next section we will find simple bounds for $I(\phi)$ and hence bracket C and R between two values. By taking the mean of the two bounds an approximation can immediately be made. The maximum possible error of this approximation is easily calculated.

§ 2. *Bounds for $I(\phi)$.* Upper bound. Introduce any arbitrary function ϕ^* . Schwarz's inequality shows at once that

$$\int_V (\nabla_1 \phi)^2 dv \int_V (\nabla_1 \phi^*)^2 dv \geq [\int_V (\nabla_1 \phi) \cdot (\nabla_1 \phi^*) dv]^2. \quad (7)$$

It is evident that

$$\begin{aligned} \int_V (\nabla_1 \phi) \cdot (\nabla_1 \phi^*) dv - \int_V (\nabla_1 \phi)^2 dv &= \int_V \nabla_1 \phi \cdot \nabla_1 (\phi^* - \phi) dv = \\ &= \int_{S_i + S_0} (\phi^* - \phi) \frac{\partial \phi}{\partial n_1} dS \end{aligned}$$

since $\nabla_1^2 \phi = 0$ in V .

This surface integral vanishes provided ϕ^* is chosen so that it takes the value ϕ_i on S_i and ϕ_0 on S_0 . We immediately see from (7) that for this choice of ϕ^*

$$I(\phi^*) \geq I(\phi), \quad (8)$$

and this gives a simple and well-known upper bound for $I(\phi)$.

Lower bound. Now introduce any \mathbf{q}^* such that $\nabla_1 \cdot \mathbf{q}^* = 0$

throughout the volume V . It is easy to see that

$$\begin{aligned} \int_V \mathbf{q}^* \cdot \nabla_1 \phi \, dv &= \int_V \nabla_1 \cdot \phi \mathbf{q}^* \, dv = \int_{S_i + S_0} \phi q^*_{n_1} \, dS = \\ &= \phi_i \int_{S_i} q^*_{n_1} \, dS + \phi_0 \int_{S_0} q^*_{n_1} \, dS = (\phi_i - \phi_0) \int_{S_i} q^*_{n_1} \, dS, \end{aligned}$$

where

$$q^*_{n_1} = l\sqrt{k_1}q_x + m\sqrt{k_2}q_y + n\sqrt{k_3}q_z.$$

Schwarz's inequality in the form

$$\int_V \mathbf{q}^{*2} \, dv \int_V (\nabla_1 \phi)^2 \, dv \geq \left(\int_V \mathbf{q}^* \cdot \nabla_1 \phi \, dv \right)^2,$$

immediately shows that

$$I(\phi) \geq (\phi_i - \phi_0)^2 \left(\int_{S_i} q^*_{n_1} \, dS \right)^2 / \int_V \mathbf{q}^{*2} \, dv, \quad (9)$$

giving a lower bound for $I(\phi)$ in terms of ϕ_i , ϕ_0 and \mathbf{q}^* defined above. If $\mathbf{q}^* = \nabla_1 \phi^{**}$, then $\nabla_1^2 \phi^{**} = 0$ in V , and the inequality (9) becomes

$$I(\phi) \geq (\phi_i - \phi_0)^2 \left(\int_{S_i} \frac{\partial \phi^{**}}{\partial n_1} \, dS \right)^2 / \int_{S_i + S_0} \phi^{**} \frac{\partial \phi^{**}}{\partial n_1} \, dS. \quad (10)$$

It is of interest to note that if electrodes form only parts T_i , T_0 of the surfaces S_i , S_0 , the remaining parts being U_i , U_0 , then for the inequality (8) to hold we should have to impose the condition that ϕ^* takes the value ϕ_i on T_i and ϕ_0 on T_0 . In the inequalities (9) (10) the surface integrals need only be taken over T_i , T_0 , provided $q^*_{n_1}$ has the extra restriction $q^*_{n_1} = 0$ over U_i , U_0 .

When determining \mathbf{q}^* , the volume may be divided into sections and a different \mathbf{q}^* may be chosen for each section, provided it is continuous across internal surfaces.

Other bounds. Let X_i be any surface internal to S_i and X_0 be any surface external to S_0 . Let $I_{\text{ext.}}(\phi)$ be the value of the dirichlet integral for ϕ which satisfies $\nabla_1^2 \phi = 0$ in the volume enclosed by X_i , X_0 , and takes the value ϕ_i on X_i and ϕ_0 on X_0 .

Now choose ϕ^* such that $\nabla_1^2 \phi^* = 0$ in the volume V between S_i , S_0 , $\phi^* = \phi_i$ in the volume enclosed by S_i , X_i and $\phi^* = \phi_0$ in the volume enclosed by S_0 , X_0 . From (8)

$$I_{\text{ext.}}(\phi) \leq I(\phi^*) = I(\phi).$$

The same argument shows that

$$I(\phi) \leq I_{\text{int.}}(\phi)$$

where $I_{\text{int.}}(\phi)$ is the corresponding dirichlet integral when we introduce boundaries Y_i , Y_0 , respectively external to S_i and internal to S_0 . We thus have another set of bounds:

$$I_{\text{ext.}}(\phi) \leq I(\phi) \leq I_{\text{int.}}(\phi). \quad (11)$$

Further bounds have recently been given, but these depend on the boundaries being star-shaped³⁾.

§ 3. *Poisson's equation.* Convenient bounds can be found for $I(\phi)$ when ϕ satisfies the differential equation $\nabla_1^2 \phi = \alpha$, α being a function of position, and such that $\phi = 0$ on both S_i , S_0 . The steady flow of viscous liquid through a straight channel of general annular cross-section would be a special case of this, with $k_1 = k_2 = k_3$ and α constant.

Let ϕ^* be any solution of $\nabla_1^2 \phi = \alpha$, then by a method similar to that used in obtaining (8) we can show that

$$I(\phi^*) \geq I(\phi), \quad (12)$$

yielding an upper bound as before. Now choose any ϕ^{**} vanishing on S_i , S_0 , then immediately we see from Schwarz's inequality,

$$I(\phi) \geq (\int_V \alpha \phi^{**} dv)^2 / I(\phi^{**}). \quad (13)$$

We thus have again bracketed $I(\phi)$ between arbitrarily-chosen admissible functions.

A lower bound can at times also be obtained by using the same ϕ^* as used in (12) for an upper bound. Assume α is positive everywhere in V , and choose ϕ^* as above so that it is positive or zero everywhere on S_i , S_0 . It can be then shown that

$$I(\phi) \geq - \int_V \phi^* \alpha dv, \quad (14)$$

and the same result will hold when α is everywhere negative in V provided ϕ^* is chosen to be negative or zero on S_i , S_0 .

The inequalities (11) still hold.

§ 4. *Two-dimensional bounds.* For two-dimensional problems, the surfaces S_i , T_i , U_i , etc. become cylinders of unit length whose cross-sectional boundaries are the curves s_i , t_i , u_i , etc. If we set

$$q_x^* = \sqrt{k_2} \frac{\partial \psi}{\partial y}, \quad q_y^* = -\sqrt{k_1} \frac{\partial \psi}{\partial x},$$

then

$\nabla_1 \cdot \mathbf{q}^* = 0$, $\nabla_1 = \mathbf{i}\sqrt{k_1} \partial/\partial x + \mathbf{j}\sqrt{k_2} \partial/\partial y$, and $q^*_{n_1} = \sqrt{(k_1 k_2)} \partial\psi/\partial s$, s being arc length of boundary. The inequality (9) immediately becomes

$$I(\phi) \geq (\phi_i - \phi_0)^2 k_1 k_2 (\psi)^2_{t_i} / \int_S (\nabla_1 \psi)^2 dS, \quad (15)$$

and any function ψ which is constant on u_i , u_0 will yield a lower bound.

Again, if we make the substitution $x = X\sqrt{k_1}$, $y = Y\sqrt{k_2}$, ϕ satisfies $\nabla^2 \phi = 0$, $\nabla^2 \equiv \partial^2/\partial X^2 + \partial^2/\partial Y^2$, and

$$I(\phi) = \sqrt{(k_1 k_2)} \int_{S_1} (\nabla \phi)^2 dS,$$

where S_1 is the area in the X, Y plane corresponding to that enclosed by the boundaries in the x, y plane. This integral is invariant under the conformal transformation $\zeta = f(Z)$, $Z = X + iY$. Let this transform the boundaries in the Z -plane into concentric circles of radii a and b ($a > b$), with S_1 corresponding to the region between them. If these circular boundaries are conductors, then $\phi = \ln |\zeta|$ is the solution to the problem in the ζ -plane and

$$\frac{1}{(\phi_i - \phi_0)^2} \int_{S_1} (\nabla \phi)^2 dS = 2\pi / \ln \left(\frac{a}{b} \right).$$

It can be shown that if A_0, A_i are the areas enclosed by the conducting boundaries in the xy plane, then $(A_0/A_i) \geq (a/b)^2$, so that

$$I(\phi) \geq 4\pi \sqrt{(k_1 k_2)} (\phi_i - \phi_0)^2 / \ln \left(\frac{A_0}{A_i} \right), \quad (16)$$

and this yields another lower bound.

§ 5. *Applications.* (a) Consider the two-dimensional capacitance problem in which there are two rectangular conductors given by

$$\left. \begin{aligned} x &= \pm c, y = \pm \beta c, \\ x &= \pm d, y = \pm \beta d, \end{aligned} \right\} \beta > 0, d > c,$$

the region between the conductors being filled with homogeneous anisotropic dielectric.

To obtain an upper bound, divide the space between the conductors into four regions, each region lying between $y = \beta x$,

$y = -\beta x$ as follows: region 1, $x > 0$; region 2, $y > 0$; region 3, $x < 0$; region 4, $y < 0$. In regions 1, 3 take $\phi^* = \ln x^2$, and in regions 2, 4 take $\phi^* = \ln (y^2/\beta^2)$, so that $\phi_i = 2 \ln c$, $\phi_0 = 2 \ln d$. Also

$$\begin{aligned} I(\phi^*) &= 2 \int_{c-\beta x}^{\frac{d}{\beta} x} \int_{-\beta x}^{\beta x} k_1 \left(\frac{2}{x} \right)^2 dy dx + 2 \int_{\beta c}^{\frac{\beta d}{\beta} y/\beta} \int_{-y/\beta}^{\frac{y}{\beta}} k_2 \left(\frac{2}{y} \right)^2 dx dy = \\ &= 16 (\beta k_1 + k_2/\beta) \ln \left(\frac{d}{c} \right). \end{aligned}$$

Thus from (4), (8)

$$C \leq (\beta k_1 + k_2/\beta)/\pi \ln (d/c). \quad (17)$$

For a lower bound, take $\phi^* = \ln \{x^2/k_1 + y^2/k_2\}^{\frac{1}{2}}$, so that

$$\begin{aligned} \left(\int_{S_i} \frac{\partial \phi^*}{\partial n_1} dS \right)^2 &= 4 \left[\int_{-\beta c}^{\beta c} \left(k_1 \frac{\partial \phi^*}{\partial x} \right)_{x=c} dy + \int_{-c}^c \left(k_2 \frac{\partial \phi^*}{\partial y} \right)_{y=-\beta c} dx \right]^2 = \\ &= 4\pi^2 k_1 k_2. \end{aligned}$$

Also

$$\begin{aligned} \int_V (\nabla_1 \phi^*)^2 dv &= 2 \int_{-\tan^{-1}\beta}^{\tan^{-1}\beta} \int_{c \operatorname{cosec} \theta}^{d \operatorname{sec} \theta} r^{-1} \left(\frac{\cos^2 \theta}{k_1} + \frac{\sin^2 \theta}{k_2} \right)^{-1} dr d\theta \\ &\quad + 2 \int_{\tan^{-1}\beta}^{\pi - \tan^{-1}\beta} \int_{\beta c \operatorname{cosec} \theta}^{\beta d \operatorname{cosec} \theta} r^{-1} \left(\frac{\cos^2 \theta}{k_1} + \frac{\sin^2 \theta}{k_2} \right)^{-1} dr d\theta \\ &= 2\pi \sqrt{(k_1 k_2)} \ln (d/c). \end{aligned}$$

Thus from (10)

$$C \geq \sqrt{(k_1 k_2)}/2 \ln (d/c). \quad (18)$$

From (17), (18)

$$(\beta k_1 + k_2/\beta)/\pi \ln (d/c) \geq C \geq \sqrt{(k_1 k_2)}/2 \ln (d/c). \quad (19)$$

These are useful bounds and may be improved by taking extra terms in ϕ^* , but it may prove difficult to get them really close. It is interesting to note that (16) yields the same lower bound as (19). Bounds can also easily be obtained by taking internal and external circular boundaries and using (11).

(b) Suppose a steady current enters a uniform rectangular metal sheet, sides a, b ($b \geq a$), through a small central internal circular electrode of radius c and flows out through an electrode which coincides with the rectangular boundary.

A close upper bound can be found simply by using (16), provided c is small compared with a, b . Here $k_1 = k_2 = \sigma$ the conductivity, and (6), (16) show that

$$2\pi\sigma R \leq \frac{1}{2} \ln(ab/\pi c^2). \quad (20)$$

It is of interest to compare the upper bound with the accurate results given by Daymond²⁾. For example, if $b = a$, $a = 225c$, the upper bound (20) takes the value 4.84 as compared with 4.80. Admittedly this is a very favourable case, but the bound is within 1% of the correct result.

A central square electrode of side $2c$ lies outside a circle of radius c and inside a circle of radius $c\sqrt{2}$. Interpolating Daymond's results for the same ratios of a, b and c as above, we see that in this case

$$4.38 \leq 2\pi\sigma R \leq 4.80,$$

and the mean value of 4.59 will be quite accurate.

(c) Often we can obtain quite reasonable bounds by the use of the inequality (11) alone. For example, consider the capacitance of a conducting solid formed by revolving an ellipse whose major axis is $2a$ and eccentricity e about the tangent at the end of the major axis; the solid may be regarded as a form of closed torus.

The exact solution is not known to the author. The body can contain a circular disk of radius $2a$, and can be contained within an oblate spheroid whose generating ellipse has a major axis of length $4a$, eccentricity E , and a radius of curvature at the ends of the major axes equal to $a(1 - e^2)$. This requires $E^2 = \frac{1}{2}(e^2 + 1)$. Now the capacitance of a disk and oblate spheroid are well known. Using these results and (11) the capacitance C satisfies the inequality

$$\frac{2aE}{\sin^{-1}E} \leq C \leq \frac{4a}{\pi}.$$

For example if $e^2 = 0.8$, $E^2 = 0.9$, and we see that this inequality yields

$$1.27a \leq C \leq 1.52a,$$

and the mean value of $1.40a$ will give a fair estimate.

(d) As an elementary example of the use of (15), consider the two-dimensional problem in which a rectangular block of anisotropic dielectric, bounded by $x = 0$, $x = d$, $y = 0$, $y = l$, has conducting plates in the edges parallel to the y -axis.

We thus have a simple condenser, and we can take $\psi = y^p$, where p is yet to be determined. We see that

$$(\psi)^2_{ti} = l^{2p}, \int_S (\nabla_1 \psi)^2 dS = k_2 d l^{2p-1} p^2 / 2p - 1,$$

so that from (4), (15)

$$C \geq \left(\frac{k_1 l}{4\pi d} \right) \left(\frac{2p - 1}{p^2} \right).$$

This has its maximum value when $p = 1$, and hence $C \geq k_1 l / 4\pi d$. With this value of p , the potential ϕ satisfies $\nabla_1^2 \phi = 0$, and the boundary conditions are satisfied, so that the equality sign holds, as is well known.

Received 11th August, 1959.

REFERENCES

- 1) Knops, R. J., Ph. D. Thesis, University of Nottingham, 1958.
- 2) Daymond, S. D., Quart. J. Mech. Appl. Math. **4** (1951) 23.
- 3) Payne, L. E. and H. F. Weinberger, Pacific J. Math. **8** (1958) 551.

ON THE INFLUENCE OF SHAPE AND VARIATIONS IN CONDUCTIVITY OF THE SAMPLE ON FOUR-POINT MEASUREMENTS

by ERIK B. HANSEN

The Haldor Topsøe Research Laboratory, Hellerup, Denmark

Summary

The influence of the finite size of the sample and of variations in conductivity through the sample on the voltage-current ratio found by four-point measurements is investigated. Expressions for this ratio are found for samples of infinite length and with rectangular or semi-circular cross-section. In the first case the influence of a finite length and of an exponential variation of the conductivity along the axis of the sample is examined. A chart showing the correction factor for a bar of rectangular cross-section is presented.

§ 1. *Introduction.* When four-point measurements are made on samples of semiconducting material the size of which is not very large, due care must be taken of the influence of the finite extension of the sample on the current-voltage ratio I/V . Usually the four probes are arranged on a straight line with the spacing s , the two outer probes being used as current contacts. The conductivity σ may then be expressed as

$$\sigma = \frac{F}{2\pi s} \frac{I}{V}, \quad (1)$$

where F , in the following referred to as the correction factor, depends on the shape of the sample. For a semi-infinite sample F is equal to 1. Thus for finite samples F is clearly greater than 1.

The problem of finding F has been considered by several authors. Valdes¹⁾ has calculated F for different positions of the four probes on a sample with plane boundaries by using the method of images. When the sample is small, this method leads to slowly converging series. The problem of improving the convergence was solved

successfully by Uhlir²⁾, who calculated some auxiliary functions encountered in problems of this kind, while Laplume³⁾ gave approximate closed form expressions for the series.

One of the purposes of the present note is to direct attention to the fact that the well-known method of solving Laplace's equation by separating the variable may be advantageous as a different way of treating problems of this kind *). In the present case this approach leads to the problem of finding the eigenfunction expansion of Green's function for the sample geometry in question. The series which is the result of calculations along these lines shows rapid convergence when the linear dimensions of the sample are not too large in comparison with s , i.e. the region of the sample sizes in which the series resulting directly from the mirror method is less practical. The present method has the additional advantage of applying also to some of those cases in which the sample is not box-shaped; further the method still applies when the conductivity is not assumed to be constant throughout the sample, but varies as a power function or an exponential function along some direction through the sample, such as in the case of drawn crystals or a zone-refined bar.

Examples of the application of the method to some of the above mentioned cases are demonstrated below. Only samples surrounded by insulating material are considered, although the method works equally well when the sample is in contact with conducting material.

§ 2. *The correction factor for box-shaped samples.* Consider a box-shaped sample $a \times h \times 2l$ as shown in fig. 1. The four probes are taken to be placed symmetrically about the xy -plane of the coordinate system shown in the figure on a line parallel to the z -axis through the point $(\Delta + \frac{1}{2}a, h, 0)$. The current field which is produced by the current $\pm I$ through the outer probes satisfies the equation

$$\nabla \cdot \mathbf{J} = 2I[\delta(\mathbf{r} - \mathbf{r}_+) - \delta(\mathbf{r} - \mathbf{r}_-)] \quad (2)$$

all over the sample, $\delta(\mathbf{r} - \mathbf{r}_+)$ and $\delta(\mathbf{r} - \mathbf{r}_-)$ being the Dirac delta-functions for the source in $\mathbf{r}_+ = (\Delta + \frac{1}{2}a, h, -\frac{3}{2}s)$ and the sink in

*) After the work described in the present note was finished, the author became aware that formulae for the two-dimensional case derived by Ollendorff in a similar way as the one used here have been applied by F. M. Smits for the case of diffused surface layers⁴⁾.

$\mathbf{r}_- = (\Delta + \frac{1}{2}a, h, \frac{3}{2}s)$ respectively. The boundary condition for \mathbf{J} is expressed by the requirement that the normal component of \mathbf{J} should vanish at every point of the boundary except at the source and the sink points. By means of the relation $\mathbf{J} = -\sigma \nabla \varphi$, where φ is the electric potential, (2) may be replaced by a differential equation in φ . In this and the following section σ is taken to be a constant; thus the equation in φ becomes

$$\nabla^2 \varphi = -\frac{2I}{\sigma} [\delta(\mathbf{r} - \mathbf{r}_+) - \delta(\mathbf{r} - \mathbf{r}_-)]. \quad (3)$$

At the same time the boundary condition becomes $\partial \varphi / \partial n = 0$ all over the boundary except at the source and the sink points. In order to obtain a region on the surface to which the boundary

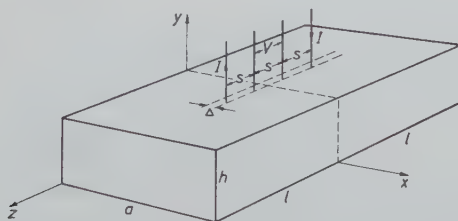


Fig. 1. Location of the probes on a box-shaped sample.

condition applies in every point, the region under consideration is extended to be the one which is bounded by the planes $x = 0$, $x = a$, $y = 0$, $y = 2h$ and $z = \pm l$. Because of the symmetry about the plane $y = h$, the current field in the upper half of this region will develop as a mirror image of the current field in the lower half of the region and hence the boundary condition $\partial \varphi / \partial n = 0$ should be satisfied all over the boundary of the extended region.

A solution of the homogeneous equation derived from (3) satisfying the boundary condition on the four planes parallel to the z -axis is given by

$$\varphi = \sum_{m=0}^{\infty} \sum_{n=0}^{\infty} A_{\alpha} \cos\left(\frac{m\pi x}{a}\right) \cos\left(\frac{n\pi y}{2h}\right) [\exp(\alpha z) + B_{\alpha} \exp(-\alpha z)], \quad (4)$$

where $\alpha = (\pi/a)[m^2 + (na/2h)^2]^{\frac{1}{2}}$. This solution applies in each of the three subregions characterized by $-l < z < -\frac{3}{2}s$, $-\frac{3}{2}s < z < \frac{3}{2}s$, and $\frac{3}{2}s < z < l$, but with different expressions for the

coefficients A_α and B_α . Because of the antisymmetry about the xy -plane the six constants for each α are reduced to three, of which the one is determined by the boundary condition at $z = \pm l$, while the second is expressed in terms of the third by the requirement of a continuous fit at $z = \pm \frac{3}{2}s$. In order to find the resulting single constant the delta function behaviour of $\nabla^2\varphi$ must be taken into account. This is simply done by calculating $\nabla^2\varphi$ from (4) and equating this expression with the Fourier expansion in x and y of the right side of (3); when the resulting equation is integrated along z over a small interval around $z = -\frac{3}{2}s$, the last coefficient is found. A calculation along these lines leads to the following expression for the potential which is valid in the region $|z| < \frac{3}{2}s$:

$$\begin{aligned} \varphi(x, y, z) = & -\frac{Iz}{\sigma ah} \\ & -\frac{4I}{\sigma ah} \sum_{\substack{m=0 \\ (m,n) \neq (0,0)}}^{\infty} \sum_{n=0}^{\infty} \frac{\cos m\pi(\Delta/a + \frac{1}{2}) \cos(n\pi/2) \cosh \alpha(l - 3s/2)}{(1 + \delta_{0,m})(1 + \delta_{0,n}) \alpha \cosh \alpha l} \\ & \cos\left(\frac{m\pi x}{a}\right) \cos\left(\frac{n\pi y}{2h}\right) \sinh \alpha z. \end{aligned} \quad (5)$$

Here α is the parameter introduced in connection with (4) and $\delta_{r,s}$ is Kronecker's delta. Insertion of the voltage between the inner probes found from (5) in (1) gives the following expression for the correction factor:

$$\begin{aligned} F = & \frac{2\pi s^2}{ah} + \frac{16\pi s}{ah} \sum_{\substack{m=0 \\ (m,n) \neq (0,0)}}^{\infty} \sum_{n=0}^{\infty} \frac{\cosh \beta(l - 3s/2) \sinh(\beta s/2)}{(1 + \delta_{0,m})(1 + \delta_{0,n}) \beta \cosh \beta l} + \\ & + \frac{16\pi s}{ah} \sum_{m=1}^{\infty} \sum_{n=0}^{\infty} \frac{(-1)^{m-1} \sin^2(m\pi\Delta/a) \cosh \gamma(l - 3s/2) \sinh(\gamma s/2)}{(1 + \delta_{0,n}) \gamma \cosh \gamma l}, \end{aligned} \quad (6)$$

where

$$\beta = (2\pi/a)[m^2 + (na/2h)^2]^{\frac{1}{2}} \text{ and } \gamma = (\pi/a)[m^2 + (na/h)^2]^{\frac{1}{2}}.$$

The general character of (6) may be checked by the following comparison with simple physical considerations. As mentioned above this formula becomes still more suitable for numerical calculations as a/s and h/s decrease; indeed, if a/s and h/s tend to zero, the two series expressions vanish, so that only the first term in (6) remains. This term is most directly interpreted physically from (5),

showing φ to behave like the potential along a filament with rectangular cross-section, in which the current is distributed homogeneously. When l increases, every term in both series in (6) decreases, so the same is true for the total correction factor F , as it should be when the size of the sample is increased. The numerical values of the terms in the second series in (6) are (of course) essentially decreasing for increasing γ , so the sum of the series is positive. Further this sum varies like Δ^2 when Δ is small. This is to be expected as F must have a minimum for the centre of gravity of the contacts being located at the central point of the upper surface of the sample. A calculation of the change in F caused by a deviation along the z -axis from the central position affirms that the same dependence on the deviation is true in this case. However, for reasons which are given below, this calculation has been omitted here. When a/s tends to infinity, the second series in (6) vanishes as this series refers to the influence of an unsymmetrical position of the probes. Formally this occurs because of the fact that the difference between the numerical values of one term and the subsequent one tends to zero as a/s tends to infinity, while the sign of the terms remains alternating throughout the series. Of course the series vanishes too when the probes are placed exactly on the centreline of the sample.

A particularly attractive feature of (6) is that the influence of a sideways displacement of the probes is separated from the main body of the formula. Also it is desirable to alter the formula so that the influence of the finite length of the sample occurs in a similar way. This may be done by expanding the denominator in a power series in $\exp(-2\beta l)$, and this in turn makes it possible to rearrange the terms in a way which improves the convergence somewhat, as will be shown below. The first series in (6) may be written as

$$\frac{8\pi s}{ah} \sum_{\substack{m=0 \\ (m,n) \neq (0,0)}}^{\infty} \sum_{n=0}^{\infty} \frac{\exp(-\beta s) - \exp(-2\beta s)}{(1 + \delta_{0,m})(1 + \delta_{0,n})\beta} [1 + \exp \beta(3s - 2l)] \sum_{r=0}^{\infty} (-1)^r \exp(-2r\beta l). \quad (7)$$

Now the coefficients β may be arranged in an infinite number of sequences $\beta_q, 2\beta_q, \dots, p\beta_q, \dots, q=1, 2, \dots$, where $\beta_1 \leq \beta_2 \leq \dots$ are those β 's $\neq 0$ for which m and n have no common divisor. If $a/2h > 1$, $\beta_1 = 2\pi/a$ and $\beta_2 = \pi/h$; if $a/2h < 1$, β_1 and β_2 are interchanged.

Thus (7) may be rewritten in the following form:

$$\frac{8\pi s}{ah} \sum_{q=1}^{\infty} \sum_{p=1}^{\infty} \frac{\exp(-p\beta_q s) - \exp(-2p\beta_q s)}{(1 + \delta_{1,q})(1 + \delta_{2,q})p\beta_q} [1 + \exp(p\beta_q(3s - 2l))] \sum_{r=0}^{\infty} (-1)^r \exp(-2rp\beta_q l). \quad (8)$$

This series may be split into four series of the form

$$\sum_{p=1}^{\infty} \frac{\exp(-p\beta_q u)}{p\beta_q} = \int_u^{\infty} \sum_{p=1}^{\infty} \exp(-p\beta_q v) dv = -\frac{1}{\beta_q} \ln[1 - \exp(-\beta_q u)], \quad (9)$$

so that the correction factor for $\Delta = 0$ becomes

$$F(\Delta = 0) = \frac{2\pi s^2}{ah} + \frac{8\pi s}{ah} \sum_{q=1}^{\infty} \frac{\ln[1 + \exp(-\beta_q s)]}{(1 + \delta_{1,q})(1 + \delta_{2,q})\beta_q} + \frac{8\pi s}{ah} \sum_{q=1}^{\infty} \sum_{r=1}^{\infty} \frac{(-1)^r}{(1 + \delta_{1,q})(1 + \delta_{2,q})\beta_q} \ln \left\{ \frac{1 - \exp[-\beta_q(2rl + 2s)]}{1 - \exp[-\beta_q(2rl + s)]} \frac{1 - \exp[-\beta_q(2rl - 2s)]}{1 - \exp[-\beta_q(2rl - s)]} \right\}, \quad (10)$$

where $\beta_q = (2\pi/a)(m^2 + (na/2h)^2)^{\frac{1}{2}}$ is the q 'th element of the sequence of those β 's $\neq 0$ for which m and n have no common divisor.

The general case covered by (6) was not considered by Uhlir ²⁾ and seems – at least as far as the Δ -dependence is concerned – not directly manageable by means of the functions calculated by this author. On the other hand, when $\Delta = 0$ and $l \rightarrow \infty$, a numerical comparison with Uhlir's formulae may be carried out. For $h = a = \frac{3}{2}$ s the same value $F = 3.150$ is found from formula (37) of reference ²⁾ and from (10) when a minor misprint in ²⁾ which was pointed out later by Uhlir is taken into account ⁵⁾. When a tends to infinity so that the bar degenerates into an infinite slice of thickness h , the comparison with Uhlir's formula becomes especially simple. In this case F is expressed by

$$F(a \rightarrow \infty, l \rightarrow \infty) = \lim_{a \rightarrow \infty} \frac{8\pi s}{ah} \sum_{\substack{m=0 \\ (m,n) \neq (0,0)}}^{\infty} \sum_{n=0}^{\infty} \frac{[1 - \exp(-\beta s)] \exp(-\beta s)}{(1 + \delta_{0,m})(1 + \delta_{0,n})\beta}. \quad (11)$$

This limiting value may be found by the following argument. For every value of m the difference between two terms in (11) denoted by $(n, m) = (n', m')$ and $(n, m) = (n', m' + 1)$ tends to zero when a tends to infinity. So the approximation which consists of replacing the summation over m by an integration becomes still better as a increases and eventually gives exactly the correct result when a becomes infinite. Thus (11) may be written as

$$F(a \rightarrow \infty, l \rightarrow \infty) = \lim_{a \rightarrow \infty} \frac{2s}{h} \sum_{m=1}^{\infty} \frac{[1 - \exp(-2\pi ms/a)] \exp(-2\pi ms/a)}{m} + \\ + \frac{8\pi s}{h} \sum_{n=1}^{\infty} \int_0^{\infty} \frac{[1 - \exp(-\beta s)] \exp(-\beta s)}{\beta a} dm. \quad (12)$$

By means of (9) the limiting value of the first series in (12) is shown to be $(2s/h) \ln 2$, while the integrals in the second series by means of the substitution $m = (na/2h) \sinh u$ are found to be equal to $K_0(n\pi s/h) - K_0(2n\pi s/h)$; here $K_0(z)$ is the modified Bessel function of the second kind of order zero. Thus the correction factor for an infinite slice of thickness h becomes

$$F(a \rightarrow \infty, l \rightarrow \infty) = \frac{2s}{h} \left\{ \ln 2 + 2 \sum_{n=0}^{\infty} K_0 \left[\frac{(2n+1)\pi s}{h} \right] \right\}. \quad (13)$$

This expression is identical with the corresponding expression derived by Uhlir (equation (13) of reference 2)). By a similar argument it may be verified that (13) tends to unity when h tends to infinity.

From (10) the correction factor was computed for an infinite bar as a function of a/s , with a/h as a parameter. The results which exhibit the predicted behaviour are shown in fig. 2.

The finite length of the bar gives rise to an alteration of the correction factor given by the second series in (10). Besides getting zero when l tends to infinity the sum of this series vanishes when a/s and h/s tend to zero as the current then is restricted to the region between the current electrodes. This behaviour is recognized in fig. 3 where the increment ΔF of the correction factor due to the finite length of a bar for which $h = \frac{1}{2}a$ and $2l = 3s + \frac{1}{2}a$ is shown. The most striking property of the additional term ΔF of the correction factor is probably its very small size even for a sample as short as the one considered here. However, in the case of thicker

samples one should expect the influence from the finite length to be greater as the "shielding" of the outer regions $|z| > \frac{3}{2}s$ is then less effective. This conclusion may find some support from fig. 3, which shows that ΔF falls more slowly for large than for small values of a/s , this being caused by the fact that the current lines penetrate deeper into the outer regions for large than for small values of a/s .

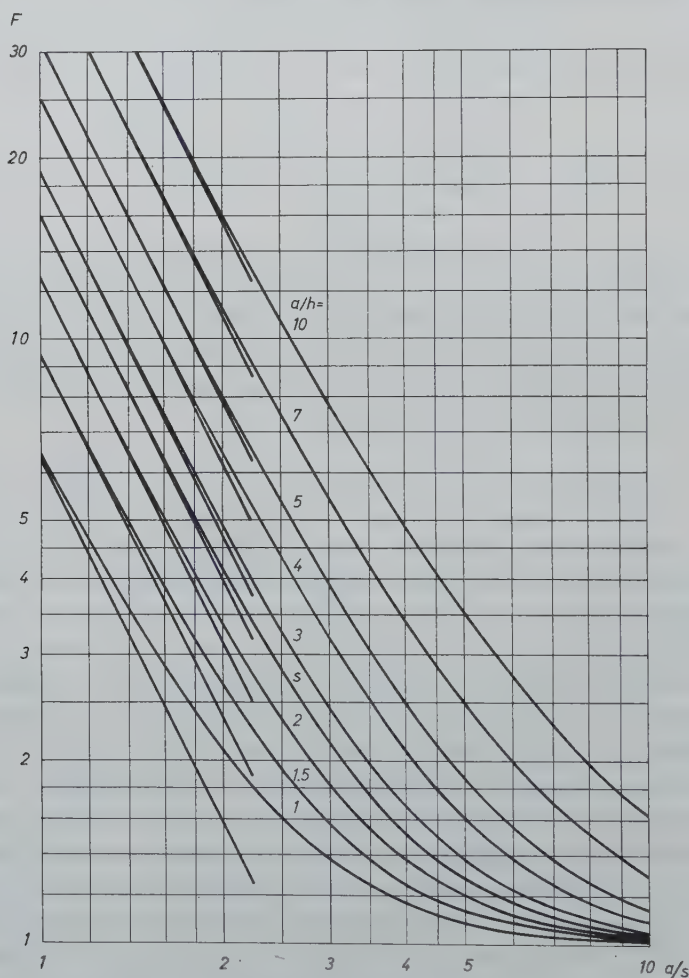


Fig. 2. The correction factor for an infinite bar of rectangular cross-section $a \times h$ and for an infinite bar of semi-circular cross-section (indicated by an s). The straight lines correspond to a homogeneous current distribution. The geometrical arrangements are shown in fig. 1 and fig. 4 respectively.

The use of small samples has the advantage of giving large correction factors, i.e. large potential differences between the voltage contacts; besides small samples will probably be more homogeneous than large ones. On the other hand, when small samples are used, it might be expected that correct positioning of the probes becomes very important. Now, as mentioned above, the error due to a displacement Δ in the x -direction from the symmetrical position of

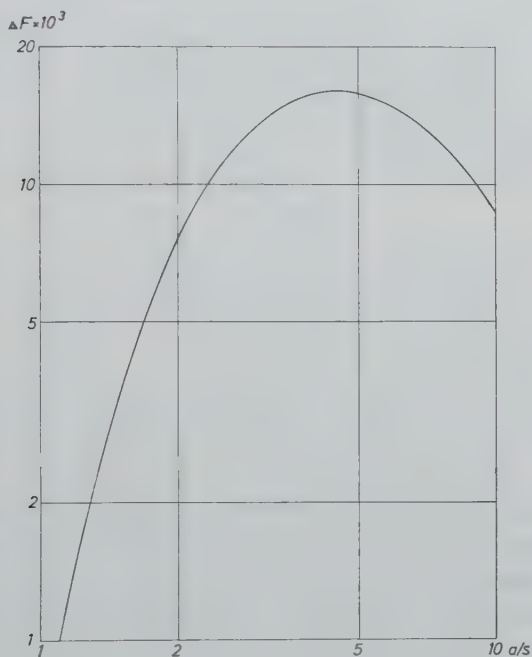


Fig. 3. The increment ΔF of the correction factor F due to the finite length of the sample; $2l = 3s + \frac{1}{2}a$; $h = \frac{1}{2}a$.

the probes tends to zero when a/s tends to zero as well as when a/s tends to infinity. Therefore the largest error should be expected to occur for some intermediate value. As an example the increment of F for $\Delta = s/5$ was computed from (6) for $a = 2.5s$, $h = 0.5a$, and $1 \rightarrow \infty$. The value was found to be as small as $\Delta F = 0.022$, which should be compared with the corresponding value of $F = 2.335$.

As mentioned above, a displacement ε of the probes along the z -axis gives rise to another increment of the correction factor. This

increment, which is proportional to ε^2 for ε small compared with $2l$, will only give rise to a correction of the l -dependent series in (10), which in turn was found to give rise to a rather small alteration of the correction factor for an infinite bar. Thus a small displacement of this kind may be expected to be unimportant; therefore a closer examination of its influence has been omitted in the present note.

§ 3. *The correction factor for samples of semi-circular cross-section.* As mentioned in § 1 the method applied in this note is also applicable when dealing with sample geometries different from the box-shaped one. Mainly the calculations are performed in a way similar to the one described in § 2.

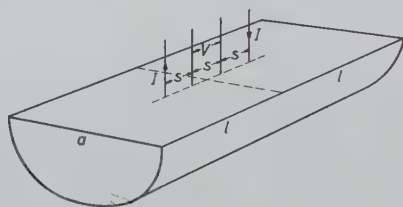


Fig. 4. Location of the probes on a sample of semi-circular cross-section.

As an example, the correction factor for a bar of length $2l$, the cross-section of which is half of a circle with diameter a was calculated. The probes were taken to be placed on the centre line as shown in fig. 4. This geometry corresponds fairly well to the one encountered in measurements on crystals grown in a boat. The correction factor defined by (1) turned out to be

$$F = 16 \left(\frac{s}{a} \right)^2 + 8 \frac{s}{a} \sum_{n=1}^{\infty} \frac{\{1 + \exp[x_n(6s - 4l)/a]\} [1 - \exp(-2x_n s/a)] \exp(-2x_n s/a)}{[1 + \exp(-4x_n l/a)] x_n [J_0(x_n)]^2}, \quad (14)$$

where x_n is the n 'th non-vanishing root of the equation $J_1(x) = 0$. Formula (14) may be checked in the same way as was done with (6). Thus, when a/s tends to zero, the series vanishes, leaving F equal to the first term in (14). This case corresponds to a homogeneous distribution of the current in the bar. Similarly, when a and l tend to infinity, the term $16(s/a)^2$ and the first terms of the series vanish

whereas the terms for which $x \gtrsim a$ remain finite. Thus if a is chosen big enough, the series may be replaced by an integral over x_n with any desired accuracy. The resulting integral is easily shown to be equal to 1.

Numerical values of the correction factor were computed as a function of a/s for $1 \rightarrow \infty$. The results are shown in fig. 2 (curve s). As could be expected this curve lies higher than the corresponding curve for a bar with rectangular cross-section $a \times \frac{1}{2}a$.

The present method works for every location of the probes on a sample like the one shown in fig. 4 as well as for circular disc-shaped samples. Furthermore this approach may be used when dealing with bars of semi-elliptic cross-section, in which case elliptic cylinder coordinates should be applied, leading to series in Mathieu functions.

§ 4. *The correction factor for samples through which the conductivity varies.* Until now only homogeneous samples have been considered. However, in samples cut out of real crystals the conductivity as a rule varies throughout the sample. The method of eigenfunctions used in this note has the particular property of being able to take into account such a variation of the conductivity. Consequently exact expressions for the correction factor may be obtained in cases of exponential or power-dependence of the conductivity on the coordinates as is encountered in zone-refined bars or in drawn crystals. When dealing with box-shaped samples, cases of conductivity variations in all the three directions at the same time are soluble while for semi-circular or semi-elliptic cross-sections only the case of a variation along the axis can be treated.

For the sake of simplicity only an infinitely long sample of rectangular cross-section, the conductivity of which varies along the z -axis as $\sigma = \sigma_0 \exp(z/d)$ is considered here. The probes are taken to be placed on the centreline of the upper surface of the samples as shown in fig. 1 ($\Delta = 0$).

In this case the potential satisfies the differential equation

$$\nabla^2 \varphi + \frac{1}{d} \frac{\partial \varphi}{\partial z} = -2I \left(\frac{\delta(\mathbf{r} - \mathbf{r}_+)}{\sigma_+} - \frac{\delta(\mathbf{r} - \mathbf{r}_-)}{\sigma_-} \right), \quad (15)$$

where $\sigma_+ = \sigma_0 \exp(-3s/2d)$ and $\sigma_- = \sigma_0 \exp(3s/2d)$ are the conductivities in the immediate neighbourhood of the current con-

tacts, together with the boundary condition of vanishing normal derivative on the surface of the sample, except at the source and sink points. This differential equation may be separated in the same way as was done with (3). Thus the calculations, following nearly the same lines as described in § 2, lead to the correction factor

$$F = \frac{8\pi s}{ah} \sum_{m=0}^{\infty} \sum_{n=0}^{\infty} \frac{\cosh(s/d) - \cosh(s/2d) \exp(-\alpha s)}{(1 + \delta_{0,m})(1 + \delta_{0,n})\alpha} \exp(-\alpha s) \quad (16)$$

if the conductivity in (1) is taken to be the conductivity at the centrepoint of the system of probes; here

$$\alpha = (2\pi/a)[m^2 + (na/2h)^2 + (a/4\pi d)^2]^{\frac{1}{2}}.$$

As is easily seen (16) reduces to (6) with $l \rightarrow \infty$ and $\Delta = 0$ for $d \rightarrow \infty$. Usually d is very large compared with s ; being a second order effect the shift in F caused by the variation of the conductivity hence is negligible. As an example the correction factor was computed for $h = 0.5a$, $a = 2.5s$, and $s/d = 0.1$. The increment of F when s/d is raised from zero to 0.1 turned out to be 2×10^{-3} .

Acknowledgements. The work described in the present note was performed at the Haldor Topsøe Research Laboratory, Hellestrup, Denmark. The author wishes to express his gratitude to Mr. Haldor Topsøe for permission to carry out this investigation and to publish the results. Thanks are also due to Miss Aase Schou who performed most of the numerical calculations.

Received 15th June, 1959.

REFERENCES

- 1) Valdes, L. B., Proc. Inst. Radio Engrs., **42** (1954) 420.
- 2) Uhler, A., Bell. Syst. Tech. J., **34** (1955) 105.
- 3) Laplume, J., Onde Electrique **35** (1955) 113.
- 4) Smits, F. M., Bell Syst. Tech. J., **37** (1958) 711.
- 5) Uhler, A., Bell Syst. Tech. J. **34** (1955) 994.

A CORNER EFFECT IN PLANE DIFFUSION THEORY *)

by HAROLD LEVINE

Applied Mathematics and Statistics Laboratory, Stanford University, Stanford, U.S.A.

Summary

The partial differential equation of diffusion type is studied in a plane sector of arbitrary angle, with the solution specified at the boundaries, and various expressions are obtained for the integrated normal derivative or flux thereto. Alternative methods of analysis are described for the right angle sector, which include an integral equation reformulation of the boundary value problem and its reduction to a functional or difference equation by Fourier transformation.

§ *Introduction.* Diffusion phenomena are characteristic of many physical problems, both time-independent and -dependent. In reactor theory, for example, it is the diffusion of neutrons which claims attention, whereas in the phenomenological theory of superconductors the magnetic field behaviour is fundamental. A unified mathematical approach to these problems is suggested by their formulation in terms of partial differential or integral equations. In this paper, some aspects of the mathematical technique are discussed with reference to plane problems where the boundaries are defined by straight lines; other features which are appropriate to curved boundaries will be described in a separate account.

The explicit statement of a problem may be associated with neutron absorption in control rods embedded within a medium where the neutron diffusion length is L (Hurwitz and Roe¹). If the spatial function ψ denotes the rate of neutron absorption per

*) This work was supported by the Office of Naval Research, contract Nour-225 (11).

unit volume, and the neutron source strength is S , the steady diffusion equation takes the form

$$-L^2 \nabla^2 \psi + \psi = S. \quad (1.1)$$

A 'black' control rod is characterized in the limit of small neutron free path by the boundary condition of vanishing ψ . In the approximation of constant source strength, then, a solution of (1) is desired, which vanishes at a control rod and approaches the value S asymptotically with distance therefrom. For plane problems, the Laplacian in (1) is a two-dimensional operator, referring to a section normal to the control rod axis. The neutron flow into a rod is determined by the normal derivative of ψ at its surface, and the integrated flow (relative to S) defines a rod absorption area. If S is constant, the function $\varphi = \psi - S$ satisfies a homogeneous differential equation

$$-L^2 \nabla^2 \varphi + \varphi = 0 \quad (1.2)$$

and assumes the boundary value $\varphi = -S$; this function may be identified with the magnetic field (of the phenomenological theory) within a cylindrical superconductor on whose boundary there is prescribed a uniform field.

A plane diffusion problem, which is central to the approximate solution for a control rod of general cross-section when L is small, pertains to the angular region formed by two semi-infinite radial lines. For if the diffusion length L is small compared to the local radius of curvature of the cross-section, the latter may be regarded as of polygonal form, and the corners do not appreciably interact if their separation greatly exceeds L . The absorption area is then equal to L times the perimeter, and the effect of each isolated corner is equivalent to a change in perimeter by the amount $LD(\vartheta_0)$, which implies a contribution $L^2 D(\vartheta_0)$ to the absorption area. Here $D(\vartheta_0)$ is a dimensionless corner correction that changes only with the angle itself and vanishes for $\vartheta_0 = \pi$.

An evaluation of D for the corner with specifications $0 < \vartheta < \vartheta_0$, $0 < r < \infty$ has been carried out by Hurwitz and Roe, who begin with a solution of (1) in the form

$$\psi(r, \vartheta) = \sum_{n=0}^{\infty} \psi_n(\rho) \sin(2n+1) \frac{\pi \vartheta}{\vartheta_0}, \quad \rho = r/L, \quad (1.3)$$

consequent to the choice

$$S = 1 = \frac{4}{\pi} \sum_{n=0}^{\infty} \frac{\sin[(2n+1)\pi\vartheta/\vartheta_0]}{2n+1}, \quad 0 < \vartheta < \vartheta_0. \quad (1.4)$$

The function $\psi_n(\rho)$ is obtained from the solution of an ordinary differential equation, and after substitution in (3)

$$D(\vartheta_0) = 2 \int_0^{\infty} \left[\frac{1}{\rho} \frac{\partial}{\partial \vartheta} \sum_{n=0}^{\infty} \psi_n(\rho) \sin(2n+1) \frac{\pi\vartheta}{\vartheta_0} \Big|_{\vartheta=0} - 1 \right] d\rho, \quad (1.5)$$

where the factor 2 reflects the equality of neutron flux into the surfaces $\vartheta = 0$ and $\vartheta = \vartheta_0$. A convergence factor is employed in effecting the summation with respect to n , and there results finally

$$D(\vartheta_0) = 4 \sum_{n=1}^{n_0} (-1)^n \cot n\vartheta_0 + \frac{4}{\vartheta_0} \int_0^{\infty} \tanh x \frac{\sinh(\pi x \cdot \vartheta_0) \cos(\pi^2/2\vartheta_0)}{\sinh^2(\pi x \cdot \vartheta_0) + \sin^2(\pi^2/2\vartheta_0)} dx, \quad (1.6)$$

where n_0 denotes the largest integer less than $\pi/2\vartheta_0$.

The next section, § 2, contains a different approach to the problem which does not require series development and subsequent summation and is distinguished by a greater adaptability to the study of various aspects of the solution. The method rests on a pair of integral transform relations, the so-called Grünberg modification of the Kontorovich-Lebedev reciprocal formulas.

A discussion of the local flux, or normal derivative of ψ at the boundary, is given in § 3, with reference to the right angle corner, $\vartheta_0 = \frac{1}{2}\pi$. The derivative, or more precisely, its deviation from a constant value reached at large distances from the corner, may be characterized by an inhomogeneous integral equation with semi-infinite domain. The complex Fourier transform of this distribution satisfies a simple type of functional or difference relation and can be explicitly obtained by a further application of the same transformation*). The normal derivative at the boundary is again

*) The occurrence of difference relations in boundary value problems based on differential or integral equations has been noted by Koiter²⁾ and more recently by Azpeitia and Newell³⁾.

calculated in § 4, to illustrate a technique for employing directly an integral representation of the ψ function within the corner region.

§ 2. *Solution of the corner problem for an arbitrary angle.*

Suppose the basic differential equation is written

$$(\nabla^2 - \alpha^2)\psi(r, \vartheta) = 1 \quad (2.1)$$

($\alpha = 1/L$, $S = -1/L^2$), and let it be required to find its solution in the domain $0 < \vartheta < \vartheta_0$, $0 < r < \infty$, subject to the conditions

$$\psi = 0 \text{ at } \vartheta = 0, \text{ and } \vartheta = \vartheta_0. \quad (2.2)$$

Introducing the explicit form of the Laplacian and multiplying with r^2 , (2.1) becomes

$$r^2 \frac{\partial^2 \psi}{\partial r^2} + r \frac{\partial \psi}{\partial r} + \frac{\partial^2 \psi}{\partial \vartheta^2} - \alpha^2 r^2 \psi = r^2. \quad (2.3)$$

Define the transform of ψ with respect to the radial coordinate by

$$\varphi(s, \vartheta) = \int_0^\infty \psi(r, \vartheta) K_s(\alpha r) dr/r, \quad (2.4)$$

where $K_s(\alpha r)$ denotes a cylinder function such that

$$\left[r^2 \frac{d^2}{dr^2} + r \frac{d}{dr} - (\alpha^2 r^2 + s^2) \right] K_s(\alpha r) = 0. \quad (2.5)$$

A differential equation for $\varphi(s, \vartheta)$ follows from (3) on multiplication with $K_s(\alpha r)/r$ and subsequent integration over r , namely

$$\frac{\partial^2 \varphi}{\partial \vartheta^2} + s^2 \varphi = \int_0^\infty r K_s(\alpha r) dr = \frac{\pi s}{2\alpha^2} \csc \frac{s\pi}{2}, \quad (2.6)$$

provided the real part of s is sufficiently small, so that the null value of ψ at $r = 0$ compensates for the singularity of $K_s(\alpha r)$, and the integrals in (2.4) and (2.6) are convergent. The solution of (2.6) which vanishes at $\vartheta = 0$ and $\vartheta = \vartheta_0$ is

$$\varphi(s, \vartheta) = \frac{\pi}{2\alpha^2 s} \csc \frac{s\pi}{2} \left[\frac{\sin s\vartheta_0 - \sin s\vartheta - \sin s(\vartheta_0 - \vartheta)}{\sin s\vartheta_0} \right] \quad (2.7)$$

and describes, in particular, an even function of s ,

$$\varphi(-s, \vartheta) = \varphi(s, \vartheta). \quad (2.8)$$

Having thus determined $\varphi(s, \vartheta)$, the inverse relation to (2.4) supplies $\psi(r, \vartheta)$, namely (Grünberg 4))

$$\psi(r, \vartheta) = \frac{1}{\pi i} \int_{\varepsilon - i\infty}^{\varepsilon + i\infty} \varphi(s, \vartheta) I_s(\alpha r) s \, ds, \quad \varepsilon > 0, \quad (2.9)$$

where $I_s(\alpha r)$ is a second solution of the differential equation (2.5), regular at $r = 0$. It is possible to express the integral (2.9) as a residue series, arising from the singularities of $\varphi(s, \vartheta)$ in the half-plane $\operatorname{Re} s > 0$, but then a summation problem occurs (with some details indicated at the end of this section). An alternative procedure which eliminates this feature, is based on a preliminary transformation of the relation (2.9). Utilizing the symmetry property (2.8), and reflection of the integration path in (2.9), it follows that

$$\begin{aligned} \psi(r, \vartheta) &= \frac{1}{2\pi i} \int_{-i\infty}^{i\infty} [I_s(\alpha r) - I_{-s}(\alpha r)] \varphi(s, \vartheta) s \, ds = \\ &= \frac{1}{2\pi i} \int_{-i\infty}^{i\infty} \left[-\frac{2}{\pi} \sin s\pi K_s(\alpha r) \right] \varphi(s, \vartheta) s \, ds. \end{aligned} \quad (2.10)$$

Let us now introduce the integral representation

$$K_s(x) = \frac{1}{\cos \frac{1}{2}s\pi} \int_0^\infty \cos(x \sinh t) \cosh st \, dt, \quad x > 0, \quad -1 < \operatorname{Re} s < 1, \quad (2.11)$$

and obtain

$$\begin{aligned} \psi(r, \vartheta) &= \frac{i}{2\pi\alpha^2} \int_{-\infty}^{\infty} e^{-i\alpha r \sinh t} \cdot \\ &\quad \cdot dt \int_{-i\infty}^{i\infty} \cosh st \left[1 - \frac{\sin s\vartheta + \sin s(\vartheta_0 - \vartheta)}{\sin s\vartheta_0} \right] ds \\ &= -\frac{1}{\alpha^2} - \frac{i}{2\pi\alpha^2} \int_{-\infty}^{\infty} e^{-i\alpha r \sinh t} dt \int_{-\infty}^{\infty} \cosh st \frac{\sin s\vartheta + \sin s(\vartheta_0 - \vartheta)}{\sin s\vartheta_0} ds. \end{aligned} \quad (2.12)$$

A change of variable $s = iu$ in the last integral yields

$$\begin{aligned} \int_{-i\infty}^{i\infty} \cosh st \frac{\sin s\vartheta + \sin s(\vartheta_0 - \vartheta)}{\sin s\vartheta_0} ds = \\ = i \int_{-\infty}^{\infty} \cos ut \frac{\sinh u\vartheta + \sinh u(\vartheta_0 - \vartheta)}{\sinh u\vartheta_0} du, \end{aligned} \quad (2.13)$$

and furthermore

$$\begin{aligned} \int_{-\infty}^{\infty} \cos ut \frac{\sinh u\vartheta}{\sinh u\vartheta_0} du &= \frac{1}{2\vartheta_0} \int_0^{\infty} \frac{dz}{z^2 - 1} [(z^\alpha - z^{-\alpha}) + (z^\beta - z^{-\beta})] = \\ &= \frac{\pi}{4\vartheta_0} \left[\cot \frac{\pi}{2} (1 - \alpha) - \cot \frac{\pi}{2} (1 + \alpha) + \cot \frac{\pi}{2} (1 - \beta) - \right. \\ &\quad \left. - \cot \frac{\pi}{2} (1 + \beta) \right] = \\ &= \frac{\pi}{2\vartheta_0} \left[\tan \frac{\pi\alpha}{2} + \tan \frac{\pi\beta}{2} \right], \quad \alpha = \frac{\vartheta + it}{\vartheta_0}, \quad \beta = \frac{\vartheta - it}{\vartheta_0}, \end{aligned} \quad (2.14)$$

while

$$\begin{aligned} \int_{-\infty}^{\infty} \cos ut \frac{\sinh u(\vartheta_0 - \vartheta)}{\sinh u\vartheta_0} du \\ = \frac{\pi}{2\vartheta_0} \left[\tan \frac{\pi\alpha'}{2} + \tan \frac{\pi\beta'}{2} \right], \quad \alpha' = 1 - \beta, \quad \beta' = 1 - \alpha. \end{aligned} \quad (2.15)$$

Thus

$$\begin{aligned} \int_{-\infty}^{\infty} \cos ut \frac{\sinh u\vartheta + \sinh u(\vartheta_0 - \vartheta)}{\sinh u\vartheta_0} du \\ = \frac{\pi}{2\vartheta_0} \left[\tan \frac{\pi\alpha}{2} + \tan \frac{\pi}{2} (1 - \alpha) + \tan \frac{\pi\beta}{2} + \tan \frac{\pi}{2} (1 - \beta) \right] \\ = \frac{\pi}{\vartheta_0} (\csc \pi\alpha + \csc \pi\beta) = \frac{2\pi}{\vartheta_0} \frac{\sin \pi\vartheta/\vartheta_0 \cosh \pi t/\vartheta_0}{\sin^2 \pi\vartheta/\vartheta_0 + \sinh^2 \pi t/\vartheta_0}, \end{aligned} \quad (2.16)$$

and

$$\psi(r, \vartheta) = -\frac{1}{\alpha^2} + \frac{1}{\alpha^2 \vartheta_0} \int_{-\infty}^{\infty} e^{-i\alpha r \sinh t} \frac{\sin \pi \vartheta / \vartheta_0 \cosh \pi t / \vartheta_0}{\sin^2 \pi \vartheta / \vartheta_0 + \sinh^2 \pi t / \vartheta_0} dt, \quad (2.17)$$

or

$$\begin{aligned} \psi(r, \vartheta) = -\frac{1}{\alpha^2} + \frac{1}{2\alpha^2 \vartheta_0} \int_{-\infty}^{\infty} e^{-i\alpha r \sinh t} & \left(\csc \pi \frac{\vartheta + it}{\vartheta_0} + \right. \\ & \left. + \csc \pi \frac{\vartheta - it}{\vartheta_0} \right) dt. \end{aligned} \quad (2.18)$$

The expression (2.17) for $\psi(r, \vartheta)$ conforms to the boundary conditions (2.2) in virtue of the behaviour

$$\lim_{\vartheta \rightarrow 0, \vartheta_0} \frac{\sin \pi \vartheta / \vartheta_0}{\sin^2 \pi \vartheta / \vartheta_0 + \sinh^2 \pi t / \vartheta_0} = \vartheta_0 \delta(t), \quad (2.19)$$

where δ denotes the Dirac delta function. Note that in the special case $\vartheta_0 = \pi$ (no corner) and $\vartheta = \frac{1}{2}\pi$, $y = r \sin \vartheta = r$,

$$\begin{aligned} \psi(y) &= -\frac{1}{\alpha^2} + \frac{2}{\pi \alpha^2} \int_0^{\infty} \cos(\alpha y \sinh t) \frac{dt}{\cosh t} \\ &= -\frac{1}{\alpha^2} + \frac{2}{\pi \alpha^2} \int_0^{\infty} \frac{\cos \alpha y p}{1 + p^2} dp = -\frac{1}{\alpha^2} + \frac{1}{\alpha^2} e^{-\alpha y}, \end{aligned} \quad (2.20)$$

as anticipated.

Having the singular limit (2.19) in mind, the representation (2.18) is suggested for the calculation of the normal derivative of ψ at $\vartheta = 0$ (or ϑ_0). Now

$$\begin{aligned} \vartheta_{\vartheta} \psi &= \frac{1}{2\alpha^2 \vartheta_0} \int_{-\infty}^{\infty} e^{-i\alpha r \sinh t} \frac{\partial}{\partial \vartheta} \left(\csc \pi \frac{\vartheta + it}{\vartheta_0} + \csc \pi \frac{\vartheta - it}{\vartheta_0} \right) dt = \\ &= \frac{1}{2i\alpha^2 \vartheta_0} \int_{-\infty}^{\infty} e^{-i\alpha r \sinh t} \frac{\partial}{\partial t} \left(\csc \pi \frac{\vartheta + it}{\vartheta_0} - \csc \pi \frac{\vartheta - it}{\vartheta_0} \right) dt \\ &= \frac{r}{2\alpha \vartheta_0} \int_{-\infty}^{\infty} \cosh t e^{-i\alpha r \sinh t} \left(\csc \pi \frac{\vartheta + it}{\vartheta_0} - \csc \pi \frac{\vartheta - it}{\vartheta_0} \right) dt, \end{aligned} \quad (2.21)$$

after an integration by parts, and consequently

$$\partial_n \psi|_{\vartheta=0} = \frac{1}{r} \partial_{\vartheta} \psi|_{\vartheta=0} = -\frac{1}{\alpha \vartheta_0} \int_{-\infty}^{\infty} \frac{\cosh t}{\sinh \pi t / \vartheta_0} \sin(\alpha r \sinh t) dt, \quad r > 0. \quad (2.22)$$

When $\vartheta_0 = \pi$, a constant value of the derivative obtains, namely $-1/\alpha$, $r > 0$, and if this be subtracted from (2.22), there results the function

$$f(x) = \frac{1}{\alpha} \int_{-\infty}^{\infty} \cosh t \sin(\alpha x \sinh t) \left[\frac{1}{\pi \sinh t} - \frac{1}{\vartheta_0 \sinh \pi t / \vartheta_0} \right] dt, \quad x > 0, \quad (2.23)$$

which tends to zero as the distance x from the corner increases. The corner correction $\Delta(\vartheta_0)$, defined by

$$\frac{1}{\alpha^2} \Delta(\vartheta_0) = 2 \int_0^{\infty} f(x) dx, \quad (2.24)$$

is therefore

$$\Delta(\vartheta_0) = 2 \int_{-\infty}^{\infty} \frac{\cosh t}{\sinh t} \left[\frac{1}{\pi \sinh t} - \frac{1}{\vartheta_0 \sinh \pi t / \vartheta_0} \right] dt. \quad (2.25)$$

The quantities $\Delta(\vartheta_0)$ and $D(\vartheta_0)$ (cf. (1.5)) differ only by their sign, and the paper of Hurwitz and Roe may be consulted for the plot of D vs. ϑ_0 ; a few special values, easily obtained by evaluation of (2.25), or (1.6), are:

$$\Delta(\pi/3) = 4/\sqrt{3}, \quad \Delta(\pi/2) = 4/\pi, \quad \Delta(\pi) = 0, \quad \Delta(2\pi) = -1.$$

Additional features of the correction factor are revealed, and its evaluation facilitated by further transformation, with the representation as a convenient basis. A finite integral expression is secured via the change of variable $\exp(\gamma t) = x^{\frac{1}{\gamma}}$,

$$\gamma = \pi/\vartheta_0, \quad \frac{1}{2} < \gamma < \infty, \quad (2.26)$$

which yields

$$\Delta(\gamma) = \frac{2}{\pi} \int_0^{\infty} \frac{x^{1/\gamma} + 1}{x^{1/\gamma} - 1} \left(\frac{x^{-\frac{1}{2}}}{1-x} - \frac{\gamma^{-1} x^{1/2\gamma-1}}{1-x^{1/\gamma}} \right) dx, \quad (2.27)$$

whence, on dividing the range of integration $0 < x < \infty$ at $x = 1$

and substituting $x = 1/v$ in $1 < x < \infty$,

$$\Delta(\gamma) = \frac{4}{\pi} \int_0^1 \frac{x^{1/\gamma} + 1}{x^{1/\gamma} - 1} \left(\frac{x^{-1/2}}{1-x} - \frac{\gamma^{-1} x^{1/2\gamma-1}}{1-x^{1/\gamma}} \right) dx. \quad (2.28)$$

The hyperbolic form

$$\Delta(\gamma) = \frac{4}{\pi} \int_0^\infty \coth t \left(\frac{1}{\sinh t} - \frac{\gamma}{\sinh \gamma t} \right) dt \quad (2.29)$$

lends itself to reduction, starting with the partial fraction development

$$\coth t = \frac{1}{t} + 2t \sum_{n=1}^\infty \frac{1}{t^2 + n^2\pi^2}. \quad (2.30)$$

Since

$$\int_0^\infty \left(\frac{q}{\sinh qx} - \frac{p}{\sinh px} \right) \frac{dx}{x} = (p - q) \ln 2, \quad (pq > 0) \quad (2.31)$$

it follows that

$$\Delta(\gamma) = \frac{4}{\pi} (\gamma - 1) \ln 2 + \frac{8}{\pi} \sum_{n=1}^\infty \int_0^\infty \frac{1}{t^2 + n^2\pi^2} \left(\frac{t}{\sinh t} - \frac{\gamma t}{\sinh \gamma t} \right) dt. \quad (2.32)$$

Further,

$$\frac{t}{\sinh t} = 1 + 2t^2 \sum_{k=1}^\infty \frac{(-1)^k}{t^2 + k^2\pi^2}, \quad (2.33)$$

and

$$\int_0^\infty \frac{1}{t^2 + n^2\pi^2} \frac{t}{\sinh t} dt = \frac{1}{2n} + \sum_{k=1}^\infty \frac{(-1)^k}{n + k}, \quad (2.34)$$

whence

$$\Delta(\gamma) = \frac{4}{\pi} (\gamma - 1) \ln 2 + \frac{8}{\pi} \sum_{n=1}^\infty \sum_{k=1}^\infty (-1)^k \left(\frac{1}{n+k} - \frac{1}{n+k/\gamma} \right). \quad (2.35)$$

The sum over k may be expressed in terms of the beta function $\beta(x)$, or the *psi*-function $\psi(x) = (d/dx) \ln \Gamma(x)$, namely

$$\sum_{k=1}^\infty \frac{(-1)^{k-1}}{k+l} = \beta(l+1) = \frac{1}{2} \left[\psi\left(\frac{l+2}{2}\right) - \psi\left(\frac{l+1}{2}\right) \right], \quad (2.36)$$

which implies that

$$\Delta(\gamma) = \frac{4}{\pi} (\gamma - 1) \ln 2 + \frac{4}{\pi} \sum_{n=1}^{\infty} \left\{ \gamma \left[\psi \left(\frac{\gamma n + 2}{2} \right) - \psi \left(\frac{\gamma n + 1}{2} \right) \right] - \psi \left(\frac{n+2}{2} \right) + \psi \left(\frac{n+1}{2} \right) \right\}. \quad (2.37)$$

Alternatively, the integral representation

$$\beta(l+1) = \int_0^1 \frac{x^l}{1+x} dx \quad (2.38)$$

enables us to write

$$\begin{aligned} \Delta(\gamma) &= \frac{4}{\pi} (\gamma - 1) \ln 2 + \frac{8}{\pi} \sum_{n=1}^{\infty} \int_0^1 \frac{dx}{1+x} (\gamma x^{n\gamma} - x^n) \\ &= \frac{4}{\pi} (\gamma - 1) \ln 2 + \frac{8}{\pi} \int_0^1 \frac{dx}{1+x} \left(\frac{\gamma x^\gamma}{1-x^\gamma} - \frac{x}{1-x} \right) \\ &= \frac{4}{\pi} \int_0^1 \frac{dx}{1+x} \left(\frac{\gamma(1+x^\gamma)}{1-x^\gamma} - \frac{1+x}{1-x} \right), \end{aligned} \quad (2.39)$$

a form complementary to (2.28).

The contribution $(4/\pi)(\gamma - 1) \ln 2$ dominates in $\Delta(\gamma)$ when $\gamma = \pi/\vartheta_0 \gg 1$ and the corner angle is small, as noted by Hurwitz and Roe. On expansion of $(t^2 + n^2\pi^2)^{-1}$ in rising powers of t , the relation (2.32) becomes

$$\begin{aligned} \Delta(\gamma) &= \frac{4}{\pi} (\gamma - 1) \ln 2 + \\ &+ \frac{8}{\pi} \sum_{n=1}^{\infty} \sum_{j=1}^{\infty} (-1)^{j-1} \int_0^{\infty} \frac{t^{2j-2}}{(n\pi)^{2j}} \left(\frac{t}{\sinh t} - \frac{\gamma t}{\sinh \gamma t} \right) dt \\ &= \frac{4}{\pi} (\gamma - 1) \ln 2 + \\ &+ \frac{8}{\pi} \sum_{j=1}^{\infty} (-1)^{j-1} \pi^{-2j} \zeta(2j) \int_0^{\infty} \left(\frac{t^{2j-1}}{\sinh t} - \frac{\gamma t^{2j-1}}{\sinh \gamma t} \right) dt \end{aligned} \quad (2.40a)$$

$$\begin{aligned}
&= \frac{4}{\pi} (\gamma - 1) \ln 2 + \\
&\quad + \frac{1}{\pi} \sum_{j=1}^{\infty} (-1)^{j-1} \frac{(2\pi)^{2j}}{(2j)!} \frac{2^{2j}-1}{j} (B_{2j})^2 \left(1 - \frac{1}{\gamma^{2j-1}}\right) \\
&= \frac{4}{\pi} (\gamma - 1 \ln 2 + \\
&\quad + \frac{\pi}{6} \left[\left(1 - \frac{1}{\gamma}\right) - \frac{\pi^2}{30} \left(1 - \frac{1}{\gamma^3}\right) + \frac{2\pi^4}{315} \left(1 - \frac{1}{\gamma^5}\right) - \dots \right], \gamma > 1,
\end{aligned} \tag{2.40b}$$

where $\zeta(2j)$ denotes the Riemann zeta-function and B_{2j} the Bernoulli number, with

$$\zeta(2j) = \frac{2^{2j-1}}{(2j)!} \pi^{2j} |B_{2j}|.$$

When γ is close to unity, $\vartheta_0 \doteq \pi$, the development (2.40) is ill-conditioned, and it is appropriate to expand the terms

$$\frac{1}{n+k} - \frac{\gamma}{\gamma n+k}$$

of (2.35) in powers of $\gamma - 1$; retaining only the first power gives the approximation

$$\Delta(\gamma)|_{\gamma \rightarrow 1} = \frac{4}{\pi} (\gamma - 1) \left[\ln 2 - 2 \sum_{n=1}^{\infty} \sum_{k=1}^{\infty} (-1)^k \frac{k}{(n+k)^2} \right].$$

As

$$\int_0^1 \frac{x^{p-1}}{1+x^q} dx = \sum_{k=0}^{\infty} \frac{(-1)^k}{p+kq},$$

it follows on differentiating with respect to q and then setting $q = 1$ that

$$\sum_{k=0}^{\infty} \frac{(-1)^k k}{(p+k)^2} = \int_0^1 \frac{x^p}{(1+x)^2} \ln x dx,$$

whence

$$\begin{aligned}
 \Delta(\gamma)|_{\gamma \rightarrow 1} &= \frac{4}{\pi} (\gamma - 1) \left[\ln 2 - 2 \sum_{n=1}^{\infty} \int_0^1 \frac{x^n}{(1+x)^2} \ln x \, dx \right] \\
 &= \frac{4}{\pi} (\gamma - 1) \left[\ln 2 - 2 \int_0^1 \frac{1}{(1+x)^2} \frac{x}{1-x} \ln x \, dx \right] \\
 &= \frac{\pi}{2} (\gamma - 1),
 \end{aligned} \tag{2.41}$$

or

$$\Delta(\vartheta_0) = \frac{1}{2}(\pi - \vartheta_0), \vartheta_0 \rightarrow \pi \tag{2.42}$$

as also observed by Hurwitz and Roe.

Before concluding this section it is of some interest to describe an evaluation of the inversion formula (2.9) without transformation to the form (2.10), and employment of an integral representation for the cylinder function *).

Consider the special value $\vartheta_0 = \pi$, when

$$\varphi(s, \vartheta) = \frac{\pi}{2\alpha^2 s} \csc \frac{s\pi}{2} \left[\frac{\sin s\pi - \sin s\vartheta - \sin s(\pi - \vartheta)}{\sin s\pi} \right],$$

and

$$\psi(r, \vartheta) = \frac{1}{2i\alpha^2} \int_{\varepsilon-i\infty}^{\varepsilon+i\infty} I_s(\alpha r) \left[\frac{\sin s\pi - \sin s\vartheta - \sin s(\pi - \vartheta)}{\sin s\pi} \right] \csc \frac{s\pi}{2} \, ds.$$

In the right half plane, $\text{Re } s > 0$, the integrand has simple poles at $s = 2m - 1$, $m = 1, 2, \dots$, and double poles at $s = 2n$, $n = 1, 2, \dots$, arising from the factor $\varphi(s, \vartheta)$, and the path may be closed about these singularities without further contribution, thanks to the rapid diminution of $I_s(\alpha r)$ for $\text{Re } s \rightarrow \infty$. The residue contribution of the first set of poles is

$$\frac{2}{\alpha^2} \sum_{m=1}^{\infty} (-1)^m I_{2m-1}(\alpha r) \sin (2m - 1) \vartheta,$$

*) Both forms are utilized in a study of diffraction of a cylindrical pulse by a semi-infinite plane screen (Turner ⁵) and evaluated as residue sums.

while that of the second set is

$$\begin{aligned}
 & -\frac{2}{\pi\alpha^2} \sum_{n=1}^{\infty} (-1)^n I_{2n}(\alpha r) \frac{d}{ds} [\sin s\pi - \sin s\vartheta - \sin s(\pi - \vartheta)]_{s=2n} \\
 & = -\frac{2}{\alpha^2} \sum_{n=1}^{\infty} (-1)^n I_{2n}(\alpha r) (1 - \cos 2n\vartheta) \\
 & = -\frac{1}{\alpha^2} + \frac{1}{\alpha^2} I_0(\alpha r) + \frac{2}{\alpha^2} \sum_{n=1}^{\infty} (-1)^n I_{2n}(\alpha r) \cos 2n\vartheta.
 \end{aligned}$$

Adding the results,

$$\begin{aligned}
 \psi(r, \vartheta) & = -\frac{1}{\alpha^2} + \frac{1}{\alpha^2} \left[I_0(\alpha r) + 2 \sum_{k=1}^{\infty} (-1)^k I_k(\alpha r) \cos k \left(\vartheta - \frac{\pi}{2} \right) \right] \\
 & = -\frac{1}{\alpha^2} + \frac{1}{\alpha^2} e^{-\alpha y}, \quad y = r \sin \vartheta,
 \end{aligned}$$

in accord with (2.20).

§ 3. *The right angle corner.* According to (2.24) the corner correction $\Delta(\vartheta_0)$ is proportional to the integral of the local normal flux $f(x)$ at either boundary of the corner. This measure of the flux corresponds to a particular value of the Fourier transform

$$\bar{f}(\zeta) = \int_0^{\infty} e^{-i\zeta x} f(x) dx, \quad (3.1)$$

namely that for argument $\zeta = 0$. A direct evaluation of the transform $\bar{f}(\zeta)$ is therefore of interest and will be accomplished for the right angle corner by starting with an integral equation characterization of $f(x)$. The integral equation, with semi-infinite domain, $0 < x < \infty$, involves a composite kernel which is not of the convolution form, so that the technique of solution merits attention.

Information about $f(x)$ and $\bar{f}(\zeta)$ is evidently available from the work of the previous section and may be recorded for comparison later on. Choosing $\vartheta_0 = \frac{1}{2}\pi$ in (2.23), it follows after the change of variable $\sinh t = u$, that

$$f(x) = \frac{2}{\pi\alpha} \int_0^{\infty} \frac{\sin(\alpha x u)}{u} \left(1 - \frac{1}{\sqrt{1+u^2}} \right) du, \quad x > 0. \quad (3.2)$$

To reduce the expression further, observe that if

$$P(x) = \int_0^{\infty} \frac{\sin xu}{u} \frac{du}{\sqrt{1+u^2}}, \quad P(\infty) = \frac{1}{2}\pi, \quad (3.3)$$

then

$$\frac{dP}{dx} = \int_0^{\infty} \frac{\cos xu}{\sqrt{1+u^2}} du = K_0(x) \quad (3.4)$$

and hence

$$P(x) = \frac{\pi}{2} - \int_x^{\infty} K_0(t) dt. \quad (3.5)$$

Thus,

$$f(x) = \frac{1}{\alpha} \left[1 - \left(1 - \frac{2}{\pi} \int_{\alpha x}^{\infty} K_0(t) dt \right) \right] = \frac{2}{\pi \alpha} \int_{\alpha x}^{\infty} K_0(t) dt, \quad x > 0. \quad (3.6)$$

As a check, note that

$$\begin{aligned} 2 \int_0^{\infty} f(x) dx &= 2 \bar{f}(0) = -\frac{4}{\pi \alpha} \int_0^{\infty} x \left(\frac{d}{dx} \int_{\alpha x}^{\infty} K_0(t) dt \right) dx \\ &= \frac{4}{\pi} \int_0^{\infty} x K_0(\alpha x) dx = \frac{4}{\pi \alpha^2} = \frac{1}{\alpha^2} \Delta(\pi/2), \end{aligned} \quad (3.7)$$

whence the value $\Delta(\pi/2) = 4/\pi$ is confirmed.

The representation (3.3) permits ready estimate of $f(x)$ for $x \rightarrow 0$ and $x \rightarrow \infty$, with the results

$$f(x) \doteq 1/\alpha, \quad x \rightarrow 0, \quad (3.8)$$

and

$$f(x) \simeq \sqrt{\frac{2}{\pi \alpha x}} e^{-\alpha x}, \quad x \rightarrow \infty. \quad (3.9)$$

Additionally, the use of (3.3) in computing the transform $\bar{f}(\zeta)$ yields

$$\bar{f}(\zeta) = \int_0^{\infty} (d e^{-i\zeta x} / -i\zeta) f(x) = \frac{1}{i\zeta \alpha} - \frac{2}{i\pi \zeta} \int_0^{\infty} e^{-i\zeta x} K_0(\alpha x) dx =$$

$$\begin{aligned}
 &= \frac{1}{i\zeta\alpha} \left(1 - \frac{1 - \frac{2i}{\pi} \operatorname{arc} \sinh \zeta/\alpha}{\sqrt{\zeta^2/\alpha^2 + 1}} \right) = \\
 &= \frac{1}{i\zeta\alpha} \left[1 - \frac{1 - \frac{2i}{\pi} \ln \left(\frac{\zeta}{\alpha} + \sqrt{\frac{\zeta^2}{\alpha^2} + 1} \right)}{\sqrt{\zeta^2/\alpha^2 + 1}} \right], \quad (3.10)
 \end{aligned}$$

and by appeal to the asymptotic form (3.9) it is evident that the function $\bar{f}(\zeta)$ is regular in the half plane $\operatorname{Im} \zeta < \alpha$. To verify the latter aspect directly, consider the function

$$p(z) = \frac{1 - \frac{2i}{\pi} \ln(z + \sqrt{z^2 + 1})}{\sqrt{z^2 + 1}} \quad (3.11)$$

and introduce the transformation

$$w = z + \sqrt{z^2 + 1}, \quad (3.12)$$

which describes a conformal mapping of the z -plane cut along the segment $(-i, i)$ onto the exterior of the unit circle $|w| = 1$. Let $w = e^{r+i\varphi}$, $r \geq 0$, $-\pi < \varphi < \pi$, whence

$$z = \sinh(r + i\varphi) = \sinh r \cos \varphi + i \cosh r \sin \varphi, \quad (3.13)$$

$$\sqrt{z^2 + 1} = \cosh(r + i\varphi) = \cosh r \cos \varphi + i \sinh r \sin \varphi, \quad (3.14)$$

and

$$\ln(z + \sqrt{z^2 + 1}) = \ln w = r + i\varphi. \quad (3.15)$$

It follows that z and $\sqrt{z^2 + 1}$ are located in the same quadrant of the z plane, whose lower half corresponds to the range $-\pi < \varphi < 0$. If use is made of (3.14), (3.15) to display $p(z)$ in the form

$$p(r, \varphi) = -\frac{\left(1 + \frac{2\varphi}{\pi}\right) - \frac{2i}{\pi} r}{\cosh(r + i\varphi)}, \quad (3.16)$$

the resulting function has no singularities in the lower half of the z plane, including the point $z = -i$ ($r = 0$, $\varphi = -\frac{1}{2}\pi$), and a singularity is first encountered at $z = i$ ($r = 0$, $\varphi = \frac{1}{2}\pi$) on entering the upper half plane.

An independent method will be described next for obtaining the transform $\bar{f}(\zeta)$ through the integral equation specifying $f(x)$. In the analysis of the preceding section, it is advantageous to stipulate a null boundary value for ψ , since the transform (2.4) contains singular factors at the corner. For present purposes, the boundary value problem is conveniently restated in terms of the function $\varphi = \psi + 1/\alpha^2$, which satisfies the homogeneous differential equation

$$(\partial_x^2 + \partial_y^2 - \alpha^2) \varphi(x, y) = 0, \quad x, y > 0, \quad (3.17)$$

and assumes the uniform boundary value

$$\varphi = \frac{1}{\alpha^2}, \quad \text{at} \begin{cases} x > 0, & y = 0 (\vartheta = 0), \\ x = 0, & y > 0 (\vartheta = \pi/2). \end{cases} \quad (3.18)$$

Clearly, the derivatives of ψ and φ are equal.

For points remote from the corner and near the boundary $\vartheta = 0 (x \rightarrow \infty, y \rightarrow 0+)$ the differential equation (3.17) is approximately one-dimensional and has the unique solution

$$\varphi = \frac{1}{\alpha^2} e^{-\alpha y}, \quad \partial_y \varphi|_{y=0} = -\frac{1}{\alpha},$$

that exhibits the requisite attenuation with distance from the boundary. Let us therefore write

$$F(x) \equiv \partial_y \varphi(x, y)|_{y=0} = f(x) - 1/\alpha, \quad x > 0, \quad (3.19)$$

and also, taking cognizance of the symmetry in boundary distributions,

$$F(y) \equiv \partial_x \varphi(x, y)|_{x=0} = f(y) - 1/\alpha, \quad y > 0. \quad (3.20)$$

The function $f(x)$ so defined is identical with the normal derivative studied above.

A fundamental solution of the inhomogeneous equation related to (3.17),

$$(\partial_x^2 + \partial_y^2 - \alpha^2) G(x, y; x', y') = -\delta(x - x') \delta(y - y'). \quad (3.21)$$

defined in the entire plane, with logarithmic singularity at $x = x'$, $y = y'$ and a null value for $\sqrt{x^2 + y^2} \rightarrow \infty$, is the Green's function

$$G(x, y; x', y') = \frac{1}{2\pi} K_0(\alpha \sqrt{(x - x')^2 + (y - y')^2}). \quad (3.22)$$

By reflection of the 'source point' x', y' in the lines $x = 0$ and $y = 0$, a solution of (3.21) is obtained in the quadrant $x, x', y, y' > 0$, namely

$$\begin{aligned} G_1(x, y; x', y') = & \frac{1}{2\pi} [K_0(\alpha \sqrt{(x-x')^2 + (y-y')^2}) + \\ & + K_0(\alpha \sqrt{(x-x')^2 + (y+y')^2}) + \\ & + K_0(\alpha \sqrt{(x+x')^2 + (y-y')^2}) + K_0(\alpha \sqrt{(x+x')^2 + (y+y')^2})] \end{aligned} \quad (3.23)$$

which has a vanishing normal derivative at the boundaries thereto. Employing the integral form of Green's second identity in the domain, there results a representation

$$\varphi(x, y) = - \int_0^\infty F(x') G_1(x, y; x', 0) dx' - \int_0^\infty F(y') G_1(x, y; 0, y') dy' \quad (3.24)$$

of the function $\varphi(x, y)$ at an arbitrary interior point in terms of its normal derivative at the boundaries. Substituting from (3.19) and making use of the relations

$$K_0[\alpha \sqrt{(x-x')^2 + (y-y')^2}] = \frac{1}{2\pi} \int_{-\infty}^\infty \frac{e^{i\xi(x-x') + i\eta(y-y')}}{\xi^2 + \eta^2 + \alpha^2} d\xi d\eta, \quad (3.25)$$

$$\int_{-\infty}^\infty K_0[\alpha \sqrt{(x-x')^2 + y^2}] dx' = \int_{-\infty}^\infty \frac{e^{i\eta y}}{\eta^2 + \alpha^2} d\eta = \frac{\pi}{\alpha} e^{-\alpha y}, \quad y > 0, \quad (3.26)$$

the expression (3.24) becomes

$$\begin{aligned} \varphi(x, y) = & \frac{1}{\alpha^2} (e^{-\alpha x} + e^{-\alpha y}) - \\ & - \int_0^\infty f(x') G_1(x, y; x', 0) dx' - \int_0^\infty f(y') G_1(x, y; 0, y') dy', \quad x, y > 0. \end{aligned} \quad (3.27)$$

When the boundary (3.18) is imposed (at either side of the right angle), an integral equation results, namely

$$\frac{1}{\alpha^2} e^{-\alpha x} = \int_0^\infty f(x') G_1(x, 0; x', 0) dx' + \int_0^\infty f(y') G_1(x, 0; 0, y) dy', \quad x > 0,$$

or

$$\frac{\pi}{2\alpha^2} e^{-\alpha x} = \int_0^\infty f(x') \left[\frac{1}{2} K_0(\alpha|x-x'|) + \frac{1}{2} K_0(\alpha|x+x'|) + K_0(\alpha\sqrt{x^2+x'^2}) \right] dx', \quad x > 0 \quad (3.28)$$

which provides a characterization of $f(x)$. If $f(x)$ is continued to the domain $-\infty < x < 0$ in the symmetric fashion,

$$f(-x) = f(x), \quad (3.29)$$

the integral equation may be recast in the form

$$\frac{\pi}{\alpha^2} e^{-\alpha|x|} = \int_{-\infty}^\infty f(x') \left[K_0(\alpha|x-x'|) + K_0(\alpha\sqrt{x^2+x'^2}) \right] dx', \quad -\infty < x < \infty. \quad (3.30)$$

The concomitant transform relation, valid within the strip $|\operatorname{Im} \zeta| < \alpha$, is

$$\frac{2\pi}{\alpha(\zeta^2 + \alpha^2)} = \frac{\pi}{\sqrt{\zeta^2 + \alpha^2}} [\bar{f}(\zeta) + \bar{f}(-\zeta)] + \int_{-\infty}^\infty \frac{\bar{f}(\eta) + \bar{f}(-\eta)}{\eta^2 + \zeta^2 + \alpha^2} d\eta, \quad (3.31)$$

being obtained from (3.30) on multiplication by $e^{-i\zeta x}$ and integration over x , with use of the integral representation (3.25) and

$$K_0(\alpha|x-x'|) = \frac{1}{2} \int_0^\infty \frac{e^{i\xi(x-x')}}{\sqrt{\xi^2 + \alpha^2}} d\xi. \quad (3.32)$$

On account of symmetry,

$$\int_{-\infty}^\infty \frac{\bar{f}(\eta) + \bar{f}(-\eta)}{\eta^2 + \zeta^2 + \alpha^2} d\eta = 2 \int_{-\infty}^\infty \frac{\bar{f}(\eta)}{\eta^2 + \zeta^2 + \alpha^2} d\eta, \quad (3.33)$$

and the latter integral may be evaluated by residue calculation in the lower half of the η plane, with the result

$$\int_{-\infty}^\infty \frac{\bar{f}(\eta)}{\eta^2 + \zeta^2 + \alpha^2} d\eta = \frac{\pi}{\sqrt{\zeta^2 + \alpha^2}} \bar{f}(-i\sqrt{\zeta^2 + \alpha^2}), \quad \operatorname{Re} \sqrt{\zeta^2 + \alpha^2} > 0. \quad (3.34)$$

The relation (3.31) becomes, accordingly,

$$\bar{f}(\zeta) + \bar{f}(-\zeta) + 2\bar{f}(-i\sqrt{\zeta^2 + \alpha^2}) = 2/\sqrt{\zeta^2 + \alpha^2}, \quad (3.35)$$

which is further simplified by the transformation

$$\zeta = \alpha \sinh w \equiv \alpha \sinh(u + iv), \quad (3.36)$$

so that

$$\bar{f}(\alpha \sinh w) + \bar{f}(-\alpha \sinh w) + 2\bar{f}(-i\alpha \cosh w) = 2\alpha^{-2} \operatorname{sech} w. \quad (3.37)$$

(3.36) describes a mapping of the entire ζ plane into an infinite strip of the w plane, namely $-\frac{1}{2}\pi < v < \frac{1}{2}\pi$, $-\infty < u < \infty$, with the correspondence $\operatorname{Im} \zeta > 0$, $v > 0$ and $\operatorname{Im} \zeta < 0$, $v < 0$. Thus $\bar{f}(\alpha \sinh w)$ is regular in the strip $-\frac{1}{2}\pi < v < 0$ and may be continued to $\operatorname{Im} w < -\frac{1}{2}\pi$, since $\sinh(-\frac{1}{2}i\pi + w) = \sinh(-\frac{1}{2}i\pi - w)$. Hence (3.37) corresponds to the functional relation

$$\begin{aligned} \bar{f}(\alpha \sinh w) + \bar{f}(\alpha \sinh(w - i\pi)) + \\ + 2\bar{f}(\alpha \sinh(w - \tfrac{1}{2}i\pi)) = 2\alpha^{-2} \operatorname{sech} w, \end{aligned} \quad (3.38)$$

or, formally

$$F(w) + 2F(w - \tfrac{1}{2}i\pi) + F(w - i\pi) = G(w). \quad (3.39)$$

The solution of (3.39) is achieved by Fourier decomposition,

$$F(w) = \frac{1}{2\pi} \int_{-\infty}^{\infty} \bar{F}(s) e^{iws} ds, \quad G(w) = \frac{1}{2\pi} \int_{-\infty}^{\infty} \bar{G}(s) e^{iws} ds, \quad (3.40)$$

which yields

$$\bar{F}(s) = \frac{\bar{G}(s)}{(1 + e^{\frac{1}{2}s\pi})^2}, \quad (3.41)$$

and thus

$$F(w) = \frac{1}{2\pi} \int_{-\infty}^{\infty} \frac{\bar{G}(s) e^{iws}}{(1 + e^{\frac{1}{2}s\pi})^2} ds. \quad (3.42)$$

In particular, with $G(w) = 2\alpha^{-2} \operatorname{sech} w$,

$$\bar{G}(s) = \int_{-\infty}^{\infty} G(w) e^{-iws} dw = \frac{4}{\alpha^2} \int_{-\infty}^{\infty} \frac{\cos sw}{\cosh w} dw = \frac{2\pi}{\alpha^2} \operatorname{sech} \frac{s\pi}{2}, \quad (3.43)$$

and consequently

$$F(w) = \frac{1}{\alpha^2} \int_{-\infty}^{\infty} \frac{e^{iws} ds}{\cosh \frac{s\pi}{2} (1 + e^{\frac{1}{2}s\pi})^2}. \quad (3.44)$$

To evaluate the integral, a preliminary change of variable is appropriate, namely $e^{\frac{1}{2}s\pi} = x$, whence

$$F(w) = \frac{4}{\pi\alpha^2} \int_0^{\infty} \frac{x^{2iw/\pi}}{(x^2 + 1)(x + 1)^2} dx. \quad (3.45)$$

Now

$$\int_0^{\infty} \frac{x^p dx}{(x^2 + 1)(x + 1)^2} = \frac{1}{2} \int_0^{\infty} x^{p-1} \left(\frac{1}{x^2 + 1} - \frac{1}{(x + 1)^2} \right) dx,$$

where

$$\begin{aligned} \int_0^{\infty} \frac{x^{p-1}}{(x + 1)^2} dx &= -\frac{d}{d\lambda} \left(\int_0^{\infty} \frac{x^{p-1}}{x + \lambda} dx \right)_{\lambda=1} = \\ &= -\frac{d}{d\lambda} \left(\frac{\pi\lambda^{p-1}}{\sin p\pi} \right)_{\lambda=1} = -\frac{\pi(p-1)}{\sin p\pi}, \quad 0 < p < 1, \end{aligned} \quad (3.46)$$

and

$$\int_0^{\infty} \frac{x^{p-1}}{1 + x^2} dx = \frac{1}{2} \int_0^{\infty} \frac{y^{p-1}}{1 + y} dy = \frac{\pi}{2 \sin \frac{1}{2}p\pi}, \quad 0 < p < 2, \quad (3.47)$$

so that

$$\begin{aligned} \int_0^{\infty} \frac{x^p dx}{(x^2 + 1)(1 + x)^2} &= \frac{\pi}{4} \frac{1}{\sin \frac{1}{2}p\pi} + \frac{\pi}{2} \frac{p-1}{\sin p\pi} = \\ &= \frac{\pi}{4} \frac{1}{\sin \frac{1}{2}p\pi} \left(1 + \frac{p-1}{\cos \frac{1}{2}p\pi} \right), \quad -1 < p < 3. \end{aligned} \quad (3.48)$$

The result (3.48) also holds for complex values of the exponent p and $-1 < \operatorname{Re} p < 3$. Let $p = 2iw/\pi$, and the combination of (3.45) and (3.48) yields

$$F(w) \equiv \tilde{f}(\alpha \sinh w) = \frac{1}{i\alpha^2 \sinh w} \left(1 - \frac{1 - 2iw/\pi}{\cosh w} \right), \quad (3.49)$$

which agrees precisely with (3.10) if the substitution $\zeta = \alpha \sinh w$ is made therein. An integral equation formulation of the boundary value problem thus lends itself to complete analysis.

§ 4. *Another solution for the right angle corner.* In the preceding section, a reformulation of the boundary value problem is given which provides an integral equation for direct calculation of the desired boundary distribution $f(x)$. This distribution can also be obtained by differentiation of the function $\varphi(x, y)$, after the latter is determined within the corner region. If the representation of $\varphi(x, y)$ in terms of its boundary value evidences a non-uniform behaviour, the procedure calls for differentiation and subsequent passage to the boundary from within the region.

To illustrate the technique, consider the right angle corner, and introduce a (second) Green's function therein,

$$G_2(x, y; x', y') = \frac{1}{2\pi} [K_0(\alpha \sqrt{(x - x')^2 + (y - y')^2}) - K_0(\alpha \sqrt{(x - x')^2 + (y + y')^2}) + K_0(\alpha \sqrt{(x + x')^2 + (y + y')^2}) - K_0(\alpha \sqrt{(x + x')^2 + (y - y')^2})],$$

$$x, y, x', y' > 0, \quad (4.1)$$

which satisfies the differential equation (3.21) and vanishes on both the boundaries $x > 0, y = 0$ and $x = 0, y > 0$; the solution of (3.17), (3.18) can then be represented in the form

$$\varphi(x, y) = \frac{1}{\alpha^2} \int_0^\infty \frac{\partial}{\partial y'} G_2|_{y'=0} dx' + \frac{1}{\alpha^2} \int_0^\infty \frac{\partial}{\partial x'} G_2|_{x'=0} dy', \quad x, y > 0, \quad (4.2)$$

where $\varphi \rightarrow 1/\alpha^2$ if the point x, y approaches a boundary.

The formal differentiation of $\varphi(x, y)$ results in singular integrals if executed at the boundaries, and preliminary transformation of (4.2) is therefore appropriate. With the help of the Fourier integral representation (3.25), it follows that

$$\int_0^\infty e^{-\epsilon x'} \frac{\partial}{\partial y'} G_2|_{y'=0} dx' = \frac{1}{\pi} \int_0^\infty e^{-\epsilon x'} \frac{\partial}{\partial y'} [K_0(\alpha \sqrt{(x - x')^2 + (y - y')^2}) +$$

$$\begin{aligned}
& + K_0(\alpha\sqrt{(x+x')^2 + (y+y')^2})]_{y'=0} dx' = \\
& = \frac{1}{2\pi^2} \int_0^\infty e^{-\varepsilon x'} \frac{\partial}{\partial y'} \left[\int_{-\infty}^\infty \frac{d\xi d\eta}{\xi^2 + \eta^2 + \alpha^2} (e^{i\xi(x-x') + i\eta(y-y')} + \right. \\
& \quad \left. + e^{i\xi(x+x') + i\eta(y-y')}) \right] dx' = \\
& = \frac{i}{2\pi^2} \int_0^\infty e^{-\varepsilon x'} \int_{-\infty}^\infty \frac{\eta d\xi d\eta}{\xi^2 + \eta^2 + \alpha^2} (e^{i\xi(x+x') + i\eta y} - e^{i\xi(x-x') + i\eta y}) dx' = \\
& = \frac{i}{2\pi^2} \int_0^\infty \frac{\eta d\xi d\eta}{\xi^2 + \eta^2 + \alpha^2} e^{i\xi x + i\eta y} \left(\frac{\varepsilon + i\xi}{\varepsilon^2 + \xi^2} - \frac{\varepsilon - i\xi}{\varepsilon^2 + \xi^2} \right) = \\
& = -\frac{1}{\pi^2} \int_{-\infty}^\infty \frac{\eta d\xi d\eta}{\xi^2 + \eta^2 + \alpha^2} \frac{\xi}{\xi^2 + \varepsilon^2} e^{i\xi x + i\eta y}, \quad (4.3)
\end{aligned}$$

and thus

$$\alpha^2 \varphi_\varepsilon(x, y) = -\frac{1}{\pi^2} \int_{-\infty}^\infty \frac{\eta d\xi d\eta}{\xi^2 + \eta^2 + \alpha^2} \frac{\xi}{\xi^2 + \varepsilon^2} (e^{i\xi x + i\eta y} + e^{i\xi y + i\eta x}). \quad (4.4)$$

The reduction of (4) to single integrals is easily accomplished, and there results, in the limit $\varepsilon \rightarrow 0$,

$$\varphi(x, y) = \frac{1}{\pi\alpha^2} \left(\int_{-\infty}^\infty \frac{\sin \xi x}{\xi} e^{-\sqrt{\xi^2 + \alpha^2} y} d\xi + \int_{-\infty}^\infty \frac{\sin \xi y}{\xi} e^{-\sqrt{\xi^2 + \alpha^2} x} d\xi, \right. \\
\left. x, y > 0, \right. \quad (4.5)$$

which confirms that $\varphi \rightarrow 1/\alpha^2$ if $y \rightarrow 0+$, $x > 0$, or $x \rightarrow 0+$, $y > 0$.

Employing (4.4), differentiation with respect to y yields

$$\begin{aligned}
& i\pi^2 \alpha^2 \partial_y \varphi_\varepsilon(x, y) = \\
& = \int_{-\infty}^\infty \frac{\eta^2}{\xi^2 + \eta^2 + \alpha^2} \frac{\xi}{\xi^2 + \varepsilon^2} e^{i\xi x + i\eta y} d\xi d\eta + \\
& \quad + \int_{-\infty}^\infty \frac{\eta}{\xi^2 + \eta^2 + \alpha^2} \frac{\xi^2}{\xi^2 + \varepsilon^2} e^{i\xi y + i\eta x} d\xi d\eta = \\
& = \int_{-\infty}^\infty \left(1 - \frac{\xi^2 + \alpha^2}{\xi^2 + \eta^2 + \alpha^2} \right) \frac{\xi}{\xi^2 + \varepsilon^2} e^{i\xi x + i\eta y} d\xi d\eta
\end{aligned}$$

$$+ \int_{-\infty}^{\infty} \frac{\eta}{\xi^2 + \eta^2 + \alpha^2} \frac{\xi^2}{\xi^2 + \epsilon^2} e^{i\xi y + i\eta x} d\xi d\eta. \quad (4.6)$$

That part of the first integral which contains the term unity in parentheses has a null value if $y > 0$, for the η integration defines the Dirac singular function of y . The limit $\epsilon \rightarrow 0$ may be taken in the remainder, and after an interchange of variables in the last integral, it follows that

$$\begin{aligned} \hat{c}_y \varphi(x, 0+) &= \frac{i}{\pi^2 \alpha^2} \int_{-\infty}^{\infty} \frac{e^{i\xi x}}{\xi^2 + \eta^2 + \alpha^2} \left(\frac{\xi^2 + \alpha^2}{\xi} - \xi \right) d\xi d\eta, \quad x > 0 \\ &= -\frac{1}{\pi^2} \int_{-\infty}^{\infty} \frac{\sin \xi x}{\xi} \frac{d\xi d\eta}{\xi^2 + \eta^2 + \alpha^2} = -\frac{1}{\pi} \int_{-\infty}^{\infty} \frac{\sin \xi x}{\xi} \frac{d\xi}{\sqrt{\xi^2 + \alpha^2}}. \end{aligned} \quad (4.7)$$

For large x , the last integral is asymptotically equal to $\alpha^{-1} \int_{-\infty}^{\infty} \sin \xi x d\xi/\xi = \pi/\alpha$, whence

$$\hat{c}_y \varphi(x, 0+) = -\frac{1}{\alpha} + \frac{2}{\pi} \int_0^{\infty} \frac{\sin \xi x}{\xi} \left(\frac{1}{\alpha} - \frac{1}{\sqrt{\xi^2 + \alpha^2}} \right) d\xi = -\frac{1}{\alpha} + f(x), \quad (4.8)$$

where $f(x)$ agrees with the expression in (3.2).

Received 22nd August, 1959.

REFERENCES

- 1) Hurwitz, H. Ir. and G. M. Roe, J. Nuclear Energy **2** (1955) 85.
- 2) Koiter, W. T., Quart. J. Mech. Appl. Math. **8** (1955) 164.
- 3) Azpeitia, A. G. and G. F. Newell, Z. angew. Math. Phys. **10** (1959) 15.
- 4) Grünberg, G. A., J. Phys. USSR **3** (1940) 401.
- 5) Turner, R. D., Quart. Appl. Math. **14** (1956) 63.

ON THE SPECIFIC HEAT OF Mn Zn-AND Ni Zn-FERRITE BETWEEN 20°C AND 350°C

by J. L. VERHAEGHE, G. G. ROBBRECHT and
W. M. BRUYNOOGHE

Natuurkundig Laboratorium der Rijksuniversiteit, Ghent, Belgium

Summary

The specific heat of two ferrites with respective chemical composition $\text{Mn}_{1-a}\text{Zn}_a\text{Fe}_2\text{O}_4$ ($a \approx 0.38$) and $\text{Ni}_{1-a}\text{Zn}_a\text{Fe}_2\text{O}_4$ ($a \approx 0.50$) has been measured with a Nernst adiabatic calorimeter in the temperature range 20°C–350°C. Associated with the ferrimagnetic transition an enhanced specific heat, due to the magnetic contribution, is observed, having a maximum at the Curie-point (172°C and 308.5°C respectively). The results of the measurements are tabulated and discussed.

§ 1. *Introduction.* Experimental investigation of the specific heat of ferromagnetics in the vicinity of the Curie temperature is of interest as a test for the validity of the theories of ferromagnetism. The collective electron theory developed by Stoner¹⁾ and Wohlfart²⁾ gives the magnetic and electronic contribution to the specific heat, whereas statistical theories by Firgau³⁾ and Weiss⁴⁾ lead to expressions for the magnitude of the discontinuity in passing the Curie temperature.

Much experimental material has been collected regarding the more familiar ferromagnetics Fe, Ni and Co. Some work has also been done on compounds such as MnAs, MnP and a Heusler alloy⁵⁾. More recent are measurements on pure Gd-metal by Griffel et al⁶⁾. Practically no attention has been paid up to now to the lately found ferrimagnetics, of which ferrites are the prototype. Except for measurements by P. Weiss et al⁷⁾ on magnetite, Fe_3O_4 , which was then still considered as a ferromagnetic, and a Russian publication⁸⁾ on Mg–Zn ferrite, no mention has been made in the literature, to the authors' knowledge, of anomalies in the specific heat of ferrimagnetics. Measurements by Bates and Sherry⁹⁾

on the related magneto-thermal effect (heat exchanges accompanying magnetization processes) for Ni-Zn ferrite have been published.

We have tried to fill up this gap, and the purpose of this paper is to offer some new caloric measurements on two ferrimagnetics, namely Mn-Zn- and Ni-Zn-ferrite. The specific heat vs. temperature curve of these compounds for the range 20°C–350°C will be given, drawing special attention to the behaviour in the ferri-magnetic-paramagnetic transition region.

§ 2. *Apparatus and experimental procedure.* A vacuum adiabatic calorimeter of the classical Nernst type was used. This apparatus, shown diagrammatically in fig. 1, consists of a copper vessel heated

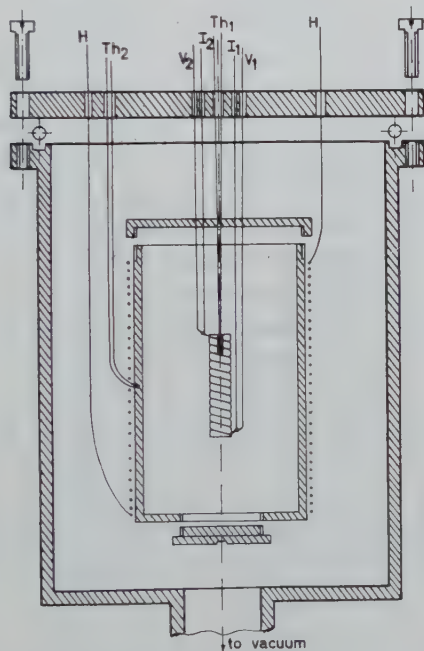


Fig. 1. Cross-sectional view of the calorimeter.

from the outside by a nickel-chromium wire, electrically insulated from the wall by a thin mica sheet. The vessel acts as an adiabatic wall and reduces the heat exchange between the sample and its surroundings. Thermal leaks are kept as small as possible by adjusting the temperature of the shielding. The sample is centrally

suspended in the calorimeter space. A helical groove of about 1 mm depth is cut in the surface of the ferrite samples by means of a diamond disk. In this groove a heating coil of 0.2 mm thick constantan wire is non-inductively wound. Current and potential wires are connected to the ends of the coil. A known amount of heat is applied to the ferrite by passing an electric direct current through the heating coil during an exactly known time interval. Calibrated silver-constantan thermocouples determine the temperatures of the sample and the adiabatic wall: one contact is introduced in a small hole in the ferrite and the wall respectively, while the other is immersed in melting ice. A small amount of waterglass insures good thermal contact between sample and thermoelement. Heat losses by conduction in the leads of the thermoelements were minimized by reducing the wire diameters. The thermo-e.m.f.'s are measured with a Diesselhorst compensator and a calibrated standard cell. The accuracy is of the order of $0.5 \mu\text{V}$, corresponding to an error in temperature smaller than 0.01°C . The entire system is suspended in a vacuum-sealed jar provided with vacuumtight connections for the thermocouples and the electric leads. All experiments are made in a vacuum better than $5 \times 10^{-5} \text{ mm Hg}$ provided by an oil diffusion pump. Calorimetric measurements are made as follows. The shielding wall and the ferrite are heated to a certain temperature θ_1 . When equilibrium is reached, heat (calculated from Joule's law) is supplied to the ferrite during a fixed time interval (2 to $2\frac{1}{2}$ min). As a consequence the temperature of the ferrite increases to θ_2 , calculated by means of the corresponding rise in the thermo-e.m.f. ($\theta_2 - \theta_1 \approx 1^\circ\text{C}$ to 1.5°C). With these experimental data, C_p at the temperature $\theta = \theta_1 + \frac{1}{2}(\theta_2 - \theta_1)$ is determined. Necessary corrections are made for the experimentally defined thermal leaks, using the small drift of temperature before and after the heating period.

§ 3. *Samples.* The measurements mentioned are made on commercially available sintered polycrystalline ferrites, namely a manganese-zinc ferrite ($\text{Mn}_{1-a}\text{Zn}_a\text{Fe}_2\text{O}_4$, $a \approx 0.38$, and a nickel-zinc ferrite $\text{Ni}_{1-a}\text{Zn}_a\text{Fe}_2\text{O}_4$, $a \approx 0.50$). The stoichiometric parameter a is determined without taking eventual impurities into account. These impurities can influence the molecular weight to some degree and account for small errors in the values of C_p .

TABLE I

The specific heat of $\text{Mn}_{1-a}\text{Zn}_a\text{Fe}_2\text{O}_4$ ($a \approx 0.38$)			
Temperature °C	Specific Heat cal degree ⁻¹ mole ⁻¹	Temperature °C	Specific Heat cal degree ⁻¹ mole ⁻¹
20	62.4	140	80
30	63.8	150	81.6
42.5	65.5	154.5	82.4
52	66.9	160	83.9
60	68.3	164	85.0
67.5	69.2	166	85.6
75	70.4	169	86.6
90	72.6	170	87.1
99	73.8	171	87.6
107.5	75.0	172	88.1
111	75.6	173.5	76.7
116	76.3	176.5	77.4
120	76.9	180	78.2
124.5	77.5	195	81.6
131.5	78.4	201	82.4

TABLE II

The specific heat of $\text{Ni}_{1-a}\text{Zn}_a\text{Fe}_2\text{O}_4$ ($a \approx 0.50$)			
Temperature °C	Specific Heat cal degree ⁻¹ mole ⁻¹	Temperature °C	Specific Heat cal degree ⁻¹ mole ⁻¹
22	43.5	263	59.0
30	43.8	272	59.7
43	44.3	285	60.6
52	45.0	291	61.1
75	45.7	296	61.6
89	46.2	299	61.9
100	46.9	301	62.1
110	47.5	304	62.4
124	48.4	308	62.8
137	49.2	313	53.5
148	50.2	316	53.7
160	51.1	319	54.0
171	51.8	326	54.5
185	53.0	331	55.9
196	53.7	342	57.7
207	54.6	355	58.5
220	55.6	360	59.0
230	56.4	371	59.7
239	57.1	380	60.4
251	58.0		

The measured samples were cylindrical rods with diameter and weight:

Mn-Zn ferrite: $2r = 5.2$ mm, $m = 2.037$ g,

Ni-Zn ferrite: $2r = 10.0$ mm, $m = 9.543$ g.

Better accuracy would have been obtained if larger quantities had been available. A difficulty arises from the rather small thermal conductivity of the ferrites. An interesting point is to know whether the applied heat is homogeneously distributed in the entire ferrite. This was experimentally checked, and we may conclude that as a

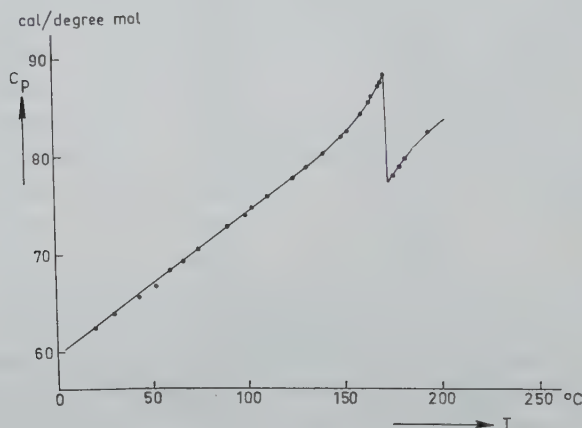


Fig. 2. Plot of the specific heat vs. temperature for a Mn Zn-ferrite.

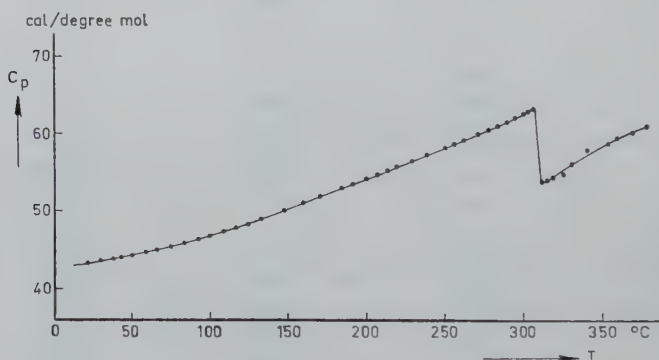


Fig. 3. Plot of the specific heat vs. temperature for a Ni Zn-ferrite.

consequence of the relatively small diameter of the cylinder and the rather deep cutting of the heater coil in the ferrite, homogeneous temperature distribution is rapidly attained. Starting from a constant homogeneously distributed temperature and changing abruptly the surface temperature, we have observed that the homogeneity was practically restored in less than one minute.

§ 4. *Results and discussion.* The measured data are tabulated in table I (Mn-Zn ferrite) and table II (Ni-Zn ferrite). These values are also plotted in fig. 2 and fig. 3 which show that the specific heat varies almost linearly with the temperature except in the region 150°C–180°C (Mn-Zn ferrite), 285°C–320°C (Ni-Zn ferrite), where it first rises and then sharply falls, also displaying the well known anomaly for ferromagnetics at the Curie-temperature. All the experimental points lie within 1% of the smooth curve. The Curie-temperatures following from our measurements are in good agreement with the values stated by Guillaud¹⁰). The temperatures where maxima are found for C_p are independent of the way these temperatures are reached. The curve was measured with rising and falling temperature, no thermal hysteresis being observed.

The quantitative interpretation of specific heat data for ferromagnetics is still rudimentary; no theory exists for ferrimagnetics except the possible application of the spinwave method at very low temperatures¹¹). Experiments of the type considered may in time serve as a guide for further modifications and adjustments of the theory of ferrimagnetism. More experimental work, especially at low temperatures, would be desirable. This would enable one to split the measured specific heat data into their different components and perhaps to compute the Debye-temperature and the thermodynamic functions; then it would be possible to compare results with those of the collective electron theory and the spinwave theory.

Our measurements reveal another interesting point that we would wish to consider: the magnitude of the discontinuity at the Curie-point. Shul'ha⁸) found a jump of approximately $2R \approx 4 \text{ cal/deg}^{-1} \text{ mole}^{-1}$ for a magnesium-zinc ferrite (exact composition unknown). For our manganese-zinc ferrite a discontinuity of approximately $6R \approx 12 \text{ cal/deg}^{-1} \text{ mole}^{-1}$ was found while for the nickel-zinc ferrite we found a jump of $4.6 R \approx 9.28 \text{ cal/deg}^{-1} \text{ mole}^{-1}$. (R is the universal gas-constant). If one takes values for the saturation moment n_B of these ferrites, as reported by Guillaud¹⁰) and Gorter¹²), a constant value of 1.7 for $\Delta C_p/n_B$ is found (table III). Accepting $\Delta C_p/n_B = 1.7$ for the MgZn ferrite in Shul'ha's experiment, we would find the value 2.35 for n_B . As Gorter¹²) gives values for n_B varying with the composition between 1 and 3.5, this result seems plausible. Research as to whether the mentioned proportionality between the anomaly in the specific heat and the magnitude of the saturation

TABLE III

Ferrite	ΔC_p (cal deg ⁻¹ mole ⁻¹)	n_B	$\Delta C_p/n_B$
Mn _{1-a} Zn _a Fe ₂ O ₄ $a \approx 0.38$	12.0 *)	6.7 **)	1.7
Ni _{1-a} Zn _a Fe ₂ O ₄ $a \approx 0.50$	9.28 *)	5.4 **)	1.7
Mg _{1-?} Zn _? Fe ₂ O ₄	4 ***)		

*) our measurements.

**) Guillaud¹⁰⁾, Gorter¹²⁾.

***) Shul'ha⁸⁾.

moment is accidental or a general law, is in progress. A general law would not be so unexpected as it could be qualitatively interpreted as a generalization for spinels of the results found for cubic structures by Firgau³⁾.

Acknowledgement. We are greatly indebted to the Nationaal Fonds voor Wetenschappelijk Onderzoek for sponsoring a research program of which this work is a part. It is also a pleasure to thank the technical staff of this laboratory for the careful construction of the mechanical equipment.

Received 11th June, 1959.

REFERENCES

- 1) Stoner, E. C., Proc. Roy. Soc. A **169** (1939) 339.
- 2) Wohlfart, E. P., Rev. Mod. Phys. **25** (1953) 211.
- 3) Firgau, V., Ann. Phys. Lpz. **40** (1941) 295.
- 4) Weiss, P. R., Phys. Rev. **74** (1948) 1493.
- 5) A comprehensive bibliography presents J. Jaffray, Ann. Phys. Paris **3** (1948) 5.
- 6) Griffel, M. et al., Phys. Rev. **93** (1954) 657.
- 7) Weiss, P., A. Piccard and A. Carrard, Arch. Sci. Phys. Nat. **43** (1917) 113.
- 8) Shul'ha, M. S., Ukrayin fiz. Zh. Dotatok **2** (1957) 54. (Physics Abstracts no. 6929, 1958).
- 9) Bates, L. F. and V. P. R. Sherry, Proc. Phys. Soc. B **68** (1955) 304.
- 10) Guillaud, C., J. Phys. Radium **13** (1951) 239.
- 11) Kranendonk, J. H. Van and J. H. Van Vleck, Rev. Mod. Phys. **30** (1958) 1.
- 12) Gorter, E. W., Saturation magnetization and crystal chemistry of ferrimagnetic oxides, Thesis Leiden 1954.

A RECIPROCITY THEOREM FOR THE ELECTROMAGNETIC FIELD SCATTERED BY AN OBSTACLE

by A. T. DE HOOP

Laboratorium voor Theoretische Elektrotechniek en Elektromagnetische Straling,
Technische Hogeschool, Delft, Netherlands

Summary

When a time-harmonic plane electromagnetic wave is incident upon a scattering obstacle of finite dimensions, the far-zone scattered field satisfies a reciprocity relation. This reciprocity relation is derived with the aid of H. A. Lorentz's theorem. The result is valid under rather general assumptions as far as the electromagnetic properties of the obstacle are concerned. As a special case, the result for a perfectly conducting obstacle is obtained.

§ 1. *Introduction.* In several branches of electromagnetic theory some kind of reciprocity theorem holds. Restricting ourselves to those branches where the field concept plays an essential role, we mention the relations between the transmitting and receiving properties of antennas ¹⁾²⁾ and the symmetry of the impedance (or admittance) matrix characterizing the properties of a waveguide junction ³⁾⁴⁾. The cited literature shows that the proof of the reciprocity relations under consideration is based upon a theorem due to H. A. Lorentz ⁵⁾.

When the scattering of a plane electromagnetic wave by an obstacle of finite dimensions is considered, it can be shown that a reciprocity relation exists for the far-zone scattered field. The special case of perfectly conducting obstacles has been investigated by Levine and Schwinger ⁶⁾ (scattering by a plane obstacle of vanishing thickness) and by Storer and Sevick ⁷⁾ (scattering by an obstacle of arbitrary shape). The proof given by these authors is based upon the integral equation to be satisfied by the surface-current density at the boundary of the obstacle.

In the present paper it is shown that the relevant reciprocity

relation holds in case the obstacle has rather general electromagnetic properties (for the precise conditions, see § 3) and is surrounded by a homogeneous, isotropic, non-conducting medium. The proof is based upon Lorentz's theorem.

Reciprocity relations in electromagnetic scattering problems have also been studied by Saxon⁸⁾. In studying Saxon's paper, the present author encountered some difficulties in understanding the physical meaning of his separation of the field at infinity into incident and outgoing spherical waves. In any case, the proof in the present paper is mathematically rigorous and the theorem applies to an idealization (plane-wave excitation) of a physically realizable situation. Our results agree with Saxon's reciprocity relation for plane-wave scattering.

§ 2. *The field outside the obstacle.* A time-harmonic, elliptically polarized, plane electromagnetic wave is incident upon an obstacle of finite dimensions. The boundary of the obstacle is a sufficiently regular closed surface S . The electric and magnetic properties of the obstacle are assumed to be linear; they will be specified in § 3. The medium in the domain outside S is assumed to be homogeneous, isotropic and non-conducting (which includes the case of free space), with permittivity ϵ_0 and permeability μ_0 . In the exterior domain, the electric field vector \mathbf{E} and the magnetic field vector \mathbf{H} are written as the sum of the incident field $\mathbf{E}^i, \mathbf{H}^i$ and the scattered field $\mathbf{E}^s, \mathbf{H}^s$:

$$\mathbf{E} = \mathbf{E}^i + \mathbf{E}^s, \quad (2.1)$$

$$\mathbf{H} = \mathbf{H}^i + \mathbf{H}^s. \quad (2.2)$$

Both the incident and the scattered field satisfy Maxwell's equations

$$\text{curl } \mathbf{H} = -i\omega\epsilon_0\mathbf{E}, \quad (2.3)$$

$$\text{curl } \mathbf{E} = i\omega\mu_0\mathbf{H}, \quad (2.4)$$

where ω is the angular frequency of the exponential time dependence of the form $\exp(-i\omega t)$. This factor, which is common to all field components, has been omitted throughout. In addition, the scattered field shall satisfy the radiation condition^{9)*)}

$$\int_{S_R} |\mathbf{E}^s - (\mu_0/\epsilon_0)^{1/2} (\mathbf{H}^s \times \mathbf{i}_R)|^2 dS = o(1) \quad (R \rightarrow \infty), \quad (2.5)$$

) For a vector \mathbf{A} whose components are complex numbers, we have $|\mathbf{A}|^2 = \mathbf{A} \cdot \mathbf{A}^$, where \mathbf{A}^* denotes the complex conjugate to \mathbf{A} .

where S_R is the surface of a sphere of radius R around some point of observation and \mathbf{i}_R is the unit vector in the direction of the outward normal to S_R .

Let $\mathbf{r} = (x, y, z)$ be the radius vector from a fixed origin to the point of observation. The origin is located at some finite distance from the obstacle. Further, the unit vector $\boldsymbol{\theta}$ in the direction of observation is introduced. Then, $\mathbf{r} = r\boldsymbol{\theta}$. If, now, the scattered field satisfies (2.3), (2.4) and (2.5), the following expansion holds¹⁰:

$$\mathbf{E}^s(\mathbf{r}) = \mathbf{F}(\boldsymbol{\theta}) \frac{e^{ikr}}{ikr} + O(r^{-2}) \quad (r \rightarrow \infty), \quad (2.6)$$

$$(\mu_0' \varepsilon_0)^{\frac{1}{2}} \mathbf{H}^s(\mathbf{r}) = [\boldsymbol{\theta} \times \mathbf{F}(\boldsymbol{\theta})] \frac{e^{ikr}}{ikr} + O(r^{-2}) \quad (r \rightarrow \infty), \quad (2.7)$$

where the (complex) factor $\mathbf{F}(\boldsymbol{\theta})$ is given by

$$4\pi \mathbf{F}(\boldsymbol{\theta}) = -k^2 \boldsymbol{\theta} \times \int_S [\mathbf{n} \times \mathbf{E}^s(\boldsymbol{\varrho})] \exp(-ik\boldsymbol{\theta} \cdot \boldsymbol{\varrho}) dS + \\ + (\mu_0' \varepsilon_0)^{\frac{1}{2}} k^2 \boldsymbol{\theta} \times \{ \boldsymbol{\theta} \times \int_S [\mathbf{n} \times \mathbf{H}^s(\boldsymbol{\varrho})] \exp(-ik\boldsymbol{\theta} \cdot \boldsymbol{\varrho}) dS \}, \quad (2.8)$$

in which $\boldsymbol{\varrho} = (\xi, \eta, \zeta)$ is the radius vector to the point of integration, and

$$k = \omega(\varepsilon_0 \mu_0)^{\frac{1}{2}} = 2\pi/\lambda, \quad (2.9)$$

λ being the wavelength in the medium outside the obstacle. The first term of the right-hand side of (2.6) and (2.7) is called the "far-zone approximation". Although S in (2.8) could be any sufficiently regular bounded closed surface completely surrounding the obstacle, it will be convenient to take S to be the boundary of the obstacle.

§ 3. *The field inside the obstacle.* The total field inside the obstacle, too, will be denoted by \mathbf{E} , \mathbf{H} . The electromagnetic properties of the obstacle are characterized by its tensor permittivity ε_{ij} , its tensor conductivity σ_{ij} and its tensor permeability μ_{ij} ($i, j = 1, 2, 3$). The field vectors $\mathbf{E} = (E_1, E_2, E_3)$ and $\mathbf{H} = (H_1, H_2, H_3)$ satisfy Maxwell's equations, which, in subscript notation, are

$$(\text{curl } \mathbf{H})_i = \sum_{j=1}^3 (\sigma_{ij} - i\omega\varepsilon_{ij}) E_j \quad (i = 1, 2, 3), \quad (3.1)$$

$$(\text{curl } \mathbf{E})_i = i\omega \sum_{j=1}^3 \mu_{ij} H_j \quad (i = 1, 2, 3). \quad (3.2)$$

It is assumed that ε_{ij} , σ_{ij} and μ_{ij} are symmetric tensors, i.e. $\varepsilon_{ij} = \varepsilon_{ji}$, $\sigma_{ij} = \sigma_{ji}$, $\mu_{ij} = \mu_{ji}$. Further, we impose the restriction that ε_{ij} , σ_{ij} and μ_{ij} are independent of the electric and magnetic field vector (thus excluding non-linear effects) and are continuous functions of position with the possible exception of a finite number of sufficiently regular bounded surfaces across which they may jump by finite amounts. If these conditions are satisfied, Lorentz's theorem holds¹¹).

Let \mathbf{E}_a , \mathbf{H}_a and \mathbf{E}_b , \mathbf{H}_b denote two vector fields which satisfy Maxwell's equations (3.1) and (3.2) in a certain domain, bounded by a sufficiently regular closed surface S . If \mathbf{n} is the unit vector in the direction of the outward normal to S , we have

$$\int_S (\mathbf{E}_a \times \mathbf{H}_b - \mathbf{E}_b \times \mathbf{H}_a) \cdot \mathbf{n} \, dS = 0. \quad (3.3)$$

Equation (3.3) is called Lorentz's theorem. The proof is easily obtained by making use of Maxwell's equations and Green's divergence theorem. Although S in (3.3) could be any sufficiently regular bounded closed surface, it will be convenient to take S to be the boundary of the obstacle.

§ 4. *Proof of the reciprocity theorem.* The vector fields \mathbf{E}_a , \mathbf{H}_a and \mathbf{E}_b , \mathbf{H}_b are chosen as follows. The field \mathbf{E}_a , \mathbf{H}_a is the total field due to an incident plane wave of the form

$$\mathbf{E}_a^i(\mathbf{r}) = \mathbf{A} \exp(-ik\boldsymbol{\alpha} \cdot \mathbf{r}), \quad (4.1)$$

$$\mathbf{H}_a^i(\mathbf{r}) = (\varepsilon_0/\mu_0)^{\frac{1}{2}} (\mathbf{A} \times \boldsymbol{\alpha}) \exp(-ik\boldsymbol{\alpha} \cdot \mathbf{r}), \quad (4.2)$$

where \mathbf{A} specifies the polarization of the wave (in general, elliptic) and $\boldsymbol{\alpha}$ is the unit vector pointing *towards* the source at infinity. Similarly \mathbf{E}_b , \mathbf{H}_b is the total field due to an incident plane wave of the form

$$\mathbf{E}_b^i(\mathbf{r}) = \mathbf{B} \exp(-ik\boldsymbol{\beta} \cdot \mathbf{r}), \quad (4.3)$$

$$\mathbf{H}_b^i(\mathbf{r}) = (\varepsilon_0/\mu_0)^{\frac{1}{2}} (\mathbf{B} \times \boldsymbol{\beta}) \exp(-ik\boldsymbol{\beta} \cdot \mathbf{r}). \quad (4.4)$$

Since the waves are transverse, we have $\mathbf{A} \cdot \boldsymbol{\alpha} = 0$ and $\mathbf{B} \cdot \boldsymbol{\beta} = 0$. From Lorentz's theorem (3.3) it follows that

$$\int_S (\mathbf{E}_a \times \mathbf{H}_b - \mathbf{E}_b \times \mathbf{H}_a) \cdot \mathbf{n} \, dS = 0, \quad (4.5)$$

where S is the boundary of the obstacle. Since $\mathbf{n} \times \mathbf{E}_{a,b}$ and

$\mathbf{n} \times \mathbf{H}_{a,b}$ are continuous across S , we need not indicate whether S is approached from the inside or the outside, respectively, when evaluating the integrand of (4.5).

In the first place we observe that

$$\int_{S_r} (\mathbf{E}_a^s \times \mathbf{H}_b^s - \mathbf{E}_b^s \times \mathbf{H}_a^s) \cdot \mathbf{n} \, dS = O(r^{-1}) \quad (r \rightarrow \infty), \quad (4.6)$$

where S_r is a sphere of radius r around the origin. This relation is proved by substituting (2.6) and (2.7) in the left-hand side of (4.6). Since Lorentz's theorem also applies to the domain bounded internally by S and externally by S_r , (4.6) implies that

$$\int_S (\mathbf{E}_a^s \times \mathbf{H}_b^s - \mathbf{E}_b^s \times \mathbf{H}_a^s) \cdot \mathbf{n} \, dS = 0. \quad (4.7)$$

Secondly, it can be shown that

$$\int_S (\mathbf{E}_a^i \times \mathbf{H}_b^i - \mathbf{E}_b^i \times \mathbf{H}_a^i) \cdot \mathbf{n} \, dS = 0. \quad (4.8)$$

Consequently, we obtain from (4.5), (4.7) and (4.8)

$$\begin{aligned} \int_S (\mathbf{E}_a^s \times \mathbf{H}_b^i - \mathbf{E}_b^i \times \mathbf{H}_a^s) \cdot \mathbf{n} \, dS = \\ = \int_S (\mathbf{E}_b^s \times \mathbf{H}_a^i - \mathbf{E}_a^i \times \mathbf{H}_b^s) \cdot \mathbf{n} \, dS. \end{aligned} \quad (4.9)$$

Now, we have from (2.8), using (4.3) and (4.4),

$$4\pi \mathbf{B} \cdot \mathbf{F}_a(\beta) = -(\mu_0/\epsilon_0)^{\frac{1}{2}} k^2 \int_S (\mathbf{E}_a^s \times \mathbf{H}_b^i - \mathbf{E}_b^i \times \mathbf{H}_a^s) \cdot \mathbf{n} \, dS. \quad (4.10)$$

Application of the identity (4.9) to the right-hand side of (4.10) yields the result

$$\mathbf{B} \cdot \mathbf{F}_a(\beta) = \mathbf{A} \cdot \mathbf{F}_b(\alpha). \quad (4.11)$$

Equation (4.11) is the reciprocity theorem to be proved.

The proof given above also applies to the case of a perfectly conducting obstacle. For, in this case each term of the left-hand side of (4.5) vanishes by virtue of the boundary condition: $\mathbf{n} \times \mathbf{E}_{a,b} = \mathbf{0}$ on S .

Received 19th June, 1959.

REFERENCES

- 1) Stevenson, A. F., Quart. Appl. Math. **5** (1948) 369.
- 2) King, R. W. P., Electromagnetic Engineering, Vol. I, McGraw-Hill Book Company, Inc., New York, 1945; p. 311.
- 3) Montgomery, C. G. et al., Principles of Microwave Circuits, M. I. T. Radiation Laboratory Series, Vol. 8, McGraw-Hill Book Company, Inc., New York, 1948; p. 141.
- 4) Flügge, S., Handbuch der Physik, Bd. 16, Elektrische Felder und Wellen, Springer, Berlin, 1958. Article by F. E. Borgnis and C. H. Papas; p. 399.
- 5) Lorentz, H. A., Versl. Kon. Akad. Wetensch. Amsterdam **4** (1895) 176.
- 6) Levine, H. and J. Schwinger, Comm. Pure Appl. Math. **3** (1950) 355.
- 7) Storer, J. E. and J. Seveck, J. Appl. Phys. **25** (1954) 369.
- 8) Saxon, D. S., Phys. Rev. **100** (1955) 1771.
- 9) Wilcox, C. H., Comm. Pure Appl. Math. **9** (1956) 115.
- 10) Hoop, A. T. de, Appl. sci. Res. **B 7** (1959) 463.
- 11) Stevenson, A. F., Ref. ¹⁾, Appendix.

WAVE PROPAGATION IN AN INHOMOGENEOUS TRANSVERSELY MAGNETIZED RECTANGULAR WAVEGUIDE

CHEN TO TAI

Instituto Tecnológico de Aeronáutica, São José dos Campos, Brasil

Summary

Wave propagation in an inhomogeneous transversely magnetized rectangular waveguide is studied with the aid of a modified Sturm-Liouville differential equation. A detailed discussion is given of the power relationship. Application of the Rayleigh-Ritz method to the approximate calculation of the eigenvalues is outlined, yielding a general secular determinantal equation. Several models are proposed to illustrate how the exact eigenvalues of this new class of boundary-value problems are to be determined.

§ 1. *Introduction.* Ever since Kales, Chait, and Sakiot¹⁾ first formulated the problem of a gyromagnetic slab in a rectangular waveguide magnetized by a transverse d.c. magnetic field, the same problem and similar ones have been studied by many others²⁻⁸⁾. In spite of these contributions there are still several important questions remaining unanswered. Among them we may mention the unidirectional paradox of Lax and Button³⁾ and the related problem concerning the nature of the evanescent modes. Little has been disclosed about the spectral distribution of the propagation constant pertaining to the evanescent modes.

In this article the problem is studied from a more general point of view. It is assumed that the medium is inhomogeneous in the broadside direction of the guide. The inhomogeneity can be either continuous or discontinuous. In these cases we obtained a differential equation for the electric field of the TE_{n0} modes. The equation is similar to the Sturm-Liouville differential equation, but with the eigenvalue appearing in a linear as well as in a quadratic term. Consequently, it has a very different characteristic from the

ordinary Sturm-Liouville equation. Many of the physical properties of such a waveguide can then be analyzed with the aid of that equation. This paper reports some preliminary results which have been obtained by this approach.

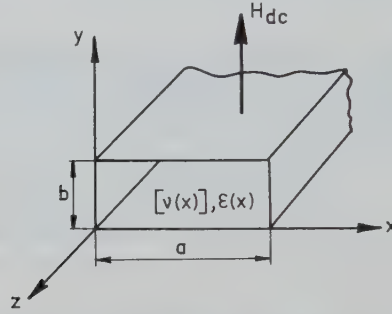


Fig. 1. An inhomogeneous gyromagnetic rectangular wave guide with a d.c. magnetic field applying in the y -direction.

§ 2. *Formulation.* The Maxwell equations for a harmonically oscillating field in a gyromagnetic inhomogeneous medium can be written in the form

$$\nabla \times \mathbf{E} = i\omega \mathbf{B}, \quad (1)$$

$$\nabla \times [\nu] \mathbf{B} = -i\omega \epsilon \mathbf{E}. \quad (2)$$

It is assumed that the time factor is $e^{-i\omega t}$. The magnetic reluctivity tensor $[\nu]$ and the dielectric constant ϵ are in general functions of position. It can be verified that in the case of an inhomogeneous gyromagnetic waveguide as shown in fig. 1, where the magnetic reluctivity tensor and the dielectric constant are only functions of x , there exists a set of transverse electric modes, the electric field of which has only one non-vanishing component E_y . By eliminating \mathbf{B} between (1) and (2) and assuming that the dependence of E_y upon x and z has the form of a guided wave, namely

$$E_y = E(x) e^{i\beta z}, \quad (3)$$

one obtains the following differential equation for $E(x)$:

$$\frac{d}{dx} \left[\nu_1 \frac{dE(x)}{dx} \right] + \left(-\beta^2 \nu_1 - \beta \frac{d\nu_2}{dx} + \omega^2 \epsilon \right) E(x) = 0, \quad (4)$$

where ν_1 and ν_2 are the elements of the magnetic reluctivity tensor

defined by

$$[\nu] = [\mu]^{-1} = \begin{bmatrix} \nu_1 & 0 & i\nu_2 \\ 0 & \nu_3 & 0 \\ -i\nu_2 & 0 & \nu_1 \end{bmatrix}. \quad (5)$$

It is to be remembered that ν_1 , ν_2 and ε are assumed to be functions of x only. In the case of a wave guide partially filled with gyromagnetic material with a constant applied magnetic field ν_1 , ν_2 and ε are given as three step functions.

§ 3. *Orthogonality and power relationship.* From (4) several important characteristics of the modes can be deduced. First of all, one observes that (4) differs from the ordinary Sturm-Liouville equation by the appearance of a linear term in β . Let us denote a typical eigenfunction by f_n and the corresponding eigenvalue by β_n ; then f_n satisfies the equation

$$\frac{d}{dx} \left(\nu_1 \frac{df_n}{dx} \right) + (-\beta_n^2 \nu_1 - \beta_n \frac{d\nu_2}{dx} + \omega^2 \varepsilon) f_n = 0. \quad (6)$$

The boundary condition for f_n is

$$f_n(0) = f_n(a) = 0. \quad (7)$$

For a lossless medium $[\nu]$ is hermitian. Under this condition it can be shown by means of (6) and a similar equation for f_m that the following orthogonal relationship exists between f_n and f_m :

$$(\beta_n - \beta_m^*) \int_0^a \left[(\beta_n + \beta_m^*) \nu_1 + \frac{d\nu_2}{dx} \right] f_n f_m^* dx = 0. \quad (8)$$

Equation (8) is a special case of a more general orthogonal relationship obtained previously by Walker⁹). There is, however, an apparent difference between the two derivations. In Walker's analysis, the relationship was derived by means of a divergence identity. The behaviour of the guided wave at infinity, therefore, must be postulated. Such an assertion is not required in the present derivation. Another orthogonal relationship, with no restriction to the hermitian property of $[\nu]$, is

$$(\beta_n - \beta_m) \int_0^a \left[(\beta_n + \beta_m) \nu_1 + \frac{d\nu_2}{dx} \right] f_n f_m dx = 0. \quad (9)$$

By using the known solutions for a rectangular waveguide partially filled with gyromagnetic material ^{1,2)} we have verified the validity of (8) and (9). The fact that the weighting factor in (8) and (9) contains the eigenvalues, imposes a serious limitation upon the normal expansion of an arbitrary function in terms of these "pseudo-orthogonal" functions. However, we are going to show that as a result of (8) there is no coupling of power between the different TE_{n0} modes, and in addition, the evanescent modes are not carriers of power flowing in the guide in spite of the fact that they are characterized by a complex propagation constant.

Thus, if we let

$$E_y = \sum A_n f_n e^{-i\beta_n z}, \quad (10)$$

then the power flowing in the guide in the positive direction of z is given by

$$\begin{aligned} P(z) &= -\frac{1}{4} \iint (E_y H_x^* + E_y^* H_x) dS = \\ &= \frac{b}{2\omega} \sum |A_n|^2 e^{i(\beta_n - \beta_n^*)z} \int_0^a \left[(\beta_n + \beta_n^*) v_1 + \frac{dv_2}{dx} \right] |f_n|^2 dx. \end{aligned} \quad (11)$$

In deriving (11) we have already made use of (8) for $n \neq m$. It is seen from (8) that when $n = m$ and β_n is complex, corresponding to the propagation constant of the evanescent mode,

$$\int_0^a \left[(\beta_n + \beta_n^*) v_1 + \frac{dv_2}{dx} \right] |f_n|^2 dx = 0; \quad (12)$$

hence, the terms in (11) which are responsible for the transport of power in the guide are those with β_n real. The net power flow is then given by

$$P = \frac{b}{2\omega} \sum |A_n|^2 \int_0^a \left(2\beta_n v_1 + \frac{dv_2}{dx} \right) |f_n|^2 dx. \quad (13)$$

The summation is to be taken over all the real β_n . Since P is independent of z , the result is compatible with the hermitian property of $[v]$.

§ 4. *Application of the Rayleigh-Ritz method to the approximate calculation of the eigenvalues.* Although we have not yet found an elegant method to analyze the spectral distribution of the eigen-

values pertaining to the modified Sturm-Liouville equation, it may be of some interest to present here a formal extension of the Rayleigh-Ritz method originally devised for the ordinary Sturm-Liouville differential equation. By multiplying (6) by f_n and integrating with respect to x from 0 to a one obtains

$$A\beta_n^2 + B\beta_n + C = 0, \quad (14)$$

where

$$A = \int_0^a v_1 f_n^2 dx, \quad (15)$$

$$B = \int_0^a \frac{dv_2}{dx} f_n^2 dx, \quad (16)$$

$$C = \int_0^a \left[v_1 \left(\frac{df_n}{dx} \right)^2 - \omega^2 \epsilon f_n^2 \right] dx. \quad (17)$$

It can be verified that (14) is a variational expression for β_n . It is a special case of a more general one obtainable by means of Rumsey's reaction method as cited by Berk¹⁰). For the approximate calculation of β_n we let

$$f_n = \sum_{p=1}^N k_p u_p, \quad (18)$$

where u_p denotes a set of orthogonal functions satisfying the orthogonal relation

$$\int_0^a v_1 u_p u_q dx = \delta_{pq} \quad (19)$$

and the boundary condition $u_p(0) = 0$ and $u_p(a) = 0$. In (19), δ_{pq} denotes the Kronecker delta function. Following the usual procedure, which leads to a secular determinantal equation, one finds

$$\text{Det } |\beta_n^2 \delta_{pq} + \beta_n B_{pq} + C_{pq}| = 0 \quad (20)$$

with $p, q = 1, 2, \dots, N$, where

$$B_{pq} = \int_0^a \frac{dv_2}{dx} u_p u_q dx, \quad (21)$$

$$C_{pq} = \int_0^a \left(v_1 \frac{du_p}{dx} \frac{du_q}{dx} - \omega^2 \epsilon u_p u_q \right) dx. \quad (22)$$

In the case that $dv_2/dx = 0$, leading to $B_{pq} = 0$, (6) reduces to the ordinary Sturm-Liouville equation, and (20) becomes the well-known secular determinantal equation for that case.

It is also evident from (14) that the condition for the existence of the reciprocal modes, with $\beta_n^+ = -\beta_n^-$, requires B to be zero. To meet this requirement v_2 has to be a symmetrical function of x with respect to the centre of the guide. Non-reciprocal modes prevail when v_2 is not symmetrical.

§ 5. *Some models for studying the spectral distribution of the eigenvalues.* While little is yet known about the general theory concerning the spectral distribution of the eigenvalues of the modified Sturm-Liouville equation, several "academic" models are proposed here to illustrate how the exact eigenvalues of some specific problems can be determined. We would like to remark here that the inhomogeneity of v_1 and v_2 can be attributed either to an inhomogeneous d.c. magnetic field or to an inhomogeneous medium. Thus, one has a certain freedom in choosing the functional dependence of v_1 , v_2 and ε upon x . We list here a few cases in which (4) can be solved in terms of known functions.

Case I.

$$\varepsilon = c_0 e^{\alpha x}, \quad v_1 = c_1 e^{\alpha x}, \quad dv_2/dx = c_2 e^{\alpha x}.$$

In this case, the solution for (4) is relatively simple, being given by

$$E(x) = A e^{-\frac{1}{2}\alpha x} \sin(k^2 - \frac{1}{4}\alpha^2 - s\beta - \beta^2)^{\frac{1}{2}}, \quad (23)$$

where $k^2 = \omega^2 c_0' c_1$ and $s = c_2' c_1$. The characteristic equation for determining β_n is

$$k^2 - \frac{1}{4}\alpha^2 - s\beta_n - \beta_n^2 = \left(\frac{n\pi}{a}\right)^2, \quad n = 1, 2, \dots \quad (24)$$

It is to be observed that when v_1 is linear in dv_2/dx , the modified Sturm-Liouville equation is reducible to the ordinary type. However as far as the eigenvalues β_n are concerned, we still have in general two different values of $|\beta_n|$ pertaining to the two non-reciprocal modes of the same order.

Case II.

$$\varepsilon = c_0, \quad v_1 = c_1 e^{\alpha x}, \quad dv_2/dx = c_2 e^{\alpha x}.$$

By changing the independent variable to ξ , defined by

$$\xi = e^{-\alpha x}, \quad (25)$$

the solution for $E(\xi)$ is found to be

$$E(\xi) = \xi^{\frac{1}{2}} Z_{\mu} \left(\frac{2k}{\alpha} \xi \right), \quad (26)$$

where Z denotes a general cylindrical function and

$$\mu = [1 + \frac{4}{\alpha^2} (\beta^2 + s\beta)]^{\frac{1}{2}}, \quad k = \omega \left(\frac{c_0}{c_1} \right)^{\frac{1}{2}}, \quad s = \frac{c_2}{c_1}.$$

It is noticed that the order of the cylindrical function is dependent upon the eigenvalue. The latter is to be determined by imposing the boundary condition that at $\xi = 1$ and $\xi = e^{-\alpha a}$ the function vanishes.

Case III.

$$\varepsilon = c_0(1 + \alpha x), \quad v_1 = c_1(1 + \alpha x), \quad dv_2/dx = c_2\alpha.$$

By changing the independent variable to η , defined by

$$\eta = 1 + \alpha x, \quad (27)$$

(4) can be transformed into the confluent hypergeometric equation. The solution for $E(\eta)$ is then given by

$$E(\eta) = \eta^{-\frac{1}{2}} W_{k,0} [2(\lambda^2 - h^2)^{\frac{1}{2}} \eta], \quad (28)$$

where $W_{k,0}$ denotes a general Whittaker function with order m equal to zero and

$$h^2 = \left(\frac{\omega}{\alpha} \right)^2 \frac{c_0}{c_1}, \quad \lambda^2 = \left(\frac{\beta}{\alpha} \right)^2,$$

$$k^2 = -\frac{1}{2} s \lambda (\lambda^2 - h^2)^{-\frac{1}{2}}, \quad s = c_2/c_1.$$

The eigenvalue β is to be determined by imposing the boundary condition that at $\eta = 1$ and $\eta = 1 + \alpha a$ the function must vanish.

Analytically, the computation of β for cases II and III is not simple at all. These examples serve mainly to illustrate the intricate nature of this class of boundary-value problems.

Finally, we may mention that the modified Sturm-Liouville equation occurs also in problems dealing with an inhomogeneous

circular or sectorial waveguide with the d.c. magnetic field applying in the axial direction. In either case the electric field component E_ϕ pertaining to the TE_{n0} modes satisfies the following differential equation:

$$\frac{d}{dr} \left[\frac{\nu_1}{r} \frac{d}{dr} (r E_\phi) \right] + \left[-\beta^2 \nu_1 + \beta \left(\frac{\nu_2}{r} - \frac{d\nu_2}{dr} \right) + \omega^2 \varepsilon \right] E_\phi = 0, \quad (29)$$

where ν_1 , ν_2 and ε have the same significance as previously except that they are now functions of r . For the homogeneous case, corresponding to constant ν_1 , ν_2 and ε , the equation can be transformed into the confluent hypergeometric equation. Solutions for the open domain have been studied by Suhl and Walker¹¹). It is obvious that the treatment which we have given to the rectangular case, such as the orthogonality and the variational method, can readily be applied to (29) with slight modifications.

Acknowledgement. The author is grateful to Professor Yutze Chow and Professor Guido Beck for many valuable discussions during the course of this study.

Received 22nd September, 1959.

REFERENCES

- 1) Kales, M. L., H. N. Chait and N. G. Sakiotis, J. Appl. Phys. **24** (1953) 816.
- 2) Lax, B., K. J. Button and L. M. Roth, J. Appl. Phys. **25** (1954) 1413.
- 3) Lax, B. and K. J. Button, J. Appl. Phys. **26** (1955) 1184.
- 4) Weibaum, S. and H. Boyet, J. Appl. Phys. **27** (1956) 519.
- 5) Seidel, H., J. Appl. Phys. **28** (1957) 218; **36** (1957) 409 Bell Sys. Techn. J.
- 6) Morganthaler, F. R., Proc. Instn Radio Engrs **45** (1957) 1407.
- 7) Straus, T. M., Wescon Record, Part I, pp. 135-146. Institute of Radio Engineers, 1958.
- 8) Soohoo, R. F., Proc. Instn Radio Engrs **46** (1958) 788.
- 9) Walker, L. R., J. Appl. Phys. **28** (1957) 377.
- 10) Berk, A. D., Trans. Prof. Group of Antennas and Propagation Instn Radio Engrs, AP-4 (1956) 104.
- 11) Suhl, H., and L. R. Walker, Bell. Sys. Tech. J. **33** (1954) 939.

INFRARED SPECTRA OF ION-PRODUCING SPECIES IN HYDROCARBONS

by ANDREW GEMANT

Engineering Research Department, The Detroit Edison Company, Detroit, Michigan,
U.S.A.

Summary

Infrared absorption spectroscopy is applied to the study of liquid hydrocarbons having high electrical conductivities. In conjunction with other methods, this technique permits conclusions to be drawn concerning the reaction mechanism, notably addition-compound formation, which precedes dissociation into free ions. Results with two particular systems, one of which involves oxidation with ozone, are presented.

Measurements of the electrical conductivity of hydrocarbon dielectrics have established that ions are generated as a result of oxidation. One of the major problems in this connection concerns the reaction mechanism that leads to the formation of ion-producing species in the hydrocarbon solvent. In the writer's previous studies ¹⁾, elucidation of the reaction mechanism was attempted by means of several approaches, such as: 1. use of reactants with known primary reaction products; 2. action of certain inhibitors which prevent ion-formation; 3. absorption spectroscopy in the ultraviolet; and 4. use of radioactively labeled reactants and adsorption on ion-exchange resins ²⁾.

Absorption spectroscopy in the infrared has now been tried in addition to these methods. Infrared spectra are particularly suitable for establishing groups and bonds present in unknown species, and it was thought promising to use that technique in connection with the problem at hand. The results of that study are presented in this paper.

As a well-defined and reproducible system of an oxidized hydrocarbon, ozonized solutions of an aromatic compound in the pre-

sence of an aliphatic acid in an alicyclic solvent were used; such a system was previously studied and described by the writer ¹). The aromatic hydrocarbon chosen for this study was naphthalene, and the aliphatic acid was lauric acid, both in 50 mM/l concentration. The solvent was methylcyclohexane, replaced in some tests by CCl_4 . The former transmits infrared radiations satisfactorily in the wave-number region between 1200 and 650 cm^{-1} , and the latter between 5000 and 1200 cm^{-1} . Successive use of both solvents gives a fairly complete absorption spectrum. Ozonization was carried out at room temperature for 15 or 30 minutes, with a constant current in the ozonizer. A Beckman IR-5 infrared spectrophotometer was used in conjunction with a NaCl cell having a length of 0.1 mm.

In the presentation and analysis of absorption spectra only those bands will be considered that show characteristic changes as a result of O_3 action. It is realized that caution is required in arriving at conclusions from infrared spectra, and that the evidence for the presence of certain groups and bonds has value only in conjunction with proofs of other nature.

Figs 1 and 2 present the absorption spectra of the system in

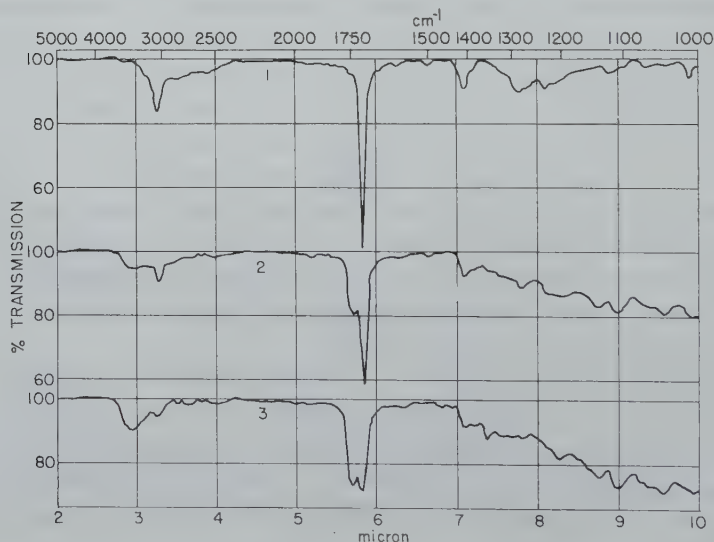


Fig. 1. Infrared spectra of naphthalene and lauric acid (each 50 mM/l) in methylcyclohexane. Range of spectrum from 5000 to 1000 cm^{-1} . Time of ozonization for curve 1, none; curve 2, 15 minutes; curve 3, 30 minutes.

methylcyclohexane in the wave-number regions of 5000 to 1000 and 1000 to 650 cm^{-1} respectively. Each figure contains three absorption spectra referring to zero, 15 and 30 minutes of ozonization times. Four significant changes, observable in the course of ozonization, are found in the absorption curves. These changes will now be discussed.

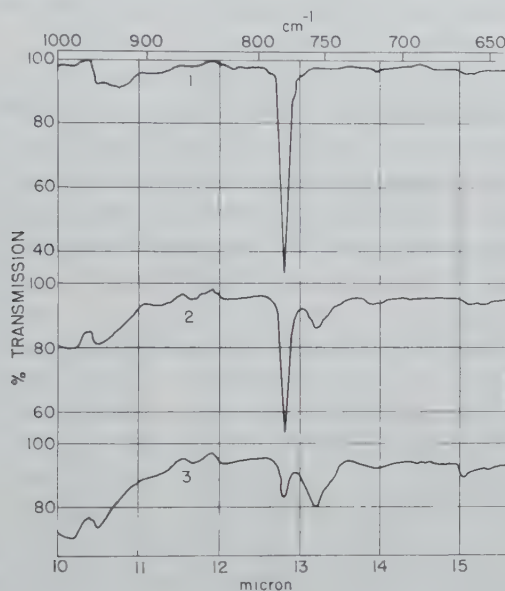


Fig. 2. Infrared spectra of naphthalene and lauric acid (each 50 mM/l) in methylcyclohexane. Range of spectrum from 1000 to 650 cm^{-1} . Time of ozonization for curve 1, none; curve 2, 15 minutes; curve 3, 30 minutes.

In fig. 1, curve 1 a broad peak is seen with a maximum at 3050 cm^{-1} , which is characteristic of the stretching frequency of the dimerized OH group in carboxylic acids³⁾. In curves 2 and 3 this peak decreases and is replaced by another broad peak whose maximum is at 3400 cm^{-1} . This peak is generally considered⁴⁾ as due to OH intermolecularly bonded in polymeric association, its location being 3400 to 3200 cm^{-1} . Thus the bond of OH in the carboxyl dimers changes in the course of O_3 action to an intermolecular bond with another molecule. This conclusion will be utilized in the course of analysis of further bands.

The second major change as a result of ozonization is found in

the sharp peak at 1710 cm^{-1} of curve 1. This peak is due to the stretching frequency of CO which in saturated carboxylic acids is found at that location ⁵). During ozonization this peak gradually diminishes from 59 per cent absorption to 42 per cent at 15 minutes O_3 action, and 29 per cent after 30 minutes. Simultaneously another peak appears, shifted to a higher frequency, about 1750 cm^{-1} ; this peaks corresponds to 20 per cent absorption after 15 minutes and 27 per cent after 30 minutes.

If, according to the shift of the OH peak, the hydroxyl becomes bound to another molecule, the CO group, too, must be associated with the other molecule, and its shift of frequency is explainable on that basis. Whereas the identity of the compound molecule cannot be stated, there are many observations to the effect that a shift of the CO band to higher frequencies take place when the carbonyl is joined to another group. A theoretical explanation of such an effect was given by Halford ⁶).

Various examples of such an effect may be quoted, such as lactone formation. The writer found the CO peak in butyrolactone in solution to be at 1780 cm^{-1} . Extensive studies along these lines were carried out by Rasmussen ⁷) and Marion ⁸). Another instance of a similar kind is ester formation ⁹). The writer examined ethyl myristate in solution and found the peak at 1740 cm^{-1} , close to where it is found in fig. 1, curve 3. There is, accordingly, agreement between the interpretation of the OH and CO shifts observed.

The third change occurs mainly between 1200 and 1000 cm^{-1} : various broad peaks of high intensity, not present in curve 1, are found developed in curves 2 and 3. The most likely explanation of these bands is formation of ozonides from the aromatic compound. Criegee ¹⁰) as well as Briner ¹¹) established the main region of ozonide bands at $1060\text{--}1040\text{ cm}^{-1}$. It can be seen that the maximum of the bands in the present instance lies between 1100 and 1000 cm^{-1} . Ozonide precursor formation is actually the first reaction to take place in the system under consideration, leading, in the absence of the acid, to a precipitate. The solution remains clear in the presence of the acid.

The fourth significant change refers to the sharp peak at 780 cm^{-1} , fig. 2, curve 1. This peak is appreciably reduced in the course of the reaction. From 67 per cent absorption it is reduced to 47 per cent after 15 minutes and 17 per cent after 30 minutes. A new broader

peak at 755 cm^{-1} appears with 14 per cent intensity after 15, and 20 per cent intensity after 30 minutes.

The original peak is characteristic of naphthalene¹²⁾ and is usually interpreted as out-of-plane deformation vibration of the CH bond in the aromatic ring. The position of this peak depends, however, on the nature of substitutions. Ortho-di-substituted aromatic rings absorb at frequencies between 770 and 735 cm^{-1} ¹³⁾. Orr and Thompson¹⁴⁾ observed a strong band near 750 cm^{-1} with ortho-di-substituted compounds. Measuring the absorption of o-xylene, the writer found the peak at 740 cm^{-1} . The coincidence of these positions with the one observed in fig. 2 points to the formation of o-substituted compounds from naphthalene. Since the OH and CO peaks of the acid indicated an attachment of the latter to another molecule, a plausible explanation of the shift of the aromatic band is the formation of an addition compound between an acid molecule and an aromatic molecule in the o-position. This compound is formed following the formation of the ozonide precursor (see later).

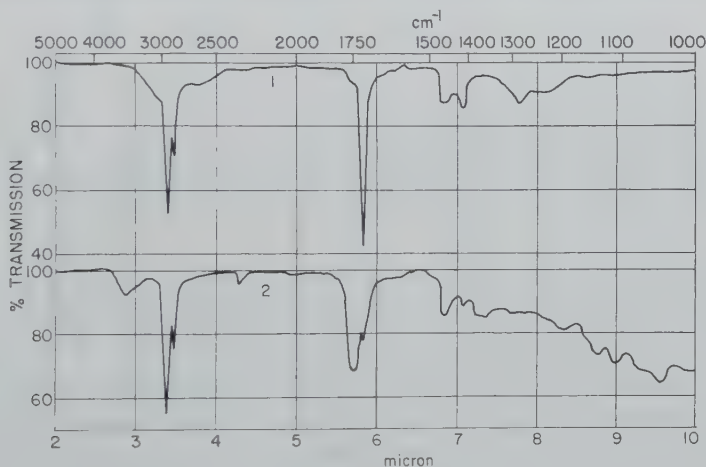


Fig. 3. Infrared spectra of naphthalene and lauric acid (each 50 mM/l) in carbon tetrachloride. Time of ozonization for curve 1, none; curve 2, 30 minutes.

In fig. 3 corresponding absorption spectra in carbon tetrachloride are presented. Since that solvent absorbs strongly between 800 and 700 cm^{-1} , the aromatic peaks are missing and the extension of the curves beyond 1000 cm^{-1} is not shown. There are two sharp

peaks between 2900 and 2800 cm^{-1} , characteristic of the CH_2 stretching frequency; these are not pronounced in fig. 1 since methylcyclohexane absorbs in that region. These peaks are superimposed on the OH dimer band in curve 1 and are unaffected by O_3 , as was to be expected. The shift of the bonded OH band to 3400 cm^{-1} is pronounced. The behaviour of the CO band is also similar to that in methylcyclohexane, a shift from 1710 to 1750 cm^{-1} taking place. The same conclusions can therefore be drawn from an analysis of absorption curves in both solvents.

Beside aliphatic acids cholesterol was found to lead to high electrical conductivities when oxidized in the manner described. It was surmised that acids formed upon ozonization of cholesterol act similarly to aliphatic acids. Such a system was examined by means of the infrared technique; the result is shown in fig. 4.

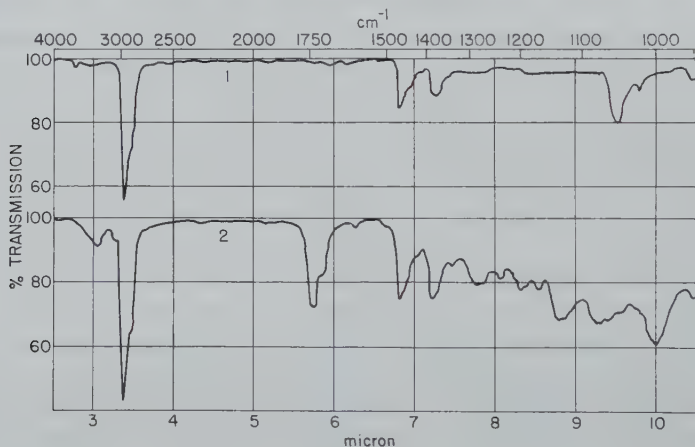


Fig. 4. Infrared spectra of naphthalene and cholesterol (each 50 mM/l) in carbon tetrachloride. Time of ozonization for curve 1, none; curve 2, 15 minutes.

Curve 1 indicates a small peak at 3600 cm^{-1} due to the free OH of cholesterol. No carboxyl peaks, of course, are found. In curve 2, OH bonded appears at 3300 cm^{-1} . Two peaks appear at 1700 and 1740 cm^{-1} , the latter larger than the former. This confirms the view that carboxyl is formed, which subsequently becomes attached to another molecule. The location of this carboxyl is very likely the side chain of cholesterol, as in cholic acid. Various

ozonide peaks, such as at 1000, 1080 and 1130 cm^{-1} , are also to be seen in curve 2.

In the previous work it was observed that certain compounds, notably unsaturated hydrocarbons and alcohols, inhibited the production of conductivities, i.e., of a high ion content. As for the olefins, they probably compete with the aromatic compound for ozone. Concerning the alcohol, the mechanism is a different one.

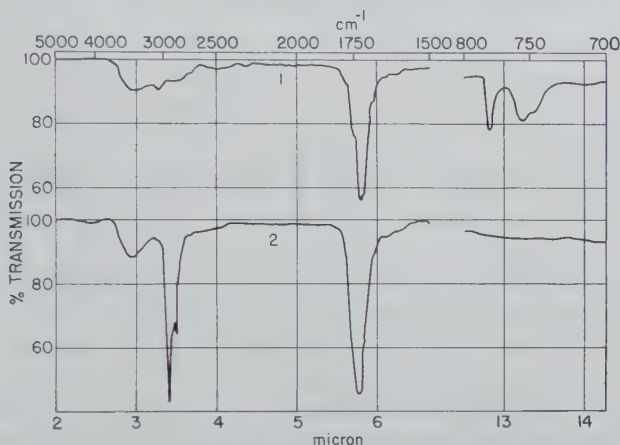


Fig. 5. Infrared spectra of naphthalene, lauric acid (each 50 mM/l) and *n*-butyl alcohol (100 mM/l) in methylcyclohexane (curve 1) and carbon tetrachloride (curve 2). Ozonization for 30 minutes.

Fig. 5 shows absorption spectra for the naphthalene system, containing, in addition, 100 mM/l *n*-butylalcohol. Curve 1 refers to methylcyclohexane, curve 2 to carbon tetrachloride, both after 30 minutes ozonization. These are to be compared with curves 3 of figs 1 and 2, and curve 2 of fig. 3, referring to the corresponding alcohol-free systems. The OH peaks, as well as those resulting from the aromatic are the same, whether the alcohol is present or not. This shows that hydrogen bonding to the ozonide precursor is present in both cases.

A difference, however, is found in the CO peaks. They are neither the original sharp peaks at 1710 cm^{-1} , nor do they show the broad peak at 1750 cm^{-1} , having rather an intermediate shape between the two. It follows from this that alcohol interferes with the formation of an addition compound between the acid and the aromatic.

Alcohol thus competes with the acid for the ozonide precursor, and, although acid probably binds part of the precursor, the bulk of the latter is being combined with alcohol. The new addition compound has no tendency to dissociate into ions, hence the suppression of high electrical conductivities. This mechanism of the action of an alcohol, which is borne out by the infrared spectrum, was suggested as a possible one in the previous publication. It is also confirmed by the radioactive method mentioned ²⁾.

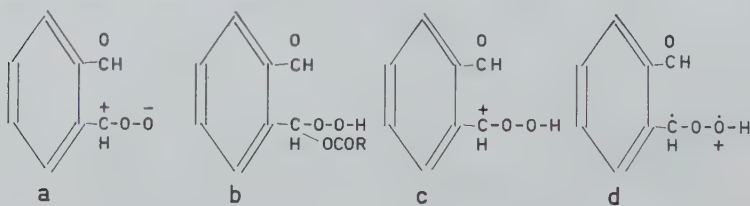


Fig. 6. Ionic species as developed from the zwitterion (a), after combining with an aliphatic acid (b) and subsequent dissociation (c). Stabilization by resonance with other ionic structures (d).

It may be pointed out that infrared spectroscopy, like the technique using ion-exchange resins, does not give specific information on free ions. These methods do not differentiate between an ion-forming compound and the free ion if the concentration of the latter is much smaller than that of the former, such as aniline and aniline cation in a solution of the base, for instance. The infrared spectra do, however, show that in the present instance acid forms an addition compound with an ozonide precursor of the aromatic. This addition compound may be considered as crypto-ionic which to a small extent dissociates into free ions; the cation is in all probability the aromatic ²⁾, the anion the aliphatic structure. Infrared spectra in conjunction with other methods thus appear to give sufficient information on the problem.

The results of the present study as well as the previous results of the author ¹⁾ are in agreement with recent studies of Criegee ¹⁵⁾ and Bailey ¹⁶⁾ on ozonolysis of aromatics. The main precursor is assumed to be the zwitterion, fig. 6a, which, in the presence of an aliphatic acid, for instance, adds to the latter (fig. 6b). This addition compound is probably the one inferred by the present author. The ionic species observed may be due to dissociation into

an aliphatic acid anion and a carbonium cation (fig. 6c). This cation is probably stabilized by resonance with other structures, such as a diradical oxonium cation (fig. 6d), similar to the structures ascribed to anthraquinone and fluorenone cations¹⁷).

In conclusion, infrared spectra of a related, although different kind of conducting solution in hydrocarbons, in which no oxidation is involved, are presented in fig. 7. These solutions, containing an aliphatic acid, an amine and a phenol in hydrocarbon were observed and described earlier by the writer¹⁸). Phenol was considered as a hydrogen bonded solvating compound for the ions formed by dissociation of the acid-amine salt.

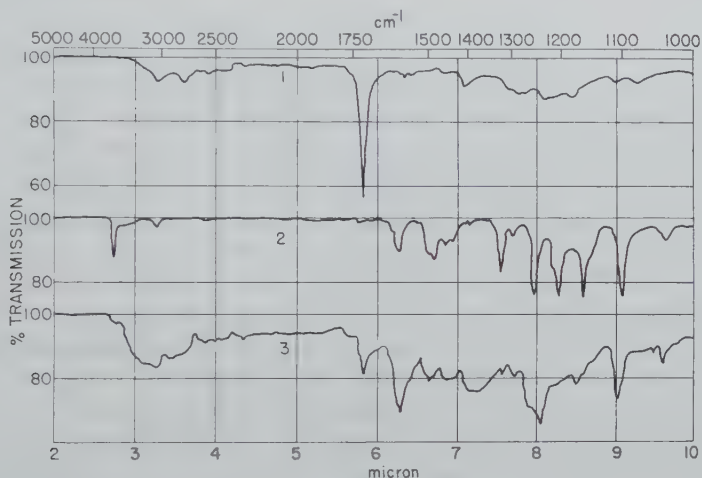


Fig. 7. Infrared spectra of lauric acid, tri-*n*-butylamine (each 50 mM/l) and *o*-cresol (70 mM/l) in methylcyclohexane, curve 1: acid and amine, curve 2: cresol, curve 3: acid, amine and cresol.

Curve 1, acid and amine, shows the OH dimer frequency at 3000, and the free CO frequency of lauric acid at 1720 cm^{-1} . Curve 2, *o*-cresol, shows free OH vibration at 3650 cm^{-1} and a peak at 1590 cm^{-1} due to the C=C stretching vibration. The CH vibration frequency of the *o*-substituted aromatic ring is at 748 cm^{-1} (not shown). When the three compounds are combined, the absorption curve shows the following changes (curve 3).

Free OH is practically absent; instead, a broad band from 3500 to 2700 cm^{-1} appears, indicating OH bonded. This bands may be due to bonding of hydroxyl of both lauric acid and cresol. The

free Co peak is reduced from 43 to 19 per cent, indicating a combination of the acid to amine; there is no noticeable second peak at a higher frequency. The C=C aromatic peak at 1590 cm^{-1} is increased from 11 to 31 per cent. According to Bellamy¹⁹ this is a sign of the presence of a carbonyl in the vicinity of the ring and subsequent conjugation. It could be interpreted in this case as hydrogen bonding of the cresol hydroxyl to the carboxyl of lauric acid, substantiating the earlier assumption concerning addition compound formation between cresol and acid-amine salt.

Received 9th October, 1959.

REFERENCES

- 1) Gemant, A., J. Electrochem. Soc. **102** (1955) 454; Appl. Sci. Res. **A6** (1956) 1.
- 2) Gemant, A., Z. physik. Chemie N.F. (1960) in print.
- 3) Corish, P. J. and D. Chapman, J. Chem. Soc. (1957) 1746.
- 4) Kuhn, L. P., J. Amer. Chem. Soc. **74** (1952) 2492.
- 5) Flett, M. S. C., J. Chem. Soc. (1951) 962.
- 6) Halford, J. O., J. Chem. Phys. **24** (1956) 830.
- 7) Rasmussen, R. S. and R. R. Brattain, J. Amer. Chem. Soc. **71** (1949) 1073.
- 8) Marion, L. et al, J. Amer. Chem. Soc. **73** (1951) 305.
- 9) Hampton, R. R. and J. E. Newell, Analyt. Chem. **21** (1949) 914.
- 10) Criegee, R., et al., Chem. Ber. **88** (1955) 1878.
- 11) Briner, E. and E. Dallwigk, Helv. Chim. Acta **39** (1956) 1446.
- 12) Eucken, A. and K. H. Hellwege, Landolt-Börnstein Zahlenwerte und Funktionen, 6th ed., Vol. I, part 2/I., p. 400, Springer, Berlin 1951.
- 13) Colthup, N. B., J. Opt. Soc. Amer. **40** (1950) 397.
- 14) Orr, S. F. D. and H. W. Thompson, J. Chem. Soc. (1950) 218.
- 15) Criegee, R., Record Chem. Progress **18** (1957) 111.
- 16) Bailey, P. S., Chem. Rev. **58** (1958) 925.
- 17) Leffler, J. E., The reactive Intermediates of Organic Chemistry, p. 44, Interscience, New York 1956.
- 18) Gemant, A., J. Phys. Chem. **54** (1950) 569.
- 19) Bellamy, L. J., Infrared Spectra of Complex Molecules, 2nd ed. p. 72, Methuen, London 1958.

ON THE MOTION OF A CHARGED PARTICLE IN AN ALMOST HOMOGENEOUS MAGNETIC FIELD

by L. J. F. BROER and L. VAN WIJNGAARDEN

Mededeling no. 91 uit het Laboratorium voor Aero- en Hydrodynamica van de
Technische Hogeschool te Delft, Netherlands

Summary

In the first part of this paper the motion of a particle in a slowly varying homogeneous field is studied. An expansion is given for the dominating spiralling part of the motion. It is found that the centre of this motion will drift slowly. Calculation of the drift amounts to the determination of the reflection in an equivalent wave propagation problem. In the remaining section the motion in constant, nearly homogeneous fields is treated, partly using the same method. In a few representative cases it is shown that the first approximation reproduces results given by Alfvén and Spitzer, while some results are given in second approximations.

§ 1. *Introduction.* The problem of an electrically charged particle moving in a slowly varying homogeneous magnetic field is an old one. It has been considered already in connection with the classical theory of diamagnetism. Due to the recent development of magneto-hydrodynamics and the theory of plasmas the interest in this problem and in the related one of the motion in a constant, nearly homogeneous field has been revived.

The classical result is that, when the homogeneous field is varied slowly, the magnetic moment of the particle is constant. Assuming that this result is also valid in a steady inhomogeneous field Alfvén¹⁾ and Spitzer²⁾ discussed the secular drift of spiralling particles in this case, using more or less heuristic arguments. In a paper by Hellwig³⁾ the author comes to the conclusion that the magnetic moment is a constant during the motion at least up to a second approximation. Hertweck and Schlüter⁴⁾ investigated the motion in a homogeneous field starting from a constant initial value and tending to a definite limit. They showed that the limit of the magnetic moment differs from the initial value at most in terms of exponential order.

As we will show, the former investigation must contain an error. Hertweck and Schlüter's work, although quite correct as it stands, is based on a modified form of the equation of motion and therefore does not decide the question of the asymptotical behaviour of the solution of the exact equation. We therefore will present in this paper some investigations on this exact equation, using a different method. Furthermore we will treat some simple cases of motion in a steady inhomogeneous field by means of analytical methods of approximation. It will be seen that these results are in support of the conclusions drawn by Alfvén and Spitzer as far as the first approximation goes*).

Further approximations are laborious to obtain. These are investigated rather summarily therefore, mainly in order to get an idea of their nature and order of magnitude. If one requires numerical information on trajectories with an accuracy beyond that supplied by the constant moment approximation, direct integration of the equations of motions by means of a computer as a rule will be the only practicable method.

§ 2. *Motion in a homogeneous field.* We consider a particle of mass m and electric charge e moving in the x - y plane under influence of a homogeneous magnetic field B in the z -direction and the inductive electric field associated with the variation of B in time. Relativistic effects are neglected.

Strictly speaking the variable field cannot be homogeneous as it has to satisfy the wave equation. We restrict ourselves therefore to field variations slow enough to ensure that the associated wave length is large compared with the orbital radius of the particle. This condition will give no difficulties in the above-mentioned applications.

The equations of motion now are

$$\begin{aligned} m \frac{d^2x}{dt^2} &= e B \frac{dy}{dt} + e E_x, \\ m \frac{d^2y}{dt^2} &= -e B \frac{dx}{dt} + e E_y, \end{aligned} \tag{1}$$

*) *Note added in proof:* After submission of this paper results closely similar to those of § 2—§ 5 have been given by S. Chandrasekhar in "the Plasma in a Magnetic Field", Stanford 1958 p. 3-23.

where

$$E_x = -\frac{y}{2} \frac{dB}{dt}, \quad E_y = \frac{x}{2} \frac{dB}{dt} \quad (2)$$

is the appropriate solution of the induction equation $\text{rot } \mathbf{E} + \dot{\mathbf{B}} = 0$.

The z -component of the magnetic moment of the particle with respect to the origin is, apart from a constant,

$$\mu = -x \frac{dy}{dt} + y \frac{dx}{dt}. \quad (3)$$

The equations (1) can be combined into a single one by introducing the complex variable $u = x + iy$. We obtain from (1) and (2)

$$\frac{d^2 u}{dt^2} + i\omega \frac{du}{dt} + \frac{i}{2} \frac{d\omega}{dt} u = 0, \quad (4)$$

where the cyclotron frequency $\omega = eB/m$ is a known function of time. Instead of (3) we now write

$$\mu = \frac{i}{2} \left(u^* \frac{du}{dt} - u \frac{du^*}{dt} \right). \quad (5)$$

Differentiating this equation, eliminating the second derivatives by means of (4) and integrating again yields the useful relation

$$2\mu - \omega u^* u = \mu_0, \quad (6)$$

where μ_0 is a constant of integration.

Equation (4) is homogeneous, linear and of the second order. It has therefore two independent fundamental solutions, from which the general solution can be found as linear combination. When the field is constant, this general solution is

$$u = C + A \exp(-i\omega t), \quad (7)$$

which represents a circular motion around a centre located at C .

The moment associated with this motion is found to be

$$\mu = \omega A^* A + \frac{1}{2} \omega (A^* C + C^* A) \cos \omega t. \quad (8)$$

The time average of the moment, which from a physical point of view often is a more interesting quantity, therefore is simply

$$\bar{\mu} = \omega A^* A. \quad (9)$$

When the field varies slowly, which means that the field variation is small during one period of the spiralling motion, one would expect to find a "fast" fundamental solution related to $A \exp(-i\omega t)$ and a "slow" one, related to C . The first is a spiralling motion around the origin, the second is a slow motion, the nature of which remains to be investigated.

A complication of the problem is due to the fact that the statement in the last paragraph is not exactly true but only in the limit of zero rate of variation. If we start with a purely fast solution, we will find in general that after some time there will be a small slow term. This means that in a variable field the centre of the spiral will move around slowly.

This shift of the centre has a direct bearing on Hertweck and Schlüter's problem. Let the field have the limits ω_1 and ω_2 for $t \rightarrow -\infty$ and $+\infty$ respectively and suppose that the solution of (4) tends asymptotically to

$$u_1 = A_1 \exp(-i\omega_1 t) \text{ for } t \rightarrow -\infty \quad (10a)$$

and

$$u_2 = A_2 \exp(-i\omega_2 t) + C_2 \text{ for } t \rightarrow +\infty. \quad (10b)$$

Application of (6) and (8) then yields

$$\omega_1 A_1^* A_1 = \omega_2 (A_2^* A_2 - C_2^* C_2)$$

and therefore, on account of (9),

$$\bar{\mu}_2 - \mu_1 = \omega_2 |C_2|^2. \quad (11)$$

The eventual increase of the moment is directly proportional to the square of the shift, and Hertweck and Schlüter's problem is equivalent to that of finding the connection between the two asymptotic limits of the solution. An approximate connection formula will be derived in § 4. It will be found then that the shift is very small indeed.

Therefore, when we are on the other hand interested in the behaviour of μ during the transition, we can, at any rate for a relatively short time, forget about the shift and suppose that there exists a purely fast solution. A short time here is an interval covering many orbital periods but only a small part of the total field change. An approximation on this line will be developed in the next section.

§ 3. *Approximate solutions.* In order to obtain these solutions we represent u by means of its amplitude and phase functions, putting

$$u = a \exp[-i \int f dt], \quad (12)$$

where a and f are real functions of time. For a motion around the origin, that is a purely fast solution, a and f will vary slowly and f will differ little from ω . In a slow solution f will be very small. In a solution of mixed type a and f will have fluctuating parts. We observe that the moment now becomes

$$\mu = a^2 f. \quad (13)$$

When (12) is substituted into (4), we obtain after separating real and imaginary terms

$$\frac{d^2 a}{dt^2} - a f(f - \omega) = 0, \quad (14)$$

$$-2f \frac{da}{dt} - a \frac{df}{dt} + \omega \frac{da}{dt} + \frac{1}{2} a \frac{d\omega}{dt} = 0. \quad (15)$$

The latter equation can be integrated at once, yielding

$$a^2(2f - \omega) = \mu_0, \quad (16)$$

a result which also could have been deduced from (6). As for a fast solution $f - \omega$ is small, the integration constant μ_0 is positive in this case.

From the foregoing equations, in which no approximations have yet been made, some interesting relations can be deduced. Eliminating f between (14) and (16) we obtain

$$\omega^2 = \frac{\mu_0^2}{a^4} \left(1 - \frac{4a^3}{\mu_0^2} \frac{d^2 a}{dt^2} \right). \quad (17)$$

When a suitable slowly varying function $a(t)$ has been chosen, the field required to realize a motion around the origin with this amplitude function can be calculated from (17). This field then will vary slowly too. Purely fast motions therefore are certainly possible. However, choosing an arbitrary slowly varying ω , one would upon solving (17) for a in general find a solution containing small fluctuating terms.

The magnetic moment for this type of motion is not a constant. Eliminating ω and f between (13) (16) and (17) we find

$$2 \frac{\mu}{\mu_0} = 1 + \left(1 - \frac{4a^3}{\mu_0^2} \frac{d^2 a}{dt^2} \right)^{\frac{1}{2}}. \quad (18)$$

We now turn to the approximate solution of (14) and (15). For a fast solution $d^2 a/dt^2$ and $f - \omega$ will be small. Therefore a first approximation is $f_1 = \omega$ and from (16)

$$a_1 = \mu_0^{\frac{1}{2}} \omega^{-\frac{1}{2}}. \quad (19)$$

In this approximation $\mu_1 = \mu_0$. Higher approximations now can be derived from (17) by iteration according to the formula

$$f_n = \omega + \frac{1}{a_{n-1} f_{n-1}} \frac{d^2}{dt^2} a_{n-1},$$

$$a_n = \mu_0^{\frac{1}{2}} (2f_n - \omega)^{-\frac{1}{2}}.$$

The result after the second stage is

$$u_2 = \mu_0^{\frac{1}{2}} \left(\omega + 2\omega^{-\frac{1}{2}} \frac{d^2}{dt^2} \omega^{-\frac{1}{2}} \right)^{-\frac{1}{2}} \exp \left[-i \int \omega \left(1 + \omega^{-3/2} \frac{d^2}{dt^2} \omega^{-\frac{1}{2}} \right) dt \right],$$

$$\frac{\mu_2}{\mu_0} = \frac{1 + \omega^{-3/2} d^2 \omega^{-1}/dt^2}{1 + 2\omega^{-3/2} d^2 \omega^{-1}/dt^2}. \quad (20)$$

When it is required that the field varies slowly, an expression of the type $\omega^{-(n+1)} d\omega^n/dt$ must be of the first order in some parameter indicating the „degree of slowness”. Second order quantities are, besides squares of first order ones, expressions like $\omega^{-(n+2)} d^2/dt^2 \omega^n$. The magnetic moment therefore is not a constant of the motion to the second order in this sense. An analogous conclusion could have been drawn from (18) of course.

Approximations to a slow solution can be obtained in the same way. In this case we have to start with

$$f_1 = 0, \quad a_1 = (-\mu_0)^{\frac{1}{2}} \omega^{-\frac{1}{2}}, \quad (21)$$

as μ_0 is negative now. After one iteration we now find

$$u_2 = (-\mu_0)^{\frac{1}{2}} \left(\omega - \omega^{\frac{1}{2}} \frac{d^2}{dt^2} \omega^{-\frac{1}{2}} \right) \exp \left(i \int \omega^{\frac{1}{2}} \frac{d^2}{dt^2} \omega^{-\frac{1}{2}} dt \right). \quad (22)$$

The physical nature of this type of solution will become clear

upon observing that (21) satisfies (4) when the first term is neglected. It represents a radial motion in which the tangential Lorentz force balances the inductive force. The neglected acceleration is taken into account in the next approximation by allowing f to differ from zero. From this ensues a tangential component of the motion and hence a radial component of the Lorentz force which is required for the radial acceleration implied by (21).

§ 4. *Shift of the centre.* We consider a motion satisfying the conditions (10). The problem is to determine the small quantity C_2 in terms of ω . It must be stated at the outset that this is a difficult question. Approximation methods lead to expressions of C_2 in terms of integrals over fluctuating functions which are hard to estimate. As we are interested only in the order of magnitude of C_2 , which fortunately turns out to be very small, we will not go into this problem too deeply but restrict ourselves to a simple derivation of an expression which has at any rate the required order of magnitude.

This can be done by introducing a new variable c by means of the relation

$$i\omega c = \frac{du}{dt} + i\omega u. \quad (23)$$

It is seen from (10) that $c_1 = 0$, $c_2 = C_2$.

Clearly $c(t_0)$ is the centre of the circular motion when the field is kept at the constant value $\omega(t_0)$ for $t \geq t_0$. Differentiating (23) we obtain, using (4) to eliminate d^2c/dt^2 ,

$$\frac{d}{dt}(\omega c) = \frac{1}{2} \frac{d\omega}{dt} u.$$

Therefore we have

$$C_2 = \frac{1}{2\omega_2} \int_{-\infty}^{+\infty} \frac{d\omega}{dt} u \, dt. \quad (24)$$

On account of the results of the last section we estimate the integral by replacing u by $u_1 = A_2(\omega_2/\omega)^{\frac{1}{2}} \exp(-i \int \omega \, dt)$. Therefore

$$C_2 = A_2\omega_2^{-\frac{1}{2}} \int_{-\infty}^{+\infty} \frac{d}{dt} \omega^{\frac{1}{2}} \exp(-i \int \omega \, dt') \, dt. \quad (25)$$

Admittedly this result might be rather inaccurate as we know that u_1 is not a very good approximation of u over the whole range. It gets out of phase and it neglects the fact that the centre of the spiralling motion wanders slowly around the origin. However, as u_1 occurs only in the integrand, these inaccuracies will average out to a large extent. Moreover it can be shown that by quite different methods analogous results for C_2 can be derived.

We will use (25) only to show that C_2 is of exponential order. As it stands, it is the integral of a first order quantity multiplied by a fluctuating function. However, as all derivatives of $\omega(t)$ vanish as $|t|$ goes to infinity, the order of the integrand can be reduced at will by partial integration. We have for instance

$$\begin{aligned} \int_{-\infty}^{+\infty} \frac{d}{dt} \omega^{\frac{1}{2}} \exp(-i \int \omega dt') dt &= \int_{-\infty}^{+\infty} -i \omega^{-1} \frac{d}{dt} \omega^{\frac{1}{2}} d[\exp(-i \int \omega dt)] = \\ &= i \int_{-\infty}^{+\infty} \frac{d}{dt} (\omega^{-1} \frac{d}{dt} \omega^{\frac{1}{2}}) \exp(-i \int \omega dt') dt. \quad \text{etc.} \end{aligned}$$

Therefore C_2 is not of finite order.

Finally we remark that the results of this and the last section are closely related to well-established methods of approximation of the wave equation. As a matter of fact, if we put

$$u = \varphi \exp(-\frac{1}{2}i \int \omega dt),$$

that is if we use a coordinate system rotating with half the orbital angular velocity, we obtain from (4)

$$\frac{d^2 \varphi}{dt^2} + \frac{\omega^2}{4} \varphi = 0.$$

If this equation is treated by the W.K.B. method, the results of § 3 are obtained, whereas an approximation essentially the same as (25) can be found by means of a method due to Bremmer⁵⁾. The shift of the centre of motion in our problem in this way becomes the equivalent of the reflection of the waves in a gradient of the refractive index which, as is well known, is neglected in the W.K.B. method.

§ 5. *An exact solution.* As an example we consider the field

$$\omega = \omega_0(1 + \Delta \tanh vt), \quad (26)$$

increasing steadily from $\omega_1 = \omega_0(1 - \Delta)$ to $\omega_2 = \omega_0(1 + \Delta)$. The ratio ν/ω_0 is a convenient measure for the slowness of the change. We make the substitutions

$$\varphi = u \exp \frac{1}{2} i \int \omega \, dt \quad (27a)$$

and

$$y = -\exp 2\nu t \quad (27b)$$

and obtain from (4)

$$\frac{d^2\varphi}{dy^2} + \frac{1}{y} \frac{d\varphi}{dy} + \frac{\omega^2}{16\nu^2 y^2} \varphi = 0, \quad (28)$$

where from (26)

$$\omega = \omega_0 \frac{(1 - \Delta) - (1 + \Delta)y}{1 - y}$$

and y runs from 0 to $-\infty$.

It turns out that (28) can be solved in terms of hypergeometric functions. The connection between the behaviour at $y = 0$ and $y \rightarrow -\infty$ can be found from the theorem on the analytical continuation of the hypergeometric function (see e.g. Morse and Feshbach ⁶). When $\nu \ll \omega_0$ the result is

$$\left| \frac{C_2}{A_2} \right| = 2^{\frac{1}{2}} \exp \left[-\frac{\pi \omega_0 (1 - \Delta)}{2\nu} \right]. \quad (29)$$

The shift therefore is indeed of exponential order. Details of this calculation are given in Appendix I.

§ 6. *Motion in converging field.* In a steady field the particle moves under influence of the Lorentz force only. The equation of motion is in vector notation

$$m \frac{d^2 \mathbf{r}}{dt^2} = e \frac{d\mathbf{r}}{dt} \times \mathbf{B}.$$

The magnetic field \mathbf{B} has no curl and divergence, therefore

$$\mathbf{B} = \text{grad } \psi, \quad \Delta \psi = 0.$$

When the field has rotational symmetry around the z -axis, ψ

can be expanded in zonal harmonics. We take two terms only, writing

$$\psi = B_0 z - \frac{B_0}{4l} (x^2 + y^2 - 2z^2),$$

where l^{-1} is a measure of the degree of inhomogeneity of the field. Therefore

$$\vec{B}_x = -\frac{B_0}{2} \frac{x}{l}, \quad B_y = \frac{B_0}{2} \frac{y}{l}, \quad B_z = B_0 \left(1 + \frac{z}{l}\right).$$

The equations of motion now become

$$\begin{aligned} \frac{d^2 x}{dt^2} &= \left(\omega \frac{dy}{dt} + \frac{\omega'}{2} \frac{dz}{dt} y \right) \\ \frac{d^2 y}{dt^2} &= - \left(\omega \frac{dx}{dt} + \frac{\omega'}{2} \frac{dz}{dt} x \right), \\ \frac{d^2 z}{dt^2} &= \frac{\omega'}{2} \left(x \frac{dy}{dt} - y \frac{dx}{dt} \right), \end{aligned} \quad (30)$$

where

$$\omega = \frac{e}{m} B_0 \left(1 + \frac{z}{l}\right) = \omega_0 \left(1 + \frac{z}{l}\right), \quad \omega' = \frac{e B_0}{m l} = \frac{d\omega}{dz}. \quad (31)$$

We observe that $\omega' dz/dt = d\omega/dt$. The two first equations in (30) therefore are formally equivalent to (4) and can be treated in the same manner when $\omega(t)$ is known. The third equation now reduces to

$$\frac{d^2 z}{dt^2} = - \frac{\omega_0}{2l} \mu, \quad (32)$$

or, on account of (31),

$$\frac{d^2 \omega}{dt^2} = - \omega'^2 \frac{\mu}{2}.$$

A solution of (4) would enable us to express μ in terms of ω and its derivatives. Then (32) is an equation for $\omega(t)$.

An approximate solution of this problem can be constructed from the results of § 3. We start with the approximation

$$x + iy = u_1 = a_0 \left(\frac{\omega_0}{\omega} \right)^{\frac{1}{2}} \exp(-i \int \omega dt), \quad \mu_1 = \mu_0 = a_0^2 \omega_0.$$

In these relations a_0 is the orbital radius, $V_n = a_0\omega_0$ the velocity normal to the z -axis in the plane $z = 0$. It is assumed that the centre of the spiral moves along the z -axis, the shift effect being therefore neglected.

If it is assumed that the particle passes the plane $z = 0$ at the line $t = 0$ with an axial speed V_a we obtain from (32):

$$z = V_a t - \frac{V_n^2}{4l} t^2.$$

Therefore in this approximation

$$\omega = \omega_0 \left(1 + \frac{V_a}{l} t - \frac{V_n^2}{4l^2} t^2 \right). \quad (33)$$

A second approximation now can be found by evaluating μ from (20) by means of (33). Substitution of the result in (32) yields the axial motion in this approximation. The normal component then can be found from the first equation (20).

This operation could be repeated any number of times. The resulting expressions would be quite complicated and not very instructive. On the other hand, the simple formula (32) is quite clear; it is equivalent to the accelerated motion of a particle of mass m and constant moment μ_0 along the z -axis. According to the point of view stated at the end of the first section we will restrict ourselves to indicating the nature of the first small deviations from the heuristic constant moment approximations. Therefore we confine ourselves to relatively small intervals of time and expand u in ascending powers of t . In this way we obtain from (33)

$$\omega^{-3/2} \frac{d^2}{dt^2} \omega^{-1/2} = \frac{V^2}{4\omega_0^2 l^2} [(1 + 2 \cos^2 \alpha) + \frac{Vt}{l} 6 \cos \alpha (1 + 3 \cos^2 \alpha) + \dots],$$

where $V_a = V \cos \alpha$, $V_n = V \sin \alpha$. Using this result and (20) to integrate (32) we obtain

$$z = V \cos \alpha t - \frac{V^2 \sin^2 \alpha}{4l} t^2 + a_0^2 \frac{V^3 t^3}{8l^4} \cos \alpha (1 + 3 \cos^2 \alpha) + \dots \quad (34)$$

In this expression a small contribution to the second term has been omitted. This arises from the fact that in the second approximation the initial tangential velocity $V \sin \alpha$ is not exactly equal to $a_0\omega_0$.

It is seen from (34) that, as long as t does not exceed l/V , which is of the order of the time of passage through the field, the ratio of the third term to the second is of the order a_0^2/l^2 . The effect of the variation of the moment in this field therefore is of the second order in the ratio of orbital radius to length of the field.

More complicated, but not essential different results can be derived when B_z on the axis does not vary linearly. In this case B_z is no longer constant in each plane normal to the axis. The leading terms of the magnetic potential are then

$$\psi = B_0 \left[z - \frac{x^2 + y^2 - 2z^2}{4l} - \frac{3z(x^2 + y^2) - 2z^3}{6d^2} \right]. \quad (35)$$

One could consider l as the length, d as the diameter of the field. It is shown in the Appendix II that the equations of motion in the x and y direction can be treated by a method analogous to that of § 3 and that the first approximation is again

$$x + iy = a_0(\omega_0/\omega)^{\frac{1}{2}} \exp(-i \int \omega \, dt),$$

where

$$\omega = \frac{eB_0}{m} \left(1 + \frac{z}{l} + \frac{z^2}{d^2} \right),$$

which is the orbital frequency calculated from the field on the z -axis. For the validity of this approximation it is required that $a_0 \ll d$.

The equation for the axial motion now turns out to be:

$$\frac{d^2z}{dt^2} = -V_n^2 \left(\frac{1}{2l} + \frac{z}{d^2} \right).$$

The initial conditions are $z = 0$, $dz/dt = V_a$ for $t = 0$. The solution then is

$$z = \frac{d^2}{2l} \left(\cos \frac{V_n t}{d} - 1 \right) + d \frac{V_a}{V_n} \sin \frac{V_n t}{d}.$$

In order to compare this with (34) we expand in terms of t , obtaining

$$z = V_a t \cos \alpha - \frac{V^2 t^2}{2l} \sin^2 \alpha - \frac{V^3 t^3}{6d^2} \cos \alpha \sin^2 \alpha \dots$$

This expansion is useful only for $t \ll d/V$. It is seen that the correction term then is larger than that in (34), being of the order of $l^4/a_0^2 d^2$.

§ 7. *Drift.* It has been shown by Alfvén¹⁾ and Spitzer²⁾ that a charged particle spiralling along a curved magnetic field line will have a slow secular motion in the direction of the bi-normal of this line. In a first approximation this drift velocity is

$$V_a = \frac{1}{\omega R} (V_{\parallel}^2 + \frac{1}{2} V_{\perp}^2), \quad (36)$$

where ω is again the orbital frequency eB/m , R the radius of curvature of the field lines and V_{\parallel} and V_{\perp} the components of the particle velocity parallel and normal to the field.

It is difficult to improve upon this result in a general field. We will therefore only derive a second approximation for a simple case, viz. the field of an infinite straight electrical current which can be found by a straightforward calculation.

We take the current along the z -axis and use cylinder coordinates. The only field component then is $B_0 = I/2\pi r$ and the equations of motion now read

$$\frac{d^2 r}{dt^2} - r \left(\frac{d\theta}{dt} \right)^2 = - \frac{e}{m} \frac{dz}{dt} \frac{I}{2\pi r}, \quad (37)$$

$$r \frac{d^2 \theta}{dt^2} + 2 \frac{dr}{dt} \frac{d\theta}{dt} = 0, \quad (38)$$

$$\frac{d^2 z}{dt^2} = \frac{e}{m} \frac{dr}{dt} \frac{I}{2\pi r}. \quad (39)$$

Three first integrals of this set can be written down at once. In the first place we will have the energy integral

$$2T = \left(\frac{dr}{dt} \right)^2 + r^2 \left(\frac{d\theta}{dt} \right)^2 + \left(\frac{dz}{dt} \right)^2, \quad (40)$$

as no work is done on a particle in a steady field. Integrating (38) we obtain

$$r^2 \frac{d\theta}{dt} = M, \quad (41)$$

and integrating (39)

$$\frac{dz}{dt} = \frac{eI}{2\pi m} \ln \frac{r}{R}. \quad (42)$$

Substituting these into the energy equation we obtain a first order differential equation for r in the form

$$2T = \left(\frac{dr}{dt}\right)^2 + \frac{M^2}{r^2} + \left(\frac{eI}{2\pi m}\right)^2 \left(\ln \frac{r}{R}\right)^2. \quad (43)$$

The integration constant R is the distance from the axis at which the vertical component of the motion vanishes. R will be practically equal to the radius of the field line along which the particle would spiral when no drift would occur. For the other constants of integration we write

$$M = RV_{\parallel}, \quad 2T = (V_{\parallel}^2 + V_{\perp}^2).$$

Clearly V_{\parallel} and V_{\perp} are the velocity components in the θ and r directions when $r = R$. At this distance the field is $B_0 = I/2\pi R$, the orbital frequency $\omega_0 = eI/2\pi mR$.

When $T \ll \omega_0^2 R^2$, the radius of the spiral is small compared with R , so r and R do not differ very much. We put $r = R + \rho$ and expand the right hand side of (43) in terms of ρ/R , terminating the series after terms of the fourth degree. The result is

$$\begin{aligned} \left(\frac{d\rho}{dt}\right)^2 &= V_{\perp}^2 - \omega_0^2 \rho^2 + \\ &+ \frac{1}{R} (2V_{\parallel}^2 \rho + \omega_0^2 \rho^3) - \frac{1}{R^2} (3V_{\parallel}^2 \rho^2 + \frac{11}{12} \omega_0^2 \rho^4). \end{aligned} \quad (44)$$

This equation could be solved in terms of elliptic functions. The algebraic work involved in this solution is considerable but can be avoided in the following way.

When R goes to infinity, we clearly would obtain a geometric function, corresponding to a spiralling motion in a constant field. The parameter of the elliptic function therefore will be small. Expansion of the function with respect to the parameter is known to be equivalent to Fourier expansion. Therefore we introduce this Fourier expansion of ρ directly into (44) and equalize corresponding coefficients on both sides. As the right hand side of (44) has five coefficients and the period of the Fourier series is not known beforehand, we have to take four terms of this series in order to get a well-determined problem. The result can be written

in the form

$$\frac{\omega_0 \rho}{V_{\perp}} = \sin n\omega_0 t + \varepsilon \left[\left(\alpha + \frac{3}{4} \right) + \frac{1}{4} \cos 2n\omega_0 t \right] + \\ + \varepsilon^2 \left[\left(\frac{\alpha^2}{2} + 3\alpha + \frac{37}{48} \right) \sin n\omega_0 t - \frac{1}{48} \sin 3n\omega_0 t \right],$$

where

$$n = 1 - (3\alpha + \frac{4}{3}) \varepsilon^2, \quad \varepsilon = V_{\perp}/\omega_0 R \text{ and } \alpha = V_{\parallel}^2/V_{\perp}^2.$$

The drift now is found by introducing this solution into (42), expanding in terms of ε and averaging over a period. We find

$$V_d = \left(\frac{dz}{dt} \right)_{Ar} = \omega_0 R \left[\varepsilon^2 \left(\alpha + \frac{1}{2} \right) - \varepsilon^4 \left(\frac{3\alpha^2}{4} + \frac{4}{7} \alpha + \frac{59}{192} \right) \right].$$

It is seen that the first term corresponds exactly to (36). The second term is of the order R^{-3} ; therefore the simple expression for the drift is correct to the second order in this case.

Appendix I.

In (28) we substitute

$$\varphi = y^n (y - 1)^m P(y). \quad (45)$$

Next we determine m and n such that in the resulting equation the coefficient of $P(y)$ reduces to a constant. This condition is satisfied by

$$m = \frac{1}{2} \left(1 - i \sqrt{\frac{\Delta^2 \omega_0^2}{v^2} - 1} \right), \quad n = - \frac{i(1 - \Delta)\omega_0}{4v}. \quad (46)$$

With these values of m and n the substitution (45) leads to a hypergeometric equation for $P(y)$:

$$y(1 - y) \frac{d^2 P}{dy^2} + [c - (a + b + 1)y] \frac{dP}{dy} - abP = 0, \quad (47)$$

where

$$a = \frac{1}{2} \left[1 - i \left(\sqrt{\frac{\Delta^2 \omega_0^2}{v^2} - 1} + \frac{\omega_0}{v} \right) \right], \\ b = \frac{1}{2} \left[1 - i \left(\sqrt{\frac{\Delta^2 \omega_0^2}{v^2} - 1} - \frac{\Delta \omega_0}{v} \right) \right], \quad (48) \\ c = 1 - \frac{i(1 - \Delta)\omega_0}{2v}.$$

The solution of (47) is the hypergeometric function $F(a, b; c; y)$, multiplied by a constant, say β :

$$P = \beta F(a, b; c; y). \quad (49)$$

We can find the behaviour of P when $y \rightarrow -\infty$ from the relation

$$F(a, b; c; y) = (-y)^{-a} \frac{\Gamma(c) \Gamma(b-a)}{\Gamma(b) \Gamma(c-a)} F\left(a, 1-c+a; 1-b+a; \frac{1}{y}\right) \\ + (-y)^{-b} \frac{\Gamma(c) \Gamma(a-b)}{\Gamma(a) \Gamma(c-b)} F\left(b, 1-c+b; 1-a+b; \frac{1}{y}\right). \quad (50)$$

(see e.g. Morse and Feshbach ⁶)

For $y \rightarrow -\infty$ the hypergeometric functions at the right hand side of (50) reduce to unity, and thus we obtain from (45) and (49), applying (50),

$$\varphi_{y \rightarrow -\infty} = (-1)^{m+n} \beta \left[\frac{\Gamma(c) \Gamma(b-a)}{\Gamma(b) \Gamma(c-a)} (-y)^{m+n-a} + \right. \\ \left. + \frac{\Gamma(c) \Gamma(a-b)}{\Gamma(a) \Gamma(c-b)} (-y)^{m+n-b} \right].$$

Substituting this result in (27a) leads with the help of (46), (48), (27b) and (26) to

$$u_2 = (-1)^{m+n} \beta \left[\frac{\Gamma(c) \Gamma(a-b)}{\Gamma(a) \Gamma(c-b)} \exp - i(1 + \Delta) \omega_0 t + \right. \\ \left. + \frac{\Gamma(c) \Gamma(b-a)}{\Gamma(b) \Gamma(c-a)} \right]. \quad (51)$$

The calculation involved in evaluating the Gamma functions can be simplified by considering that $\nu \ll \omega_0$. (48) then reduces to

$$a = \frac{1}{2} \left[1 - \frac{i(1 + \Delta)\omega_0}{2\nu} \right], \quad b = \frac{1}{2}, \quad c = 1 - \frac{i(1 - \Delta)\omega_0}{2\nu}.$$

With the use of the properties of Gamma functions (see e.g. Whittaker and Watson ⁷) we find, comparing (51) with (10),

$$\left| \frac{C_2}{A_2} \right| = \sqrt{\frac{2 \cosh \pi \Delta \omega_0 / \nu}{\cosh \pi \omega_0 / \nu + \cosh \pi \Delta \omega_0 / \nu}}.$$

In the case under consideration ($\nu \ll \omega_0$) this can be further approximated to

$$\left| \frac{C_2}{A_2} \right| = 2^{\frac{1}{2}} \exp \frac{-\pi(1-\Delta)\omega_0}{2\nu}.$$

Appendix II

From the magnetic potential ψ as given in (35) we derive the equations of motion in the form

$$m \frac{d^2x}{dt^2} = eB_0 \left[\frac{dy}{dt} \left(1 + \frac{z}{l} + \frac{z^2}{d^2} - \frac{x^2 + y^2}{2d^2} \right) + \frac{dz}{dt} \left(\frac{x}{2l} + \frac{xz}{d^2} \right) \right],$$

$$m \frac{d^2y}{dt^2} = -eB_0 \left[\frac{dx}{dt} \left(1 + \frac{z}{l} + \frac{z^2}{d^2} - \frac{x^2 + y^2}{2d^2} \right) + \frac{dz}{dt} \left(\frac{y}{2l} + \frac{yz}{d^2} \right) \right],$$

When we put again $x + iy = u$, we obtain

$$\frac{d^2u}{dt^2} + i\omega \frac{du}{dt} + \frac{i}{2} \frac{d\omega}{dt} u = \frac{i\omega_0 u u^*}{2d^2} \frac{du}{dt},$$

where

$$\omega_0 = \frac{eB_0}{m}, \quad \omega = \frac{eB_0}{m} \left(1 + \frac{z}{l} + \frac{z^2}{d^2} \right).$$

Next we substitute $u = a \exp(-i \int f dt)$ and separate real and imaginary terms. This yields

$$\frac{d^2u}{dt^2} - af(f - \omega) - \frac{\omega_0}{2d^2} a^3 f = 0,$$

$$2 \frac{da}{dt} f + a \frac{df}{dt} - \omega \frac{da}{dt} - \frac{1}{2} a \frac{d\omega}{dt} + \frac{\omega_0}{2d^2} a^2 \frac{da}{dt} = 0.$$

When a varies slowly and moreover $a^2 \ll d^2$, an iteration process analogous to that in § 3 can be set up by writing these equations in the form

$$f - \omega = \frac{1}{af} \frac{d^2a}{dt^2} - \frac{\omega_0}{2} \frac{a^2}{d^2},$$

$$\frac{d}{dt} [a(2f - \omega)^{\frac{1}{2}}] = - \frac{\omega_0 a^2}{2d^2} (2f - \omega)^{-\frac{1}{2}} \frac{da}{dt}.$$

In the first stage the righthand sides of these equations are neglected. This yields the familiar solution

$$f = \omega, a = a_0(\omega_0/\omega)^{\frac{1}{2}},$$

which has been used in § 6. Calculation of further approximations, which is straightforward, is not required in this section and is therefore not given here.

Received 5th November, 1959.

REFERENCES

- 1) Alfvén, H., *Cosmical Electrodynamics*, Clarendon Press, Oxford 1950.
- 2) Spitzer, jr., L., *Physics of Fully Ionized Gases*, Interscience Publishers Inc., New York 1956.
- 3) Hellwig, G., *Z. Naturforschung* **10a** (1955) 508.
- 4) Hertweck, F. and A. Schlüter, *Z. Naturforschung* **12a** (1957) 844.
- 5) Bremmer, H., *Geometrisch-optische benadering van de golfvergelijking*. Handelingen van het 27^e Nederlands Natuur en Geneeskundig Congres, p. 88, Ruygrok en Co, Haarlem 1939.
- 6) Morse, Ph. and H. Feshbach, *Methods of Theoretical Physics* Vol. I, p. 581, McGraw-Hill Book Comp. Inc. 1953.
- 7) Whittaker, E. T. and G. N. Watson, *A Course of Modern Analysis* Chapter XII. Cambridge At the University Press 1952.

SUSCEPTIBILITY MEASUREMENTS OF Nb BETWEEN ROOM TEMPERATURE AND LIQUID HELIUM TEMPERATURES

by A. VAN ITTERBEEK, W. PEELAERS *) and F. STEFFENS

Instituut voor Lage Temperaturen en Technische Fysica, Leuven, Belgium

Summary

Measurements have been carried out on bulk Nb between room temperature and liquid helium temperatures. The susceptibility shows an increase of 1% per 100 degrees for decreasing temperatures. No field dependence could be detected up to liquid hydrogen temperature. This is in agreement with the results obtained by other authors. In the liquid He region some anomalies appear, notwithstanding fields were used higher than the critical one. It is supposed that the sample was not completely in the normal state.

§ 1. *Introduction.* Nb is a paramagnetic substance and moreover it is a superconductor. The susceptibility of niobium has been measured some years ago by De Haas and Van Alphen¹⁾ and by Kriessman and Callen²⁾. These measurements cover the temperature region from liquid hydrogen up to 1600°C. They found an increase of the magnetic susceptibility for decreasing temperatures. The purpose of our measurements was to check whether this increase still subsists in the liquid helium region.

§ 2. *Experimental method and calibration of the field.* A. Method. Faraday's method has been used. A detailed description has been given in a paper of one of us together with Duchateau³⁾ and Pollentier⁴⁾. Since then some refinements concerning the electrical circuit of the coils have been introduced. The two coils with which we compensate the force acting on the sample have been

*) Research fellow of the I.W.O.N.L. (Instituut tot Aanmoediging van het Wetenschappelijk Onderzoek in Nijverheid en Landbouw).

placed in series, so that one and the same variable current I flows in both. The advantages of the system are the following:

1) the measurements can be done much faster because only one current has to be measured;

2) greater variations in the current introduce the possibility of extending the field of investigation to substances with greater susceptibilities.

The following formula has been used:

$$c\Delta I^2 = m\chi H (dH/dx),$$

in which c is the constant of the microgram balance that has been used to measure the susceptibility, $\Delta I^2 = I_H^2 - I_0^2$ the difference between the square of the current I_H with magnetic field on and I_0 without field in the two coils, m the mass of the sample, χ the mass susceptibility and dH/dx the gradient of the magnetic field.

B. Calibration of the field. We determined the position between the pole pieces of the magnet where the constant $C_1 = c[H (dH/dx)]^{-1}$ is a minimum, or $H(dH/dx)$ a maximum.

After this we determined C_1 for four field strenghts, because one of our purposes was to make an investigation about the field dependence of the sample. These values are listed in table I.

TABLE I

$H (\text{\AA})$	$C_1 \times 10^6 (\text{e.m.u.})$
6875.6	1.4440
8727.6	0.8959
11202.5	0.5707
13759.4	0.4253

The calibration has been carried out with two samples, one of Cr and another of Ge. Both are spectrographically pure and have the following characteristics:

Cr: Origin: Johnson and Matthey.

Lines detected:	Copper	} faintly visible
	Silicium	
	Calcium	
	Na	} very faintly visible
	Pb	
	Mg	

mass: 45 mg.

Ge: Origin: Professor Breckpot, Chemistry department of the University of Louvain.

Specific resistance: $60 \Omega \text{ cm}$ at 20°C .

Number of atoms impurity: $3 \times 10^{12}/\text{cm}^3$ Ge.

Type: n .

Hall constant at 20°C : $-125000 \text{ cm}^3/\text{Coulomb}$.

Form: parallelepipedum (height 5.5 mm, width 5 mm).

Monocrystal.

Mass: 745.2 mg.

As value for the susceptibility of Ge we used that obtained by Stevens *et al.*⁵⁾: $\chi_{\text{mass}} = -0.106 \times 10^{-6}$ at room temperature. This value has also been checked by one of us together with Duchateau³⁾.

For the determination of the position where H (dH/dx) is a maximum we used the Cr sample. Once this position was known, we placed the Ge sample with its centre in this position and measured ΔI^2 . After this had been done, we made again use of the Cr sample to measure step by step the ΔI^2 over the height of the Ge sample. A numerical integration has been carried out to obtain the values listed in table I.

§ 3. *Measurements and discussion of the precautions to be taken in the liquid He region.* Measurements between 1.18°K and room temperature have been done on a sample of Nb furnished by Johnson and Matthey which has the following spectrographic composition:

<i>Element</i>	<i>Lines detected</i>	<i>Degree of visibility</i>
Tantalum	3311.162 3218.840	Very faintly visible
Magnesium	2852.129	Very faintly visible
Silicium	2516.123	Very faintly visible
Copper	3273.962	Hardly visible

Lines of: Ag, Al, Ca, Co, Cr, Fe, K, Li, Mn, Mo, Na, Ni, Pb, Sb, Sn, Ti, V, W, Zn, Zr were not detected.

In spite of the fact that no traces of iron could be detected, we checked the sample on ferromagnetic impurities with the method of Honda and Owen⁶⁾. One calculates:

$$\chi_H = \chi_\infty + c\sigma_s/H,$$

with χ_H the apparent susceptibility, χ_∞ the exact susceptibility, c the number of iron atoms/g and σ_s the magnetic moment of one Fe atom.

We can write that the magnetisation $\sigma = \chi H$ and find out how σ depends upon the magnetic field H . At great field strengths, σ has to increase linearly with the magnetic field. If we extrapolate this straight line to the lower field region, it would not pass through the origin if ferromagnetic impurities are present. In order to obtain the concentration of the ferromagnetic impurities, we have to draw a line parallel to the extrapolated one and going through the origin. The distance between the two lines gives $c\sigma_s$, the concentration of ferromagnetic impurities present in the sample.

No ferromagnetic impurities could be detected in the sample of Nb. We were specially interested in the variation of the susceptibility with temperature and the eventual field dependence of the sample. The values obtained are listed in table II.

TABLE II

T ($^{\circ}\text{K}$)	Between H (\AA) $\neq 0$ and $H = 0$	$\chi \times 10^6$
293	13759.4	2.39
	11202.5	2.39
	8727.6	2.39
77.4	13759.4	2.45
	11202.5	2.46
	8727.6	2.44
	6875.6	2.43
64.7	13759.4	2.43
20.21	13759.4	2.47
	11202.5	2.47
	8727.6	2.47
	6875.6	2.49
16.46	13759.4	2.47
14.89	13759.4	2.48
4.23		(2.48)
3.01	between	(2.42)
1.99	11202.5	(2.43)
1.69		(2.42)
1.18	and 13759.4	(2.36)

The accidental error in the susceptibility measurement is of the order of 1% for the strongest field (13759.4 O) and increases to about 2% for the lowest field (6875.6 O).

The values obtained for χ in the liquid He range have been put between brackets for the following reason. It is known that Nb is one of the metals that becomes superconducting at a temperature of 8°K and has a critical field of 2600 O extrapolated to 0°K ⁷⁾. These values were obtained by measurements on thin wires. Our sample had a triangular shape, was very small (height 0.8 mm; breadth 4 mm), but nevertheless it can be considered as matter in bulk.

Now, in order to measure at liquid He temperatures in the non-superconducting state, the measurements were carried out in magnetic fields much higher than the critical one. These field strengths are indicated in table II.

The values of the susceptibility are calculated by means of equation

$$\chi = \frac{1}{m} \frac{C_{120} C_{190}}{C_{120} - C_{190}} (I_{190}^2 - I_{120}^2),$$

in which C_{120} and C_{190} are the values of the constant C_1 corresponding respectively to a field of 11202.5 O and 13759.4 O (see table I). It should be emphasised that this equation is only valid if χ does not depend on the field strength.

§ 4. *Discussion of the results obtained for Nb.* As can be seen from table II, there was a slight increase in the susceptibility with decreasing temperature. The increase is of the order of 1% per hundred degrees and agrees very well with that obtained by Kriessman ²⁾ in the high temperature region (from 0°C to 1600°C) and Van Alphen ¹⁾ in the low temperature region (from 289°K to 14.2°K). It is to be noticed that nevertheless there exists a difference between the absolute values at room temperature for the susceptibility given by them (2.24×10^{-6} and 2.28×10^{-6}) and ours (2.39×10^{-6}). This is probably due to a difference in the calibration.

No field dependence could be detected up to liquid hydrogen temperature, as was also found by Van Alphen. At liquid He temperatures, we first used a field of 8727.6 O; that is more than

three times the critical value at 0°K for Nb in the form of a thin wire, this to avoid the superconducting state. Nevertheless it was impossible to stabilise the microgram balance and measurements could not be done. The instability disappeared at 11202.5 Ø. A possible explanation may be the incomplete disappearance of superconductivity in the sample at 8727.6 Ø.

The results in the liquid He region (table II), indicate a decrease in the susceptibility of about 5%. We believe that the sample was not completely in the normal state.

We take the opportunity to express our sincere thanks to the I.W.O.N.L. (Instituut tot Aanmoediging van het Wetenschappelijk Onderzoek in Nijverheid en Landbouw) of which one of us obtained a research fellowship. Further we express our gratitude to the Union Minière du Haut-Katanga for its financial help during these measurements.

Received 30th November, 1959.

REFERENCES

- 1) Alphen, P. H. van, Thesis Leiden 1933.
- 2) Kriessman, C. J. and H. B. Callen, Phys. Rev. **94** (1954) 837.
- 3) Itterbeek, A. van, L. de Greve and W. Duchateau, Appl. Sci. Res. B **4** (1955) 300.
- 4) Itterbeek, A. van, R. Pollentier, and W. Peelaers, Appl. Sci. Res. B **7** (1959) 329.
- 5) Stevens, D. K. and H. C. Schweinler, Phys. Rev. **100** (1955) 1084.
- 6) Honda, K., Ann Phys. Lpz. **32** (1910) 1048; M. Owen, Ann. Phys. Lpz **37** (1912) 637.
- 7) Shoenberg, D., Superconductivity, Cambridge University Press, 1952.

CHARACTERISTIC PARAMETERS OF GAS-TUBE PROPORTIONAL COUNTERS

I. METHANE, METHANE-ARGON, AND ETHANOL-ARGON COUNTERS *).

ROBERT W. KISER

Department of Chemistry, Kansas State University, Manhattan, Kansas, U.S.A.

Summary

The gas multiplication factor A_0 was determined in cylindrical counters at specific counter wire voltages and varied pressures, wire radii and counter shell radii for methane and various methane-argon mixtures, as used in proportional counters. It is seen that the Rose-Korff and the Curran-Craggs-modified Rose-Korff theory do not agree with the experimental results. Use of the Diethorn expression is made in presenting the results in terms of two parameters \overline{AV} and \overline{K} , characteristic of the gas filling. The meaning and values of \overline{AV} and \overline{K} are discussed, and the recent results of van Duuren and Sizoo for an ethanol-argon mixture are reinterpreted in terms of these characteristic parameters.

§ 1. *Introduction.* Rossi and Staub¹⁾ have shown that any expression which is to relate the gas multiplication factor A_0 to the counter and gas-filling parameters must satisfy the condition

$$A_0 = f[p a, V/\ln(b/a)], \quad (1)$$

where p is the pressure, a is the centre wire radius, V is the voltage on the counter and b is the counter shell radius.

Rose and Korff²⁾ derived the following equation to express the change in A_0 with the various factors:

$$A_0 = \exp\{2(\alpha N_m C_c a V)^\dagger [(V/V_0)^\dagger - 1]\}, \quad (2)$$

*) A portion of the work reported herein was abstracted from the Ph. D. thesis of Robert W. Kiser, Purdue University, Lafayette, Indiana, January, 1958 (Available from University MicroFilms, Ann Arbor, Michigan, L.C. Card No. Mic-58-1792). This work was supported in part by the United States Atomic Energy Commission under Contracts At(11-1)-166 with Purdue University and At-(11-1)-751 with Kansas State University.

where $\alpha = \text{constant}$, $N_m = \text{number of molecules per unit volume}$, $C_e = \text{capacitance of the counter per cm length}$, $V = \text{the voltage on the counter}$ and V_0 is the proportional region threshold voltage at which $A_0 = (1 + \delta)$, δ being only infinitesimally greater than zero. (It is to be noted that the experimental determination of V_0 is most difficult).

Since $N_m = N_0 p$, where $N_0 = (6.023 \times 10^{23} / 760 \times 22414)$ molecules/cm³, and p is the pressure, and since from basic electrostatics the capacitance of a coaxial cylindrical counter is given by

$$C_e = 0.556 / \ln (b/a), \quad (3)$$

we may rewrite equation (2) in the form

$$\ln A_0 = 2 \left[\frac{\beta N_0 V a p}{\ln(b/a)} \right]^{\frac{1}{2}} [(V/V_0)^{\frac{1}{2}} - 1]. \quad (4)$$

We see that (4) satisfies the conditions of Rossi and Staub.

Curran and Craggs³⁾ modified the Rose-Korff theory to give

$$\ln A_0 = 2 \left[\frac{\gamma V a}{\ln(b/a)} \right]^{\frac{1}{2}} \left[\left(\frac{V \bar{L}_e}{I_p a \ln(b/a)} \right)^{\frac{1}{2}} - 1 \right], \quad (5)$$

where I_p is the ionization potential of the gas or gas mixture, γ is a constant, and \bar{L}_e is the mean free path of the electron to restore the energy lost in collision. Assuming that \bar{L}_e varies as $1/p$, i.e.,

$$\bar{L}_e = k/p \quad (6)$$

and substituting

$$K_1/K_2 = k/I_p, \quad (7)$$

where

$$K_2 = \gamma^{\frac{1}{2}}, \quad (8)$$

we obtain the expression

$$\ln A_0 \left[\frac{\ln(b/a)}{4Va} \right]^{\frac{1}{2}} = K_1 \left[\frac{V}{pa \ln(b/a)} \right]^{\frac{1}{2}} - K_2. \quad (9)$$

K_1 and K_2 therefore should be characteristic of the counter gas only. If this is true, and if (9) holds, then all of the experimental data should fall on a single straight line when $\ln A_0 \{ [\ln(b/a)] / 4aV \}^{\frac{1}{2}}$ is plotted against $[V/pa \ln(b/a)]^{\frac{1}{2}}$. It will be shown later that, although (9) satisfies the Rossi-Staub conditions, the Curran-Craggs-modified Rose-Korff theory does not correctly describe the ex-

perimental results for either the 10% ethanol—90% argon proportional counter or the methane proportional counters.

Diethorn⁴⁾ has derived a somewhat different relationship between the gas multiplication factor and the various parameters of the counters and gases or gas mixtures:

$$\ln A_0 = \frac{V \ln 2}{\overline{\Delta V} \ln(b/a)} \ln \left[\frac{V}{\bar{K} p a \ln(b/a)} \right], \quad (10)$$

where $\overline{\Delta V}$ and \bar{K} are constants characteristic of the gas. It is noted that this relation obeys the Rossi-Staub conditions. Rearranging (10), we obtain

$$\left[\frac{\ln A_0 \ln(b/a)}{V} \right] = \frac{\ln 2}{\overline{\Delta V}} \ln \left[\frac{V}{p a \ln(b/a)} \right] - \left[\frac{\ln 2 \ln \bar{K}}{\overline{\Delta V}} \right]. \quad (11)$$

A plot of $[\ln A_0 \ln(b/a)]/V$ versus $\ln [V/pa \ln(b/a)]$ should yield a straight line if the experimental data are to verify the use of the Diethorn expression. It will be shown below that the Diethorn expression indeed does represent correctly the experimental results of these investigations.

The two parameters which should be characteristic of the gaseous countertube filling are $\overline{\Delta V}$ and \bar{K} . $\overline{\Delta V}$ will be obtained from the slope of the plot made according to the above-given directions and \bar{K} from the intercept. The slope is given by $\ln 2/\overline{\Delta V}$ and the intercept by $-\ln 2 \ln \bar{K}/\overline{\Delta V}$.

An order of magnitude value of $\overline{\Delta V}$ can be calculated. Since $\overline{\Delta V}$ is the mean kinetic energy imparted to the electron between successive ionizing collisions, and since this energy must be sufficient to ionize, it must at least be equal to the ionization potential I_p if the ionizing electron losses all of its kinetic energy in the collision. Since excitation of the gas molecules to low-lying excited states also is quite probable, and in addition, since the electron may not lose all of its kinetic energy in a collision, $\overline{\Delta V}$ is expected to be considerably greater than I_p and possibly nearer to the value of W , i.e., about 30 V. Such an approximate value of the electron energy has also been taken by others, e.g., Korft⁵⁾.

Another approach to an order of magnitude calculation of $\overline{\Delta V}$ is to consider $\overline{\Delta V}$ to be proportional to the critical field, E_c . Then for a proportional counter voltage of about 2000 V.

$$\overline{\Delta V} \cong 2000 \bar{L}_e/r_c \ln(b/a), \quad (12)$$

where r_c is the radius of the critical field for gas multiplication. Since $(r_c/\bar{L}_e) \cong 10$, and $\ln(b/a) \cong 6$ for many of the proportional counters used in this study,

$$\overline{\Delta V} \cong 33 \text{ (in V)}, \quad (13)$$

in good agreement with the previous estimate. It will be seen from the results that both of these estimates are in excellent agreement with the experimental data.

To estimate an order of magnitude for \bar{K} , we need to note that according to Diethorn $\bar{K} < \bar{E}/p$. Assuming \bar{E} to be given by $V/r_c \ln(b/a)$,

$$\bar{K} < V/r_c p \ln(b/a). \quad (14)$$

Assuming $r_c \cong 0.010$ in, $p = 100$ mm Hg, and $\ln(b/a) \cong 6$, at a voltage of 2000 V:

$$\bar{K} < 2000/6 \cong 300 \text{ (in V/in mm Hg)}. \quad (15)$$

We shall see later that this estimate also is in reasonable accord with the experimental findings.

It was the purpose of these investigations, then to determine values of A_0 for various proportional counter gases and gas mixtures and to use the experimental findings to evaluate these proportional counter theories. As the Diethorn expression was found to be the most useful, an attempt has been made to determine the significance of the two characteristic parameters, $\overline{\Delta V}$ and \bar{K} , for these counters. The values of $\overline{\Delta V}$ and \bar{K} determined are tabulated for these gases and provide a very convenient basis for calculation of the necessary voltage to produce a predetermined value of A_0 for any given counter and wire diameters and pressures for the gases and gas mixtures studied.

§ 2. *Measurement of the gas multiplication factor A_0 .* The gas multiplication factor A_0 is given by

$$A_0 = (\overline{N_e/N_i}), \quad (16)$$

where N_e = number of electrons collected in the proportional pulse initiated by N_i initial electrons.

The magnitude of the pulse appearing on the centre wire is

$$J = N_e (q/C) \quad (17)$$

or

$$A_0 = CJ/qN_i, \quad (18)$$

where q is the electronic charge, 1.602×10^{-19} C, and C is the distributed capacitance of the system, in F. It has here been assumed that the effect of the movement of the positive ion sheath away from the centre wire after the electron collection is negligible. Although this assumption is reasonably valid for small values of A_0 , it becomes poorer as A_0 becomes large, i.e., as the counter voltage is increased.

N_i is obtained from a knowledge of the average energy W necessary to produce an ion pair for the given gas, and the energy E lost in the counter by the initial event:

$$N_i = E/W. \quad (19)$$

Then

$$A_0 = CWJ/qE. \quad (20)$$

Since we employed additional amplification so that the pulses could be analyzed and then registered by a scaler, we must account for the electronic amplification G by noting that

$$J' = JG \quad (21)$$

and therefore

$$A_0 = CWJ'/qEG, \quad (22)$$

where J' is the final output voltage.

By calibrating the electronic amplifiers used with a pulse generator, possessing variable characteristics of pulse shape, G may be obtained. Thus, the pulse shapes used for calibration were made identical to those produced by the counters employed. The results of calibration of G for the preamplifier and amplifier employed in this study showed excellent linearity.

In these calibrations we employed X-radiation of 2.82 keV. This radiation was obtained from the electron-capture decay of argon-37, which was admixed with the counting gas. The average energy W to produce an ion pair, varies with the nature of the counter gas filling. The values of W for various gases which have been used in these investigations are: CH₄, 28.9; C₂H₅OH, 32.6; and Ar, 26.5 V/ion pair.

The capacitance of these counters possessing coaxial cylindrical geometry is given by

$$C_e = \frac{0.556 L}{\ln (b/a)}, \quad (23)$$

where L is length of the counter. C_c is then given in pF. Calculated and measured values of the counters employed agreed within experimental error. The determination of the remaining distributed capacitance was carried out by changing the length of the signal cable between the counter and the preamplifier. The output pulse of the preamplifier was observed as a function of the change in signal cable length at a constant counter voltage. The capacitance of the Amphenol RG-114/U cable employed is 6.5 pF per foot. A plot of $1/J'$ versus the total capacitance of the unit yields a straight line which passes through the origin. An illustration of this technique is given in fig. 1. In all measurements of A_0 , the length of the signal cable to the preamplifier was minimized.

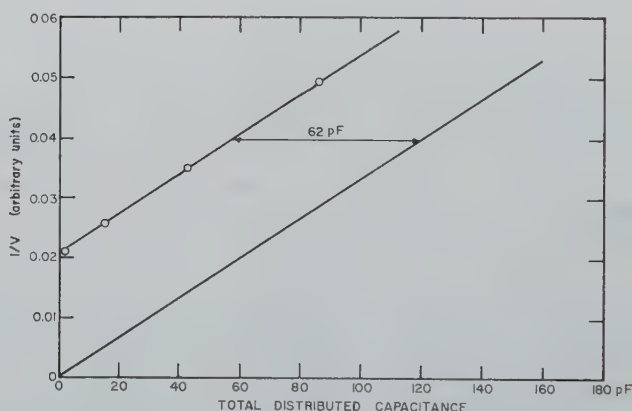


Fig. 1. Determination of the distributed capacitance of the proportional counter spectrometer.

Finally J' was accurately known from a calibration of the pulse height analyzers employed. The calibration showed that the zero energy of the analyzer was channel 2.0, and that the slope was 0.865 V/channel.

Thus

$$A_0 = \frac{0.865 CWJ''}{1.602 \times 10^{-19} EG} \quad (24)$$

or

$$A_0 = (CQJ''/EG) \times 5.40 \times 10^{18}, \quad (25)$$

where J'' is expressed in terms of channel numbers. The values of

C , W , J'' , E , and G are then inserted into (25) and the experimental value of A_0 obtained.

The methane, used in the experiments described in this work, was obtained from Matheson Company. The methane was of C. P. grade and was stated to have a minimum purity of 99.0%. The argon was also from Matheson and was stated to be at least 99.9% pure. These gases were not subjected to further purification when withdrawn from their containers.

All mixtures were blended in approximately two-liter storage bulbs in the vacuum system, using manometric techniques. Samples were withdrawn when desired from these storage bulbs for filling the counters. It is to be noted that in all cases very small quantities of argon-37 were added to these gases and gas mixtures.

All signal cables were of Amphenol RG-114.U. The preamplifier were products of the Bay Engineering Company and possessed a combined electronic gain range of 1.17×10^3 to 2.15×10^5 . The noise level of the preamplifier was found to be about 70 μ V.

The stable high voltage supply employed was the John Fluke Model 400BDA, with an output variable from 500 V to 5100 V d.c., positive or negative, at a current drain of 0 to 1 mA. The stability was better than 0.01% per hour. The ripple was less than 5 mV at any output voltage and current, and the voltage resolution was 50 mV at any output voltage.

For much of this work the RIDL model 3300 100-channel pulse height analyser was employed. This analyzer uses the Wilkinson type analog-to-digital converter, and information is accumulated in a magnetic core memory unit composed of sixteen ten-by-ten wafers. Complementing controls permitted the internal automatic subtraction of background. Also employed was the RIDL model 33-2 single-channel pulse height analyzer. The analyzers were shown, through the use of scintillation counter and proportional counter inputs, to possess excellent linearity and stability.

The Tektronix model 535 oscilloscope, with types 35A and 53/54E plug-in amplifiers, and the model 515 oscilloscope were used in the calibrations and also for the observation of the proportional spectra.

The counters which were used were constructed specifically for this work, except for 8334, which was obtained from N. Wood Counter Laboratories. The detailed parameters of the counters used are given in table I. The two-mil diameter tungsten wire was

obtained from Sylvania Electric Company. The five-mil diameter platinum wire was a J. Bishop and Co. product. All wires were cleaned before insertion into the counters with an absolute ethanol-soaked cleansing tissue. Centre wires always were pulled and maintained taut. Every effort was made to achieve good coaxiality. All counter shells were carefully cleaned before assembly. Counter 2182 was sealed using polystyrene end-plugs and Apiezon-W wax. No effects were noticed from the possible degassing of these plastic closures. Throughout, the stopcocks and all vacuum seals were greased with Apiezon-N. During the measurements the counters were maintained in either a brass or an aluminium electrostatic shield. The resolution of the *KX*-ray from the decay of argon-37 was 12–14% in the counters used.

TABLE I

Physical constants of the counters employed							
Counter No.	Shell	Wall thickness (in.)	Cathode	Internal shell radius (in.)	Centre wire	Centre wire radius (in.)	Length (in.)
II	Pyrex	0.010	external	0.48	tungsten	0.0010	10.2
III	Pyrex	0.010	external	0.51	tungsten	0.0010	8.3
XV	soda-lime	0.039	external	1.00	tungsten	0.0010	15.0
2182	brass	0.066	brass	0.94	platinum	0.0025	10.5
8334	Pyrex	0.039	silver	0.44	tungsten	0.0010	10.2

§ 3. *Comparison of the modified Rose-Korff and the Diethorn theories with experiment.* The results of the determinations of the gas multiplication factors for methane are given in tables II and III. These results are shown graphically in fig. 2, using the Curran-Craggs-modified Rose-Korff theory. It is obvious from the fact that one single straight line is not obtained that this theory does not correctly describe the experimental results, although the theory does satisfy the Rossi-Staub conditions. These same experimental results are plotted in fig. 3 using the Diethorn expression, and it is readily observed that this expression accounts for the experimental results in good fashion.

Diethorn⁴⁾ also studied the methane case, and although he used distinctly different counters and pressures, his data and the data presented here are in excellent agreement. Further, the results of Rossi and Staub¹⁾ for their 85% methane (–15%?) agree

TABLE II

The gas multiplication factors for 99.8% CH ₄ -0.2% Ar							
Counter II $p = 159$ mm		Counter II $p = 301$ mm		Counter II $p = 357$ mm		Counter II $p = 450$ mm	
V	$\ln A_0$	V	$\ln A_0$	V	$\ln A_0$	V	$\ln A_0$
1300	6.801	1600	6.370	1750	6.136	1900	6.250
1350	7.185	1650	6.685	1800	6.399	1950	6.513
1400	7.586	1700	6.969	1850	6.789	2000	6.822
1450	7.975	1750	7.352	1900	7.170	2050	7.192
1500	8.421	1800	7.674	1950	7.534	2100	7.505
1550	8.854	1850	8.055	2000	7.916	2150	7.840
1600	9.306	1900	8.420	2050	8.350	2200	8.202
1650	9.752	1950	8.804	2100	8.755	2250	8.571
1700	10.182	2000	9.232	2150	9.147	2300	8.935
1750	10.638	2050	9.616	2200	9.532	2350	9.300
1800	11.084	2100	10.023	2250	9.938	2400	9.683
1850	11.556	2150	10.401	2300	10.345	2450	10.055
1900	12.064	2200	10.789	2350	10.725	2500	10.427
1950	12.521	2250	11.163	2400	11.130	2550	10.798
		2300	11.551	2450	11.523	2600	11.160
		2350	11.966	2500	11.857	2650	11.509
		2400	12.488	2550	12.226	2700	11.821
						2750	12.150

TABLE III

The gas multiplication factors for 99.8% CH ₄ -0.2% Ar							
Counter II $p = 597$ mm		Counter III $p = 357$ mm		Counter XV $p = 233$ mm		Counter XV $p = 359$ mm	
V	$\ln A_0$	V	$\ln A_0$	V	$\ln A_0$	V	$\ln A_0$
2250	6.544	1700	6.057	1650	6.430	1900	5.938
2300	6.879	1750	6.347	1700	6.717	1950	6.256
2350	7.160	1800	6.697	1750	7.065	2000	6.683
2400	7.457	1850	6.994	1800	7.409	2050	6.947
2450	7.784	1900	7.352	1850	7.762	2100	7.265
2500	8.079	1950	7.741	1900	8.134	2150	7.565
2550	8.400	2000	8.189	1950	8.507	2200	7.894
2600	8.727	2050	8.527	2000	8.885	2250	8.237
2650	9.010	2100	8.916	2050	9.269	2300	8.566
2700	9.313	2150	9.324	2100	9.655	2350	8.920
2750	9.610	2200	9.674	2150	10.061	2400	9.269
2800	9.911	2250	10.077	2200	10.449	2450	9.609
2850	10.228	2300	10.472	2250	10.851	2500	9.962
2900	10.535	2350	10.845	2300	11.240	2550	10.322
2950	10.827	2400	11.228	2350	11.644	2600	10.664
3000	11.126	2450	11.552	2400	12.049	2650	11.032
3050	11.431	2500	11.932	2450	12.441	2700	11.363
3100	11.736	2550	12.278			2750	11.712
3150	12.026					2800	12.038
3200	12.318					2850	12.346

fairly well with our data for 99.8% CH₄-0.2% Ar, particularly in considering their statement that, "... no effort was made to reach

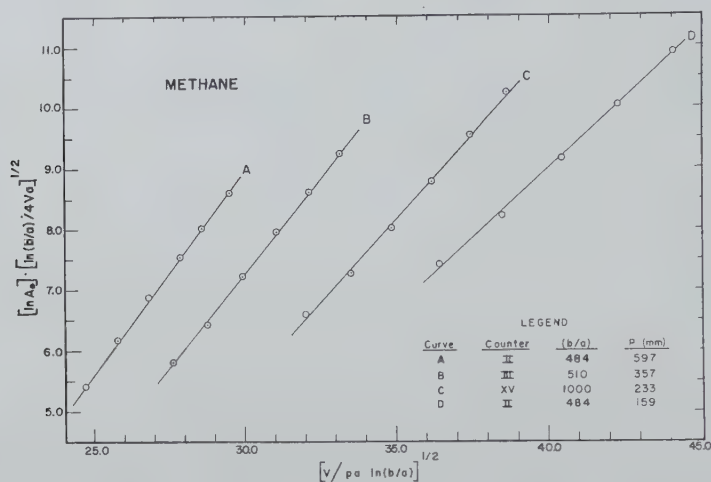


Fig. 2. Test of the Curran-Craggs-modified Rose-Korff theory using methane.

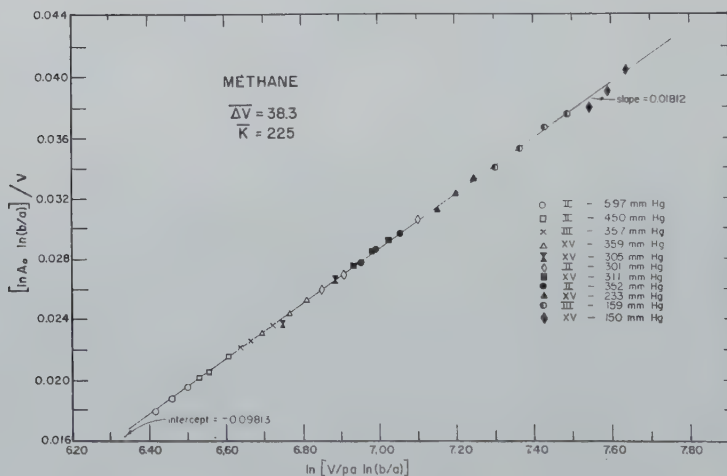


Fig. 3. Test of the Diethorn expression using methane.

any high degree of accuracy in obtaining the experimental data presented...". Finally, the data presented by Kumabe and Sonoda⁶⁾ for pure methane in their counter B, a cylindrical

coaxial Maze counter, agree quite well this data, as shown in table IV, where their data are compared with values of A_0 calculated from the values of $\overline{\Delta V}$ and \overline{K} given. The value of 190 for $\overline{\Delta V}$ is that obtained by Diethorn. Considering that both Rossi and Staub's work and Kumabe and Sonoda's work were done at low values of A_0 , using $Po-\alpha$ particles, and this author used argon-37 while Diethorn used iron-55, the agreement is considered excellent.

TABLE IV

The gas multiplication factors for a methane counter with $a = 0.00197$ in., $b = 0.453$ in. and $p = 400$ mm Hg.		
V	gas multiplication factor A_0	
	Kumabe and Sonoda ⁶⁾	Calculated ($\overline{\Delta V} = 38.3$; $\overline{K} = 190$)
700	1.2	0.71
800	1.6	0.96
900	1.8	1.4
1000	2.1	2.0
1100	3.	3.0
1200	4.	4.8
1300	5.5	7.6
1400	8.6	12.6
1500	16.	21.
1600	31.	37.
1700	59.	64.
1800	105.	118.
1900	170.	210.

It is noted here also that the results given by Rose and Korff ²⁾ for 100% methane do not agree with any of the results described in this paragraph and that the results presented by Rose and Ramsey ⁷⁾ for methane are insufficient for purpose of comparison.

The results of the determinations of A_0 for the 7.9% CH_4 -92.1% Ar mixture are given in table V. In fig. 4 these results have been plotted using the Diethorn expression. Again, a good fit of the data with a single straight line is possible. The values of $\ln A_0$ for the 76.5% CH_4 -23.5% Ar and for the 90.3% CH_4 -9.7% Ar mixtures are tabulated in table VI. Unfortunately the results presented by Bertolini, Bisi and Zappa ⁸⁾ for 10% CH_4 -90% Ar are only relative and therefore cannot be compared with our results for 7.9% CH_4 -92.1% Ar.

TABLE V

The gas multiplication factors for 7.9% CH ₄ -92.1%			
Counter II $p = 595$ mm		Counter 2182 $p = 592$ mm	
V	$\ln A_0$	V	$\ln A_0$
1250	5.645	1950	6.023
1300	6.052	2000	6.299
1350	6.452	2050	6.561
1400	6.852	2100	6.899
1450	7.237	2150	7.227
1500	7.705	2200	7.605
1550	8.180	2250	7.992
1600	8.659	2300	8.390
1650	9.111	2350	8.806
1700	9.575	2400	9.208
1750	10.026	2450	9.660
1800	10.483	2500	10.083
		2550	10.526
		2600	10.981
		2650	11.458
		2700	11.891
		2750	12.376
		2800	12.851
		2850	13.428
		2900	13.938

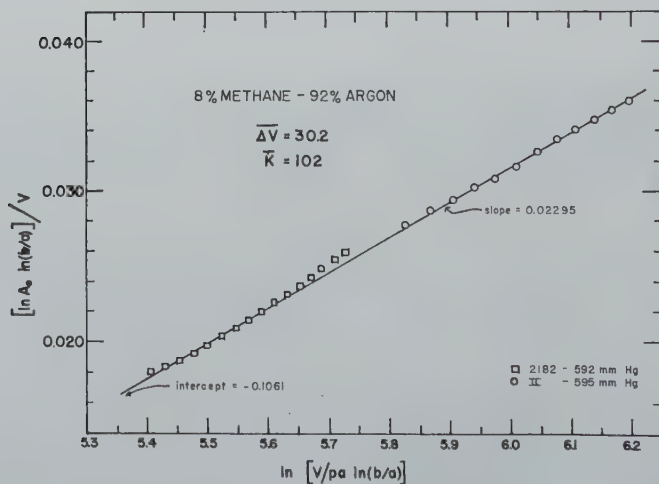


Fig. 4. Diethorn plot for 7.9% Methane — 92.1% Argon.

Rose and Korff²⁾ determined values of A_0 at various counter voltages for 50, 75 and 90% CH_4 counters, the diluent in each case being argon. However, the five different sets of data for 90% CH_4 -10% Ar do not fit a single straight line when plotted in terms of the Diethorn expression. Two of these sets are at the same pressures and yet appear as distinctly different relations. The very small counters which they used may be the cause, in the absence of any other plausible explanation, of the poor fit of the experimental data by the Diethorn expression.

TABLE VI

Gas multiplication factors for other CH_4 -Ar mixtures			
76.5% CH_4 -23.5% Ar Counter 8334 $p = 591$ mm		90.3% CH_4 -9.7% Ar Counter III $p = 503$ mm	
V	$\ln A_0$	V	$\ln A_0$
2200	6.114	2000	6.293
2250	6.477	2050	6.645
2300	6.771	2100	6.947
2350	7.107	2150	7.320
2400	7.427	2200	7.683
2450	7.737	2250	8.029
2500	8.065	2300	8.401
2550	8.401	2350	8.784
2600	8.772	2400	9.167
2650	9.131	2450	9.532
2700	9.473	2500	9.904
2750	9.836	2550	10.265
2800	10.173	2600	10.678
2850	10.553	2650	11.062
2900	10.904	2700	11.427
2950	11.260	2750	11.791
3000	11.599	2800	12.106
3050	11.938	2850	12.437
3100	12.241		
3150	12.557		
3200	12.811		
3250	13.048		
3300	13.271		

Van Duuren and Sizoo⁹⁾ recently attempted to verify the use of the Rose-Korff theory, using their experimental results on the proportional operation of counters filled with 10% ethanol-90% argon. They found rather large discrepancies between the theory and their results, especially for low values of E/p , and considered this

as probably due to the nature of the simplifying assumptions used in the theory. Since, in general, the values of A_0 determined in this work ranged from about 400 to approximately 40000 whereas the values in van Duuren and Sizoo's studies ranged from slightly greater than one to about 1000 or so, it would be most interesting to see if the Diethorn expression would hold for their ethanol-argon studies. The original data of van Duuren and Sizoo were recalculated and plotted in terms of the Diethorn expression. The resultant graph is shown in fig. 5. It is observed that their data can be readily interpreted using the Diethorn theory, except at extremely low values of A_0 (below approximately $A_0 = 3$).

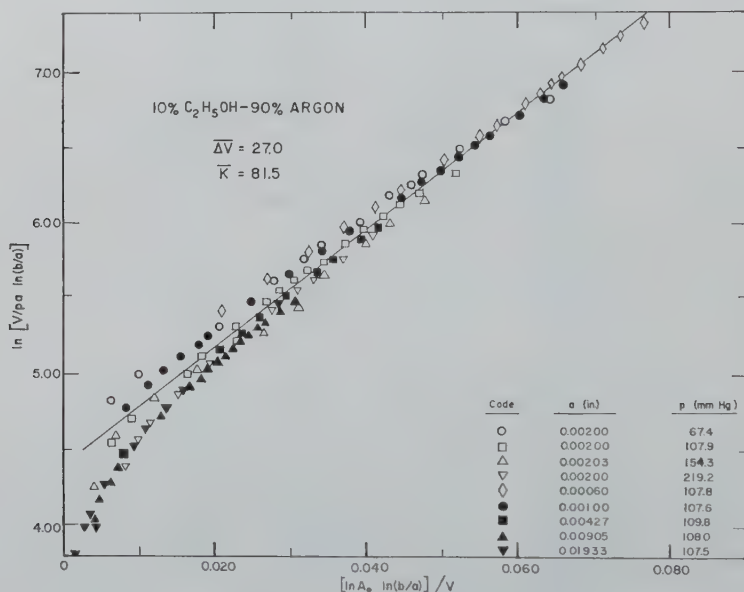


Fig. 5. Diethorn plot of Van Duuren and Sizoo's data for 10% Ethanol-90% Argon.

It is concluded, therefore, that the Diethorn expression more correctly describes the experimental values of the gas multiplication factor than do the Rose-Korff and the Curan-Craggs-modified Rose-Korff theories. We shall now examine the values of $\overline{\Delta V}$ and \overline{K} , the characteristic parameters of the counting gases, and discuss their physical meaning.

§ 4. *The characteristic parameters, $\overline{\Delta V}$ and \overline{K} .* Earlier in this paper we obtained approximate values of $\overline{\Delta V}$ and \overline{K} which we expected to be in reasonable agreement with the experimental results; i.e., $\overline{\Delta V} \cong 30$ V (equation (13)) and $\overline{K} \cong 300$ V/in. mm Hg (equation (15)). In table VII are summarized the various values of $\overline{\Delta V}$ and \overline{K} which have been obtained from Diethorn plots of the experimental data, along with values of W for the gases or gas mixtures. It is immediately seen that the values of $\overline{\Delta V}$ are in excellent agreement with the predicted approximate value of 30 V. The fact that $\overline{\Delta V}$ was expected to be near the value of W is also shown in table VII, where it is seen that for these proportional gases $\overline{\Delta V} \geq W$. It is noted then that $\overline{\Delta V} \geq W$ for these proportional counting gases, and this fact may be used in predicting the values of $\overline{\Delta V}$ for other proportional gases. If $\overline{\Delta V}$ is estimated to within 10%, the value of A_0 would be correct to within a factor of about 2. If then \overline{K} could be predicted, one would be able to calculate conveniently the operational characteristics of any desired proportional counter.

TABLE VII

Characteristic parameters of proportional counting gases			
Filling	$\overline{\Delta V}$ (V)	\overline{K} (V/in mm Hg)	W (eV) ^c
99.8% CH ₄ -0.2% Ar	38.3	225.	28.9
100% CH ₄ (Diethorn) ^a	40.3	190.	28.9
7.9% CH ₄ -92.1% Ar	30.2	102.	26.7
76.5% CH ₄ -23.5% Ar	36.2	258.	28.3
90.3% CH ₄ -9.7% Ar	28.3	287.	28.7
10.0% EtOH-90.0% Ar ^b	27.0	81.5	27.1

a) See Diethorn ⁴).

b) Recalculated results of Van Duuren and Sizoo ⁹).

c) Values for mixtures have been obtained using the methods outlined by H. J. Moe, T. E. Bortner and G. S. Hurst (J. Phys. Chem. **61** (1957) 422) and G. Bertolini, N. Bettoni and A. Bisi (Phys. Rev. **92** (1953) 1586).

From Diethorn's derivation, $\overline{K} < \overline{E}/p$ when the probability that ionization will occur upon impact is proportional to \overline{E}/p . Therefore, we shall assume that

$$\overline{K} = 0.6 \overline{E}/p. \quad (26)$$

However

$$E = \overline{\Delta V}/\overline{L}_e, \quad (27)$$

thus

$$\overline{K} = 0.6 \overline{\Delta V}/p \overline{L}_e. \quad (28)$$

The mean free path of an electron in a gas is given by

$$\bar{L}_e = 5.66 \bar{L}_g = 5.66/n\pi d^2 \quad (29)$$

and therefore

$$\bar{K} = 0.6 n\pi d^2 \bar{\Delta V}/5.66p. \quad (30)$$

Assuming the ideal gas law to hold,

$$\bar{K} = (0.6\pi d^2 (\bar{\Delta V}/5.66) (1/RT)). \quad (31)$$

Then

$$d^2 = 5.15 \times 10^{-17} K/\bar{\Delta V}, \quad (32)$$

where K is in units of $V/\text{in mm Hg}$, $\bar{\Delta V}$ is in V , and d^2 is in cm^2 ,

From an examination of the data on ionization cross-sections for nitrogen, oxygen, nitric oxide, carbon monoxide and acetylene, as given by Massey and Burhop¹⁰), we see that the ionization cross-section at electron energies equal to W is approximately 0.5 times that at 75 eV. Essentially the same results are obtained from the theoretical results given by Massey and Burhop¹⁰). We then correct (32) for this electron energy effect, and obtain

$$d_{75}^2 = 1.03 \times 10^{-16} \bar{K}/\bar{\Delta V}. \quad (33)$$

However, the cross-section Q is given by

$$Q = \pi r^2 = \pi d^2/4. \quad (34)$$

Therefore, for 75 V electrons, the ionization cross-section is

$$_{75}Q_i = 8.1 \times 10^{-17} \bar{K}/\bar{\Delta V}. \quad (35)$$

Calculation of $_{75}Q_i$ for methane gives

$$_{75}Q_i = 8.1 \times 10^{-17} \times (225/38.3) = 4.75 \times 10^{-16} \text{ (in cm}^2\text{)}, \quad (36)$$

which is in good agreement with the value of $4.65 \times 10^{-16} \text{ cm}^2$ as given by Lampe, Franklin and Field¹¹).

If we calculate $_{75}Q_i$ for the methane-argon mixtures studied in this work and assume the additivity of values of $_{75}Q_i$ as individual components of a mixture, we may calculate the value of $_{75}Q_i$ for argon. Doing so, we find that $_{75}Q_i$ (Ar) varies from 2.7 to $39.0 \times 10^{-16} \text{ cm}^2$ and is in no manner constant. Therefore, the additivity assumption is likely incorrect. Upon re-examination of the variation of \bar{K} with concentration, as listed in table VII, we see that \bar{K} does

not vary linearly with concentration. However, at low concentration of the organic substance in the inert gas the deviation from this assumption is not too serious¹²⁾, and accordingly we calculate a value of $2.7 \times 10^{-16} \text{ cm}^2$ for ${}_{75}Q_i$ of argon from the 7.9% CH_4 -92.1% Ar data. This is to be compared with the value of $3.52 \times 10^{-16} \text{ cm}^2$ as listed by Massey and Burhop¹⁰⁾. It is obvious that the data could be made to give still better agreement, but without any good reason for other choices which might be made.

From the results of the 10.0% ethanol-90.0% Ar data of Van Duuren and Sizoo⁹⁾, assuming the additivity of values of ${}_{75}Q_i$ at this concentration to be valid, a negative value of ${}_{75}Q_i$ would result for ethanol, using the literature value of $3.5 \times 10^{-16} \text{ cm}^2$ for argon. Although Lampe, Franklin and Field¹¹⁾ do not give an experimental value for ${}_{75}Q_i(\text{C}_2\text{H}_5\text{OH})$, the relationship they give relating the polarizability α_0 of molecules and their ionization cross-sections can be used to find an approximate value of ${}_{75}Q_i$. Taking $\alpha_0 = 5.63 \times 10^{-24} \text{ cm}^3$, ${}_{75}Q_i(\text{C}_2\text{H}_5\text{OH}) = 10.0 \times 10^{-16} \text{ cm}^2$. The negative value of ${}_{75}Q_i$ obtained above from Van Duuren and Sizoo's proportional counter data then is likely in error. If we use the value of $\bar{K} = 130$, as determined by Storrs and Kiser¹²⁾ from Geiger-Müller counter studies, $\bar{\Delta V} = 27.0$, and assume the additivity of values of ${}_{75}Q_i$, we calculate ${}_{75}Q_i(\text{C}_2\text{H}_5\text{OH}) = 7.5 \times 10^{-16} \text{ cm}^2$, having taken ${}_{75}Q_i(\text{Ar}) = 3.5 \times 10^{-16} \text{ cm}^2$. This calculated value of ${}_{75}Q_i[\text{EtOH}]$ is in fair agreement with the estimated value of $10 \times 10^{-16} \text{ cm}^2$. It is noted that, although the ${}_{75}Q_i$ additivity assumption is admittedly poor, it does allow approximative insights into these results.

It is concluded, then, that for the gases studied and reported herein the calculation of ${}_{75}Q_i$ from the counting gas parameter \bar{K} is possible. Investigations of other proportional counting gases are presently being made, and preliminary results appear to verify this conclusion for other systems than those reported here. We have, then, a new approach for the determination of values of Q_i .

Alternatively, for gases whose values of Q_i are known \bar{K} may be calculated if $\bar{\Delta V}$ is known. Since $\bar{\Delta V} \geq W$ for proportional gases, this is possible. From the knowledge of $\bar{\Delta V}$ and \bar{K} the operational characteristics of a particular counter with a given gaseous filling can be calculated using the Diethorn expression.

Investigations of other proportional gases are presently underway in these laboratories in an attempt to further test the ideas discussed.

Acknowledgement. The author wishes to express his appreciation to Drs. Werner H. Wahl and William H. Johnston for many helpful discussions of this work.

Received 1st December, 1959.

REFERENCES

- 1) Rossi, B. B. and H. H. Staub, *Ionization Chambers and Counters*, McGraw-Hill Book Co., Inc., New York 1949, pp. 73-74 and 77.
- 2) Rose, M. E. and S. A. Korff, *Phys. Rev.* **59** (1941) 850.
- 3) Curran, S. C. and J. D. Craggs, *Counting Tubes*, Academic Press, Inc., New York 1949, pp. 32-33.
- 4) Diethorn, W., *A Methane Proportional Counter System for Natural Radiocarbon Measurements*, NYO-6628, March 16, 1956.
- 5) Korff, S. A., *Electron and Nuclear Counters*, 2nd Edition, D. Van Nostrand Co., Inc., New York 1955, p. 61.
- 6) Kumabe, I. and M. Sonoda, *J. Phys. Soc. Japan* **9** (1954) 877.
- 7) Rose, M. E. and W. E. Ramsey, *Phys. Rev.* **61** (1942) 198.
- 8) Bertolini, G., A. Bisi and L. Zappa, *Nuovo Cimento* **10** (1953) 1424.
- 9) Duuren, K. van and G. J. Sizoo, *Appl. Sci. Res.* **B7** (1959) 379.
- 10) Massey, H. S. W. and E. H. S. Burhop, *Electronic and Ionic Impact Phenomena*, Oxford at the Clarendon Press, London 1956, pp. 38-39, 141 and 265.
- 11) Lampe, F. W., J. L. Franklin and F. H. Field, *J. Amer. Chem. Soc.* **79** (1957) 6129.
- 12) Storrs, C. D. and R. W. Kiser, *Abstracts of Papers*, 134th American Chemical Society Meeting, Chicago, Sept. 7-12, 1958, p. 56S.

ON THE SOLUTION OF AN EIGENVALUE EQUATION OF THE WIENER-HOPF TYPE IN FINITE AND INFINITE RANGES *)

by R. MITTRA

Antenna Laboratory, Department of Electrical Engineering, University of Illinois, Urbana, Illinois, U.S.A.

Summary

The purpose of the paper is to present a formulation of the eigenvalue matrix equation of the Wiener-Hopf integral equation defined in finite and infinite ranges. The method provides a simple means for obtaining the eigenvalue equation and indicates a way for obtaining the eigenfunctions and the eigenvalue. The important contribution of the paper is the direct rather than the transform method of solution. Such a formulation is also helpful in the solution of inhomogeneous Wiener-Hopf equations in finite and infinite ranges.

§ 1. *Introduction.* In this paper we consider the eigenvalue problem defined by the equation

$$\varphi(t) = \lambda \int_0^T \varphi(\tau) K |t - \tau| d\tau, \quad 0 < T < \infty, \quad (1.1)$$

$$K |t| = \sum_{r=1}^n C_r \exp(-k_r |t|), \quad (1.2)$$

which is encountered in a class of problems in probability theory. The origin of (1.1) and a transform method of solution has been discussed by Youla¹⁾ in a recent paper. The purpose of the paper is to show that the eigenvalue problem can be formulated in terms of a determinantal equation without resorting to the transform method of formulation. The direct method of formulation is simple and involves comparatively less amount of work. From the assumed form of the kernel it is seen that the method is limited to the

*) The research reported in this paper was carried out under Contract No. AF 33 (616)-6079 at the University of Illinois.

special type of kernels of the type (1.2) or to those which can be expanded in the form of (1.2).

§ 2. *The eigenvalue matrix.* In this section we shall obtain the eigenvalue determinant for the problem. As a first step assume an expansion for $\varphi(t)$ in the form

$$\varphi(t) = \sum_{m=1}^n (A_m e^{-\gamma_m t} + B_m e^{\gamma_m t}), \quad 0 < t < T. \quad (2.1)$$

Such a form is dictated by the fact that the integral I , defined by

$$I = \int_0^T e^{-\gamma_m t} K |t - \tau| d\tau, \quad (2.2)$$

yields $\exp(-\gamma_m \tau)$ multiplied by a constant, plus some other terms of the type $\exp(-k_r \tau)$ and $\exp(+k_r \tau)$. If by adjusting A_m and B_m we can make the coefficients of $\exp(-k_r \tau)$ and $\exp(k_r \tau)$ in the integrated expression of

$$\int_0^T \varphi(\tau) K |t - \tau| d\tau$$

equal to zero, we will have the solution to our eigenvalue problem.

When (2.1) is substituted in (1.1), the evaluation of the resulting integrals involves integrals of the type

$$\int_0^T e^{p\tau} e^{-k_r |t - \tau|} d\tau = -\frac{2k_r e^{pt}}{p^2 - k_r^2} - \frac{e^{-k_r t}}{p + k_r} + \frac{e^{k_r t + (p - k_r)T}}{p - k_r}.$$

Using the above one has

$$\begin{aligned} \frac{1}{\lambda} \varphi(t) &= \frac{1}{\lambda} \left[\sum_{m=1}^n A_m e^{-\gamma_m t} + \sum_{m=1}^n B_m e^{\gamma_m t} \right] = \int_0^T \varphi(\tau) K |t - \tau| d\tau = \\ &= \sum_{m=1}^n \int_0^T A_m e^{-\gamma_m t} \sum_{r=1}^n e^{-k_r |t - \tau|} + \sum_{m=1}^n \int_0^T B_m e^{\gamma_m t} \sum_r C_r e^{-k_r |t - \tau|} d\tau = \\ &= -2 \sum_{m,r} \frac{k_r A_m C_r e^{-\gamma_m t}}{\gamma_m^2 - k_r^2} - \sum_{m,r} \frac{A_m C_r e^{-k_r t}}{k_r - \gamma_m + k_r} - \sum_{m,r} \frac{A_m C_r e^{k_r t - (k_r + \gamma_m)T}}{k_r + \gamma_m} \\ &\quad - 2 \sum_{m,r} \frac{k_r B_m C_r e^{\gamma_m t}}{\gamma_m^2 - k_r^2} - \sum_{m,r} \frac{B_m C_r e^{-k_r t}}{k_r + \gamma_m} - \sum_{m,r} \frac{B_m C_r e^{k_r t - (k_r - \gamma_m)T}}{k_r - \gamma_m}. \quad (2.3) \end{aligned}$$

If (2.3) is to be true for all t , the coefficients of $e^{-\gamma_m t}$ and $e^{\gamma_m t}$ should agree on both sides of the equation and the coefficients of $\exp(k_r t)$

and $\exp(-k_r t)$ must vanish for all r . Applying this condition we get from (2.3):

Coeff. of $e^{k_r t} = 0$, or,

$$\sum_{m=1}^n \frac{A_m}{k_r - \gamma_m} + \sum_m \frac{B_m}{k_r + \gamma_m} = 0, \quad (2.4)$$

coeff. of $e^{-k_r t} = 0$, or,

$$\sum_{m=1}^n \frac{A_m e^{-\gamma_m t}}{k_r + \gamma_m} + \sum_m \frac{B_m e^{\gamma_m t}}{k_r - \gamma_m} = 0. \quad (2.5)$$

Equations (2.4) and (2.5) are a homogeneous set of $2n$ equations for the coefficients A_m and B_m .

Also by equating the coefficients of $e^{-\gamma_m t}$ or $e^{\gamma_m t}$ for each m in both sides of (2.3), we get

$$\frac{1}{\lambda} = -2 \sum_r \frac{k_r C_r}{\gamma_m^2 - k_r^2}, \quad r = 1, 2, \dots, n. \quad (2.6)$$

Equations (2.4), (2.5) and (2.6) are the desired eigenvalue equations.

§ 3. *Routine for solution.* The routine for calculating λ and the unknowns in the expansion of the eigenfunction, viz., A_m , B_m , and γ_m is outlined in the following. Noting that (2.6) is an algebraic equation of n^{th} order for γ_m^2 and that the coefficients of this equation involve λ , the following steps may be followed for the eigenvalue calculation.

1. Find n roots of γ_m^2 , viz., $\gamma_1^2, \gamma_2^2, \dots, \gamma_n^2$ from (2.6). Note that the roots will be functions of λ .

2. Substitute $\gamma_1, \gamma_2, \dots$, etc. in (2.4), and (2.5). Since (2.4) is a homogeneous equation, A_m and B_m , the determinant $\Delta(\lambda)$ of the equation must equal zero.

3. Using $\Delta(\lambda) = 0$, solve the resulting equation of λ . For each λ , say λ_p , calculate γ_{mp} ($m = 1, \dots, n$) from the expressions for γ_m in step 1.

4. Substitute these γ_{mp} 's in (2.4) and (2.5) and solve for A_{mp} 's and B_{mp} 's corresponding to the p^{th} eigenvalue λ_p . Note that the coefficients can be determined only within a multiplicative constant (this of course is always the case in an eigenvalue problem). The expression for the p^{th} eigenfunction is

$$\varphi_p = \sum_{m=1}^n A_{mp} e^{-\gamma_{mp} t} + \sum B_{mp} e^{\gamma_{mp} t}. \quad (3.1)$$

Although the formal routine is outlined above, it is pertinent to point out the difficulties in working out a practical case. Firstly the difficulty is in solving for the n roots of (2.6) since the coefficients involve the unknown λ . Even more difficult is the solution of the determinantal equation $\Delta(\lambda) = 0$ since it is usually a transcendental equation for λ . One must therefore resort to numerical methods and expect only approximate solutions.

§ 4. *Example.* To illustrate the routine, an example will be worked out in this section. Consider the case

$$K |t - \tau| = e^{-k|t - \tau|}.$$

Equation (2.6) for this case of $n = 1$ is

$$\frac{1}{\lambda} + \frac{2k}{\gamma^2 - k^2} = 0 \quad (4.1)$$

or

$$\gamma = (k^2 - 2k\lambda)^{\frac{1}{2}}. \quad (4.2)$$

From (2.4) and (2.5) we have

$$\frac{A}{k - \gamma} + \frac{B}{k + \gamma} = 0, \quad (4.3)$$

$$\frac{A e^{-\gamma t}}{k + \gamma} + \frac{B e^{\gamma t}}{k - \gamma} = 0. \quad (4.4)$$

Hence,

$$\Delta = \begin{vmatrix} \frac{1}{k - \gamma} & \frac{1}{k + \gamma} \\ \frac{e^{-\gamma T}}{k + \gamma} & \frac{e^{\gamma T}}{k - \gamma} \end{vmatrix} = 0. \quad (4.5)$$

From (4.5)

$$\frac{e^{\gamma T}}{(k - \gamma)^2} - \frac{e^{-\gamma T}}{(k + \gamma)^2} = 0$$

or

$$e^{\gamma T} = \frac{\pm (k - \gamma)}{k + \gamma}. \quad (4.6)$$

Substituting (4.2) in (4.6), there results,

$$e^{(k^2 - 2k\lambda)^{\frac{1}{2}} T} = \frac{\pm (k - (k^2 - 2k\lambda)^{\frac{1}{2}})}{k + (k^2 - 2k\lambda)^{\frac{1}{2}}}. \quad (4.7)$$

Solutions of (4.7), which is a transcendental equation, are the eigenvalues λ of the problem.

For a particular λ , say λ_p , we have from (4.2) and (4.3)

$$\begin{aligned} \gamma_p &= (k^2 - 2k\lambda_p)^{\frac{1}{2}}, \\ B_p &= \frac{k + \gamma_p}{\gamma_p - k} A_p. \end{aligned} \quad (4.8)$$

Hence,

$$\varphi_p = A_p \left[e^{-\gamma_p t} + \frac{k + \gamma_p}{k - \gamma_p} e^{\gamma_p t} \right]. \quad (4.9)$$

Equation (4.9) rearranged reads

$$\varphi_p = \frac{k}{\gamma_p} (\sinh \gamma_p t + \cosh \gamma_p t),$$

where the constant factor has been dropped. The same solution was obtained by Youla¹⁾ by using a different method of formulation.

§ 5. *Upper limit infinity.* It is of interest to consider the case when T , the upper limit of the integral equation (1.1), is infinity. The formulation discussed above is still valid, but there results certain simplifications of the process of obtaining λ and φ . This is the subject of the discussion below.

We notice first of all that because of the infinite range of the integral equation, continuous eigenvalues will result for the type of kernel considered. In order for the integral

$$\int_0^\infty (\sum C_r e^{-k_r t}) (A_r e^{-\gamma_r t} + B_r e^{\gamma_r t}) dt$$

to converge, it is essential that, if $\text{Re}(\gamma_r) = \gamma_{r1} (\gamma_{r1} > 0)$, then $\gamma_{n1} < k_1$, k_r real. It has been assumed that $k_1 < k_2 < \dots < k_n$ and $\gamma_{11} < \dots < \gamma_{n1}$. It is to be noted that since $\gamma_{r1} > 0$, all γ_r 's are admissible.

Since the γ 's involve the eigenvalue λ , this sets a limit to the

values that λ can take. Consider again the simple example in which

$$K |t - \tau| = e^{-k|t - \tau|}.$$

Then the substitution of

$$\varphi(\tau) = A e^{-\gamma\tau} + B e^{\gamma\tau} \quad (5.1)$$

in the integral equation

$$\varphi(t) = \lambda \int_0^\infty \varphi(\tau) e^{-k|t - \tau|} d\tau, \quad k \text{ real}, \quad (5.2)$$

yields

$$\frac{1}{\lambda} (A e^{\gamma t} + B e^{-\gamma t}) = -\frac{2kA e^{-\gamma t}}{\gamma^2 - k^2} - \frac{A e^{-kt}}{\gamma + k} - \frac{2kB e^{\gamma t}}{\gamma^2 - k^2} - \frac{B e^{-kt}}{-\gamma + k}. \quad (5.3)$$

Hence,

$$\frac{1}{\lambda} + \frac{2k}{\gamma^2 - k^2} = 0 \quad (5.4)$$

and

$$\frac{A}{\gamma + k} - \frac{B}{\gamma - k} = 0. \quad (5.5)$$

From (5.4)

$$\gamma = \sqrt{k^2 - 2k\lambda}. \quad (5.6)$$

In (5.5) A can be arbitrarily chosen, and solving for B we get

$$B = \frac{\gamma - k}{\gamma + k} A. \quad (5.7)$$

Note that (5.5) can be satisfied for all γ 's by the choice of B/A . Therefore the eigenvalue equation (5.5) is satisfied for a continuous range of λ . The solution $\varphi(t)$ is

$$\varphi(t) = A \left[e^{-\sqrt{k^2 - 2k\lambda}t} + \frac{\sqrt{k^2 - 2k\lambda} - k}{\sqrt{k^2 - 2k\lambda} + k} e^{\sqrt{k^2 - 2k\lambda}t} \right]. \quad (5.7)$$

Note also that if $\text{Re } \lambda < 0$, then $\text{Re } (\gamma) > k$; hence negative values of $\text{Re } (\gamma)$ are inadmissible. Equation (5.2) has also been solved by Wiener-Hopf technique and appears as an example in the book by Morse and Feshbach²⁾.

§ 6. *Conclusion.* In this paper we have considered the eigenvalue problem for the finite and infinite function range Wiener-Hopf equation with a kernel function $K |t|$ which can be expressed as a series of exponentials.

The equation occurs in the field of probability theory, the details of the origin and certain applications have been given by Youla ¹⁾, and the discussion in this paper has presented a method of solving the eigenvalue problem in terms of a set of simultaneous equations derived in a rather simple manner. The technique outlined here is also useful in solving the inhomogeneous Wiener-Hopf equation with finite and infinite ranges without resorting to the method of Fourier transforms. The details of this and the contents of the paper have been published in a technical report ³⁾ by the author.

Received 16th November, 1959.

REFERENCES

- 1) Youla, D. C., The Solution of a Homogeneous Wiener-Hopf Integral Equation, IRE Trans. on Information Theory, Vol IT-3, No. 3, Sept. 1957.
- 2) Morse, P. M. and H. Feshbach, Methods of Theoretical Physics, Pt. I, p. 981, McGraw-Hill.
- 3) Mittra, R., On the Solution of a Class of Wiener-Hopf Integral Equation for Finite and Infinite Ranges, Technical Report No. 37, Antenna Laboratory, University of Illinois.

HEATING OF AN IONIZED GAS SHEATH BY MICROWAVES *)

by MAHENDRA SINGH SODHA

Physics Division Armour Research Foundation Chicago, Illinois, U.S.A.

Summary

In this communication the author has discussed the heating of an isothermal rigid uniform sheath by the incidence of microwaves, a problem of importance in space physics. The physical processes considered are as follows: The temperature of the sheath rises due to the absorption of microwaves, which in turn increases the electron density and thereby affects the absorption. This continues until the absorbed microwave energy equals the energy lost by radiation.

§ 1. *Introduction.* The study of the interaction of electromagnetic energy with an ionized gas occupies a prominent place in space physics. Since 1933 considerable effort has been devoted to the study of phenomena induced in the ionosphere by radio-waves, particularly the Luxemburg effect. However, these investigations were concerned with radio-waves of low energy. In this communication the author has considered the incidence of high energy microwaves on a plasma sheath. The physical processes involved can easily be visualized. The temperature of the sheath rises due to absorption of the microwaves, which in turn increases the electron density and thereby affects the absorption. Thus the temperature of the sheath continues rising until the absorbed microwave energy equals the energy lost by radiation.

A straightforward method for analysis would be to attempt the solution of the hydrodynamic equations, involved in the formation of the plasma sheath, as modified by the electromagnetic energy. Besides being very difficult to obtain, this solution would strongly

*) Work supported by Rome Air Development Center and Air Research Development command under contract number AF 30(602)-2034.

depend on the way the sheath is formed and hence be of little value in other cases. Hence the author has taken recourse to a rather idealized model in the hope that the results obtained will indicate the orders of magnitude and the importance of various parameters which are involved.

It is obvious that a sheath left to itself will dissipate by diffusion, and this is certainly not the case for sheaths one may possibly be interested in. The confining hydrodynamic forces keep the sheath unchanged in form or in other words, rigid. It is conceivable that absorption of electromagnetic energy will change the form of the sheath. However, we can as a first approximation assume the sheath to retain its form even under the influence of high energy microwaves. To simplify analysis we may further assume the sheath to be uniform and isothermal and the microwaves to be incident normally.

§ 2. *Basic equations.* The basic equations and implied assumptions are as follows:

1. Rigidity and absence of doubly and multiply charged ions require

$$N_0 + (N_e + N_i)/2 = N, \quad (1)$$

where N_0 , N_e and N_i denote the numbers per unit volume of neutral molecules, electrons and ions. N denotes the number of neutral molecules in the absence of ionization.

2. Electric neutrality of plasma requires

$$N_e = N_i. \quad (2)$$

3. Thermodynamic equilibrium requires

$$K_1 = N_e N_i P / N_0 (N_e + N_0 + N_i), \quad (3)$$

where K_1 is the equilibrium constant and P is the pressure given by

$$P = (N_e + N_0 + N_i) kT, \quad (4)$$

k and T being the Boltzmann constant and temperature respectively

Further, Saha's equation provides

$$K_1 = AT^{5/2} \exp(-B/T), \quad (5)$$

where A and B are characteristic of the element of which the sheath consists.

4. If the microwave is a plane wave described by

$$E_y \propto \exp\{i[\omega t - (a - ib)x]\}, \quad (6)$$

Margenau's ¹⁾ results may be expressed as

$$2a^2 = \frac{\omega^2}{c^2} \{[1 - (4\pi\sigma_i/\omega)]^2 + (2\pi\sigma_\gamma/\omega)^2\}^{1/2} + \frac{\omega^2}{c^2} [1 - (4\pi\sigma_i/\omega)] \quad (7)$$

and

$$2b^2 = \frac{\omega^2}{c^2} \{[1 - (4\pi\sigma_i/\omega)]^2 + (2\pi\sigma_\gamma/\omega)^2\}^{1/2} - \frac{\omega^2}{c^2} [1 - (4\pi\sigma_i/\omega)] \quad (8)$$

where $\sigma_\gamma - i\sigma_i$ is the a.c. conductivity of the gas given by

$$\sigma_\gamma = \frac{N_e e^2}{3m} \left\langle \frac{1}{v^2} \frac{d}{dv} \left(\frac{v v^3}{v^2 + \omega^2} \right) \right\rangle, \quad (9)$$

$$\sigma_i = \frac{N_e e^2}{3m} \left\langle \frac{1}{v^2} \frac{d}{dv} \left(\frac{\omega v^3}{v^2 + \omega^2} \right) \right\rangle. \quad (10)$$

E is the electric vector, ω is the microwave frequency, e is the charge of an electron in e.s.u., m is the mass of electron, v is the electron velocity, ν is the collision frequency of the electron and $\langle \rangle$ denotes the average over the electron velocity distribution.

The collision frequency of an electron is given by

$$\nu = \nu_0 + \nu_{e,i}, \quad (11)$$

where the subscripts 0 and e, i refer to collisions with neutral molecules and ions and other electrons.

The collision frequency ν_0 is given by

$$\nu_0 = N_0 v Q(v), \quad (12)$$

where $Q(v)$ is the cross-section of collision and is tabulated for most gases as a function of v .

For singly charged ions $\nu_{e,i}$ is approximately given by ²⁾

$$\nu_{e,i} = (4\pi e^4/m^2)(1/1.432)(m/2k_0T)^{0.778} N_i \ln A/v^{1.444}, \quad (13)$$

where $\ln A$ is tabulated by Spitzer ³⁾ for various values of N_e and T and may be treated as a constant (≈ 10).

The calculation of the distribution function with all these sources of scattering, appreciable absorption and multiple reflections is

rather complicated and we will not attempt to treat it here. Moreover, since we are interested only in orders of magnitude, in our crude model a Maxwellian distribution should suffice.

It may be easily seen that the coefficient of intensity reflection at the boundary of the sheath and vacuum for normal incidence is given by

$$R = \frac{[a - (\omega/c)]^2 + b^2}{[a + (\omega/c)]^2 + b^2}. \quad (14)$$

It is obvious that the coefficient of intensity absorption is $2b$.

5. Taking into account the multiple reflections at the boundary of the sheath, it may be shown that the energy absorbed in the sheath per unit time per unit area is given by

$$\Phi = I(1 - R) \left[1 - \frac{e^{-2bl}(1 - R)}{1 - R e^{-2bl}} \right], \quad (15a)$$

where I is the intensity of the microwave or the energy incident per unit area per unit time and l is the thickness of the sheath. If one of the boundaries of the sheath is a metallic wall with perfect reflection, expression (15a) should be replaced by

$$\Phi' = I(1 - R) \left[1 - \frac{e^{-4bl}(1 - R)}{1 - R e^{-4bl}} \right]. \quad (15b)$$

In what follows we shall use only (15a).

6. The energy equation for the sheath may be written as

$$\frac{3}{2}kl(N_0 + N_e + N_i) dT/dt = \Phi - 2\sigma(T^4 - T_1^4), \quad (16)$$

where $\frac{3}{2}k(N_0 + N_e + N_i)$ is the heat capacity per unit volume of the sheath, dT/dt is the rate of rise of temperature, and $2\sigma(T^4 - T_1^4)$ is the energy lost per unit area by radiation from the two surfaces, assuming the sheath to be a black body. The last term in (16) has to be modified if one of the boundaries loses heat by conduction to a thick metallic surface.

§ 3. *Solution.* From (1), (2), (3), (4) and (5) one obtains

$$N_i = N_e = \frac{1}{2} \left\{ \left[\frac{A^2}{k^2} T^3 e^{-2B/T} + \frac{4NA T^{3/2}}{k} e^{-B/T} \right]^{1/2} - \frac{A}{k} T^{3/2} e^{-B/T} \right\} \quad (17)$$

and

$$N_0 = N - N_e. \quad (18)$$

Using (6) to (15b) and (17) and (18) we can calculate Φ as a function of T for given N , ω , l and I . Hence from (16) we may write the solution as

$$t = \int_0^t dt = \int_{T_0}^T \frac{\frac{3}{2}kl(N + N_e)}{\Phi(T) - 2\sigma(T^4 - T_1^4)} dT. \quad (19)$$

The integration can be performed numerically in a straightforward manner since $\Phi(T)$ and N_e are known functions of T .

The maximum or steady state temperature may be obtained by putting $dT/dt = 0$ in (16) and solving for T graphically.

§ 4. *Discussion.* When l is small, the power loss by radiation is given by ⁴⁾

$$1.54 \times 10^{-27} N_e^2 T^{1/2}$$

per unit volume. Hence $2\sigma(T^4 - T_1^4)$ must be replaced by $1.54 \times 10^{-27} N_e^2 T^{1/2} l$ in all the equations.

The present treatment is very crude but it

i) brings out the important parameters in the problem.

ii) gives the order of magnitude of the temperature that can be reached under given conditions.

iii) gives the order of magnitude of the time needed to reach a given fraction of the steady state temperature so that laboratory experiments with pulses of microwaves can be planned.

Received 18th December, 1959.

REFERENCES

- 1) Margenau, H. Phys. Rev. **69** (1946) 508.
- 2) Sodha, M. S. and Y. P. Varshni, Phys. Rev. **114** (1959) 717.
- 3) Spitzer, L., Physics of Fully Ionized Gases, Interscience Publishers Inc., New York 1956, 0. 73.
- 4) Thompson, W. B., Radiation from a Plasma, Atomic Energy Research Establishment, Harwell, AERETM/73, 1957.

PROPAGATION OF ELECTROMAGNETIC PULSES
IN A HOMOGENEOUS CONDUCTING EARTH

JAMES R. WAIT*)

Newmont Exploration Limited, Danbury, Connecticut, U.S.A.

Summary

A general analysis for the electromagnetic response of conducting media due to pulse excitation is presented. The treatment is based on the Laplace transform theory. First, a survey of the field is made and the limitations and scope of the previous work are pointed out. The theory of propagation of a plane wave pulse in a conducting and homogeneous medium of infinite extent is then reviewed. The form of these results enable one to evaluate the relative importance of the conductivity and the dielectric constant. It is indicated, for sufficiently large times in the transient response, that displacement currents may be safely neglected for sea water and for most geological media. Under this assumption, the waveform of the electric field in a conducting medium is illustrated for the case where the source is an electric dipole energized by a step-function current. Results are also presented for exponential and bell-shaped source functions. The pulse shape of the field components is profoundly modified as they propagate through the medium. It is suggested that this property may be utilized in measuring distances in the earth's crust. The more difficult problem of propagation in non-infinite conducting media is also considered. To account for the presence of the interface in a conducting half space, (i.e. homogeneous flat ground) a rather involved analytical expression for the transient fields is required. Certain special cases, such as a horizontal electric dipole at the interface, are illustrated by numerical results. The transient excitation of a wire loop lying on the surface of a homogeneous ground is also considered. Finally, transient coupling between pairs of parallel insulated wires grounded at their end points is treated as an extension of the earlier results.

§ 1. *Introduction.* It is traditional in the theoretical study of electromagnetic waves to assume a time dependence of the form $\exp(i\omega t)$. The resulting solutions are thus valid only in the steady state. In many applications this assumption is justified in a crude sense even when the signal is a "burst" of a continuous wave such

*) Present address: National Bureau of Standards, Boulder, Colorado, U.S.A.

as a radar pulse. However, if one is interested in the precise form of the leading edge or trailing edge of the pulse, the solution for harmonic time dependences tells you exactly nothing. The problem becomes rather critical when the wave suffers dispersion such as would be the case for propagation in a conducting or ionized medium.

It is the purpose of the present paper to consider the propagation of an electromagnetic pulse signal in conducting media under various assumptions. Taken together it is believed that these results shed some light on the behaviour of pulse propagation in actual terrestrial media such as soils and rocks and sea water. There has been some attention already given to this general problem and it seems desirable to review this past work and mention any limitations of the results.

Using an operational approach Riordan ¹⁾ calculated voltages during transient conditions in a grounded wire lying on the earth's surface due to a suddenly applied current in a second grounded wire. In his treatment, the displacement currents in the air and the ground were neglected. Furthermore, his starting point was a formula due to Foster ²⁾ for the mutual impedance between grounded wires which assumed that the insulation was perfect in the sense that the current in the primary wire was constant throughout its length and the induced terminal voltage was the line integral of the electric field along the length of the secondary wire. Since Foster's results are valid when typical dimensions D in the problem are small compared to the free-space wavelength, the formulae of Riordan are valid at times t much greater than D/c where c is the velocity of light in vacuo. Many interesting related problems are discussed by Sunde ³⁾ in his text.

The author ⁴⁾ has derived explicit formulae and presented numerical results for the fields of electric and magnetic dipoles which are excited by a step-function current. The surrounding conducting medium was assumed to be infinite and homogeneous, and displacement currents were neglected. The results are thus not valid for small times. Under similar assumptions the transient fields of a magnetic dipole over a layered conductor were calculated under various conditions ⁵⁾. The author has also presented an exact solution for the fields of a magnetic dipole with step function current excitation in a homogeneous conducting medium ⁶⁾. In

this work displacement currents were accounted for and it was shown that at sufficiently large times (after the initiation of the source pulse) the previously derived approximate formulae were regained ⁴).

More recently, a series of papers by Bhattacharyya have appeared dealing with this subject. Since they are closely related to the above described work they will be mentioned in turn. In his first ⁷) and second ⁸) paper, he presents a solution for the transient fields of an electric dipole excited by a ramp current source and located in an infinite homogeneous conducting medium. This ramp source is a current which rises linearly with time t from 0 to t_1 after which it is a constant. In these solutions displacement currents are neglected. Bhattacharyya illustrates that the electric and magnetic field intensities exhibit time gradients varying with the shortness of the rise time t_1 . This author prefers the ramp source as a theoretical model in preference to a step function source. In fact, he says "an electric pulse rising instantaneously from one value to another is not physically realizable". It is only proper to point out, however, that Bhattacharyya's ramp source is also not physically realizable as there are discontinuities in the derivatives at both $t = 0$ and $t = t_1$. Actually, the response calculated for a step function source is more basic since the response for arbitrary excitation may be computed readily by superposition therefrom.

In a third paper Bhattacharyya ⁹) has presented formulas for the fields of a small loop (i.e. magnetic dipole), lying on the surface of a conducting half-space, energized by ramp-function source currents. For zero rise time these results reduce to those given by Wait ⁵). Displacement currents are again neglected.

In a fourth paper, Bhattacharyya ¹⁰) discusses the fields of an electric dipole energized by a step function current. The conducting surrounding medium is assumed infinite and homogeneous, but displacement currents are considered. The inversion of the relevant Laplace transforms is carried out by numerical means. The transforms are similar in form to the results given by Wait for the corresponding problem of a magnetic dipole. Finally in a fifth paper, Bhattacharyya ¹¹) obtains results for the fields of a small loop on the surface of the conducting homogeneous earth, taking full account of the displacement currents in both the air and the

ground. Again the inversion of the Laplace transforms is carried out partly by numerical means.

It should be emphasized that in both these latter two papers of Bhattacharyya ¹⁰⁾¹¹⁾ and an earlier paper by Wait ⁶⁾ the conductivity and dielectric constant of the medium are assumed to be constant with respect to frequency. In the case of sea water this is a good assumption, but on the other hand the electrical "constants" of soils and rocks are very frequency-dependent. In fact, in the region of 10 Hz to 10 kHz, the dielectric constant varies approximately as the inverse of frequency for many geological media ¹²⁾. This fact should be borne in mind in the interpretation of electrical transient measurements *in situ*.

A further paper on the subject by Richards ¹³⁾ has appeared recently. The stated purpose of his paper was to extend Wait's result for the electric fields of a transient magnetic dipole to give explicit expressions for the magnetic field components. Richards results are given in the form of convolution integrals and thus are not really "explicit", although they appear to be consistent with the results of Bhattacharyya and Wait when specialized to step-function source functions. Richards also points out that for ranges of interest in most practical problems the waveforms of the received fields are not influenced by the displacement currents.

Recently a paper by Grumet ¹⁴⁾ has appeared which considers propagation into a semi-infinite conductor when a step-function electric field is applied to the plane interface. How this is to be accomplished is not stated. The problem as formulated is one-dimensional and is entirely equivalent to calculating the voltage at any point on a uniform transmission line whose series resistance, series inductance and shunt capacitance per unit length are specified ¹⁵⁾.

In addition to the investigations mentioned above, there are a number of recent papers ¹⁶⁻²¹⁾ which deal with the propagation along the surface of the earth to great distances. Usually these are confined to the radiation field of the antenna, and attention is limited to the space above or on the surface of the earth. As has been pointed out very recently by Keilson and Row ²²⁾, however, the convolution theorem may be applied to calculate the waveform at some subsurface point in terms of the field at the surface. In the example they used, the electromagnetic disturbance

postulated at the interface was a pure Zenneck surface wave. Such a wave bears little similarity to that set up by a physical source. Despite this fact, the conclusions reached by Keilson and Row, in the main, are valid.

The possibility that transient electromagnetic waves may be used in geophysical prospecting has been discussed quite frequently in recent years. White ²³⁾, in particular, has proposed that the buildup of the voltage between two grounded electrodes resulting from a suddenly applied current at two other electrodes is indicative of the sub-surface features. This problem has also been studied in some detail by Wait ²⁴⁾ who treated the transient electromagnetic response of a stratified conductor ⁵⁾, thin slabs ²⁵⁾ and spheres ²⁶⁾ for various sources. Transient coupling, between pairs of parallel insulated wires grounded at their end points in a conducting medium, was also considered ²⁷⁾.

The geological and geophysical applications of transients have been discussed extensively by Belluigi ²⁸⁻³¹⁾ in Italy and similar studies have been made by Yost ³²⁾ in the U.S.A.

The use of transient electromagnetic pulses to probe geological structures is apparently highly developed in the U.S.S.R. A number of papers, mainly theoretical, have appeared in the Russian literature in the last decade. Their developments have been apparently carried out independently of that done elsewhere. Virtually no references are given to the "western" literature, although very similar problems have been treated. Tikhonov ³³⁾³⁴⁾, in particular, has treated formally the electric transient fields on the surface of both a homogeneous and a layered half space for both plane wave and dipole sources. Skugarevskaya ³⁵⁾³⁶⁾, in collaboration with Tikhonov, has further developed the theory and was able to evaluate approximately the infinite integrals corresponding to small or large times in the transient response. Chetayev ³⁷⁾, also in the U.S.S.R., has published a solution for the transient fields of a loop lying on the surface of a homogeneous conducting half space. He also developed an approximate correction term to account for the presence of a layer. He gave no numerical results.

In the above mentioned Russian work on this subject, the displacement currents are consistently neglected and the conductivity is assumed to be a constant with respect to frequency or time. For this reason, it would appear that the suggested interpretation of

experimental data as proposed by Skugarevskaya ³⁶⁾ should be considered with a certain caution. The variability of the electrical properties of the geological materials could very well give rise to anomalous results ¹²⁾. Nevertheless, the results of Russian workers are very valuable and are leading to a better understanding of transient electromagnetic waves in conducting layered media.

§ 2. *Propagation of transients in unbounded media.* The simplest case to consider is when the fields only depend on one coordinate. Furthermore, if the medium is homogeneous with conductivity σ , dielectric constant ϵ and permeability μ , the field components for a time harmonic plane wave may be represented by

$$H_y(i\omega) = H_0(i\omega) e^{-\gamma x} e^{i\omega t} \quad (1)$$

and

$$(\sigma + i\epsilon\omega) E_z(i\omega) = \gamma H_0(i\omega) e^{-\gamma x} e^{i\omega t} \quad (2)$$

where

$$\gamma = [i\mu\omega(\sigma + i\epsilon\omega)]^{\frac{1}{2}}, \quad (3)$$

ω is the angular frequency and H_0 is the magnitude of the H_y field at $x = 0$. The cartesian coordinate system (x, y, z) has been chosen so that the direction of propagation is parallel to the x axis and the magnetic and electric field vectors are parallel to the y and z directions respectively.

Now if in the plane $x = 0$ the y component of the magnetic field is specified as some function of time, say $h_0(t)$, then the problem is to determine the form of the magnetic field $h_y(t)$ and electric field $e_z(t)$ at some finite value of x . This may be accomplished by representing the transient fields as Fourier integrals and then using the known results for the corresponding time-harmonic problem. For example, $h_0(t)$ may be written in the form

$$h_0(t) = \frac{1}{2\pi} \int_{-\infty}^{+\infty} H_0(i\omega) e^{i\omega t} d\omega = \frac{1}{2\pi i} \int_{-i\infty}^{+i\infty} H_0(s) e^{st} ds \quad (4)$$

and thus

$$H_0(i\omega) = \int_0^{\infty} h_0(t) e^{-i\omega t} dt = \int_0^{\infty} h_0(t) e^{-st} dt = H_0(s), \quad (5)$$

assuming that $h_0(t) = 0$ for $t < 0$. As is indicated above, the quantity s can be identified with $i\omega$. In this s notation, $H_0(s)$ is the

Laplace transform of $h_0(t)$, which may be written symbolically as

$$H_0(s) = Lh_0(t) \quad (6)$$

or

$$h_0(t) = L^{-1}H_0(s). \quad (7)$$

The formal results for the field components are thus

$$h_y(t) = L^{-1}H_y(s) = L^{-1}H_0(s) e^{-\gamma(s)x} \quad (8)$$

and

$$e_z(t) = L^{-1}E_z(s) = L^{-1} \frac{\mu(s)}{\gamma(s)} H_0(s) e^{-\gamma(s)x}, \quad (9)$$

where

$$\gamma(s) = [\mu s(\sigma + \epsilon s)]^{\frac{1}{2}}. \quad (10)$$

It will now be assumed that the driving function $h_0(t)$ is a unit impulse, that is

$$h_0(t) = H_0 \delta(t) \quad (11)$$

where $\delta(t)$ is the Dirac function at $t = 0$. Thus

$$H_0(s) = H_0 \quad (12)$$

and

$$h_y(t) = L^{-1}H_0 e^{-\gamma(s)x} = L^{-1}H_0 \exp\{-[s(s + a)]^{\frac{1}{2}}k\}, \quad (13)$$

where

$$k = (\epsilon\mu)^{\frac{1}{2}}x \text{ and } a = \sigma/\epsilon. \quad (14)$$

Consulting the tables of Laplace transform pairs in Magnus *et al.*³⁸⁾ or Campbell and Foster³⁹⁾ it is possible to write down the result

$$\begin{aligned} h_y(t) = & H_0 e^{-\frac{1}{2}at} \delta(t - k) + \\ & + H_0 a k e^{-\frac{1}{2}at} \frac{I_1[\frac{1}{2}a(t^2 - k^2)^{\frac{1}{2}}]}{2(t^2 - k^2)^{\frac{1}{2}}} u(t - k), \end{aligned} \quad (15)$$

also

$$\begin{aligned} e_z(t) = & (\mu/\epsilon)^{\frac{1}{2}} H_0 e^{-\frac{1}{2}at} \delta(t - k) + \\ & + (\mu/\epsilon)^{\frac{1}{2}} \frac{H_0 a}{2} e^{-\frac{1}{2}at} \left\{ \frac{t}{(t^2 - k^2)^{\frac{1}{2}}} I_1[\frac{1}{2}a(t^2 - k^2)^{\frac{1}{2}}] - \right. \\ & \left. - I_0 \left[\frac{a}{2} (t^2 - k^2)^{\frac{1}{2}} \right] \right\} u(t - k). \end{aligned} \quad (16)$$

The corresponding responses $\bar{h}_y(t)$ and $\bar{e}_z(t)$ for an arbitrary excitation $h_0(t)$ may be expressed formally in terms of the impulse responses quoted above as follows:

$$\bar{h}_y(t) = \frac{1}{H_0} \int_0^t h_y(\tau) h_0(t - \tau) d\tau \quad (17)$$

and

$$\bar{e}_z(t) = \frac{1}{H_0} \int_0^t e_z(\tau) e_0(t - \tau) d\tau. \quad (18)$$

For example if the exciting magnetic field in the plane $x = 0$ is a stepfunction, that is if

$$h_0(t) = H_0 u(t), \quad (19)$$

the corresponding step-function responses are given by

$$\bar{h}_y(t) = \int_0^t h_y(\tau) d\tau \quad (20)$$

and

$$\bar{e}_z(t) = \int_0^t e_z(\tau) d\tau, \quad (21)$$

being simply integrals over the impulse responses. The resulting integration over the impulse functions is simple, i.e.

$$\int_0^t \delta(\tau - k) d\tau = u(t - k), \quad (22)$$

leading to a step-function. The integration of the second factor in the right of (15) apparently is not expressible in closed form. However, integration of the right hand side of equation (21) may be easily carried out and the result is

$$\bar{e}_z(t) = (\mu/\varepsilon)^{\frac{1}{2}} H_0 e^{-\frac{1}{2}at} I_0[\frac{1}{2}a(t^2 - k^2)^{\frac{1}{2}}] u(t - k). \quad (23)$$

This is an exact result. It is interesting to study the limiting case of this formula when the medium is highly conducting since this sheds some light on the nature of approximations that are used later in more complicated situations. If

$$(t^2 - k^2)^{\frac{1}{2}} \gg 2\varepsilon/\sigma, \quad (24)$$

the Bessel function I_0 may be replaced by the first term of its

asymptotic expansion, thus

$$\tilde{e}_z(t) \cong (\mu/\sigma)^{\frac{1}{2}} H_0(\pi t)^{-\frac{1}{2}} \exp(-\sigma\mu r^2/4t). \quad (25)$$

This is the result which could be obtained if displacement currents were neglected at the outset. For example if ε was set equal to zero and the exciting magnetic field on the plane $x = 0$ has the form $H_0 u(t)$, then it follows directly that

$$\tilde{e}_z(t) \cong L^{-1}(\mu/\sigma)^{\frac{1}{2}} H_0 s^{-\frac{1}{2}} \exp[-(\sigma\mu s)^{\frac{1}{2}} x], \quad (26)$$

which is consistent with (9) above.

§ 3. *Transient fields of dipoles in unbounded and homogeneous media.*

3a. *Exact Solutions.* The fields of a dipole in an infinite and homogeneous conducting medium may be expressed formally in terms of Bessel functions in the same manner as in the previous section.

The electric dipole of length ds is located at the centre of a spherical coordinate system (r, θ, ϕ) and oriented in the polar ($\theta = 0$) direction. The expressions for the Laplace transforms of the field components may be written down immediately since they have the same form as the corresponding time-harmonic expressions. Thus

$$E_r(s) = \frac{I(s) ds}{2\pi(\sigma + \varepsilon s)} \frac{e^{-\gamma r}}{r^3} (1 + \gamma r) \cos \theta, \quad (27)$$

$$E_\theta(s) = \frac{I(s) ds}{4\pi(\sigma + \varepsilon s)} \frac{e^{-\gamma r}}{r^3} (1 + \gamma r + \gamma^2 r^2) \sin \theta, \quad (28)$$

$$H_\phi(s) = \frac{I(s) ds}{4\pi r^2} e^{-\gamma r} (1 + \gamma r) \sin \theta, \quad (29)$$

where $\gamma = [\mu s(\sigma + \varepsilon s)]^{\frac{1}{2}}$ and $I(s)$ is the transform of the current $i(t)$ in the dipole. If

$$i(t) = I_0 \delta(t), \quad (30)$$

then, of course, $I(s) = I_0$. The magnetic field response as a function of time is then to be obtained from

$$h_\phi(t) = \frac{I_0 ds}{4\pi r^2} \sin \theta \cdot \Phi(t), \quad (31)$$

where

$$\Phi(t) = L^{-1} e^{-\sqrt{s(s+a)}k} [1 + \sqrt{s(s+a)}k]. \quad (32)$$

This transform was inverted in a previous paper ⁶⁾ and the result may be written as

$$\begin{aligned} \Phi(t) = & \left[1 + \frac{ak}{2} \left(1 + \frac{ak}{4} \right) \right] e^{-\frac{1}{2}ak} \delta(t-k) + k e^{-\frac{1}{2}ak} \delta'(t-k) + \\ & + \frac{a^2 k^3 e^{-\frac{1}{2}at}}{4(t^2 - k^2)} I_2 \left[\frac{1}{2}(t^2 - k^2)^{\frac{1}{2}} a \right] u(t-k), \end{aligned} \quad (33)$$

where $\delta'(t-k)$ is the doublet impulse function ^{*}) at $t=k$.

The expressions for the electric field components are not expressible in closed form. They may be formally written in terms of convolution integral as follows

$$e_r(t) = \frac{I_0 ds}{2\pi\epsilon r^3} \cos \theta e^{-at} \int_0^t e^{a\tau} \Phi(\tau) d\tau \quad (34)$$

and

$$e_\theta(t) = \frac{I_0 ds}{4\pi\epsilon r} \left[\frac{\partial}{\partial r} \frac{1}{r} e^{-at} \int_0^t e^{a\tau} \Phi(\tau) d\tau \right] \sin \theta. \quad (35)$$

The function $\Phi(t)$ also occurs in the solution for the electric field $\tilde{e}_\phi(t)$, produced by a magnetic dipole or small loop of area da excited by a step-function current $I_0 u(t)$. Explicitly,

$$\tilde{e}_\phi(t) = \frac{-\mu I_0 da}{4\pi r^2} \Phi(t) \sin \theta. \quad (36)$$

From the viewpoint of the reciprocity theorem this is not at all surprising. The corresponding magnetic field components are formally given by

$$\tilde{h}_r(t) = \frac{I_0 da}{2\pi r^3} \left[\int_0^t \Phi(\tau) d\tau \right] \cos \theta \quad (37)$$

and

$$\tilde{h}_\theta(t) = \frac{I_0 da}{4\pi r} \left[\frac{\partial}{\partial r} \frac{1}{r} \int_0^t \Phi(\tau) d\tau \right] \sin \theta, \quad (38)$$

which are obtained by an integration of Maxwell's equations.

^{*}) Formally, $L\delta'(t-k) = s e^{-ks}$.

3b. Approximate solutions for high conductivity. It is possible to simplify the results in the previous section when the conductivity is high and the response times are not small. As mentioned earlier, the simplification amounts to the neglect of displacement currents. In the case of the electric dipole the Laplace transforms of the field components may be written as

$$E_r(s) = \frac{I(s) \, ds}{2\pi\sigma r^3} (1 + \alpha s^{\frac{1}{2}}) \exp(-\alpha s^{\frac{1}{2}}) \cos \theta, \quad (39)$$

$$E_\theta(s) = \frac{I(s) \, ds}{4\pi\sigma r^3} (1 + \alpha s^{\frac{1}{2}} + \alpha^2 s) \exp(-\alpha s^{\frac{1}{2}}) \sin \theta, \quad (40)$$

$$H_\phi(s) = \frac{I(s) \, ds}{4\pi r^2} (1 + \alpha s^{\frac{1}{2}}) \exp(-\alpha s^{\frac{1}{2}}) \sin \theta, \quad (41)$$

where $\alpha^2 = \sigma\mu r^2$. For a step-function current source, $I(s) = I_0/s$, the transforms may be readily inverted as was demonstrated in an earlier paper ⁴). The responses are given by

$$\tilde{e}_r(t) = \frac{I_0 \, ds}{2\pi\sigma r^3} A\left(\frac{\alpha}{2t^{\frac{1}{2}}}\right) u(t) \cos \theta, \quad (42)$$

$$\tilde{e}_\theta(t) = \frac{I_0 \, ds}{4\pi\sigma r^3} B\left(\frac{\alpha}{2t^{\frac{1}{2}}}\right) u(t) \sin \theta, \quad (43)$$

$$\tilde{h}_\phi(t) = \frac{I_0 \, ds}{4\pi r^2} A\left(\frac{\alpha}{2t^{\frac{1}{2}}}\right) u(t) \sin \theta, \quad (44)$$

where

$$A(x) = \operatorname{erfc}(x) + x \operatorname{erf}'(x) \quad (45)$$

and

$$B(x) = \operatorname{erfc}(x) + (x + 2x^3) \operatorname{erf}'(x), \quad (46)$$

with

$$\operatorname{erfc}(x) = 1 - \operatorname{erf}(x) = \frac{2}{\sqrt{\pi}} \int_x^\infty e^{-y^2} dy \quad (47)$$

and

$$\operatorname{erf}'(x) = \frac{d}{dx} \operatorname{erf}(x) = \frac{2}{\sqrt{\pi}} e^{-x^2}. \quad (48)$$

The error function and its derivative occurring in the above ex-

pressions are extensively tabulated; the argument x is the real quantity $\alpha/(2t^{\frac{1}{2}})$.

The corresponding expressions for the fields of a magnetic dipole or small loop excited by a step-function current are very similar. Explicitly

$$\tilde{h}_r(t) = \frac{I_0 da}{2\pi r^3} A\left(\frac{\alpha}{2t^{\frac{1}{2}}}\right) u(t) \cos \theta, \quad (49)$$

$$\tilde{h}_\theta(t) = \frac{I_0 da}{4\pi r^3} B\left(\frac{\alpha}{2t^{\frac{1}{2}}}\right) u(t) \sin \theta, \quad (50)$$

$$\begin{aligned} \tilde{e}_\phi(t) &= \frac{-\mu I_0 da}{4\pi r^2} \frac{d}{dt} A\left(\frac{\alpha}{2t^{\frac{1}{2}}}\right) u(t) \sin \theta \\ &= \frac{-I_0 da}{2\pi \sigma r^4} C\left(\frac{\alpha}{2t^{\frac{1}{2}}}\right) u(t) \sin \theta. \end{aligned} \quad (51)$$

where the A and B functions are as given above and the new C function is given by

$$C(x) = x^4 \operatorname{erf}''(x) = \frac{-4x^5}{\pi^{\frac{1}{2}}} e^{-x^2}. \quad (52)$$

The response functions A , B and C characterize the field responses for an electric and magnetic dipole source with step-function excitation of current. They are approximate in the sense that displacement currents have been neglected. This restricts the range of application to times t such that

$$(t^2 - k^2)^{\frac{1}{2}} \gg 2\varepsilon/\sigma \text{ where } k = (\varepsilon\mu)^{\frac{1}{2}} r. \quad (53)$$

The relatively simple analytical form of the Laplace transforms in (39) to (41) enables one to investigate more realistic source functions. For example if the source current in either the electric or magnetic dipole has the form

$$I(t) = I_0 e^{-\beta t} u(t), \quad (54)$$

the transform for the source function is

$$I(s) = \frac{I_0}{s + \beta}. \quad (55)$$

The required inversions may be effected by using the known result³⁹⁾

$$\frac{e^{-\alpha s^{\frac{1}{2}}}}{s + \beta} = L \operatorname{Re} e^{-\beta t} e^{-i\beta^{\frac{1}{2}}\alpha} \operatorname{erfc}\left(\frac{\alpha}{2t^{\frac{1}{2}}} - i\beta^{\frac{1}{2}}t^{\frac{1}{2}}\right) u(t), \quad (56)$$

and the following results are obtained by differentiating the above with respect to α and t , respectively:

$$\frac{\alpha s^{\frac{1}{2}} e^{-\alpha s^{\frac{1}{2}}}}{s + \beta} = L \left[\operatorname{Re} i\alpha\beta^{\frac{1}{2}} e^{-\beta t} e^{-i\beta^{\frac{1}{2}}\alpha} \operatorname{erfc} \left(\frac{\alpha}{2t^{\frac{1}{2}}} - i\beta^{\frac{1}{2}}t^{\frac{1}{2}} \right) + \frac{2}{\pi^{\frac{1}{2}}} e^{-\alpha^2/4t} \left(\frac{\alpha}{2t^{\frac{1}{2}}} \right) \right] u(t) \quad (57)$$

and

$$\frac{\alpha^2 s e^{-\alpha s^{\frac{1}{2}}}}{s + \beta} = L \left\{ -\alpha^2 \beta e^{-\beta t} \operatorname{Re} \left[e^{-i\beta^{\frac{1}{2}}\alpha} \operatorname{erfc} \left(\frac{\alpha}{2t^{\frac{1}{2}}} - i\beta^{\frac{1}{2}}t^{\frac{1}{2}} \right) \right] + \frac{4}{\pi^{\frac{1}{2}}} e^{-\alpha^2/4t} \left(\frac{\alpha}{2t^{\frac{1}{2}}} \right)^3 \right\} u(t). \quad (58)$$

Re indicates that the real part is to be taken. The explicit expressions for the electric field components of the electric dipole are then given by

$$E_r = \frac{I_0 \, ds}{2\pi\sigma r^3} A(\beta, t) \cos \theta \quad (59)$$

and

$$E_\theta = \frac{I_0 \, ds}{4\pi\sigma r^3} B(\beta, t) \sin \theta, \quad (60)$$

where

$$A(\beta, t) = \left\{ \operatorname{Re} \left[e^{-\beta t} e^{-i\beta^{\frac{1}{2}}\alpha} (1 + i\beta^{\frac{1}{2}}\alpha) \operatorname{erfc} \left(\frac{\alpha}{2t^{\frac{1}{2}}} - i\beta^{\frac{1}{2}}t^{\frac{1}{2}} \right) \right] + \frac{2}{\pi^{\frac{1}{2}}} \left(\frac{\alpha}{2t^{\frac{1}{2}}} \right) e^{-\alpha^2/4t} \right\} u(t) \quad (61)$$

and

$$B(\beta, t) = \left\{ \operatorname{Re} \left[e^{-\beta t} e^{-i\beta^{\frac{1}{2}}\alpha} (1 + i\beta^{\frac{1}{2}}\alpha - \beta\alpha^2) \operatorname{erfc} \left(\frac{\alpha}{2t^{\frac{1}{2}}} - i\beta^{\frac{1}{2}}t^{\frac{1}{2}} \right) \right] + \frac{2}{\pi^{\frac{1}{2}}} \left[\left(\frac{\alpha}{2t^{\frac{1}{2}}} \right) + 2 \left(\frac{\alpha}{2t^{\frac{1}{2}}} \right)^3 \right] e^{-\alpha^2/4t} \right\} u(t). \quad (62)$$

The magnetic field components of the magnetic dipole or small loop excited by the exponential current have the same form:

$$H_r = \frac{I_0 \, da}{2\pi r^3} A(\beta, t) \cos \theta \quad (63)$$

and

$$H_\theta = \frac{I_0 da}{4\pi r^3} B(\beta, t) \sin \theta. \quad (64)$$

Two interesting special cases are immediately deduced. If the time constant of the exponential is very large (i.e. β very small), the response for the step-function current source is recovered, that is

$$A(\beta, t) = A(t) \quad \text{Lim } \beta \rightarrow 0 \quad (65)$$

and

$$B(\beta, t) = B(t). \quad \text{Lim } \beta \rightarrow 0 \quad (66)$$

If the excitation is of the form $\exp(i\omega t) u(t)$, then the response functions are simply $A(i\omega, t)$ and $B(i\omega, t)$, respectively, and they are functions of the angular frequency ω . The corresponding steady state solutions, denoted by $A(\omega)$ and $B(\omega)$, are then recovered by noting that

$$A(i\omega, t) = A(\omega) = (1 + \gamma r) e^{-\gamma r} \quad \text{Lim } t \rightarrow \infty \quad (67)$$

and

$$B(i\omega, t) = B(\omega) = (1 + \gamma r + \gamma^2 r^2) e^{-\gamma r}, \quad \text{Lim } t \rightarrow \infty \quad (68)$$

where

$$\gamma r = (i\omega)^{\frac{1}{2}} \alpha = (i\sigma\mu\omega)^{\frac{1}{2}} r. \quad (69)$$

The responses for an exponentially rising step may also be easily computed, for example if the source current has the form

$$I(t) = I_0(1 - e^{-\beta t}) u(t). \quad (70)$$

The corresponding responses for the r and θ field components are respectively given by

$$U(\beta, t) = A(t) - A(\beta, t) \quad (71)$$

and

$$V(\beta, t) = B(t) - B(\beta, t). \quad (72)$$

As the time constant becomes small, the step-function responses are again recovered. For example,

$$U(\beta, t) = A(t) \quad \text{Lim } \beta \rightarrow \infty \quad (73)$$

and

$$V(\beta, t) = B(t). \quad \text{Lim } \beta \rightarrow \infty \quad (74)$$

3c. Illustrations of certain features of the transient response in an infinite medium. Some of the characteristics of transient propagation in a conducting medium are best illustrated by a graphical presentation of results. The functions $A(t)$ and $B(t)$ characterize the step-function response of the r and θ components of the dipole fields, respectively. They are shown plotted in fig. 1 as a function of $x^2/4$ or $t/\sigma\mu r^2$, which is a time parameter. It is interesting to note that the function $A(x)$ corresponding to the radial field component rises monotonically with time and approaches the static value of unity. On the other hand, the function $B(x)$ corresponding to the tangential field component rises much more rapidly and tends to overshoot the static value by about 40%. It then decays monotonically to its static value.

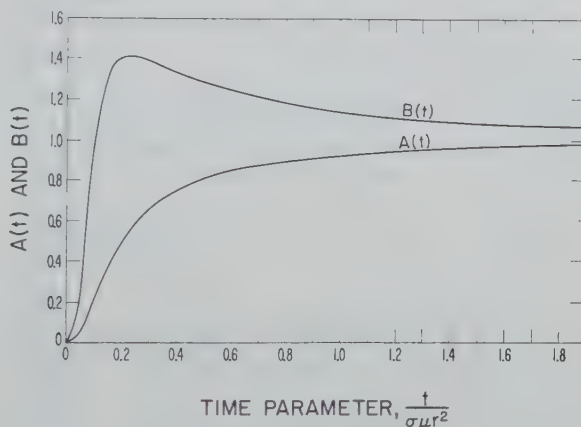


Fig. 1. Transient dipole field functions for step functions current source.

The corresponding dipole field responses $A(\beta, t)$ and $B(\beta, t)$ for an exponential source function may be calculated from (61) and (62) or directly from the superposition of the step-function responses. An example is shown in fig. 2 where $A(\beta, t)$ and $B(\beta, t)$ are plotted as a function of $t/\sigma\mu r^2$ for an exponential current source given by $I = I_0 e^{-\beta t}$ where $\beta = 1/\sigma\mu r^2$. Here it may be noted that both functions go to a maximum and eventually diminish to zero at very large times.

Another interesting case is when the source current in the dipole is a half-cycle of a sine wave. For example, $I(t) = I_0 \sin \beta t$ for

$0 < \beta t < \pi$. The half-period length π/β is taken to be equal to $0.9/\sigma\mu r^2$ for purposes of illustration. The resulting response functions $A_s(t)$ and $B_s(t)$ for the radial and tangential field responses are

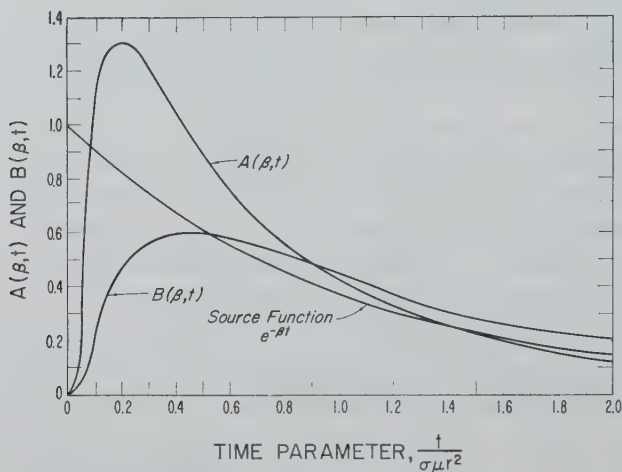


Fig. 2. Response of a dipole energized by an exponential current $I = I_0 e^{-\beta t}$, where $\beta = 1/\sigma\mu r^2$.

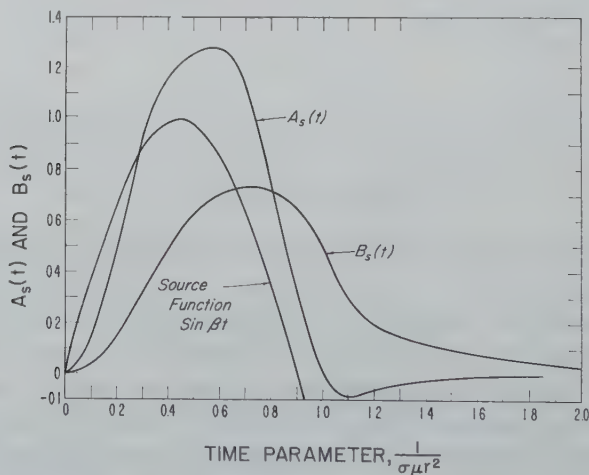


Fig. 3. Electric dipole energized by a half sine wave current $I_0 \sin \beta t$, for half period $= 0.9/\sigma\mu r^2$.

shown in fig. 3 for this example. It can be noted here that the radial field response rises to a broad maximum and diminishes monotoni-

cally to zero. On the other hand, the tangential field response rises to a more pronounced maximum and then "undershoots" the zero axis to form a "tail" to the pulse.

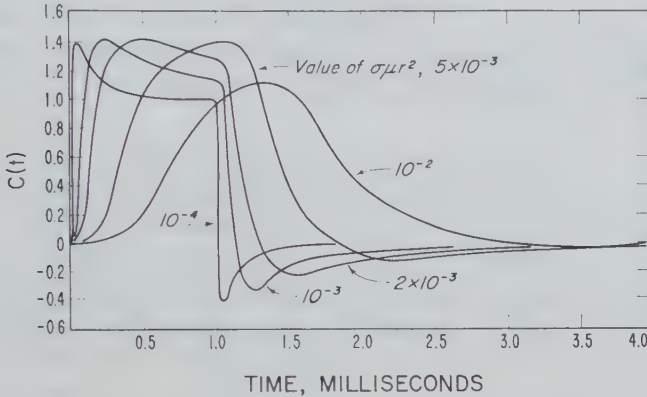


Fig. 4. Transient dipole field function for rectangular current source pulse. Source pulse time $\tau = 10^{-3}$ s, $E_{\theta} = (I \, ds / 4\pi\sigma r^3) B_r(t) \sin \theta$.

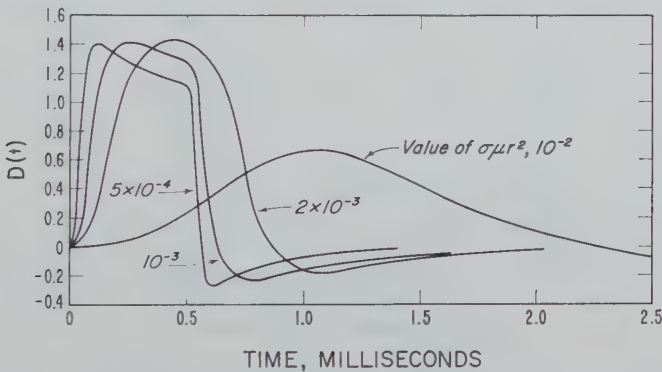


Fig. 5. Transient dipole field function for rectangular current source pulse. Source pulse time $\tau = 0.5 \times 10^{-3}$ s, $E_{\theta} = (I \, ds / 4\pi\sigma r^3) B_r(t) \sin \theta$.

A further illustration of the nature of the dispersion of the pulse is shown in figs. 4 and 5 for a rectangular source pulse. The specific form of the current is

$$I(t) = I_0[u(t) - u(t - \tau)] \quad (75)$$

where τ is the length of the source pulse. The corresponding tangen-

tial field response $B_r(t)$ is thus given by

$$B_r(t) = B(t) - B(t - \tau). \quad (76)$$

This is the function which is plotted in fig. 4 and 5 for $\tau = 1.0$ and 0.5 ms respectively. The appropriate values of the parameter $\sigma\mu r^2$ are indicated on the curves. These curves illustrate the increased dispersion as the pulse travels to greater distances.

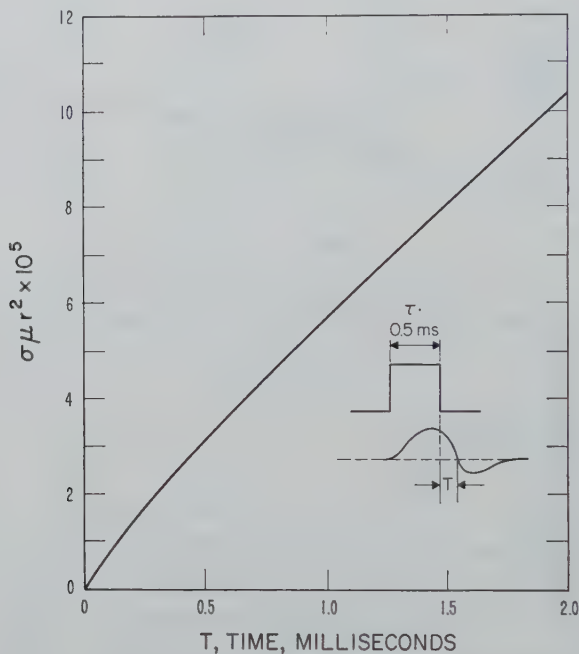


Fig. 6. Parameter $\sigma\mu r^2$ versus T .

The following values would be typical of sea water

$$\sigma = 4 \text{ mhos/m,}$$

$$\epsilon = 80 \times 8.854 \times 10^{-12} \text{ F/m,}$$

$$\mu = 4\pi \times 10^{-7} \text{ H/m.}$$

Then for a distance r of, say, 20 meters, it follows that

$$\sigma\mu r^2 = 2 \times 10^{-3}, \quad (77)$$

which is one of the curves plotted in fig. 4 and 5. It should also be

noted that for this example

$$k = (\epsilon\mu)^{\frac{1}{2}}r = 0.6 \times 10^{-6} \text{ s}, \quad (78)$$

and

$$1/a = \epsilon/\sigma = 1.77 \times 10^{-10} \text{ s}. \quad (79)$$

Thus the response curves shown in figs. 4 and 5 are not valid within a few microseconds of the leading and trailing edge of the source pulse.

The possibility exists that the shape of an electromagnetic pulse in a conducting medium is an indication of the distance to its origin. A useful criterion in the case of the rectangular source pulse is the time T from the end of the source pulse to the instant where the electric field passes through zero. This is indicated in fig. 6 where $\sigma\mu r^2$ is plotted as a function of T . The quantity T appears to be almost a linear function of $\sigma\mu r^2$.

§ 4. *Transient fields in a semi-infinite conducting medium.* 4a. **Horizontal electric dipole excitation.** The propagation of electromagnetic pulses as discussed in previous sections is based

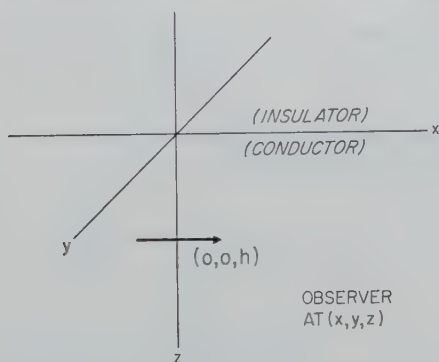


Fig. 7. Coordinate system for horizontal electric dipole in conducting half space.

on the idealization of an infinite medium. The effect of an interface between a non-conducting and a conducting medium is now investigated. The model adopted initially is a horizontal electric dipole located in a semi-infinite conducting medium at depth h from a plane interface. Choosing a cartesian coordinate system, the conducting medium is defined by the space $z > 0$ whereas the

insulating region above it is the space $z < 0$. The coordinates of the electric dipole are $(0, 0, h)$ and it is oriented parallel to the x axis as indicated in fig. 7.

The formal solution of this problem for harmonic time dependence is well known. As shown by Sommerfeld⁴⁰⁾, the fields may be derived from a Hertz vector which has both an x and a z component. To simplify the subsequent analysis somewhat, the displacement currents are neglected. As discussed in previous sections, this is justified for low frequencies in the time harmonic problem or large times in the transient problem. With this simplification, Sommerfeld's expressions for the components of the Hertz vector are

$$\Pi_x = \frac{I \, dl}{4\pi\sigma} \left[\frac{e^{-\gamma r_0}}{r_0} - \frac{e^{-\gamma r}}{r} + 2 \int_0^\infty \frac{e^{-u(z+h)}}{\lambda + u} J_0(\lambda\rho) \lambda \, d\lambda \right],$$

$$\Pi_y = 0, \quad (80)$$

$$\Pi_z = -\frac{I \, dl}{2\pi\sigma} \frac{\partial}{\partial x} \int_0^\infty \frac{e^{-u(z+h)}}{u + \lambda} J_0(\lambda\rho) \, d\lambda, \quad (81)$$

where

$$r_0 = [(z - h)^2 + \rho^2]^{\frac{1}{2}}, \quad r = [(z + h)^2 + \rho^2]^{\frac{1}{2}},$$

$$\rho = [x^2 + y^2]^{\frac{1}{2}}, \quad u = (\lambda^2 + \gamma^2)^{\frac{1}{2}},$$

and dl is the infinitesimal length of the dipole.

It may be readily verified that

$$\Pi_x = \frac{I \, dl}{4\pi\sigma} \left[\frac{e^{-\gamma r_0}}{r_0} - P + \frac{2}{\gamma^2} \left(\frac{\partial^2 P}{\partial z^2} + \frac{\partial^3 N}{\partial z^3} - \gamma^2 \frac{\partial N}{\partial z} \right) \right] \quad (82)$$

and

$$\Pi_z = -\frac{I \, dl}{2\pi\sigma\gamma^2} \left(\frac{\partial^3 N}{\partial x \partial z^2} + \frac{\partial^2 P}{\partial x \partial z} \right), \quad (83)$$

where

$$N = \int_0^\infty \frac{e^{-u(z+h)}}{u} J_0(\lambda\rho) \, d\lambda \quad (84)$$

and

$$P = \int_0^\infty \frac{e^{-u(z+h)}}{u} J_0(\lambda\rho) \lambda \, d\lambda. \quad (85)$$

The integrals N and P are known. From Foster ²⁾ or Magnus *et al.*³⁸⁾

$$N = I_0[\tfrac{1}{2}\gamma(r - z)] K_0[\tfrac{1}{2}\gamma(r + z)] \quad (86)$$

and from Sommerfeld ²⁵⁾

$$P = e^{-\gamma r}/r. \quad (87)$$

The transform of the electric field in the conducting half-space may be obtained from the relation

$$\mathbf{E} = -\gamma^2 \mathbf{\Pi} + \text{grad div } \mathbf{\Pi}, \quad (88)$$

where $i\omega$ is replaced formally by s . Furthermore, on utilizing the fact that N satisfies the wave equation

$$\left(\frac{\partial^2}{\partial x^2} + \frac{\partial^2}{\partial y^2} + \frac{\partial^2}{\partial z^2} - \gamma^2 \right) N = 0, \quad (89)$$

it is not difficult to show that

$$E_x = \frac{I(s)}{4\pi\sigma} \left[\left(-\frac{\partial^2}{\partial y^2} - \frac{\partial^2}{\partial z^2} \right) (P_0 - P) + 2 \left(\frac{\partial^3 N}{\partial y^2 \partial z} - \frac{\partial^2 P}{\partial z^2} \right) \right], \quad (90)$$

$$E_y = \frac{I(s)}{4\pi\sigma} \left[\frac{\partial^2}{\partial x \partial y} (P_0 - P) - 2 \frac{\partial^3 N}{\partial x \partial y \partial z} \right], \quad (91)$$

$$E_z = \frac{I(s)}{4\pi\sigma} \left[\frac{\partial^2}{\partial x \partial z} (P_0 + P) \right], \quad (92)$$

where

$$P_0 = \exp[-(\sigma\mu s)^{\frac{1}{2}}r_0]/r_0, \quad (93)$$

$$P = \exp[-(\sigma\mu s)^{\frac{1}{2}}r]/r, \quad (94)$$

and

$$N = I_0 [\tfrac{1}{2}(\sigma\mu s)^{\frac{1}{2}}(r - z)] K_0[\tfrac{1}{2}(\sigma\mu s)^{\frac{1}{2}}(r + z)]. \quad (95)$$

The current in the dipole is taken to be of the form $I\delta(t)$ where I is a constant. Thus $I(s)$ may be replaced by I . The required transform pairs are ³⁹⁾

$$P_0 = Lp(r_0, t) u(t), \quad (96)$$

$$P = Lp(r, t) u(t), \quad (97)$$

$$N = Ln(r, t) u(t), \quad (98)$$

where

$$p(r, t) = \left(\frac{2}{\pi}\right)^{\frac{1}{2}} \frac{8}{\sigma\mu T^{3/2}} \exp(-2r^2/T), \quad (99)$$

$$n(r, t) = \left(\frac{4}{\sigma\mu T}\right) I_0(\rho^2/T) \exp(-\rho^2/T) \exp[-2(z+h)^2/T] \quad (100)$$

and

$$T = 8t/(\sigma\mu).$$

$[p(r_0, t)]$ is obtained by replacing r with r_0 in $p(r, t)$.

Carrying out the differentiations, indicated in (90), (91) and (92), leads to explicit expression for the components of the transient fields resulting from an impulsive current source. These are

$$\begin{aligned} e_x(t) = \frac{4I \, dl}{\pi\sigma} & \left\{ \left[\frac{1}{2T} - \left(\frac{y}{T}\right)^2 - \left(\frac{z-h}{T}\right)^2 \right] p(r_0, t) \right. \\ & - \left[\frac{1}{2T} - \left(\frac{y}{T}\right)^2 - \left(\frac{z+h}{T}\right)^2 \right] p(r, t) - \\ & - \frac{(z+h)}{Tt} \left[\frac{I_1 - I_0}{2T} + \left(\frac{y}{T}\right)^2 (I_1' - 2I_1 + I_0) \right] \exp(-\rho^2/T) \\ & \cdot [\exp - 2(z+h)^2/T] - \left[2\left(\frac{z+h}{T}\right)^2 - \frac{1}{2T} \right] p(r, t) \Big\}, \quad (101) \end{aligned}$$

$$\begin{aligned} e_y(t) = \frac{4I \, dl}{\pi\sigma} & \left\{ \frac{xy}{T^2} [p(r_0, t) - p(r, t)] + \right. \\ & \left. + \frac{xyz}{T^3 t} (I_1' - 2I_1 + I_0) \exp(-\rho^2/T) \exp[-2(z+h)^2/T] \right\}, \quad (102) \end{aligned}$$

$$e_z(t) = \frac{4I \, dl}{\pi\sigma} \left(\frac{x}{T}\right) \left[-\frac{(z-h)}{T} p(r_0, t) + \frac{(z+h)}{T} p(r, t) \right]. \quad (103)$$

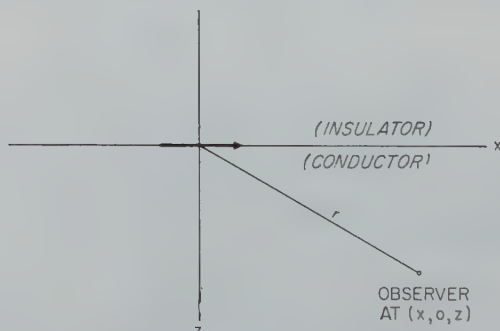


Fig. 8. Situation where the source dipole is on the surface of the half space and the observer is in the $y = 0$ plane.

The argument of the Bessel functions I_0 , I_1 and I_1' is ρ^2/T ; the prime on I_1 indicates a derivative with respect to the argument.

To simplify the discussion, the fields in the principal plane $y = 0$ are considered and the dipole is located at the surface, i.e. $h = 0$, as indicated in fig. 8. The $e_y(t)$ component now vanishes, which is to be expected because of symmetry. The other two components may be written in the form

$$e_x(t) = \frac{I \, dl}{2\pi\sigma r^3} \left(\frac{8}{\sigma\mu r^2} \right) f_x(\tau), \quad (104)$$

$$e_z(t) = \frac{I \, dl}{2\pi\sigma r^3} \left(\frac{8}{\sigma\mu r^2} \right) f_z(\tau), \quad (105)$$

where

$$\begin{aligned} f_x(\tau) = & -\frac{4 \cos \theta}{\tau^3} [I_1(\sin^2\theta/\tau) - I_0(\sin^2\theta/\tau)] \cdot \exp(-\sin^2\theta/\tau) \exp(-2 \cos^2\theta/\tau) - \\ & - \left(\frac{2}{\pi} \right)^{\frac{1}{2}} \frac{16}{\tau^{5/2}} \left(\frac{\cos^2 \theta}{\tau} - \frac{1}{4} \right) \exp(-2/\tau) \end{aligned} \quad (106)$$

and

$$f_z(\tau) = \left(\frac{2}{\pi} \right)^{\frac{1}{2}} \frac{16}{\tau^{7/2}} (\sin \theta \cos \theta) \exp(-2/\tau) \quad (107)$$

with

$$\tau = T/r^2 = 8t/(\sigma\mu r^2), \quad r^2 = z^2 + x^2, \quad \text{and} \quad \tan \theta = x/z.$$

If the medium is infinite in extent, the corresponding expressions are

$$e_x^0(t) = \frac{I \, dl}{4\pi\sigma r^3} \left(\frac{8}{\sigma\mu r^2} \right) f_x^0(\tau) \quad (108)$$

and

$$e_z^0(t) = \frac{I \, dl}{4\pi\sigma r^3} \left(\frac{8}{\sigma\mu r^2} \right) f_z^0(\tau), \quad (109)$$

where

$$f_x^0(\tau) = 8 \sqrt{\frac{2}{\pi}} \left(1 - \frac{2 \cos^2 \theta}{\tau} \right) \frac{1}{\tau^{5/2}} \exp(-2/\tau) \quad (110)$$

and

$$f_z^0(\tau) = f_z(\tau). \quad (111)$$

The latter identity is rather interesting since it indicates that the form of the transient is not modified by the presence of the interface. However, the behaviour of $f_x(\tau)$ for the semi-infinite medium and $f_x^0(\tau)$ for the infinite medium are quite different.

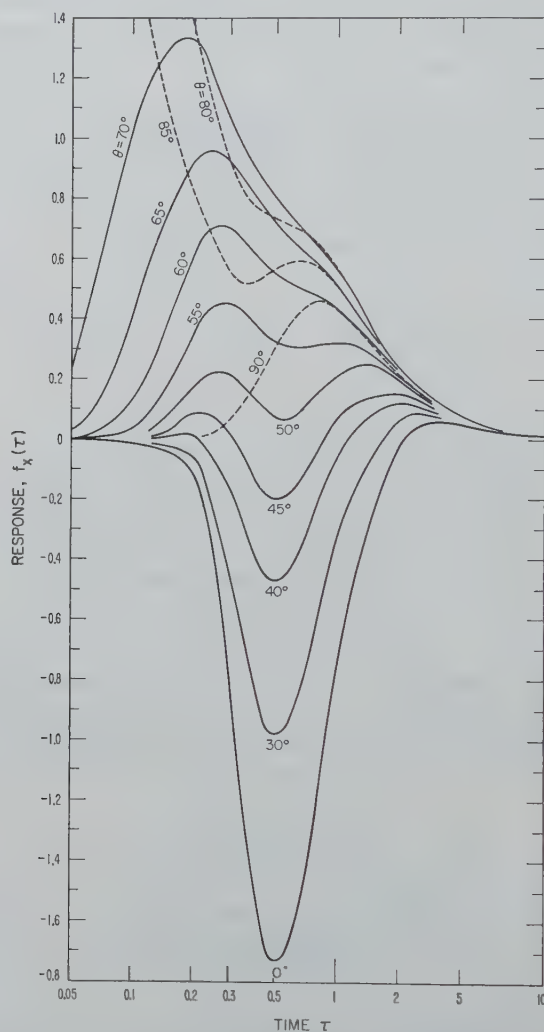


Fig. 9. Response function $f_x(\tau)$ for horizontal field in half space.

The response functions $f_x(\tau)$, $f_x^0(\tau)$ and $f_z(\tau)$ are shown plotted in figs. 9, 10 and 11 respectively. The abscissae in each of these

curves is τ , which is proportional to time. The angle to the observer in the conductor is θ and indicated on the curves. $\theta = 0$, of course, corresponds to the situation where the observer is directly under the source dipole. On the other hand, $\theta = 90^\circ$ corresponds to the observer being at some other point on the surface.

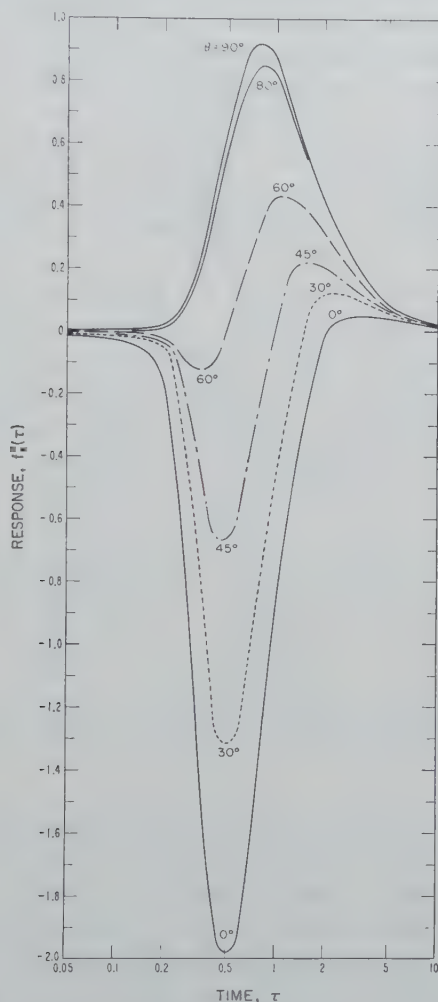


Fig. 10. Response function $f_x^0(\tau)$ for horizontal field in infinite space.

It may be noted that the waveform for the horizontal electric field in the half space (proportional to $f_x(\tau)$) undergoes a considerable

rable change as θ varies from 0 to 90° . This is to be compared with the waveform for the horizontal electric field in the infinite space (proportional to $f_x^0(\tau)$). In these two cases the waveforms are similar for propagation steeply into the conductor (i.e. smaller values of θ); there is a considerable difference, however, in the case of propagation in the horizontal or near horizontal direction (i.e. θ near 90°).

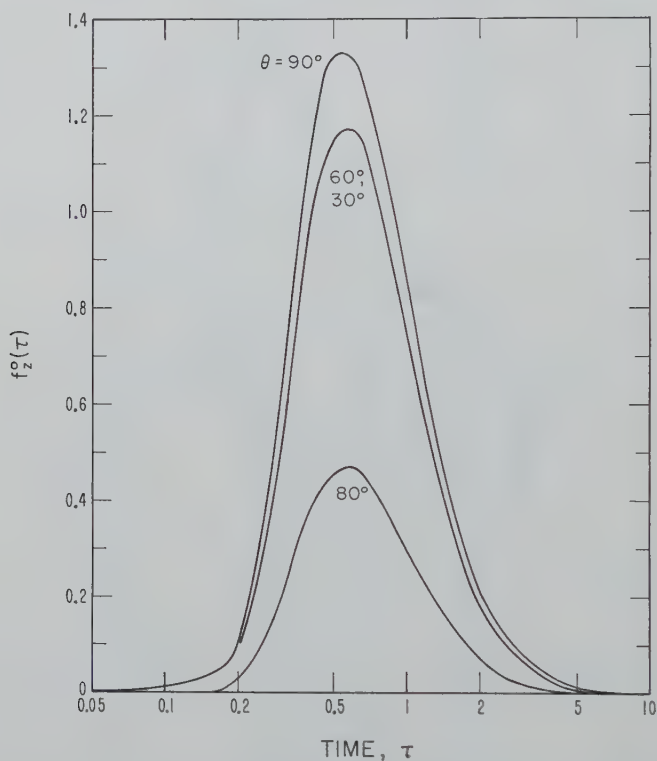


Fig. 11. Response functions $f_z^0(\tau)$ or $f_z(\tau)$ for vertical field.

In fact, at $\theta = 90^\circ$ it is not difficult to show that

$$f_x(\tau) = \delta(\tau) + \sqrt{\frac{2}{\pi}} \frac{4}{\tau^{5/2}} e^{-2/\tau} u(\tau) \quad (112a)$$

and

$$f_x^0(\tau) = \sqrt{\frac{2}{\pi}} \frac{8}{\tau^{5/2}} e^{-2/\tau} u(\tau), \quad (112b)$$

where $\delta(\tau)$ is a unit impulse function defined such that

$$\lim_{\epsilon \rightarrow 0} \int_0^{+\epsilon} \delta(\tau) d\tau = 1.$$

The presence of the impulse function is related to the presence of the insulator interface. Since all displacement currents have been neglected, the immediate arrival of a disturbance at the observer is reconciled. For any depth of the observer (i.e. $\theta < 90^\circ$), the unit delta impulse is replaced by a pulse of finite duration and finite "rise time". This is illustrated clearly in fig. 9.

It is rather interesting that the vertical electric fields behave the same way in both a conducting half space and an infinite conducting space. This is indicated by the identical analytical forms for $f_z(\tau)$ and $f_z^0(\tau)$.

The theoretical development in this section has been restricted to an impulse current excitation. Unfortunately, the inversion of the relevant Laplace transforms is only possible in this case. However, the response for other source functions may be obtained by invoking the principle of superposition. For example, in the case of a stepfunction current source, the responses are obtained in the usual way by integrating the impulse responses with respect to time from 0 to t .

In the case where the source dipole is located at the surface and the observer is at $(x, 0, z)$ the step-function responses may be obtained from

$$\bar{e}_x = \frac{I ds}{2\pi\sigma r^3} \int_0^\tau f_x(\tau) d\tau \quad (113)$$

and

$$\bar{e}_z = \frac{I ds}{2\pi\sigma r^3} \int_0^\tau f_z(\tau) d\tau. \quad (114)$$

The first of these integrals cannot be evaluated in closed form as far as this writer has been able to ascertain. However, if $\theta = 90^\circ$, corresponding to the observer as well as the source being on the surface of the half space, it easily follows that

$$\bar{e}_x = \frac{I ds}{2\pi\sigma r^3} \left\{ 1 + A \left[\left(\frac{\sigma\mu}{t} \right)^{\frac{1}{2}} \frac{r}{2} \right] \right\}, \quad (115)$$

where the function $A(x)$ has been plotted in fig. 1 as a function of $\frac{1}{4}x^2$ or $t/(\sigma\mu r^2)$. The square bracket term on the right hand side of (115) thus varies from unity for small times to 2 for large times.

4b. Wire loop or magnetic dipole excitation. Another obvious method to excite transient fields in a semi-infinite medium is by a closed wire loop lying on the surface. When the area becomes small, the loop may be represented adequately by a magnetic dipole. For sake of generality the loop is taken to have a finite radius a as indicated in fig. 12.

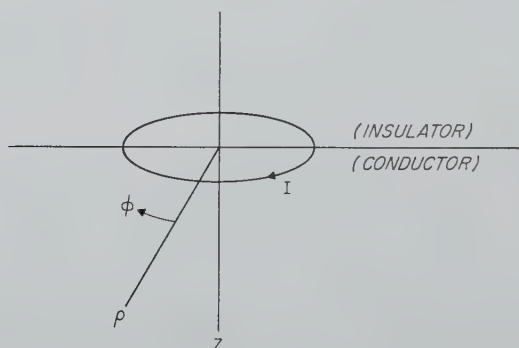


Fig. 12. Cylindrical coordinate system and the circular wire loop lying on the surface of the half space.

In terms of a cylindrical coordinate system (ρ, ϕ, z) the conductor fills the half-space $z > 0$ and the loop is defined by $\rho = a$ and $z = 0$. For a constant current $I \exp(i\omega t)$ the harmonic solution for the electric field may be written for $z > 0$ ⁵⁾

$$E_{\phi} = \partial F / \partial \rho, \quad (116)$$

where

$$F = \frac{i\mu\omega a^2 I}{4} \int_0^{\infty} \frac{2\lambda}{u + u_0} f_0(\lambda) e^{-uz} J_0(\lambda\rho) d\lambda \quad (117)$$

with

$$f_0(\lambda) = \frac{2J_1(\lambda a)}{\lambda a}$$

and

$$u = (\lambda^2 + \gamma^2)^{\frac{1}{2}}, \quad u_0 = (\lambda^2 + \gamma_0^2)^{\frac{1}{2}}, \\ \gamma^2 = i\mu\omega(\sigma + i\varepsilon\omega), \quad \gamma_0^2 = i\mu\omega(i\varepsilon_0\omega).$$

The solution for the insulating space (i.e. for $z < 0$) has the same form except that e^{-uz} is replaced by e^{+u_0z} .

Now, since

$$\left[\frac{1}{\rho} \frac{\partial}{\partial \rho} \left(\rho \frac{\partial}{\partial \rho} \right) + \lambda^2 \right] J_0(\lambda \rho) = 0 \quad (118)$$

and

$$J_1(x) = \sum_0^{\infty} \frac{(-1)^m x^{2m+1}}{m!(m+1)! 2^{2m+1}}, \quad (119)$$

it follows that

$$\lambda^{2m} J_0(\lambda \rho) = \left[-\frac{1}{\rho} \frac{\partial}{\partial \rho} \left(\rho \frac{\partial}{\partial \rho} \right) \right]^m J_0(\lambda \rho) \quad (120)$$

and

$$f_0(\lambda a) J_0(\lambda \rho) = \sum_{m=0}^{\infty} \frac{(a/2)^{2m}}{m!(m+1)!} \left[\frac{1}{\rho} \frac{\partial}{\partial \rho} \left(\rho \frac{\partial}{\partial \rho} \right) \right]^m J_0(\lambda \rho). \quad (121)$$

Therefore

$$F = \sum_{m=0}^{\infty} \frac{(\frac{1}{2}a)^{2m}}{m!(m+1)!} \left[\frac{1}{\rho} \frac{\partial}{\partial \rho} \left(\rho \frac{\partial}{\partial \rho} \right) \right]^m G, \quad (122)$$

where

$$G = \frac{a^2 I}{2\sigma} \int_0^{\infty} (u - \lambda) e^{-uz} \lambda J_0(\lambda \rho) d\lambda. \quad (123)$$

Equation (122) may be written operationally as $F = \Gamma G$ where Γ signifies the required summation and differentiation. When $a \ll \rho$, corresponding to a small loop only, the term $m = 0$ is important. Then $F \cong G$, which is the contribution of the magnetic dipole. Higher terms in the series correspond to the multipole terms. It is seen that the field of the finite circular loop is thus easily calculated from the field of the magnetic dipole by suitable differentiation with respect to ρ .

The basic function G may be expressed in terms of the known integrals N and P introduced in the previous section. This readily leads to

$$\begin{aligned} G &= \frac{a^2 I}{2\sigma} \left[\frac{\partial^2 P}{\partial z^2} - \frac{\partial}{\partial z} \left(\gamma^2 N - \frac{\partial^2 N}{\partial z^2} \right) \right] = \\ &= \frac{a^2 I}{2\sigma} \left[\frac{\partial^2 P}{\partial z^2} - \frac{\partial}{\partial z} \left(\frac{1}{\rho} \frac{\partial}{\partial \rho} \rho \frac{\partial}{\partial \rho} \right) N \right]. \end{aligned} \quad (124)$$

For an impulse current in the loop [i.e. $I(t) = I\delta(t)$], the transient response is then expressed as

$$e_\phi(t) = \Gamma \frac{\partial g(t)}{\partial \rho}, \quad (125)$$

where

$$g(t) = \frac{a^2 I}{2\sigma} \left[\frac{\partial^2 p(t)}{\partial z^2} - \frac{\partial}{\partial z} \left(\frac{1}{\rho} \frac{\partial}{\partial \rho} \rho \frac{\partial}{\partial \rho} \right) n(t) \right], \quad (126)$$

in terms of the functions $n(t)$ and $p(t)$ used in the previous section. Closed form expressions for the field $e_\phi(t)$ are obtained after the differentiations have been effected. The response for a step-function current is then given by

$$\tilde{e}_\phi(t) = \int_0^t e_\phi(t) dt. \quad (127)$$

It appears that this integration must be carried out by numerical means in the general case. However, if the observer is in the interface (i.e. $z = 0$), the step-function response $\tilde{e}(t)$ may be expressed in simple form:

$$\tilde{e}_\phi(t) = \frac{I da}{2\pi\sigma\rho^4} H(t) u(t), \quad (128)$$

where

$$H(t) = 3 \operatorname{erf} \left(\frac{\alpha}{2t^{\frac{1}{2}}} \right) - \left[\frac{3\alpha}{2t^{\frac{1}{2}}} + 2 \left(\frac{\alpha}{2t^{\frac{1}{2}}} \right)^3 \right] \operatorname{erf}' \left(\frac{\alpha}{2t^{\frac{1}{2}}} \right) \quad (129)$$

and $\alpha = (\sigma\mu)^{\frac{1}{2}}\rho$. The function $H(t)$ is shown plotted in fig. 13 as a function of the time parameter $t/\sigma\mu\rho^2$. It is simply a unit directional pulse starting at a value of 3.0 and decaying gradually to zero.

§ 5. *Transient coupling in grounded circuits of finite length.*

5a. *Infinite medium case.* In the foregoing discussion it has been tacitly assumed that the current elements have dimensions which are effectively infinitesimal. When other dimensions in the problem are not relatively large, it is necessary to consider the finite size of the source and receiving antennae. This is particularly true in applications to geophysical prospecting where the source may consist of two electrodes located in a bore hole, which are energized by a current pulse. The transient voltage response is developed between two additional electrodes.

An expression is now developed for the transient fields due to a step function of current in a wire of length $B-A$ embedded in an infinite medium of conductivity σ and permeability μ . The coordi-

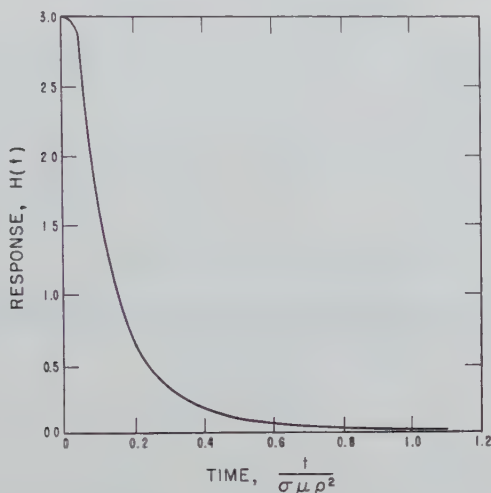


Fig. 13. Electric field response of a small loop lying on the earth's surface.

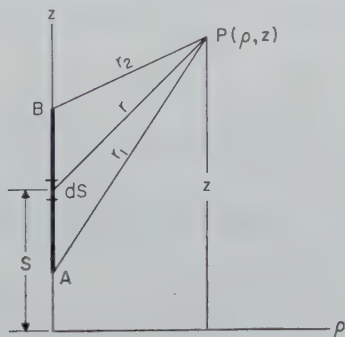


Fig. 14. The coordinate system for the finite current element extending from A to B in a conducting medium of infinite extent.

nate system is shown in fig. 14. The fields at the point $P(\rho, z)$ due to a current $i(s) ds$ at $(0, S)$, in transform notation, is

$$e_z(s)/i(s) = dS[P(r) + (\partial^2/\partial S \partial z) Q(r)] \quad (130)$$

and

$$e_\rho(s)/i(s) = dS[\partial^2 Q(r)/\partial S \partial \rho], \quad (131)$$

where

$$P(r) = \mu s \exp(-\gamma r)/4\pi r \quad (132)$$

and

$$Q(r) = \exp(-\gamma r)/4\pi\sigma r. \quad (133)$$

This follows from (27) and (28) when cylindrical coordinates are used. The expressions for the field transforms at P due to current transform $i(s)$ throughout the length of the wire is given by

$$e_z(s)/i(s) = \int_A^B P(r) dS + [(\partial/\partial z) Q(r)]_{S=A}^B \quad (134)$$

and

$$e_\rho(s)/i(s) = [(\partial/\partial \rho) Q(r)]_{S=A}^B. \quad (135)$$

The current in the wire will be assumed to be constant throughout its length and is of a step function type

$$i(s) = L[Iu(t)] = I/s. \quad (136)$$

Then

$$\begin{aligned} e_z(s)/I &= \\ &= \mu/4\pi \int_A^B \exp[-(\sigma\mu s)^{\frac{1}{2}}r]/r dS + \frac{1}{4\pi\sigma s} \{(\partial/\partial z) \exp[-(\sigma\mu s)^{\frac{1}{2}}r]/r\}_{S=A}^B \end{aligned} \quad (137)$$

and

$$e_\rho(s)/I = \frac{1}{4\pi\sigma s} \{(\partial/\partial \rho) \exp[-(\sigma\mu s)^{\frac{1}{2}}r]/r\}_{S=A}^B. \quad (138)$$

The expressions for the fields using (137) and (138) are then

$$\begin{aligned} E_z(t) &= \mu I/4\pi \int_A^B (1/2)(\sigma\mu/\pi t^3)^{\frac{1}{2}} \exp(-\sigma\mu r^2/4t) dS + \\ &+ \frac{I}{4\pi\sigma} (\partial/\partial z) \left\{ \frac{1}{r} - \operatorname{erf} \left[\frac{r}{2} \left(\frac{\sigma\mu}{t} \right)^{\frac{1}{2}} \right] / r \right\}_{S=A}^B \end{aligned} \quad (139)$$

and

$$E_\rho(t) = \frac{I}{4\pi\sigma} (\partial/\partial \rho) \left\{ \frac{1}{r} - \operatorname{erf} \left[\frac{r}{2} \left(\frac{\sigma\mu}{t} \right)^{\frac{1}{2}} \right] / r \right\}_{S=A}^B. \quad (140)$$

The integral in the above expression is now evaluated:

$$\int_A^B \exp(-\sigma\mu r^2/4t) dS = \exp(-\beta^2\rho^2) \int_A^B \exp[-\beta^2(S-z)^2] dS, \quad (141)$$

where $r^2 = \rho^2 + (S - z)^2$ and $\beta^2 = \sigma\mu/4t$. Then

$$\int_A^B \exp(-\beta^2 r^2) dS = \frac{\exp(-\beta^2 \rho^2)}{\beta} \int_{\beta(A-z)}^{\beta(B-z)} \exp(-x^2) dx =$$

$$= \frac{\sqrt{\pi}}{2} \frac{\exp(-\beta^2 \rho^2)}{\beta} \{\operatorname{erf}[\beta(B-z)] - \operatorname{erf}[\beta(A-z)]\}. \quad (142)$$

Using the above relation and carrying out the differentiations in (139) and (140), the complete expressions become

$$E_z(t) = \mu I / (8\pi t) \exp(-\beta^2 \rho^2) \{\operatorname{erf}[\beta(B-z)] - \operatorname{erf}[\beta(A-z)]\} +$$

$$+ (I/4\pi\sigma)[M(r_1) - M(r_2)] \quad (143)$$

and

$$E_\rho(t) = (I/4\pi\sigma)[N(r_1) - N(r_2)], \quad (144)$$

where

$$M(r) = (z - S)/r^3 [1 - \operatorname{erf}(\beta r) + \beta r \operatorname{erf}'(\beta r)], \quad (145)$$

$$N(r) = \rho/r^3 [1 - \operatorname{erf}(\beta r) + \beta r \operatorname{erf}'(\beta r)], \quad (146)$$

$$r_1 = [(A - z)^2 + \rho^2]^{\frac{1}{2}},$$

$$r_2 = [(B - z)^2 + \rho^2]^{\frac{1}{2}}.$$

The physical counterpart of this case could be a linear insulated wire which is grounded at its end points. The step function current generator is anywhere between its end points. The assumption that the current is constant throughout its length implies that the propagation constant is negligibly small for important times in the transient response. This is certainly the case for most types of insulation where the shunt admittance is relatively small.

It can also be shown that the insulation has a negligible effect on the radiation from the wire into the conducting medium as long as the over-all radius R_0 of the insulated wire is such that $R_0 \ll \ll (2t/\sigma\mu)^{\frac{1}{2}}$ where σ and μ are the properties of the external medium and t is the time that the transient is measured, following the application of the step function current. This follows from the fact that the radial wave impedance at the insulation-medium boundary is almost identical for the insulation material and conducting medium when R_0 satisfies the above inequality.

An interesting check on the above method is to find the expression

for the fields when the source wire is infinite. When $-A$ and $+B$ go to infinity, the fields become

$$\begin{aligned} E_z(t) &= (\mu I/8\pi)(\sigma\mu/\pi t^3)^{\frac{1}{2}} \exp(-\beta^2\rho^2) \int_{-\infty}^{+\infty} \exp(-\beta x^2) dx = \\ &= (\mu/4\pi t) \exp(-\beta^2\rho^2). \end{aligned} \quad (147)$$

and

$$E_\rho(t) = 0.$$

Now since

$$L[E_z(t)/I] = \mu/2\pi\{K_0[(\sigma\mu s)^{\frac{1}{2}}\rho]\}, \quad (148)$$

it follows that

$$e_z(s)/i(s) = (\mu s/2\pi)K_0[(\sigma\mu s)^{\frac{1}{2}}\rho]. \quad (149)$$

If the current is of the form $I \exp(i\omega t)$, then the steady state field is

$$e_z(i\omega) \exp(i\omega t)/I = (i\mu\omega/2\pi)K_0[(i\sigma\mu\omega)^{\frac{1}{2}}\rho] \exp(i\omega t), \quad (150)$$

which is well-known.

The transient voltage response in one finite grounded circuit due to a step function current in another similar circuit, which is itself parallel to the first, is now calculated. The circuit consists of an insulated wire embedded in an infinite and isotropic medium with a conductivity σ and magnetic permeability μ . The wire is grounded at the points A and B as shown in fig. 15.

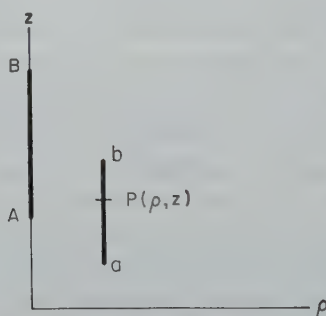


Fig. 15. Illustrating two parallel insulated wires grounded at their end points.

By some means a unit step-function current is caused to flow in the wire throughout its length. The open-circuit voltage $v(t)$ induced in a finite insulated circuit, grounded at the points a and b and separated from the first circuit by a constant separation

ρ , is then

$$v(t) = \int_a^b E_z(t) dz. \quad (151)$$

This can be rewritten in the following form:

$$v(t) = (I/4\pi\sigma) \int_a^b \frac{\partial}{\partial z} \left[\frac{\operatorname{erfc}(\beta r_2)}{r_2} - \frac{\operatorname{erfc}(\beta r_1)}{r_1} \right] dz \quad (152)$$

$$+ (\mu/8\pi t) \exp(-\beta^2 \rho^2) \int_a^b \{ \operatorname{erf}[\beta(B-z)] - \operatorname{erf}[\beta(A-z)] \} dz.$$

The following integral relation can be easily verified:

$$\beta \int \operatorname{erf}(\beta x) dx = \beta x \operatorname{erf}(\beta x) + \frac{1}{2} \operatorname{erf}'(\beta x) = \psi(\beta x), \quad (153)$$

and this defines the function $\psi(\beta x)$. Employing this result, the required integrations can be carried out to yield

$$v(t) = (I/4\pi\sigma) \left\{ \frac{\operatorname{erfc}[\beta B \cdot b]}{B \cdot b} + \right.$$

$$+ \frac{\operatorname{erfc}[\beta A \cdot a]}{A \cdot a} - \frac{\operatorname{erfc}(\beta B \cdot a)}{B \cdot a} - \frac{\operatorname{erfc}(\beta A \cdot b)}{A \cdot b} \left. \right\} +$$

$$+ \frac{I}{4\pi} \left(\frac{\mu}{\sigma t} \right)^{\frac{1}{2}} \exp(-\beta^2 \rho^2) \{ \psi[\beta(B-a)] + \psi[\beta(A-b)] -$$

$$- \psi[\beta(A-a)] - \psi[\beta(B-b)] \}, \quad (154)$$

where the dot between the points signifies a linear dimension equal to the actual separation of the points. That is

$$B \cdot b = [\rho^2 + (B-b)^2]^{\frac{1}{2}}, \text{ etc.} \quad (155)$$

The above rather complicated expression will give the open circuit voltage, in volts, in the circuit ba for a suddenly applied current of I amperes applied to the circuit BA which is parallel and at a separation ρ .

A common electrode array used in resistivity prospecting in wells or drill holes is the three electrode collinear array of equal spacings. This is represented by the following special case of the general formulation:

$$B = +\infty, A-a=2l, A-b=l \text{ and } \rho=0.$$

The current line in this case is assumed to act in an equivalent

manner as a semi-infinite wire. This is effected by positioning the electrode B at a sufficiently great distance from the other electrodes. The voltage developed in the circuit ba is then measured by a high impedance voltmeter. The voltage $v(t)$ corresponding to this case is given by

$$-8\pi\sigma l \frac{v(t)}{I} = 2 \operatorname{erfc}(\beta l) - \operatorname{erfc}(2\beta l) - 4\beta^2 l^2 [1 + (\psi(\beta l) - \psi(2\beta l))/\beta l]. \quad (156)$$

The quantity on the right hand side of this equation is plotted in fig. 16 as a function of the parameter $4t/\sigma\mu l^2$, where t is the response time in seconds, l is the electrode spacing in meters and σ is the conductivity in mhos per meter. This quantity approaches the value one for long times and represents the static condition of current flow.

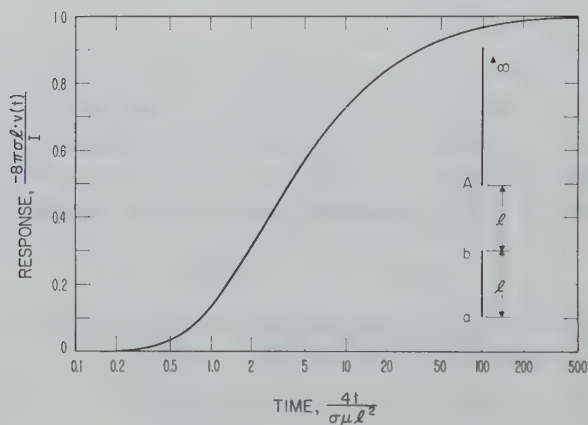


Fig. 16. Transient voltage developed in circuit ab due to a step function current in the semi-infinite wire grounded at A .

5b. Semi-infinite medium case. The method used in the previous section may be applied to the case where the wires are in the interface between the air and a conducting half-space. Choosing an (x, y, z) coordinate system, the half-space is defined by $z > 0$ and the insulator (i.e. the air) by $z < 0$. The coordinate system is shown in fig. 17. The source is taken to be a linear wire extending from A to B in the interface $z = 0$.

The fields at the point $P(x, y)$ in the interface due to a current

element $i(s) dS$ at $(0, S)$ may be written as

$$e_x(s)/i(s) = dS[\bar{P}(r) + (\partial^2/\partial S \partial x) \bar{Q}(r)] \quad (157)$$

and

$$e_y(s)/i(s) = dS[\partial^2 \bar{Q}(r)/\partial S \partial x], \quad (158)$$

where

$$\bar{P}(r) = \frac{1}{2\pi\sigma r^3} [1 - (1 + \gamma r) e^{-\gamma r}], \quad (159)$$

$$\bar{Q}(r) = \frac{1}{2\pi\sigma r} \quad \text{and} \quad \gamma^2 = \sigma\mu s. \quad (160)$$

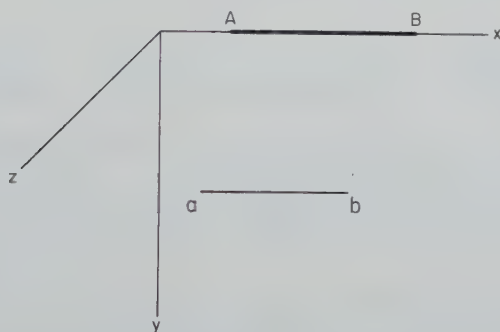


Fig. 17. Illustrating two parallel insulated wires lying at the interface $z = 0$ and grounded at their end points.

This follows from § 3a or more directly from the work of Foster²⁾

Again the source current is taken to be a step function $Iu(t)$. The transient field at $P(x, y)$ may then be written as

$$E_x(t) = \frac{I}{2\pi\sigma} \int_A^B \left\{ \frac{\partial^2}{\partial S \partial x} \frac{1}{r} + \frac{1}{r^3} \operatorname{erf} \left[\frac{r}{2} \left(\frac{\sigma\mu}{t} \right)^{\frac{1}{2}} \right] - \frac{1}{r^2} \left(\frac{\sigma\mu}{\pi t} \right)^{\frac{1}{2}} \exp(-\sigma\mu r^2/4t) \right\} dS. \quad (161)$$

Carrying out the integration leads to

$$E_x(t) = \frac{I}{2\pi\sigma} \left[\frac{B-x}{[y^2 + (B-x)^2]^{3/2}} - \frac{A-x}{[y^2 + (A-x)^2]^{3/2}} + \Phi(x-A) - \Phi(x-B) \right] u(t), \quad (162)$$

where

$$\Phi(u) = \frac{u}{y^2(y^2 + u^2)^{\frac{1}{2}}} \operatorname{erf}(\beta \sqrt{y^2 + u^2}) - \frac{1}{y^2} e^{-\beta^2 y^2} \operatorname{erf}(\beta u) \quad (163)$$

with $\beta^2 = \sigma\mu/4t$. If $-A$ and $+B$ approach infinity, it is seen that

$$E_x(t) = \frac{I}{\pi\sigma y^2} (1 - e^{-\beta^2 y^2}) u(t),$$

which is the field parallel to an infinite wire carrying a step-function current.

Returning to the general case, the other field component is given by

$$E_y = -\frac{Iy}{2\pi\sigma} \left\{ \frac{1}{[y^2 + (B-x)^2]^{3/2}} - \frac{1}{[y^2 + (A-x)^2]^{3/2}} \right\} u(t), \quad (164)$$

which, to the extent that displacement currents may be neglected, is a positive step at $t = 0$. This appears to be rather an interesting result and suggests that the transverse field in the interface follows the form of the current in the source wire to a high approximation.

The transient coupling between two parallel grounded circuits may also be calculated in a straightforward manner. Again neglecting all displacement currents the voltage $v(t)$ induced in the linear insulated circuit, grounded at points a and b and separated from the first circuit by a constant separation y is then

$$v(t) = \int_a^b E_x(t) dx. \quad (165)$$

Following Riordan¹⁾ the integrations may be carried out to yield

$$v(t) = \frac{I}{2\pi\sigma y} [\psi(b-A) - \psi(b-B) - \psi(a-A) + \psi(a-B)] u(t), \quad (166)$$

where

$$\begin{aligned} \psi(u) = & -\frac{y}{\sqrt{y^2 + u^2}} + \frac{\sqrt{y^2 + u^2}}{y} \operatorname{erf}(\beta \sqrt{y^2 + u^2}) - \\ & - \frac{u}{y} e^{-\beta^2 y^2} \operatorname{erf}(\beta u). \end{aligned} \quad (167)$$

If again $+B$ and $-A$ tend to $+\infty$, the result simplifies con-

siderably to

$$v(t) = \frac{(b-a)I}{\pi\sigma y^2} (1 - e^{-\beta^2 v^2}) u(t). \quad (168)$$

The latter formula is applicable in an approximate sense to parallel wires if one of the wires is long compared to the other. For the general case it is necessary to employ (166).

§ 6. *Concluding remarks.* While the problems treated in this paper are idealized, it is felt that they may help one to understand the nature of pulse propagation in actual conducting media such as sea water or rocks and soils. The main feature of an electromagnetic signal in conducting media is that it changes its shape or waveform as it propagates away from the source. The consequence is that steep leading edges of transmitting pulses are not preserved and thus radar-type distance measurements are virtually impossible. On the other hand, the distortion of the pulse shape is a possible criterion of distance of travel. This phenomenon may find application in detection of buried objects in the ground or the distance of geological substrata.

The extension of the theory to more complicated structures such as a layered conducting half space and spherical conductors is desirable. Some progress has already been made in this direction as mentioned in the introduction. Unfortunately, the integrals which are involved in the formal solutions are exceedingly complicated and they apparently are not expressible in terms of tabulated functions. With the availability of large automatic computers it is possible to evaluate many of these integrals by numerical methods. This would seem to be the direction in which to proceed.

Acknowledgements. The author would like to thank Dr. A. A. Brant for his suggestions and advice during the course of this work. He is also grateful to Mrs. Patrica Murdock for assistance in preparing the manuscript, to John Harman for drafting the illustrations and to Mrs. Anabeth Murphy for carrying out the calculations required for figs. 9, 10 and 11.

REFERENCES

- 1) Riordan, J., Bell Syst. Tech. J. **12** (1933) 420.
- 2) Foster, R. M., Bell Syst. Tech. J. **10** (1931) 408.
- 3) Sunde, E., Earth Conduction Effect in Transmission Systems, Van Nostrand and Co Ltd., New York 1949.
- 4) Wait, J. R., Geophysics **16** (1951) 213.
- 5) Wait, J. R., Can. J. Phys. **29** (1951) 577.
- 6) Wait, J. R., J. Appl. Phys. **24** (1953) 341.
- 7) Bhattacharyya, B. K., Geophysics **20** (1955) 959.
- 8) Bhattacharyya, B. K., Geophysics **22** (1957) 75.
- 9) Bhattacharyya, B. K., J. Technology **1** (1956) 152.
- 10) Bhattacharyya, B. K., Geophysics **22** (1957) 905.
- 11) Bhattacharyya, B. K., Geophysics **24** (1959) 89.
- 12) Wait, J. R., A. A. Brant, H. O. Seigel *et al.*, Overvoltage Research and Geophysical Applications, Pergamon Press, London and New York, 1959.
- 13) Richards, P. I., Transients in Conducting Media, Trans. I.R.E. Vol. AP-6, pp. 178-182, April 1958.
- 14) Grumet, A., J. Appl. Phys. **30** (1959) 682.
- 15) Heaviside, O., Electromagnetic Theory, Vol. 3, The Electrician Printing and Publishing Co., London 1912, also see H. J. Josephs, Heaviside's Electric Circuit Theory, Methuen and Co., Ltd., London 1946.
- 16) Wait, J. R., Can. J. Res. **34** (1956) 27.
- 17) Wait, J. R., The Transient Behaviour of the Electromagnetic Ground Wave over a Spherical Earth, Trans. I.R.E. on Antennas and Propagation, Vol. AP-5, pp. 198-202, April 1957.
- 18) Johler, J. R., Geofis. Pura Appl. **37** (1957) 116; also J. Res. Nat. Bur. Stand., Wash. **60** (1958) 281.
- 19) Wait, J. R., Can. J. Phys. **35** (1957) 1146.
- 20) Levy, B. R. and J. B. Keller, Propagation of Electromagnetic Pulses around the Earth Trans I.R.E. on Antennas and Propagation, Vol. AP-6, pp. 56-61, January 1958.
- 21) Johler, J. R., and L. C. Walters, Propagation of a Ground Wave Pulse around a Finitely Conducting Spherical Earth from a Damped Sinusoidal Source Current, Trans. I.R.E. on Antennas and Propagation, Vol. AP-7, No. 1, pp. 1-10, January 1959.
- 22) Keilson, J. and R. V. Row, J. Appl. Phys. **30** (1959) 1595.
- 23) White, G. E., Trans. Amer. Inst. Min. Metall. **164** (1945) 170.
- 24) Wait, J. R., A Basis of Electrical Prospecting Employing Time-Varying Electromagnetic Fields, Ph. D. University of Toronto, March, 1951. Also available from Library, Colorado School of Mines, Golden, Colorado.
- 25) Wait, J. R., Can. J. Phys. **34** (1956) 890.
- 26) Wait, J. R., Geophysics **16** (1951) 666.
- 27) Wait, J. R., Geophysics **18** (1953) 138.
- 28) Belluigi, A., Fondamenti teorici dei Geoltrans, Bollettino del Servizio Geologico d'Italia, Vol. LXXIV, 1952.
- 29) Belluigi, A., L'eccitazione transitoria E. M. d'un terreno stratificato con dipolo magnetico pulsante verticale, Tipografia Del Senato, Vol. LXXV, 1954.
- 30) Belluigi, A., Geofis. Pura Appl. **25** (1953) 29.
- 31) Belluigi, A., Annali di Geofis. **7** (1954) 1.
- 32) Jacque Yost, W., R. L. Caldwell, C. I. Beard, C. D. McClure and E. N. Skomal, Geophysics **17** (1952) 806.

- 33) Tikhonov, A. N., The Establishment of an Electric Current in a Homogeneous Conducting Half Space, *Bull. Acad. Sci. U.S.S.R. Ser. Geogr. and Geophys.* No. 3, 1946.
- 34) Tikhonov, A. N., The Establishment of an Electric Current in an Inhomogeneous Layered Medium, *Bull. Acad. Sci. U.S.S.R. Ser. Geogr.* No. 3, 1950, also No. 6, 1951.
- 35) Skugarevskaya, O. A., The Initial (and Final) Stage of the Process of Establishment of an Electric Current in a Layer which lies on an Ideally Conducting Foundation, *Bull. Acad. Sci. U.S.S.R. Ser. Geophys.* No. 6, 1951.
- 36) Tikhonov, A. N., and O. A. Skugarevskaya, The Interpretation of the Process of the Establishing an Electric Field in Layer Media, *Bull. Acad. Sci. U.S.S.R. Ser. Geophys.* No. 3 pp. 358-362, 1958.
- 37) Chetayev, D. N., Theory of Sounding Using D.C. Impulses in a Non-grounded Loop, *Bull. Acad. Sci. U.S.S.R. Ser. Geophys.* No. 5, pp. 595-598, 1956.
- 38) Magnus, W. and F. Oberhettinger, *Functions of Mathematical Physics*, Chelsea Publishing Co., New York 1954, p. 133.
- 39) Campbell, G. and R. M. Foster, *Fourier Integrals for Practical Application*, Van Nostrand Co Ltd., New York 1949.
- 40) Sommerfeld, A. N., *Partial Differential Equations*, Academic Press, New York 1949.

SPHERE AND CIRCLE THEOREMS INVOLVING
SURFACE DISCONTINUITIES OF POTENTIAL

by G. POWER

Nottingham University, England

and H. L. W. JACKSON

Nottingham Technical College, England

Summary

New sphere and circle theorems are presented which allow for discontinuities of potential at the surface of separation and are thus of special importance in heat problems where the 'radiation' boundary condition applies. Moreover these theorems permit results to be obtained in particular cases which agree with those deduced from previous theorems.

§ 1. *Introduction.* Yeh, Martinek and Ludford ¹⁾ have given a sphere theorem of sufficient generality to cover most boundary conditions in hydrodynamics, heat, magnetism and electricity when the fields under consideration are harmonic. The corresponding theorem in two dimensions has been given by Power and Jackson ²⁾. However, the results depend on the continuity of potential distribution across the boundary surface and hence cannot be used for heat problems in which the 'radiation' boundary condition applies. The term 'radiation' is perhaps a little misleading but is used in most classical works when there is a rate of transfer of heat between two surfaces in contact proportional to the temperature difference.

Sphere and circle theorems are here presented which not only allow for this type of boundary condition, but which also can be employed to deduce, in special cases, results which agree with those given by previous theorems. The usual uniqueness theorems hold.

§ 2. *Sphere theorem.* With the usual notation, let $\phi_0(r) \equiv \phi_0(r, \theta, w)$ be the harmonic potential distribution lying entirely

outside the sphere $r = a$, and $\phi_1(r) \equiv \phi_1(r, \theta, w)$ the harmonic potential distribution lying entirely within this sphere. The function $\phi(r) \equiv \phi(r, \theta, w)$ given by

$$\begin{aligned} \phi(r) = \phi_e(r) = \phi_0(r) + \frac{B}{r} \phi_0\left(\frac{a^2}{r}\right) + \frac{1}{r} \int_0^1 F(s) \phi_0\left(\frac{sa^2}{r}\right) ds + \\ + C \phi_1(r) + \int_1^\infty G(s) \phi_1(sr) ds, \quad (r \geq a) \end{aligned} \quad (1)$$

$$\begin{aligned} \phi(r) = \phi_i(r) = \phi_1(r) + \frac{b}{r} \phi_1\left(\frac{a^2}{r}\right) + \frac{1}{r} \int_1^\infty g(s) \phi_1\left(\frac{sa^2}{r}\right) ds + \\ + c \phi_0(r) + \int_0^1 f(s) \phi_0(sr) ds, \quad (r \leq a) \end{aligned}$$

with $c = C = 0$, $b = B = a$,

$$F(s) = P_1 s^{\alpha_1} + P_2 s^{\alpha_2}, \quad f(s) = Q_1 s^{\alpha_1} + Q_2 s^{\alpha_2},$$

$$G(s) = R_1 s^{\gamma_1} + R_2 s^{\gamma_2}, \quad g(s) = S_1 s^{\gamma_1} + S_2 s^{\gamma_2},$$

$$\begin{aligned} P_1 = \frac{av_3(1+\alpha_1)(1+2\alpha_1)}{v_1\alpha_1(\alpha_2-\alpha_1)}, \quad P_2 = \frac{av_3(1+\alpha_2)(1+2\alpha_2)}{v_1\alpha_2(\alpha_1-\alpha_2)}, \\ Q_1 = \frac{-v_3(1+2\alpha_1)}{v_2(\alpha_2-\alpha_1)}, \quad Q_2 = \frac{-v_3(1+2\alpha_2)}{v_2(\alpha_1-\alpha_2)}, \end{aligned} \quad (2)$$

$$R_1 = \frac{v_4(1+2\gamma_1)}{v_1(\gamma_1-\gamma_2)}, \quad R_2 = \frac{v_4(1+2\gamma_2)}{v_1(\gamma_2-\gamma_1)},$$

$$S_1 = \frac{-av_4(1+\gamma_1)(1+2\gamma_1)}{v_2\gamma_1(\gamma_1-\gamma_2)}, \quad S_2 = \frac{-av_4(1+\gamma_1)(1+2\gamma_2)}{v_2\gamma_2(\gamma_2-\gamma_1)},$$

where α_1, α_2 are roots of the equation $\alpha^2 + \alpha(1+k) - v_3/v_1 = 0$, γ_1, γ_2 are the roots of $\gamma^2 + \gamma(1+k) + v_4/v_2 = 0$, where $k = -(v_4/v_2 + v_3/v_1)$, and all the integrals are uniformly convergent, has the following properties:

$$\begin{aligned} \nabla^2(\phi - \phi_0) &= 0 & \text{for } r \geq a, \\ \nabla^2(\phi - \phi_1) &= 0 & \text{for } r \leq a, \end{aligned} \quad (3)$$

$$v_1 \frac{a \partial \phi_e}{\partial r} = v_2 \frac{a \partial \phi_i}{\partial r} = v_3 \phi_e - v_4 \phi_i \quad \text{on } r = a,$$

v_1, v_2, v_3, v_4 being constants.

The constants given in (2) are obtained either by assuming series expansions for ϕ_0 and ϕ_1 and equating coefficients or by using a method similar to that of Yeh, Martinek and Ludford¹⁾. It is therefore not necessary to give any detailed working here. It is to be noted that the roots α , γ are related in general by $\alpha + \gamma = -1$, although care has to be taken in the use of this relationship when dealing with degenerate cases.

§ 3. *Applications.* The most obvious use of this theorem is in the case of steady heat flow when there is a spherical surface of separation of two media of different conductivities. In most cases, heat transfer between the two media takes place with the rate of transfer between the two surfaces in contact being proportional to their temperature difference. Thus the properties (3) are immediately relevant to this type of problem where $\nu_3 = \nu_4$ is the surface conductance.

Moreover results obtained by the previous sphere theorem¹⁾ with $\phi_e = \phi_i$ on $r = a$ as one boundary condition can also be deduced. Consider, for example, the electrical problem in which there is a homogeneous sphere of dielectric constant k_i set in a homogeneous medium of dielectric constant k_0 with field generators in the region $r > a$ only. We set $\phi_1 = 0$, $\nu_3 = \nu_4$, $\nu_1/\nu_2 = k_0/k_i$, and then let $\nu_1 \rightarrow 0$. From (2) we see that there is one finite root $\alpha_1 = -k_i/(k_0 + k_i)$, and one root α_2 which becomes infinite in the limit. The root α_1 yields

$$P_1 = \frac{ak_0(k_i - k_0)}{(k_i + k_0)^2}, \quad Q_1 = \frac{k_0(k_i - k_0)}{(k_i + k_0)^2}.$$

The root α_2 and the constants P_2 , Q_2 combine to give

$$c = \frac{2k_0}{(k_i + k_0)}, \quad B = \frac{a(k_0 - k_i)}{(k_i + k_0)}.$$

This is the exterior sphere theorem as given by Power³⁾.

If in the above system the field generators are in the region $r < a$, we put $\phi_0 = 0$, $\nu_3 = \nu_4$, $\nu_1/\nu_2 = k_0/k_i$, and let $\nu_1 \rightarrow 0$ as before. Again there is one finite root $\gamma_1 = -k_0/(k_i + k_0)$ and one root γ_2 which becomes infinite in the limit. The root γ_1 gives

$$R_1 = \frac{k_i(k_i - k_0)}{(k_i + k_0)^2}, \quad S_1 = \frac{ak_i(k_i - k_0)}{(k_i + k_0)^2}.$$

The root γ_2 and R_2, S_2 in the limit combine to give

$$C = \frac{2k_i}{(k_i + k_0)}, \quad b = \frac{a(k_i - k_0)}{(k_i + k_0)}.$$

This is the interior sphere theorem as given by Power³⁾.

Both the external and internal hydrodynamical problems involving a rigid sphere at rest in a perfect fluid moving steadily and irrotationally are merely particular cases of the above results.

To obtain the exterior heat solution given in ¹⁾ we simply set $v_4 = 0, v_3 = v_1 ah$ in ϕ_e . The interior solution is found by setting $v_3 = 0, v_4 = v_2 ah$ in ϕ_i .

§ 4. *Circle theorem.* Let $f_0(z)$ be the complex potential of a distribution lying entirely outside the circle $|z| = a$, and $f_1(z)$ the complex potential of a distribution entirely within the circle. Then $w(z)$ defined by

$$\begin{aligned} w_e(z) = f_0(z) + A\bar{f}_0\left(\frac{a^2}{z}\right) + \int_0^1 F(t)\bar{f}_0\left(\frac{ta^2}{z}\right) dt + \\ + Bf_1(z) + \int_1^\infty G(t)f_1(tz) dt, \quad |z| \geq a, \\ w_i(z) = f_1(z) + C\bar{f}_1\left(\frac{a^2}{z}\right) + \int_1^\infty H(t)\bar{f}_1\left(\frac{ta^2}{z}\right) dt + \\ + Df_0(z) + \int_0^1 K(t)f_0(tz) dt, \quad |z| \leq a, \end{aligned} \quad (4)$$

with $B = D = 0, A = C = 1$,

$$\begin{aligned} F(t) = \frac{-2v_3}{v_1} t^\alpha, \quad K(t) = \frac{2v_3}{v_2} t^\alpha, \quad G(t) = \frac{2v_4}{v_1} t^\gamma, \\ H(t) = -(2v_4/v_2)t^\gamma, \quad \alpha = -(1+k), \quad \gamma = (k-1), \end{aligned}$$

where k is defined as in § 2, and all the integrals are uniformly convergent, has the following properties:

$$\begin{aligned} \nabla^2 R[w(z) - f_0(z)] &= 0, & \text{when } |z| \geq a, \\ \nabla^2 R[w(z) - f_1(z)] &= 0, & \text{when } |z| \leq a, \end{aligned} \quad (5)$$

$$R\left(v_1 \frac{a\partial w_e}{\partial|z|}\right) = R\left(v_2 \frac{a\partial w_i}{\partial|z|}\right) = R(v_3 w_e - v_4 w_i) \quad \text{when } |z| = a.$$

It is to be noticed that in this case $\alpha + \gamma = -2$, and $\nu_1, \nu_2, \nu_3, \nu_4$ are again constants. Care has to be exercised in using these results when logarithmic singularities occur, and slight modification may be necessary.

Although no detailed working need be given, the results can be obtained either by considering the real parts of the complex potential functions as given or by expanding them in series. The properties (5) are again immediately relevant for 'radiation' boundary problems where $\nu_3 = \nu_4$ is the surface conductance. Also the exterior and interior circle theorems as given by Power and Jackson ²⁾ for electrostatics, magnetism, hydrodynamics and heat can be deduced as in § 3.

Received 19th January, 1960.

REFERENCES

- 1) Yeh, G. C. K., J. Martinek and G. S. S. Ludford, *Z. angew. Math. Mech.* **36** (1956) 111.
- 2) Power, G. and H. L. W. Jackson, *Appl. Sci. Res.* **B6** (1957) 456.
- 3) Power, G., *Pac. J. Math.* **4** (1954) 79.

LETTER TO THE EDITOR

A mechanical Hall effect

We consider a non-viscous gas with conductivity σ moving between two infinite parallel plates under the influence of a constant driving force \mathbf{P} , parallel to the plates. We assume a constant magnetic field \mathbf{B}_0 , normal to the plates, applied from outside. The plates are taken to be perfect conductors.

Furthermore we assume that the gas is electrically neutral and is in equilibrium at a constant temperature. The partial electron pressure then is $\frac{1}{2}p$, and the equations of plasma theory (cf. Spitzer¹) read (in M.K.S. units):

$$\begin{aligned}\operatorname{div} \mathbf{V} &= 0, & \mathbf{P} + \operatorname{grad} p + \mathbf{J} \times \mathbf{B} &= 0, \\ \operatorname{div} \mathbf{B} &= 0, & \operatorname{rot} \mathbf{B} &= \mu \mathbf{J}, \\ \mathbf{E} + \mathbf{V} \times \mathbf{B} - \frac{\mathbf{J}}{\sigma} &= \frac{\mathbf{P} + \operatorname{grad} p}{2en} + \frac{\mathbf{J} \times \mathbf{B}}{en},\end{aligned}$$

where n is the electron number density. The terms on the right hand side of the last equation are characteristic of plasma theory proper. They are neglected in "one-component" magnetohydrodynamics.

We take the origin halfway between the plates, the x -axis in the direction of \mathbf{P} and the z -axis in the direction of \mathbf{B}_0 . The appropriate solution of the equations then is found to be:

$$\begin{aligned}V_x &= \frac{P}{\sigma B_0^2}, & V_y &= -\frac{P}{2neB_0}, \\ B_x &= -\frac{\mu P}{B_0}z, & B_z &= B_0, \\ J_y &= -\frac{P}{B_0}, & \frac{dp}{dz} &= -\frac{\mu P^2}{B_0^2}z,\end{aligned}$$

all other components, including those of \mathbf{B} , being zero. Outside the medium $B_x = 0$, the discontinuity in B_x being connected with the return current flowing in the plates.

It is easily seen that in the "one component" theory the same solution is obtained apart from V_y , which is zero then. Clearly this solution means that there is an angle θ between the flow and the driving force. We have

$$\operatorname{tg} \theta = V_y/V_x = -\sigma B_0/2ne.$$

In a dilute gas σ can be expressed by means of an effective collision time τ as $\sigma = e^2 n \tau / m$, where m is the electron mass. Introducing the cyclotron frequency $\omega = e B_0 / m$ we obtain

$$\operatorname{tg} \theta = -\frac{1}{2} \omega \tau.$$

We now construct a rectangular duct by inserting two walls parallel to \mathbf{V} and the z -axis. The result obtained above then means that a pressure gradient $P \operatorname{tg} \theta$ across the duct is set up when the gas is driven through the field by a force P . This is a mechanical analogue to the Hall-effect.

Finally we point out that this effect eventually is due to the mass difference between electrons and ions. The mass-ratio, however, does not occur explicitly in the result. The reason for this is that the equations of plasma theory in the form used are not exact but constitute an approximation for large mass ratio.

L. J. F. BROER,
L. A. PELETIER and
L. VAN WIJNGAARDEN

Laboratory for Aero- and Hydrodynamics
Technische Hogeschool, Delft, Netherlands.

Received 8th January, 1960.

REFERENCE

- 1) Spitzer jr., L., Physics of fully ionized gases, Interscience Publishers Inc., New York 1956.

A HARMONIC GENERATOR AND DETECTOR FOR THE SHORT MILLIMETER WAVE REGION

by H. W. DE WIJN

Zeeman-Laboratorium der Universiteit van Amsterdam, Nederland

Summary

The design of a millimeter wave harmonic generator and detector of the open crystal type is described. The construction of the instruments is rigid. Tolerances and backlash of the adjusting mechanism are kept small. The operation under different conditions is discussed.

§ 1. *Introduction.* It is well-known that below 6 mm wavelength the useful effect of microwave harmonic multipliers and detectors with commercial cartridge crystals rapidly falls off with decreasing wavelength. As previously reported by Klein *et al.*¹⁾, Johnson *et al.*²⁾ and King *et al.*³⁾, considerable improvement in millimeter wave harmonic generation and detection can be obtained if the rectifying element is placed directly in the millimeter waveguide. This may be realized by introducing the semiconductor crystal and the fine tungsten wire separately each from one side into the millimeter waveguide, after which the crystal is brought into contact with the tungsten wire by means of a mechanical system.

§ 2. *Description of the instruments.* A cross-section of the harmonic multiplier is given in fig. 1. With a few exceptions all parts are made of brass. The primary waveguide (I.D. 7.11×3.56 mm) and the millimeter waveguide (I.D. 2.80×1.27 mm) are soldered perpendicular to each other in a housing, after which the whole has been gold-plated inside as well as outside. Both waveguides are short-circuited at one end with a plunger. The tungsten wire with a diameter of 50μ is bent in the desired shape and copper-plated and soldered upon a nickel-plated steel pin with a diameter of 0.7 mm. The point is cone-shaped, 0.2 mm in height, and has at the

top a radius of curvature of about $2\ \mu$. It is formed by electrolytic etching in a 5 n KOH solution with an a.c. current from a 6 V, 50 Hz source. To obtain a sharp point the tungsten wire should be cleaned carefully and attention should be paid to the length of the

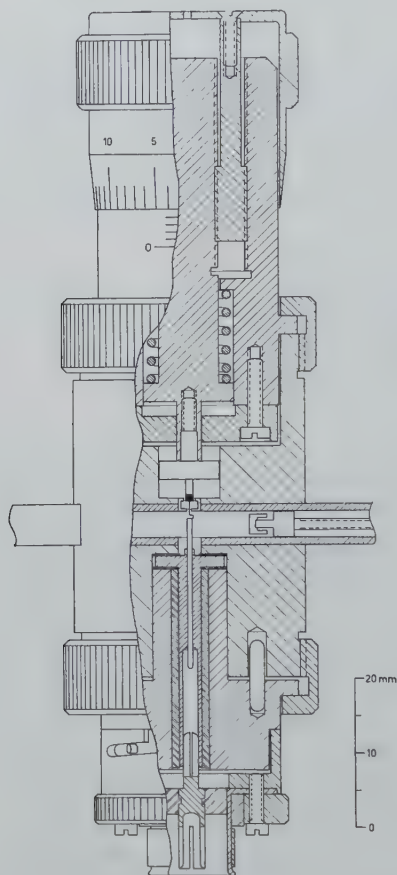


Fig. 1. Cross-section of the millimeter wave harmonic multiplier. The millimeter waveguide is perpendicular to the page. Insulating materials are indicated by shading with double lines.

wire immersed in the solution, in this case 0.7 mm. The steel pin, which serves as antenna in the primary waveguide, is put into the insulated inner conductor of a holder, after which the holder is set tight at the bottom of the housing by means of a swivel. The disk of the inner conductor is thereby jammed between two mica washer

plates near the waveguide in order to obtain a rigid construction. The antenna is now terminated at the lower side by a coaxial system, $1/4$ wavelength in length, acting as a choke for microwaves. A plug, electrically connected with the tungsten wire, has been fitted to the holder with a bayonet-catch. For a moment the plug socket is replaced by an accessory with which the antenna is pushed up until the tungsten wire has the correct position in the millimeter waveguide, i.e. until the point is at the height of the upper inner surface of the millimeter waveguide. The crystals, pieces of silicon broken from the slabs of Sylvania 1N26 diodes, have a diameter of about 0.5 mm and are soldered upon a cartridge which is screwed tight in a differential screw mechanism. The inner axis of the differential screw, which has an effective pitch of $50\text{ }\mu$, is anchored in a slot. The backlash of the screw is reduced by a spring. The differential screw is fixed in the housing by means of a second swivel. The crystal is centered with respect to the housing by the disk of its cartridge, so that defects in the centering of the differential screw are of no influence. The crystal and the point of the tungsten wire can now be brought into contact by means of the differential screw. The instant of first contact is observed with an ohmmeter. Further adjusting of the pressure between the crystal and the point of the wire must occur when the multiplier is in operation. There is an optimum pressure, though not very critical.

The design of the detector is analogous to the design of the multiplier. Except for the housing, which contains only a millimeter waveguide, all parts of multipliers and detectors are interchangeable. The tungsten wire sticks into the millimeter waveguide through a hole with a diameter of 0.3 mm. The detector is adjusted in the same way as the multiplier.

§ 3. *Operation of the instruments.* The instruments are mechanically of a rigid and stable construction. Once adjusted they remained during three months without considerable loss in useful effect, even after severe shocks. With a klystron, operating at 8.2 mm wavelength, microwave power at 1.4 mm wavelength is easily observed behind a waveguide filter with a cut-off wavelength of 1.6 mm and a length of 40 mm, using the conventional video detection method. The second harmonic of a 10 mm klystron is estimated to be obtained with a conversion loss of about 10 to 15 dB.

For the second harmonic the largest power is gained if the tungsten wire element is short-circuited for direct current. For higher harmonics a bias resistance of several kilo-ohms leads to the best results. Experimentally it has been found that the power available in the higher harmonics is about proportional to 10^λ , λ being the wavelength expressed in millimeters. A bias tension from a battery did not result in better performance. At a wavelength of 5 mm the detector is more than 10 times as sensitive as a detector with a commercial 1N53 cartridge crystal, at 4 mm about 50 times as sensitive. Germanium has also been tested as crystal material in the detector, but silicon appeared to be superior.

Acknowledgements. This work has been carried out under the auspices of the Stichting voor Fundamenteel Onderzoek der Materie (F.O.M.), financially supported by the Nederlandse Organisatie voor Zuiver Wetenschappelijk Onderzoek (Z.W.O.). The author is indebted to Prof. Dr. G. W. Rathenau and Dr. F. W. Heineken for the stimulating interest and to Mr. Th. M. Huymans for the accurate machining of the instruments.

Received 10th February, 1960.

REFERENCES

- 1) Klein, J. A., J. H. N. Loubser, A. H. Nethercot and C. H. Townes, *Rev. Sci. Instrum.* **23** (1952) 78.
- 2) Johnson, C. M., D. M. Slager, and D. D. King, *Rev. Sci. Instrum.* **25** (1954) 213.
- 3) King, W. C. and W. Gordy, *Phys. Rev.* **93** (1954) 407.

A CRITERION FOR THE EFFICIENCY OF IRON CORE ELECTROMAGNETS

by D. DE KLERK and C. J. GORTER

Commun. Suppl. No. 117a from the Kamerlingh Onnes Laboratorium,
Leiden, Netherlands

Summary

A criterion is proposed for the efficiency of iron core electromagnets. This criterion is applied to a number of magnets on which data have been published. The differences in efficiency are quite high and correspond to a ratio in volume (and weight) up to almost one hundred. Short conical pole cores (see fig. 4g and 4h) apparently present great advantages.

§ 1. *Introduction.* In general the numerical data on the performance of electromagnets as quoted in the literature cannot be compared with each other. The maximum fields are usually given for completely different diameters and distances of the pole faces, so that it is practically impossible to find out which magnet works most efficiently. For this reason we have tried to find an efficiency criterion for electromagnets *).

As early as 1872 Lord Kelvin ¹⁾ proved the following theorem: If all linear dimensions of an electromagnet (including those of the field space) as well as the number of ampere turns are multiplied by the same factor, the field strength at corresponding points of the field pattern remains the same.

In 1889 Stefan ²⁾³⁾ derived a formula for the field between cylindrical poles with pole tips in the shape of truncated cones. Assuming that the apexes of the cones coincide and that the magnetization in the iron is homogeneous and parallel to the axis of revolution, he found:

$$H = 4\pi M_0[(1 - \cos \varphi) + \sin^2 \varphi \cos \varphi \ln (r_2/r_1)], \quad (1)$$

*) This criterion was already given in a simplified form by one of the authors (D. de Klerk) in Ned. T. Natuurkunde **26** (1960) 65.

where M_0 is the magnetization per unit volume of the iron, φ is the halfangle of the pole tip, r_1 is the radius of the pole face and r_2 is the radius of the cylindrical core.

Stefan's supposition that the magnetization in the iron is homogeneous and parallel to the axis does not correspond to reality. It is well-known, for instance, that the optimum angle derived from formula (1) is $54^\circ 44'$, whereas in practice 60° gives better results. Further, the application of cylindrical pole cores is not very favourable in order to obtain strong fields.

Other models were treated by Bitter ⁴⁾ and De Klerk ⁵⁾, the latter also finding a linear relation between $H/4\pi M_0$ and $\ln r_2/r_1$, with a different coefficient for $\ln (r_2/r_1)^*$, while Dreyfus ⁶⁾ developed a more complicated relation, which for $H > 8\pi M_0$ does not differ much from linearity.

As far as we know, the only formula for the case that the apexes of the pole tips do not coincide has been given by Walter ⁷⁾. His rather complicated expression was further based on the same assumptions as Stefan's formula (1). For given values of M_0 , r_1 , r_2 and φ the field increases with decreasing distance between the pole faces and tends to an asymptotic value when d approaches zero.

§ 2. In view of the linear relation between H and $\ln (r_2/r_1)$ for the case of coinciding apexes of the cones ($2r_1/d = \sqrt{3}$ if $\varphi = 60^\circ$) we wondered whether such a relation would also apply to other values of $2r_1/d$ (non-coinciding apexes).

For this reason we plotted the highest fields H_h mentioned in the descriptions against $\log (V/v)$ for a number of electromagnets ^{**)}. Here V is the volume of the magnet (iron and copper) and v the volume of the field space ($\pi r_1^2 d$). Since for one magnet $\log (V/v)$ is a linear function of $\ln (r_2/r_1)$, one should expect to find, for each value of $2r_1/d$, a linear relation between H_h and $\log (V/v)$, while the use of the ratio (V/v) guarantees that, according to Kelvin's theorem, the same relation is found for magnets of the same shape.

Fig. 1 shows the data for two "halfring electromagnets" as described by Du Bois ⁸⁾⁹⁾ for which rather detailed field data have

*) An error occurred in the paper of De Klerk. The $\cos \varphi$ in the denominator of the formula on page 11 must be removed.

**) Throughout this paper the natural logarithms are denoted by \ln , the Briggian logarithms by \log .

been published. The values are also collected in tables I and II. The weights of the magnets were 360 and 200 kilograms respectively.

Each curve of fig. 1 corresponds to a certain value of r_2/r_1 , whereas each point of a curve represents a value of $2r_1/d$. The

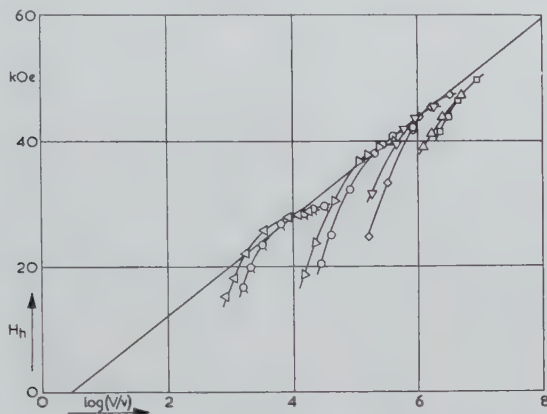


Fig. 1. Highest field strengths as a function of $\log(V/v)$ for Du Bois' halfring electromagnets.

360 kg magnet:	200 kg magnet:
□ $r_2/r_1 = 25.8$	△ $r_2/r_1 = 22.2$
◇ $r_2/r_1 = 15.5$	▽ $r_2/r_1 = 13.3$
○ $r_2/r_1 = 7.75$	▷ $r_2/r_1 = 6.67$
⊙ $r_2/r_1 = 2.16$	◁ $r_2/r_1 = 1.86$

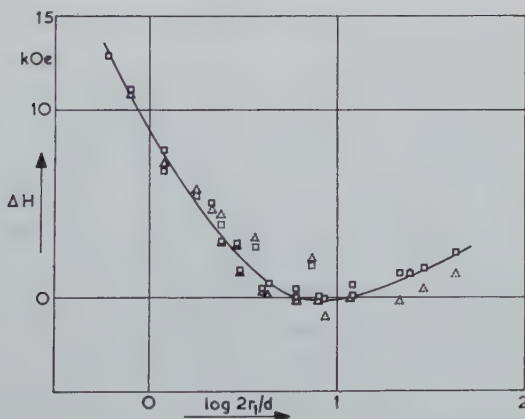


Fig. 2. Deviations from the common tangent for Du Bois' halfring electromagnets.

□ 360 kg magnet	△ 200 kg magnet
-----------------	-----------------

TABLE I

Du Bois' halfring electromagnet; 360 kg, $2r_2 = 9.3$ cm; no cobalt steel pole tips					
$2r_1$	d	V/v	H_h	$2r_1/d$	ΔH
0.36 cm	0.05 cm	9.05×10^6	49 700 Oe	7.2	1600 Oe
	0.10	4.52	46 400	3.6	2600
	0.15	3.02	43 800	2.4	3800
	0.20	2.26	41 200	1.8	5300
0.6	0.05	3.27×10^6	47 300	12	600
	0.10	1.63	45 400	6	0
	0.15	1.09	43 700	4	400
	0.20	0.814	41 600	3	1400
	0.50	0.327	33 200	1.2	6700
	1.00	0.163	24 700	0.6	12800
1.2	0.05	8.16×10^5	41 800	24	1100
	0.10	4.08	40 700	12	0
	0.15	2.73	39 300	8	0
	0.20	2.04	37 900	6	400
	0.50	0.816	32 300	2.4	2900
	1.00	0.408	25 000	1.2	7800
	1.50	0.273	20 400	0.8	11000
4.3	0.10	3.18×10^4	29 600	43	2300
	0.15	2.11	29 000	28.6	1500
	0.20	1.59	28 400	21.5	1200
	0.50	0.636	26 700	8.6	-200
	1.00	0.318	23 400	4.3	700
	1.50	0.211	19 800	2.9	2800
	2.00	0.159	16 700	2.15	5000

shapes of the curves are in reasonable agreement with Walter's formula, mentioned above.

The curves of the one magnet fit very nicely between those of the other one. The curves have, with reasonable precision, a common tangent, and points of different curves with the same value of $2r_1/d$ are on straight lines, parallel to the tangent. This is illustrated in fig. 2, where the differences ΔH between the tangent and the curves are plotted against $\log(2r_1/d)$. A single curve is found for all the ΔH -values derived from different curves of fig. 1. In the region $4 < 2r_1/d < 25$ ΔH is below 1000 Oe.

At this point we like to make some comments.

The slope of the tangent of fig. 1 is 7900 Oe. The second term of equation (1) may be written as

$$4\pi M_0 \frac{\sin^2 \varphi \cos \varphi}{3 \log e} \log \left(\frac{r_2}{r_1} \right)^3.$$

TABLE II

Du Bois' halfring electromagnet; 200 kg, $2r_2 = 8$ cm; no cobalt steel pole tips					
$2r_1$	d	V/v	H_n	$2r_1/d$	ΔH
0.36 cm	0.05 cm	5.04×10^6	47 200 Oe	7.2	200 Oe
	0.10	2.52	43 800	3.6	3100
	0.15	1.68	41 100	2.4	4400
	0.20	1.26	38 900	1.8	5600
0.6	0.05	1.82×10^6	45 200	12	600
	0.10	0.908	43 400	6	0
	0.15	0.606	41 700	4	300
	0.20	0.454	39 300	3	1300
	0.50	0.182	31 500	1.2	6500
1.2	0.05	4.55×10^5	39 800	24	1100
	0.10	2.27	38 900	12	-100
	0.15	1.52	37 500	8	-200
	0.20	1.13	36 600	6	-200
	0.50	0.455	30 300	2.4	2900
	1.00	0.227	23 700	1.2	7100
	1.50	0.152	18 500	0.8	10700
4.3	0.10	17.8×10^3	28 700	43	1200
	0.15	11.8	28 200	28.6	400
	0.20	8.6	27 800	21.5	-300
	0.50	3.55	25 700	8.6	-1100
	1.00	1.78	22 000	4.3	100
	1.50	1.18	18 100	2.9	2600
	2.00	0.86	15 000	2.15	4600

With $q = 60^\circ$, $4\pi M_0 = 22000$ gauss the coefficient of $\log(r_2/r_1)^3$ becomes 6400 Oe. Since De Klerk's formula (see § 1) gives a higher value for this coefficient, the value 7900 Oe seems not unreasonable.

The dotted points in fig. 2 were derived from the curves of fig. 1 which, for some unknown reason, deviate markedly from the tangent. It appears that in the region $2r_1/d < 3$ these points do not deviate much from the curve. This is important because, in § 3, this part of the curve will in particular be used for further computations.

Some field values were given by Du Bois, using cobalt steel pole tips and extra coils between the poles of the magnet. The points fall somewhat above the curves of fig. 1, but in general the data show the same character.

Du Bois constructed two more halfring electromagnets, one of 1400 kg and one of 50 kg. The data for these, however, are less detailed. We left them out of the discussion.

§ 3. We would suggest that, if other types of electromagnets give rise to similar diagrams, the positions of the tangents in the $H_h, \log(V/v)$ -diagrams might give a useful indication of the efficiencies of the various types of magnets. Unfortunately, however, the data published for most electromagnets are very incomplete. Often, for each value of r_1 there is only one maximum field available, the ratio $2r_1/d$ being about 1.5 or 2, so that the correction ΔH of fig. 2 is not negligible at all.

For this reason we adopted a different procedure. We took the field values from the literature (preferably data with the highest values of the ratio $2r_1/d$), corrected them with the help of the curve of fig. 2 and plotted these values in the $H, \log(V/v)$ -diagram. The

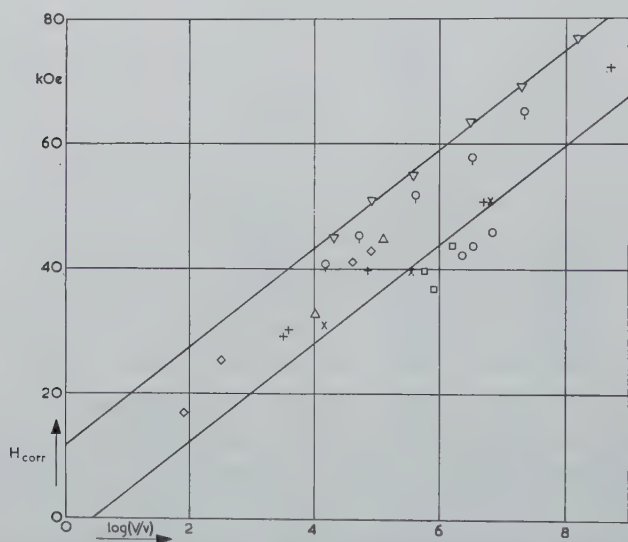


Fig. 3. Highest field strengths, after correction, as a function of $\log(V/v)$ for several electromagnets.

Lower line: Du Bois' halfring magnets (fig. 1).

Upper line: Uppsala University magnet.

- Du Bois' ring magnet.
- Du Bois' older halfring magnet.
- × Weiss-magnet.
- + Weiss-magnet of the Kamerlingh Onnes Laboratory.
- △ Bellevue magnet.
- ◇ Bitter's A.D. Little-magnet.
- Oerlikon-magnet.
- ▽ Uppsala University magnet.

TABLE III

Electromagnet of Uppsala University; 37000 kg, $2r_2 = 59$ cm; cobalt steel pole tips						
$2r_1$	d	V/v	H_h	$2r_1/d$	ΔH	H_{corr}
0.5 cm	0.2 cm	121×10^6	74 000 Oe	2.5	2900 Oe	76 900 Oe
1.0	0.3	20.2	67 500	3.3	1700	69 200
2.0	0.5	3.02	62 500	4.0	1000	63 500
4.0	1.0	0.378	54 000	4.0	1000	55 000
6.0	2.0	0.084	49 000	3.0	2000	51 000
12.0	2.0	0.021	45 000	6.0	0	45 000

TABLE IV

Du Bois' older halfring electromagnet; 175 kg, $2r_2 = 8$ cm; no cobalt steel pole tips						
$2r_1$	d	V/v	H_h	$2r_1/d$	ΔH	H_{corr}
0.6 cm	0.1 cm	8.15×10^5	36 700 Oe	6.0	0 Oe	36 700 Oe
0.5	0.2	5.8	36 800	2.5	2900	39 700
0.3	0.2	16.1	38 000	1.5	5900	43 900

TABLE V

Du Bois' ringelectromagnet; 275 kg, $2r_2 = 10$ cm; no cobalt steel pole tips						
$2r_1$	d	V/v	H_h	$2r_1/d$	ΔH	H_{corr}
0.36 cm	0.05 cm	6.91×10^6	46 000 Oe	7.2	-100 Oe	45 900 Oe
0.36	0.10	3.45	42 500	3.6	1300	43 800
0.36	0.15	2.30	39 000	2.4	3200	42 200
0.30	0.20	2.50	38 000	1.5	5900	43 900

results for several magnets are shown in fig. 3. The data are also given in tables III till X.

The lower line is the common tangent for Du Bois' halfring electromagnets as given in fig. 1. The upper line represents the large electromagnet of the University of Uppsala ⁶⁾¹⁰⁾, constructed by Dreyfus. For this magnet some data are available with $2r_1/d$ of the order of 3, see table III. Within the experimental precision the two lines have the same slope (7900 Oe). For most of the other magnets the corrections ΔH are quite appreciable.

It appears that an older halfring magnet of Du Bois ¹¹⁾¹²⁾ and his original ring magnet ¹³⁾ (tables IV and V) are below the lower line of fig. 3. The well-known Weiss-magnet ¹⁴⁾, developed in 1907 (table VI), is not better than Du Bois' halfring magnets. The big Weiss-magnet at the Kamerlingh Onnes Laboratory ¹⁵⁾ (table VII), however, proves to operate more efficiently than Weiss' original model. The points of the big magnet of the French Académie des

TABLE VI

Weiss-magnet; 1000 kg, $2r_2 = 15$ cm; no cobalt steel pole tips						
$2r_1$	d	V/v	H_h	$2r_1/d$	ΔH	H_{corr}
0.36 cm	0.192 cm	6.53×10^6	46 300 Oe	1.88	4500 Oe	50 800 Oe
1.0	0.445	3.66×10^5	36 000	2.25	3500	39 500
2.5	2.00	1.37×10^4	24 100	1.25	6900	31 000

TABLE VII

Weiss-magnet of the Kamerlingh Onnes Laboratory; 12000 kg, $2r_2 = 40$ cm, no cobalt steel pole tips						
$2r_1$	d	V/v	H_h	$2r_1/d$	ΔH	H_{corr}
0.18 cm	0.12 cm	5.03×10^8	67 000 Oe	1.66	5200 Oe	72 200 Oe
0.8	0.6	5.08×10^6	54 000	1.33	6600	60 600
4	1.7	7.18×10^4	36 400	2.35	3300	39 700
10	5.0	3.90×10^3	26 000	2.00	4200	30 200
10	6.0	3.27×10^3	24 000	1.67	5200	29 200

TABLE VIII

Bellevue electromagnet; 120000 kg, $2r_2 = 75$ cm; cobalt steel pole tips						
$2r_1$	d	V/v	H_h	$2r_1/d$	ΔH	H_{corr}
0.3 cm	0.2 cm	1.08×10^9	70 000 Oe	1.50	5900 Oe	75 900 Oe
6.09	4	1.30×10^5	39 000	1.52	5700	44 700
25	3	1.04×10^4	32 800	8.33	-100	32 700

TABLE IX

A.D. Little-electromagnet; 2000 kg, $2r_2 = 28$ cm; cobalt steel pole tips						
$2r_1$	d	V/v	H_h	$2r_1/d$	ΔH	H_{corr}
2.5 cm	1.25 cm	4.16×10^4	37 000 Oe	2.00	4100 Oe	41 100 Oe
14	5	3.31×10^2	23 000	2.80	2400	25 400
28	5	8.27×10^1	17 000	5.60	100	17 100
2.5	0.6	8.73×10^4	42 000	4.17	800	42 800

TABLE X

Oerlikon-electromagnet; 3000 kg, $2r_2 = 20$ cm; cobalt steel pole tips						
$2r_1$	d	V/v	H_h	$2r_1/d$	ΔH	H_{corr}
0.33 cm	0.2 cm	2.25×10^7	60 000 Oe	1.65	5200 Oe	65 200 Oe
0.6	0.4	3.41×10^6	52 000	1.50	5900	57 900
1.2	0.8	4.26×10^5	46 000	1.50	5900	51 900
2.4	1.6	5.32×10^4	39 500	1.50	5900	45 400
3.6	2.4	1.57×10^4	35 000	1.50	5900	40 900

Sciences at Bellevue ¹⁶⁾ (table VIII) and those of the American A.D. Little-magnet, constructed by Bitter and Reed ¹⁷⁾ (table IX), are higher. The Swiss Oerlikon-magnet ¹⁸⁾ (table X) is still higher, but it remains well below the line of the Uppsala magnet.

§ 4. Fig. 4 shows the cross-sections of the poles and winding spaces of the magnets discussed in this paper, the sequence being from low to high efficiency. The scales were chosen in such a way that r_2 (the radius of the basis of the pole tip) has the same value for all of them. The pole tips were drawn with the traditional angle of 60° , and r_2/r_1 was arbitrarily chosen equal to five. The only exception is the A.D. Little-magnet, which is commercially available with pole tips of another shape.

Unfortunately some descriptions in the literature are rather incomplete, so that some details in fig. 4 had to be guessed. We are not sure that the drawings *b*, *f* and *g* are precise. Nevertheless, some conclusions may be drawn.

In fig. 3 Du Bois' halfring magnet and the Weiss-magnet have the same efficiency. It may be seen in fig. 4*b* and 4*c* that both have pole cores of constant diameter, so that, with increasing number of ampere turns, saturation starts in the cores and not in the pole tips. The relatively thicker yoke of the Weiss-magnet does not make much difference, the yokes not reaching saturation.

The Weiss-magnet of the Kamerlingh Onnes Laboratory (fig. 4*d*) is better than Weiss' original model (fig. 4*c*). This may be due to the fact that the pole cylinders and the coils are relatively much shorter, which apparently influences the saturation in a favourable way.

Pole cores of conical shape are better than cylinders, and the steeper and shorter they are built, the higher the efficiency is. The Bellevue and A.D. Little-magnets (figs 4*e* and 4*f*) are apparently better than the Weiss-magnet; the Oerlikon-magnet (fig. 4*g*) is still better, but the most efficient magnet is the one of Uppsala University (fig. 4*h*). The pole cores have a slope of 45° and their length is hardly larger than r_1 .

§ 5. The quality criterion, as given here, is, for a variety of reasons, only a rough one indeed.

For the diagram of fig. 3 we used, in the calculations, the strongest field value given for a certain field space for each magnet. It is not certain, however, that the degree of saturation of the cores was approximately the same in all the cases.

The curve of fig. 2, which was used for the calculation of the corrections, is valid for Du Bois' halfring electromagnets. It is not

certain, however, that it is justified to apply it (as we did) for other types of magnets. This is probably the explanation of the fact that in fig. 3, some magnets do not yield nice straight lines. It seems

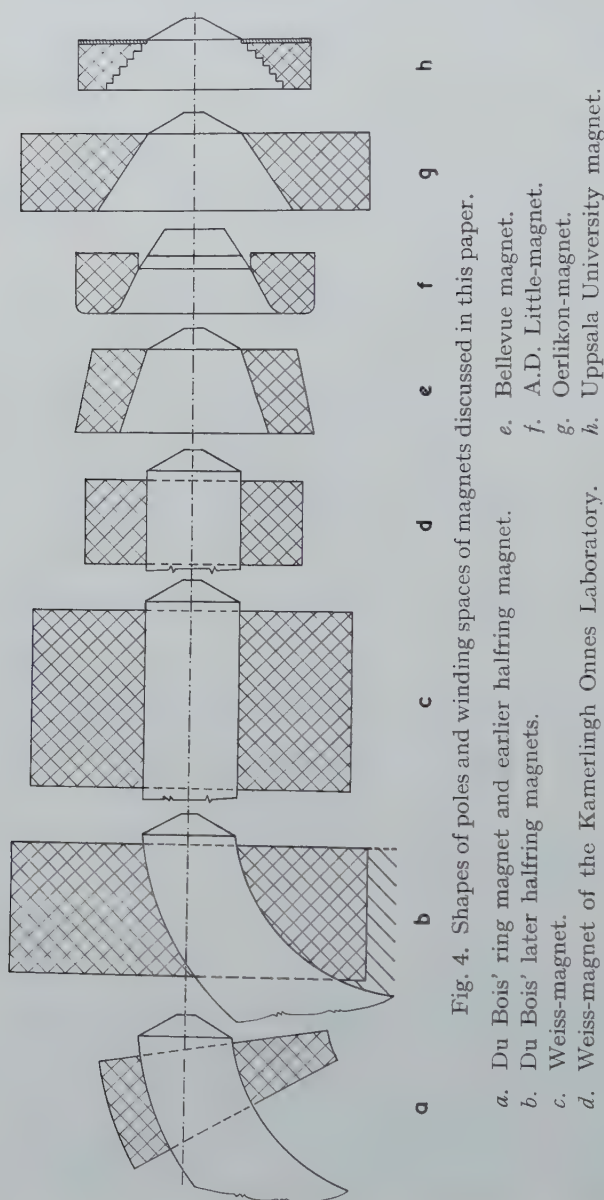


Fig. 4. Shapes of poles and winding spaces of magnets discussed in this paper.

- a.* Du Bois' ring magnet.
- b.* Du Bois' later halfring magnet.
- c.* Weiss-magnet.
- d.* Weiss-magnet of the Kamerlingh Onnes Laboratory.
- e.* Bellevue magnet.
- f.* A.D. Little-magnet.
- g.* Oerlikon-magnet.
- h.* Uppsala University magnet.

rather improbable, however, that this seriously affects the relative positions of the magnets in the diagram.

Usually the volume of a magnet is not given. For this reason we took, in our computations, the weights as given in the literature, and divided them by 7.8 (roughly the density of iron and copper). We doubt, however, whether a weight, quoted as "roughly three tons", is accurate within 10%. Moreover, some magnets have a heavy iron foot, and it is not always clear from the paper whether this is included in the given weight or not.

Pole tips of cobalt steel give an increase in the field strength of a few kilo oersted, and in some cases it is not stated whether the magnet has cobalt steel pole tips or not.

§ 6. The power consumption of the magnet has been left out of consideration in our efficiency criterion. This point entails some complications, because the fraction of the time the magnet is in actual use plays the predominant role.

Consider a large electromagnet, used in a low temperature laboratory for adiabatic demagnetization work. Let us suppose there are on the average two helium runs per week, and ten demagnetizations per run. For each demagnetization the magnet is in actual use during at the most half an hour, but not always at full power. It is obvious that, in this case, depreciation and interest are financially much more important than the power consumption.

In the case of a smaller magnet, more or less constantly in use for Zeeman splittings or resonance work, the costs of power consumption will outweigh the other running costs of the magnet, including writing off.

§ 7. Let us consider the Uppsala magnet as an "efficient" magnet and the Du Bois and original Weiss-magnets as "inefficient". It follows from fig. 3 that, for a given weight of iron and copper, an efficient construction may produce a gain of roughly 15000 Oe. Even more impressive is the statement that, in order to obtain the same gain in field with the inefficient magnet, one has to increase the weight by a factor of almost one hundred!

The diagrams of fig. 2 and 3 may be useful for the calculation of new electromagnets. Suppose one wants to build a magnet which gives 30000 Oe in a pole gap of 8 cm, and pole faces of 12 cm diameter.

In this case we have $2r_1/d = 1.5$, $\Delta H = 6000$ Oe, $H_{\text{corr.}} = 36000$ Oe. For a magnet with the efficiency of the Uppsala magnet it follows: $V/v = 1250$, so that a weight of almost 9 tons would be required. For a magnet with the efficiency of the Oerlikon-magnet (the second best) one gets $V/v = 4000$, hence a weight of 28 tons.

It seems that the efficiency criterion could be improved. It is obvious, for instance, that the straight lines of fig. 3 cannot be correct down to very small values of (V/v) . The authors hope, however, that the criterion in its provisional form may be of some use if one wants to compare the performances of different types of electromagnets.

Received 8th April, 1960

REFERENCES

- 1) Thomson, W., Pap. Electrostat. and Magnetism, 1872, p. 564.
- 2) Stefan, J., Ann. Phys. Lpz. **33** (1889) 440.
- 3) Bates, L. F., Modern Magnetism, third edition, Cambridge 1951, p. 77.
- 4) Bitter, F., Rev. Sci. Instrum. **7** (1936) 479.
- 5) De Klerk, D., Ned. T. Natuurkde **26** (1960) 1.
- 6) Dreyfus, L., Elektrotechnik und Maschinenbau **53** (1935) 205.
- 7) Walter, B., Ann. Phys. Lpz. **14** (1904) 106.
- 8) Du Bois, H., Z. Instrumkde **31** (1911) 362.
- 9) Du Bois, H., Ann. Phys. Lpz. **42** (1913) 953.
- 10) Dreyfus, L., Asea J. **12** (1935) 8.
- 11) Du Bois, H., Z. Instrumkde **19** (1899) 357.
- 12) Du Bois, H., Ann. Phys. Lpz. **1** (1900) 199.
- 13) Du Bois, H., Ann. Phys. Lpz. **51** (1894) 537.
- 14) Weiss, P., J. de Phys. **6** (1907) 353.
- 15) Häder, G., Siemens Zeitschr. **10** (1930) 481.
- 16) Cotton, A. and Dupouy, G., C. R. Acad. Sci. Paris **190** (1930) 544.
- 17) Bitter, F. and Reed, F. E., Rev. Sci. Instrum. **22** (1951) 171.
- 18) Data taken from a proposal by Oerlikon to the Delft Institute of Technology, 1954.

THE SURFACE CHARGE OF A SEMI-INFINITE CYLINDER DUE TO AN AXIAL POINT CHARGE *)

by H. A. LAUWERIER

Mathematical Centre, Amsterdam, Netherlands

Summary

In this paper we determine the surface charge density of a semi-infinite conducting cylinder due to an axial point charge. The problem can be reduced to an integral equation of the Wiener-Hopf type. The relevant factorization problem is studied in detail.

§ 1. *Introduction.* The problem of the determination of the field of an axial point charge inside a hollow infinitely long conducting cylinder has been considered by various writers ¹⁾.

If there is a point charge -1 at the origin and if in cartesian coordinates (x, y, z) the position of the cylinder is determined by $-\infty < x < \infty$, $r = \sqrt{y^2 + z^2} = 1$ the surface charge at the cylinder is

$$\sigma(x) = \frac{1}{2\pi^2} \int_0^{\infty} \frac{\cos tx}{I_0(t)} dt. \quad (1.1)$$

In this paper we shall consider the equivalent problem for a semi-infinite cylinder $0 < x < \infty$, $r = 1$. This problem is much more complicated. The determination of the surface charge $\sigma(x)$, which also depends on the position of the point charge on the axis, involves the solving of a Wiener-Hopf equation of the first kind

$$\int_0^{\infty} h(x-t) \sigma(t) dt = g(x), \quad x > 0 \quad (1.2)$$

with $h(x) \sim -\ln x^2$ for $x \rightarrow 0$. If $\sigma(x)$ is known, the electrostatic

*) This paper is a revised version of a solution of a prize question put by the Wiskundig Genootschap in 1955.

field $V(r, x)$ may be easily determined (cf. (2.3)). We shall therefore confine our attention to the determination of $\sigma(x)$ from (1.2).

The Wiener-Hopf equation (1.2) cannot be solved by the familiar methods since in this case the strip of convergence is absent. There is only a line of convergence, the real axis, upon which the Fourier transform of the kernel function has a logarithmic singularity at the origin. However, the integral equation (1.2) may be solved by means of the methods developed by Muskhelishvili ²⁾; cf. also ³⁾ and ⁴⁾. In particular the notion of sectionally holomorphic functions plays an important role in the solution of (1.2) ⁵⁾. In § 3 this will be discussed in detail. An explicit expression is obtained for the Fourier transform of the surface charge $\sigma(x)$ depending on the proper factorization of the Fourier transform $H(x)$ of $h(x)$.

The explicit factorization is carried out in § 4. Various integral representations and series expansions are derived. This may lead to an expansion of $\sigma(x)$ for small x in § 5, or for large x in § 7. If the point charge is at the open end $(0, 0)$ of the cylinder $0 < x < \infty$, $r = 1$, we have e.g.

$$2\pi\sigma(x) = 0.337x^{-1/2} + 0.527x^{1/2} - 0.782^{3/2} - 0.961^{5/2} \dots \quad (1.3)$$

Special expressions are derived in § 6 for the case that the point charge is far inside or outside the cylinder.

§ 2. *Reduction of the problem to an integral equation.* The electrostatic field $V(r, x)$ of a point charge at $(0, a)$ of intensity -1 in the presence of a semi-infinite conducting cylinder $r = 1$, $0 < x < \infty$ is determined by

$$\frac{1}{r} \frac{\partial}{\partial r} \left(r \frac{\partial V}{\partial r} \right) + \frac{\partial^2 V}{\partial x^2} = 0, \quad (2.1)$$

$$V = 0 \quad \text{for} \quad r = 1, x > 0,$$

$$V = -[r^2 + (x - a)^2]^{-\frac{1}{2}} + O(1) \quad \text{for} \quad r^2 + (x - a)^2 \rightarrow 0.$$

The induced charge density at the cylinder is

$$\sigma(x) = -\frac{1}{4\pi} \frac{\partial V}{\partial r} \bigg|_{r=1}^{1+0}. \quad (2.2)$$

Conversely, if $\sigma(x)$ is known, the potential $V(r, x)$ may be deter-

mined from

$$V(r, x) = -[r^2 + (x - a)^2]^{-\frac{1}{2}} + \\ + \int_0^{\infty} \sigma(t) dt \int_0^{2\pi} [r^2 + 1 + 2r \cos \theta + (x - t)^2]^{-\frac{1}{2}} d\theta$$

or

$$V(r, x) = -[r^2 + (x - a)^2]^{-\frac{1}{2}} + \int_0^{\infty} h(r, x - t) \sigma(t) dt, \quad (2.3)$$

where

$$h(r, x) = 4[(r + 1)^2 + x^2]^{-\frac{1}{2}} K\{2r^{\frac{1}{2}}[(r + 1)^2 + x^2]^{-\frac{1}{2}}\}. \quad (2.4)$$

The function $K(k)$ is the complete elliptic integral

$$K(k) = \int_0^{\frac{\pi}{2}} (1 - k^2 \sin^2 \varphi)^{-\frac{1}{2}} d\varphi = \frac{1}{2}\pi F(\frac{1}{2}, \frac{1}{2}; 1; k^2).$$

For $r = 1$, $x > 0$ from (2.3) the following integral equation for $\sigma(x)$ is obtained:

$$\int_0^{\infty} h(x - t) \sigma(t) dt = g(x), \quad (2.5)$$

where

$$h(x) = 4(x^2 + 4)^{-\frac{1}{2}} K[2(x^2 + 4)^{-\frac{1}{2}}], \quad (2.6)$$

and

$$g(x) = [1 + (x - a)^2]^{-\frac{1}{2}}. \quad (2.7)$$

Equation (2.5) is of the well-known Wiener-Hopf type. In view of

$$h(x) \sim -\ln x^2, \quad x \rightarrow 0$$

the integral equation is singular.

§ 3. *Solution of the integral equation.* By $F^+(z)$ we shall understand a function of the complex variable $z = x + iy$ which is holomorphic in the upper half-plane $y > 0$ and which vanishes at infinity. In a similar way $F^-(z)$ is holomorphic in the lower half-plane $y < 0$ and vanishes at infinity. At the real axis we define

$$F^+(x) = \lim_{y \downarrow 0} F^+(x + iy) \quad F^-(x) = \lim_{y \uparrow 0} F^-(x + iy).$$

Consider now the Wiener-Hopf equation (2.5) in the form

$$\int_0^{\infty} h(x - t) \sigma(t) dt = \begin{cases} g(x) & x > 0, \\ \chi(x) & x < 0, \end{cases} \quad (3.1)$$

where $\sigma(x)$, $x > 0$ and $\chi(x)$, $x < 0$ are unknown functions. Let $H(x)$, $S^+(z)$, $G^+(z)$, $X^-(z)$ represent the following Fourier transforms:

$$\begin{aligned} H(x) &= \int_{-\infty}^{\infty} e^{itx} h(t) dt, \\ S^+(z) &= \int_0^{\infty} e^{itz} \sigma(t) dt, \quad G^+(z) = \int_0^{\infty} e^{itz} g(t) dt, \\ X^-(z) &= \int_{-\infty}^0 e^{itz} \chi(t) dt, \end{aligned}$$

then Fourier transformation of (3.1) gives

$$H(x)S^+(x) = G^+(x) + X^-(x). \quad (3.2)$$

The kernel function $H(x)$ can be factorized as the product of limit functions of sectionally holomorphic functions $H^+(z)$ and $H^-(z)$:

$$H(x) = H^+(x) H^-(x). \quad (3.3)$$

Then (3.2) may be written as follows:

$$H^+(x) S^+(x) - \frac{X^-(x)}{H^-(x)} = \frac{G^+(x)}{H^-(x)}. \quad (3.4)$$

If the factorization (3.3) is carried out properly, the relation (3.4) is of the form

$$\phi^+(x) - \phi^-(x) = \varphi(x). \quad (3.5)$$

The solution of the problem (3.5) is unique if ϕ^+ , ϕ^- and φ belong to any finite L^2 -class, i.e. for $-A < x < A$ for any positive A . We have

$$\phi^{\pm}(z) = \frac{1}{2\pi i} \int_{-\infty}^{\infty} \frac{\varphi(t)}{t - z} dt, \quad (3.6)$$

and

$$\phi^+(x) = \frac{1}{2} \varphi(x) + \frac{1}{2\pi i} \int_{-\infty}^{\infty} \frac{\varphi(t)}{t - x} dt, \quad (3.7)$$

where

$$\int_{-\infty}^{\infty} \frac{\varphi(t)}{t - x} dt \stackrel{\text{def}}{=} \lim_{\varepsilon \rightarrow 0} \int_{\varepsilon}^{\infty} \frac{\varphi(x+t) - \varphi(x-t)}{t} dt. \quad (3.8)$$

Thus the following explicit solution of (3.2) is obtained:

$$S^+(z) = \frac{1}{2\pi i H^+(z)} \int_{-\infty}^{\infty} \frac{G^+(t)}{H^-(t)} \frac{dt}{t-z}. \quad (3.9)$$

From $S(z)$ the surface charge $\sigma(x)$ may be derived by inverse Fourier transformation.

In view of

$$\int_{-\infty}^{\infty} \phi^-(t) \frac{dt}{t-z} = 0 \quad \text{for } \operatorname{Im} z > 0$$

the right-hand side of (3.9) may be replaced by

$$S^+(z) = \frac{1}{2\pi i H^+(z)} \int_{-\infty}^{\infty} \frac{G(t)}{H^-(t)} \frac{dt}{t-z}, \quad (3.10)$$

where

$$G(x) = \int_{-\infty}^{\infty} e^{itx} g(t) dt.$$

We have

$$G(x) = 2e^{iax} K_0(|x|) \quad (3.11)$$

and

$$H(x) = 4\pi I_0(x) K_0(|x|), \quad (3.12)$$

cf. Erdélyi, Tables of Integral Transforms (1.14.13).

§ 4. *Factorization of $H(x)$.* Introduce the function

$$L(x) \stackrel{\text{def}}{=} \frac{|x|}{2\pi} H(x) = 2|x| I_0(x) K_0(|x|). \quad (4.1)$$

For $x \rightarrow \infty$ we have

$$\ln L(x) = \frac{1}{8x^2} + \frac{13}{64x^4} + O(x^{-6}). \quad (4.2)$$

Then the factorization of $H(x)$ is obtained as follows

$$H^+(z) = \left(\frac{2\pi}{z}\right)^{\frac{1}{2}} \exp \left[\frac{\pi i}{4} + \frac{1}{2\pi i} \int_{-\infty}^{\infty} \frac{\ln L(t)}{t-z} dt \right], \quad \operatorname{Im} z \geq 0, \quad (4.3)$$

$$H^-(z) = \left(\frac{2\pi}{z}\right)^{\frac{1}{2}} \exp \left[-\frac{\pi i}{4} - \frac{1}{2\pi i} \int_{-\infty}^{\infty} \frac{\ln L(t)}{t-z} dt \right], \quad \text{Im } z \leq 0. \quad (4.4)$$

From (4.3) we obtain for $z \rightarrow x$

$$H^+(x) = 2 [\pi I_0(x) K_0(|x|)]^{\frac{1}{2}} \exp \left[\frac{\pi i}{4} \operatorname{sgn} x + \frac{1}{2\pi i} \int_{-\infty}^{\infty} \frac{\ln L(t)}{t-x} dt \right]; \quad (4.5)$$

also

$$H^-(x) = \overline{H^+(x)}, \quad (4.6)$$

$$\left. \begin{aligned} H^+(xe^{\pi i}) &= H^-(x), \\ H^-(xe^{-\pi i}) &= H^+(x), \end{aligned} \right\} \quad \text{for } x > 0. \quad (4.7)$$

The asymptotic behaviour of $H^+(z)$ may be determined as follows. We have

$$\frac{1}{2\pi i} \int_{-\infty}^{\infty} \frac{\ln L(t)}{t-z} dt = \sum_1 \frac{\alpha_k}{s^k}$$

where $s = -iz$, $\operatorname{Re} s > 0$. The first few coefficients are

$$\begin{aligned} \alpha_1 &= \frac{1}{\pi} \int_0^{\infty} \ln L(t) dt = -0.0280, \quad \alpha_2 = -\frac{1}{16}, \\ \alpha_3 &= -\frac{1}{\pi} \int_0^{\infty} t^2 \left[\ln L(t) - \frac{1}{8t^2} \right] dt = -0.00298, \quad \alpha_4 = \frac{13}{128}. \end{aligned}$$

Hence we have

$$z \rightarrow \infty \quad H^+(z) = \left(\frac{2\pi}{s}\right)^{\frac{1}{2}} \exp \sum_1 \frac{\alpha_k}{s^k}, \quad s = -iz. \quad (4.8)$$

For $H^+(x)$ an alternative expression may be derived in the following way. We need the auxiliary function

$$\Omega(x) \stackrel{\text{def}}{=} \arg [-Y_0(x) + iJ_0(x)], \quad x > 0, \quad (4.9)$$

with $0 \leq \Omega(x) \leq \pi$. Without proof we mention the following simple properties of this function:

$$\Omega'(x) = \frac{2}{\pi x [J_0^2(x) + Y_0^2(x)]}. \quad (4.10)$$

For $x \rightarrow \infty$ we have

$$\Omega'(x) = 1 + \frac{1}{8x^2} - \frac{25}{128x^4} + O(x^{-6}). \quad (4.11)$$

For $x \rightarrow +0$ we have

$$\Omega(x) = \frac{\pi}{2 \ln (2/x)} + O\left(\ln^{-2} \frac{2}{x}\right). \quad (4.12)$$

At the k th zero β_k of $J_0(x)$, $k \geq 1$, we have

$$\Omega(\beta_k - 0) = 0, \quad \Omega(\beta_k + 0) = \pi. \quad (4.13)$$

We shall now prove the following formula:

$$\arg H^+(x) = \frac{x}{\pi} \int_0^\infty \frac{\Omega(t)}{t^2 + x^2} dt. \quad (4.14)$$

According to (4.5) we have

$$\arg H^+(x) = \frac{\pi}{4} \operatorname{sgn} x - \frac{x}{\pi} \int_0^\infty \frac{\ln L(t)}{t^2 - x^2} dt. \quad (4.15)$$

This odd function is the sine transform of the even function

$$\frac{1}{2y} + \frac{1}{\pi} \int_0^\infty \cos yt \ln L(t) dt, \quad y > 0.$$

This function may be reduced as follows

$$\begin{aligned} & \frac{1}{2y} - \frac{1}{\pi y} \int_0^\infty \sin yt \frac{L'(t)}{L(t)} dt = \\ & = \frac{1}{2y} - \frac{1}{\pi y} \operatorname{Im} \int_0^\infty e^{iyt} \left[\frac{1}{t} + \frac{I_0'(t)}{I_0(t)} + \frac{K_0'(t)}{K_0(t)} \right] dt = \\ & = -\frac{1}{y} \sum_1^\infty e^{-\beta_k y} + \frac{1}{\pi y} \operatorname{Im} \int_0^\infty e^{-yt} \frac{J_0'(t) - iY_0'(t)}{J_0(t) - iY_0(t)} dt = \\ & = -\frac{1}{y} \left[\sum_1^\infty e^{-\beta_k y} - \frac{1}{\pi} \int_0^\infty e^{-yt} \Omega'(t) dt \right] = \frac{1}{\pi} \int_0^\infty e^{-yt} \Omega(t) dt. \end{aligned}$$

The expression last obtained is the sine transform of the righthand side of (4.14). Thus we have

$$H^+(x) = 2[\pi I_0(x) K_0(|x|)]^{\frac{1}{2}} \exp \frac{\pi i}{\pi} \int_0^{\infty} \frac{\Omega(t)}{t^2 + x^2} dt. \quad (4.16)$$

We note that for a purely imaginary z the function $H^+(z)$ is real. We have from (4.3) and (4.4)

$$H^+(si) = H^-(-si) = \left(\frac{2\pi}{s}\right)^{\frac{1}{2}} \exp \frac{s}{\pi} \int_0^{\infty} \frac{\ln L(t)}{t^2 + s^2} dt. \quad (4.17)$$

Finally we shall consider the behaviour of $H^+(z)$ near the origin. For $x > 0$ we have

$$\ln L(x) = \ln 2x + \ln \ln \frac{2}{x} + O\left(\ln^{-1} \frac{2}{x}\right).$$

Since

$$\frac{z}{\pi i} \int_0^{\infty} \frac{\ln 2t}{t^2 - z^2} dt = \frac{1}{2} \ln 2z - \frac{\pi i}{4}, \quad \text{Im } z > 0,$$

and

$$\frac{z}{\pi i} \int_0^{\infty} \frac{\ln \ln 2/t}{t^2 - z^2} dt = \frac{1}{2} \ln \ln \frac{2}{z} + O\left(\ln^{-1} \frac{2}{z}\right), \quad \text{Im } z > 0,$$

we obtain

$$z \rightarrow 0, \quad H^+(z) = 2\left(\pi \ln \frac{2}{z}\right)^{\frac{1}{2}} \left[1 + O\left(\ln^{-1} \frac{2}{z}\right)\right]. \quad (4.18)$$

At the positive real axis we have

$$\begin{aligned} H^+(x) &= 2\left(\pi \ln \frac{2}{x}\right)^{\frac{1}{2}} \left[1 + \frac{\gamma - \frac{1}{2}\pi i}{2 \ln \frac{1}{2}x} + O\left(\ln^{-2} \frac{2}{x}\right)\right], \\ H^-(x) &= 2\left(\pi \ln \frac{2}{x}\right)^{\frac{1}{2}} \left[1 + \frac{\gamma + \frac{1}{2}\pi i}{2 \ln \frac{1}{2}x} + O\left(\ln^{-2} \frac{2}{x}\right)\right]. \end{aligned} \quad (4.19)$$

The argument of $H^+(x)$ as a function of x is given in table I.

TABLE I

x	$\arg. H^+(x)$	x	$\arg. H^+(x)$
0.00	0	1.4	0.739
0.05	0.278	1.6	0.749
0.1	0.349	1.8	0.757
0.15	0.401	2	0.762
0.2	0.441	3	0.772
0.3	0.506	4	0.778
0.4	0.554	5	0.779
0.5	0.593	6	0.780
0.6	0.624	7	0.781
0.8	0.670	8	0.781
1.0	0.701	9	0.782
1.2	0.723	10	0.782
		∞	$\pi/4 = 0.785$

§ 5. *Expansion of $\sigma(x)$ for small x .* The properties of the functions $H^\pm(z)$ derived in the previous section validate the derivation of the solution of the Wiener-Hopf equation (2.5). We have obtained according to (3.10) and (3.11).

$$S^+(z) = \frac{1}{\pi i H^+(z)} \int_{-\infty}^{\infty} e^{iat} \frac{K_0(|t|)}{H^-(t)} \frac{dt}{t-z}, \quad (5.1)$$

or

$$S^+(z) = \frac{1}{4\pi^2 i H^+(z)} \int_{-\infty}^{\infty} e^{iat} \frac{H^+(t)}{I_0(t)} \frac{dt}{t-z}. \quad (5.2)$$

The asymptotic expansion of $S^+(z)$ for $z \rightarrow \infty$ may be determined as follows.

According to (4.8) we have

$$\frac{1}{H^+(z)} = \left(\frac{s}{2\pi}\right)^{\frac{1}{2}} \exp - \sum_1 \frac{\alpha_k}{s^k},$$

where $s = -iz$, $\text{Re } s > 0$. This may be brought into the form

$$\frac{1}{H^+(z)} = \left(\frac{s}{2\pi}\right)^{\frac{1}{2}} \sum_0 \frac{a_k}{s^k}, \quad (5.3)$$

where

$$a_0 = 1, \quad a_1 = -\alpha_1 = 0.0280,$$

$$a_2 = -\alpha_2 + \frac{\alpha_1^2}{2} = -0.0629, \quad a_3 = -\alpha_3 + \alpha_1 \alpha_2 - \frac{\alpha_1^3}{6} = 0.00473.$$

Furthermore we have the asymptotic expansion

$$\frac{1}{\pi i} \int_{-\infty}^{\infty} e^{iat} \frac{K_0(|t|)}{H^-(t)} \frac{dt}{t-z} = 2^{-\frac{1}{2}} \sum_0 \frac{b_k}{s^{k+1}}, \quad (5.4)$$

where

$$b_k = \frac{2^{-\frac{1}{2}}}{\pi} \operatorname{Re} \int_0^{\infty} \exp \left[i \left(\frac{k\pi}{2} - at \right) \right] t^k \frac{K_0(t)}{H^+(t)} dt$$

or, in view of (4.16),

$$b_k = \frac{1}{\pi} \sqrt{\frac{2}{\pi}} \int_0^{\infty} t^k \left[\frac{K_0(t)}{I_0(t)} \right]^{\frac{1}{2}} \cos \left[\frac{k\pi}{2} - A(t) - at \right] dt, \quad (5.5)$$

where

$$A(x) \stackrel{\text{def}}{=} \arg H^+(x) = \frac{x}{\pi} \int_0^{\infty} \frac{\Omega(t)}{t^2 + x^2} dt. \quad (5.6)$$

By means of (5.3) and (5.4) we obtain from (5.1)

$$2\pi S^+(z) = \sqrt{\pi} \sum_0^{\infty} c_k s^{-k-\frac{1}{2}}, \quad z = si \quad (5.7)$$

where

$$c_k = \sum_0^k a_j b_{k-j}. \quad (5.8)$$

Accordingly we obtain for the inverse Fourier transform $\sigma(x)$ the following expansion, presumably convergent for small x :

$$2\pi\sigma(x) = \sum_0^{\infty} \frac{\Gamma(\frac{1}{2})}{\Gamma(k + \frac{1}{2})} c_k x^{k-\frac{1}{2}}. \quad (5.9)$$

In the case $a = 0$ the first few coefficients are

$$\begin{array}{ll} b_0 = 0.337, & c_0 = 0.337, \\ b_1 = 0.254, & c_1 = 0.263, \\ b_2 = -0.614, & c_2 = -0.586, \\ b_3 = -1.803, & c_3 = -1.803, \end{array}$$

so that

$$2\pi\sigma(x) = 0.337 x^{-\frac{1}{2}} (1 + 1.56x - 2.32x^2 - 2.85x^3 \dots). \quad (5.10)$$

From this we obtain $\sigma(x)$ for a few x values (table II).

TABLE II

x	$\sigma(x)$	x	$\sigma(x)$
0.001	10.69	0.02	2.46
0.002	7.57	0.05	1.62
0.003	6.19	0.1	1.21
0.004	5.37	0.2	0.92
0.005	4.81	0.5	0.57
0.01	3.43		

§ 6. *Expressions for large $|a|$.* We shall consider the case $a > 0$ and $a < 0$ separately. If $a > 0$, we have from (5.2)

$$S^+(z) = \frac{e^{iaz}}{2\pi I_0(z)} - \frac{1}{2\pi H^+(z)} \sum_1^\infty \frac{h_k e^{-a\beta_k}}{(iz + \beta_k) J_1(\beta_k)}, \quad (6.1)$$

where

$$h_k = H^+(i\beta_k).$$

The inverse transformation of (6.1) gives

$$\sigma(x) = \sigma_0(x - a) + \frac{1}{2\pi} \sum_1^\infty \frac{h_k e^{-a\beta_k}}{J_1(\beta_k)} B(\beta_k, x), \quad (6.2)$$

where $\sigma_0(x - a)$ represents the surface charge of a double-infinite cylinder due to a point charge -1 at $x = a$, $r = 1$, and where the function $B(\beta, x)$ is the inverse Fourier transform of

$$[H^+(z)(-iz - \beta)]^{-1}$$

or

$$B(\beta, x) = \frac{1}{2\pi} \int_{-\infty}^{\infty} e^{-itx} \frac{dt}{H^+(t)(-it - \beta)}. \quad (6.3)$$

If $a < 0$, we obtain from (5.1) by taking both sides of the negative imaginary axis as new path of integration

$$S^+(z) = \frac{1}{H^+(z)} \int_0^\infty e^{at} \frac{J_0(t)}{H^+(ti)} \frac{dt}{t - iz}, \quad (6.4)$$

from which

$$\sigma(x) = \int_0^\infty e^{at} \frac{J_0(t)}{H^+(ti)} B(-t, x) dt. \quad (6.5)$$

The expressions (6.2) and (6.5) are useful if $|a|$ is large. If, however, $|a|$ is small, we may proceed as follows. From (5.1) or (5.2) we obtain at once by inverse transformation

$$\sigma(x) = \sigma_0(x - a) + \frac{1}{2\pi^2 i} \int_L \frac{e^{-iux}}{H^+(u)} du \int_{-\infty}^{\infty} e^{iat} \frac{K_0(|t|)}{H^-(t)} \frac{dt}{t - u},$$

where L is a contour along both sides of the negative imaginary axis. This may be written as

$$\sigma(x) = \sigma_0(x - a) + \frac{1}{\pi} \int_{-\infty}^{\infty} e^{iat} \frac{K_0(|t|)}{H^-(t)} B(-ti, x) dt, \quad (6.6)$$

where

$$B(\beta, x) = \frac{1}{2\pi} \int_L e^{-itx} \frac{dt}{H^+(t)(-it - \beta)}, \quad \arg \beta = -\frac{\pi}{2}. \quad (6.7)$$

The functions $B(\beta, x)$ which are used in (6.2), (6.5) and (6.6) may be reduced as follows

a. β real and positive:

$$\begin{aligned} B(\beta, x) &= \frac{1}{8\pi^2} \int_0^{\infty} e^{-itx} \frac{H^-(t)}{I_0(t) K_0(|t|)} \frac{dt}{-it - \beta} = \\ &= \frac{1}{8\pi^2} \int_{-\infty}^{\infty} e^{-itx} \left[\frac{I_0'(t)}{I_0(t)} - \frac{t}{|t|} \frac{K_0'(|t|)}{K_0(|t|)} \right] \frac{tH^-(t)}{-it - \beta} dt = \\ &= \frac{1}{4\pi} \sum_1 \frac{\beta_j h_j}{\beta_j + \beta} e^{-\beta_j x} - \frac{1}{4\pi^2} \operatorname{Re} \int_0^{\infty} e^{-tx} \frac{K_0'(-ti)}{K_0(-ti)} \frac{tH^-(ti)}{t + \beta} dt \end{aligned}$$

and finally

$$B(\beta, x) = \frac{1}{4\pi} \sum_1 \frac{\beta_j h_j}{\beta_j + \beta} e^{-\beta_j x} + \frac{1}{2\pi^3} \int_0^{\infty} e^{-tx} \frac{H^+(ti)}{J_0^2(t) + Y_0^2(t)} \frac{dt}{t + \beta}. \quad (6.8)$$

b. β real and negative:

In a similar way we obtain

$$\begin{aligned} B(\beta, x) &= \frac{1}{4\pi} \sum_1 \frac{\beta_j h_j}{\beta_j + \beta} e^{-\beta_j x} - \frac{\beta J_1(\beta)}{4\pi J_0(\beta)} H^+(-\beta i) e^{\beta x} + \\ &+ \frac{1}{2\pi^3} \int_0^{\infty} e^{-tx} \frac{H^+(ti)}{J_0^2(t) + Y_0^2(t)} \frac{dt}{t + \beta} \end{aligned} \quad (6.9)$$

c. β purely imaginary:

In this case the expression (6.8) may be used.

The expressions (6.8) and (6.9) are reasonable convergent if x is large. For small x we better take the expansion derived in the previous section.

§ 7. *Behaviour of $\sigma(x)$ for $x \rightarrow \infty$.* The behaviour of $\sigma(x)$ for $x \rightarrow \infty$ may be determined from the behaviour of $S^+(z)$ for $z \rightarrow 0$. From (5.2) we obtain for small z

$$S^+(z) = \frac{e^{iaz}}{2\pi I_0(z)} + \frac{1}{4\pi^2 i H^+(z)} \int_{L'} e^{iat} \frac{H^+(t)}{I_0(t)} \frac{dt}{t-z}, \quad (7.1)$$

where L' is the real axis with a semi-circular indentation at the origin which separates z from the poles $i\beta_k$, $k = 1, 2 \dots$ of $I_0^{-1}(t)$. Then for $z \rightarrow 0$ we obtain from (7.1) in view of (4.18)

$$2\pi S^+(z) = 1 - \frac{C}{2} \left(\pi \ln \frac{2}{z} \right)^{-\frac{1}{2}} + O \left[\left(\ln \frac{2}{z} \right)^{-3/2} \right], \quad (7.2)$$

where

$$C = - \frac{1}{2\pi i} \int_{L'} e^{iat} \frac{H^+(t)}{t I_0(t)} dt. \quad (7.3)$$

For $\sigma(x)$ we find accordingly

$$\sigma(x) = \frac{C}{8\pi^{\frac{1}{2}}} \frac{1}{x(\ln x)^{3/2}} + O[x^{-1} (\ln x)^{-5/2}]. \quad (7.4)$$

The coefficient C may be expressed as follows for $a > 0$:

$$C = \sum_1^{\infty} \frac{H^+(i\beta_k) e^{-a\beta_k}}{\beta_k J_1(\beta_k)}. \quad (7.5)$$

Received 10th February, 1960.

REFERENCES

- 1) Bouwkamp, C. J. and N. G. de Bruijn, J. Appl. Phys. **18** (1947) 562.
- 2) Muskhelishvili, N. I., Singular integral equations, Groningen, 1953.
- 3) Titchmarsh, E. C., Theory of Fourier integrals, Oxford 1937. See in particular Ch. 5 on Hilbert transforms.
- 4) Sparenberg, J. A., Proc. K. Ned. Akad. Wet. A **59** (1956) 29.
- 5) See ref.²⁾, § 15 and § 26.

SCATTERING OF ELECTROMAGNETIC WAVES BY COAXIAL FERRITE CYLINDERS OF DIFFERENT TENSOR PERMEABILITIES

by YUTZE CHOW

Instituto Tecnológico de Aeronáutica, São José dos Campos, S. P., Brazil

Summary

The boundary value problem of the scattering of a plane electromagnetic wave normally incident on coaxial ferrite cylinders of different tensor permeabilities is investigated. The expressions for the scattered field are derived in terms of Bessel and Neumann functions of different orders.

§ 1. *Introduction.* Scattering of an electromagnetic wave by coaxial cylinders of isotropic materials has previously been investigated¹⁾, the scattered field due to a plane wave normally incident upon the coaxial cylinders being symmetrical in nature with respect to the direction of incidence. For anisotropic materials, however, the symmetry of the scattered fields is no longer preserved. The case of scattering by a single ferrite cylinder has been studied by Tai *et al*²⁾. The present paper extends their treatment to the case of two coaxial cylinders of different materials.

§ 2. *The boundary value problem.* Consider the three regions (fig. 1):

Region 1: air, (μ_0, ϵ_0) , $\rho \geq b$.

Region 2: ferrite tube, $a \leq \rho \leq b$, with tensor permeability $\|\mu'\|$ defined by

$$\|\mu'\| = \begin{vmatrix} \mu_1' & i\mu_2' & 0 \\ -i\mu_2' & \mu_1' & 0 \\ 0 & 0 & \mu_0 \end{vmatrix}.$$

Region 3: central ferrite cylinder, $\rho \leq a$, with a tensor permeability $\|\mu''\|$ defined by

$$\|\mu''\| = \begin{vmatrix} \mu_1'' & i\mu_2'' & 0 \\ -i\mu_2'' & \mu_1'' & 0 \\ 0 & 0 & \mu_0 \end{vmatrix}. \quad (2)$$

We assume that the incident plane wave is propagated in the positive x -direction and has a time dependence $\exp(-i\omega t)$. The electric field of the incident wave is assumed to be along the positive

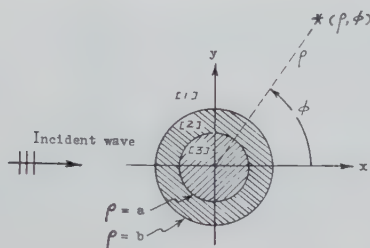


Fig. 1. Scattering by coaxial cylinders of different tensor permeabilities.

Region (1): (μ_0, ϵ_0) ; region (2): $(\|\mu'\|, \epsilon')$; region (3): $(\|\mu''\|, \epsilon'')$.

z -direction (in fig. 1 pointing out of the paper); the incident electric field can be expanded into a series of Bessel functions:

$$\begin{aligned} \mathbf{E}^i &= \hat{\mathbf{z}} E_z^i = \hat{\mathbf{z}} E_0 \exp(ik_0 x) = \\ &= \hat{\mathbf{z}} E_0 \sum_{m=-\infty}^{\infty} (i)^m J_m(k_0 \rho) \exp(-im\phi). \end{aligned} \quad (3)$$

The magnetic field of the incident wave is given by

$$\begin{aligned} \mathbf{H}^i &= (i\omega\mu_0)^{-1} \nabla \times \mathbf{E}^i = \\ &= (i\omega\mu_0)^{-1} \left(\hat{\rho} \frac{\partial}{\rho \partial \phi} - \hat{\phi} \frac{\partial}{\partial \rho} \right) E_z^i = \hat{\rho} H_\rho^i + \hat{\phi} H_\phi^i. \end{aligned} \quad (4)$$

For our present purpose we are interested only in H_ϕ^i which is given by

$$H_\phi^i = i(\omega\mu_0)^{-1} \frac{\partial E_z^i}{\partial \rho} = i\eta_0^{-1} E_0 \sum_{m=-\infty}^{\infty} (i)^m J_m'(k_0 \rho) \exp(-im\phi), \quad (5)$$

where

$$J_m'(s) \equiv \partial J_m(s) / \partial s \text{ and } \eta_0 = (\mu_0 / \epsilon_0)^{\frac{1}{2}}, \quad k_0 = (\omega^2 \mu_0 \epsilon_0)^{\frac{1}{2}}.$$

Region 1. The reflected fields in region (1) may be expanded into

a series of Hankel functions of the first kind:

$$\mathbf{E}^r = zE_z^r = zE_0 \sum_{m=-\infty}^{\infty} (i)^m A_m H_m^{(1)}(k_0 \rho) \exp(-im\phi) \quad (6)$$

and

$$H_\phi^r = i\eta_0^{-1} E_0 \sum_{m=-\infty}^{\infty} (i)^m A_m H_m'^{(1)}(k_0 \rho) \exp(-im\phi). \quad (7)$$

Region 2.

$$\mathbf{H} = (i\omega)^{-1} \|\mu'\|^{-1} \cdot \nabla \times \mathbf{E} \quad (8)$$

with

$$\|\mu'\|^{-1} = \left\| \begin{array}{ccc} v_1' & iv_2' & 0 \\ -iv_2' & v_1' & 0 \\ 0 & 0 & v_0 \end{array} \right\| \quad (9)$$

where

$$v_1' \equiv \mu_1'(\mu_1'^2 - \mu_2'^2)^{-1}, v_2' \equiv -\mu_2'(\mu_1'^2 - \mu_2'^2)^{-1}, v_0 = \mu_0^{-1}.$$

Also, we have

$$\nabla \times (\|\mu'\|^{-1} \cdot \nabla \times \mathbf{E}) - \omega^2 \varepsilon \mathbf{E} = 0. \quad (10)$$

In our particular case the incident wave has an electric field parallel to the z -direction, so (10) is simply

$$(\omega^2 \varepsilon + v_1' \nabla^2) E_{z2} = 0$$

or

$$(\nabla_p^2 + \kappa'^2) E_{z2} = 0, \quad (11)$$

where

$$\nabla_p^2 \equiv \left(\frac{\partial^2}{\partial \rho^2} + \frac{\partial}{\rho \partial \rho} + \frac{1}{\rho^2} \frac{\partial^2}{\partial \phi^2} \right), \quad (12)$$

$$\kappa'^2 \equiv \omega^2 \varepsilon' v_1'^{-1} = \kappa_1'^2 (1 - \alpha'^2), \kappa_1'^2 \equiv \omega^2 \varepsilon' \mu_1', \alpha' \equiv \mu_2' \mu_1'^{-1}.$$

The solution of (11) is of the form $J_m(k'\rho) \exp(-im\phi)$, so we can write down the general solution in a series form as

$$E_{z2} = E_0 \sum_{m=-\infty}^{\infty} (i)^m [B_m J_m(\kappa' \rho) + C_m N_m(\kappa' \rho)] \exp(-im\phi), \quad (13)$$

where B_m and C_m are coefficients to be determined, and N_m is the Neumann function.

The magnetic field of the wave in region 2 is given by

$$\begin{aligned} \mathbf{H}_2 &= (i\omega)^{-1} \cdot \|\mu'\|^{-1} \cdot \nabla \times \mathbf{E}_2 \\ &= (i\omega)^{-1} \left\| \begin{array}{ccc} v_1' & iv_2' & 0 \\ -iv_2' & v_1' & 0 \\ 0 & 0 & v_2 \end{array} \right\| \cdot \nabla \times (\hat{z} E_{z2}) \end{aligned}$$

or

$$\left\| \begin{array}{c} H_{\rho 2} \\ H_{\phi 2} \end{array} \right\| = (i\omega)^{-1} \left\| \begin{array}{c} \left(v_1' \frac{\partial}{\rho \partial \phi} - iv_2' \frac{\partial}{\partial \rho} \right) \\ \left(-iv_2' \frac{\partial}{\rho \partial \phi} - v_1' \frac{\partial}{\partial \rho} \right) \end{array} \right\| E_{z2}. \quad (14)$$

In our case, we are interested in the $H_{\phi z}$ component:

$$\begin{aligned} H_{\phi 2} &= \frac{1}{i\omega} E_0 \sum_{m=-\infty}^{\infty} (i)^m \left\{ \frac{-v_2' m}{\rho} [B_m J_m(\kappa' \rho) + C_m N_m(\kappa' \rho)] - \right. \\ &\quad \left. - v_1' \kappa' [B_m J_m'(\kappa' \rho) + C_m N_m'(\kappa' \rho)] \right\} \exp(L - im\phi) = \\ &= -\frac{1}{i\omega} E_0 \sum_{m=-\infty}^{\infty} (i)^m \left\{ B_m \left[\frac{mv_2'}{\rho} J_m(\kappa' \rho) + v_1' \kappa' J_m'(\kappa' \rho) \right] + \right. \\ &\quad \left. + C_m \left[\frac{mv_2'}{\rho} N_m(\kappa' \rho) + v_1' \kappa' N_m'(\kappa' \rho) \right] \right\} \exp(L - im\phi). \quad (15) \end{aligned}$$

In region 3. We have

$$\mathbf{E}_3 = \hat{z} E_{z3} = \hat{z} E_0 \sum_{m=-\infty}^{\infty} (i)^m D_m J_m(\kappa'' \rho) \exp(-im\phi), \quad (16)$$

$$\mathbf{H}_3 = \frac{1}{i\omega} \|\hat{\rho} \hat{\phi}\| \cdot \left\| \begin{array}{c} \left(v_1'' \frac{\partial}{\rho \partial \phi} - iv_2'' \frac{\partial}{\partial \rho} \right) \\ \left(-iv_2'' \frac{\partial}{\rho \partial \phi} - v_1'' \frac{\partial}{\partial \rho} \right) \end{array} \right\| E_{z3}, \quad (17)$$

$$\begin{aligned} H_{\phi 3} &= -(i\omega)^{-1} E_0 \sum_{m=-\infty}^{\infty} (i)^m D_m \left[\frac{mv_2''}{\rho} J_m(\kappa'' \rho) + v_1'' \kappa'' J_m'(\kappa'' \rho) \right] \cdot \\ &\quad \cdot \exp(-im\phi), \quad (18) \end{aligned}$$

where

$$\kappa''^2 = \omega^2 \varepsilon'' v_1''^{-1} = \kappa_1''^2 (1 - \alpha''^2), \quad \kappa_1''^2 = \omega^2 \varepsilon'' \mu_1'', \quad \alpha'' = \mu_2'' / \mu_1''.$$

§ 3. *The boundary conditions.* At the boundaries the following conditions must be fulfilled:

$$(E_{z2} - E_{z3})|_{\rho=a} = 0, \quad (19)$$

$$(H_{\phi 2} - H_{\phi 3})|_{\rho=a} = 0, \quad (20)$$

$$(E_z^i + E_z^r - E_{z2})|_{\rho=b} = 0, \quad (21)$$

$$(H_{\phi}^i + H_{\phi}^r - H_{\phi 2})|_{\rho=b} = 0. \quad (22)$$

Therefore, from (19) we have

$$B_m J_m(k'a) + C_m N_m(k'a) - D_m J_m(k''a) = 0. \quad (23)$$

In like manner we get from (20), (21), (22)

$$B_m \left[\frac{mv_2'}{a} J_m(k'a) + v_1' k' J_m(k'a) \right] + C_m \left[\frac{mv_2'}{a} N_m(k'a) + v_1' k' N_m'(k'a) \right] - D_m \left[\frac{mv_2''}{a} J_m(k''a) + v_1'' k'' J_m'(k''a) \right] = 0, \quad (24)$$

$$- A_m H_m^{(1)}(k_0 b) + B_m J_m(k'b) + C_m N_m(k'b) = J_m(k_0 b), \quad (25)$$

$$- A_m H_m^{(1)}(k_0 b) + B_m \left(\frac{\eta_0}{\omega} \right) \left[\frac{mv_2'}{b} J_m(k'b) + v_1' k' J_m'(k'b) \right] +$$

$$+ C_m \left(\frac{\eta_0}{\omega} \right) \left[\frac{mv_2'}{b} N_m(k'b) + v_1' k' N_m'(k'b) \right] = J_m'(k_0 b), \quad (26)$$

From these four simultaneous equations the coefficients may thus be computed, for example the amplitude of the reflected wave in region (1) may be calculated from the coefficients of the series:

$$\begin{aligned} A_m = \frac{1}{A} \left\{ \left(\frac{\eta_0}{\omega} \right) J_m(k_0 b) \left[J_m(k''a) \left(\left(\frac{mv_2'}{a} N_m(k'a) + \right. \right. \right. \right. \\ \left. \left. \left. + \frac{\omega}{\eta'} N_m'(k'a) \right) \left(\frac{mv_2'}{b} J_m(k'b) + \frac{\omega}{\eta'} J_m'(k'b) \right) \right] - \right. \\ \left. - \left(\frac{mv_2'}{a} J_m(k'a) + \frac{\omega}{\eta'} J_m(k'a) \right) \left(\frac{mv_2'}{b} N_m(k'b) + \frac{\omega}{\eta'} N_m'(k'b) \right) \right) + \\ \left. + \left(\frac{\omega v_2''}{a} J_m(k''a) + \frac{\omega}{\eta''} J_m'(k''a) \right) \left(J_m(k'a) \left(\frac{mv_2'}{b} N_m(k'b) + \right. \right. \right. \\ \left. \left. \left. + \frac{\omega}{\eta'} N_m'(k'b) \right) - N_m(k'a) \left(\frac{mv_2'}{b} J_m(k'b) + \frac{\omega}{\eta'} J_m'(k'b) \right) \right) \right] - \end{aligned}$$

$$\begin{aligned}
& -J_m'(k_0b) \left[J_m(k''a) \left(J_m(k'b) \left(\frac{mv_2'}{a} N_m(k'a) + \frac{\omega}{\eta'} N_m'(k'a) \right) - \right. \right. \\
& \quad \left. \left. - N_m(k'b) \left(\frac{mv_2'}{a} J_m(k'a) + \frac{\omega}{\eta'} J_m(k'a) \right) \right) + \left(\frac{mv_2''}{a} J_m(k''a) + \right. \right. \\
& \quad \left. \left. + \frac{\omega}{\eta''} J_m'(k''a) \right) \left(J_m(k'a) N_m(k'b) - J_m(k'b) N_m(k'a) \right) \right] \Big\}
\end{aligned}$$

for

$$\begin{aligned}
\Delta = & - \left\{ \left(\frac{\eta_0}{\omega} \right) H_m^{(1)}(k_0b) \left[J_m(k''a) \left(\left(\frac{mv_2'}{a} N_m(k'a) + \right. \right. \right. \\
& \quad \left. \left. + \frac{\omega}{\eta'} N_m'(k'a) \right) \left(-\frac{mv_2'}{b} J_m(k'b) + \frac{\omega}{\eta'} J_m'(k'b) \right) - \right. \right. \\
& \quad \left. \left. - \left(\frac{mv_2'}{a} J_m(k'a) + \frac{\omega}{\eta'} J_m(k'a) \right) \left(\frac{mv_2'}{b} N_m(k'b) + \frac{\omega}{\eta'} N_m'(k'b) \right) \right) + \right. \\
& \quad \left. + \left(\frac{mv_2''}{a} J_m(k''a) + \frac{\omega}{\eta''} J_m'(k''a) \right) \left(J_m(k'a) \left(\frac{mv_2'}{b} N_m(k'b) + \right. \right. \right. \\
& \quad \left. \left. + \frac{\omega}{\eta'} N_m'(k'b) \right) - N_m(k'a) \left(\frac{mv_2'}{b} J_m(k'b) + \frac{\omega}{\eta'} J_m'(k'b) \right) \right) \right] - \\
& - H_m^{(1)'}(k_0b) \left[J_m(k''a) \left(J_m(k'b) \left(\frac{mv_2'}{a} N_m(k'a) + \frac{\omega}{\eta'} N_m'(k'a) \right) - \right. \right. \\
& \quad \left. \left. - N_m(k'b) \left(\frac{mv_2'}{a} J_m(k'a) + \frac{\omega}{\eta'} J_m(k'a) \right) \right) + \left(\frac{mv_2''}{a} J_m(k''a) + \right. \right. \\
& \quad \left. \left. + \frac{\omega}{\eta''} J_m'(k''a) \right) \left(J_m(k'a) N_m(k'b) - J_m(k'b) N_m(k'a) \right) \right] \Big\}
\end{aligned}$$

and

$$\eta' = (v_1' \varepsilon')^{-\frac{1}{2}}, \quad \eta'' = (v_1'' \varepsilon'')^{-\frac{1}{2}}$$

Thus, if all the parameters are known quantities, then the numerical calculations may be carried out.

§ 4. *The special case of a dielectric outer cylinder.* This special case of a dielectric outer cylinder is of interest for two reasons: first, the expressions for the coefficients are somewhat simplified,

and second, from the experimental point of view it is easier to make different sizes of dielectric tubes to fit an inner ferrite cylinder.

In this case the coefficient A_m is given by

$$A_m = \frac{1}{A} \left\{ \frac{\omega}{\eta'} J_m(k''a) [J_m'(k'a) J_m'(k_0b) N_m(k'b) - \right. \\ - J_m(k'b) J_m'(k_0b) N_m'(k'a) + \xi J_m(K_0b) J_m'(k'b) N_m'(k'a) - \\ - \xi J_m'(k'a) J_m(k_0b) N_m'(k'b)] + \left[\frac{mv_2''}{a} J_m(k''b) + \right. \\ \left. + \frac{\omega}{\eta''} J_m'(k''a) \right] [J_m(k'b) J_m'(k_0b) N_m(k'a) - \\ - J_m(k'a) J_m'(k_0b) N_m'(k'a) + \\ \left. + \xi J_m(k_0b) J_m(k'a) N_m'(k'b) - \xi J_m(k_0b) J_m'(k'b) N_m(k'a)] \right\},$$

where

$$\xi = (\epsilon'/\epsilon_0)^{\frac{1}{2}},$$

and

$$A = \left(\frac{\omega}{\eta'} \right) J_m(k''a) [J_m(k'b) H_m^{(1)'}(k_0b) N_m'(k'a) - \\ - J_m'(k'a) H_m^{(1)'}(k_0b) N_m(k'b) + \xi J_m'(k'a) H_m^{(1)}(k_0b) N_m'(k'b) - \\ - \xi H_m^{(1)}(k_0b) J_m'(k'b) N_m'(k'a)] + \\ + \left[\frac{mv_2''}{a} J_m(k''a) + \frac{\omega}{\eta''} J_m'(k''a) \right] [J_m(k'a) H_m^{(1)'}(k_0b) N_m(k'b) - \\ - J_m(k'b) H_m^{(1)'}(k_0b) N_m(k'a) + \xi H_m^{(1)}(k_0b) J_m'(k'b) N_m(k'a) - \\ - \xi H_m^{(1)}(k_0b) J_m(k'a) N_m'(k'b)],$$

while the coefficient B_m is given by

$$B_m = \frac{1}{A} [J_m(k_0b) \cdot H_m^{(1)'}(k_0b) - J_m'(k_0b) H_m^{(1)}(k_0b)] \\ \left[\left(\frac{\omega}{\eta'} \right) J_m(k''a) N_m'(k'a) - \right. \\ \left. - \left(\frac{mv_2''}{a} \right) J_m(k''a) N_m(k'a) - \left(\frac{\omega}{\eta''} \right) J_m'(k''a) N_m(k'a) \right],$$

the coefficient C_m is given by

$$C_m = \frac{1}{\Delta} [J_m'(k_0 b) H_m^{(1)}(k_0 b) - J_m(k_0 b) H_m^{(1)'}(k_0 b)] \\ \left[\left(\frac{\omega}{\eta'} \right) J_m(k'' a) J_m'(k' a) - \right. \\ \left. - \left(\frac{m v_2''}{a} \right) J_m(k' a) J_m(k'' a) - \left(\frac{\omega}{\eta''} \right) J_m(k' a) J_m'(k'' a) \right]$$

and D_m is given by

$$D_m = \frac{1}{\Delta} [H_m^{(1)'}(k_0 b) J_m(k_0 b) - H_m^{(1)}(k_0 b) J_m'(k_0 b)] \left(\frac{\omega}{\eta'} \right) \\ [J_m(k' a) N_m'(k' a) - J_m'(k' a) N_m(k' a)].$$

§ 5. *The special case of a perfectly conducting inner cylinder.* In this case, the calculation is much simpler than in the previous case. The coefficient A_m is given by

$$A_m = \frac{1}{\Delta} \left\{ J_m'(k_0 b) [J_m(k' a) N_m(k' b) - J_m(k' b) N_m(k' a)] - \right. \\ \left. - \left(\frac{\eta_0}{\omega} \right) J_m(k_0 b) \left[\left(\frac{m v_2'}{b} \right) (J_m(k' a) N_m(k' b) - J_m(k' b) N_m(k' a)) + \right. \right. \\ \left. \left. + \left(\frac{\omega}{\eta'} \right) (J_m(k' a) N_m'(k' b) - J_m'(k' b) N_m(k' a)) \right] \right\}$$

and the denominator is given by

$$\Delta = \left(\frac{\eta_0}{\omega} \right) H_m^{(1)}(k_0 b) \left[\left(\frac{m v_2'}{b} \right) (J_m(k' a) N_m(k' b) - J_m(k' b) N_m(k' a)) + \right. \\ \left. + \left(\frac{\omega}{\eta'} \right) (J_m(k' a) N_m'(k' b) - J_m'(k' b) N_m(k' a)) \right] - \\ - H_m^{(1)'}(k_0 b) [J_m(k' a) N_m(k' b) - J_m(k' b) N_m(k' a)],$$

the coefficient B_m is given by

$$B_m = \frac{1}{\Delta} N_m(k' a) [J_m(k_0 b) H_m^{(1)'}(k_0 b) - J_m'(k_0 b) H_m^{(1)}(k_0 b)]$$

and the coefficient C_m is given by

$$C_m = \frac{1}{A} J_m(k'a) [J_m'(k_0b) H_m^{(1)}(k_0b) - J_m(k_0b) H_m^{(1)'}(k_0b)].$$

Acknowledgement. The writer is grateful to Dr. C. T. Tai for his kind encouragement.

Received 22nd March, 1960.

REFERENCES

- 1) Adey, A. W., Canad. J. Phys. **34** (1956) 510.
- 2) Tai, C. T. and Yutze Chow, ITA Engenharia, **2** (1959) 71.

PLASMA DYNAMICS IN AN ARC FORMED BY LOW-VOLTAGE SPARKOVER OF A LIQUID DIELECTRIC *)

by P. K. ECKMAN

Jet Propulsion Laboratory, California Institute of Technology
Pasadena, California, U.S.A.

and E. M. WILLIAMS

Electrical Engineering Department, Carnegie Institute of Technology
Pittsburgh, Pennsylvania, U.S.A.

Summary

An algorithm is derived for the physical conditions in a low-current electrical discharge initiated by low-voltage sparkover between plane electrodes immersed in a liquid dielectric. Calculated results are concerned with column-pressure, temperature, voltage gradient, electron density and column radius for a discharge in a liquid nitrogen dielectric. Of these only column radius can be studied experimentally; experimental results are shown to compare reasonably well with predicted results.

§ 1. *Introduction.* This paper is concerned with the physical phenomena accompanying the radial growth of the ionized gas columns of electric arcs formed by low-voltage sparkover of gaps between closely-spaced electrodes immersed in a liquid dielectric. The period of interest in this work is the first microsecond after arc formation. Some previous works ¹⁾²⁾ have dealt with the results of experimental studies of the electrode phenomena at the termini of the discharges; this paper deals with deductions from physical theory concerning the state and dynamics of the ionized column itself.

*) Work supported in part by the National Science Foundation, U.S.A., under Grants G3072 and G10520. The work described is abstracted from a dissertation submitted by P. K. Eckman in partial fulfillment of the requirements for the degree of Doctor of Philosophy at Carnegie Institute of Technology.

Electrical sparkover between metallic electrodes immersed in a liquid dielectric is followed by a high current density arc discharge, the removal of electrode material and the formation of well-defined and characteristic electrode craters. The associated phenomena have been the subject of experimental studies ³⁾⁴⁾, originally with emphasis on the formation of colloidal suspensions of the particles eroded from the electrodes, and, more recently, in connection with 'electrical' machining ⁵⁾ processes in which the electrode-material removal is adapted for purposes analogous to those encountered in conventional machine tools. Despite the development of an extensive art in electrical machining the physical phenomena involved have been incompletely understood. Moreover, although refined experimental techniques ¹⁾ are available for the study of the erosion of the electrodes, there is very little possibility of a direct experimental investigation of the discharge dynamics. These considerations have led to the study, the results of which are reported in this paper.

§ 2. *Rationale of solution.* This study commenced with the selection of a model configuration for the electrodes, discharge path, and dielectric channels as encountered under simplified circumstances in the relevant technology. This configuration, shown in fig. 1, comprises two plane-parallel electrodes, separated by a small spacing, with a cylindrical discharge column centered in the space between the electrodes. These elements are immersed in a liquid dielectric.

The object of the mathematical analysis is the description of the system after initial sparkover and formation of the discharge column. The liquid dielectric surrounding the discharge was assumed to be incompressible. The analysis proceeded by applying the Navier-Stokes equations, written for a cylindrical coordinate system, to a gas column expanding radially from the centre of the model configuration. Conditions of the material within the gas column were determined by approximating an energy balance between the power delivered to the gap and power dissipated from the discharge column. The expanding gas column is considered to be of high enough temperature, pressure and density so that it may be treated as a plasma. Quasi-equilibrium equations permit calculation of the state of the gas-column as the expansion continues.

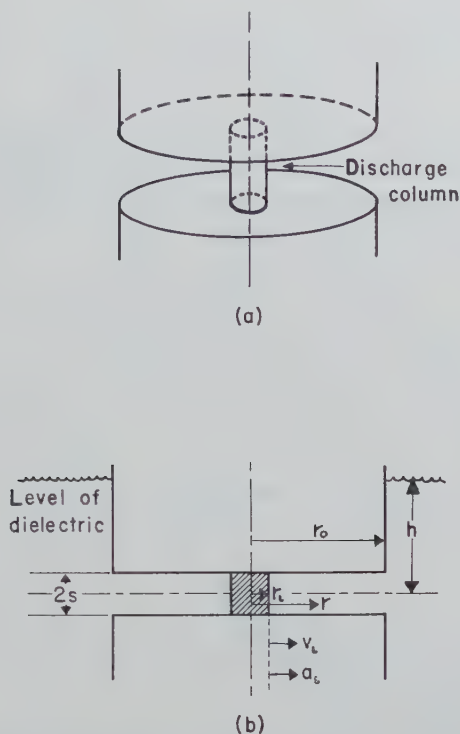


Fig. 1. (a) Configuration selected as a model of a discharge column formed in a liquid dielectric by sparkover between closely-spaced plane-parallel electrodes, (b) coordinates used in analysis. The radius of the discharge column is r_i and v_i and a_i represent the velocity and acceleration, respectively, of the boundary of this column. $v(r)$ and $a(r)$ represent the velocity and acceleration, respectively, of the fluid outside the discharge column at a radius r from the center of the column.

§ 3. *Details of solution.* The general expression of the simplified Navier-Stokes equation for incompressible-fluid flow is given as ⁶⁾

$$\rho \frac{d}{dt}(\omega) = F - \text{grad } p + \mu \nabla^2 \omega, \quad (1)$$

in which

- ρ = mass density,
- μ = viscosity
- p = pressure,
- ω = velocity (generalized),
- F = body forces (generalized).

The continuity expression

$$\operatorname{div} \boldsymbol{\omega} = 0, \quad (2)$$

is also used.

For the configuration employed, cylindrical coordinates are most suitable, and r , θ , and z will denote the radial, angular, and axial coordinates, respectively. If we assume (a) radial flow only, (b) zero viscosity and (c) no body forces, then

$$\omega_\theta, \omega_z = 0, \quad \frac{\partial p}{\partial \theta}, \frac{\partial p}{\partial z} = 0,$$

$$\mu = 0, \quad F_r, F_\theta, F_z = 0,$$

and we obtain

$$\rho \left(\frac{\partial \omega_r}{\partial t} + \omega_r \frac{\partial \omega_r}{\partial r} \right) = - \frac{\partial p_r}{\partial r} \quad (3)$$

and

$$\frac{\partial \omega_r}{\partial r} + \frac{\omega_r}{r} = 0. \quad (4)$$

Using the dimensions of fig. 1.

$$\rho \left[\frac{\partial v(r)}{\partial t} + v(r) \frac{\partial v(r)}{\partial r} \right] = - \frac{\partial p(r)}{\partial r} \quad (5)$$

and, since

$$v(r) = v_i \frac{r_i}{r},$$

(4) becomes

$$\frac{\partial v(r)}{\partial r} = - \frac{v_i r_i}{r^2}, \quad (6)$$

in which v_i, r_i are not functions of r but only of t . Thus (5) becomes

$$\rho \left[\frac{\partial v(r)}{\partial t} - \frac{v_i^2 r_i^2}{r^3} \right] = - \frac{\partial p(r)}{\partial r}. \quad (7)$$

Since

$$a(r) = \frac{\partial v(r)}{\partial t} = \frac{\partial v_i}{\partial t} \frac{r_i}{r} + \frac{v_i}{r} \frac{\partial r_i}{\partial t}$$

and

$$\frac{\partial v_i}{\partial t} = a_i, \quad \frac{\partial r_i}{\partial t} = v_i,$$

(7) may be written

$$\rho \left(\frac{a_i r_i}{r} + \frac{v_i^2}{r} - \frac{v_i^2 r_i^2}{r^3} \right) = - \frac{\partial p(r)}{\partial r}. \quad (8)$$

Integration of (8) from $r = r_i$ to $r = r_0$ yields

$$\frac{p_i - p_0}{\rho} = a_i r_i \ln \left(\frac{r_0}{r_i} \right) + v_i^2 \left[\ln \left(\frac{r_0}{r_i} \right) + \frac{r_i^2}{2r_0^2} - \frac{1}{2} \right]. \quad (9)$$

Solving for a_i we find

$$a_i = \frac{\frac{p_i - p_0}{\rho} - v_i^2 \ln \left(\frac{r_0}{r_i} \right) + \frac{v_i^2 (r_0^2 - r_i^2)}{2r_0^2}}{r_i \ln \left(\frac{r_0}{r_i} \right)}, \quad (10)$$

in which r_0 , ρ and p_0 are fixed, p_i varies as r_i , and r_i and v_i vary with a_i .

§ 4. *Computation methods.* Results have been calculated with an IBM-650 Data-Processing System. The computation procedure has involved a systematic study of the effects of various parameters upon discharge column growth.

Using (10) and assuming that $(r_i)_0$ and $v_i(0)$ are specified, we can find r_i and v_i at any time $t > 0$ by a purely iterative process, taking increments of t small enough so that none of the significant parameters of the problem changes by more than a few percent with each iteration. For most of the computation $(v_i)_0$ is assumed to be zero (sample calculations have shown that the initial choice of $(v_i)_0$ and $(r_i)_0$ have a negligible effect on the solution for $t > 10^{-8}$ seconds).

The major problem is to relate p_i to the size of the gas column. To do this, three quite general equations are used: (a) the ionization equation, (b) the resistivity equation, (c) the total-radiation equation. With the extremes of current-density and pressure of this problem, three independent variables in these equations enable us to describe the discharge conditions. This is in marked contrast to

the complexities encountered under other discharge conditions. As developed in the Appendix, these equations are for (a), (b) and (c) respectively

$$\frac{N_e^2}{N_n} = 2.43 \times 10^{21} T_e^{\frac{3}{2}} \exp\left(\frac{eV_i}{KT_e}\right), \quad (11)$$

$$\frac{E}{J} = \frac{221}{T_e^{\frac{3}{2}}} \log_{10}\left(\frac{6.25 \times 10^4}{N_e^{\frac{1}{2}}}\right), \quad (12)$$

$$E \cdot J = 1.42 \times 10^{-40} N_e^2 T_e^{\frac{1}{2}}, \quad (13)$$

E = electric-field intensity and $|E| = V_g/2s$,

J = current density, and $|J| = I/\pi r_i^2$,

$2s$ = length of electrode gap,

V_g = the positive-column gap voltage,

I = the total discharge current,

K = Boltzmann's constant,

N_e = the density of electrons in the discharge column,

N_n = the density of neutral atoms,

T_e = the electron temperature,

e = the electronic charge,

V_i = the ionization potential of the dielectric material.

We also have the continuity relations

$$N_0 = N_e + N_n \quad (14)$$

and

$$(N_0)_t = (N_0)_0 (r_i)_0^2 / (r_i)_t^2, \quad (15)$$

in which N_0 = the total density of the particles in the dielectric.

It is assumed, at the start, that $t = 0$ is the instant at which breakdown has occurred. That is, conduction is present and the current flowing is determined by the properties of the energy source, circuit, and the arc drop. The formative period¹) of the spark has passed ($25\text{--}50 \times 10^{-9}$ seconds).

If we start by specifying the initial voltage across the gap and assume that the initial particle density $(N_0)_0$ is the same as that of the liquid prior to breakdown, the simultaneous solution of (11) through (14) will yield $(r_i)_0$, $(J)_0$, $(N_e)_0$, $(T_e)_0$ and $(p_i)_0$. Assuming that $(v_i)_0 = 0$, it follows from (10) that $a_i = f(p_i, v_i, r_i)$ and the

growth of the discharge interface can be calculated by choosing small increments of time Δt and letting

$$r_{j+1} = r_j + v_j \Delta t + \frac{1}{2} a_j (\Delta t)^2$$

and

$$v_{j+1} = V_j + a_j \Delta t.$$

At the end of each Δt interval (11) through (14) are again solved, and new values of J , N_e , T_e , p_i , and a new V_g are found. From (10) a new a_i is found, and similar successive iterations permit determination of r_i as a continuing function of time.

Most of the calculations of this work were carried out for a liquid-nitrogen dielectric. Liquid nitrogen was advantageous for use in both the theoretical and experimental work of this study because its ionization potential (15.4 volts) and initial particle-density ($3.49 \times 10^{28} \text{ m}^{-3}$) are more accurately known than those of the hydrocarbon-mixture dielectrics commonly employed in electric-spark machining.

§ 5. Discussion of approximations employed.

A. Assumption of non-viscous flow. The fluid-flow problem has been treated with the assumption of zero viscosity. The validity of this assumption can be tested by calculating the pressure drop across the fluid due to viscous flow (in the steady state) and comparing this with the pressure drop found in the non-viscous solution. Such considerations show that the pressure drop across the liquid between the electrode gap (see fig. 1) is

$$p_i - p_0 = \frac{3r_i v_i}{s^2} \mu \ln \frac{r_0}{r_i}, \quad (16)$$

while a continuous check of the quantity $p_i - p_0$ during the various stages of the problem-solution has shown that the viscous pressure never exceeds 1% of the column pressure for the dielectric and configuration employed.

B. Assumption of symmetry in the discharge configuration. In the model chosen it was assumed that the discharge occurs along the axis of symmetry. Although discharges seldom occur at the exact centre of the configuration, it is clear that if the discharge column diameter is small compared with the electrode diameter, the electrode configuration approximates that of two infinite planes in any case, symmetrical or asymmetrical.

C. Zero arc-formation interval. This work is confined to the phenomena encountered after the arc is established; it is implicitly assumed that the formative time of the arc is zero. The solution is thus unrealistic in the vicinity of $t = 0$; however, since the formative time is very much smaller than the time interval under study, the solution becomes more realistic, in so far as this assumption is concerned, as time increases.

D. Potential distribution between the anode and cathode. The potential difference between electrodes comprises three rather distinct parts, the cathode drop V_c , the anode drop V_a and the discharge column drop V_g , which is necessary to maintain an electric field inside the plasma or ionized gas between the anode and cathode.

The voltage-drop V_c occurs over a distance of an electron mean-free-path from the cathode surface (corresponding to the very high gradient necessary to account for the extremely high current-densities measured in typical instances)¹⁾⁷⁾⁸⁾, while the voltage drop V_a covers a distance of several mean free paths from the anode surface. Both V_c and V_a are of the order of 6 to 8 V, generally of the same order as the ionization potential of the electrode material, and remain relatively constant during a discharge.

The major component of the gap-voltage drop V_g occurs across the 'positive column' of the discharge. This voltage is expected to vary with time, depending upon the initial over-voltage across the gap, the dielectric particle density, current density and the radial expansion of the discharge column.

E. Conditions in the plasma. In the discharge column the E field is relatively uniform over the entire length. The power developed in the column is

$$\mathbf{E} \cdot \mathbf{J} = P_{rad} + \frac{3}{2} N_e K \frac{\partial T_e}{\partial t}, \quad (17)$$

in which P_{rad} = "free-free" radiation (from a plasma).

A uniform current density within the arc channel is assumed. Furthermore, by assuming zero viscosity and infinite thermal conductivity (in the plasma); it has been implied that particle density (and drift velocity along the discharge axis) is constant across the discharge cross-section.

Some question might arise as to whether there is temperature

equilibrium in the classical sense. In low-pressure discharges, it is often true that equilibrium does not exist between the electrons, ions and gas molecules. However, at higher and higher pressures the electron temperature and gas temperature approach the same value. Spitzer⁹⁾ considers an electron-proton gas, the velocity and distribution of which is arbitrarily altered (perhaps by sudden changes in the E field, density and/or temperature) and shows that equipartition will be established between electrons and protons in a time

$$\tau_{eg} = \frac{5.9 \times 10^8 T_e^{\frac{3}{2}}}{N_e \ln \Omega}, \text{ in which } \Omega = \frac{3}{2e^3} \left(\frac{K^3 T_e^3}{\pi N_e} \right)^{\frac{1}{2}}.$$

Calculation of the equipartition times throughout the problem has shown that these times are of roughly the same time scale as the time increments used in the computation. As long as

$$\frac{\partial E}{\partial t} \Delta t \ll E, \quad \frac{\partial N_e}{\partial t} \Delta t \ll N_e \quad \text{and} \quad \frac{\partial T_e}{\partial t} \Delta t \ll T_e$$

and the increment Δt is as great or greater than t_{eq} , we may apply the thermal-ionization equation with reasonable accuracy. Recently Braginski¹⁰⁾ has applied such equilibrium conditions to the growth of sparks in a high-density gas and found excellent agreement with experiment.

F. Heat losses. In the simple cylindrical model chosen, heat loss will occur by conduction into the electrodes at the ends of the column and by conduction and mixing at the boundary between the plasma and the surrounding fluid. Both phenomena act to retard column growth.

It has been assumed that the rate of heat loss to the electrode is of the form

$$Q_1 = h_1 A \theta, \quad (18)$$

in which

h_1 = a heat conduction coefficient at the electrode,

A = cross-sectional area of the discharge column,

θ = temperature difference between the column and the electrode surface.

Values of h_1 may be obtained by considering the heat flow into a semi-infinite slab at a point on its surface. It can be shown⁸⁾ that if a steady heat flow Q_1 is begun at $t = 0$, then at any later time t ,

at a distance r from the source, the temperature of the slab is increased by an amount

$$\theta(r, t) = \left(\frac{Q_1}{2\pi h_c r} \right) \left[1 - \operatorname{erf} \left(\frac{br}{t^{1/2}} \right) \right], \quad (19)$$

in which

$$b = \frac{\rho^{1/2} c^{1/2}}{2h_c^{1/2}}$$

and

ρ = density,

c = electrode thermal capacity,

h_c = electrode thermal conductivity.

Since there is little evidence ¹⁾²⁾ of electrode melting (except for electrodes with melting points below about 700°C), we can place an upper bound on Q_1 at any time by means of (19) and an upper bound on h_1 by (18). For short-duration discharges, values of h_1 as high as 1×10^4 J/m²s°C may occur.

At the interface between the discharge column and the liquid dielectric conditions are quite obscure. Certainly there are turbulent and mixing effects and other phenomena occurring. An estimate for heat loss here has been made in the form

$$Q_2 = h_2(2\pi r_1)(2a) T_e, \quad (20)$$

in which h_2 is an interface heat conduction coefficient. Such a correction has been applied to the calculation of radial growth.

G. Single-multiple ionization. All calculations are based on an assumed single ionization of the dielectric material. The extent of any multiple ionization varies during the discharge and depends upon the temperature, electron density and partition function of a stage of ionization (which itself is temperature-dependent) and may be calculated by use of the general Saha ionization equation. However, the complete calculation increases the number of individual computations by at least an order of magnitude. This refinement would not be justified in view of the many other approximations and uncertainties inherent in the simple configuration and analysis employed.

H. Pinch effect. The material pressure p_i in the discharge-column is modified by a certain amount because of the "pinch

effect"¹¹). The magnetic pressure p_m is a direct result of the interaction of the current in the plasma with the magnetic field caused by that current. The pinch pressure in the plasma is

$$P_m = B/8\pi\mu \quad (21)$$

and

$$B = 2\mu I/r. \quad (22)$$

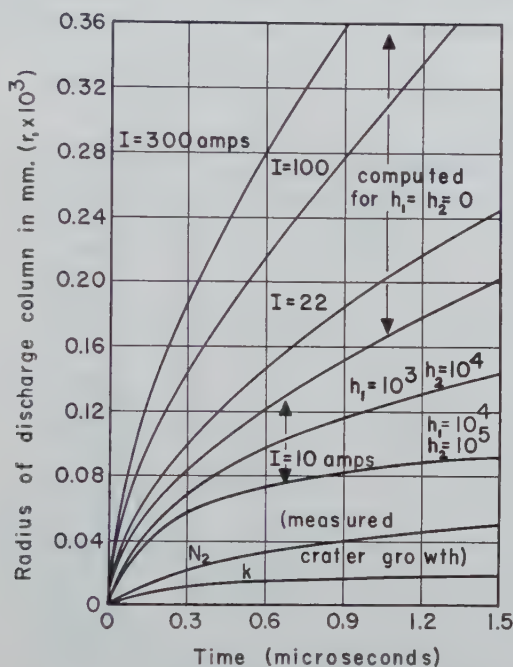


Fig. 2. Curves showing the dependence of the computed discharge-radius upon the duration of the discharge for various currents and heat-transfer constants and a curve of measured crater radius. The additional curve of measured data is for a kerosene (K) dielectric. Rough estimates of heat-transfer for copper electrodes suggest that a reasonable value of h_1 is in the range $1 \times 10^3 < h_1 < 1 \times 10^4$. No very satisfactory basis has been found for estimating h_2 . All data except the single curve for kerosene, are for a liquid-nitrogen dielectric.

Hence the magnetic pressure at the interface is given by

$$P_m = \mu I^2 / 2\pi r^2. \quad (23)$$

In the calculation performed, p_m has been found to be negligible compared to p_1 throughout the duration of the discharge considered.

§ 6. *Results.* Fig. 2 shows computed curves of discharge radius as a function of discharge duration for cases in which negligible thermal losses are assumed and cases in which more 'realistic' values of thermal loss have been taken into account, together with curves of measured discharge radius. Some of the discrepancies between measured and computed values may be accounted for by the experimental situation, as discussed below. The theoretical work of this study suggests no explanation for the markedly smaller discharge

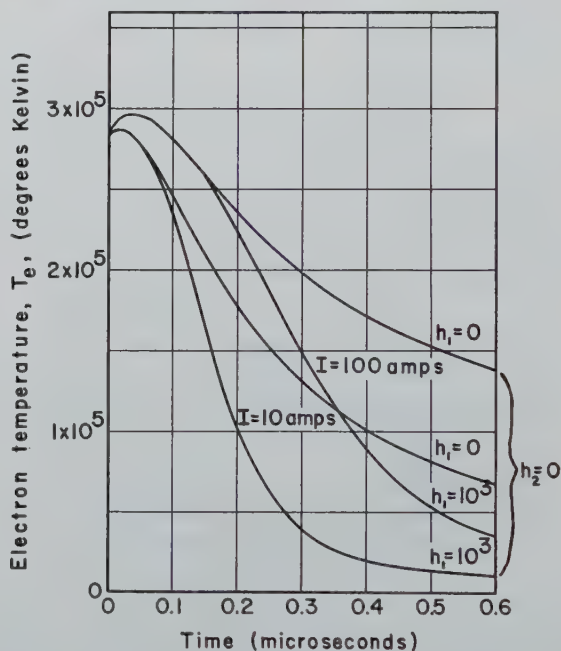


Fig. 3. Calculated time-variation of electron temperature with time, in a discharge in a liquid-nitrogen dielectric, for two values of current and two conditions of heat-transfer.

column radius encountered in the hydrocarbon dielectric, which is regarded as too chemically complicated to be analyzed by the methods of this paper. Calculations have indicated that initial particle density will have relatively small effects on discharge radius, for instance. Although one expects higher particle densities to result in higher values of p_i , the 'temperature' in the discharge is less, so that higher particle densities result in only slight increases in column radius.

Curves of current density versus discharge duration are not shown, since current density can be calculated directly from current and discharge radius. A discharge column of 10 A and 0.04 mm radius corresponds to a current density of approximately 2×10^9 A/m², for example.

Figs. 3, 4, 5 and 6 are concerned with various conditions within the discharge. In computing these data, heat transfer has been either neglected or treated somewhat less thoroughly than in the

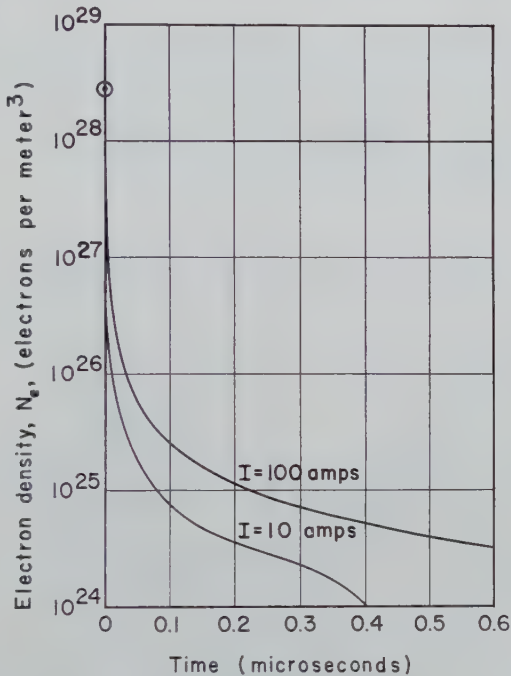


Fig. 4. Calculated time-variation of electron-density in a discharge in a liquid-nitrogen dielectric. Heat transfer has been neglected in this example.

data of fig. 2, since the authors were concerned primarily with orders of magnitude.

The variation of electron temperature with time suggests some limitations of the analysis employed. Starting with values of T_e of the order of 3×10^5 °K (fig. 3) the temperature falls as the discharge column expands and electron densities (fig. 4) drop rapidly. The "free-free" radiation equation (13) is not accurate at temperatures below 40000–50000°K since Stefan-Boltzmann (black-body) radi-

ation becomes first a significant factor as the temperature is reduced and, subsequently, a dominant factor. Thus the validity of solutions shown here is open to question after the time at which such low temperatures are reached.

By the time that the temperature has dropped to 30000°K the percentage of ionization is down to 95% and is falling rapidly. This is clear from the points of inflection in the N_e vs t and E vs t curves (figs 4 and 5).

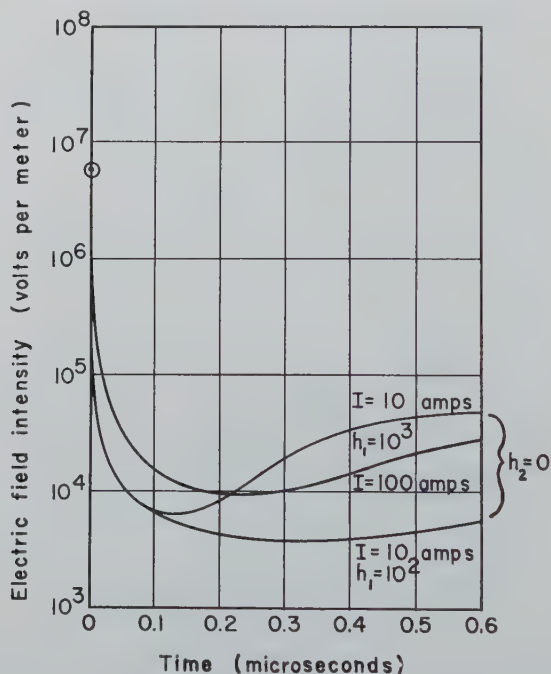


Fig. 5. Calculated time-variation of potential gradient in the discharge-column drop-region in a liquid-nitrogen dielectric.

Fig. 6 shows the material pressure p_i during typical discharges. The pressure p_i begins at high values, about 10^6 atmospheres, gradually falling (as both T_e and N_e are reduced) to values in the range of 1 to 10 atmospheres for microsecond pulses. The pinch pressure, while large for small values of t , never becomes an appreciable fraction of p_i , and its effect on column growth is negligible for the range of currents considered here. It would appear that for

high currents ($I > 1000$ A) and longer pulses the effects of pinch pressure should be included in finding the net column pressure.

§ 7. *Experimental investigation.* Experimental tests were conducted to study the effects of single, unidirectional current discharges in a liquid-nitrogen dielectric. The magnitudes and durations of the pulses employed have been limited to a range in which electrode melting will be negligible and in which the column temperature will remain high.

In the procedure used, sparkover was initiated in a liquid dielectric between polished, plane-parallel, cylindrical electrodes of 1.27 cm diameter, and the applied voltage was adjusted over the range from

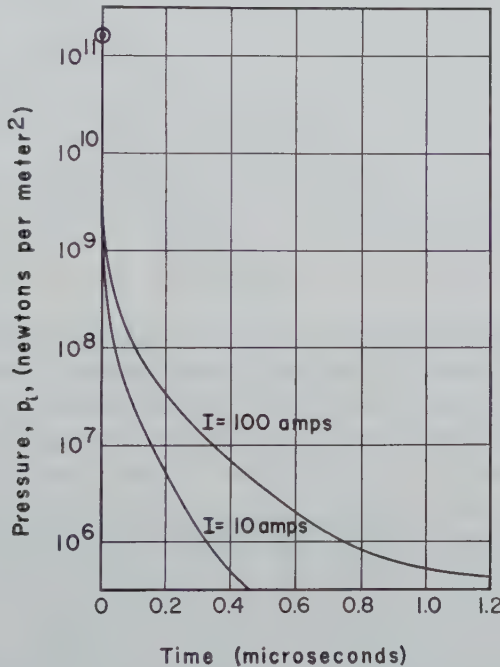


Fig. 6. Calculated time-variation of the discharge-column pressure in a liquid-nitrogen dielectric. Heat transfer has been neglected.

50 to 3000 volt. The circuit was arranged to deliver, following sparkover, a single current pulse of substantially constant amplitude and of adjustable duration from .015 to 1.50 microseconds. A "pressure head" from 1.25 to 7.50 cm of dielectric was maintained

above the gap level (see fig. 1). The apparatus utilized has been described previously by Smith and Williams¹⁾²⁾ who were concerned with a kerosene dielectric.

Following each discharge, the diameter of the electrode craters formed by the discharge was measured. It is usually assumed that the crater diameter is equal to the maximum discharge diameter. There is, of course, no assurance that thermal processes such as melting (and subsequent solidification) do not take place after the discharge itself has ceased. However, it seems even more likely that the growth of crater area may lag the growth of the discharge column. In fact, a clearly defined area of surface discoloration commonly surrounds the crater and is perhaps of twice the diameter of the craters themselves. Whether this discolored area is due to thermal processes in the electrode itself or to a column diameter of larger size is not known. It seems most reasonable that at any instant during the discharge the crater area will be less than the actual area of the discharge column. It has been observed that the electrode gap, i.e. discharge length, has no effect on electrode crater-area within the range of electrode gaps studied. The only experimental difficulty encountered was in keeping the polished electrode surfaces free from frost during immersion in the nitrogen.

§ 8. *Conclusions.* It is clear from the comparison of calculated and measured values of discharge column radius that the analytical results are accurate to better than an order of magnitude. It may be inferred that other results, such as calculated pressures, temperatures, and electric field intensities, for which direct experimental measurements are not feasible, are of comparable accuracy. It is expected that the results presented can be used to improve understanding of the perplexing process of electrode erosion in the short-duration low-current electrical discharge which is initiated by sparkover of a liquid dielectric. Also, the reasonable success of the analytical study, as demonstrated experimentally, may contribute to the growing development of analytical methods in the field of plasma dynamics.

APPENDIX

A. *Ionization equation.* The ionizing effects of the molecular collisions, radiation, and electron collisions which occur in gases at high temperature are generally classed as 'thermal ionization'. If the gas is considered as being in a state of dynamic equilibrium with "chemical" changes occurring in two different directions, we may use a thermodynamic treatment to determine the relative number of electrons (and ions) and excited atoms for a given gas as a function of its absolute temperature and pressure. Saha¹²⁾ first developed such a treatment in which the temperature and the ionization potential of the material are used to characterize the state of the gas which 'dissociates' into electrons and ions. The results have an important bearing, not only on discharge problems¹³⁾ but also in the field of astrophysics¹⁴⁾¹⁵⁾.

In its most general form, the relationship found by Saha and later derived more rigorously by Menzel¹⁶⁾ is

$$\frac{N_{q+1}}{N_q} P_e = 3.35 \times 10^{-2} T_e^{\frac{5}{2}} \left[\exp \left(\frac{-5040 V_{q+1}}{T_e} \right) \right] \left[\frac{2B_{q+1}(T_e)}{B_q(T_e)} \right], \quad (24)$$

in which

$$P_e = k N_e T_e \quad (25)$$

N_q = density of particles in the q th stage of ionization

V_q = the ionization-potential of particles in the q th stage.

The correction term

$$\frac{2B_{q+1}(T_e)}{B_q(T_e)}$$

is a function of temperature for any given atom, depending on the number and type of energy states. The term may be computed from atomic theory, and published tables⁹⁾¹⁵⁾ are available which give this correction factor. In practical calculations the correction is frequently omitted¹³⁾¹⁷⁾. If we write the ionization equation as

$$\frac{N_1}{N_0} P_e = 3.35 \times 10^{-2} T_e^{\frac{5}{2}} \exp \left(\frac{-5040 V_1}{T_e} \right). \quad (26)$$

and substitute (25) in (26), we obtain

$$\frac{N_e^2}{N_0} = 2.43 \times 10^{21} T_e^{\frac{5}{2}} \exp \left(\frac{-5040 V_1}{T_e} \right). \quad (27)$$

This assumes that $N_1 = N_e$ (single ionization only) and is the form of the ionization equation actually used in this paper.

It is important to keep in mind the limitations imposed by the assumptions made in deriving the equation. The gas is assumed to be homogeneous. Walls, turbulence and other factors are assumed not to interfere with the ideal thermal equilibrium. Ample indirect evidence from investigation of arcs¹⁸⁾ seems to justify the thermodynamic treatment, even in cases where, instead of pure thermal equilibrium, a small energy flow is present in the gas.

B. *Resistivity equation.* The resistivity of a gas supporting a high-current discharge is of the form:

$$\frac{E}{J} = \frac{K_1}{T_e^{\frac{3}{2}}} \ln \left(K_2 \frac{T_e^2}{N_e^{\frac{1}{2}}} \right). \quad (28)$$

From the definition of σ , we may use

$$\sigma = J/E \quad (29)$$

We shall determine σ in an electron gas as follows.

The force on one electron due to an electric field is eE ; this causes an electron to move parallel to the E field with an average drift-velocity v_D . The electron loses a certain momentum every time it collides with an ion; the ions are considered stationary because of their much larger mass and limited mobility, and the average momentum lost per collision is $m_e v_D$. If there are β such collisions per unit time, then the average retarding (viscous) force is given by $\beta m_e v_D$. The drift-velocity v_D adjusts itself, so that the force owing to the E field and that owing to viscosity are equal,

$$eE = \beta m_e v_D \text{ or } v_D = \frac{m_e \beta}{e} E. \quad (30)$$

In their random motion, the electrons have an average or mean free path λ_e and an average thermal velocity \bar{v} . The number of collisions per unit time β is given by

$$\beta = \bar{v}/\lambda_e, \quad (31)$$

so that we can find

$$v_D = \frac{e \lambda_e E}{m_e \bar{v}} = \mu_e E, \quad (32)$$

in which μ_e is defined as the mobility of the electrons and

$$\mu_e = e\lambda_e/m_e\bar{v}. \quad (33)$$

Now, knowing the drift velocity and the charge density eN_e , we can obtain the current density

$$J = v_D(eN_e) = eN_e\mu_e E. \quad (34)$$

A definition

$$\sigma = eN_e\mu_e \quad (35)$$

is consistent with the usual definition of σ . Since

$$\sigma = e^2 N_e \lambda_e / m_e \bar{v}, \quad (36)$$

the problem now is to find \bar{v} and λ_e . From kinetic theory

$$\bar{v} = \sqrt{3kT/m_e}, \quad (37)$$

and it can easily be shown (19) that

$$e = 1/(N_0 Q_0 + N_+ Q_+), \quad (38)$$

in which N_+ = density of positive ions, Q_+ is the effective cross-section for electron-positive ion collisions and Q_0 is the effective cross-section for electron-atom collisions. Thus, the conductivity is given as

$$\sigma = \frac{e^2 N_e}{\sqrt{3m_e kT} (N_0 Q_0 + N_+ Q_+)}. \quad (39)$$

If a plasma is actually present, $N_0 \ll N_+$, and

$$\lambda_e = 1/N_+ Q_+ \quad (40)$$

Thus, for a plasma

$$\sigma = \frac{e^2 N_e}{\sqrt{3m_e kT} N_+ Q_+} \quad (41)$$

Various authors ²⁰⁾²¹⁾ have derived expressions for Q_+ by calculating the deflection of electrons as a result of the Coulomb forces of the positive ions. On the average, in a homogeneous, uniform, positive column the electric fields of separate electrons and positive ions will neutralize each other and the average space charge is equal to zero. But at distances of the order of magnitude of the

average interval between ions, these fields are still noticeable. In such calculations it is necessary to assume a finite distance at which the field of a single positive ion is negligible compared to the other nearby ions in order that the resulting integrals converge. Thus, the results of such calculations vary in their numerical coefficients, but agree in general form and order of magnitude.

For purposes of numerical computation the relationship originally proposed by Gvosdover²²⁾ has been retained. Gvosdover reasons that if N_+ positive ions are in a unit volume, then the greatest distance d over which the field of the ion is spread is

$$d = (N_+)^{-\frac{1}{3}}.$$

When distances are smaller than d , we can assume that the interaction of ions and electrons take place according to Coulomb's law. By choosing d as the "cut-off" distance rather than the classical Debye-Hückel shielding distance, he arrives at the value

$$Q_+ = \gamma e^4 / (kT)^2 \quad (42)$$

in which

$$\gamma = \frac{\pi}{4} \ln \left(\frac{kT_e}{e^2 N_+^{\frac{1}{3}}} \right). \quad (43)$$

Using this value, we obtain

$$\frac{1}{\sigma} = \frac{\pi \sqrt{3m_e} e^2}{4(kT_e)^{\frac{3}{2}}} \ln \left(\frac{kT_e}{e^2 N_e^{\frac{1}{3}}} \right) \quad (44)$$

In this derivation it has been implicitly assumed that there is:

1. Single ionization of a gas without boundaries,
2. $N_0 \ll N_e$, and hence $N_e \approx N_+$,
3. A uniform current (and hence ion) distribution.

It should be noted that the expression given here for resistivity depends primarily on T_e and N_e , and neither the kind of gas nor the configuration appears explicitly in the equation. This expression for resistivity then holds, providing a) T_e is sufficiently high to yield an ionization of about 30% or more and (b) the power input is assumed equal to that dissipated (quasi-equilibrium).

C. Radiation equation. The dissipation of energy in the column is assumed to be

$$\int_0^a 2\pi r B N_e^2 T_e^{\frac{1}{2}} dr \quad (45)$$

in W/unit length. This follows from an expression by Cillie ²³⁾ for the power radiated per unit-volume in a high-temperature plasma. The value of the constant is $B = 1.4 \times 10^{-40}$, if N_e is electrons/m³ and T_e is in degrees Kelvin. This expression begins to break down for temperature below the range of 10^5 °K.

The expression is of this form because at higher temperatures recombination radiation (electrons becoming captured, thus emitting radiation) is negligible compared to bremsstrahlung (free-free transition-radiation). Assuming a Maxwellian velocity distribution, the total amount of energy radiated per unit volume is

$$\Sigma = \frac{N_e N_+ \pi 2^5 e^6}{3 h m_e c^2} \left(\frac{2 \pi k T_e}{3 m_e} \right)^{\frac{1}{2}} \quad (46)$$

If we have only single ionization, the $n N_e = N_+$ and

$$\Sigma = 1.42 \times 10^{-27} N_e^2 T_e^{\frac{1}{2}} \text{ ergs/cm}^3 \text{ s}$$

or the power radiated is

$$P = 1.42 \times 10^{-40} N_e^2 T_e^{\frac{1}{2}} \text{ W/m.}$$

This is based on the Born approximation ²⁴⁾²⁵⁾.

Received 20th April, 1960

REFERENCES

- 1) Williams, E. M. and R. E. Smith, Trans. Amer. Inst. Elect. Engrs **74** pt 1 (1955) 164.
- 2) Williams, E. M. and R. E. Smith, Trans. Amer. Inst. Elect. Engrs **76** pt 1 (1957) 93.
- 3) Bredig, G., Z. angew. Chemie **1** (1898) 951.
- 4) Benendicks, C., Ark. Mat. Astr. Fys. **8** (1912).
- 5) Williams, E. M., J. B. Woodford, Jr. and R. E. Smith, Trans. Amer. Inst. Elect Engrs **73** pt 2 (1954) 83.
- 6) Schlichting, H., Boundary Layer Theory, McGraw-Hill 1955.
- 7) Fromme, K. D., Proc. Soc. B **62** (1949) 805.
- 8) Germer, L. H. and F. E. Hayworth, J. Appl. Phys. **20** (1949) 1085.
- 9) Spitzer, Jr. L., Physics of Fully Ionized Gases, Interscience, London 1956.
- 10) Braginski, S. I., Soviet Physics (JETP) **34** (1958) 1068.
- 11) Post, R. F., Rev. Mod. Phys. **28** (1956) 338.
- 12) Saha, M. N., Phil. Mag. **40** (1920) 472.

- 13) Cobine, J. D., Gaseous Conductors, Dover Publications 1958.
- 14) Hynek, J. A., Astrophysics, McGraw-Hill (1951).
- 15) Aller, L. H., Astrophysics – The Atmosphere of the Sun and Stars, Ronald Press, New York 1953.
- 16) Menzel, D. M., Proc. Nat. Acad. Sci. **19** (1933) 40.
- 17) Suits, C. G., Gen. Elec. Rev. **39** (1936) 194.
- 18) King, R. B., Astrophys. J. **108** (1948) 429.
- 19) Sproull, R. L., Modern Physics, John Wiley 1956.
- 20) Chapman, S. and T. G. Cowling, The Mathematical Theory of Non-Uniform Gases, University Press, Cambridge 1953.
- 21) Maecker, H., Z. Phys. **140** (1955) 119.
- 22) Gvosdover, S. D., Physik Z. Sowjetunion **12** (1937) 164.
- 23) Cillie, C., Mon. Not. Roy. Astr. Soc. **92** (1931) 820.
- 24) Bethe, H., Handbuch der Physik XXIV/1, 1933.
- 25) Heitler, W., Quantum Theory of Radiation, Oxford Press, New York 1954.

CHARACTERISTICS OF RIDGE WAVEGUIDES

by FREDERICK YOUNG and JERE HOHMANN

Carnegie Institute of Technology, Pittsburgh, U.S.A.

Summary

The cut-off frequencies, impedances, mode separations and power capacities are accurately calculated from Maxwell's equations for several double and single ridge waveguides. For the particular guides considered the ridge dimensions are varied over a wide range to include many cases previously not available in the literature. Waveguides having width to height ratios of 1 : 1 and 2 : 1 are considered in great detail.

§ 1. *Introduction.* The ridge waveguide is useful in various microwave applications because it can be operated at a lower frequency and has a lower impedance and a wider mode separation than a simple rectangular waveguide. In this paper the single ridge and double ridge waveguides shown in fig. 1 and fig. 2 respectively, are considered.

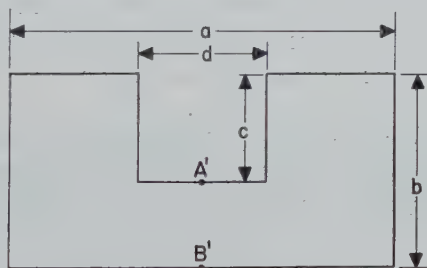


Fig. 1. The cross-section of the single ridge waveguide.

Cohn¹⁾ calculated the approximate value of the cut-off frequency and impedance of the single ridge waveguide operating in the TE₁₀ mode by consideration of the discontinuity capacitance between the edge of the ridge and the opposite wall. The values of capacitance he used are given by Ramo and Whinnery²⁾. Cohn's formulae

yield accurate results if $\frac{1}{2}(a - d) > b$. Mihran³⁾ extended Cohn's analysis by including a term for the capacitance between the ridge and side wall of the guide.

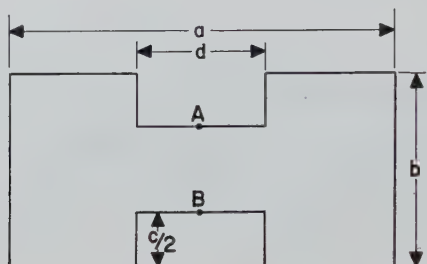


Fig. 2. The cross-section of the double ridge waveguide.

The solutions of Cohn and Mihran are both attempts to solve a field problem by lumped circuit techniques. Because an electromagnetic field is equivalent to an infinite number of lumped circuit elements, the lumped circuit approaches mentioned are limited in accuracy. The methods of Cohn and Mihran yield little information about the power capacity of the waveguide and offer no direct means of analysis for higher modes.

A more sophisticated method used by Ereteza and Spangenberg⁴⁾ approximated the ridge waveguide by a large array of inductances and capacitances arranged to satisfy the finite difference form of Maxwell's equations. Inherent in that system are undesirable losses in the circuit elements and coupling problems. Economic and practical considerations discourage the use of that method.

It is the purpose of this paper to derive from Maxwell's equations the cut-off frequencies, impedances, mode separations and power transmission capabilities of the single and double ridge waveguide.

§ 2. *Method of solution.* It is assumed that the fields vary sinusoidally with time and propagate along the length of the waveguide in the z direction. Then

$$E'(x, y, z, t) = E(x, y) e^{j\omega t - \gamma z}, \quad (1)$$

$$H'(x, y, z, t) = H(x, y) e^{j\omega t - \gamma z}. \quad (2)$$

When Maxwell's curl equations are combined and (1) and (2)

are substituted, the Helmholtz equation

$$\nabla_{xy}^2 \psi + (\mu\epsilon\omega^2 + \gamma^2)\psi = 0 \quad (3)$$

results, provided the medium bounded by the waveguide is isotropic and lossless. Here the operator

$$\nabla_{xy}^2 = \frac{\partial^2}{\partial x^2} + \frac{\partial^2}{\partial y^2} \quad (4)$$

and ψ is the axial component of either the electric or magnetic field. In this particular problem the Helmholtz equation is subject to either the Dirichlet or the Neumann boundary conditions depending on whether a TM or TE mode is being considered. By a simple variational principle it can be shown that

$$K^2 = - \frac{\iint \psi \nabla_{xy}^2 \psi \, dx \, dy}{\iint \psi^2 \, dx \, dy}, \quad (5)$$

where $K^2 = \mu\epsilon\omega^2 + \gamma^2$. The cut-off frequency of any mode is given by

$$f_c = \frac{K}{2\pi\sqrt{\mu\epsilon}}. \quad (6)$$

Because the wavefunction ψ is not known except in trivial configurations, (5) cannot be used directly to find the eigenvalue K^2 . Instead a trial wavefunction obtained by careful estimation is inserted in (5) and K^2 is calculated numerically. The eigenvalue obtained and the assumed wavefunction are substituted into

$$\nabla_{xy}^2 \psi_i + K_i^2 \psi_i = R_i. \quad (7)$$

If the assumed ψ_i is correct, $R_i = 0$ everywhere within the waveguide. If the residual R_i is not zero at all places, the assumed wavefunction must be adjusted accordingly. The new trial wavefunction ψ_{i+1} is calculated at each point inside the waveguide by the equation

$$\psi_{i+1} = \psi_i + \frac{R_i}{(4 - K_i^2 h^2)/g}. \quad (8)$$

Here h is the distance between mesh points.

The number of points considered in the waveguides are between 200 and 1000 depending upon the dimensions of the ridge. The derivatives and integrals are easily calculated by well-known finite difference

methods. The best value of g is near 1.3 and is best determined by trial and error because it varies with the configuration. It is also useful, for reasons not well understood, to make g an order of magnitude larger in one out of every 10 or 15 iterations. Such a procedure speeds the reduction of the residuals. When $g = 1$, this is the Rayleigh-Ritz method which converges too slowly to be useful in this problem. With the modified Rayleigh-Ritz method described above, about 30 iterations reduce the residuals to a negligible fraction of the wavefunction at each point in the mesh.

§ 3. *Calculation of higher modes.* Only TE and TM modes are considered in this paper because all other modes may be expressed as a linear combination of these. Assuming that the waveguide walls have infinite conductivity, the following boundary conditions exist: for TM modes the axial electric field equals zero at the conductor surface ($\psi = 0$ on S), and for TE modes the normal derivative of axial magnetic fields equals zero at the conductor surface ($\partial\psi/\partial n = 0$ on S). These conditions are known as the homogeneous Dirichlet and Neumann conditions respectively. The double subscript notation used to designate modes, such as TE_{mn} follows the notation of Ramo and Whinnery²⁾. The first integer m denotes the number of half wave lengths in the long and n the number in the short dimension of the cross-section of the waveguide. The waveguide is always oriented so that the long dimension lies parallel to the x axis.

Four modes have been considered, TE₁₀, TE₀₁, TE₂₀ and TM₁₁. Because of symmetry only half of the area bounded by the conducting surface S must be considered in the single ridge case. For the double ridge waveguide only one quadrant of is needed. Fortunately, symmetry reduces the number of mesh points needed by the numerical process.

The variational technique employed yields the absolute minimum value of K^2 when the trial function ψ_0 is the exact solution to (3). In the case of the transverse electric mode, where the entire cross-section of the waveguide was used, the Neumann condition applies at all boundaries. In that case the lowest possible mode (TE₀₀) yields

$$H_z(x, y) = 0 \quad (9)$$

everywhere inside S . To avoid this trivial solution the problem is

set as in fig. 3 and fig. 4. A similar situation occurs for the TM11 mode for which more useful boundary conditions are given in fig. 5.

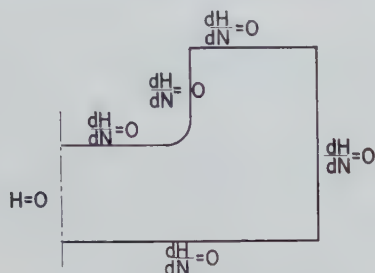


Fig. 3. The boundary conditions of the TE10 mode.

The corners of the waveguide are rounded because the finite difference techniques yield solutions to rounded configurations with fewer mesh points than they would for perfectly square configurations.

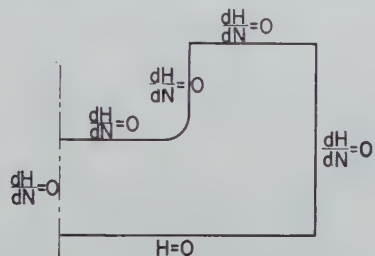
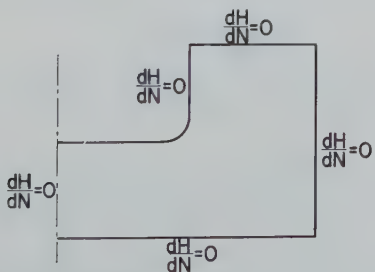


Fig. 4. (a) The boundary conditions of the TE01 mode,



(b) the TE20 mode.

tions. Only with an infinite number of mesh points can square corners be treated. The use of a finite number of mesh points automatically introduces an uncertainty which rounds the corners.

In practice sharp corners are not desirable because the high electric stress in the vicinity of the corners causes breakdown at low power levels.

For the TE₂₀ mode the boundaries of fig. 4*b* all satisfy the Neumann condition. The direct attack based on symmetry yields the trivial solution of (9). The wave functions for higher modes are all orthogonal to ψ_0 as well as to each other. A variational principle may be obtained for K_1^2 , the eigenvalue greater than K_0^2 but less than K_3^2 by restricting the admissible trial wave functions to those orthogonal to ψ_0 . Then

$$\iint \psi_1 \psi_0 \, dx \, dy = 0. \quad (10)$$

The minimum value of (5) for trial functions subject to the above condition is K_1^2 , the corresponding eigenfunction ψ_1 . This process may be continued to obtain K_2^2 by further restricting the possible trial functions to those orthogonal to ψ_0 and ψ_1 .

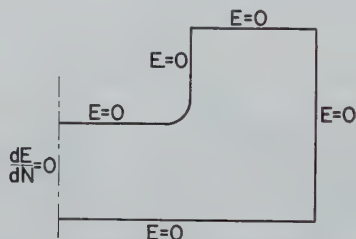


Fig. 5. The boundary conditions of the TM₁₁ mode.

For the case of the TE₂₀ mode $\psi_0 = \text{constant}$. Then

$$\iint \psi_1 \, dx \, dy = 0. \quad (11)$$

Between iterations the trial function is adjusted so that at each mesh point

$$\psi'_{i,j} = \psi_{i,j} - \frac{1}{m'} \sum_{j=1}^{m'} \psi_{i,j}. \quad (12)$$

Here $\psi_{i,j}$ is the trial function evaluated at the j th mesh point after the i th iteration, $\psi'_{i,j}$ is the adjusted trial function and m' is the total number of mesh points.

§ 4. *Cut-off frequencies.* To facilitate the presentation of the results, they are given in terms of dimensionless ratios. The relative

cut-off frequency $\xi_{m,n}$ of the ridge waveguide is the ratio of the cut-off frequency of the ridge waveguide to the cut-off frequency of an identical waveguide having no ridge.

$$\xi_{m,n} = \frac{K_{m,n}}{\pi \sqrt{(m/a)^2 + (n/b)^2}}. \quad (13)$$

Here m and n depend upon the mode being considered and $K_{m,n}$ is the eigenvalue of the ridge waveguide. The curves of relative cut-off frequency *versus* the ratio of ridge width to waveguide width for various values of the ratio of ridge to waveguide depth are shown in figs. 6 and 7. For both the single and double ridge waveguide

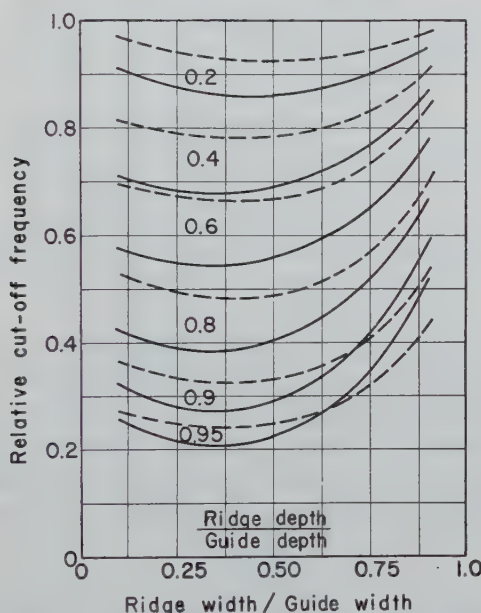


Fig. 6. The relative cut-off frequency characteristics of the single ridge waveguide operating in the TE₁₀ mode. (In this and all subsequent figures the solid lines and the dashed lines represent a guide width to depth ratio of 1 to 1 and 2 to 1 respectively)

slightly lower relative cut-off frequencies can be obtained, in some cases, by the use of a 2 : 1 rather than a 1 : 1 width to height ratio. It is interesting to note that for a given ridge depth to guide depth ratio the lowest relative cut-off frequency occurs when the ridge width to guide width is between 0.35 and 0.5.

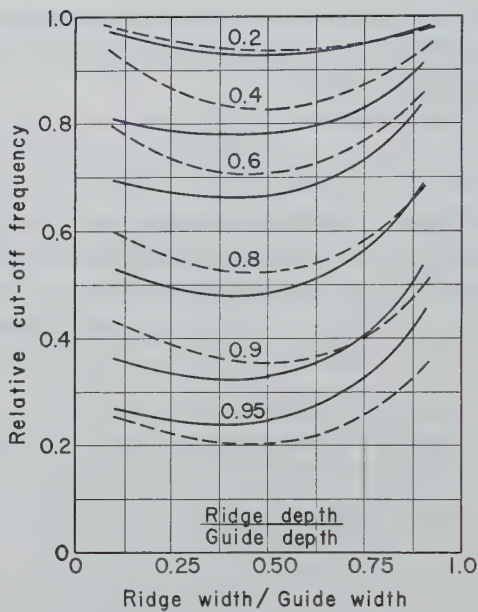


Fig. 7. The relative cut-off frequency characteristics of the double ridge waveguide operating in the TE₁₀ mode.

§ 5. *Power capacity.* The power capacity of a waveguide is limited by the maximum electric field its dielectric can tolerate without breakdown. In most cases the maximum electric field occurs at the corners of the ridges and must be kept below the breakdown strength of the dielectric. It can be shown that the power transmitted by the lossless guide through the lossless dielectric is

$$P = \frac{j\gamma\omega\mu}{2K^2} \int_s H_z^2 dS. \quad (14)$$

In this paper the surface integral of (14) is replaced by a summation of H_z^2 over all the mesh points. The power capacity of the ridge and its corresponding rectangular guide are calculated by the finite difference equivalent of (14). The ratio η of ridge waveguide to rectangular waveguide power is formed.

$$\eta = \frac{K \int_s H_{zr}^2 dS}{K_r \int_s H_z^2 dS}. \quad (15)$$

Here K and K_r , H_z and H_{zr} are the eigenvalues and axial magnetic

fields for the rectangular and ridge waveguides respectively. In (15) the power carried by each guide is evaluated close to its cut-off frequency. Before η can be calculated by (15), H_z and H_{zr} must be normalized so that the maximum value of the electric field in each of the waveguides is the breakdown field of the dielectric. In figs. 8 and 9 are plots of relative power capacity η versus the ratio of

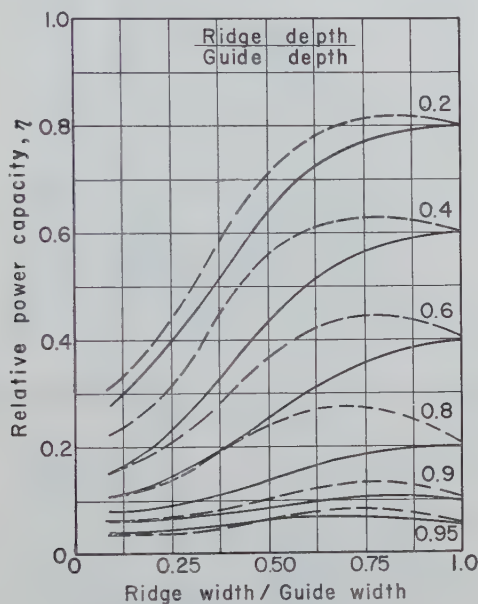


Fig. 8. The relative power capacity of the single ridge waveguide operating in the TE₁₀ mode.

ridge to guide width for various values of the ratio of ridge to guide depth. As would be expected the ridge waveguide having the greatest cross-sectional area has a slightly greater power capability than the square one. The peak relative power capacity for a given ratio of ridge to guide depth lies between a ridge to guide width ratio about 0.7 and 1.

§ 6. *Mode separation.* In many applications it is imperative that one mode be transmitted and the others quickly attenuated. This occurs if the operating frequency of the guide is above the cut-off frequency of the first mode and below the cut-off frequency of the

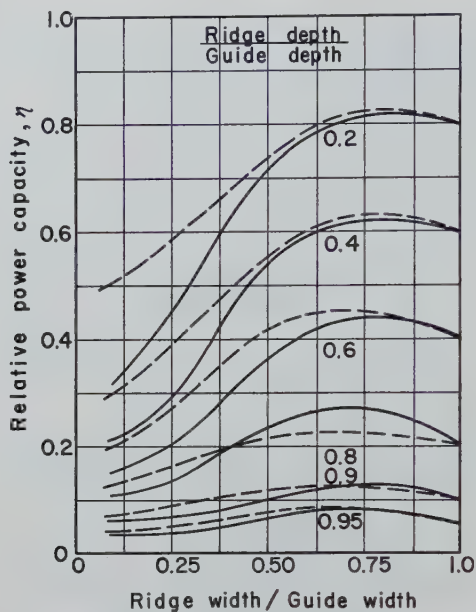


Fig. 9. The relative power capacity of the double ridge waveguide operating in the TE_{10} mode.

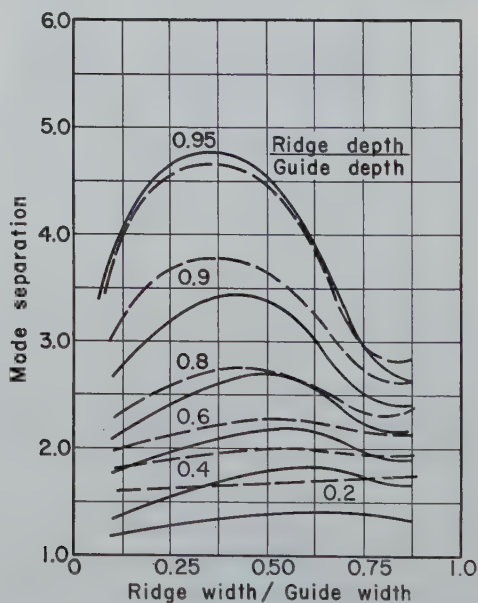


Fig. 10. The mode separation between the TE_{01} and TE_{10} modes of the single ridge waveguide.

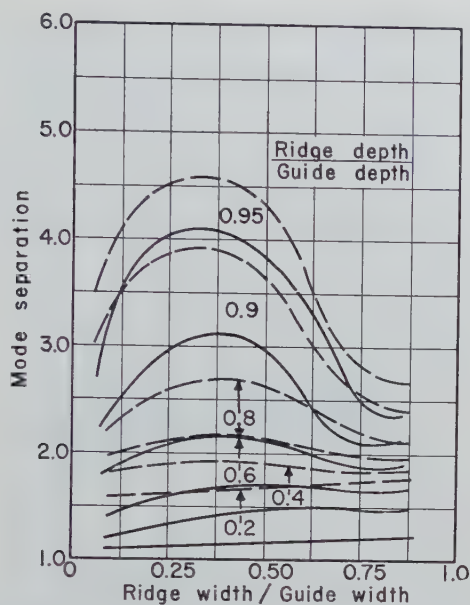


Fig. 11. The mode separation between the TE₀₁ and TE₁₀ modes of the double ridge waveguide.

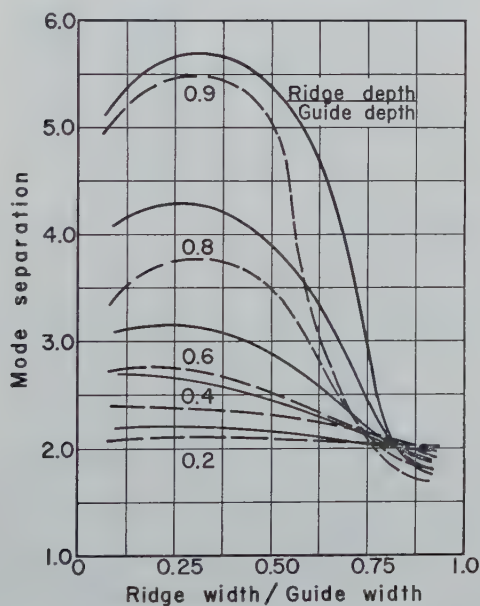


Fig. 12. The mode separation between the TE₂₀ and TE₁₀ modes of the single ridge waveguide.

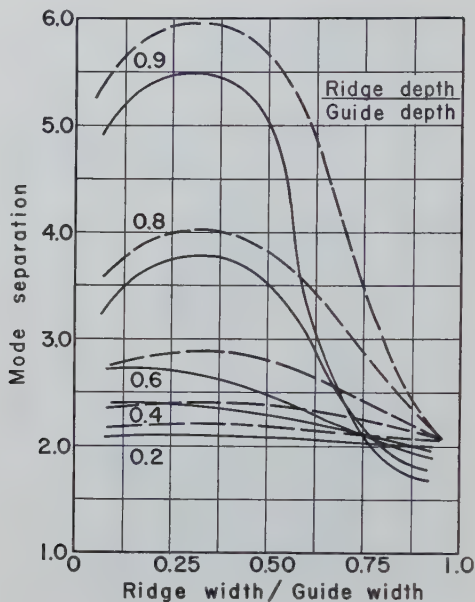


Fig. 13. The mode separation between the TE₂₀ and TE₁₀ modes of the double ridge waveguide.

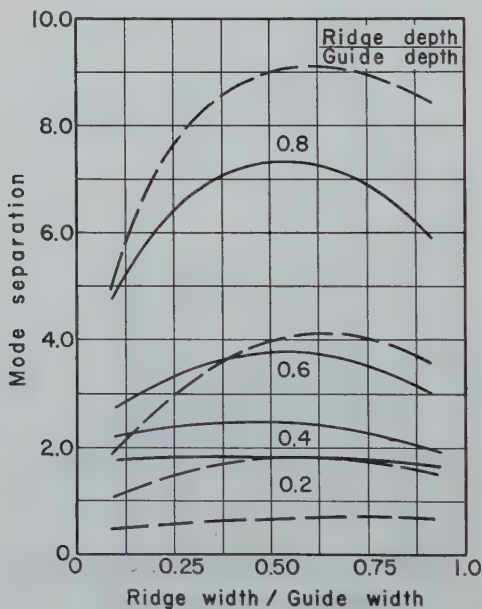


Fig. 14. The mode separation between the TM₁₁ and TE₁₀ modes of the single ridge waveguide.

second mode. The mode separation s , i.e., the ratio of K_p to K_{p+1} , for a ridge waveguide is considerably greater than that of a rectangular waveguide. Plots of mode separation factor versus the ratio of ridge to guide width for various values of the ratio of ridge to guide depth are included in figs. 10 through 15 inclusive. For a given ridge to guide depth the maximum mode separation occurs at roughly the same ridge to guide width as does the minimum cut-off frequency of the TE₁₀ mode.

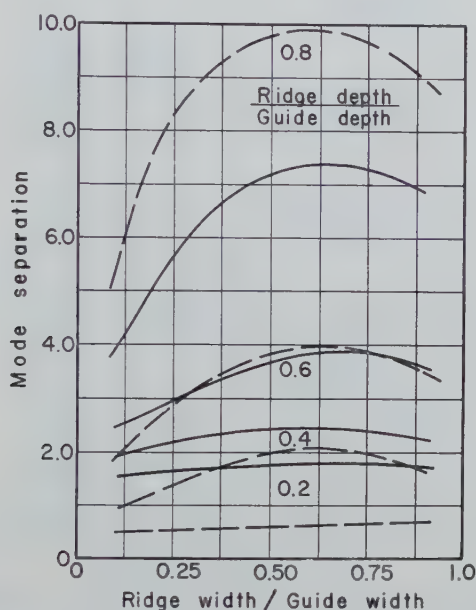


Fig. 15. The mode separation between the TM₁₁ and TE₁₀ modes of the double ridge waveguide.

§ 7. *Impedance.* The impedance of a ridge waveguide is customarily expressed in the following manner for TE modes:

$$z_0 = z_0^\infty \sqrt{\frac{\mu}{\epsilon}} \left(1 - \frac{\omega^2 \mu \epsilon}{K^2} \right)^{-\frac{1}{2}}. \quad (16)$$

The concept of z_0^∞ was introduced by Cohn and was used by Mihran and Erteza. For a rectangular guide z_0^∞ is unity. For a ridge waveguide z_0^∞ may be either greater or smaller than one depending upon the size of the ridge and the mode considered. The earlier workers evaluated z_0^∞ by calculating the voltage across the guide and dividing it by the current flowing down the walls.

When the field distributions within the guide are accurately known better, results may be obtained from (17):

$$z_0^\infty = \beta^2/\eta. \quad (17)$$

Here β^2 is the maximum relative voltage obtained by dividing the maximum value of $\int E_y dy$ for the corresponding rectangular waveguide. In (17) all quantities must first be adjusted so that the maximum electric field is the breakdown field of the dielectric. For

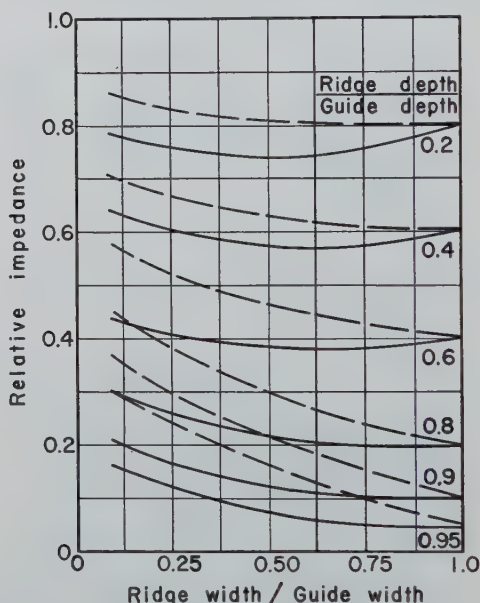


Fig. 16. The relative impedance of the single ridge waveguide operating in the Te_{10} mode.

the TE_{01} mode the voltage line integral is evaluated along lines AB and A' B' in figs. 1 and 2. In higher modes care must be taken to choose the proper path of integration. The impedance curves are given by figs. 16 and 17. It is interesting to note that the single ridge guide possesses, for a given ridge to guide depth ratio, a value of ridge to guide width ratio which minimizes the relative impedance whereas the double ridge waveguide does not.

§ 8. *Experimental evidence.* Cohn examined experimentally a double ridge waveguide with a width to height ratio of 3.7. The ridge to guide width ratio was 0.4 and the ridge depth to guide

height ratio was 0.65. For the TE₁₀ mode the measured value of cut-off frequency was 1675 MHz as compared to a value of 1685 MHz calculated by the modified Rayleigh-Ritz method. For the TE₂₀ mode the cut-off frequency measured was 5200 MHz, while the calculated value of 5170 MHz is obtained here.

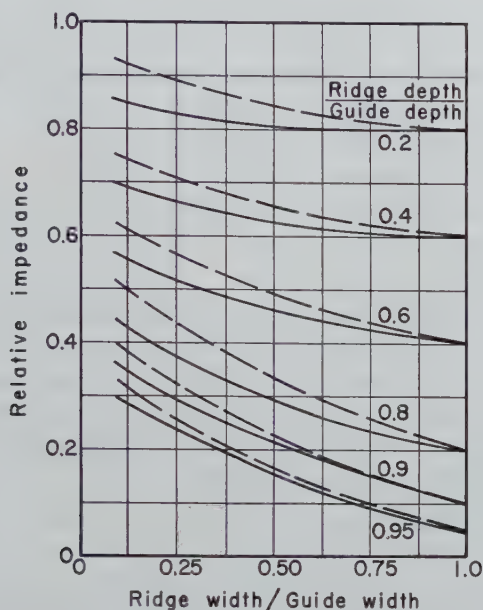


Fig. 17. The relative impedance of the double ridge waveguide operating in the TE₁₀ mode.

Anderson⁵⁾ measured the cut-off frequency of a waveguide having a guide width to height ratio of 2, a ridge to guide width ratio of 0.29 and a ridge depth to guide height ratio of 0.34. The experimental value of the cut-off frequency of the TE₁₀ mode was 4200 MHz compared to our calculated value of 4180 MHz. In each case the difference between the measured and calculated values are of the same magnitude as the errors made in interpolating graphs.

§ 9. *Conclusions.* The most important parameter in the design of ridge waveguides is the ratio of ridge to guide depth. At the cost of lower power capacity the relative cut-off frequency of the lowest mode can be made to approach zero by letting that ratio approach unity. How low in frequency a practical ridge waveguide can operate

is not known but may well be limited by mechanical and machining considerations. The ratio of ridge to guide width does not influence the characteristics of the ridge waveguide as much as does the ridge to guide depth ratio except in the cases of very narrow or wide ridges.

It is significant that the relative cut-off frequency, relative power capacity and relative impedance curves of the single ridge waveguide having a width to depth ratio of 2 : 1 are almost identical to those of the double ridge waveguide having a width to depth ratio of 1 : 1. However, the single ridge waveguide while twice as large as the double ridge waveguide has better mode separation properties than the double ridge waveguide.

The double ridge waveguide having a width to depth ratio of 2 : 1 possesses the lowest relative cut-off frequency for the TE₁₀ mode of the waveguide considered here. It also exhibits the greatest relative power capacity, and has the most favourable mode separation properties. In all cases the mode separation factor is strongly dependent upon the ridge to guide ratio. For very small values of that ratio the mode separation factor is small and almost independent of the ridge to guide width ratio. As the ridge gets deeper the ridge to guide width ratio becomes more important.

From the curves presented it can be seen that for a given ridge to guide depth ratio the ridge to guide width can be adjusted to optimize any of the characteristics except the relative impedance. However, it is harder to adjust the width to obtain the best combination of those characteristics. In specific cases the design data presented in this paper can be used to obtain the most desirable dimensions for the ridge waveguides analysed here and might develop insight into other unsolved cases. Using the method described here a new ridge waveguide can be analysed by a large high speed internally programmed digital computer (e.g. IBM 704) in times ranging from two to twenty minutes depending upon the ridge to guide depth ratio.

Received 26th April, 1960.

REFERENCES

- 1) Cohn, S. B., *Proc. Instn Radio Engrs* **34** (1947) 783.
- 2) Ramo, S. and J. R. Whinnery, *Fields and Waves in Modern Radio*, John. Wiley and Sons, Inc. New York, (1944).
- 3) Mihran, T. G., *Proc. Instn Radio Engrs* **37** (1949) 640.
- 4) Erteza, A. and K. Spangenberg, Stanford University Report 1952.
- 5) Anderson, T. N., P. G. M. T. T. (1955) 2.

THE MAGNETIC SUSCEPTIBILITY OF Ag-Mn AND Cu-Mn SOLID SOLUTIONS BETWEEN 1.2°K AND 368°K

by A. VAN ITTERBEEK, W. PEELAERS*) and F. STEFFENS**)

Instituut voor Lage Temperaturen en Technische Fysika, Leuven, Belgium

Summary

The magnetic susceptibility of Ag-Mn and Cu-Mn solid solutions containing between 0.25 and 5.3 at % Mn has been measured between 1.2 and 368°K. The alloys obey a Curie-Weiss law up to and including liquid nitrogen temperatures and p_{eff} , effective magneton number, values derived for the manganese atom are discussed and compared with other published values. At liquid hydrogen temperatures the alloys no longer obey a Curie-Weiss law. It has been found that some of the alloys show a transition from a paramagnetic into an antiferromagnetic state. This occurs at a certain temperature, known as the Néel temperature T_N . The field dependence of the susceptibility was also investigated. No field dependence occurs as long as the temperature at which measurements are done, is far above the Néel temperature T_N . Once in the neighbourhood of this transition temperature T_N field dependence is observed.

§ 1. *Introduction.* Preliminary measurements on the same subject have been described in a paper ¹⁾. Since then some refinements in the experimental set-up have taken place which are described in another paper ²⁾. The magnetic susceptibility of the solid solutions has been investigated as a function of temperature and magnetic field.

§ 2. *Experimental.* 2.1. Preparation of the alloys. The alloys were prepared from spectroscopically standardized silver, copper and manganese delivered by Johnson-Matthey and Co (London) and the American Melting and Refining company. The

*) Research Fellow of the I.W.O.N.L. (Instituut tot aanmoediging van het Wetenschappelijk Onderzoek in Nijverheid en Landbouw).

**) Research Fellow of the I.I.K.W. (Interuniversitair Instituut voor Kernwetenschappen).

constituents were accurately weighed (Sartorius balance) and placed in a silica tube, which is then evacuated.

The alloys were prepared in a high frequency furnace, the following scheme being applied:

- 1) degassing of the constituents for one hour under continuous evacuation;
- 2) melting for a period of about one hour at 1300°C;
- 3) homogenising and quenching in distilled water.

The homogeneity of the alloys is examined by measuring the susceptibility of specimens taken at different places of the ingot.

2.2. Method and calibration of the balance. The magnetic susceptibility of the alloys is determined using a microgram balance and Faraday's method. For a detailed description we refer to papers ³⁾ and ²⁾. The following expression is obtained:

$$C\Delta I^2 = m\chi H \, dH/dx.$$

ΔI^2 : the variation of I^2 between $H = 0$ and the value H

m : mass of the sample

C : constant of the microgram balance

H : magnetic field

χ : mass susceptibility

At room temperature the measurements are carried out in vacuum (10^{-3} mm Hg). At low temperatures the sample is suspended in an atmosphere of carefully purified helium gas at a pressure of 2 mm. We determined at first the position where $C_1 = C(H \, dH/dx)^{-1}$ is a minimum or $H \, dH/dx$ a maximum. The values obtained for C_1 at different magnetic field strengths are given in table I. The calibra-

TABLE I

$H(\text{Ø})$	$C_1 \times 10^6 \text{ c.g.s.u.}$
6875.6	1.3994
8727.6	0.8761
11202.5	0.5604
13759.4	0.4224

tion has been carried out at room temperature with spectroscopically standardized niobium, delivered by Johnson-Matthey and Co (London). As value of the mass susceptibility at room temperature 2.39×10^{-6} has been taken. The susceptibility of niobium is field-independent. The results obtained for C_1 have been checked afterwards with iron ammonium alum.

§ 3. *Discussion of the results.* A. Investigation of the susceptibility as a function of temperature. From measurements on the susceptibility as a function of temperature it has been possible to determine the transition between the paramagnetic and antiferromagnetic state. This transition takes place at a certain temperature T_N , known as the Néel temperature, below which the alternating arrangement of the spin starts.

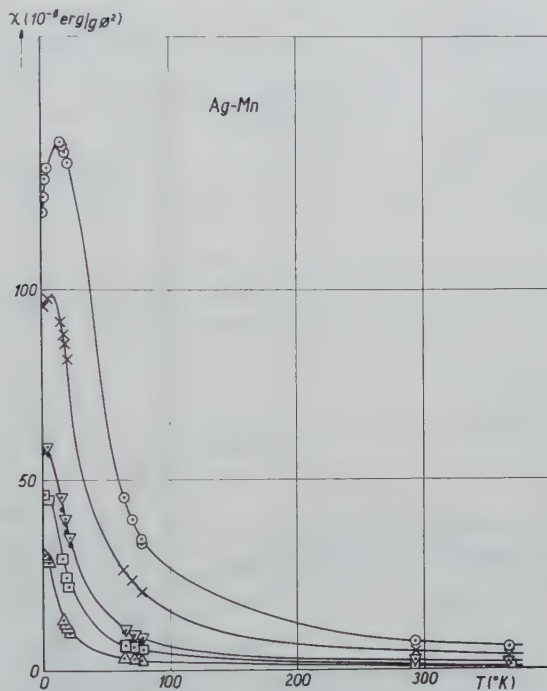


Fig. 1. The mass susceptibility of Ag-Mn alloys as a function of temperature.

- △: 0.5 at % Mn
- : 1.24 at % Mn
- : 1.67 at % Mn
- ▽: 1.75 at % Mn
- ×: 3.50 at % Mn
- : 5.30 at % Mn

This transition takes place, for certain values of the concentration of manganese in the alloys, in the temperature region 1.2°K–20°K. For low concentrations of manganese it appeared that the lowest

temperature attainable (1.2°K) with our set-up was not low enough to detect this transition. The results are plotted in figs 1, 2, 3 and 4.

Figs 1 and 3 give the change of the mass susceptibility over the whole temperature region for Ag-Mn and Cu-Mn alloys. Figs 2 and 4 give the mass susceptibility as a function of temperature for the region 1.2–20.4°K. It is from these figures that the transition temperature T_N has been determined.

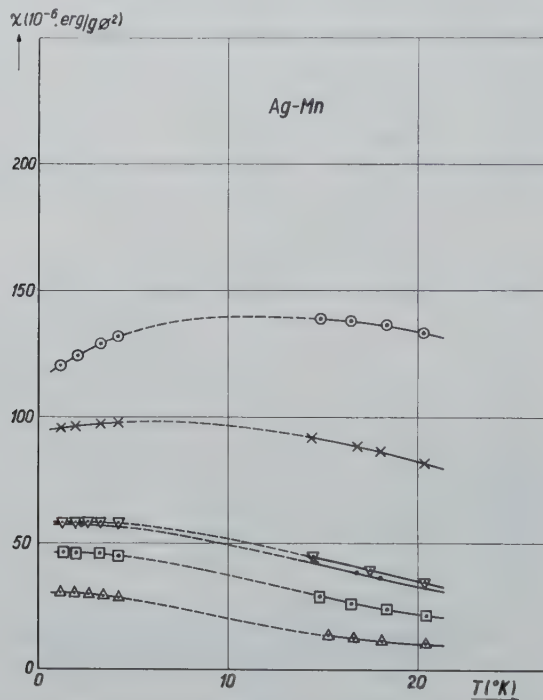


Fig. 2. The mass susceptibility of Ag-Mn alloys as a function of temperature.

- \triangle : 0.5 at % Mn
- \square : 1.24 at % Mn
- \bullet : 1.67 at % Mn
- ∇ : 1.75 at % Mn
- \times : 3.50 at % Mn
- \circ : 5.30 at % Mn

In tables II and III are given the values of T_N for the alloys. There is an increase of the Néel temperature with increasing concentration of manganese; in other words, the antiferromagnetic

TABLE II

at % Mn	Néel temp. T_N ($^{\circ}\text{K}$)
0.50	none
1.24	none
1.67	none
1.75	between 1.2 and 1.9
3.50	6
5.30	11.4

TABLE III

at % Mn	Néel temp. T_N ($^{\circ}\text{K}$)
0.25	none
1.40	4
1.61	between 1.9 and 4
2.57	10.6
4.82	11.5

state sets in at higher temperatures when the concentration of manganese is increased.

If now the results obtained for Ag-Mn and Cu-Mn are compared, we see that, for an equal concentration of manganese, antiferro-

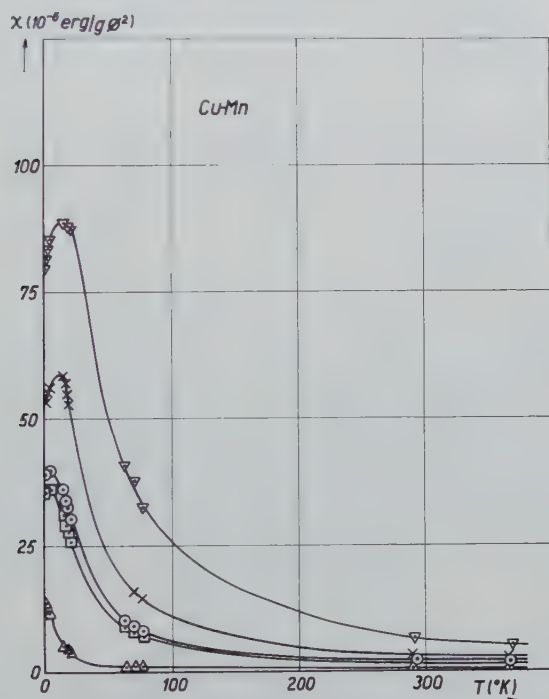


Fig. 3. The mass susceptibility of Cu-Mn alloys as a function of temperature.

- Δ : 0.25 at % Mn
- \square : 1.40 at % Mn
- \circ : 1.61 at % Mn
- \times : 2.57 at % Mn
- ∇ : 4.82 at % Mn

magnetism sets in earlier in the Cu-Mn than in the Ag-Mn alloys. One of the reasons is probably the smaller lattice spacing in copper. In silver the lattice spacing is 4.08 Å, for copper 3.61 Å, so that the dissolved manganese atoms for an equal concentration in silver and copper, are closer to each other in copper than in silver.

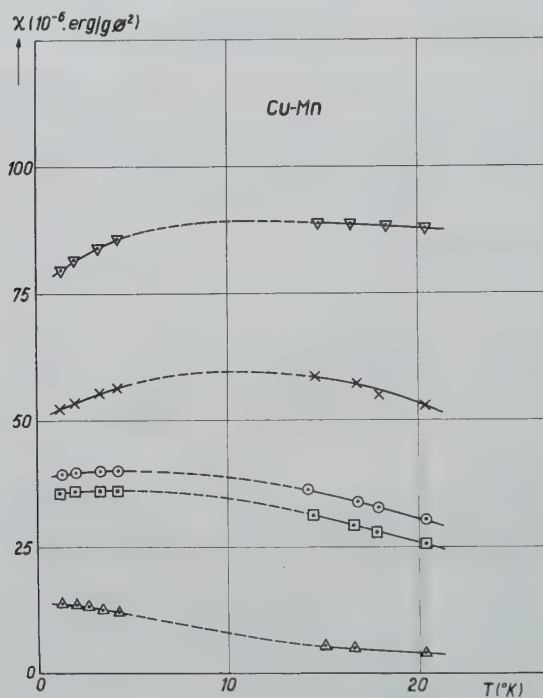


Fig. 4. The mass susceptibility of Cu-Mn alloys as a function of temperature.

- △: 0.25 at % Mn
- : 1.40 at % Mn
- : 1.61 at % Mn
- ×: 2.57 at % Mn
- ▽: 4.82 at % Mn

B. Determination of the Curie constant C and the Curie temperature for the temperature region where the alloys obey a Curie-Weiss law. The results are shown in figs. 5 and 6 as graphs of $1/\chi$ plotted against T . All these graphs are linear between 64°K–368°K, showing that the magnetic behaviour is well represented over this temperature range by a Curie-Weiss

law $\chi = C(T - \theta)$. At liquid hydrogen temperatures this law is no longer obeyed. The values of C and θ calculated from our results by the method of least mean squares are given in tables IV and V. As can be seen from these tables, there is also an increase of the values of C and θ with increasing concentration of manganese.

TABLE IV

Ag-Mn		
at % Mn	$C \times 10^4$ (erg deg./g O^2)	θ ($^{\circ}\text{K}$)
1.24	4.48	-3.2
1.67	6.15	2.3
3.50	13.0	13.8
5.10	18.8	18.6
5.30	19.6	20.6

TABLE V

Cu-Mn		
at % Mn	$C \times 10^4$ (erg deg./g O^2)	θ ($^{\circ}\text{K}$)
1.40	5.47	0.3
1.61	6.21	3.0
2.57	9.9	9.8
4.82	18.1	20.7

The values of C and θ given above refer to the alloys, but we were interested above all in the magnetic behaviour of the manganese atom. So it was first necessary to correct the measured susceptibilities for temperature-independent diamagnetism. This has been done in the conventional way by assuming that the main diamagnetic contribution comes from the silver or the copper. The measured susceptibilities were thus first converted into gram-atomic susceptibilities χ_A and the corrected susceptibilities χ_B determined from the formula

$$\chi_A = \chi_B + (1 - C_{\text{Mn}}) \chi_A^{\text{Ag}} \text{ or } \chi_A = \chi_B + (1 - C_{\text{Mn}}) \chi_A^{\text{Cu}},$$

where C_{Mn} = atomic concentration of Mn, $\chi_A^{\text{Ag}} = -19.56 \times 10^{-6}$ e.m.u. (g atom) $^{-1}$ and $\chi_A^{\text{Cu}} = -5.276 \times 10^{-6}$ e.m.u. (g atom) $^{-1}$. It was found that the χ_B values obey also a Curie-Weiss law in the same temperature range as for the alloys.

The values of C and θ calculated by the method of the least mean squares are given in tables VI and VII. The values obtained for Ag-Mn correspond to those of Gustafsson⁴⁾ and connect with

TABLE VI

Ag-Mn		
at % Mn	$C \times 10^3$	θ ($^{\circ}\text{K}$)
1.24	56.2	-13.7
1.67	73.8	-4.5
3.50	145	11.3
5.10	204	17.6
5.30	213	19

TABLE VII

Cu-Mn		
at % Mn	$C \times 10^3$	θ ($^{\circ}\text{K}$)
1.40	36.9	-3.35
1.61	41.7	-0.29
2.57	64.5	8.3
4.82	116	20

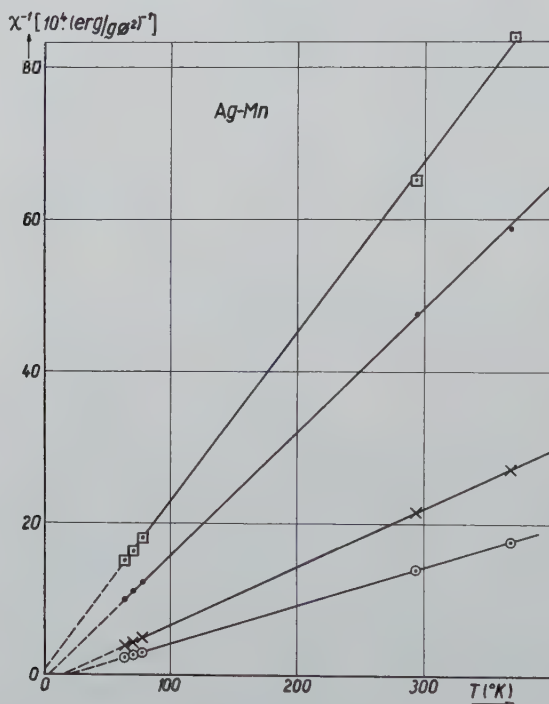


Fig. 5. Ag-Mn.

- : 1.24 at % Mn
- : 1.67 at % Mn
- ×: 3.50 at % Mn
- : 5.30 at % Mn

those of D. P. Morris and I. Williams⁵). For Cu-Mn there is agreement with the values obtained by Owen *et al*⁶).

C. Magnetic moment. It is well known that valuable information about the electronic configuration of transition metal atoms can be obtained from the magnetic susceptibility of alloys containing these atoms in solid solution.

If the susceptibility obeys a Curie-Weiss law, effective magneton numbers p_{eff} may be derived, and assuming the orbital momenta to be quenched, p_{eff} may be equated to $[4S(S+1)]^{\frac{1}{2}}$, where S is the total spin quantum number of the solute atom. Corrections were made for temperature-independent diamagnetism in the way described in § 3B.

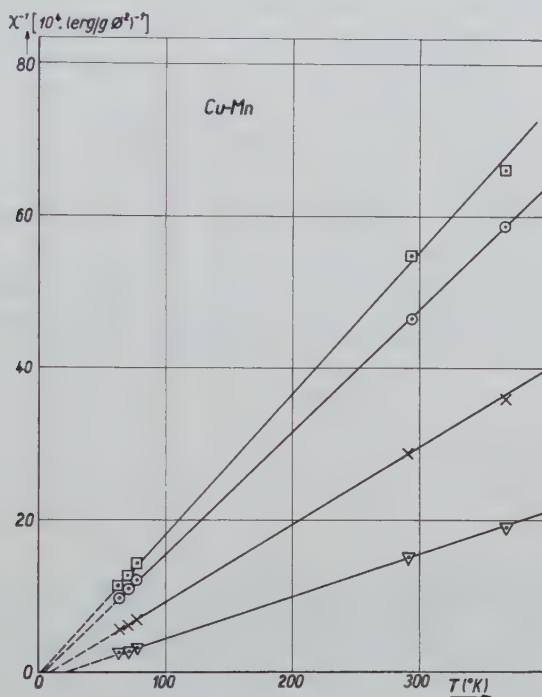


Fig. 6. Cu-Mn.

- : 1.40 at % Mn
- : 1.61 at % Mn
- ×: 2.57 at % Mn
- ▽: 4.82 at % Mn

According to the classical theory one obtains as expression for the Curie constant

$$C = N^2 p^2 / 3R.$$

p can be expressed in effective magneton numbers $p_{\text{eff}} = p/\mu_B$. So we obtain $C = N^2 p^2 \mu^2 B / 3R$ or

$$p_{\text{eff}} = 1/N\mu_B \times [3R(T - \theta) \chi_{\text{mole}}]^{\frac{1}{2}} = 1/N\mu_B \times (3RC)^{\frac{1}{2}},$$

$$N = 6.02 \times 10^{23}$$

$$R = 8.315 \times 10^7 \text{ erg/deg. mol}$$

$$\mu_B = 9.27 \times 10^{-21} \text{ e.m.u.}$$

p = magnetic moment of the atom

p_{eff} = effective magneton number

The results obtained from measurements at room temperature are given in tables VIII and IX.

TABLE VIII

Ag-Mn	
at % Mn	p_{eff}
1.24	6.03
1.67	5.89
3.50	5.74
5.10	5.66
5.30	5.65

TABLE IX

Cu-Mn	
at % Mn	p_{eff}
1.40	4.54
1.61	4.55
2.57	4.45
4.82	4.35

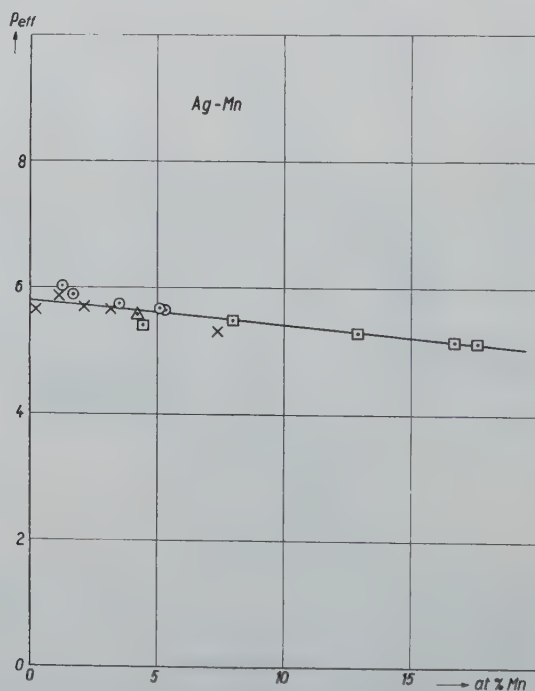


Fig. 7. p_{eff} of the Ag-Mn alloys as a function of at % Mn.

□: Morris and Williams

×: Gustafsson

△: Owen *et al*

○: present work

In fig. 7 and 8 we have plotted p_{eff} against Mn concentration including the results of Owen *et al* ⁶⁾, Gustafsson ⁴⁾, D. P. Morris and I. Williams ⁵⁾, Valentiner and Becker ⁷⁾ and Néel ⁹⁾. At high concentrations of manganese, the points are situated on a straight line. Extrapolation of this line gives a p_{eff} -value at infinite dilution of about 5.8 for the Ag-Mn and 4.9 for the Cu-Mn system. For the former the electronic configuration of the manganese atom approximates most closely to $3d^5 4s^2$ and for the latter $3d^6 4s$.

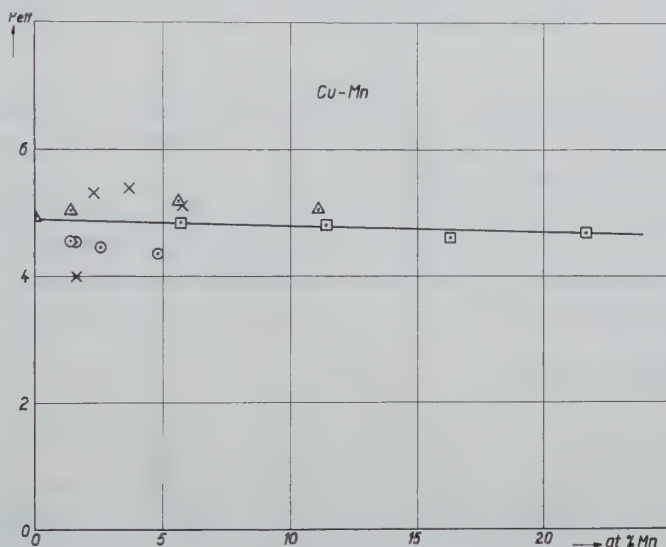


Fig. 8. p_{eff} of the Cu-Mn alloys as a function of at % Mn.

- \square : Valentiner and Becker
- \times : Néel
- Δ : Owen *et al*
- \odot : present work

As can be seen from fig. 8 there is a great scattering in the values at low concentrations of manganese. This is probably due to the sensitivity of p_{eff} to the magnitude of the diamagnetic correction and to error in composition. It is our opinion that the extrapolation of the straight line towards the low concentration region is justified.

It is also to be noted that E. Sheil *et al* ⁸⁾ derived from their measurements a p_{eff} value of 4.9 for the manganese atom as well in Ag-Mn as well as in Cu-Mn alloys.

D. Field dependence of the susceptibility. For the

Ag-Mn as well as for the Cu-Mn alloys the following conclusions can be drawn:

- a) as long as the temperature at which measurements are carried out is not in the neighbourhood of the transition temperature T_N , the susceptibility is field-independent;
- b) once in the neighbourhood of T_N , we found that the susceptibility becomes field-dependent in the paramagnetic as well as in the antiferromagnetic state;
- c) the susceptibility is field-dependent in the antiferromagnetic state.

Acknowledgements. We take the opportunity to express our sincere thanks to the Union Minière du Haut Katanga for financial help during these measurements.

We thank respectively the I.W.O.N.L. (Instituut tot aanmoediging van het Wetenschappelijk Onderzoek in Nijverheid en Landbouw) and the I.I.K.W. (Interuniversitair Instituut voor Kernwetenschappen) from which two of us obtained a fellowship.

Received 10th May, 1960.

REFERENCES

- 1) Itterbeek, A. van, R. Pollentier and W. Peelaers, Appl. Sci. Res. B **7** (1959) 329.
- 2) Itterbeek, A. van, W. Peelaers and F. Steffens, Appl. Sci. Res. B **8** (1960) 177.
- 3) Itterbeek, A. van, L. De Greve and W. Duchateau, Appl. Sci. Res. B **4** (1955) 300; A. van Itterbeek and W. Duchateau, Physica **22** (1956) 649.
- 4) Gustafsson, G., Ann. Phys. Lpz. **25** (1936) 545.
- 5) Morris, D. P. and I. Williams, Proc. Phys. Soc. **73** (1959) 422.
- 6) Owen, J., M. E. Browne, V. Arp and A. F. Kip, J. Phys. Chem. Solids **2** (1957) 85.
- 7) Valentiner, S. and G. Becker, Z. Phys. **80** (1933) 735.
- 8) Scheil, E. and E. Wachtel, Z. Metallkunde **48** (1957) 571. Also E. Scheil, E. Wachtel, E. and A. Kalkuhl, Z. Metallkunde **49** (1958) 464.
- 9) Néel, L., J. Phys. Radium **3** (1932) 160.

A MODIFICATION OF CAGNIARD'S METHOD FOR SOLVING SEISMIC PULSE PROBLEMS

by A. T. DE HOOP

Laboratorium voor Theoretische Elektrotechniek, Technische Hogeschool, Delft,
Netherlands

Summary

A modification of Cagniard's method for solving seismic pulse problems is given. In order to give a clear picture of our method, two simple problems are solved, viz. the determination of the scalar cylindrical wave generated by an impulsive line source and the scalar spherical wave generated by an impulsive point source.

§ 1. *Introduction.* The application of Cagniard's ¹⁾ method in obtaining exact solutions of three-dimensional seismic pulse problems leads to complicated expressions for the components of the displacement vector in the elastic solid. This is partly due to the fact that in a homogeneous, isotropic, elastic solid two types of waves, travelling with different velocities, occur. In order to give a clear picture of Cagniard's method, Dix ²⁾ applied it to a simple problem in scalar wave propagation, viz. the determination of the spherical wave generated by an impulsive point source located in a homogeneous, isotropic, unbounded medium. Even in this simple problem (the solution of which can also be obtained by less complicated methods) quite a number of transformations of complex contour integrals are involved.

In the present paper it is shown that Cagniard's method can be simplified considerably if the corresponding modification for two-dimensional problems as developed by the present author ^{3,4)} is taken as a guidance. Again, the aforementioned point source problem will be considered; for reference, also the solution of the corresponding line source problem will be given.

It is remarked that the resulting method is also simpler than

the technique employed by Pekeris⁵⁻¹⁰), which is slightly different from the one due to Cagniard.

§ 2. *The scalar wave generated by an impulsive line source.* Let x, y, z be Cartesian coordinates in three-dimensional space. A point in space will be located by either its Cartesian coordinates, its cylindrical coordinates r, φ, z defined through

$$x = r \cos \varphi, \quad y = r \sin \varphi, \quad z = z, \quad (2.1)$$

with $0 \leq r < \infty$, $0 \leq \varphi < 2\pi$, $-\infty < z < \infty$, or its spherical polar coordinates defined through

$$x = R \sin \theta \cos \varphi, \quad y = R \sin \theta \sin \varphi, \quad z = R \cos \theta, \quad (2.2)$$

with $0 \leq R < \infty$, $0 \leq \theta \leq \pi$, $0 \leq \varphi < 2\pi$.

The two-dimensional wave function $u = u(x, y, t)$ due to the presence of a two-dimensional line source acting at $x = 0, y = 0$, satisfies the two-dimensional scalar wave equation

$$\frac{\partial^2 u}{\partial x^2} + \frac{\partial^2 u}{\partial y^2} - \frac{1}{v^2} \frac{\partial^2 u}{\partial t^2} = -\delta(x, y) f(t), \quad (2.3)$$

where $\delta(x, y)$ denotes the two-dimensional delta function and v is the wave front velocity. The function $f(t)$ determines the strength of the line source as a function of time; it is assumed that $f(t) = 0$ when $t \leq 0$. Further, it is assumed that the medium is at rest prior to the instant $t = 0$ and that everywhere outside the source $u = u(x, y, t)$ is continuous and has continuous partial derivatives of the first and second order.

Following Cagniard, all functions of time are subjected to a one-sided Laplace transform with respect to time. Let

$$F(s) = \int_0^{\infty} \exp(-st) f(t) dt \quad (2.4)$$

and

$$U(x, y; s) = \int_0^{\infty} \exp(-st) u(x, y, t) dt, \quad (2.5)$$

where s is a real, positive, number large enough to ensure the convergence of the integrals (2.4) and (2.5) (it is assumed that the behaviour of $f(t)$ and $u(x, y, t)$ as $t \rightarrow \infty$ is such that such a number s can be found). Since u and $\partial u / \partial t$ are continuous, $U(x, y; s)$ satisfies

the differential equation

$$\frac{\partial^2 U}{\partial x^2} + \frac{\partial^2 U}{\partial y^2} - \frac{s^2}{v^2} U = -\delta(x, y) F(s). \quad (2.6)$$

In order to solve (2.6) we introduce the Fourier transform of $U(x, y; s)$ with respect to x . Let

$$\mathcal{U}(\alpha; y; s) = \int_{-\infty}^{\infty} \exp(is\alpha x) U(x, y; s) dx, \quad (2.7)$$

where the factor s in the argument of the exponential function has been included for convenience. With (2.7) the following equation for $\mathcal{U}(\alpha; y; s)$ is obtained

$$\frac{d^2 \mathcal{U}}{dy^2} - s^2 \gamma^2 \mathcal{U} = -\delta(y) F(s), \quad (2.8)$$

where

$$\gamma = \gamma(\alpha) = (\alpha^2 + 1/v^2)^{\frac{1}{2}} \quad (\operatorname{Re} \gamma \geq 0). \quad (2.9)$$

As indicated in (2.9), γ is defined as that branch of the square root at the right-hand side of (2.9) for which $\operatorname{Re} \gamma \geq 0$. The solution of (2.8) that is bounded as $|y| \rightarrow \infty$ is given by

$$\mathcal{U}(\alpha; y; s) = \frac{F(s)}{2s\gamma} \exp(-s\gamma |y|). \quad (2.10)$$

With the aid of Fourier's inversion theorem we then obtain for $U(x, y; s)$ the expression

$$U(x, y; s) = \frac{F(s)}{2\pi} \int_{-\infty}^{\infty} \exp(-is\alpha x - s\gamma |y|) \frac{1}{2\gamma} d\alpha. \quad (2.11)$$

In the right-hand side of (2.11) we write $\alpha = -ip$ and consider p as a complex variable in the p -plane. This leads to

$$U(x, y; s) = -\frac{F(s)}{2\pi i} \int_{-i\infty}^{i\infty} \exp[-s(p\alpha + \gamma |y|)] \frac{1}{2\gamma} dp, \quad (2.12)$$

in which

$$\gamma = (1/v^2 - p^2)^{\frac{1}{2}} \quad (\operatorname{Re} \gamma \geq 0). \quad (2.13)$$

The only singularities of the integrand in (2.12) are branch points at $p = 1/v$ and $p = -1/v$. In view of subsequent deformations

of the path of integration we take $\operatorname{Re} \gamma \geq 0$ everywhere in the p -plane. This implies that branch cuts are introduced along $\operatorname{Im} p = 0$, $1/v < |\operatorname{Re} p| < \infty$.

The next step towards the solution of the transient problem is to perform the integration in the p -plane along such a path that the right-hand side of (2.12) can be recognized as the Laplace transform of a certain function of time. The analysis which follows will show that the path has to be selected such that

$$px + \gamma|y| = \tau, \quad (2.14)$$

where τ is real and positive. If $r/v < \tau < \infty$, eq. (2.14) represents the branch Γ of a hyperbola, where Γ is given through

$$p = \frac{x}{r^2} \tau \pm i \frac{|y|}{r^2} (\tau^2 - r^2/v^2)^{\frac{1}{2}} \quad (r/v < \tau < \infty), \quad (2.15)$$

in which the square root is taken positive. It is easily verified that, by virtue of Cauchy's theorem and Jordan's lemma¹¹), the integral along the imaginary p -axis is equal to the integral along Γ . Along Γ we have

$$\gamma = \frac{|y|}{r^2} \tau \mp i \frac{x}{r^2} (\tau^2 - r^2/v^2)^{\frac{1}{2}} \quad (2.16)$$

and

$$\frac{\partial p}{\partial \tau} = \pm \frac{i\gamma}{(\tau^2 - r^2/v^2)^{\frac{1}{2}}}. \quad (2.17)$$

In (2.15), (2.16) and (2.17) the upper and lower signs belong together. Taking into account the symmetry of the path of integration with respect to the real axis and introducing τ as variable of integration we obtain

$$U(x, y; s) = \frac{F(s)}{2\pi} \int_{r/v}^{\infty} \exp(-s\tau) (\tau^2 - r^2/v^2)^{-\frac{1}{2}} d\tau. \quad (2.18)$$

This expression is of the general form

$$U(x, y; s) = F(s) \int_0^{\infty} \exp(-s\tau) g(x, y, \tau) d\tau, \quad (2.19)$$

where, in our case,

$$g(x, y, \tau) = \begin{cases} 0 & (0 < \tau < r/v), \\ \frac{1}{2\pi} (\tau^2 - r^2/v^2)^{-\frac{1}{2}} & (r/v < \tau < \infty). \end{cases} \quad (2.20)$$

Application of the shift rule for Laplace transforms to the function $F(s) \exp(-s\tau)$ directly yields the function $u(x, y, t)$. We obtain

$$u(x, y, t) = \int_0^t f(t - \tau) g(x, y, \tau) d\tau \quad (t > 0), \quad (2.21)$$

while, from our assumptions, $u(x, y, t) = 0$ when $t < 0$. In our case we have

$$u(x, y, t) = \begin{cases} 0 & (0 < t < r/v), \\ \frac{1}{2\pi} \int_{r/v}^t f(t - \tau) (\tau^2 - r^2/v^2)^{-\frac{1}{2}} d\tau & (r/v < t < \infty). \end{cases} \quad (2.22)$$

From the final result (2.22) it is clear that $g(x, y, t)$ can be regarded as the wave function corresponding to a delta function time dependence of the source.

§ 3. *The scalar wave generated by an impulsive point source.* The three-dimensional wave function $u = u(x, y, z, t)$ due to the presence of a point source acting at $x = 0, y = 0, z = 0$ satisfies the three-dimensional wave equation

$$\frac{\partial^2 u}{\partial x^2} + \frac{\partial^2 u}{\partial y^2} + \frac{\partial^2 u}{\partial z^2} - \frac{1}{v^2} \frac{\partial^2 u}{\partial t^2} = -\delta(x, y, z) f(t), \quad (3.1)$$

where $\delta(x, y, z)$ denotes the three-dimensional delta function. Again, we assume that, outside the source, u is continuous and has continuous partial derivatives of the first and second order. Further, $f(t) = 0$ when $t < 0$ and $u \equiv 0$ when $t < 0$. The following one-sided Laplace transforms with respect to time are introduced

$$F(s) = \int_0^\infty \exp(-st) f(t) dt \quad (3.2)$$

and

$$U(x, y, z; s) = \int_0^\infty \exp(-st) u(x, y, z, t) dt. \quad (3.3)$$

Since u and $\partial u / \partial t$ are continuous, $U(x, y, z; s)$ satisfies the differential equation

$$-\frac{\partial^2 U}{\partial x^2} + \frac{\partial^2 U}{\partial y^2} + \frac{\partial^2 U}{\partial z^2} - \frac{s^2}{v^2} U = -\delta(x, y, z) F(s). \quad (3.4)$$

In order to solve (3.4) we introduce the two-dimensional Fourier transform of $U(x, y, z; s)$ with respect to x and y . Let

$$\mathcal{U}(\alpha, \beta; z; s) = \int_{-\infty}^{\infty} dy \int_{-\infty}^{\infty} \exp[is(\alpha x + \beta y)] U(x, y, z; s) dx. \quad (3.5)$$

Then $\mathcal{U}(\alpha, \beta; z; s)$ satisfies the differential equation

$$\frac{d^2 \mathcal{U}}{dz^2} - s^2 \gamma^2 \mathcal{U} = -\delta(z) F(s), \quad (3.6)$$

where

$$\gamma = \gamma(\alpha, \beta) = (\alpha^2 + \beta^2 + 1/v^2)^{\frac{1}{2}} \quad (\text{Re } \gamma \geq 0). \quad (3.7)$$

The solution of (3.7) that is bounded as $|z| \rightarrow \infty$ is given by

$$\mathcal{U}(\alpha, \beta; z; s) = \frac{F(s)}{2s\gamma} \exp(-s\gamma |z|). \quad (3.8)$$

With the aid of Fourier's inversion theorem we obtain the following expression for $U(x, y, z; s)$:

$$U(x, y, z; s) = \frac{sF(s)}{4\pi^2} \int_{-\infty}^{\infty} d\beta \int_{-\infty}^{\infty} \exp[-is(\alpha x + \beta y) - s\gamma |z|] \frac{1}{2\gamma} d\alpha. \quad (3.9)$$

Again, we shall try to cast the integral on the right-hand side of (3.9) in such a form that $u(x, y, z, t)$ can be found more or less by inspection. It will be advantageous to transform the exponential function into a form which resembles the one occurring in the two-dimensional problem. This is accomplished by introducing new variables of integration ω and q through

$$\alpha = \omega \cos \varphi - q \sin \varphi, \quad \beta = \omega \sin \varphi + q \cos \varphi. \quad (3.10)$$

Since $d\alpha d\beta = d\omega dq$, we obtain

$$U(x, y, z; s) = \frac{sF(s)}{4\pi^2} \int_{-\infty}^{\infty} dq \int_{-\infty}^{\infty} \exp[-is\omega r - s\gamma |z|] \frac{1}{2\gamma} d\omega, \quad (3.11)$$

in which, as $\alpha^2 + \beta^2 = \omega^2 + q^2$,

$$\gamma = (\omega^2 + q^2 + 1/v^2)^{\frac{1}{2}} \quad (\operatorname{Re} \gamma \geq 0). \quad (3.12)$$

In order to bring the right-hand side of (3.11) in a form which is analogous to the two-dimensional case, we introduce the variable $p = i\omega$ and regard p as a complex variable in the p -plane, while q is kept real. The result is

$$U(x, y, z; s) = \frac{sF(s)}{4\pi^2 i} \int_{-\infty}^{\infty} dq \int_{-i\infty}^{i\infty} \exp[-s(pr + \gamma|z|)] \frac{1}{2\gamma} d\phi, \quad (3.13)$$

in which

$$\gamma = (q^2 + 1/v^2 - p^2)^{\frac{1}{2}} \quad (\operatorname{Re} \gamma \geq 0). \quad (3.14)$$

From now on, the procedure is similar to the one outlined in § 2. By virtue of Cauchy's theorem and Jordan's lemma the integration along the imaginary p -axis can be replaced by an integration along the branch Γ of a hyperbola, where Γ is given through

$$p = \frac{r}{R^2} \tau \pm i \frac{|\hat{z}|}{R^2} [\tau^2 - R^2(q^2 + 1/v^2)]^{\frac{1}{2}} \\ (R(q^2 + 1/v^2)^{\frac{1}{2}} < \tau < \infty). \quad (3.15)$$

Along Γ we have

$$\gamma = \frac{|z|}{R^2} \tau \mp i \frac{r}{R^2} [\tau^2 - R^2(q^2 + 1/v^2)]^{\frac{1}{2}} \quad (3.16)$$

and

$$\frac{\partial p}{\partial \tau} = \pm \frac{i\gamma}{[\tau^2 - R^2(q^2 + 1/v^2)]^{\frac{1}{2}}}. \quad (3.17)$$

In (3.15), (3.16) and (3.17) the upper and lower signs belong together. Taking into account the symmetry of the path of integration with respect to the real axis and introducing τ as variable of integration we obtain

$$U(x, y, z; s) = \\ = \frac{sF(s)}{4\pi^2} \int_{-\infty}^{\infty} dq \int_{R(q^2 + 1/v^2)^{\frac{1}{2}}}^{\infty} \exp(-s\tau) [\tau^2 - R^2(q^2 + 1/v^2)]^{-\frac{1}{2}} d\tau. \quad (3.18)$$

Now we interchange the order of integration, which leads to

$$\begin{aligned}
 U(x, y, z; s) &= \\
 &= \frac{sF(s)}{4\pi^2} \int_{R/v}^{\infty} \exp(-s\tau) d\tau \int_{-(\tau^2/R^2 - 1/v^2)^{1/2}}^{(\tau^2/R^2 - 1/v^2)^{1/2}} [\tau^2 - R^2(q^2 + 1/v^2)]^{-1/2} dq \\
 &= \frac{sF(s)}{4\pi R} \int_{R/v}^{\infty} \exp(-s\tau) d\tau,
 \end{aligned}$$

or

$$U(x, y, z; s) = F(s) \frac{\exp(-sR/v)}{4\pi R}. \quad (3.19)$$

Application of the shift rule yields the well-known result

$$u(x, y, z, t) = \frac{f(t - R/v)}{4\pi R}. \quad (3.20)$$

§ 4. *Conclusion.* The procedure outlined in the present paper provides a method by means of which several mixed initial-boundary value problems can be solved. For *two-dimensional problems* also other methods are available, in particular the "method of conical flow". This method has been applied by Maue¹²⁾ and, more recently, by Miles¹³⁾ to several two-dimensional problems in elastodynamics.

Received 19th May, 1960.

REFERENCES

- 1) Cagniard, L., *Réflexion et réfraction des ondes séismiques progressives*, Gauthier-Villars, Paris 1939.
- 2) Dix, C. H., *Geophysics* **19** (1954) 722.
- 3) Hoop, A. T. de, The surface line source problem, Second Annual Report Seismic Scattering Project, Institute of Geophysics, University of California, Los Angeles, California, U.S.A., 1957.
- 4) Hoop, A. T. de, Representation theorems for the displacement in an elastic solid and their application to elastodynamic diffraction theory, Thesis, Delft, Netherlands, 1958; Ch. IV.
- 5) Pekeris, C. L., *Proc. Nat. Acad. Sci.* **41** (1955) 469.
- 6) Pekeris, C. L., *Proc. Nat. Acad. Sci.* **41** (1955) 629.
- 7) Pekeris, C. L., *Proc. Nat. Acad. Sci.* **42** (1956) 439.
- 8) Pekeris, C. L. and Z. Alterman, *J. Appl. Phys.* **28** (1957) 1317.
- 9) Pekeris, C. L. and H. Lifson, *J. Acoust. Soc. Amer.* **29** (1957) 1233.
- 10) Pekeris, C. L. and I. M. Longman, *J. Acoust. Soc. Amer.* **30** (1958) 323.
- 11) Whittaker, E. T. and G. N. Watson, *A course of modern analysis*, 4th ed., p. 115, Cambridge 1950.
- 12) Maue, A. - W., *Z. angew. Math. Mech.* **34** (1954) 1.
- 13) Miles, J. W., Homogeneous solutions in elastic wave propagation. Report GM-TR-0165-00350 of Space Technology Laboratories, Ramo-Wooldridge Corporation, Los Angeles, California, U.S.A., 1958; also *Quart. Appl. Math.* **18** (1960) 37.

TRANSIENT PHENOMENA ASSOCIATED WITH
SOMMERFELD'S HORIZONTAL DIPOLE PROBLEM

by H. J. FRANKENA

Laboratorium voor Theoretische Elektrotechniek, Technische Hogeschool, Delft,
Netherlands**Summary**

A horizontal electric dipole, located above the plane interface of two non-conducting media, has a dipole moment which is an arbitrary but given function of time when $t > 0$ and which is zero when $t < 0$. Travelling electromagnetic waves, generated by this dipole, are calculated with the aid of a modification of Cagniard's method. For the electric field vector above and at the interface we obtain expressions for the direct and reflected waves in the case that the velocity of light in the medium containing the source is the larger one.

§ 1. *Introduction.* The electromagnetic radiation from an electric dipole, located above the plane interface of two media has been calculated in 1909 by Sommerfeld¹⁾ for a vertical dipole; in 1912 von Hoerschelmann²⁾ solved the corresponding problem for a horizontal dipole. The relevant solutions apply to the case that the dipole moment varies harmonically in time. In the years thereafter a large number of authors have devoted papers to this problem; a comprehensive treatment and an extensive bibliography can be found in two reports by Baños and Wesley³⁾.

The transient field from a dipole, located at the interface of two media, was the subject of recent papers by several authors. Poritsky⁴⁾ obtained results by generalizing Weyl's method for the steady-state case, while Van der Pol⁵⁾, Pekeris and Alterman⁶⁾, Bremmer⁷⁾ and Levelt⁸⁾ applied integral transforms in order to get a solution. Pekeris and Alterman have made use of a method related to a technique developed by Cagniard⁹⁾ in connection with problems in seismic wave propagation. This method in the

form, given in their paper, however, seems to be unnecessarily complicated.

In the present paper we employ a simplified procedure, based on the method developed by De Hoop^{10,11)} in relation to problems in elastic wave propagation. The expressions we derive are valid for a dipole, located above the interface of two media, whose moment is zero for negative values of time and is an arbitrary, but given, function of time for positive values of time. For simplicity, we consider only the case that the velocity of light in the medium containing the dipole is the larger one. In this medium and at the interface we calculate the electric field intensity; from this the magnetic field vector can be found with the aid of Maxwell's equations. The calculations are carried out for a horizontal *electric* dipole; the solutions for a horizontal *magnetic* dipole follow from these results by the interchanges

$$\mathbf{E} \rightarrow \mathbf{H}, \mathbf{H} \rightarrow -\mathbf{E}, \varepsilon \rightarrow \mu, \mu \rightarrow \varepsilon.$$

§ 2. *Mathematical formulation.* We introduce a system of Cartesian coordinates x, y, z . The half-space $z > 0$ is occupied by a medium with dielectric constant ε_1 and magnetic permeability μ_1 , the half-space $z < 0$ by a medium where these constants have the values ε_2 and μ_2 , respectively. Both media are homogeneous; the conductivity is assumed to be zero everywhere. A horizontal electric dipole is located at the point $x = y = 0, z = h > 0$, having a dipole moment $f(t) \mathbf{i}_x$, where $f(t) = 0$ when $t < 0$ and \mathbf{i}_x denotes the unit vector in the x -direction.

If \mathbf{E} indicates the electric field vector, we obtain from Maxwell's equations the following inhomogeneous wave equation:

$$\nabla^2 \mathbf{E} - \frac{\partial^2 \mathbf{E}}{\partial t^2} = \frac{1}{\varepsilon} \text{grad } \rho + \frac{\partial \mathbf{J}}{\partial t}, \quad (2.1)$$

where ρ and \mathbf{J} are the densities of the charge and the current, respectively. We now adopt the notation

$$\begin{aligned} \mathbf{E}(x, y, z, t) &= \mathbf{E}^{(0)}(x, y, z, t) + \mathbf{E}^{(1)}(x, y, z, t) & (z > 0), \\ \mathbf{E}(x, y, z, t) &= \mathbf{E}^{(2)}(x, y, z, t) & (z < 0). \end{aligned}$$

Here $\mathbf{E}^{(0)}$ denotes the primary field, i.e. the field, the dipole would generate if the entire space were occupied by a medium with

$\varepsilon = \varepsilon_1$, $\mu = \mu_1$ and conductivity equal to zero. From (2.1) it is seen that $\mathbf{E}^{(0)}$, $\mathbf{E}^{(1)}$ and $\mathbf{E}^{(2)}$ must satisfy the wave equations

$$\nabla^2 \mathbf{E}^{(0)} - v_1^{-2} \frac{\partial^2 \mathbf{E}^{(0)}}{\partial t^2} = \frac{1}{\varepsilon_1} \text{grad } \rho + \mu_1 \frac{\partial \mathbf{J}}{\partial t}, \quad (2.2)$$

$$\nabla^2 \mathbf{E}^{(n)} - v_n^{-2} \frac{\partial^2 \mathbf{E}^{(n)}}{\partial t^2} = \mathbf{0} \quad (n = 1, 2), \quad (2.3)$$

with

$$v_n = (\varepsilon_n \mu_n)^{-\frac{1}{2}}. \quad (2.4)$$

In (2.2) we introduce the electric moment per unit volume \mathbf{m} through

$$\mathbf{J} = \frac{\partial \mathbf{m}}{\partial t} = \frac{df(t)}{dt} \delta(x, y, z - h) \mathbf{i}_x; \quad (2.5)$$

from the conservation of charge it then follows, that

$$\rho = -f(t) \frac{\partial}{\partial x} [\delta(x, y, z - h)]. \quad (2.6)$$

Inserting this we obtain from (2.2) the equation

$$\begin{aligned} \nabla^2 \mathbf{E}^{(0)} - v_1^{-2} \frac{\partial^2 \mathbf{E}^{(0)}}{\partial t^2} = & -\frac{f(t)}{\varepsilon_1} \text{grad} \left\{ \frac{\partial}{\partial x} [\delta(x, y, z - h)] \right\} + \\ & + \mu_1 \frac{d^2 f(t)}{dt^2} \delta(x, y, z - h) \mathbf{i}_x. \end{aligned} \quad (2.7)$$

The boundary conditions at the interface require the continuity of the tangential components of the electric and magnetic field vectors. By elimination of the magnetic field vector with the aid of Maxwell's equations these conditions can be written as four linear relations between the components of $\mathbf{E}^{(0)}$, $\mathbf{E}^{(1)}$ and $\mathbf{E}^{(2)}$ at points of the interface.

Finally, the fields must be solutions of the wave equations (2.3) and (2.7) that satisfy

$$\text{div } \mathbf{E}^{(n)} = 0 \quad (n = 1, 2) \quad (2.8)$$

at each point of the appropriate half-space and

$$\text{div } \mathbf{E}^{(0)} = 0 \quad (2.9)$$

everywhere outside the source.

§ 3. *Application of integral transforms.* We now perform three integral transforms on the functions occurring in (2.3) and (2.7): a one-sided Laplace transform with respect to time and a Fourier transform with respect to x and y , respectively. Our notation is

$$\mathbf{E}(x, y, z; s) = \int_0^{\infty} \mathbf{E}(x, y, z, t) \exp(-st) dt, \quad (3.1)$$

$$\mathbf{F}(\alpha, \beta; z; s) = \int_{-\infty}^{\infty} \int_{-\infty}^{\infty} \mathbf{E}(x, y, z; s) \exp(-is\alpha x - is\beta y) dx dy. \quad (3.2)$$

Throughout the paper s is a real, positive parameter.

At first we consider the primary field. We assume this field together with its first time-derivative to be zero at $t = 0$; then its transformed components $F_k^{(0)}$ satisfy differential equations of the form

$$\frac{\partial^2 F_k^{(0)}}{\partial z^2} - s^2 \gamma_1^2 F_k^{(0)} = \frac{sf(s)}{2\varepsilon_1} X_k(\alpha, \beta; z; s), \quad (3.3)$$

where

$$\gamma_1 = (\alpha^2 + \beta^2 + v_1^{-2})^{\frac{1}{2}}, \quad (3.4)$$

$$f(s) = \int_0^{\infty} f(t) \exp(-st) dt \quad (3.5)$$

and where $X_k(\alpha, \beta; z; s)$ can be found by transformation of (2.7). The function γ_1 is chosen as that branch of the square root for which

$$\operatorname{Re} \gamma_1 \geq 0. \quad (3.6)$$

The solutions of the differential equations (3.3), which are bounded as $|z| \rightarrow \infty$, are then

$$\mathbf{F}^{(0)} = \frac{sf(s)}{2\varepsilon_1} \mathbf{A}^{(0)} \exp(-s\gamma_1 |z - h|), \quad (3.7)$$

in which the components of $\mathbf{A}^{(0)}$ are found as

$$A_x^{(0)} = -\frac{1}{\gamma_1} (\alpha^2 + v_1^{-2}), \quad (3.8)$$

$$A_y^{(0)} = -\frac{1}{\gamma_1} \alpha \beta, \quad (3.9)$$

$$A_z^{(0)} = \mp i\alpha. \quad (3.10)$$

In (3.10) the upper sign applies to the domain $z > h$, the lower sign to $z < h$.

The functions $\mathbf{F}^{(1)}$ and $\mathbf{F}^{(2)}$ are solutions of the homogeneous differential equations

$$\frac{\partial^2 \mathbf{F}^{(n)}}{\partial z^2} - s^2 \gamma_n^2 \mathbf{F}^{(n)} = \mathbf{0} \quad (n = 1, 2), \quad (3.11)$$

where

$$\gamma_n = (\alpha^2 + \beta^2 + v_n^{-2})^{\frac{1}{2}} \quad (n = 1, 2). \quad (3.12)$$

If we choose γ_n as that branch of the square root for which

$$\operatorname{Re} \gamma_n \geq 0, \quad (3.13)$$

the solutions, that are bounded as $|z| \rightarrow \infty$, can be written as

$$\mathbf{F}^{(1)} = \frac{sf(s)}{2\varepsilon_1} \mathbf{A}^{(1)} \exp[-s\gamma_1(z+h)], \quad (3.14)$$

$$\mathbf{F}^{(2)} = \frac{sf(s)}{2\varepsilon_1} \mathbf{A}^{(2)} \exp[-s\gamma_1 h + s\gamma_2 z]. \quad (3.15)$$

The functions $\mathbf{A}^{(1)}$ and $\mathbf{A}^{(2)}$ must satisfy six linear equations, two of which result from the divergence conditions (2.8) and the remaining four from the boundary conditions. The solutions of these equations are

$$A_x^{(1)} = \frac{\alpha^2}{\gamma_1} + \frac{\mu_1\gamma_2 - \mu_2\gamma_1}{v_1^2\gamma_1 D} - 2\varepsilon_1\alpha^2 \frac{\mu_1\gamma_1 + \mu_2\gamma_2}{D\Delta}, \quad (3.16)$$

$$A_y^{(1)} = \frac{\alpha\beta}{\gamma_1} - 2\varepsilon_1\alpha\beta \frac{\mu_1\gamma_1 + \mu_2\gamma_2}{D\Delta}, \quad (3.17)$$

$$A_z^{(1)} = i\alpha \frac{\varepsilon_2\gamma_1 - \varepsilon_1\gamma_2}{\Delta}, \quad (3.18)$$

$$A_x^{(2)} = -2\varepsilon_1 \frac{\mu_1\mu_2}{D} - 2\varepsilon_1\alpha^2 \frac{\mu_1\gamma_1 + \mu_2\gamma_2}{D\Delta}, \quad (3.19)$$

$$A_y^{(2)} = -2\varepsilon_1\alpha\beta \frac{\mu_1\gamma_1 + \mu_2\gamma_2}{D\Delta}, \quad (3.20)$$

$$A_z^{(2)} = 2i\varepsilon_1\alpha \frac{\gamma_1}{\Delta}, \quad (3.21)$$

with the abbreviations

$$D = \mu_1\gamma_2 + \mu_2\gamma_1 \quad (3.22)$$

and

$$\Delta = \varepsilon_1 \gamma_2 + \varepsilon_2 \gamma_1. \quad (3.23)$$

Using the inversion formula for the Fourier transform (Sneddon¹²) we obtain with (3.7), (3.14) and (3.15)

$$\begin{aligned} E^{(0)}(x, y, z; s) = & \\ = \frac{s^3 f(s)}{8\pi^2 \varepsilon_1} \int_{-\infty}^{\infty} \int_{-\infty}^{\infty} A^{(0)}(\alpha, \beta) \exp[-s|z-h| \gamma_1(\alpha, \beta) + & \\ + is\alpha x + is\beta y] d\alpha d\beta, & \quad (3.24) \end{aligned}$$

$$\begin{aligned} E^{(1)}(x, y, z; s) = & \\ = \frac{s^3 f(s)}{8\pi^2 \varepsilon_1} \int_{-\infty}^{\infty} \int_{-\infty}^{\infty} A^{(1)}(\alpha, \beta) \exp[-s(z+h) \gamma_1(\alpha, \beta) + & \\ + is\alpha x + is\beta y] d\alpha d\beta, & \quad (3.25) \end{aligned}$$

$$\begin{aligned} E^{(2)}(x, y, z; s) = & \\ = \frac{s^3 f(s)}{8\pi^2 \varepsilon_1} \int_{-\infty}^{\infty} \int_{-\infty}^{\infty} A^{(2)}(\alpha, \beta) \exp[-sh\gamma_1(\alpha, \beta) + & \\ + sz\gamma_2(\alpha, \beta) + is\alpha x + is\beta y] d\alpha d\beta. & \quad (3.26) \end{aligned}$$

§ 4. *Application of Cagniard's method.* We shall reduce the expressions (3.24) and (3.25) to a form which is directly amenable for application of Cagniard's technique. This is easily accomplished when we replace x, y, z by the cylindrical coordinates r, φ, z through the relations

$$x = r \cos \varphi, \quad y = r \sin \varphi, \quad z = z.$$

The crucial step (cf. De Hoop¹¹) now consists of replacing the variables of integration α, β by the variables p, q through

$$\alpha = p \cos \varphi - q \sin \varphi, \quad (4.1)$$

$$\beta = p \sin \varphi + q \cos \varphi. \quad (4.2)$$

Inserting this in the expressions (3.24) and (3.25) we get

$$\begin{aligned} E^{(0)}(r, \varphi, z; s) = & \\ = \frac{s^3 f(s)}{8\pi^2 \varepsilon_1} \int_{-\infty}^{\infty} \int_{-\infty}^{\infty} A^{(0)}(p, q) \exp[-s|z-h| \gamma_1(p, q) + isrp] dp dq, & \quad (4.3) \end{aligned}$$

$$\begin{aligned} \mathbf{E}^{(1)}(r, \varphi, z; s) = \\ = \frac{s^3 f(s)}{8\pi^2 \varepsilon_1} \int_{-\infty}^{\infty} \int_{-\infty}^{\infty} \mathbf{A}^{(1)}(p, q) \exp[-s(z+h) \gamma_1(p, q) + isrp] dp dq, \quad (4.4) \end{aligned}$$

where

$$\gamma_n(p, q) = (p^2 + q^2 + v_n^{-2})^{\frac{1}{2}} \quad (n = 1, 2). \quad (4.5)$$

The functions $\mathbf{A}^{(0)}(p, q)$ and $\mathbf{A}^{(1)}(p, q)$ are obtained by substitution of (4.1) and (4.2) into the forms (3.8)–(3.10) and (3.16)–(3.18).

Taking into account the condition

$$\operatorname{Re} \gamma_n \geq 0 \quad (n = 1, 2) \quad (4.6)$$

it can be verified that the only singularities of the integrands in (4.3) and (4.4) are branch points in the complex p -plane at $p = \pm i(q^2 + v_n^{-2})^{\frac{1}{2}}$. In view of subsequent modifications of the path of integration in the p -plane, we impose the condition (4.6) at any point of the p -plane; this implies that branch cuts have to be introduced along $\operatorname{Re} p = 0, |\operatorname{Im} p| \geq (q^2 + v_n^{-2})^{\frac{1}{2}}$, for both $n = 1$ and $n = 2$. The right-hand sides of (4.3) and (4.4) are now in a form which will enable us to obtain the field vectors as a function of time.

We replace the integrals along the real p -axis by integrals along such contours in the complex p -plane that the exponentials in the integrands of (4.3) and (4.4) can be written as $\exp(-s\tau)$, where τ is real and positive. If we introduce τ as a new variable of integration in stead of p and then interchange the order of integration, then, provided that $v_1 > v_2$, we obtain for the electric field vectors in the s -domain real expressions of the form

$$\mathbf{E}^{(m)}(R, \varphi, \theta; s) = s^3 f(s) \int_{R/v_1}^{\infty} \mathbf{A}^{(m)}(R, \varphi, \theta, \tau) \exp(-s\tau) d\tau \quad (m=0,1), \quad (4.7)$$

where R, φ and θ denote certain spherical polar coordinates. We introduce the functions $\Psi(s)$ and $\psi(t)$ through

$$\Psi(s) = s^3 f(s) = \int_0^{\infty} \psi(t) \exp(-st) dt; \quad (4.8)$$

then (4.7) can be written as

$$\mathbf{E}^{(m)}(R, \varphi, \theta; s) = \Psi(s) \mathbf{E}^{(m)}(R, \varphi, \theta; s) \quad (m = 0, 1), \quad (4.9)$$

where

$$\mathbf{E}^{(m)}(R, \varphi, \theta; s) = \int_{R/v_1}^{\infty} \mathbf{A}^{(m)}(R, \varphi, \theta, \tau) \exp(-s\tau) d\tau \quad (m=0,1). \quad (4.10)$$

From (4.8) and (4.9) it is seen, that $\mathbf{E}^{(m)}(R, \varphi, \theta; s)$ are the Laplace transforms of the electric field vectors corresponding to a dipole with moment $\frac{1}{2}t^2\mathbf{i}_x$ for $t > 0$. The fields $\mathbf{E}^{(m)}(R, \varphi, \theta, t)$ are now obtained as the convolution integrals

$$\mathbf{E}^{(m)}(R, \varphi, \theta, t) = \int_0^t \psi(t - \tau) \mathbf{E}^{(m)}(R, \varphi, \theta, \tau) d\tau \quad (m = 0, 1), \quad (4.11)$$

where $\mathbf{E}^{(m)}(R, \varphi, \theta, \tau)$ is the solution of the integral equation

$$\mathbf{E}^{(m)}(R, \varphi, \theta; s) = \int_0^\infty \mathbf{E}^{(m)}(R, \varphi, \theta, t) \exp(-st) dt \quad (m = 0, 1). \quad (4.12)$$

Using the uniqueness theorem for the Laplace transform (see e.g. Doetsch¹³) it is then seen from (4.10) and (4.12) that

$$\begin{aligned} \mathbf{E}^{(m)}(R, \varphi, \theta, t) &= \mathbf{0} & (t < R/v_1) \\ \mathbf{E}^{(m)}(R, \varphi, \theta, t) &= \mathbf{A}^{(m)}(R, \varphi, \theta, t) & (t > R/v_1) \end{aligned} \quad (m = 0, 1), \quad (4.13)$$

where τ is identified with the actual time t . In the next section the calculations of $\mathbf{E}^{(0)}(R, \varphi, \theta, t)$ and $\mathbf{E}^{(1)}(R, \varphi, \theta, t)$ are performed explicitly.

§ 5. *Explicit formulae for the field vectors.* At first we consider the primary field vector $\mathbf{E}^{(0)}(r, \varphi, z; s)$, given in (4.3). It will be convenient to introduce the spherical polar coordinates R_1, φ_1, θ_1 through

$$r = R_1 \sin \theta_1, \quad \varphi = \varphi_1, \quad z - h = R_1 \cos \theta_1.$$

We now change the contour of integration in the p -plane to the curve along which the exponential in the integrand of (4.3) can be written as $\exp(-s\tau)$, where τ is real and positive. This curve is one branch L of a hyperbola; its position is drawn in fig. 1. In the integrand of (4.3) the only singularities are the branch points $p = \pm i(q^2 + v_1^{-2})^{\frac{1}{2}}$; it is easily seen, that L intersects no branch cut. Making use of Cauchy's theorem the integral along the real p -axis can be replaced by the integral along L : the integrals along two additional circular arcs at infinity vanish by virtue of Jordan's lemma (Whittaker and Watson¹⁴). Along L we have

$$\tau = R_1(p^2 + q^2 + v_1^{-2})^{\frac{1}{2}} |\cos \theta_1| - iR_1 p \sin \theta_1; \quad (5.1)$$

solving this equation for p we find

$$p = i \frac{\tau}{R_1} \sin \theta_1 \pm \left[\frac{\tau^2}{R_1^2} - (q^2 + v_1^{-2}) \right]^{\frac{1}{2}} |\cos \theta_1|$$

$$((q^2 + v_1^{-2})^{\frac{1}{2}} \leq \tau < \infty). \quad (5.2)$$

Instead of p we introduce τ as a new variable of integration. We obtain from (4.3)

$$E^{(0)}(R_1, q_1, \theta_1; s) = \frac{s^3 f(s)}{4\pi^2 \varepsilon_1} \operatorname{Re} \int_{-\infty}^{\infty} dq \int_{\tau_1(q)}^{\infty} \frac{\partial \omega}{\partial \tau} A^{(0)}(\omega, q) \exp(-s\tau) d\tau, \quad (5.3)$$

in which p is replaced by ω , with

$$\omega = i \frac{\tau}{R_1} \sin \theta_1 + \left[\frac{\tau^2}{R_1^2} - (q^2 + v_1^{-2}) \right]^{\frac{1}{2}} |\cos \theta_1|, \quad (5.4)$$

and further

$$\tau_1(q) = R_1(q^2 + v_1^{-2})^{\frac{1}{2}}. \quad (5.5)$$

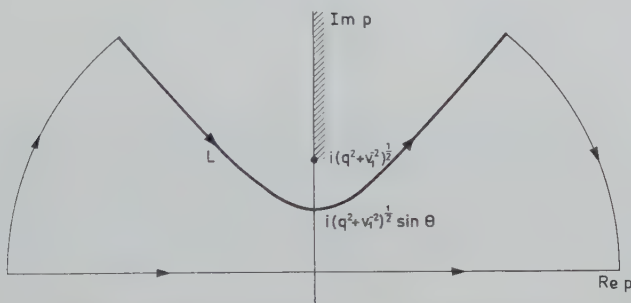


Fig. 1. Contour of integration in the p -plane.

We interchange the order of integration and find

$$E^{(0)}(R_1, q_1, \theta_1; s) =$$

$$= \frac{s^3 f(s)}{4\pi^2 \varepsilon_1 R_1} \int_{R_1/v_1}^{\infty} \exp(-s\tau) \operatorname{Re} \left[\int_{-\pi/2}^{\pi/2} \gamma_1(\tau, \psi_1) A^{(0)}(\tau, \psi_1) d\psi_1 \right] d\tau, \quad (5.6)$$

where q has been replaced by the variable ψ_1 according to

$$q = \left(\frac{\tau^2}{R_1^2} - v_1^{-2} \right)^{\frac{1}{2}} \sin \psi_1. \quad (5.7)$$

Using the substitutions (5.4) and (5.7) we find from (4.5)

$$\gamma_1(\tau, \psi_1) = \frac{\tau}{R_1} |\cos \theta_1| + i \left(\frac{\tau^2}{R_1^2} - v_1^{-2} \right)^{\frac{1}{2}} \sin \theta_1 \cos \psi_1. \quad (5.8)$$

The components of $\mathbf{A}^{(0)}(\tau, \psi_1)$ follow from substitution of (5.4), (4.1) and (4.2) into (3.8)–(3.10). Comparing (5.6) with (4.7) and making use of (4.13) it is easily seen that for the field vector $\mathbf{E}^{(0)}(R_1, \varphi_1, \theta_1, t)$, introduced at the end of the preceding section, we have

$$\begin{aligned} \mathbf{E}^{(0)}(R_1, \varphi_1, \theta_1, t) &= \mathbf{0} \quad (t < R_1/v_1), \\ \mathbf{E}^{(0)}(R_1, \varphi_1, \theta_1, t) &= \\ &= \frac{1}{4\pi^2 \varepsilon_1 R_1} \operatorname{Re} \left[\int_{-\pi/2}^{\pi/2} \gamma_1(t, \psi_1) \mathbf{A}^{(0)}(t, \psi_1) d\psi_1 \right] \quad (t > R_1/v_1). \end{aligned} \quad (5.9)$$

The primary electric field vector $\mathbf{E}^{(0)}(R_1, \varphi_1, \theta_1, t)$ is then found by insertion of (5.9) into formula (4.11).

Now we calculate the secondary field. In (4.4) we introduce another set of spherical polar coordinates R_2, φ_2, θ_2 through

$$r = R_2 \sin \theta_2, \quad \varphi = \varphi_2, \quad z + h = R_2 \cos \theta_2.$$

As before, we change the contour of integration into the curve along which the exponential in the integrand of (4.4) can be written as $\exp(-s\tau)$, where τ is real and positive. This contour is one branch of a hyperbola similar to L in fig. 1. In the case $v_1 > v_2$ this curve intersects no branch cut and we obtain, analogous to (5.6), the expression

$$\begin{aligned} \mathbf{E}^{(1)}(R_2, \varphi_2, \theta_2; s) &= \\ &= \frac{s^3 f(s)}{4\pi^2 \varepsilon_1 R_2} \int_{R_2/v_1}^{\infty} \exp(-s\tau) \operatorname{Re} \left[\int_{-\pi/2}^{\pi/2} \gamma_1(\tau, \psi_2) \mathbf{A}^{(1)}(\tau, \psi_2) d\psi_2 \right] d\tau, \end{aligned} \quad (5.10)$$

from which

$$\begin{aligned} \mathbf{E}^{(1)}(R_2, \varphi_2, \theta_2, t) &= \mathbf{0} \quad (t < R_2/v_1), \\ \mathbf{E}^{(1)}(R_2, \varphi_2, \theta_2, t) &= \\ &= \frac{1}{4\pi^2 \varepsilon_1 R_2} \operatorname{Re} \left[\int_{-\pi/2}^{\pi/2} \gamma_1(t, \psi_2) \mathbf{A}^{(1)}(t, \psi_2) d\psi_2 \right] \quad (t > R_2/v_1). \end{aligned} \quad (5.11)$$

In the latter integrand the components of $\mathbf{A}^{(1)}(t, \psi_2)$ can be found from (3.16)–(3.18) with

$$\gamma_1(t, \psi_2) = \frac{t}{R_2} \cos \theta_2 + i \left(\frac{t^2}{R_2^2} - v_1^{-2} \right)^{\frac{1}{2}} \sin \theta_2 \cos \psi_2, \quad (5.12)$$

$$\gamma_2(t, \psi_2) = [\gamma_1^2(t, \psi_2) - v_1^{-2} + v_2^{-2}]^{\frac{1}{2}}; \quad (5.13)$$

the sign of the square root in the latter expression is fixed by the condition (3.13).

§ 6. *Final remarks.* The wave fronts, corresponding to the solutions (5.9) and (5.11), are drawn in fig. 2. We remark that from the expression (5.9) the well-known formulae for the electric field of a (horizontal) dipole in free space can easily be obtained.

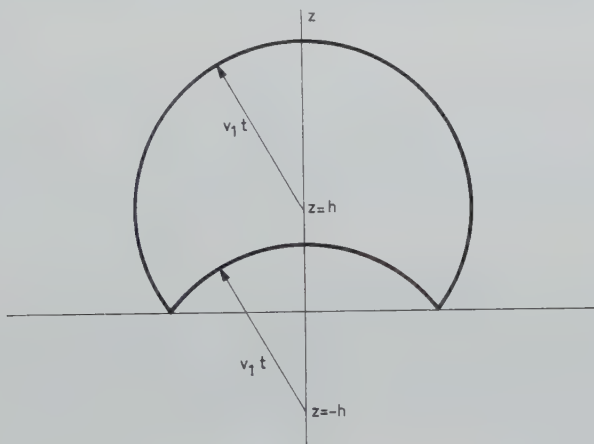


Fig. 2. Wave fronts corresponding to the two solutions given.

For field calculations when $v_1 < v_2$ the same technique as in the previous case can be applied. Then, however, the expression corresponding to (5.11) for the secondary field vector consists of several terms, corresponding to three different wave fronts (Frankena¹⁵). The additional terms arise from loop integrals around a branch cut of the complex p -plane in the domain between the real p -axis and the curve, along which the exponential in the integrand of (4.4) can be written as $\exp(-s\tau)$ (τ real and positive).

The expressions for the electric field vector below the interface can be derived from (3.26). If we introduced in this formula the

variables p and q from (4.1) and (4.2) directly, it would turn out that the presence of both square roots γ_1 and γ_2 leads to difficulties. One method of solving this problem is to reduce the integrand to a form which has an exponential function similar to those of (3.24) and (3.25). This is accomplished by writing $(s\gamma_2)^{-1} \exp(sz\gamma_2)$ as a double Fourier integral. The solution is then found again by the procedure of § 4; the field vector is obtained in the form of a representation theorem, expressing the field at a point below the interface in terms of the field at the interface.

Acknowledgement. The author is indebted to Professor J. P. Schouten and to Professor A. T. de Hoop, both of the Laboratorium voor Theoretische Elektrotechniek, Technische Hogeschool, Delft, Netherlands, for their valuable remarks and their stimulating interest in the course of this work.

Received 18th May, 1960.

REFERENCES

- 1) Sommerfeld, A., Ann. Phys., Lpz. **28** (1909) 665.
- 2) Hoerschelmann, H. von, Über die Wirkungsweise des geknickten Marconischen Senders in der drahtlosen Telegraphie, Jahrbuch der drahtlosen Telegraphie und Telephonie **5** (1912) 14-34 and 188-211.
- 3) Baños, A. Jr. and J. P. Wesley, The horizontal electric dipole in a conducting half-space, Parts I and II, University of California, Scripps Institution, 1954.
- 4) Poritsky, H., Brit. J. Appl. Phys. **6** (1955) 421.
- 5) Pol, B. van der, Trans. Instn Radio Engrs AP-4 (1956) 288.
- 6) Pekeris, C. L. and Z. Alterman, J. Appl. Phys. **28** (1957) 1317.
- 7) Bremmer, H., The surface-wave concept in connection with propagation trajectories associated with the Sommerfeld problem, paper presented at the URSI symposium on electromagnetic wave theory, held at the University of Toronto, June 15-20, 1959.
- 8) Levelt, A. H. M., Solution of the Laplace inversion problem for a special function, Mathematisch Centrum, Reports ZW 1959-010 and ZW 1959-012, Amsterdam 1959.
- 9) Cagniard, L., Réflexion et réfraction des ondes séismiques progressives, Gauthier-Villars, Paris 1939.
- 10) Hoop, A. T. de, Representation theorems for the displacement in an elastic solid and their application to elastodynamic diffraction theory, Thesis, Delft 1958.
- 11) Hoop, A. T. de, Appl. Sci. Res. B **8** (1960) 349.
- 12) Sneddon, I. N., Fourier transforms, section 3, McGraw-Hill, New York 1951.
- 13) Doetsch, G., Handbuch der Laplace-Transformation, Bd. 1, p. 74, Birkhäuser, Basel 1950.
- 14) Whittaker, E. T. and G. N. Watson, A course of modern analysis, 4th ed., p. 115, Cambridge University Press 1952.
- 15) Frankena, H. J., Transient phenomena associated with Sommerfeld's horizontal dipole problem, Report Laboratorium voor Elektrotechniek, Technische Hogeschool, Delft 1960.

RADIATION OF PULSES GENERATED BY A VERTICAL ELECTRIC DIPOLE ABOVE A PLANE, NON-CONDUCTING, EARTH

by A. T. DE HOOP and H. J. FRANKENA

Laboratorium voor Theoretische Elektrotechniek, Technische Hogeschool, Delft,
Netherlands

Summary

At a height h above a plane, non-conducting, earth a vertical electric dipole emits an impulsive electromagnetic wave. The resulting electromagnetic field in the air is determined; it consists of a reflected wave which is superimposed upon the given incident wave. The Hertzian vector corresponding to the reflected wave is expressed in terms of a single integral over a finite interval; this integral is written in such a form that its numerical evaluation can easily be performed.

§ 1. *Introduction.* In the problem of the electromagnetic radiation from a vertical electric dipole situated at a certain height h above a plane earth all field quantities are usually assumed to vary harmonically in time. One of the two well-known methods for solving this steady-state problem is due to Sommerfeld ¹⁾, the other to Weyl ²⁾. In several recent publications, however, the case is considered where the time dependence of the current in the dipole is impulsive rather than harmonic. We mention the papers by Poritsky ³⁾, Van der Pol ⁴⁾, Pekeris and Alterman ⁵⁾, Bremmer ⁶⁾ and a report by Levelt ⁷⁾. The techniques employed by these authors differ in several respects. Poritsky uses a generalization of Weyl's method to the effect that the total field is written as the superposition of a continuous system of plane pulses. Van der Pol, Pekeris and Alterman, Bremmer and Levelt make use of integral transforms or operational calculus. In this way Van der Pol obtained an elementary result when both the transmitter and the point of observation are located at the ground. Pekeris and

Alterman obtain numerical results for the field above and inside the earth in the case $h = 0$. Their technique originates from Pekeris' studies on impulsive wave propagation in elastic media. It is closely related to a similar method developed by Cagniard ⁸⁾ who, too, was concerned with the generation of seismic waves by impulsive sources.

One of the present authors developed a simplified version ⁹⁾ of the methods employed by Cagniard and by Pekeris and subsequently applied the simplified procedure to the determination of the surface displacement generated by an interior source in an elastic half-space ¹⁰⁾. In the present paper the latter technique is used to determine the electromagnetic field radiated by a vertical electric dipole located above a plane, non-conducting, earth. The electric moment of the dipole varies in time as a given function $f(t)$, with $f(t) = 0$ when $t < 0$. The attention is confined to the field in the air; unless $h = 0$ (see ⁵⁾), the determination of the field inside the earth is much more difficult. Our result is given in the form of a definite integral over a finite interval; this integral can easily be computed numerically.

§ 2. *Statement of the problem and method of solution.* We consider the electromagnetic field in either of two homogeneous, isotropic, semi-infinite media with different electromagnetic properties. A Cartesian coordinate system is introduced such that the upper medium (the air) occupies the half-space $0 < z < \infty$, while the lower medium (the earth) occupies the half-space $-\infty < z < 0$. Their common boundary is the plane $z = 0$. A point in space will be located by either its Cartesian coordinates or its cylindrical coordinates r, φ, z defined through

$$x = r \cos \varphi, \quad y = r \sin \varphi, \quad z = z, \quad (2.1)$$

with $0 \leq r < \infty$, $0 \leq \varphi < 2\pi$, $-\infty < z < \infty$. The electromagnetic properties of the media are characterized by their permittivity ε and their permeability μ ; their conductivity is assumed to be zero. For the upper medium we have $\varepsilon = \varepsilon_1$ and $\mu = \mu_1$, for the lower medium we have $\varepsilon = \varepsilon_2$ and $\mu = \mu_2$.

At $x=0, y=0, z=h$ ($h>0$) a vertical electric dipole starts to radiate at the instant $t=0$; it is assumed that prior to this instant all field quantities vanish identically. It is well-known (see, e.g., Stratton ¹¹⁾)

that the electromagnetic field generated by this vertical dipole can be derived from a Hertzian vector $\mathbf{\Pi}$ of which only the z -component is different from zero. The electric field vector \mathbf{E} and the magnetic field vector \mathbf{H} are expressed in terms of $\mathbf{\Pi}$ through the relations

$$\mathbf{E} = \text{grad div } \mathbf{\Pi} - \varepsilon\mu \frac{\partial^2 \mathbf{\Pi}}{\partial t^2}, \quad (2.2)$$

$$\mathbf{H} = \varepsilon \text{curl } \frac{\partial \mathbf{\Pi}}{\partial t}. \quad (2.3)$$

In the region $z > 0$ we write

$$\mathbf{\Pi} = (u_0 + u_1) \mathbf{i}_z \quad (0 < z < \infty), \quad (2.4)$$

where u_0 yields the incident wave, i.e. the field that would exist if the upper medium were unbounded, while u_1 accounts for the reflection of the incident wave against the interface and is defined as the difference between the actual Hertzian vector and $u_0 \mathbf{i}_z$. Similarly, in the region $z < 0$ we write

$$\mathbf{\Pi} = u_2 \mathbf{i}_z \quad (-\infty < z < 0), \quad (2.5)$$

where u_2 yields the refracted field. At any interior point of the appropriate half-spaces $u_1 = u_1(x, y, z, t)$ and $u_2 = u_2(x, y, z, t)$ are assumed to be continuous together with their first and second order partial derivatives. In the region $z > 0$ the function u_1 satisfies the homogeneous wave equation

$$\Delta u_1 - \frac{1}{v_1^2} \frac{\partial^2 u_1}{\partial t^2} = 0; \quad (2.6)$$

in the region $z < 0$ the function u_2 satisfies the differential equation

$$\Delta u_2 - \frac{1}{v_2^2} \frac{\partial^2 u_2}{\partial t^2} = 0. \quad (2.7)$$

In these equations $\Delta = \partial^2/\partial x^2 + \partial^2/\partial y^2 + \partial^2/\partial z^2$ denotes the three-dimensional Laplacian; further,

$$v_1 = (\varepsilon_1 \mu_1)^{-\frac{1}{2}} \quad (2.8)$$

and

$$v_2 = (\varepsilon_2 \mu_2)^{-\frac{1}{2}} \quad (2.9)$$

are the velocities of propagation in the upper and lower medium, respectively. The function u_0 is given by ¹²⁾

$$u_0 = \frac{1}{4\pi\epsilon_1} \frac{f(t - R_1/v_1)}{R_1}, \quad (2.10)$$

where

$$R_1 = [x^2 + y^2 + (z - h)^2]^{\frac{1}{2}}. \quad (2.11)$$

The function $f(t)$ determines the electric moment of the dipole as a function of time as can be seen from the equation

$$\Delta u_0 - \frac{1}{v_1^2} \frac{\partial^2 u_0}{\partial t^2} = -\frac{1}{\epsilon_1} \delta(x, y, z - h) f(t), \quad (2.12)$$

where $\delta(x, y, z - h)$ denotes, in a usual notation, the three-dimensional delta function. According to our assumptions, $f(t) = 0$ when $-\infty < t < 0$. The continuity of E_x , E_y , H_x and H_y at the interface is guaranteed if the following boundary conditions are satisfied:

$$\lim_{z \rightarrow +0} \left(\frac{\partial u_0}{\partial z} + \frac{\partial u_1}{\partial z} \right) = \lim_{z \rightarrow -0} \frac{\partial u_2}{\partial z}, \quad (2.13)$$

$$\epsilon_1 \lim_{z \rightarrow +0} (u_0 + u_1) = \epsilon_2 \lim_{z \rightarrow -0} u_2. \quad (2.14)$$

All field quantities occurring in the problem are now subjected to a one-sided Laplace transform with respect to time; e.g.,

$$F(s) = \int_0^{\infty} \exp(-st) f(t) dt. \quad (2.15)$$

Similarly, U_0 , U_1 and U_2 denote the Laplace transforms of u_0 , u_1 and u_2 , respectively. Following Cagniard ⁸⁾, s is restricted to real positive values large enough to ensure the convergence of the integrals of the type (2.15) (it is tacitly assumed that the behaviour of the relevant functions as $t \rightarrow \infty$ is such that such a number s can be found). Since, in particular, u_1 , $\partial u_1/\partial t$, u_2 and $\partial u_2/\partial t$ are continuous, $U_1 = U_1(x, y, z; s)$ and $U_2 = U_2(x, y, z; s)$ satisfy the differential equations

$$\Delta U_1 - \frac{s^2}{v_1^2} U_1 = 0 \quad (2.16)$$

and

$$\Delta U_2 - \frac{s^2}{v_2^2} U_2 = 0, \quad (2.17)$$

respectively. The next step is to introduce the two-dimensional Fourier transforms of $U_1(x, y, z; s)$ and $U_2(x, y, z; s)$ with respect to x and y . Let

$$\mathcal{U}_{1,2}(\alpha, \beta; z; s) = \int_{-\infty}^{\infty} dy \int_{-\infty}^{\infty} \exp[is(\alpha x + \beta y)] U_{1,2}(x, y, z; s) dx, \quad (2.18)$$

in which the (real) factor s in the argument of the exponential function has been included for convenience. If \mathcal{U}_1 and \mathcal{U}_2 were known, U_1 and U_2 could be determined from the inversion integral

$$U_{1,2}(x, y, z; s) = \frac{s^2}{4\pi^2} \int_{-\infty}^{\infty} d\beta \int_{-\infty}^{\infty} \exp[-is(\alpha x + \beta y)] \mathcal{U}_{1,2}(\alpha, \beta; z; s) d\alpha. \quad (2.19)$$

The corresponding representation of $U_0(x, y, z; s)$ is known to be ⁹⁾

$$\begin{aligned} U_0(x, y, z; s) &= \\ &= \frac{sF(s)}{4\pi^2 \varepsilon_1} \int_{-\infty}^{\infty} d\beta \int_{-\infty}^{\infty} \exp[-s(i\alpha x + i\beta y + \gamma_1 z - h)] \frac{1}{2\gamma_1} d\alpha, \end{aligned} \quad (2.20)$$

in which

$$\gamma_1 = \gamma_1(\alpha, \beta) = (\alpha^2 + \beta^2 + 1/v_1^2)^{\frac{1}{2}} \quad (\text{Re } \gamma_1 \geq 0). \quad (2.21)$$

Since the boundary conditions are independent of time, they reduce to

$$\lim_{z \rightarrow +0} \left(\frac{\partial U_0}{\partial z} + \frac{\partial U_1}{\partial z} \right) = \lim_{z \rightarrow -0} \frac{\partial U_2}{\partial z}, \quad (2.22)$$

$$\varepsilon_1 \lim_{z \rightarrow +0} (U_0 + U_1) = \varepsilon_2 \lim_{z \rightarrow -0} U_2. \quad (2.23)$$

In order to determine \mathcal{U}_1 and \mathcal{U}_2 we substitute the corresponding representations of U_1 and U_2 (compare (2.19)) in the differential equations (2.16) and (2.17). This procedure leads to two ordinary differential equations for \mathcal{U}_1 and \mathcal{U}_2 , respectively, with z as independent variable. The solutions that remain bounded as $|z| \rightarrow \infty$ can be written as

$$\mathcal{U}_1 = \frac{F(s)}{s} \mathcal{A}_1 \exp[-s\gamma_1(z + h)], \quad (2.24)$$

$$\mathcal{U}_2 = \frac{F(s)}{s} \mathcal{A}_2 \exp[s(\gamma_2 z - \gamma_1 h)], \quad (2.25)$$

where γ_1 is given by (2.21) and γ_2 by

$$\gamma_2 = \gamma_2(\alpha, \beta) = (\alpha^2 + \beta^2 + 1/v_2^2)^{\frac{1}{2}} \quad (\text{Re } \gamma_2 \geq 0). \quad (2.26)$$

The functions $\mathcal{A}_1 = \mathcal{A}_1(\alpha, \beta)$ and $\mathcal{A}_2 = \mathcal{A}_2(\alpha, \beta)$ follow from the boundary conditions at the interface. It is found that

$$\mathcal{A}_1 = \frac{\varepsilon_2 \gamma_1 - \varepsilon_1 \gamma_2}{\varepsilon_2 \gamma_1 + \varepsilon_1 \gamma_2} \frac{1}{2\varepsilon_1 \gamma_1}, \quad (2.27)$$

$$\mathcal{A}_2 = \frac{1}{\varepsilon_2 \gamma_1 + \varepsilon_1 \gamma_2}. \quad (2.28)$$

From these results the Hertzian vector in the upper medium will be determined. Since the incident wave u_0 is already known, we are left with the problem of determining the reflected wave u_1 . Equations (2.19) and (2.24) show that $U_1 = U_1(x, y, z; s)$ is of the form

$$U_1(x, y, z; s) = sF(s) G_1(x, y, z; s), \quad (2.29)$$

where

$$\begin{aligned} G_1(x, y, z; s) &= \\ &= \frac{1}{4\pi^2} \int_{-\infty}^{\infty} d\beta \int_{-\infty}^{\infty} \exp\{-s[i\alpha x + i\beta y + \gamma_1(z+h)]\} \mathcal{A}_1(\alpha, \beta) d\alpha. \end{aligned} \quad (2.30)$$

From now on we restrict the discussion to the case $v_2 < v_1$. In § 3 it will be shown that then the integral at the right-hand side of (2.30) can be transformed into

$$G_1(x, y, z; s) = \int_{R_2/v_1}^{\infty} \exp(-s\tau) g_1(x, y, z, \tau) d\tau, \quad (2.31)$$

where only *real* values of τ occur in the integration and where R_2 is given by

$$R_2 = [x^2 + y^2 + (z+h)^2]^{\frac{1}{2}} \quad (2.32)$$

(R_2 = distance from the image of the source to the point of observation). Now we observe that $sF(s) \exp(-s\tau)$ is the Laplace transform of a function of time that vanishes when $t < \tau$ and equals $df(t-\tau)/dt$ when $\tau < t$. Using the notation $df/dt = f'$ we finally obtain for the z -component of the Hertzian vector corresponding to the reflected wave

$$u_1(x, y, z, t) = \begin{cases} 0 & (0 < t < R_2/v_1), \\ \int_{R_2/v_1}^t f'(t-\tau) g_1(x, y, z, \tau) d\tau & (R_2/v_1 < t < \infty). \end{cases} \quad (2.33)$$

From the foregoing analysis it is clear that $u_1(x, y, z, t)$ reduces to $g_1(x, y, z, t)$ in case $f(t)$ is given by $f(t) = 1$ ($t > 0$), i.e. $f(t)$ is the Heaviside unit step function.

The electromagnetic field vectors in the air are obtained by using (2.4), (2.10) and (2.33) in the right-hand sides of (2.2) and (2.3).

§ 3. *Determination of the function $g_1(x, y, z, \tau)$.* In the present section it will be shown that the transformations outlined in § 3 of reference ⁹) lead to an expression for $g_1(x, y, z, \tau)$ in the form of a single integral over a finite interval. In the integral on the right-hand side of (2.30) we introduce new variables of integration ω and q through

$$\alpha = \omega \cos \varphi - q \sin \varphi, \quad (3.1)$$

$$\beta = \omega \sin \varphi + q \cos \varphi. \quad (3.2)$$

Since $d\alpha d\beta = d\omega dq$, we obtain

$$G_1(x, y, z; s) = \frac{1}{4\pi^2} \int_{-\infty}^{\infty} dq \int_{-\infty}^{\infty} \exp \{ -s[i\omega r + \gamma_1(z+h)] \} \mathcal{A}_1 d\omega, \quad (3.3)$$

in which, as $\alpha^2 + \beta^2 = \omega^2 + q^2$,

$$\gamma_{1,2} = (\omega^2 + q^2 + 1/v_{1,2}^2)^{\frac{1}{2}} \quad (\text{Re } \gamma_{1,2} \geq 0). \quad (3.4)$$

Next we introduce the variable $p = i\omega$ and regard p as a complex variable, while q is kept real. The result is

$$G_1(x, y, z; s) = \frac{1}{4\pi^2 i} \int_{-\infty}^{\infty} dq \int_{-i\infty}^{i\infty} \exp \{ -s[p r + \gamma_1(z+h)] \} \mathcal{A}_1 dp, \quad (3.5)$$

in which (compare (2.27))

$$\mathcal{A}_1 = \frac{\varepsilon_2 \gamma_1 - \varepsilon_1 \gamma_2}{\varepsilon_2 \gamma_1 + \varepsilon_1 \gamma_2} \frac{1}{2\varepsilon_1 \gamma_1}, \quad (3.6)$$

with

$$\gamma_{1,2} = (q^2 + 1/v_{1,2}^2 - p^2)^{\frac{1}{2}} \quad (\text{Re } \gamma_{1,2} \geq 0). \quad (3.7)$$

In the complex p -plane the integrand in (3.5) has branch points at $p = \pm \Omega_1(q)$ and at $p = \pm \Omega_2(q)$, where

$$\Omega_{1,2}(q) = (q^2 + 1/v_{1,2}^2)^{\frac{1}{2}} \quad (\Omega_{1,2} > 0). \quad (3.8)$$

In view of subsequent deformations of the path of integration we

take $\operatorname{Re} \gamma_1 \geq 0$ and $\operatorname{Re} \gamma_2 \geq 0$ not only on the imaginary p -axis but everywhere in the p -plane. This implies that branch cuts are introduced along $\operatorname{Im} p = 0$, $\Omega_1(q) < |\operatorname{Re} p| < \infty$ and along $\operatorname{Im} p = 0$, $\Omega_2(q) < |\operatorname{Re} p| < \infty$. It can easily be verified that, by virtue of Cauchy's theorem and Jordan's lemma¹³⁾, the integral along the imaginary p -axis in (3.5) can be replaced by an integral along the branch Γ_1 of a hyperbola, where Γ_1 is given through

$$p = (r/R_2^2)\tau \pm i(h/R_2^2)[\tau^2 - R_2^2\Omega_1^2(q)]^{\frac{1}{2}} \quad (R_2\Omega_1(q) < \tau < \infty), \quad (3.9)$$

in which the square root is taken positive or zero. The upper and lower sign in (3.9) refer to the part of Γ_1 located in the upper and lower half of the p -plane, respectively. Along Γ_1 we have

$$\gamma_1 = (h/R_2^2)\tau \mp i(r/R_2^2)[\tau^2 - R_2^2\Omega_1^2(q)]^{\frac{1}{2}} \quad (3.10)$$

and

$$\frac{\partial p}{\partial \tau} = \pm \frac{i\gamma_1}{[\tau^2 - R_2^2\Omega_1^2(q)]^{\frac{1}{2}}}. \quad (3.11)$$

In (3.9), (3.10) and (3.11) the upper and lower signs belong together. Taking into account the symmetry of the path of integration with respect to the real axis and introducing τ as variable of integration we obtain, since q , s and τ are real,

$$\begin{aligned} G_1(x, y, z; s) &= \\ &= \frac{1}{\pi^2} \int_0^\infty dq \int_{R_2\Omega_1(q)}^\infty \exp(-s\tau) \operatorname{Re} \{\mathcal{A}_1\gamma_1\} \frac{1}{[\tau^2 - R_2^2\Omega_1^2(q)]^{\frac{1}{2}}} d\tau. \end{aligned} \quad (3.12)$$

Interchanging the order of integration we have

$$\begin{aligned} G_1(x, y, z; s) &= \\ &= \int_{R_2/v_1}^\infty \exp(-s\tau) d\tau \int_0^{(\tau^2/R_2^2 - 1/v_1^2)^{\frac{1}{2}}} \frac{1}{\pi^2} \operatorname{Re} \{\mathcal{A}_1\gamma_1\} \frac{1}{[\tau^2 - R_2^2\Omega_1^2(q)]^{\frac{1}{2}}} dq. \end{aligned} \quad (3.13)$$

The integral on the right-hand side of (3.13) has the form announced in § 2, eq. (2.31). Consequently, $g_1(x, y, z, \tau)$ is given by

$$g_1(x, y, z, \tau) = \frac{1}{\pi^2 R_2} \int_0^{\frac{1}{2}\pi} \operatorname{Re} \{\mathcal{A}_1\gamma_1\} d\psi, \quad (3.14)$$

where a new variable of integration ψ has been introduced through

$$q = (\tau^2/R_2^2 - 1/v_1^2)^{\frac{1}{2}} \sin \psi \quad (0 \leq \psi \leq \frac{1}{2}\pi). \quad (3.15)$$

In the right-hand side of (3.14) we have to substitute for p and γ_1 the values (compare (3.9) and (3.10))

$$p = (r/R_2^2) \tau + i(h/R_2^2)(\tau^2 - R_2^2/v_1^2)^{\frac{1}{2}} \cos \psi, \quad (3.16)$$

$$\gamma_1 = (h/R_2^2) \tau - i(r/R_2^2)(\tau^2 - R_2^2/v_1^2)^{\frac{1}{2}} \cos \psi, \quad (3.17)$$

while q is given by (3.15). In all these expressions $R_2/v_1 < \tau < \infty$ and $R_2 = [r^2 + (z + h)^2]^{\frac{1}{2}}$.

§ 4. *Concluding remarks.* The problem of determining the Hertzian vector corresponding to the reflected wave generated by a vertical electric dipole located at a height h above a non-conducting earth with plane boundary has been reduced to the evaluation of the integrals in (2.33) and (3.14). In (2.33) the function $f'(t - \tau)$ takes into account how the electric moment of the dipole varies in time, while $g_1(x, y, z, \tau)$, given by (3.14), depends on the geometry of the boundary value problem and the physical properties of the air and the ground. As was to be expected the function g_1 is independent of q , i.e. the Hertzian vector is rotationally symmetrical about the z -axis.

Received 19th May, 1960.

REFERENCES

- 1) Sommerfeld, A., Ann. Phys., Lpz. **28** (1909) 665.
- 2) Weyl, H., Ann. Phys., Lpz. **60** (1919) 481.
- 3) Poritsky, H., Brit. J. Appl. Phys. **6** (1955) 421.
- 4) Pol, B. van der, Trans. Instn Radio Engrs AP-4 (1956) 288.
- 5) Pekeris, C. L. and Z. Alterman, J. Appl. Phys. **28** (1957) 1317.
- 6) Bremmer, H., Trans. Instn Radio Engrs AP-7, Special Supplement (1959) 175.
- 7) Levelt, A. H. M., Solution of the Laplace inversion problem for a special function, Mathematisch Centrum, Reports ZW 1959-010 and ZW 1959-012, Amsterdam 1959.
- 8) Cagniard, L., Réflexion et réfraction des ondes séismiques progressives, Gauthier-Villars, Paris 1939.
- 9) Hoop, A. T. de, Appl. sci. Res. B **8** (1960) 349.
- 10) Hoop, A. T. de, Surface motion of a uniform elastic half-space produced by a dilatational, impulsive, point-source, Report of the Laboratorium voor Theoretische Elektrotechniek, Technische Hogeschool, Delft 1960.
- 11) Stratton, J. A., Electromagnetic theory, p. 573, McGraw-Hill Book Company, New York 1941.
- 12) Stratton, J. A., loc. cit.; p. 434.
- 13) Whittaker, E. T. and G. N. Watson, A course of modern analysis, 4th ed., p. 115, Cambridge University Press 1952.

MEASUREMENTS ON THE PERMEABILITY OF HYDROGEN FROM H_2 AND H_2O THROUGH STEEL, STAINLESS STEEL AND ALUMINIUM

by F. BOESCHOTEN, W. VAN EGMOND *)
and H. M. J. KINDERDIJK

Reactor Centrum Nederland, the Hague, Netherlands

Summary

Permeation rates of hydrogen from H_2 and H_2O through steel, stainless steel and aluminium tubes of 0.1 mm thickness were determined at different temperatures, and in the case of H_2 also at different pressures; the measurements with steam were carried out with superheated steam at atmospheric pressure. For H_2 -steel the results were in accordance with the literature; for H_2 -stainless steel much lower permeation rates were found than for H_2 -ordinary steel. For H_2 -aluminium the data were not reproducible and no reliable quantitative values can be given. The permeability of hydrogen from steam through steel rises very rapidly with temperature, stronger than for stainless steel, for which latter permeation rates of the same order of magnitude were found. No permeation could be detected of hydrogen from steam through aluminium within the sensitivity limits of the apparatus, that is about 10^{-10} cm³ NTP/cm²s.

§ 1. *Apparatus.* In principle the arrangement was the same as used by Smithells and Ransley¹⁾. The permeation rate was measured of hydrogen through metal tubes of 50 mm length, 8 mm diameter and 0.1 mm wall thickness (5% tolerance).

During the measurements with H_2 the hydrogen pressure was kept constant at the outside of the tube, which was sealed at one end and which could be evacuated at the other, where it was connected to the glass tubing of the vacuum system. We measured the time in which the pressure in the tube rose from 10^{-6} tor (or lower) to 10^{-3} tor in a volume of about 320 cm³. This volume is separated from the mercury vapour pumps by a Horseling-valve⁹⁾.

*) Fysisch Laboratorium der Rijksuniversiteit te Utrecht.

In principle this is also the method used by Norton⁶). The pressure in this volume was measured with a Philips tetrode ionization gauge with sensitivities of about 2 A tor^{-1} for air and 1 A tor^{-1} for hydrogen, both sensitivities per ampere emission current of the gauge cathode. In a blank test the pressure of the gas in the closed system reached a value of about $2 \times 10^{-5} \text{ tor}$ without changing appreciably over tens of hours.

The principal parts of the arrangement are shown in fig. 1. The tube could be heated by a r.f. field (about 1 MHz); by adjusting the turns of a r.f. coil around the tube in such a way that at the ends more heat is dissipated than at the centre, a fairly uniform temperature could be obtained over the tube length. This method of heating turned out to be more satisfactory than heating by a current through the tube as used by Smithells and Ransley. The temperature was measured with a thermocouple that could be moved along the axis of the tube; it takes some minutes for the thermocouple to arrive at a constant temperature. Inevitable temperature gradients over the tube length (depending on the external gas pressure) have to be averaged exponentially. The thermocouple, being placed in the low pressure system, is heated almost entirely by radiation.

In the case of aluminium, which has a low (but not exactly known) emissivity, too low a temperature may be found because of radiation escaping at the open end of the tube. The error that may result from this effect amounts to about 5% in the absolute temperature, but is of less influence than other (mostly uncontrollable) factors.

In the measurements with superheated steam the arrangement could be much simpler, because after some time the whole tube will obtain the temperature of the steam which is easily measured. So r.f. heating and a moving thermocouple inside the tube are not necessary. The latter was used, however, for checking, and the temperature indicated by the moving thermocouple inside the tube turned out to be within 5% the same as measured in the steam. All the measurements with superheated steam were made under atmospheric pressure.

§ 2. *Experimental results.* We were mainly interested in the permeation rate through 304 stainless steel (18–20% Cr, 8–10% Ni)

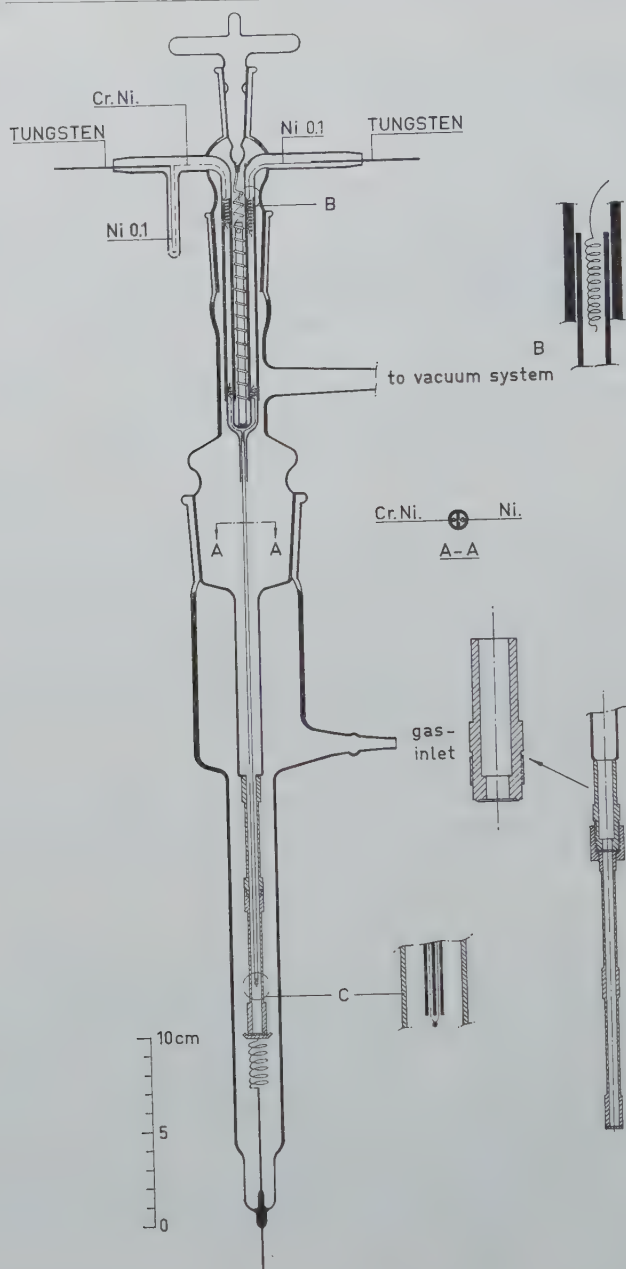


Fig. 1. Apparatus for measuring the permeability of a gas through metal tubes. The lower end of the tube is heated by placing a r.f. coil around it. The upper half has also a 0.1 mm wall, making the heat flow to the glass-metal seal as small as possible. The tube has an electrical connection through the glass envelope. The thermocouple may be moved in axial direction by turning the knob at the upper side of the system.

and 2S aluminium. But in order to get familiar with the apparatus and to obtain an impression of the effect of surface treatments, measurements with ordinary ST 37 steel, which has a much higher (and better known) permeability, were also made.

The permeation rate is often expressed as a function of temperature by 1) $q = k' e^{-b/T}$, where b is a constant *) for a certain gas-metal system and T the temperature, both in °K. Usually q and k' are expressed in cm^3 at NTP per cm^2 per second and k' is supposed to be inversely proportional to the wall thickness d of the metal and to be dependent on the pressure difference between both sides of the wall. In our case the internal pressure may be put zero. For a diatomic gas like hydrogen $k' = kd^{-1}P^{1/2}$, where k is a constant, characteristic for the gas-metal system under consideration. With d in mm and P in tor, k is given in terms of cm^3 at NTP per second and per mm thickness at one tor pressure. Values of the constants k and b for various gas-metal systems have been listed by Barrer**) 2)3). The constant b must be determined by varying the temperature at constant external gas pressure. With b known the constant k may be found by varying the gas pressure from about 1 atm to not too low values and determining the slope of the curve of q versus $P^{1/2}$. As a matter of fact this gives more reliable values than using only one point of the curve.

We were able to obtain consistent results only if the tube was heated for some time (about one hour) at the desired temperature and pressure before the measurements started. Moreover, the permeation rate may change (it generally decreases) if the metal gets older. But even with the necessary precautions considerable differences may be observed between permeability measurements on the same tube, if carried out with intervals of days; this is especially true for aluminium. Probably this is mainly caused by slightly different and uncontrollable conditions of the surface (oxide layer?), but also by recrystallization effects. Generally the constant b in the exponent is less affected than k and may be determined fairly reliably.

*) b may be written as $b = Q/R$, where Q is the activation energy per gram-atom necessary for permeation and R is the gas constant.

**) In this table the permeability is given as $P = P_0 e^{-E/RT}$, but unfortunately P is said to be expressed in $\text{cm}^3\text{s}^{-1}\text{cm}^{-2}\text{mm}^{-1}$ thickness at atmospheric pressure, whereas it is given at one tor pressure. This is probably caused by the fact, that all authors use different units. For E we may put approximately $2b$.

No simple dependence on temperature and gas pressure is known for the permeability of hydrogen from steam through metals. This is evident from the fact that the dissociation of the water molecules depends on temperature and on the surface that is in contact with the vapour.

a. Steel-hydrogen. Measurements with ordinary ST 37 steel were carried out in the temperature range of 100°C–200°C. Because our apparatus had to be extremely sensitive for the measurements with steam, the permeation rate of hydrogen through steel could be measured at lower temperatures than those in earlier measurements. In order to discover the influence of the surface treatment on the permeation rate, three type of tubes were investigated: turned (1), turned and polished with diamond (2), and turned and polished and etched with a solution of 5 cm³ nitric acid in 100 cm³ ethyl alcohol (3). No very great influence of these surface treatments was observed. Within the limits of error of about 25% no difference in permeation rate between the turned and the polished tubes could be detected. The average values for b and k are given in table I. Because of the etching treatment the permeation rate decreased to about half the value for unetched surfaces. This unexpected results may be due to poisoning effects. In table I a comparison is made between the various values of b and k (see also ref.²⁾ and ³⁾).

TABLE I

Permeability data for hydrogen-steel $q = kd^{-1}P^{\frac{1}{2}}e^{-b/T}$			
k [cm ³ NTP mm cm ² s tor ¹]	b [°K]	temperature range [°C]	authors
1.63 × 10 ⁻³	4800	780–245	Smithells and Ransley ¹⁾
1.6 × 10 ⁻³	4700	700–300	Borelius and Lindblom ⁴⁾
	4350	700–300	Post and Ham ⁵⁾
	9430	1180–900	Post and Ham ⁵⁾
0.86 × 10 ⁻³	4250	200–100	Boeschoten, van Egmond and Kinderdijk

That the values for b and k obtained from our measurements are lower than those found by other investigators, may be explained by assuming that the formula $q = k''d^{-1}P^{\frac{1}{2}}T^{\frac{1}{2}}e^{-b''/T}$ gives a somewhat better description of the permeation phenomena ²⁾. According to this formulè the values obtained for b from the relation

$q = kd^{-1}P^{\frac{1}{2}}e^{-b/T}$ are higher, the higher the temperatures at which q is determined.

b. Steel-steam. Whith our method the temperature could be varied, but not the pressure of the steam. The permeation rate at atmospheric pressure was observed to increase more rapidly than according to $e^{-b/T}$ (table II). This is not surprising because the degree of dissociation of the water vapour depends on the temperature and the surface. For comparison we also listed the permeation rate of hydrogen from water through steel as may be computed from Norton's data⁶).

TABLE II

Permeation rate of H from H ₂ O through steel of 0.1 mm thickness	
Temperature K	q cm ³ .NTP cm ⁻² s
575	274 × 10 ⁻⁸
525	10 × 10 ⁻⁸
450	1 × 10 ⁻⁸
373 (water)	9 × 10 ⁻¹⁰ (Norton)
298 (water)	1.5 × 10 ⁻¹⁰ (Norton)
373 (vapour)	immeasurable (Norton)

It may be noted that extrapolation of our data on steam to temperatures at which Norton determined the permeation rate for water, seems to indicate that the permeability for hydrogen from water does not differ greatly in order of magnitude from the permeability for hydrogen from steam of the same temperature (373°K) and pressure, though the density of water is about 2000 times the density of steam. This is not very surprising, because at the boiling point steam and water are in thermodynamical equilibrium and the presence of a steel wall will not disturb this. How Norton succeeded in finding a difference in permeation rate of at least a factor 10 has not become clear.

The tubes age rather rapidly, so that after a few minutes the permeation rate of a fresh surface already decreases. After treatment of the surface with cerosine the original permeation rates are found again.

c. Stainless steel-hydrogen. The permeation rate was measured through stainless steel (304) tubes in the temperature

range of 300°C to 550°C and at pressures ranging from 4 tor to 400 tor. Values for b as read from the slope of the $\ln q - 1/T$ curve varied from 9000°K (in the lower pressure range) to 11000°K (in the higher pressure range). As an average may be used $b = 10\,000^\circ\text{K}$ and $k = 5 \times 10^{-2} \text{ cm}^3\text{NTP mm cm}^{-2} \text{ s}^{-1} \text{ tor}^{-1}$.

d. Stainless steel-steam. Fig. 2 presents the permeation rate as a function of temperature for a stainless steel tube of 0.1 mm thickness. The temperature dependence is found to be much less pronounced than for ordinary steel. In the temperature range of 500°K–700°K the permeation rates of hydrogen from water through freshly scraped, ordinary and stainless steel, do not differ greatly. In some cases the permeability of stainless steel was even found to be larger than for ordinary steel.

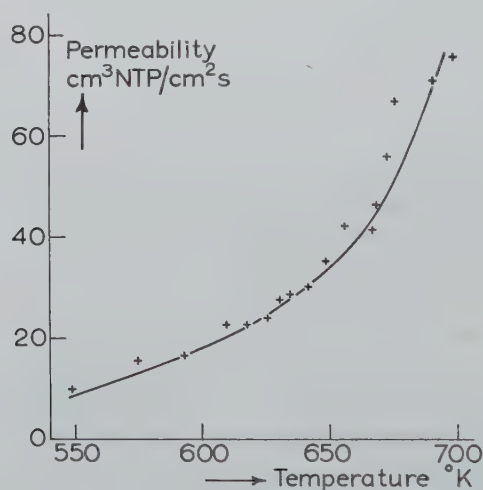


Fig. 2. The permeation rate as a function of temperature for a stainless steel tube of 0.1 mm thickness.

e. Aluminium-hydrogen. The permeation rate of hydrogen through aluminium is so variable, probably depending very strongly on the surface condition, that it hardly makes any sense to give a value for b and k . The use of these quantities implies a certain reproducibility, which is difficult if not impossible to obtain. Our measurements were made at temperatures varying from 360°C to 400°C with 2S aluminium, without any special surface treatment. The measurements were impeded by the fact that if heated at

temperatures of about 450°C or higher, our tubes collapsed even at relatively low external pressures. The result of a number of tests with tubes of 0.1 mm wall thickness are shown in table III.

TABLE III

Permeation rate q of hydrogen through 2 S aluminium of 0.1 mm thickness.			
Tube nr	Temperature [°K]	H ₂ pressure [tor]	Permeation rate q [cm ³ NTP cm ⁻² s ⁻¹]
I	635	136	0.32×10^{-9}
I	645	136	1.92
I	645	136	0.18 *)
I	655	136	1.16
II	655	9.5	0.26
II	"	34	0.52
II	"	"	1.2
II	"	"	0.84
II	"	"	0.71
II	"	136	1.92
II	675	36	3.2
II	675	9	1.3

*) After hours of heating.

TABLE IV

Values for the constant b as found in various investigations for the system aluminium hydrogen.		
b in °K	remarks	authors
15600	freshly scraped surface	Smithells and Ransley
21500	anodically oxidized	Idem
5500	from sorption measurements	Eichenauer and Pebler
about 50000	fresh aluminium, rapidly diminishing with time	Russell
about 30000	in some cases, not changing with time	Boeschoten, Kinderdijk, van Egmond

As in the work of Russell ⁷⁾ the permeation rate was found to change with time, but not always rapidly as may be seen from the observations on tube II at 655°K. On that tube we observed the permeation rate to be about five times lower than found by Smithells and Ransley ⁶⁾ for freshly scraped surfaces. It seems to be very difficult to give more or less reliable quantitative permeation rates of hydrogen through aluminium, which is, for example, possible for nickel and even for iron. This fact may be stressed by comparing the values for the constant b in the exponent

as found in various investigations. The constant k differs still more and would be a very large number if derived from Russell's or our measurements.

f. Aluminium-steam. The permeation rate of hydrogen from superheated steam of atmospheric pressure and 300°C through aluminium was immeasurably small. For tubes of 0.1 mm thickness q was less than 10^{-10} cm³NTP cm² s⁻¹.

Acknowledgement. We wish to thank Mr. P. Eykhout, Mr. L. van Ruyven and Mr. P. F. J. v. d. Most for the measurements they have done.

Received 27th April, 1960

REFERENCES

- 1) Smithells, C. J. and C. E. Ransley, Proc. Roy. Soc. A **150** (1935) 172.
- 2) Barrer, R. M., Diffusion in and through solids, Cambridge, 1941.
- 3) Jost, W., Diffusion in solids, liquids and gases, New York, 1952.
- 4) Borelius, G. and S. Lindblom, Ann. Phys. Lpz. **82** (1927) 201.
- 5) Post, C. B. and W. R. Ham, J. Chem. Phys. **5** (1937) 913.
- 6) Norton, F. J., J. Appl. Phys. **11** (1940) 262.
- 7) Smithells, C. J. and C. E. Ransley, Proc. Roy. Soc. A **152** (1935) 706.
- 8) Russell, A. S., Metal Progress, 1949, p. 827.
- 9) Horseling, J., Philips Techn. Rev. **17** (1955) 231.
- 10) Fast, J. D., Philips Techn. Rev. **6** (1941) 369 and **7** (1942) 74.
- 11) Eichenauer, W. and A. Pebler, Z. Metallk. **48** (1957) 373.

CHARACTERISTIC PARAMETERS OF GEIGER-MÜLLER COUNTER GASES.

I. ETHANOL-ARGON MIXTURES *)

by CHARLES D. STORRS ** and ROBERT W. KISER

Department of Chemistry, Kansas State University, Manhattan, Kansas, U.S.A.

Summary

The Wilkinson and the Diethorn-Kohman expressions of counter operation are reviewed. In equating these two expressions, the gas amplification factor is taken to be 10^7 at the starting potential for Geiger operation of the counter. Although the use of this numerical value has not yet been completely verified, the use of a constant is established from the results obtained for the five different ethanol-argon mixtures examined in this work. The variation of the characteristic parameters with gas composition is shown to be in general accord with the theory being formulated.

§ 1. *Introduction.* The Geiger-Müller counter and the counting process are much improved with the admixture of a small quantity of organic vapor with the inert gas in the counter. Originally developed by Trost ¹⁾²⁾, these self-quenching counters allow some increase in the speed of recovery of the counter, but more important, allow the use of simpler electronic circuitry with which to follow the counter.

Following Trost's important work, many workers began the development of a theory of gas-tube counter operation. Notable developments in theoretical approaches have been made ³⁻¹⁴⁾. From these has risen a reasonably clear physical conception of the Geiger discharge, and working theories of counter operation have been developed in general forms. Further, the decompositions of various

*) Presented at the 134th Meeting of the American Chemical Society, Chicago, Illinois, September 7-12, 1958.

**) Now at Petroleum Chemicals, Inc., Lake Charles, Louisiana.

organic quenching agents in the Geiger discharge have been shown to be in agreement with these presently accepted theories¹⁵⁻¹⁸).

Although these physical concepts and theories appear to be valid, they apparently lack a quantitative aspect. That is to say, one has been unable to predict from basic principles the operation of various gases or gas mixtures in various counters. It is in this respect that we are presently concerned with the characteristic parameters of Geiger-Müller counter gases. Basic relations and concepts have been used in attempting to arrive at the desired quantitative aspects. Ethanol-argon, investigated because of its prominent use as a counter gas, is one of the first test cases of the theory now being formulated.

§ 2. *Theoretical.* Wilkinson⁸⁾⁹⁾ has given the theoretical derivation for the equation

$$V_s \ln (k_2 V_s / p) = k_3, \quad (1)$$

where V_s is the starting potential for the Geiger region, p is the pressure, k_2 and k_3 are constants and the geometry is cylindrical. Rearranging (1), one obtains

$$\ln (V_s / p) = k_3 V_s^{-1} - \ln k_2. \quad (2)$$

If $\ln(V_s/p)$ is plotted *versus* V_s^{-1} , a linear curve with a slope of k_3 and an intercept of $-\ln k_2$ should result. Such experimental verification has already been obtained⁹⁾.

Wilkinson⁸⁾⁹⁾ also theoretically derived the relation that

$$[V_s / \ln(b/a)] \ln [V_s / k_4 a \ln(b/a)] = k_5, \quad (3)$$

where b is the radius of the counter cathode, a is the radius of the centre wire and k_4 and k_5 are constants, again for cylindrical geometry. Rearranging (3), we see that

$$\ln[V_s / a \ln(b/a)] = (k_5 / V_s) \ln(b/a) + \ln k_4. \quad (4)$$

A plot of $\ln[V_s / a \ln(b/a)]$ *versus* $(1/V_s)$ of the experimental data should result in a straight line with a slope of $k_5 \ln(b/a)$ and an intercept of $\ln k_4$. Wilkinson has shown this to hold for the investigated gases⁹⁾.

From theoretical considerations, Diethorn and Kohman¹⁹⁾ derived the following relation, wherein is expressed the operation of proportional counters:

$$\ln A_0 = [V \ln 2/\overline{\Delta V} \ln(b/a)] \ln [V/\overline{K} p a \ln(b/a)], \quad (5)$$

where A_0 is the gas multiplication factor in the proportional region at the particular value of V . V is the voltage on the centre wire. $\overline{\Delta V}$ and \overline{K} are the characteristic parameters of the counter gases. It is to be noted that the Diethorn-Kohman expression is a decided improvement over the formulae proposed by Rose and Korff⁷⁾ and Curran and Craggs²⁰⁾.

Rearrangement of equation (5) leads to:

$$[\ln A_0 \ln(b/a)]/V = \{\ln 2 \ln[V/p a \ln(b/a)]\}/\overline{\Delta V} - (\ln 2 \ln \overline{K})/\overline{\Delta V}. \quad (6)$$

A plot of $[\ln A_0 \ln(b/a)]/V$ versus $\ln[V/p a \ln(b/a)]$ should result in a straight line having a slope of $\ln 2/\overline{\Delta V}$ and an intercept of $-(\ln 2 \ln \overline{K})/\overline{\Delta V}$. It has been shown^{21) 29)} that such plots for the proportional operation of methane, ethane, carbon dioxide and methane-argon and carbon dioxide-argon mixtures do indeed give linear plots, substantiating the use of the Diethorn-Kohman expression.

In the study made by Kiser^{21) 29)} it was shown that $\overline{\Delta V} \geq W$ for the proportional gases studied, where W is the energy, in eV, necessary to create an ion pair in the gas or gas mixture. However, for the case of an 11.3% ethanol-88.7% argon mixture, a Geiger-Müller counter gas, which was studied in its proportional operation, it was found that $\overline{\Delta V} < W$, and in fact $\overline{\Delta V}$ approximated the ionization potential of ethanol. (See also results of van Duuren and Sizoo^{29) 30)}.) Kiser further observed that in treating the Geiger-Müller data of a 16.4% ethanol-83.6% argon mixture with the Diethorn equation for proportional operation, assuming $A_0 = A_g = 10^7$ at $V = V_s$, the values of $\overline{\Delta V}$ and \overline{K} compared reasonably well with the results of the proportional study on the slightly different mixture. A_g is the gas multiplication factor at the Geiger threshold, where $V = V_s$. Table I compares the preliminary results observed.

Since it appeared reasonable that one equation should describe the characteristic behaviour of both Geiger-Müller and proportional counter gases, Kiser²¹⁾ proposed that one may equate equations

TABLE I

Preliminary ethanol-argon parameters		
Filling	$\overline{\Delta V}(V)$	$\overline{K}(V/\text{in mm Hg})$
11.3% EtOH-88.7% A (from proportional studies employing equation (6)).	10.5	480.
16.4% EtOH-83.6% A (from Geiger-Müller studies employing equations (6), (2) and (4)).	11.0	440.

(2) and (4) with (6), giving then

$$k_2 = 1/\overline{K}a \ln(b/a), \quad (7)$$

$$k_3 = [\overline{\Delta V} \ln(b/a) \ln A_0]/\ln 2, \quad (8)$$

$$k_4 = \overline{K}p, \quad (9)$$

$$k_5 = \overline{\Delta V} \ln A_0/\ln 2. \quad (10)$$

Although the physical meanings of $\overline{\Delta V}$ and \overline{K} are to be discussed further in a forthcoming paper, a comparison of the values given by Kiser would indicate that $\overline{\Delta V}$ might remain nearly constant in the various mixtures of ethanol and argon. Since Lauterjung²²⁾ has shown that a description of various mixtures of the same gases used as counter fillings shows a dependence upon the concentration of quenching agent, we may then expect \overline{K} to vary with the composition of the gas mixtures.

In this paper we describe further examinations of the two proposed characteristic parameters of the counter gases, $\overline{\Delta V}$ and \overline{K} , using various ethanol-argon mixtures as the Geiger-Müller counter gases. As expected, $\overline{\Delta V}$ remains reasonably constant as the composition is varied, although the small changes observed are explained, and \overline{K} is found to vary in a regular fashion with changes in composition. The variation of \overline{K} with composition was found to be nearly linear over the range studied.

§ 3. *Experimental.* The several cylindrical counters employed were constructed in our laboratories. The shells were made of soda glass or brass and the centre wires were either of 2 mil tungsten or 25 mil silver. The counters were both of the normal and of the Maze-

type construction. Standard procedures ²¹⁾ were observed in the construction of these counters.

Normal vacuum techniques were used in evacuating and filling the counters and in blending the various mixtures for filling the counters.

The argon was obtained from the Matheson Company and was purified when withdrawn from the cylinder. "Q-gas", a commercially-available Geiger-Müller counting gas composed of 1.3% butane and 98.7% helium, was obtained from the Matheson Company. The absolute ethanol was prepared by careful and repeated distillations over barium oxide and calcium sulfate. From an examination of the ultraviolet spectrum of the absolute ethanol, it was observed that the sample contained less than 0.001% benzene. The measured density of the product was 0.78525 gm cm³ at 25°C. Dissolved gases were removed from the absolute ethanol using the common vacuum system technique of multiple freezing, pumping and thawing cycles. Finally, the ethanol-argon mixtures were blended in a two litre storage bulb from which samples could later be withdrawn for filling the counters.

Counters containing the desired composition of ethanol and argon and filled to known pressures were then irradiated with a small radioactive source. With no external quenching circuit, plateau measurements were made and pulse heights of the Geiger pulses were observed. The count rate was recorded with an RIDL model 200BD scaler which also supplied the high voltage. A Tektronix 515 oscilloscope was used to observe the Geiger pulses *) directly on the centre wire of the counter.

From the starting potentials so obtained, and the knowledge of a , b and p , curves were constructed as shown in figs 1 and 2. Values of \overline{AV} and \overline{K} were then obtained from these linear plots.

§ 4. *Results.* Figs 1 and 2 were plotted in accordance with (6), but the $\ln A_0$ term has been omitted. This is done to test the proposed

*) It is noted that we define a counter to be operating in the Geiger region if, and only if, it fulfills the following conditions: (a) the pulse height variation is to be linear with an increase in overvoltage up to the discharge region and is to be linear after the beginning of the discharge region although now the slope is to be one-half of the former value, (b) the counter is to exhibit a reasonable plateau in plotting the count rate *versus* the overvoltage, and (c) the heights of the counter pulses are all to be identical, or very nearly so. Such gases as methane and ethane and many of the organometallic vapors, then, are not Geiger-Müller counter gases. This has been emphasized previously ²¹⁾.

constancy of $A_0 = A_g = 10^7$ at $V = V_s$. The fact that linear plots were observed in these cases shows that A_0 is constant as a , b and p are varied, but does not necessarily substantiate the choice of

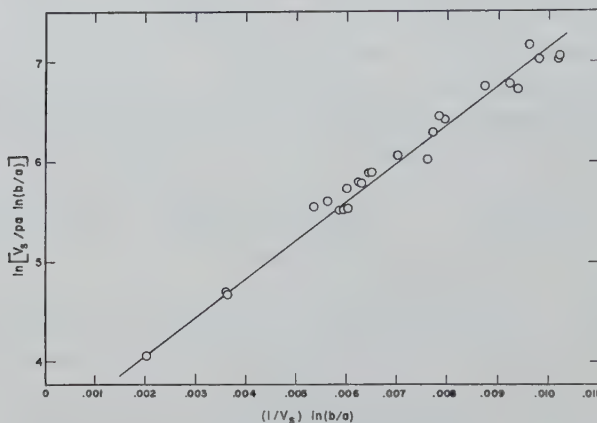


Fig. 1. Characteristic operation of commercial "Q-gas".

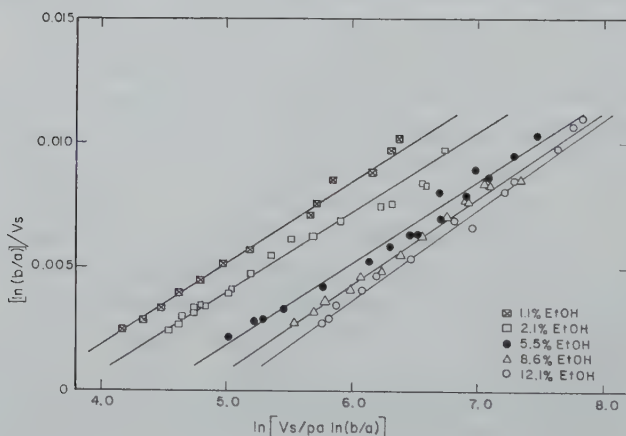


Fig. 2. Characteristic operation of various mixtures of ethanol and argon.

the value of 10^7 . The choice of 10^7 will be discussed below. From these figures, showing the linear dependence expected, much confidence is gained in the use of (6) for the Geiger-Müller counter as well as for the proportional counter.

Table II and fig. 3 summarize the values of $\overline{\Delta V}$ and \overline{K} as obtained from the slopes and intercepts of the curves of figs 1 and 2. Fig. 3 emphasizes the expected near constancy of the $\overline{\Delta V}$ values and the regular variation of \overline{K} with composition. The slight decrease in $\overline{\Delta V}$ with composition is in agreement with the work of Liebson²⁴ as will be discussed later. It should be noted that the equations developed by Lauterjung²²) involved a logarithmic relation of

TABLE II

Characteristic parameters of "Q-Gas" and ethanol-argon mixtures		
Filling	$\overline{\Delta V}(V.)$	$\overline{K}(V/\text{in mm Hg})$
"Q-Gas"	15.9	29.6
1.1% EtOH-98.9% A	12.4	33.4
2.1% EtOH-97.9% A	13.3	43.2
5.5% EtOH-94.5% A	12.7	89.7
8.6% EtOH-91.4% A	11.7	127
12.1% EtOH-97.9% A	11.1	160

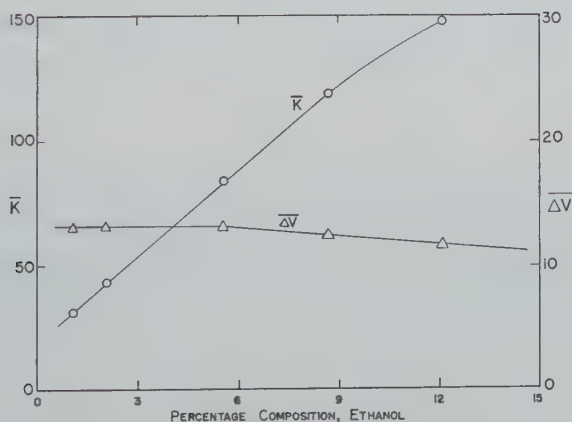


Fig. 3. Variation of $\overline{\Delta V}$ and \overline{K} with the composition of ethanol-argon mixtures.

the counter filling composition to the starting potentials. Although \overline{K} is reasonably linear over most of the region studied, \overline{K} is involved in a logarithmic term. Thus, our results are also in essential agreement with those of Lauterjung.

§ 5. *Discussion of results.* It has been observed that A_g is a constant, and it has been assumed that $A_g = 10^7$. The studies made

by Kiser ²¹⁾ and the present reported studies appear to substantiate the choice of 10^7 . The value is not at all unreasonable since the value of 10^8 is often quoted as being the gas amplification factor for a counter when operating on the plateau, and since often the size of the pulse differs by an order of magnitude at the starting potential V_s , and at a potential midway on the plateau. We feel certain then that $A_g = 10^7$ is valid to within better than an order of magnitude. Further tests of the use of $A_g = 10^7$ will be carried out in studies of the characteristic parameters of other gases and gas mixtures, employing both the proportional counter and the Geiger-Müller counter investigational techniques.

It has already been shown ^{21) 29)} that $\overline{\Delta V} \geq W$ for the gases studied in the proportional region, and we find here that $\overline{\Delta V} < W$ for the gases in the Geiger counter, in which photon spread effects very near the wire are important. From the relations discussed above,

$$\ln A \simeq k/\overline{\Delta V}. \quad (11)$$

This may be used to estimate the importance of the effect by the photon spread upon the total amplification factor by use of the relation

$$\%T = 100 A_g \overline{\Delta V}^{W-1}, \quad (12)$$

where $\%T$ is the percent contribution to the discharge and multiplication processes by the Townsend avalanche. Liebson ²⁴⁾ reported the number of photons relative to the number of ions to increase in ethanol-argon counters as the percentage of alcohol vapour increased. In that our data shows $\overline{\Delta V}$ to decrease with increasing concentration of ethanol, and since a decrease of $\overline{\Delta V}$ causes a decrease in $\%T$, indicating the increased importance of photons in the discharge, our results are in agreement with those of Liebson ²³⁾

For the 12.1% ethanol-87.9% argon counter, W is approximately 27 eV. Therefore

$$\%T \simeq 7.5 \times 10^{-3}\%,$$

which shows that, in this case, the Townsend avalanche indeed makes a relatively minor contribution to the Geiger discharge, there being a copious production of photons for continued propagation of the discharge near the centre wire after multiplication has been initiated.

On the other hand, a 90% methane-10% argon counter has

$\overline{AV} = 28.3$ V and $W = 28.7$ eV. Therefore, $\%T = 80\%$, which indicates that the photon spread effect is quite unimportant and that almost all of the amplification is due to the Townsend avalanches. Thus, it is seen that this method may serve as a means of distinguishing between proportional and Geiger-Müller operation of gases and gas mixtures. As a guide, one may consider that if $\overline{AV} \geq 0.85 W$, the gas will act in a proportional manner, and if $\overline{AV} \leq 0.6W$, the gas will act in a Geiger manner. In the intermediate range it would be expected that the gas shows properties of both types of operation. Thus, all of the gas mixtures of table II are expected to be Geiger in their operation, and such is the case.

The available data ²⁴⁻²⁸) concerning the operation of halogen-quenched Geiger-Müller counters indicate that the theory being formulated here may also apply to the halogen counters. However, more detailed study will be necessary to ascertain such applications.

It is planned that further investigations be made on other gases and gas mixtures so that the assumptions and implications given herein may be more thoroughly tested. Such studies are now in progress along with attempts to calculate \overline{AV} and \overline{K} from more basic quantities ²⁹).

Acknowledgements. The authors wish to thank Professor G. D. Johnson for the U.V. spectral measurements, Professor H. C. Moser, Dr. J. E. Lewis and Mr. C. Bouffiou for loan of some equipment and Dr. M. H. Lietzke for his comments. Further, these authors gratefully acknowledge the support of this work by the Department of Chemistry, Kansas State University.

Received 3rd May, 1960

REFERENCES

- 1) Trost, A., *Physik. Z.* **35** (1935) 801.
- 2) Trost, A., *Z. Phys.* **105** (1937) 399.
- 3) Montgomery, C. G. and D. D. Montgomery, *Phys. Rev.* **57** (1940) 1030.
- 4) Montgomery, C. G. and D. D. Montgomery, *J. Franklin Inst.* **231** (1941) 447.
- 5) Stever, H. G., *Phys. Rev.* **61** (1942) 38.
- 6) Korff, S. A. and R. D. Present, *Phys. Rev.* **65** (1944) 274.
- 7) Rose, M. E. and S. A. Korff, *Phys. Rev.* **59** (1941) 850.
- 8) Wilkinson, D. H., *Phys. Rev.* **74** (1948) 1417.
- 9) Wilkinson, D. H., *Ionization Chambers and Counters*, Cambridge at the University Press, Cambridge 1950.

- 10) Korff, S. A., *Rev. Modern Phys.* **14** (1942) 1.
- 11) Korff, S. A., *Electron and Nuclear Counters*, D. Van Nostrand Co., Inc., 2nd ed., New York 1955.
- 12) Korff, S. A., *Geiger Counters*, in *Handbuch der Physik*, Vol. 45, edited by S. Flugge and E. Creutz, Springer-Verlag, Berlin 1958, pp. 53-85.
- 13) Krumbein, A. D., *Rev. Sci. Instrum.* **22** (1951) 821.
- 14) Raether, H., *Appl. Sci. Res.* **B5** (1955) 23.
- 15) Friedland, S. S., *Phys. Rev.* **74** (1948) 898.
- 16) Farmer, E. C. and S. C. Brown, *Phys. Rev.* **74** (1948) 902.
- 17) Kiser, R. W. and W. H. Johnston, *J. Amer. Chem. Soc.* **78** (1956) 707.
- 18) Kiser, R. W. and W. H. Johnston, *J. Amer. Chem. Soc.* **79** (1957) 811.
- 19) Diethorn, W., *A Methane Proportional Counter System for Natural Radiocarbon Measurements*, NYO-6629, March 16, 1956.
- 20) Curran, S. C. and J. D. Craggs, *Counting Tubes*, Academic Press, Inc., New York 1949).
- 21) Kiser, R. W., *Radiochemical Studies with Gas-Tube Counters at Normal and Elevated Temperatures*, Doctoral Dissertation, Purdue University, Lafayette, Indiana, January, 1958. (Available from University Micro Films, Ann Arbor, Michigan, L. C. Card No. Mic-58-1792).
- 22) Lauterjung, K. H., *Z. Naturforsch.* **7A** (1952) 344.
- 23) Liebson, S. H., *Phys. Rev.* **72** (1947) 602.
- 24) Liebson, S. H. and H. Friedman, *Rev. Sci. Instrum.* **19** (1948) 303.
- 25) Liebson, S. H., *Rev. Sci. Instrum.* **20** (1949) 483.
- 26) Zoonen, D. van and G. Prast, Jr., *Appl. Sci. Res.* **B3** (1952) 1.
- 27) Zoonen, D. van, *Appl. Sci. Res.* **B3** (1953) 377.
- 28) Zoonen, D. van, *Appl. Sci. Res.* **B5** (1955) 368.
- 29) Kiser, R. W., *Appl. Sci. Res.* **B8** (1960) 183.
- 30) Duuren, K., van and G. J. Sizoo, *Appl. Sci. Res.* **B7** (1959) 379.

THE ELECTROMAGNETIC FIELDS OF A DIPOLE IN THE PRESENCE OF A THIN PLASMA SHEET

by JAMES R. WAIT

National Bureau of Standards, Boulder, Colorado, U.S.A.

Summary

The problem of electric and magnetic dipoles located near a thin planar slab or sheet of ionized material is considered. A constant and uniform magnetic field is impressed on the slab. Under the assumption that the thickness of the slab is very small, expressions for the resultant fields are obtained. As a result of the anisotropy of the sheet it is indicated that the fields are elliptically polarized in general. On carrying out a saddle-point evaluation of the integrals in the formal solution it is shown that the far fields may be split into "radiation" and "surface wave" components. The dependence of the radiation pattern and the surface wave characteristics on electron density, collision frequency and the impressed magnetic field is illustrated.

§ 1. *Introduction.* A gaseous plasma is distinguished by the presence of significant concentrations of positive (and negative) ions and free electrons such that the total number of charge carriers of each sign is the same. To a large degree, the ionosphere ¹⁾, gaseous discharges ²⁾, strong shock waves ³⁾ and flames ⁴⁾ may be described as plasma. The behaviour of microwaves incident on plasma is currently receiving a great deal of attention ⁵⁾, although in many respects such investigations are closely related to earlier studies of the ionosphere.

The presence of electrons in the plasma render it a conducting medium. The electron density, the frequency of collisions between these electrons and the ions and the operating frequency determine the extent to which the signal is absorbed, reflected or transmitted by the plasma. It is true that the electric charge of the molecular ions will also contribute to the total density but, except at es-

extremely low frequencies, their influence in this regard is negligible ¹⁾).

When an external magnetic field is impressed, the plasma becomes anisotropic in its electrical properties. These magneto-ionic effects depend not only on electron density and operating frequency but also on the strength and direction of the magnetic field. The bulk of magneto-ionic theory ¹⁾ deals with ionized media or plasma which are homogeneous and infinite in extent. On the basis of such results, inferences are drawn about the behaviour of electromagnetic waves in inhomogeneous or varying media. Such a procedure is only valid when the properties (i.e., electron density and collision frequency) are varying slowly in a distance equal to one wavelength. It is really quite surprising that such an approach has been so successful.

Another approach which has yielded to analytical treatment is the sharply bounded ionized medium ⁶⁾. For example, the lower edge of the ionosphere has been idealized as a homogeneous plasma with a plane interface, below which is free space. The rigorous treatment of this problem is, however, extremely involved, although some recent progress has been made by using automatic computers ⁷⁾. The reflection from a planar stratified ionosphere with a smooth profile of electron density has been considered at great length by Budden ⁸⁾.

Very recently Poeverlein ⁹⁾ has shown that an inhomogeneous ionosphere could be well represented by a number of parallel sub-layers. It appears that this simplified approach holds great promise for problems of more complicated geometry such as spherical, cylindrical and conical plasma sheaths.

It is the purpose of the present paper to extend Poeverlein's work for the single thin slab of ionized media. The excitation is taken to be an electric or magnetic dipole oriented normal to the slab. Particular attention is paid to the surface waves which may be excited.

§ 2. *Formulation of boundary conditions.* The model assumed is a thin planar slab of an ionized medium. A steady and constant magnetic field \mathbf{H} is impressed on the slab. The problem is to calculate the resulting electromagnetic fields in the presence of electric

and magnetic dipoles. Choosing a cylindrical coordinate system (ρ, ϕ, z) , the dipole (either electric or magnetic) is located at the origin and is oriented parallel to the z axis. The slab is taken to occupy the space $-(h + \delta/2) < z < -(h - \delta/2)$, and $0 < \rho \leq \infty$. The situation is illustrated in fig. 1.

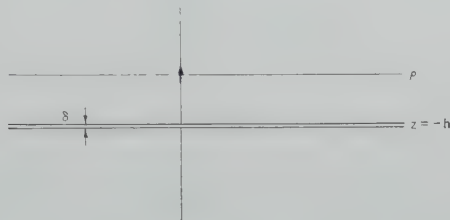


Fig. 1. Thin ionized sheet and cylindrical coordinate system. The electric (or magnetic) dipole is located at the origin and oriented normal to the sheet.

The thickness of the sheet δ is now considered to be very small compared to all other significant dimensions in the problem. A consequence is that the induced current density \mathbf{J} flows only in the transverse direction. That is, J_z may be neglected compared with J_ρ and J_ϕ . This kind of approximation has been discussed in previous papers by the author¹⁰⁾¹¹⁾. As mentioned, it has also been used by Poeeverlein⁹⁾ whose analysis was restricted to plane wave incidence. Starting with the relevant equations of motion for electrons and harmonic time dependence, (i.e., $\exp i\omega t$) it is not difficult to see that the electric field components E_ρ and E_ϕ in the sheet are related to J_ρ and J_ϕ by

$$(\nu + i\omega)J_\rho - \omega_z J_\phi = \omega_0^2 \epsilon E_\rho, \quad (1a)$$

$$\omega_z J_\rho + (\nu + i\omega)J_\phi = \omega_0^2 \epsilon E_\phi, \quad (1b)$$

where ν is the (constant) collision frequency of the electrons with the ions, ω_0^2 is the electron plasma frequency, ω_z is the z or normal component of the gyro-frequency and ϵ is the dielectric constant of free space. There is also a third equation relating J_ρ and J_ϕ with E_z . Although not required in the solution, it is given by

$$-\omega_\phi J_\rho + \omega_\rho J_\phi = \omega_0^2 \epsilon E_z. \quad (1c)$$

In what follows $\omega_\rho = \omega_\phi = 0$.

A subscript 1 will now be used to indicate the space above the

sheet (i.e., $z > -h$) and a subscript 2 for the space below the sheet (i.e., $z < -h$). Now because of the thinness of the sheet two of the boundary conditions may be written

$$H_{1\phi} - H_{2\phi} = -J_\rho\delta, \quad H_{1\rho} - H_{2\rho} = J_\phi\delta \text{ for } z \rightarrow -h. \quad (2a)$$

These are simply a statement of Ampere's law when applied to a thin rectangular circuit whose upper and lower long sides are above and below the sheet, respectively. To within the same approximation

$$E_\phi = E_{1\phi} = E_{2\phi}, \quad E_\rho = E_{1\rho} = E_{2\rho} \text{ for } z \rightarrow -h, \quad (2b)$$

which is a consequence of Faraday's law when applied to a similar rectangular circuit. In this case the line integral of E around the rectangle approaches zero since the magnetic current in the sheet is vanishingly small.

Using equations (1a) and (1b), the boundary conditions (2a) may now be written in the form

$$\begin{aligned} \eta(H_{1\phi} - H_{2\phi}) &= -ME_\rho - NE_\phi, \\ \eta(H_{1\rho} - H_{2\rho}) &= -NE_\rho + ME_\phi, \end{aligned} \quad (3)$$

where

$$M = \frac{\varepsilon\omega_0^2\delta(\nu + i\omega)}{(\nu + i\omega)^2 + \omega_z^2} \eta, \quad (4)$$

and

$$N = \frac{\varepsilon\omega_0^2\delta\omega_z}{(\nu + i\omega)^2 + \omega_z^2} \eta, \quad (5)$$

and $\eta = (\mu/\varepsilon)^{\frac{1}{2}} \cong 120\pi$.

For convenience in what follows the field is now represented in terms of two scalar functions which may be the z components of electric and magnetic Hertz vectors. Denoting these by Π and Π^* , it follows that, for axial symmetry ¹²⁾

$$\begin{aligned} E_\rho &= \frac{\partial^2}{\partial\rho\partial z} \Pi, & H_\rho &= \frac{\partial^2}{\partial\rho\partial z} \Pi^*, \\ E_\phi &= i\mu\omega \frac{\partial\Pi^*}{\partial\rho}, & H_\phi &= -i\varepsilon\omega \frac{\partial\Pi}{\partial\rho}, \\ E_z &= \left(k^2 + \frac{\partial^2}{\partial z^2}\right) \Pi, & H_z &= \left(k^2 + \frac{\partial^2}{\partial z^2}\right) \Pi^*. \end{aligned} \quad (6)$$

The four boundary conditions at the sheet (i.e., $z = -h$) now can be written conveniently in the form

$$ik(\Pi_1 - \Pi_2) = M\partial\Pi_1/\partial z + Nk\eta\Pi_1^*, \quad (7)$$

$$\eta(\partial\Pi_1^*/\partial z - \partial\Pi_2^*/\partial z) = -N\partial\Pi_1/\partial z + M\eta\Pi_1^*, \quad (8)$$

$$\Pi_1^* = \Pi_2^*, \quad (9)$$

$$\partial\Pi_1/\partial z = \partial\Pi_2/\partial z. \quad (10)$$

The boundary conditions as developed above are applicable for any exciting field which is symmetrical about the z axis.

§ 3. *Formal solution.* The source is now taken as a z -directed electric dipole at the origin. The primary fields are derived from an electric Hertz vector which has only a z component Π_p . In terms of the current I and length ds of the dipole

$$\Pi_p = \frac{Ids}{4\pi i\epsilon\omega} \frac{\exp[-ik(\rho^2 + z^2)^{\frac{1}{2}}]}{(\rho^2 + z^2)^{\frac{1}{2}}} \quad (11)$$

as is well known. This may be written in integral form as ¹²⁾

$$\Pi_p = p_e \int_0^\infty \exp(-u|z|) J_0(\lambda\rho)(\lambda/u) d\lambda \quad (12)$$

where $u = (\lambda^2 - k^2)^{\frac{1}{2}} = i(k^2 - \lambda^2)^{\frac{1}{2}}$ and $p_e = Ids/(4\pi i\epsilon\omega)$. Equation (12) may be written operationally in the form

$$\Pi_p = p_e \Gamma \exp(-uz) \text{ for } z > 0, = p_e \Gamma \exp(uz) \text{ for } z < 0,$$

where Γ is the symbolic operator for

$$\int_0^\infty \dots J_0(\lambda\rho)(\lambda/u) d\lambda. \quad (13)$$

The total fields in the regions above and below the sheet are then expressed in the general form

$$\Pi_1 = p_e \Gamma \{\exp(uz) + R_e(\lambda) \exp[-u(z + 2h)]\} \text{ for } 0 > z > -h, \quad (14)$$

$$\Pi_2 = p_e \Gamma [T_e(\lambda) \exp(uz)] \text{ for } z < -h, \quad (15)$$

$$\Pi_1^* = p_e \Gamma \{C_e(\lambda) \exp[-u(z + 2h)]\} \text{ for } 0 > z > -h, \quad (16)$$

$$\Pi_2^* = p_e \Gamma [C_e'(\lambda) \exp(uz)] \text{ for } z < -h. \quad (17)$$

These integrals satisfy the wave equation and satisfy the appropriate conditions at infinity. Furthermore, Π_1 has the proper singularity at the origin. The functions R_e , T_e , C_e and C_e are then obtained from the boundary conditions as expressed by equations (7) to (10). Thus

$$R_e(\lambda) = \frac{(2u + ikM)M + N^2ik}{ikD}, \quad (18)$$

$$T_e(\lambda) = 1 - R_e(\lambda), \quad (19)$$

$$C_e(\lambda) = C_e'(\lambda) = 2N/D\eta, \quad (20)$$

where

$$ikD = (M + 2ik/u)(2u + ikM) + N^2ik. \quad (21)$$

The formal solution for the magnetic dipole proceeds in almost the same fashion. It will suffice to sketch briefly the derivation. The primary field of the vertical magnetic dipole may be obtained from

$$\Pi_p^* = \phi_m \Gamma \exp(uz) \text{ for } z < 0, \quad (22)$$

where $\phi_m = I_m dA/4\pi$ in terms of the area dA and the circulating current I_m in the equivalent small loop. The resultant fields may then be obtained from

$$\Pi_1^* = \phi_m \Gamma \{ \exp(uz) + R_m(\lambda) \exp[-u(z + 2h)] \} \text{ for } 0 > z > -h, \quad (23)$$

$$\Pi_2^* = \phi_m \Gamma [T_m(\lambda) \exp(uz)] \text{ for } z < -h, \quad (24)$$

$$\Pi_1 = \phi_m \Gamma \{ C_m(\lambda) \exp[-u(z + 2h)] \} \text{ for } 0 > z > -h, \quad (25)$$

$$\Pi_2 = \phi_m \Gamma [C_m'(\lambda) \exp(uz)] \text{ for } z < -h, \quad (26)$$

where

$$R_m(\lambda) = - \frac{(M + 2ik/u)M + N^2}{D}, \quad (27)$$

$$C_m(\lambda) = - C_m'(\lambda) = 2\eta N/D, \quad (28)$$

$$T_m(\lambda) = 1 + R_m(\lambda). \quad (28b)$$

§ 4. *Evaluation of integrals.* The integrals occurring in the expressions for the Hertz vectors are now evaluated. First the integration variable is changed from λ to S . That is $\lambda = kS$ and conse-

quently $u = ikC$, where $C = (1 - S)^{\frac{1}{2}}$. Thus, for electric dipole excitation,

$$\Pi_1 = -ikp_e \int_0^{\infty} [e^{-ikC|z|} + R_e e^{-ikC(z+2h)}] C^{-1} J_0(k\rho S) S dS, \quad (29)$$

$$\Pi_1 = -ikp_e \int_0^{\infty} (1 - R_e) e^{ikCz} C^{-1} J_0(k\rho S) S dS, \quad (30)$$

$$\Pi_1^* = -i\varepsilon\omega p_e \int_0^{\infty} G e^{-ikC(z+2h)} C^{-1} J_0(k\rho S) S dS, \quad (31)$$

$$\Pi_2^* = -i\varepsilon\omega p_e \int_0^{\infty} G e^{ikCz} C^{-1} J_0(k\rho S) S dS, \quad (32)$$

where

$$R_e = \frac{(N^2 + M^2) + 2MC}{D}, \quad G = \frac{2N}{D}, \quad (33)$$

$$D = N^2 + (2 + M/C)(MC + 2). \quad (34)$$

Similarly for magnetic dipole excitation

$$\Pi_1^* = -ikp_m \int_0^{\infty} [e^{-ikC|z|} + R_m e^{-ikC(z+2h)}] C^{-1} J_0(k\rho S) S dS, \quad (35)$$

$$\Pi_2^* = -ikp_m \int_0^{\infty} (1 + R_m) e^{ikCz} C^{-1} J_0(k\rho S) S dS, \quad (36)$$

$$\Pi_1 = -i\mu\omega p_m \int_0^{\infty} G e^{-ikC(z+2h)} C^{-1} J_0(k\rho S) S dS, \quad (37)$$

$$\Pi_1 = +i\mu\omega p_m \int_0^{\infty} G e^{ikCz} C^{-1} J_0(k\rho S) S dS, \quad (38)$$

where

$$R_m = -\frac{N^2 + M^2 + 2M/C}{D}. \quad (39)$$

It is seen that these integrals have poles at roots of

$$D = 0. \quad (40)$$

This equation can be rewritten in the form

$$2MC^2 + (M^2 + N^2 + 4)C + 2M = 0, \quad (41)$$

which is simply a quadratic in C . Thus, the roots are given by

$$C = \frac{-(M^2 + N^2 + 4) \pm [(M^2 + N^2 + 4)^2 - 16M^2]^{\frac{1}{2}}}{4M} \quad (42)$$

and they are designated in what follows as C_a and C_b . The factors in the integrands may then be written in the following form

$$\frac{R_e}{C} = \frac{N^2 + M^2}{2M(C_a - C_b)} \left(\frac{1}{C - C_a} - \frac{1}{C - C_b} \right) + \frac{1}{C_a - C_b} \left(\frac{C_a}{C - C_a} - \frac{C_b}{C - C_b} \right), \quad (43)$$

$$\frac{R_m}{C} = -\frac{N^2 + M^2}{2M(C_a - C_b)} \left(\frac{1}{C - C_a} - \frac{1}{C - C_b} \right) + \frac{1}{(C_a - C_b)C_a} \left(\frac{1}{C} - \frac{1}{C - C_a} \right) - \frac{1}{(C_a - C_b)C_b} \left(\frac{1}{C} - \frac{1}{C - C_b} \right), \quad (44)$$

$$\frac{G}{C} = \frac{N}{M(C_a - C_b)} \left(\frac{1}{C - C_a} - \frac{1}{C - C_b} \right). \quad (45)$$

Thus we are concerned with the two basic integrals

$$P_0(\alpha) = \int_0^\infty e^{-ikC\alpha} C^{-1} J_0(k\rho S) S dS, \quad (46)$$

$$Q(\alpha, \Delta) = \int_0^\infty e^{-ikC\alpha} (C + \Delta)^{-1} J_0(k\rho S) S dS, \quad (47)$$

where $C = (1 - S^2)^{\frac{1}{2}}$.

The first integral is well known and is given by

$$P_0(\alpha) = \frac{\exp[-ik(\alpha^2 + \rho^2)^{\frac{1}{2}}]}{-ik(\alpha^2 + \rho^2)^{\frac{1}{2}}}. \quad (48)$$

The other integral is not so simple; however, it yields to a saddle-point integration¹³⁾¹⁴⁾. In this case, proper attention should be paid to the location of the pole at $C = -\Delta$ in relation to the deformed path of integration through the saddle-point. The result is

$$Q(\alpha, \Delta) \cong \frac{\cos \theta}{\cos \theta + \Delta} \frac{e^{-ikR}}{(-ikR)} + qQ_s(\alpha, \Delta) \quad (49)$$

where $\cos \theta = \alpha/(\alpha^2 + \rho^2)^{\frac{1}{2}}$, $R = (\alpha^2 + \rho^2)^{\frac{1}{2}}$,

$$Q_s(\alpha, \Delta) = -i\pi\Delta e^{ikR\Delta \cos \theta} H_2^{(2)}(kR \sin \theta \sqrt{1 - \Delta^2}), \quad (50)$$

and

$$q = 1 \text{ for } \arg \left[\sin \frac{1}{2} \left(\frac{\pi}{2} - \theta + \arcsin \Delta \right) \right] > \frac{\pi}{4},$$

$$= 0 \text{ for } \arg \left[\sin \frac{1}{2} \left(\frac{\pi}{2} - \theta + \arcsin \Delta \right) \right] < \frac{\pi}{4}.$$

$H_0^{(2)}(Z)$ is the Hankel function of the second kind of order zero.

The first term in (49) is the contribution from the saddle-point, and the second term is the residue of the pole which may or may not be captured in the resulting deformation of the contour to its path of steepest descent through the saddle-point. The above expression for $Q(\alpha, \Delta)$ is valid in the far field such that terms which vary as $1/R^2$, $1/R^3$, etc., may be neglected. Furthermore, there is also a restriction that the pole and the saddle-point are not too close. This is violated for example if θ is near $\pi/2$ and $|\Delta|$ is small. In this situation, however, the integral for $Q(\alpha, \Delta)$ may be evaluated by a modified saddle-point technique. In this case ¹³⁾

$$Q(\alpha, \Delta) \cong \left\{ \frac{\cos \theta}{\cos \theta + \Delta} + \frac{\Delta}{\cos \theta + \Delta} \cdot [1 - i\sqrt{\pi p} e^{-p} \operatorname{erfc}(ip^{1/2})] \right\} \frac{e^{-ikR}}{(-ikR)}, \quad (51)$$

where $p = -\frac{1}{2}ik\Delta^2(\alpha^2 + \rho^2)^{1/2}$. This result is valid for $|\Delta|^2 \ll 1$ and $k\rho \gg 1$.

It is now a simple matter to express the Hertz vectors in terms of the basic integrals $P_0(\alpha)$ and $Q(\alpha, \Delta)$. For example, in the region above the ionized sheet (i.e., $z > 0$) and for electric dipole excitation,

$$\frac{\Pi_1}{-ikp_e} = P_0(|z|) + \frac{N^2 + M^2}{2M(C_a - C_b)} (Q_a - Q_b) + \frac{1}{(C_a - C_b)} (C_a Q_a - C_b Q_b), \quad (52)$$

$$\frac{\Pi_1^*}{-i\epsilon\omega p_e} = \frac{N}{M(C_a - C_b)} (Q_a - Q_b), \quad (53)$$

while for magnetic dipole excitation

$$\begin{aligned} \frac{H_1^*}{-ikp_m} = & P_0(|z|) - \frac{N^2 + M^2}{2M(C_a - C_b)} (Q_a - Q_b) + \\ & + \frac{1}{(C_a - C_b)C_a} [P_0(2h + z) - Q_a] - \frac{1}{(C_a - C_b)C_b} [P_0(2h + z) - Q_b] \end{aligned} \quad (54)$$

and

$$\frac{H_1}{-i\mu\omega p_m} = \frac{N}{M(C_a - C_b)} (Q_a - Q_b), \quad (55)$$

where $Q_a = Q(2h + z, -C_a)$ and $Q_b = Q(2h + z, -C_b)$.

§ 5. *The radiation and surface wave fields.* Carrying out the differentiations indicated by (6), explicit expressions for the field components are readily obtained. The resultant electric field in the far field may be conveniently written as

$$\mathbf{E} = \mathbf{E}^{(R)} + \mathbf{E}^{(S)}, \quad (56)$$

where $\mathbf{E}^{(R)}$ is the radiation field and $\mathbf{E}^{(S)}$ is the surface wave field.



Fig. 2. Thin ionized sheet with dipole and spherical coordinate system for radiation pattern computation.

These are respectively connected with the saddle-point and the pole contribution. The radiation field is conveniently written in terms of a spherical coordinate system (r, θ, ϕ) centered at the dipole. Thus the far fields for electric dipole excitation have the form

$$E_\theta^{(R)} \cong -p_e k^2 P_e(\theta) \exp(-ikr)/r$$

and

$$E_\phi^{(R)} \cong p_e k^2 Z_e(\theta) \exp(-ikr)/r, \quad (58)$$

where $P_e(\theta)$ and $Z_e(\theta)$ are by definition the patterns of the in-

polarized and cross-polarized radiation. These have the form, for $0 < \theta < \pi/2$,

$$P_e(\theta) \cong \left[1 + \frac{N^2 + M^2 + 2M \cos \theta}{D(\cos \theta)} e^{-i2kh \cos \theta} \right] \sin \theta, \quad (59)$$

$$Z_e(\theta) \cong 2N/D(\cos \theta) \quad (60)$$

while for $\pi/2 < \theta < \pi$,

$$P_e(\theta) \cong \left[1 - \frac{N^2 + M^2 - 2M \cos \theta}{D(-\cos \theta)} \right] \sin \theta, \quad (61)$$

$$Z_e(\theta) \cong 2N/D(-\cos \theta) \quad (62)$$

where

$$D(\cos \theta) = N^2 + \left(2 + \frac{M}{\cos \theta} \right) (M \cos \theta + 2). \quad (63)$$

Similarly for magnetic dipole excitation,

$$E_\phi^{(R)} \cong p_m k^2 P_m(\theta) \exp(-ikr)/r \quad (64)$$

and

$$E_\theta^{(R)} \cong -p_m k^2 Z_m(\theta) \exp(-ikr)/r, \quad (65)$$

For $0 < \theta < \pi/2$, the patterns are given by

$$P_m(\theta) \cong \left[1 - \frac{N^2 + M^2 + 2M/\cos \theta}{D(\cos \theta)} e^{-i2kh \cos \theta} \right] \sin \theta, \quad (66)$$

$$Z_m(\theta) \cong 2N/D(\cos \theta); \quad (67)$$

while, for $\pi/2 < \theta < \pi$, they are given by

$$P_m(\theta) \cong \left[\frac{N^2 + M^2 - 2M/\cos \theta}{D(-\cos \theta)} \right] \sin \theta \quad (68)$$

and

$$Z_m(\theta) \cong 2N/D(-\cos \theta). \quad (69)$$

The surface wave fields are associated with the contribution from the pole. Normally, for a particular situation, only one of the roots C_a and C_b satisfies the condition

$$\arg \left[\sin \frac{1}{2} \left(\frac{\pi}{2} - \theta + \arcsin \Delta \right) \right] > \frac{\pi}{4},$$

where $\Delta = -C_a$ or $-C_b$. The root which does satisfy this condition

is designated C_a . In the case of electric dipole excitation, the surface wave fields may be derived from the following Hertz vectors:

$$\Pi_{1S} = -ikp_e \left[\frac{N^2 + M^2 + 2MC_a}{2M(C_a - C_b)} \right] Q_S(2h + z, -C_a) \quad (70)$$

and

$$\Pi_{1S}^* = -i\epsilon\omega p_e \frac{N}{M(C_a - C_b)} Q_S(2h + z, -C_a), \quad (71)$$

where the function Q_S is given by (50).

Similarly for magnetic dipole excitation

$$\Pi_{1S}^* = ikp_m \left[-\frac{N^2 + M^2 + 2M/C_a}{2M(C_a - C_b)} \right] Q_S(2h + z, -C_a) \quad (72)$$

and

$$\Pi_{1S} = -i\mu\omega p_m \frac{N}{M(C_a - C_b)} Q_S(2h + z, -C_a). \quad (73)$$

Explicit expressions for the field components are then obtained by carrying out the differentiations indicated in (6).

In terms of cylindrical coordinates (ρ, ϕ, z) it is not difficult to show that, for electric dipole excitation and for $k\rho \gg 1$,

$$(E_z)_{1S} \cong -k^3 p_e \frac{N^2 + M^2 + 2MC_a}{2M(C_a - C_b)} \left(\frac{2\pi i}{k\rho} \right)^{\frac{1}{2}} S_a^{\frac{1}{2}} \cdot e^{-ikS_a z} e^{-ikC_a(z+2h)}, \quad (74)$$

where $S_a = (1 - C_a^2)^{\frac{1}{2}}$.

In the case of magnetic dipole excitation

$$(E_\phi)_{1S} \cong k^2 \mu \omega p_m \frac{N^2 + M^2 + 2M/C_a}{2M(C_a - C_b)} \left(\frac{2\pi i}{k\rho} \right)^{\frac{1}{2}} S_a^{\frac{1}{2}} \cdot e^{-ikS_a z} e^{-ikC_a(z+2h)}. \quad (75)$$

It is clearly evident that these have the form of a cylindrical surface wave. The horizontal component of the phase velocity is $1/\text{Re } S_a$ relative to c ; it is thus a "slow wave." The attenuation in the horizontal direction is $-\text{Im } kS_a$ nepers per unit length and the attenuation in the vertical direction is $-\text{Im } kC_a$ nepers per unit length.

A revealing property of the surface wave is its polarization of the electric vector in the plane normal to the sheet. In the case of

electric dipole excitation, the polarization factor $(\text{Pol.})_e$ is given by

$$(\text{Pol.})_e = \left(\frac{E_\phi}{E_z} \right)_{1S} = \frac{1}{S_a} \frac{2N}{N^2 + M^2 + 2MC_a}, \quad (76)$$

whereas, for magnetic dipole excitation, the polarization factor $(\text{Pol.})_m$ is given by

$$(\text{Pol.})_m = \left(\frac{E_z}{E_\phi} \right)_{1S} = - \frac{2NS_a}{N^2 + M^2 + 2M/C_a}. \quad (77)$$

These expressions are also applicable for the region below the sheet. In this case it is just necessary to change the sign on the right-hand side of (76) and (77). It is rather interesting to note that the $(\text{Pol.})_e$ and $(\text{Pol.})_m$ are real quantities if the collision frequency is zero. Thus the surface wave is linearly polarized in this loss-free case.

§ 6. *Presentation of results.* Using the formulae developed in the preceding sections, calculations of the radiation and surface wave

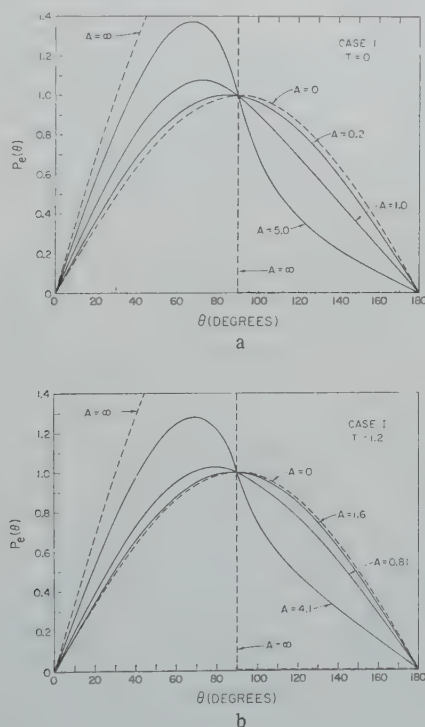


Fig. 3. The in-polarized radiation patterns for an electric dipole oriented perpendicular to a thin plasma sheet for $\nu \gg \omega$.

fields have been carried out for two limiting cases. The first of these is denoted as case I, and the collision frequency ν is assumed to be very large compared to ω . Thus $\nu + i\omega$, where it occurs in the expression for M and N , can be replaced by ν . It then follows that

$$M = A \frac{1}{1 + T^2}, \quad N = A \frac{T}{1 + T^2},$$

where $A = \delta\omega_0^2/c\nu$ and $T = \omega_z/\nu$.

The pattern $P_e(\theta)$ for this case is shown in figs. 3a and 3b for $T = 0$ and 1.2, respectively, for a range of values for A and for $kh = 0$. The shapes of the curves are very similar. It appears that the influence of a magnetic field (i.e., $T > 0$) is to slightly decrease the reflectivity at low grazing angles. Furthermore, in both cases, the reflectivity increases as A becomes large. In the limiting case of $A = \infty$ there is perfect reflection and zero transmission through the sheet.

The pattern $Z_e(\theta)$ for the cross-polarized radiation from the vertical dipole is shown in figs. 4a and 4b for $T = 0.6$ and 1.2

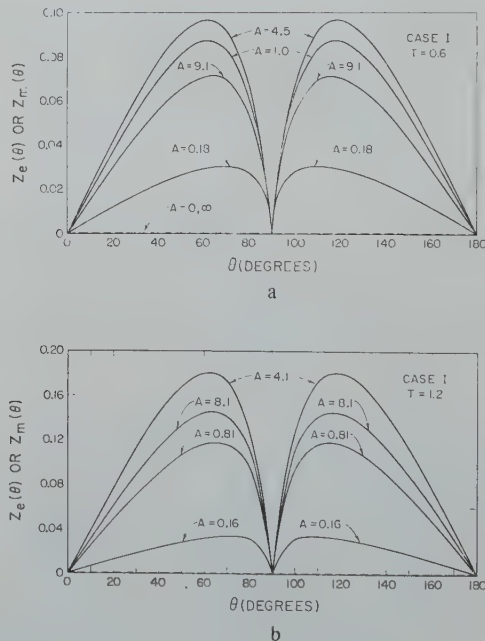


Fig. 4. The cross-polarized radiation pattern for electric or magnetic dipole oriented perpendicular to a thin plasma sheet for $\nu \gg \omega$.

respectively. The corresponding pattern for $T = 0$ is simply zero as the cross-polarized field vanishes when the magnetic field is removed. The pattern $Z_e(\theta)$ is symmetrical about $\theta = 90^\circ$ which is not surprising since the direct radiation from the source dipole, in this polarization, is zero. It is also interesting to note that the cross-polarized radiation apparently reaches a maximum for A equal to about 5 for the two values of T chosen. Another important factor is that the pattern $Z_e(\theta)$ does not depend on the height h of the dipole, provided, of course, that the distance R to the observer is much greater than h .

The radiation pattern $Z_m(\theta)$ for the cross-polarized fields of a magnetic dipole is also shown in Figs. 4a and 4b. Because of the normalization $Z_m(\theta)$ is identical with $Z_e(\theta)$.

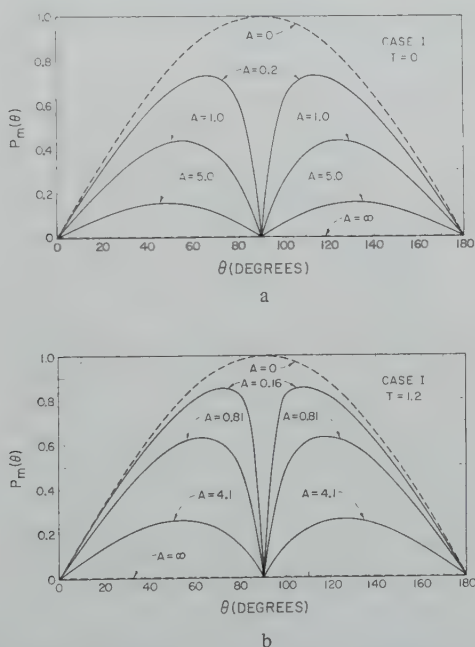


Fig. 5. The in-polarized radiation patterns for a magnetic dipole oriented perpendicular to a thin plasma sheet for $\nu \gg \omega$.

The pattern $P_m(\theta)$ for the in-polarized radiation from the magnetic dipole is shown in Figs. 5a and 5b for $T = 0$ and 1.2, respectively. Since $kh = 0$, these patterns are also symmetrical. In the limiting case $A = \infty$ the sheet tends to cancel the fields completely.

The radiation pattern functions $P_e(\theta)$, $Z_e(\theta)$, $P_m(\theta)$ and $Z_m(\theta)$ are adequate descriptions of the total radiation field for case I since the surface wave contribution is negligible in most cases. This follows from the fact that the surface wave contribution Q_s in (49) is not excited. Furthermore, even at grazing angles and large values of A , it may be established from (51) that

$$Q(\alpha, \Delta) \cong \frac{\cos \theta}{\cos \theta + \Delta} \frac{e^{-ikR}}{(-ikR)},$$

provided $|p| \gg 1$ and $\arg \Delta < \pi/4$.

The other limiting situation, denoted as case II, occurs when the collision frequency ν is much less than ω . Then $\nu + i\omega$ may be replaced by $i\omega$ in the expressions for M and N . Thus

$$M = iB \frac{1}{Q^2 - 1}, \quad N = B \frac{Q}{Q^2 - 1},$$

where $B = \delta\omega_0^2/c\omega$ and $Q = \omega_z/\omega$.

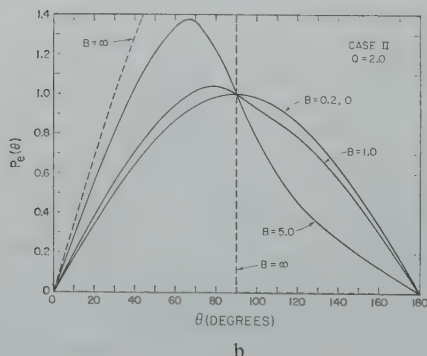
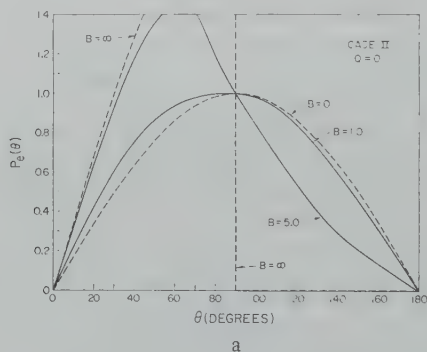


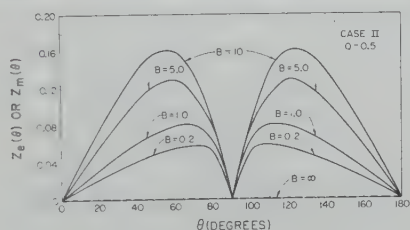
Fig. 6. The in-polarized radiation patterns for an electric dipole oriented perpendicular to a thin plasma sheet for $\nu \ll \omega$.

It is noted that for $Q < 1$, M is a positive imaginary number and N is a positive real number. For $Q > 1$, M is a negative imaginary number and N is a negative real number.

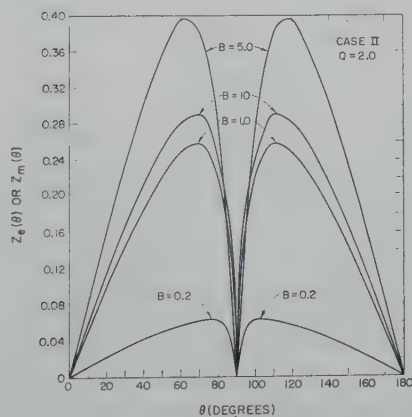
The patterns $P_e(\theta)$, $Z_e(\theta)$, $P_m(\theta)$ and $Z_m(\theta)$ are plotted in figs. 6 to 8 for $kh = 0$. In many respects these are quite similar to the corresponding patterns for case I. Thus B is somewhat analogous to A , and Q is somewhat analogous to T . This is provided Q is not near unity. In fact in this limiting case the sheet behaves as a perfect reflector and thus

$$\begin{aligned} P_e(\theta) &\cong \sin \theta \quad \text{for } 0 < \theta < 90^\circ, \\ &\cong 0 \quad \text{for } 90^\circ < \theta < 180^\circ, \\ Z_e(\theta) = Z_m(\theta) &\cong 0, \quad P_m(\theta) \cong 0. \end{aligned}$$

Further computations would be required to adequately describe the behaviour of the patterns in the transition region on either side of $Q=1$.



a



b

Fig. 7. The cross-polarized radiation pattern for electric or magnetic dipole oriented perpendicular to a thin plasma sheet for $\nu \ll \omega$.

In case II the surface wave cannot be neglected. In fact, near the sheet and at large distances from the source the surface wave considerably exceeds the radiation field. The characteristics of the surface wave excited by either the electric or magnetic dipole are related to the roots C_a and C_b of (42). In the present case C_a is a

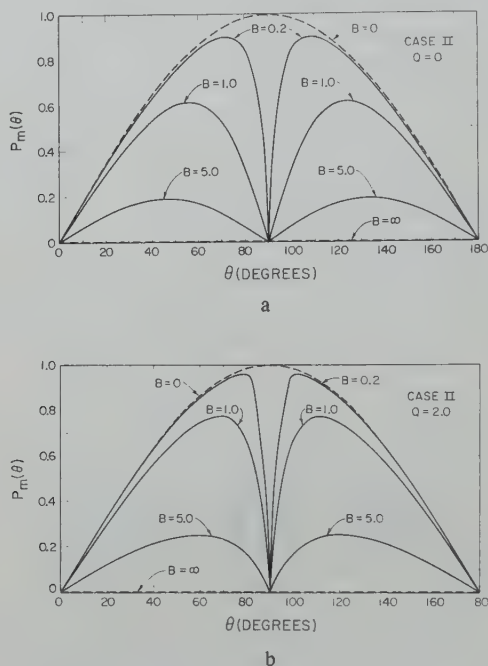


Fig. 8. The in-polarized radiation patterns for a magnetic dipole oriented perpendicular to a thin plasma sheet for $\nu \ll \omega$.

negative imaginary quantity and C_b has a positive imaginary part. In fig. 9a the positive real quantity iC_a is plotted as a function of B for a range of Q values. In fig. 9b the negative real quantity iC_b is plotted in a similar fashion. The vertical decay of the surface wave is numerically equal to ikC_a in nepers per meter and this is proportional to the ordinate in fig. 9a. A strongly trapped wave corresponds to large values of iC_a .

The quantity $-iC_b$ shown in fig. 9b does not correspond to a physical wave. If for no other reason it would be rejected since it would correspond to a wave increasing with height and thus cannot be excited by any sensible launching device. On the other hand, the

quantity C_b does enter into the amplitude coefficient of the wave as indicated by (74) and (76) for example.

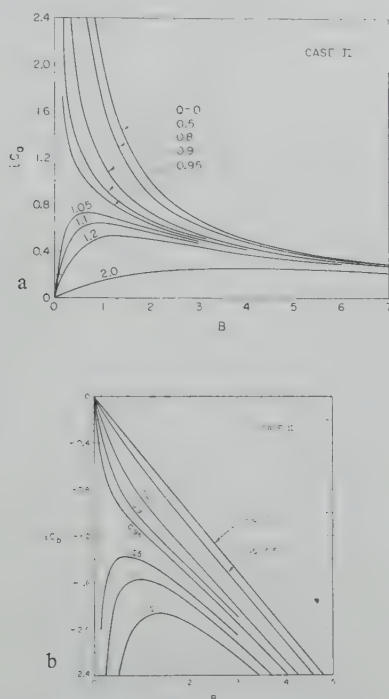


Fig. 9. *a*) The positive real quantity iC_a as a function of the parameter B for $\nu \ll \omega$. The ordinate is a measure of the decay of the surface wave normal to the sheet while the abscissa is proportional to the electrical thickness of the sheet.

b) The negative real quantity iC_b as a function of the parameters B for $\nu \ll \omega$. Unlike C_a this does not correspond to a trapped surface wave.

The phase velocity of the surface wave, relative to c , is shown in fig. 10. The ordinate is the quantity $1/\text{Re } S_a$ where

$$S_a(1 - C_a^2)^{\frac{1}{2}} = (1 + |C_a|^2)^{\frac{1}{2}}.$$

In general it is a "slow wave". The retardation is greatest when the value of B is small and Q is less than one. As Q approaches one, that is as the operating approaches the gyro-frequency, there is a rather abrupt transition of the behaviour of the phase velocity.

Finally, the polarization factors $(\text{Pol.})_e$ and $(\text{Pol.})_m$ are shown in figs. 11*a* and 11*b*. These are plotted as a function of B for various

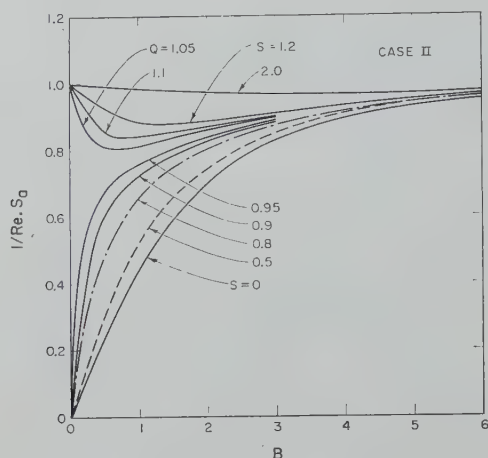


Fig. 10. The relative phase velocity of the surface wave as a function of B for $\nu \ll \omega$.

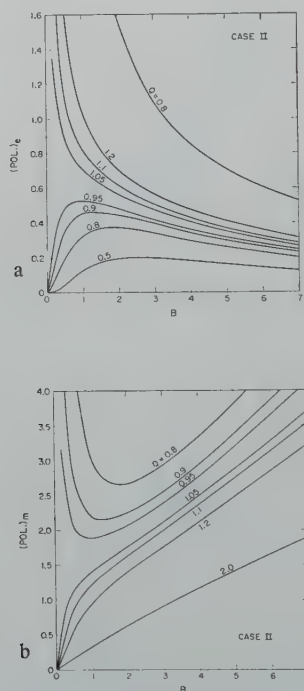


Fig. 11. *a*) The wave polarization of the surface wave excited by an electric dipole for $\nu \ll \omega$. The ordinate is the ratio of the electric field components normal to the direction of propagation of the surface wave.

b) The wave polarization of the surface wave excited by a magnetic dipole. N.B. $(\text{POL.})_e \times (\text{POL.})_m = 1$.

values of Q . The factor $(\text{Pol.})_e$, which is appropriate for electric dipole excitation, is seen to be small for $Q < 1$, which means that the surface wave is essentially vertically polarized. As Q is increased, it is seen that the horizontally polarized component increases. There is again an abrupt transition at $Q = 1$.

The situation is somewhat different for magnetic dipole excitation as seen in fig. 11*b*. The cross-polarized component is now vertically polarized, and it appears to be quite large particularly if $Q < 1$.

§ 7. *Conclusions.* The representation of a planar slab of ionized media by a thin sheet with appropriate boundary conditions appears to be a very useful technique. The simplification of the problem is attained, however, at the expense of a loss in generality. It is only when the thickness of the sheet is very small compared to other significant dimensions that this idealization is expected to be of any practical use. Nevertheless, the behaviour of the solution brings to light many interesting features which could be present in situations where waves are propagating along interfaces between isotropic and anisotropic media.

Acknowledgements. I would like to thank Mrs. Nancy Carter and Mrs. Alyce Conda for carrying out the computations and Mrs. Eileen Brackett for her assistance in preparing the manuscript. I am particularly indebted to Bernard Wieder for his critical reading of the manuscript. The work in this paper was supported by the U.S. Air Force Cambridge Research Laboratories.

Received 12th July, 1960.

REFERENCES

- 1) Ratcliffe, J. A., *Magneto-ionic theory*, Cambridge University Press, 1959.
- 2) Goldstein, L., *Electrical discharges in gases and modern electronics*, in Vol. VII of *Adv. in Electronics and Electron Physics*, Academic Press, New York, 1958.
- 3) Lamb, L. and S. C. Lin, *J. Appl. Phys.* **28** (1957) 754.
- 4) Adler, F. P., *Appl. J. Phys.*, **25** (1954) 903.
- 5) Goldstein, L., *Trans. Instn. Radio Engrs Vol. MTT-6* (1958) 19.
- 6) Bremmer, H., *Terrestrial radio waves*, Elsevier Publ. Co., Amsterdam 1949.
- 7) Johler, J. R. and L. C. Walters, *Nat. Bur. Stand. J. Res.* **64D** (1960) 269.
- 8) Budden, K. G., *Phil. Trans. Roy. Soc. London, A* **248** (1955) 45.
- 9) Poeverlein, H., *J. Atmos. Terr. Phys.* **12** (1958) 126.
- 10) Wait, J. R., *Can. J. Phys.* **29** (1951) 577.
- 11) Wait, J. R., *Appl. Sci. Res. B* **3** (1953) 230.
- 12) Wait, J. R., *Electromagnetic radiation from cylindrical structures*, Pergamon Press, London 1959.
- 13) Wait, J. R., *Nat. Bur. Stand. J. Res.* **59** (1957) 365.
- 14) Furutsu, K., *J. Rad. Res. Lab. (Tokyo)* **6** (1959) 269.

IMPEDANCE BOUNDARY CONDITIONS FOR IMPERFECTLY CONDUCTING SURFACES

by T. B. A. SENIOR

The University of Michigan, The Radiation Laboratory, Ann Arbor, Michigan, U.S.A

Summary

It is shown how the exact electromagnetic boundary conditions at the surface of a material of large refractive index can be approximated to yield the usual impedance or Leontovich boundary conditions. These conditions relate the tangential components of the electric and magnetic fields (or the normal components and their normal derivatives) via a surface impedance which is a function only of the electromagnetic properties of the material. They are valid for surfaces whose radii of curvature are large compared with the penetration depth, and also for materials which are not homogeneous but whose properties vary slowly from point to point. As the refractive index (or conductivity) increases to infinity, the conditions go over uniformly to the conditions for perfect conductivity.

§ 1. *Introduction.* In its most straightforward form an impedance boundary condition is one which relates the tangential components of the electric and magnetic fields via an impedance factor which is a function of the properties of the surface and, possibly, of the field which is incident upon it. The concept of a surface impedance is, of course, not new, and has long been used in a variety of engineering calculations. On the other hand, the idea of incorporating this impedance into the initial formulation of a boundary value problem appears to date only from the beginning of the last war.

During the early 1940's a considerable number of Russian papers were published dealing with various aspects of propagation over the earth, and in these an attempt was made to take into account the properties of actual ground materials by specifying an impedance boundary condition at the surface. This represented a departure from the (then) accepted practice of studying in complete detail certain problems of a very idealized nature, and paved the way for a

discussion of propagation over an inhomogeneous, as well as a rough, earth. It was shown that the impedance boundary condition is a valid approximation to the exact condition when the refractive index of the ground is large compared with unity, and the surface impedance can be expressed directly in terms of the electromagnetic properties of the material. These boundary conditions are usually attributed to Leontovich (see, for example, Fock ¹) and were described by Leontovich ²) himself in 1948. They were first applied to a physical problem by Alpert ³) in 1940, and were used extensively in Russian work throughout the war. A short summary of their application to propagation problems has been given by Feinberg ⁴).

Unfortunately, the proofs associated with these conditions are not readily accessible. Although the conditions are frequently employed in modern electromagnetic theory, it would often appear that either their degree of generality or the restrictions which they require are not fully appreciated. It is the purpose of the present paper to collect in one place some of the proofs associated with these conditions as they apply to the surface of a material of large but finite refractive index. This also serves to provide the necessary background for a subsequent paper in which impedance boundary conditions are developed for a surface which is perfectly conducting but geometrically rough.

In § 2 the exact electromagnetic boundary conditions are briefly discussed. The approximate conditions for a flat interface between a homogeneous isotropic medium and free space are derived in § 3, and the flat interface is generalized to a surface of large radius of curvature in § 4. The necessary modifications when the properties of the medium vary from point to point are given in § 5.

§ 2. *Exact boundary conditions.* At the interface between two homogeneous isotropic media neither of which is perfectly conducting, an electromagnetic field satisfies the boundary conditions

$$[\hat{n} \times \mathbf{E}] = 0, \quad (1)$$

$$[\hat{n} \cdot \mathbf{D}] = 0, \quad (2)$$

$$[\hat{n} \times \mathbf{H}] = 0, \quad (3)$$

$$[\hat{n} \cdot \mathbf{B}] = 0, \quad (4)$$

where \mathbf{n} is a unit vector normal and the square brackets denote the discontinuities in the corresponding field components on crossing the boundary. In these equations \mathbf{E} and \mathbf{H} are the electric and magnetic field vectors in terms of which $\mathbf{B} = \mu\mathbf{H}$, where μ is the permeability, and $\mathbf{D} = \epsilon\mathbf{E}$, where ϵ is the complex permittivity *)

$$\epsilon = \epsilon' + i \frac{\sigma}{\omega}.$$

A consequence of using a complex (rather than a real) permittivity is that no surface charge distribution appears on the right-hand side of (2).

Equations (1) through (4) are not all independent and therefore constitute a set of boundary conditions at the interface which are more than sufficient. If, for example, the first two are selected, the use of Maxwell's equations shows that (3) and (4) are satisfied automatically. Similarly if the conditions (3) and (4) upon the magnetic field are selected; and indeed, a specification of all the tangential components (\mathbf{E} and \mathbf{H}), or both normal components will suffice. On the other hand, (1) and (4) or (2) and (3) do not constitute sufficient sets since, for example, (1) is not independent of (4).

It should be emphasized that in spite of the so-called "proofs" presented in many textbooks the boundary conditions (1) through (4) cannot be verified by experiments carried out in a homogeneous medium, nor is the author aware of any method by which they can be deduced from Maxwell's equations. In consequence, it appears necessary to regard them as an essential postulate of electromagnetic theory, and the consequent agreement between theory and experiment then provides the evidence in favour of their validity.

It will be observed that the boundary conditions relate the field in the first medium (which we shall henceforth regard as free space) to that in the second medium, and in practice are not always easy to apply in the solution of problems. When the second medium is perfectly conducting, however, the fields therein are identically zero and the only fields to be considered are those in free space. In this case (1) and (4) reduce to

$$\hat{\mathbf{n}} \times \mathbf{E} = 0, \quad (5)$$

$$\hat{\mathbf{n}} \cdot \mathbf{B} = 0, \quad (6)$$

*) A time variation $e^{i\omega t}$ is assumed.

but (2) and (3) are replaced by

$$\hat{n} \cdot \mathbf{D} = \delta, \quad (7)$$

$$\hat{n} \times \mathbf{H} = \mathbf{K}, \quad (8)$$

where δ and \mathbf{K} are surface distributions of charge and current respectively. Since these are known only when the fields \mathbf{E} and \mathbf{H} have been determined, (7) and (8) do not represent boundary conditions in the usual sense, and we are therefore left with (5) and (6) from which to determine the fields in free space. On the other hand, a further degeneracy now appears and whereas two conditions were required when the medium was not perfectly conducting, a single equation now suffices. Thus, for example, (5) alone *) specifies the fields at all points, and (6), (7) and (8) can all be deduced therefrom.

When the refractive index N of the second medium relative to free space is large compared with unity, boundary conditions can be derived which are analogous to (5) and (6) in that the only fields which appear are those in free space (medium 1). This permits a considerable simplification in the analysis of any scattering or diffraction problem involving bodies which are not perfectly conducting, since it avoids the need to calculate the fields within the body. These new conditions are an approximation to (1) through (4), and their derivation is based on the neglect of terms $O(1/N^2)$ in comparison with unity. We shall first obtain the conditions for an infinite flat interface and later generalize the results so as to apply to a more practical set of circumstances.

§ 3. *Approximate boundary conditions for a flat interface.* Consider a homogeneous isotropic medium whose permittivity, permeability and conductivity are ϵ' , μ and σ respectively. It is assumed that this medium occupies the region $z < 0$ of a Cartesian coordinate system (x, y, z) . The halfspace $z > 0$ is free space, the permittivity and permeability of which are ϵ_0 and μ_0 .

Relative to free space the complex refractive index of the medium is

$$N = \sqrt{\frac{\mu}{\mu_0} \left(\frac{\epsilon'}{\epsilon_0} + i \frac{\sigma}{\omega \epsilon_0} \right)},$$

*) Although a radiation condition (or its equivalent) must also be imposed if the region is infinite in extent, and an edge condition if this is appropriate.

and boundary conditions at the interface $z = 0$ will now be derived under the assumption that $|N|$ is large compared with unity. It will be appreciated that this requirement is satisfied by a material whose dielectric constant ϵ'/ϵ_0 is large, as well as by a material of high conductivity. For the purposes of the analysis it is convenient to introduce the parameter η defined by $\eta = \mu/(\mu_0 N)$; thus

$$\eta = \frac{1}{\sqrt{\frac{\mu_0}{\mu} \left(\frac{\epsilon'}{\epsilon_0} + i \frac{\sigma}{\omega \epsilon_0} \right)}} \quad (9)$$

and is zero for perfect conductivity.

Let us denote by (\mathbf{E}, \mathbf{H}) the electromagnetic field in $z > 0$, and by $(\mathbf{E}', \mathbf{H}')$ the field in $z < 0$. From the divergence condition we have

$$\frac{\partial E_x}{\partial x} + \frac{\partial E_y}{\partial y} + \frac{\partial E_z}{\partial z} = 0 \quad (10)$$

and similarly

$$\frac{\partial E'_x}{\partial x} + \frac{\partial E'_y}{\partial y} + \frac{\partial E'_z}{\partial z} = 0. \quad (11)$$

At the interface $z = 0$ the tangential components of the electric field are continuous, so that

$$E_x = E'_x, \quad E_y = E'_y$$

and hence, by tangential differentiation,

$$\frac{\partial E_x}{\partial x} = \frac{\partial E'_x}{\partial x}, \quad \frac{\partial E_y}{\partial y} = \frac{\partial E'_y}{\partial y}.$$

Eq. (10) and (11) then give

$$\frac{\partial E_z}{\partial z} = \frac{\partial E'_z}{\partial z}. \quad (12)$$

In the medium, however,

$$\frac{\partial^2 E'_z}{\partial x^2} + \frac{\partial^2 E'_z}{\partial y^2} + \frac{\partial^2 E'_z}{\partial z^2} + k^2 N^2 E'_z = 0 \quad (13)$$

where k is the propagation constant in free space. If $|N| \gg 1$, the field is rapidly varying in the z direction, leading to a large value of

$\partial^2 E_z' / \partial z^2$, and by comparison with this the x and y derivatives are small. This fact is, perhaps, most clearly seen by considering a plane wave incident on the boundary from the direction of free space. Because of the large value of $|N|$, application of Snell's law shows that the transmitted field is deflected toward the normal. For a fixed direction of incidence, the angle between the direction of the transmitted field and the normal is $O(1/|N|)$, which implies that $\partial^2 E_z' / \partial x^2$ and $\partial^2 E_z' / \partial y^2$ are smaller than $\partial^2 E_z' / \partial z^2$ by a factor of order $|N|^2$. Accordingly, in (13) the first two derivatives can be neglected in comparisons with the third, and the equation then becomes

$$\frac{\partial^2 E_z'}{\partial z^2} + k^2 N^2 E_z' = 0. \quad (14)$$

The solution of this is

$$E_z' = A e^{i k N z} + B e^{-i k N z}, \quad (15)$$

where A and B are constants as yet undetermined. If N is defined to have positive imaginary part, the fact that the medium is infinite in extent implies that A must be zero, since the field E_z' must correspond to propagation in the negative z direction. Hence

$$E_z' = B e^{-i k N z} \quad (16)$$

from which we obtain

$$\frac{\partial E_z'}{\partial z} = -i k N E_z'. \quad (17)$$

But from (2)

$$E_z' = \frac{\epsilon_0}{\epsilon} E_z \quad (18)$$

at the interface, and this can be combined with equation (17) to give

$$\frac{\partial E_z'}{\partial z} = i k N \frac{\epsilon_0}{\epsilon} E_z = -i k \eta E_z \quad (19)$$

at $z = 0$. Using (12) we now have

$$\frac{\partial E_z}{\partial z} = -i k \eta E_z, \quad (20)$$

and this is one of the required boundary conditions at the interface. Eq. (20) is accurate to the first order in η .

A similar analysis can be developed for the normal component of the magnetic field. From the divergence condition we obtain

$$\frac{\partial H_z}{\partial z} = \frac{\partial H_z'}{\partial z},$$

(cf (12)) and since we also have

$$\frac{\partial H_z'}{\partial z} = -ikNH_z',$$

(cf (17)) it follows that

$$\frac{\partial H_z}{\partial z} = -ikNH_z'.$$

But at the boundary $z = 0$

$$H_z' = \frac{\mu_0}{\mu} H_z$$

and hence

$$\frac{\partial H_z}{\partial z} = -\frac{ik}{\eta} H_z. \quad (21)$$

This is the second of two boundary conditions at the interface, and is accurate to order η .

It will be observed that (21) differs from (20) in having η replaced by $1/\eta$, and this is in accordance with the interpretation of η as an impedance associated with the surface. The point will be elaborated upon in a moment, but for the time being it is sufficient to note that (20) and (21) specify the behaviour of the normal components of both \mathbf{E} and \mathbf{H} at the interface, and therefore represent a sufficient set of boundary conditions.

For some applications an alternative (but entirely equivalent) representation of these boundary conditions proves more convenient. Taking first (20), since

$$\mathbf{E} = -\frac{Z}{ik} \nabla \times \mathbf{H}$$

where $Z = 1/Y = \sqrt{\mu_0/\epsilon_0}$ is the intrinsic impedance of free space, and since $\nabla \cdot \mathbf{E} = 0$, the boundary condition can be written as

$$\frac{\partial}{\partial x} (E_x + \eta Z H_y) = -\frac{\partial}{\partial y} (E_y - \eta Z H_x). \quad (22)$$

Similarly, the boundary condition (21) gives

$$\frac{\partial}{\partial y} (E_x + \eta Z H_y) = \frac{\partial}{\partial x} (E_y - \eta Z H_x) \quad (23)$$

and by eliminating $E_x + \eta Z H_y$ and $E_y - \eta Z H_x$ successively between these equations, we have

$$\frac{\partial^2 \Phi}{\partial x^2} + \frac{\partial^2 \Phi}{\partial y^2} = 0, \quad (24)$$

where $\Phi = E_x + \eta Z H_y$ or $E_y - \eta Z H_x$. This equation can be solved by assuming a separable form for Φ . If $\Phi = \Phi_1(x)\Phi_2(y)$, then

$$-\frac{\partial^2 \Phi_1}{\partial x^2} + a^2 \Phi_1 = 0, \quad \frac{\partial^2 \Phi_2}{\partial y^2} - a^2 \Phi_2 = 0,$$

where a^2 is some separation constant, and the solutions are

$$\Phi_1 = A_1 e^{iax} + B_1 e^{-iax},$$

$$\Phi_2 = A_2 e^{ay} + B_2 e^{-ay}$$

where A_1, B_1, A_2 and B_2 are constants as yet undefined. If a is not purely real, both A_1 and B_1 must be identically zero since otherwise Φ_1 would become exponentially large for large x (either positive or negative). In this case Φ_1 , and hence Φ , is zero. If a is purely real, the same argument applied to the variable y shows that Φ_2 is zero, leading to the same conclusion as regards Φ . Since Φ is therefore zero,

$$E_x = -\eta Z H_y, \quad (25)$$

$$E_y = \eta Z H_x, \quad (26)$$

and this is the alternative statement of the boundary conditions at the interface $z = 0$. In this form the conditions simply state that ηZ is the effective impedance of the surface as seen by a field in free space. For comparison with this, the impedance of a perfectly conducting surface is zero.

§ 4. *Extension to a curved interface.* In order to generalize these conditions for application to surfaces which are not flat, it is first necessary to express (20) and (21), (25) and (26) in forms which do not explicitly involve the coordinate system. If E_n and H_n are the

field components normal to the boundary, and if n is a coordinate whose positive direction is outwards as regards the medium, (20) and (21) can be written as

$$\frac{\partial E_n}{\partial n} = -ik\eta E_n, \quad (27)$$

$$\frac{\partial H_n}{\partial n} = -\frac{ik}{\eta} H_n. \quad (28)$$

For the second pair of conditions a vector form is more convenient, and following Leontovich ²⁾, (25) and (26) are combined to give

$$\mathbf{E} - (\hat{\mathbf{n}} \cdot \mathbf{E})\hat{\mathbf{n}} = \eta Z \hat{\mathbf{n}} \times \mathbf{H}. \quad (29)$$

Of the three scalar equations contained herein, only two are independent.

We now turn to a consideration of the boundary conditions at a curved interface between the medium and free space. As in the case of the flat interface the object is to determine approximate boundary conditions in which only the fields in free space appear. It is clear, however, that unless restrictions are placed upon the shape of the boundary, these conditions will involve the geometrical properties of the surface as well as the electrical parameters of the medium and in consequence may vary from point to point on the surface. Such conditions would be of little practical value. On the other hand, by restricting the type of surface to be allowed, the curvature effects can be made negligible, and the boundary conditions then reduce to those obtained for an infinite flat surface.

A rigorous derivation of the restrictions which must be placed on the type of surface in order that (27) through (29) be valid is beyond the scope of this paper, and for details of the analysis reference is made to Rytov ⁵⁾ and Leontovich ²⁾. The actual limitations, however, can be arrived at by a semi-intuitive argument.

It will be recalled that in the analysis of the flat boundary the assumption was made that

$$|N| \gg 1, \quad (30)$$

and this is sufficient to ensure that within the medium the field is slowly varying along the surface and behaves essentially as a plane wave propagating in the direction of the inward normal. Let us now seek to apply (29) or (27) and (28) to each point on a curved surface.

In order that the field shall vary little within a wavelength along the surface, a restriction must be placed upon the radii of curvature, and a trivial analysis shows that the requirement is

$$|N| k\rho \gg 1, \quad (31)$$

where ρ is the smallest radius of curvature at the point in question. If (31) is satisfied, any correction to the boundary condition (29) consequent upon the curvature is negligible (see Leontovich²).

For a surface which is open (implying that the medium is infinite in extent) and which has no inward normal intersecting the surface in a second point, the restrictions (30) and (31) are sufficient to justify the application of the flat surface conditions. For a closed surface, however, a difficulty arises when the conduction current in the medium is negligible compared with the displacement current. The inward travelling field then suffers little or no attenuation, and accordingly may appear as an outward travelling field on the farther side of the surface. This is contrary to the assumption made in the derivation of the flat surface condition. For this reason it is necessary for the field within the medium to be attenuated at a rate such that the penetration depth δ is small compared with ρ , giving rise to the additional restriction

$$\delta \ll \rho. \quad (32)$$

If $\sigma \gg \omega\epsilon'$, (32) can be written as

$$\sqrt{\frac{\mu}{\mu_0} \frac{\sigma}{2\omega\epsilon_0}} k\rho \gg 1,$$

which in turn reduces to the inequality (31) if the conduction current dominates. On the other hand, if the displacement current dominates, the inequality (32) represents an additional restriction which is stronger than (31).

The difficulty which arises with a dielectric medium has been noted by Leontovich², who also points out that for a body made of this material the boundary condition (29) can be justified only under very restricted circumstances. For a body of general shape the boundary conditions are only applicable if the medium is conducting and satisfies the inequality (32). The importance of this restriction, rather than (31), can be seen from a study of the few exact solutions which are known for bodies which are not perfectly

conducting. For example, if a plane wave is incident on a sphere of radius ρ , the exact solution can be found as a sum of vector wave functions whose coefficients are functions of N . If it is now assumed that $|N|k\rho \gg 1$, these coefficients reduce to the forms which would have been obtained by using the condition (29) apart from additional terms involving $\tan Nk\rho$. Such terms only disappear if $\tan Nk\rho$ can be replaced by $-i$ to the leading order in N , i.e. if $|\operatorname{Im} N|k\rho \gg 1$. Similarly, if a field is incident upon an infinite slab of (uniform) thickness d , the exact solution contains an exponential factor e^{2iNkd} corresponding to internal reflection from the lower surface, and the approximate boundary conditions would then be valid only if the terms containing this factor can be taken zero. This in turn requires an attenuation of the inward travelling field subject to a restriction of the form (32) with ρ replaced by d . It is of interest to note that (32) is here required even though the surface is flat.

In summary, we now have that for a homogeneous isotropic body whose refractive index N and smallest radius of curvature or dimension ρ are such that

$$|N| \gg 1, \quad (30)$$

$$|\operatorname{Im} N|k\rho \gg 1, \quad (33)$$

the boundary conditions at its surface can be written as

$$\frac{\partial E_n}{\partial n} = -ik\eta E_n, \quad (27)$$

$$\frac{\partial H_n}{\partial n} = -\frac{ik}{\eta} H_n, \quad (28)$$

where $\eta = \mu/(\mu_0 N)$. These are equivalent to the single vector condition

$$\mathbf{E} - (\hat{\mathbf{n}} \cdot \mathbf{E})\hat{\mathbf{n}} = \eta Z \hat{\mathbf{n}} \times \mathbf{H}. \quad (29)$$

In some circumstances it may be possible to replace (33) by the weaker restriction

$$|N|k\rho \gg 1, \quad (31)$$

but such cases must be regarded as exceptional. In this connection it is of interest to note that Fock¹⁾ in his discussion of these boundary conditions ignores the distinction between dielectric and conducting media, and gives only the restrictions (30) and (31).

Eq. (27) through (29) are approximations to the exact boundary conditions correct to the first order in η , and accordingly in any solution obtained using these conditions there is no (physical) justification for retaining terms which are of a higher order in η . A consequence of this is that if the fields are capable of expansion in series of ascending (positive) powers of η , the perfectly conducting approximation (corresponding to $\eta = 0$) can be inserted into the right-hand sides of (27) and (29) and into the left-hand side of (28). In general, such expansions will be valid, though a problem in which this is not true is the incidence of an H -polarized plane wave on an imperfectly conducting half-plane (Senior ⁶)⁷). In this case, however, the failure may well be due to the additional assumption of a "thin" body *) implicit in the problem.

§ 5. *An inhomogeneous medium.* Let us now go on to consider the problem in which the medium is not homogeneous, so that the refractive index varies from point to point. This variation will be attributed to ϵ alone and μ will be regarded as spatially invariant. We shall again begin by assuming an infinite flat interface between the medium and free space.

At any point (x, y, z) within the medium

$$\nabla \cdot (\epsilon \mathbf{E}') = 0, \quad (34)$$

and since

$$\nabla \cdot (\epsilon \mathbf{E}') = \epsilon \nabla \cdot \mathbf{E}' + \mathbf{E}' \cdot \nabla \epsilon,$$

(34) can be written as

$$\frac{\partial E_x'}{\partial x} + \frac{\partial E_y'}{\partial y} = - \frac{\partial E_z'}{\partial z} - \frac{1}{\epsilon} \mathbf{E}' \cdot \nabla \epsilon. \quad (35)$$

In free space, however,

$$\nabla \cdot \mathbf{E} = 0, \quad (36)$$

and using the continuity of the tangential components across the interface, we now have

$$\frac{\partial E_z}{\partial z} = - \frac{\partial E_x'}{\partial x} - \frac{\partial E_y'}{\partial y} = \frac{\partial E_z'}{\partial z} + \frac{1}{\epsilon} \mathbf{E}' \cdot \nabla \epsilon \quad (37)$$

*) The mathematical requirement here is $d \ll \lambda$, where d is the thickness of the half-plane, and by assuming that the half-plane is tipped with a semi-circular cylinder it can be shown that the boundary conditions are applicable if $\delta \ll d \ll \lambda$.

at $z = 0$. In terms of η , however, $\varepsilon = (\mu/\mu_0)(\varepsilon_0/\eta^2)$, so that $(1/\varepsilon)\nabla\varepsilon = (-2/\eta)\nabla\eta$, and this can be inserted into (37) to give

$$\frac{\partial E_z}{\partial z} = \frac{\partial E_z'}{\partial z} - \frac{2}{\eta} \left(E_x' \frac{\partial \eta}{\partial x} + E_y' \frac{\partial \eta}{\partial y} + E_z' \frac{\partial \eta}{\partial z} \right) \quad (38)$$

at $z = 0$. But at the interface

$$E_x' = E_x, \quad E_y' = E_y, \quad E_z' = (\mu_0/\mu)\eta^2 E_z,$$

and using these relations (38) becomes

$$\frac{\partial E_z}{\partial z} = \frac{\partial E_z'}{\partial z} - \frac{2}{\eta} \left(E_x \frac{\partial \eta}{\partial x} + E_y \frac{\partial \eta}{\partial y} + \frac{\mu_0}{\mu} \eta^2 E_z \frac{\partial \eta}{\partial z} \right). \quad (39)$$

In arriving at this equation no approximations have been made, and the second term on the right-hand side can be interpreted as a correction to the boundary condition resulting from the variation of η throughout the medium. If

$$\left| \frac{1}{k\eta} \nabla \eta \right| \ll 1, \quad (40)$$

which implies that the relative variation is small, E_x , E_y and E_z will not differ substantially from the values appropriate to a homogeneous medium. For such a medium it was shown in § 3 that

$$E_x, E_y = O(\eta), \quad E_z = O(1),$$

and in (39) it is now seen that the lateral variation of η is more important than the normal variation. Indeed, if $\partial\eta/\partial x$, $\partial\eta/\partial y$ and $\partial\eta/\partial z$ are all comparable with one another, the effect produced by the z variation of η is smaller by an order of magnitude. The z variation can therefore be neglected and henceforth η will be assumed to be a function of x and y only.

The next step is to obtain an expression for $\partial E_z'/\partial z$ in terms of the free space field. From the field equations

$$\mathbf{E}' = -\frac{\sqrt{\mu_0\varepsilon_0}}{ik\varepsilon} \nabla \times \mathbf{H}', \quad (41)$$

$$\mathbf{H}' = \frac{\sqrt{\mu_0\varepsilon_0}}{ik\mu} \nabla \times \mathbf{E}' \quad (42)$$

we have

$$\mathbf{E}' = \frac{1}{k^2 N^2} \nabla \times \nabla \times \mathbf{E}', \quad (43)$$

and since

$$\begin{aligned}\nabla \times \nabla \times \mathbf{E}' &= \nabla(\nabla \cdot \mathbf{E}') - \nabla^2 \mathbf{E}' \\ &= -\nabla \left(\frac{1}{\varepsilon} \mathbf{E}' \cdot \nabla \varepsilon \right) - \nabla^2 \mathbf{E}',\end{aligned}$$

the equation for the field within the medium can be written

$$\nabla^2 \mathbf{E}' + k^2 N^2 \mathbf{E}' + \nabla \left(\frac{1}{\varepsilon} \mathbf{E}' \cdot \nabla \varepsilon \right) = 0. \quad (44)$$

If ε is now expressed in terms of the refractive index N using

$$\varepsilon = \frac{\mu_0}{\mu} \varepsilon_0 N^2,$$

(44) becomes

$$\nabla^2 \mathbf{E}' + k^2 N^2 \mathbf{E}' + 2\nabla \left(\frac{1}{N} \mathbf{E}' \cdot \nabla N \right) = 0, \quad (45)$$

and since the tangential derivatives of \mathbf{E}' are again negligible in comparison with the normal derivative, (45) reduces to

$$\frac{\partial^2 \mathbf{E}'}{\partial z^2} + k^2 N^2 \mathbf{E}' + 2\nabla \left(\frac{1}{N} \mathbf{E}' \cdot \nabla N \right) = 0. \quad (46)$$

In particular,

$$\frac{\partial^2 E_z'}{\partial z^2} + k^2 N^2 E_z' + 2 \frac{\partial}{\partial z} \left[\frac{1}{N} \left(E_x' \frac{\partial N}{\partial x} + E_y' \frac{\partial N}{\partial y} \right) \right] = 0. \quad (47)$$

In order to determine E_z' from (47) it is necessary to know the variation of E_x' and E_y' in the z direction, and for this purpose the x and y components of (46) are employed. To the first order the variation of N can be neglected, and we then have

$$-\frac{\partial^2 E_x'}{\partial z^2} + k^2 N^2 E_x' = 0,$$

the solution of which is

$$E_x' = (E_x')_{z=0} e^{-ikNz}, \quad (48)$$

since the field in the medium must behave as a wave travelling in the negative z -direction. Moreover, at $z = 0$, $E_x' = E_x$ and hence

$$E_x' = E_x e^{-ikNz}. \quad (49)$$

Similarly,

$$E_y' = E_y e^{-ikNz}, \quad (50)$$

and (47) can now be written as

$$\frac{\partial^2 E_z'}{\partial z^2} + k^2 N^2 E_z' + \alpha e^{-ikNz} = 0, \quad (51)$$

where

$$\alpha = -2ik \left(E_x \frac{\partial N}{\partial x} + E_y \frac{\partial N}{\partial y} \right). \quad (52)$$

α is, of course, independent of z .

The complete solution of (51) is obtained by adding a particular integral to the general solution Ae^{-ikNz} , where A is some constant. The former can be taken as

$$\frac{\alpha z}{2ikN} e^{-ikNz},$$

giving

$$E_z' = e^{-ikNz} \left(A + \frac{\alpha z}{2ikN} \right). \quad (53)$$

Hence

$$\frac{\partial E_z'}{\partial z} = -ikNE_z' + \frac{\alpha}{2ikN} e^{-ikNz},$$

and at $z = 0$ this reduces to

$$\begin{aligned} \frac{\partial E_z'}{\partial z} &= -ikNE_z' + \frac{\alpha}{2ikN} = \\ &= -ik\eta E_z + \frac{1}{\eta} \left(E_x \frac{\partial \eta}{\partial x} + E_y \frac{\partial \eta}{\partial y} \right) \end{aligned} \quad (54)$$

by using the expression for α . If this is now inserted into (34) bearing in mind that $\partial \eta / \partial z = 0$, a boundary condition is obtained in the form

$$\frac{\partial E_z}{\partial z} = -ik\eta E_z - \frac{1}{\eta} \left(E_x \frac{\partial \eta}{\partial x} + E_y \frac{\partial \eta}{\partial y} \right) \quad (55)$$

at the interface $z = 0$. Apart from the presence of the tangential components E_x and E_y consequent upon the variation of ϵ through the medium this equation is the same as (20).

A boundary condition for the normal component of the magnetic field can be obtained by an analysis similar to the above. Since $\nabla \cdot \mathbf{H} = \nabla \cdot \mathbf{H}' = 0$, the continuity of the tangential components of \mathbf{H} across the interface leads to the equation

$$\frac{\partial H_z}{\partial z} = \frac{\partial H_z'}{\partial z} \quad (56)$$

(cf (37)) at $z = 0$. Inside the medium the field equations give

$$\begin{aligned} \mathbf{H}' &= \frac{\mu_0 \epsilon_0}{\mu k^2} \nabla \times \left(\frac{1}{\epsilon} \nabla \times \mathbf{H}' \right) \\ &= \frac{\mu_0 \epsilon_0}{\mu k^2} \left[\frac{1}{\epsilon} \nabla \times \nabla \times \mathbf{H}' + \nabla \frac{1}{\epsilon} \times (\nabla \times \mathbf{H}') \right] \\ &= -\frac{1}{k^2 N^2} \left(\nabla^2 \mathbf{H}' + 2ikN \frac{\mu_0}{\mu} \mathbf{Y} \mathbf{E}' \times \nabla N \right) \end{aligned}$$

and hence

$$\nabla^2 \mathbf{H}' + k^2 N^2 \mathbf{H}' + 2ikN \frac{\mu_0}{\mu} \mathbf{Y} \mathbf{E}' \times \nabla N = 0. \quad (57)$$

In particular, the z -component of (57) is

$$\frac{\partial^2 H_z'}{\partial z^2} + k^2 N^2 H_z' + 2ikN \frac{\mu_0}{\mu} Y \left(E_x' \frac{\partial N}{\partial y} - E_y' \frac{\partial N}{\partial x} \right) = 0,$$

where the x and y derivatives have been neglected in comparison with the z , and by using the expressions for E_x' and E_y' given by (49) and (50) respectively we arrive at the equation

$$\frac{\partial^2 H_z'}{\partial z^2} + k^2 N^2 H_z' + \beta e^{-ikNz} = 0 \quad (58)$$

(cf (51)), where

$$\beta = 2ikN \frac{\mu_0}{\mu} Y \left(E_x \frac{\partial N}{\partial y} - E_y \frac{\partial N}{\partial x} \right) \quad (59)$$

(cf (52)). The solution of (58) is

$$H_z' = e^{-ikNz} \left(B + \frac{\beta z}{2ikN} \right) \quad (60)$$

(cf (53)), where B is some constant, and hence at $z = 0$

$$\begin{aligned}\frac{\partial H_z'}{\partial z} &= -ikNH_z' + \frac{\beta}{2ikN} = \\ &= -ikN \frac{\mu_0}{\mu} H_z + \frac{\mu_0}{\mu} Y \left(E_x \frac{\partial N}{\partial y} - E_y \frac{\partial N}{\partial x} \right) \quad (61) \\ &= -\frac{ik}{\eta} H_z + \frac{Y}{\eta} \left(E_y \frac{\partial \eta}{\partial x} - E_x \frac{\partial \eta}{\partial y} \right).\end{aligned}$$

If this is substituted into (56), the boundary condition on the normal component of \mathbf{H} at the interface is

$$\frac{\partial H_z}{\partial z} = -\frac{ik}{\eta} H_z + \frac{Y}{\eta} \left(E_y \frac{\partial \eta}{\partial x} - E_x \frac{\partial \eta}{\partial y} \right), \quad (62)$$

which is analogous to the condition (21). As with the condition (55), the variation of η has introduced the tangential components E_x and E_y into a boundary condition which is otherwise the same as for a homogeneous medium.

From (55) and (62) boundary conditions can be derived involving only the tangential components of \mathbf{E} and \mathbf{H} . Using the equation $\nabla \cdot \mathbf{E} = 0$ and the expression for E_z in terms of H_x and H_y , (55) becomes

$$\frac{\partial E_x}{\partial x} - \frac{1}{\eta} E_x \frac{\partial \eta}{\partial x} + \eta Z \frac{\partial H_y}{\partial x} = -\frac{\partial E_y}{\partial y} - \frac{1}{\eta} E_y \frac{\partial \eta}{\partial y} - \eta Z \frac{\partial H_x}{\partial y}$$

which reduces to

$$\frac{\partial}{\partial x} \left(\frac{E_x}{\eta} + ZH_y \right) = -\frac{\partial}{\partial y} \left(\frac{E_y}{\eta} - ZH_x \right).$$

Similarly (62) can be written as

$$\frac{\partial}{\partial y} \left(\frac{E_x}{\eta} + ZH_y \right) = \frac{\partial}{\partial x} \left(\frac{E_y}{\eta} - ZH_x \right)$$

and by means of the analysis given in § 3 (eq. (24) et seq.) it now follows that $(E_x/\eta + ZH_y)$ and $(E_y/\eta - ZH_x)$ are both identically zero at the interface. Hence,

$$E_x = -\eta ZH_y, \quad (63)$$

$$E_y = \eta ZH_x, \quad (64)$$

which are of precisely the same form as the conditions (25) and (26) for a homogeneous medium. In particular, the tangential derivatives of η do not enter into these equations in spite of the fact that they appear in (55) and (62). Thus, the conditions (63) and (64) are relatively insensitive to changes in the medium, and any correction terms arising from the inhomogeneity must be of higher order than those considered here. Indeed, if η is regarded as a function of z as well as x and y , it can be shown that

$$E_x = -\eta Z H_y \left[1 + O\left(\frac{1}{k} \frac{\partial \eta}{\partial z}\right) \right]$$

(see Rytov ⁵), and by virtue of (40) $k^{-1} \partial \eta / \partial z \ll \eta$.

In spite of the simplicity of equations (63) and (64), these boundary conditions are of little practical value as they stand. Although the coordinates x and y do not occur explicitly in these equations, the material parameter η is itself a function of x and y , and accordingly the boundary conditions vary with position on the interface. This is a source of difficulty in any attempt to employ these conditions in the solution of an actual problem.

On the other hand, if it is assumed that the variations of η are random but uniform in some statistical sense, the difficulty can be overcome in a manner which is satisfactory for many practical applications. Such an assumption is, of course, additional to the restriction (40) and implies that if a large sample of the surface is chosen, the values of η within this sample are substantially the same independently of the portion of the surface from which the sample is taken. Under these circumstances it is to be expected that the field will (in general) be a function of the statistical properties of the surface, rather than of individual features, and this leads us to consider an average field satisfying an averaged boundary condition. Such an average is obtained either by moving the transmitter and receiver whilst maintaining their positions relative to the plane $z = 0$ (so that different samples of surface appear beneath them), or by replacing the given surface by others of a family whose statistical properties are the same. The boundary conditions satisfied by the average field (\mathbf{E} , \mathbf{H}) can be found by the simple process of averaging equations (63) and (64). Bearing in mind that to the first order in η , H_x and H_y can be replaced by the components H_x^0 and H_y^0 for a

perfectly conducting surface, (63) and (64) give

$$\bar{E}_x = -\bar{\eta}ZH_y^0, \quad E_y = \bar{\eta}ZH_x^0,$$

which can be replaced by

$$\bar{E}_x = -\bar{\eta}Z\bar{H}_y, \quad (65)$$

$$\bar{E}_y = \bar{\eta}Z\bar{H}_x. \quad (66)$$

to the first order in η . Similarly, if the correction terms in (55) and (62) are neglected, the averaged versions are

$$\frac{\partial \bar{E}_z}{\partial z} = -ik\bar{\eta}\bar{E}_z, \quad (67)$$

$$\frac{\partial \bar{H}_z}{\partial z} = -\frac{ik}{\bar{\eta}}\bar{H}_z. \quad (68)$$

The above results are valid for statistically uniform surfaces whose refractive index $N = \mu/(\mu_0\eta)$ satisfies the restrictions (30) and (40). It will be observed that the average fields are determined by the average value of η , and not by the average values of ε or σ . This is in accordance with the conclusion reached by Feinberg⁸⁾ under the same restrictions but by a somewhat circuitous analysis.

These boundary conditions can be generalized so as to apply to a curved surface in the manner described in § 4. The restrictions under which this is valid are the same as in § 4, and will not be repeated here.

Acknowledgement. This research was sponsored by the Rome Air Development Center of the U.S. Air Force under Contract AF-30-(602)-2099.

Received 26th July, 1960.

REFERENCES

- 1) Fock, V. A., J. Phys. USSR **10** (1946) 13.
- 2) Leontovich, M. A., Investigations of Propagation of Radiowaves, Part II, Moscow 1948.
- 3) Alpert, J. L., J. Tech. Phys. USSR **10** (1940) 1358.
- 4) Feinberg, E. L., Supplemento, Nuovo Cim. **11** (1959) 60.
- 5) Rytov, S. M., J. Exp. Theor. Phys. USSR **10** (1940) 120.
- 6) Senior, T. B. A., Proc. Roy. Soc. London A **213** (1952) 436.
- 7) Senior, T. B. A., Comm. Pure Appl. Math. **12** (1959) 337.
- 8) Feinberg, E. L., J. Phys. USSR **8** (1944) 317.

IMPEDANCE BOUNDARY CONDITIONS FOR STATISTICALLY ROUGH SURFACES

by T. B. A. SENIOR

The University of Michigan, The Radiation Laboratory, Ann Arbor, Michigan, U.S.A.

Summary

It is shown that for an electromagnetic field incident on a perfectly conducting surface having small geometrical irregularities which are distributed at random but in a statistically uniform and isotropic manner, the boundary condition can be replaced by a generalized impedance condition applied at a neighbouring mean surface. The surface impedance is a tensor function of the direction at which the field is incident as well as of the statistical properties of the irregularities, but simplifies in certain particular cases. Although the detailed analysis is carried out for a mean surface which is flat, the boundary condition is applicable to a curved surface providing the radii of curvature are large in comparison with the wavelength. It is believed that this approach is of value in studying the effect of minor surface roughnesses on the scattering of electromagnetic waves.

§ 1. *Introduction.* In recent years an increasing amount of attention has been devoted to the effect of surface irregularities on the propagation and scattering of electromagnetic waves. In the course of this work many types of irregularity have been studied ranging from isolated bumps of simple mathematical form, through specific (or even periodic) arrangements of particular protuberances, to random distributions of general irregularities. Since the ultimate goal is a knowledge of the scattered field, most analyses have aimed at the direct calculation of this quantity, and this in turn has usually required that a separate mathematical treatment be provided for every shape of background surface on which the bumps are placed. In view of the complications associated with anything but a flat surface, an infinite plane background surface has been studied almost to the exclusion of any other shape.

The present paper is concerned only with the case of a surface

having small geometrical irregularities which are distributed in a random but statistically uniform and isotropic manner, and is prompted by disagreements which have arisen about the influence of minor surface roughnesses in model scattering experiments. In order to achieve a degree of generality which is, perhaps, not otherwise obtainable, attention is directed at the boundary condition rather than at the scattered field. By taking the actual surface to be perfectly conducting, it is shown that the boundary condition can be replaced by a form of impedance boundary condition applied at a neighbouring (fictitious) mean surface. The effective surface impedance is a tensor function of the statistical properties of the irregularities and of the direction at which the field is incident. The analysis is given in detail for a mean surface which is flat, but the boundary condition is also applicable to a curved surface (and hence to a finite body) providing the radii of curvature (and the minimum dimensions) are all large in comparison with the wavelength.

In certain cases the surface impedance can be taken as a scalar, and the boundary condition then reduces to one of the Leontovich type. This is the standard impedance boundary condition for a surface of large but finite conductivity (see, for example, Senior ¹) and implies that the surface roughness has the same effect as changing the conductivity of the surface. Although this may seem strange at first sight, a direct consequence of the roughness is that the tangential components of the electric field at a nearby mean surface are related to the other field components through small parameters characteristic of the surface imperfections. If a suitable averaging process is applied, the conditions on the field at the mean surface reduce to a boundary condition of the type discussed in ¹), and to this degree of approximation the geometrical imperfections are therefore equivalent to a conductivity change.

A description of the surface which is considered is given in § 2, and the appropriate boundary condition is derived in § 3 through § 5 for the particular case in which the mean surface is an infinite plane. The effective surface impedance is obtained explicitly in § 6 and § 7, and some numerical values are presented (§ 8). A general discussion which includes the application of these conditions to a curved surface is given in § 9.

§ 2. *The surface.* The problem to be discussed is one in which an electromagnetic field is incident upon a perfectly conducting surface which varies in a statistically uniform manner about some mean surface. To begin with it is assumed for simplicity that the surface is infinite in extent and obtained by perturbation of a plane. This allows the mean surface to be taken as the plane $z = 0$ in a Cartesian system of coordinates (x, y, z) , and only later is the problem generalized to the case of a mean surface which is curved.

The method which is used is based on one proposed by Feinberg²⁾³⁾ for a study of ground wave propagation over a rough earth. The equation of the surface is taken as

$$z = \zeta(x, y), \quad (1)$$

and the height and scale of the variation of ζ about its mean are denoted by the length parameters ζ_0 and l respectively. The first stage in the analysis is the expression of the boundary conditions on the actual surface as conditions upon the field components at the (fictitious) mean surface. This is accomplished by a Taylor expansion of the field about a point (x, y) on the mean surface, and it is clear that the expansion will only be valid if the behaviour of the field at the mean surface differs but slightly from the behaviour on the actual surface. This immediately places a restriction upon the type of surface which can be considered and also upon the location of the mean surface. In particular, large gradients or abrupt changes in gradient cannot be allowed since such perturbations may produce significant changes in the field in their immediate vicinity.

In the course of the Taylor expansion it is found that ζ and its first derivatives occur, and the typical (or root mean square) values of these make up the three parameters of smallness which are present in the problem. For a surface which is statistically isotropic, the typical values of ζ , $\partial\zeta/\partial x$ and $\partial\zeta/\partial y$ are equal ($= \gamma_0$, say), and only this case will be considered. The number of small parameters is now reduced to two, and the restriction to small surface gradients requires that

$$\gamma_0 \ll 1. \quad (2)$$

Moreover, in the practical case to be investigated here, the scale length will never exceed *) the wavelength of the incident field, and

*) It will usually be considerably less than this.

if the mean surface is drawn so that $\zeta_0 \sim l\gamma_0$, equation (2) gives

$$\zeta_0 \ll l, \quad (3)$$

which is a sufficient restriction on ζ_0 . It should be remarked, however, that (3) is not a necessary condition, and Feinberg²⁾ has shown that the higher terms in the Taylor expansion can still be neglected if

$$k\zeta_0 \ll \sqrt{\frac{l}{\lambda}}. \quad (4)$$

By choosing l/λ large compared with unity it becomes possible to allow surface imperfections which are not small in comparison with the wavelength providing the slopes are small. Such cases, however, will not be discussed.

§ 3. *First order boundary conditions.* Since the actual surface is perfectly conducting, the boundary condition at $z = \zeta$ is

$$\hat{\mathbf{n}} \times \mathbf{E} = 0, \quad (5)$$

where $\hat{\mathbf{n}}$ is a unit vector normal, and from this we obtain

$$E_x = -\frac{\partial \zeta}{\partial x} E_z, \quad (6)$$

$$E_y = -\frac{\partial \zeta}{\partial y} E_z. \quad (7)$$

The above equations specify relations which must be satisfied by the field components at $z = \zeta$, and once these conditions have been imposed the surface can be removed without affecting the field in the region above. The next task is to express (6) and (7) as conditions upon the field components at a mean surface, and this is done by expanding the field components in Taylor series. Since the field is finite and continuous everywhere throughout the free space region except at the source, we have

$$E_x(x, y, \zeta) = E_x(x, y, 0) + \zeta \frac{\partial}{\partial z} E_x(x, y, 0) + \frac{\zeta^2}{2} \frac{\partial^2}{\partial z^2} E_x(x, y, 0) + \dots$$

where the differentiation must be carried out before z is put equal to zero. But if the incident field possesses a non-zero component E_z

(as will be assumed), E_z for the total field will be $O(1)$, and since (6) then shows that E_x is of the first order in small quantities (denoted collectively by δ),

$$E_x(x, y, \zeta) = E_x + \zeta(\partial E_x / \partial z) + O(\delta^3).$$

The field components on the right are evaluated at $z = 0$. Similarly

$$E_y(x, y, \zeta) = E_y + \zeta(\partial E_y / \partial z) + O(\delta^3),$$

$$E_z(x, y, \zeta) = E_z + \zeta(\partial E_z / \partial z) + O(\delta^2).$$

Substituting into (6) and (7),

$$E_x = -\zeta_x E_z - \zeta \frac{\partial E_x}{\partial z} - \zeta \zeta_x \frac{\partial E_z}{\partial z} + O(\delta^3), \quad (8)$$

$$E_y = -\zeta_y E_z - \zeta \frac{\partial E_y}{\partial z} - \zeta \zeta_y \frac{\partial E_z}{\partial z} + O(\delta^3), \quad (9)$$

where $\zeta_x = \partial \zeta / \partial x$, etc. and these are the equivalent boundary conditions at the mean surface $z = 0$.

A little simplification can be achieved by using the fact that the divergence relation

$$\frac{\partial E_z}{\partial z} = -\frac{\partial E_x}{\partial x} - \frac{\partial E_y}{\partial y} \quad (10)$$

holds at all points including those on the mean surface. If the expressions for E_x and E_y on $z = 0$ are inserted, it is seen that $\partial E_z / \partial z = O(\delta)$ and hence (12) and (13) can be written as

$$E_x = -\zeta_x E_z - \zeta(\partial E_x / \partial z) + O(\delta^3), \quad (11)$$

$$E_y = -\zeta_y E_z - \zeta(\partial E_y / \partial z) + O(\delta^3) \quad (12)$$

for $z = 0$. In combination with (10) we now have

$$\frac{\partial E_z}{\partial z} = \frac{\partial}{\partial x} \left(\zeta_x E_z + \zeta \frac{\partial E_x}{\partial z} \right) + \frac{\partial}{\partial y} \left(\zeta_y E_z + \zeta \frac{\partial E_y}{\partial z} \right) + O(\delta^3), \quad (13)$$

which is identical to the equation obtained by Feinberg.

The significance of the above results becomes apparent on using the field equation *)

$$\nabla \times \mathbf{E} = ikZH$$

*) M.k.s. units are employed with a time factor $e^{-i\omega t}$.

to eliminate the normal derivatives from (11) and (12), which then become

$$E_x = ikZ\bar{\zeta}H_y - \frac{\partial}{\partial x}(\bar{\zeta}E_z) + O(\delta^3), \quad (14)$$

$$E_y = -ikZ\bar{\zeta}H_x - \frac{\partial}{\partial y}(\bar{\zeta}E_z) + O(\delta^3), \quad (15)$$

where $Z = 1/Y$ is the intrinsic impedance of free space. In this form the equations differ from the Leontovich boundary condition only in the presence of the terms involving E_z on the right hand sides, and these terms apart, the equations are the same as for an imperfectly conducting material having a surface impedance $-ik\bar{\zeta}$. For a statistically rough surface, however, such an interpretation is dependent on the choice of the mean surface. To order δ the field components for a smooth surface can be inserted into the right hand sides of (14) and (15), and if the mean surface is chosen so that $\bar{\xi} = 0$, where the bar denotes an average taken over the whole xy plane, the boundary conditions satisfied by the average fields are

$$E_x = E_y = 0 + O(\delta^2).$$

These are the conditions for a perfectly conducting smooth surface at $z = 0$, showing that the terms of order δ produce no conductivity effect. This conclusion, however, is a consequence of choosing a particular mean surface. If this does not coincide with the "average" surface, the roughness will produce a first order effect, as is to be expected since the boundary conditions are then being applied on a surface which is displaced even in the limit of zero roughness.

In the practical case of a surface having a statistical type of roughness, it is natural to choose a mean surface which coincides with the average, and if the resulting boundary conditions are to take this roughness into account, it is necessary to retain the second order terms in, for example, (11) and (12). This in turn requires us to obtain expressions for E_z , $\partial E_x/\partial z$ and $\partial E_y/\partial z$ on the surface accurate to $O(\delta)$, which expressions can be substituted into (11) and (12) to make explicit the terms of order δ^2 .

§ 4. *Second order boundary conditions.* At any point in space the electric and magnetic fields can be written as integrals involving the

field components on the surface. Thus, from Stratton ⁴⁾ we have

$$\mathbf{E}(x, y, z) = \frac{1}{2}\mathbf{E}_A + \frac{1}{4\pi} \int_S [ikZ(\hat{\mathbf{n}} \times \mathbf{H})\phi + \hat{\mathbf{n}} \times \mathbf{E} \times \nabla\phi + (\hat{\mathbf{n}} \cdot \mathbf{E})\nabla\phi] dS, \quad (16)$$

where the differentiation is with respect to the surface coordinates (x_1, y_1, z_1) and $\hat{\mathbf{n}}$ is a unit vector normal to the mean surface S drawn inwards as regards free space. The symbol \mathbf{E}_A denotes a surface integral over an infinite hemisphere if the incident field is a plane wave, or over a small sphere surrounding the source if this is at a finite distance; \mathbf{E}_A is therefore a function of the incident field alone and is independent of the characteristics of the surface S . ϕ is the free space Green's function $\phi = \rho^{-1}e^{ik\rho}$, with

$$\rho = \sqrt{(x - x_1)^2 + (y - y_1)^2 + (z - z_1)^2}.$$

Taking the surface S to be the plane $z = 0$, we have $\hat{\mathbf{n}} = (0, 0, 1)$ and hence

$$\begin{aligned} \mathbf{E}(x, y, z) = \frac{1}{2}\mathbf{E}_A(x, y, z) + \frac{1}{4\pi} \iint \left[ikZ(-H_y, H_x, 0)\phi + \right. \\ \left. + \left(E_x \frac{\partial\phi}{\partial z_1}, E_y \frac{\partial\phi}{\partial z_1}, -E_x \frac{\partial\phi}{\partial x_1} - E_y \frac{\partial\phi}{\partial y_1} \right) + \right. \\ \left. + E_z \left(\frac{\partial\phi}{\partial x_1}, \frac{\partial\phi}{\partial y_1}, \frac{\partial\phi}{\partial z_1} \right) \right] dx_1 dy_1. \quad (17) \end{aligned}$$

In particular,

$$E_z(x, y, z) = \frac{1}{2}E_{Az}(x, y, z) + \frac{1}{4\pi} \iint \left(-E_x \frac{\partial\phi}{\partial x_1} - E_y \frac{\partial\phi}{\partial y_1} + E_z \frac{\partial\phi}{\partial z_1} \right) dx_1 dy_1$$

and by applying partial integration to the first two terms of the integrand, the equation becomes

$$\begin{aligned} E_z(x, y, z) &= \frac{1}{2}E_{Az} + \frac{1}{4\pi} \iint \left[\left(\frac{\partial E_x}{\partial x_1} + \frac{\partial E_y}{\partial y_1} \right) \phi + E_z \frac{\partial\phi}{\partial z_1} \right] dx_1 dy_1 \\ &= \frac{1}{2}E_{Az} - \frac{1}{4\pi} \iint \left(\frac{\partial E_x}{\partial z_1} \phi - E_z \frac{\partial\phi}{\partial z_1} \right) dx_1 dy_1. \end{aligned}$$

If the observation point is now allowed to approach the surface S , the fact that

$$\lim_{z \rightarrow 0} \iint E_z \frac{\partial\phi}{\partial z_1} dx_1 dy_1 = 2\pi E_z(x, y, 0)$$

leads to the result

$$E_z(x, y, 0) = E_{Az}(x, y, 0) - \frac{1}{2\pi} \iint \frac{\partial E_z}{\partial z_1} \phi \, dx_1 dy_1. \quad (18)$$

The final step is to use the expression for $\partial E_z/\partial z$ at a point on the mean surface. From (13)

$$\begin{aligned} \frac{\partial E_z}{\partial z_1} &= ikZ \left[\frac{\partial}{\partial x_1} (\zeta_1 H_y) - \frac{\partial}{\partial y_1} (\zeta_1 H_x) \right] + \left(\frac{\partial^2}{\partial x_1^2} + \frac{\partial^2}{\partial y_1^2} \right) (\zeta_1 E_z) \\ &= ikZ (\zeta_{x_1} H_y - \zeta_{y_1} H_x) + \left(k^2 + \frac{\partial^2}{\partial x_1^2} + \frac{\partial^2}{\partial y_1^2} \right) (\zeta_1 E_z), \end{aligned}$$

which can be substituted into (18) to give

$$\begin{aligned} E_z &= E_{Az} - \frac{1}{2\pi} \iint \left[ikZ (\zeta_{x_1} H_y - \zeta_{y_1} H_x) + \right. \\ &\quad \left. + \left(k^2 + \frac{\partial^2}{\partial x_1^2} + \frac{\partial^2}{\partial y_1^2} \right) (\zeta_1 E_z) \right] \phi \, dx_1 dy_1 + O(\delta^3) \quad (19) \end{aligned}$$

at any point (x, y) on the surface $z = 0$.

Turning now to the x component of (17) we have

$$\begin{aligned} E_x(x, y, z) &= \frac{1}{2} E_{Ax}(x, y, z) + \frac{1}{4\pi} \iint \left(-ikZ H_y \phi + E_x \frac{\partial \phi}{\partial z_1} + E_z \frac{\partial \phi}{\partial x_1} \right) dx_1 dy_1 \\ &= \frac{1}{2} E_{Ax}(x, y, z) + \frac{1}{4\pi} \iint \left(\frac{\partial E_z}{\partial x_1} \phi + E_z \frac{\partial \phi}{\partial x_1} + E_x \frac{\partial \phi}{\partial z_1} - \frac{\partial E_x}{\partial z_1} \phi \right) dx_1 dy_1 \end{aligned}$$

and since the first two terms of the integrand integrate to zero,

$$E_x(x, y, z) = \frac{1}{2} E_{Ax}(x, y, z) + \frac{1}{4\pi} \iint \left(E_x \frac{\partial \phi}{\partial z_1} - \frac{\partial E_x}{\partial z_1} \phi \right) dx_1 dy_1.$$

Hence,

$$\begin{aligned} \frac{\partial}{\partial z} E_x(x, y, z) &= \\ &= \frac{1}{2} \frac{\partial}{\partial z} E_{Ax}(x, y, z) - \frac{1}{4\pi} \iint \left(E_x \frac{\partial^2 \phi}{\partial z_1^2} - \frac{\partial E_x}{\partial z_1} \frac{\partial \phi}{\partial z_1} \right) dx_1 dy_1 \end{aligned}$$

and in the limit of an observation point on the mean surface,

$$\begin{aligned} \frac{\partial}{\partial z} E_x(x, y, 0) &= \frac{\partial}{\partial z} E_{Ax}(x, y, 0) - \frac{1}{2\pi} \lim_{z \rightarrow 0} \iint E_x \frac{\partial^2 \phi}{\partial z_1^2} dx_1 dy_1 \\ &= \frac{\partial}{\partial z} E_{Ax}(x, y, 0) + \frac{1}{2\pi} \iint \left(k^2 E_x + \frac{\partial^2 E_x}{\partial x_1^2} + \frac{\partial^2 E_x}{\partial y_1^2} \right) \phi \, dx_1 dy_1. \end{aligned}$$

If the expression for E_x given by (14) is substituted into this integral, the boundary value of $\partial E_x / \partial z$ is found to be

$$\frac{\partial E_x}{\partial z} = \frac{\partial E_{Ax}}{\partial z} - \frac{1}{2\pi} \iint \left\{ \left(k^2 + \frac{\partial^2}{\partial x_1^2} + \frac{\partial^2}{\partial y_1^2} \right) \left[-ikZ\zeta_1 H_y + \frac{\partial}{\partial x_1} (\zeta_1 E_z) \right] \right\} \phi \, dx_1 dy_1 + O(\delta^3), \quad (20)$$

which can be combined with (14) and (19) to give

$$E_x = -\zeta_x E_{Az} - \zeta \frac{\partial E_{Ax}}{\partial z} + \frac{1}{2\pi} \iint P_x \phi \, dx_1 dy_1 + O(\delta^3), \quad (21)$$

where

$$P_x = ikZ(\zeta_x \zeta_{x_1} H_y - \zeta_x \zeta_{y_1} H_x) + ikZ \left(k^2 + \frac{\partial^2}{\partial x_1^2} + \frac{\partial^2}{\partial y_1^2} \right) (\zeta \zeta_1 H_y) + \left(k^2 + \frac{\partial^2}{\partial x_1^2} + \frac{\partial^2}{\partial y_1^2} \right) \left(\frac{\partial}{\partial x} + \frac{\partial}{\partial x_1} \right) (\zeta \zeta_1 E_z). \quad (22)$$

By an analysis similar in all respects to the above it can also be shown that on the mean surface

$$\frac{\partial E_y}{\partial z} = \frac{\partial E_{Ay}}{\partial z} - \frac{1}{2\pi} \iint \left\{ \left(k^2 + \frac{\partial^2}{\partial x_1^2} + \frac{\partial^2}{\partial y_1^2} \right) \left[ikZ\zeta_1 H_x + \frac{\partial}{\partial y_1} (\zeta_1 E_z) \right] \right\} \phi \, dx_1 dy_1 + O(\delta^3), \quad (23)$$

and by using (15), (19) and (23) we have

$$E_y = -\zeta_y E_{Az} - \zeta \frac{\partial E_{Ay}}{\partial z} + \frac{1}{2\pi} \iint P_y \phi \, dx_1 dy_1 + O(\delta^3), \quad (24)$$

where

$$P_y = ikZ(\zeta_y \zeta_{x_1} H_y - \zeta_y \zeta_{y_1} H_x) - ikZ \left(k^2 + \frac{\partial^2}{\partial x_1^2} + \frac{\partial^2}{\partial y_1^2} \right) (\zeta \zeta_1 H_x) + \left(k^2 + \frac{\partial^2}{\partial x_1^2} + \frac{\partial^2}{\partial y_1^2} \right) \left(\frac{\partial}{\partial y} + \frac{\partial}{\partial y_1} \right) (\zeta \zeta_1 E_z). \quad (25)$$

These equations express the tangential components of the electric field on the mean surface in a way which makes explicit the factors of order δ^2 . To this order, it is sufficient to insert into the formulae

for P_x and P_y the field components for a perfectly conducting (smooth) surface at $z = 0$, but before doing so we shall consider the averaging processes which must be applied to (21) and (25) if the actual surface is defined in a statistical manner.

§ 5. *Averaged boundary conditions.* In order to discuss the effect of roughness with any degree of generality, it is necessary to assume that the surface is known only as regards its statistical properties. Let us therefore consider a surface which is statistically uniform and isotropic, but which is otherwise defined by its statistical parameters alone. The field behaviour near to the surface can now be determined only in some average sense, leading to the concept of averaged boundary conditions. Such conditions can be obtained from (21) and (24) by applying either of two averaging processes. In the first of these the points (x, y) , (x_1, y_1) are allowed to roam over a surface having the required statistical properties, the relative positions of the two points being kept constant. At every point the field is evaluated and the results are then averaged over all x and y . This is essentially a "space average" applied to one particular surface.

The second type of average is obtained by keeping the points (x, y) , (x_1, y_1) fixed and introducing different samples of surface into the region between them. All the surfaces are, of course, members of the same statistical family and, in consequence, the averages are here "ensemble averages." Although the two averaging processes are equivalent in most practical cases, the second kind proves most convenient in the present work and will be used throughout the subsequent analysis.

The surface parameters which appear in (22) and (25) are ζ , $\zeta\zeta_1$ and their derivatives. In specifying their average values we first observe that $\bar{\zeta}$ involves the location of the mean surface, and by choosing this such that the departure of the actual surface is zero on the average, we have

$$\bar{\zeta} = \bar{\zeta}_x = \bar{\zeta}_y = 0, \quad (26)$$

thereby justifying the description "mean". For $\zeta\zeta_1$ the average value represents an effective correlation function, and since the surface is uniform and isotropic, this will be defined as

$$\overline{\zeta(x, y)\zeta(x_1, y_1)} = \zeta_0^2 F(\rho), \quad (27)$$

where ζ_0 is the standard deviation (or root mean square departure from the mean), and $F(\rho)$ is real and a function only of the distance ρ separating the two points (x, y) and (x_1, y_1) . $F(\rho)$ has a maximum value of unity at $\rho = 0$ (at which point $\partial F/\partial \rho = 0$), and falls rapidly to zero for increasing $\rho > l$, where l is typical of the roughness scale. It is assumed that ζ_0^2 and $F(\rho)$ are known for the surface under consideration.

If the averaging process is now applied to (21) and (24), the boundary conditions become

$$E_x = \frac{\zeta_0^2}{2\pi} \iint \bar{P}_x \phi dx_1 dy_1 + O(\delta^3), \quad (28)$$

where

$$\begin{aligned} \bar{P}_x = ikZ & \left(-\frac{\partial^2 F}{\partial x \partial x_1} H_y - \frac{\partial^2 F}{\partial x \partial y_1} H_x \right) + \\ & + ikZ \left(k^2 + \frac{\partial^2}{\partial x_1^2} + \frac{\partial^2}{\partial y_1^2} \right) (F H_x) + \\ & + \left(k^2 + \frac{\partial^2}{\partial x_1^2} + \frac{\partial^2}{\partial y_1^2} \right) \left(\frac{\partial}{\partial x} + \frac{\partial}{\partial x_1} \right) (F E_z), \quad (29) \end{aligned}$$

and similarly for E_y . To the required order in δ , the field components H_x , H_y and E_z can be replaced by the corresponding components for a smooth surface, and for this reason they have been excluded from the averaging process.

Since $F(\rho)$ is a function only of the variable ρ , it follows that

$$\left(\frac{\partial}{\partial x} + \frac{\partial}{\partial x_1} \right) F = 0$$

and hence

$$\left(\frac{\partial}{\partial x} + \frac{\partial}{\partial x_1} \right) (F E_z) = F \frac{\partial E_z}{\partial x_1} = i \frac{Z}{k} F \left(\frac{\partial^2 H_y}{\partial x_1^2} - \frac{\partial^2 H_x}{\partial x_1 \partial y_1} \right),$$

which enables \bar{P}_x to be expressed as a function of the components H_x and H_y in the form

$$\begin{aligned} \bar{P}_x = ikZ & \left\{ \left[-\frac{\partial^2 F}{\partial x \partial x_1} + \Gamma \left(1 + \frac{1}{k^2} \frac{\partial^2}{\partial x_1^2} \right) \right] H_y - \right. \\ & \left. - \left[\frac{\partial^2 F}{\partial x \partial y_1} + \frac{\Gamma}{k^2} \frac{\partial^2}{\partial x_1 \partial y_1} \right] H_x \right\} \quad (30) \end{aligned}$$

with

$$\Gamma = F \left(k^2 + \frac{\partial^2}{\partial x_1^2} + \frac{\partial^2}{\partial y_1^2} \right) + \frac{\partial^2 F}{\partial x_1^2} + \frac{\partial^2 F}{\partial y_1^2} + 2 \frac{\partial F}{\partial x_1} \frac{\partial}{\partial x_1} + 2 \frac{\partial F}{\partial y_1} \frac{\partial}{\partial y_1}. \quad (31)$$

Similarly,

$$\bar{P}_y = ikZ \left\{ \left[\frac{\partial^2 F}{\partial x \partial y_1} + \frac{\Gamma}{k^2} \frac{\partial^2}{\partial x_1 \partial y_1} \right] H_y - \left[\frac{\partial^2 F}{\partial y \partial y_1} + \Gamma \left(1 + \frac{1}{k^2} \frac{\partial^2}{\partial y_1^2} \right) \right] H_x \right\}, \quad (32)$$

and these results give rise to the following matrix equation

$$(\bar{P}_x, \bar{P}_y) = \begin{pmatrix} a_{11} & a_{12} \\ a_{21} & a_{22} \end{pmatrix} \begin{pmatrix} -ZH_y \\ ZH_x \end{pmatrix}, \quad (33)$$

where

$$a_{11} = -ik \left[\frac{\partial^2 F}{\partial x \partial x_1} + \Gamma \left(1 + \frac{1}{k^2} \frac{\partial^2}{\partial x_1^2} \right) \right], \quad (34)$$

$$\begin{aligned} a_{12} &= a_{21} \\ &= -ik \left[\frac{\partial^2 F}{\partial x \partial y_1} + \frac{\Gamma}{k^2} \frac{\partial^2}{\partial x_1 \partial y_1} \right], \end{aligned} \quad (35)$$

$$a_{22} = -ik \left[\frac{\partial^2 F}{\partial y \partial y_1} + \Gamma \left(1 + \frac{1}{k^2} \frac{\partial^2}{\partial y_1^2} \right) \right]. \quad (36)$$

Although the elements a_{ij} are differential operators, we note the interesting fact that as written above the matrix is symmetric.

§ 6. *The surface impedance matrix.* In order to evaluate the matrix representing the effective surface impedance, it is necessary to integrate the elements a_{ij} in the manner shown in (28). This in turn requires us to insert into (28) the dependence of the components H_x and H_y on the surface coordinates x_1, y_1 in a neighbourhood of the point (x, y) .

Since the surface can be regarded as smooth as far as these components are concerned, we can write

$$H_x(x_1, y_1, 0) = H_x(x, y, 0) \exp i[k_x(x_1 - x) + k_y(y_1 - y)],$$

$$H_y(x_1, y_1, 0) = H_y(x, y, 0) \exp i[k_x(x_1 - x) + k_y(y_1 - y)],$$

where k_x and k_y can be assumed constant throughout the integration. If the incident field is produced by a point source at a finite distance from the surface, k_x and k_y are the direction cosines of the source relative to the point (x, y) and are therefore functions of x and y . Equations (37) and (38) are then valid unless the source is within a wavelength or so of the surface, and even in this case the equations fail only for that portion of the surface which is in the immediate vicinity of the source. If, on the other hand, the incident field is a plane wave (corresponding to a source at infinity), k_x and k_y are the tangential components of the propagation vector and are the same at all points of the surface. For a plane wave incident in a direction making angles α and β with the positive x and negative z axes respectively,

$$k_x = k \cos \alpha \sin \beta, \quad (39)$$

$$k_y = k \sin \alpha \sin \beta, \quad (40)$$

and we note in passing that $k^2 - k_x^2 - k_y^2 \neq 0$ except for grazing incidence ($\beta = \pm \pi/2$).

Using the above expressions for H_x and H_y , equations (34) through (36) become

$$a_{11} = ik \left[\frac{\partial^2 F}{\partial x \partial x_1} + \left(1 - \frac{k_x^2}{k^2} \right) \Gamma \right],$$

$$a_{12}, a_{21} = -ik \left[\frac{\partial^2 F}{\partial x \partial y_1} - \frac{k_x k_y}{k^2} \Gamma \right],$$

$$a_{22} = -ik \left[\frac{\partial^2 F}{\partial y \partial y_1} + \left(1 - \frac{k_y^2}{k^2} \right) \Gamma \right]$$

with

$$\Gamma = (k^2 - k_x^2 - k_y^2)F + \frac{\partial^2 F}{\partial x_1^2} + \frac{\partial^2 F}{\partial y_1^2} + 2i \left(k_x \frac{\partial F}{\partial x_1} + k_y \frac{\partial F}{\partial y_1} \right),$$

and to the second order in δ the boundary condition on the mean surface can now be written as

$$(E_x, E_y) = \begin{pmatrix} A_{11} & A_{12} \\ A_{21} & A_{22} \end{pmatrix} \begin{pmatrix} -ZH_y \\ ZH_x \end{pmatrix}, \quad (41)$$

where

$$A_{ij} = \frac{\zeta_0^2}{2\pi} \iint a_{ij} \exp i[k_x(x_1 - x) + k_y(y_1 - y)] \phi dx_1 dy_1. \quad (42)$$

The matrix A_{ij} is, of course, symmetric, and (41) represents a generalized form of the usual impedance boundary condition.

The integration in (42) is most easily carried out by introducing the polar coordinates (ρ, θ) , where

$$x_1 = x + \rho \cos \theta, \quad y_1 = y + \rho \sin \theta.$$

If, in addition, we place

$$k_x = \tau \cos \alpha, \quad k_y = \tau \sin \alpha$$

with $\tau = \sqrt{k_x^2 + k_y^2}$, then

$$A_{ij} = \frac{\zeta_0^2}{2\pi} \int_0^\infty \int_0^{2\pi} a_{ij} \exp i\rho[k + \tau \cos(\theta - \alpha)] d\theta d\rho,$$

and since F is only a function of ρ , the θ integration can be carried out immediately to give

$$A_{11} = -ik\zeta_0^2 \int_0^\infty \left[\left(1 - \frac{k_x^2}{k^2}\right) B - \frac{1}{2} \left(\frac{\partial^2 F}{\partial \rho^2} + \frac{1}{\rho} \frac{\partial F}{\partial \rho} \right) J_0(\tau\rho) + \frac{1}{2} \left(\frac{\partial^2 F}{\partial \rho^2} - \frac{1}{\rho} \frac{\partial F}{\partial \rho} \right) \cos 2\alpha J_2(\tau\rho) \right] e^{ik\rho} d\rho, \quad (43)$$

$$A_{12}, A_{21} = i \frac{k_x k_y \zeta_0^2}{k} \int_0^\infty \left[B - \left(\frac{k}{\tau} \right)^2 \left(\frac{\partial^2 F}{\partial \rho^2} - \frac{1}{\rho} \frac{\partial F}{\partial \rho} \right) J_2(\tau\rho) \right] e^{ik\rho} d\rho, \quad (44)$$

$$A_{22} = -ik\zeta_0^2 \int_0^\infty \left[\left(1 - \frac{k_y^2}{k^2}\right) B - \frac{1}{2} \left(\frac{\partial^2 F}{\partial \rho^2} + \frac{1}{\rho} \frac{\partial F}{\partial \rho} \right) J_0(\tau\rho) - \frac{1}{2} \left(\frac{\partial^2 F}{\partial \rho^2} - \frac{1}{\rho} \frac{\partial F}{\partial \rho} \right) \cos 2\alpha J_2(\tau\rho) \right] e^{ik\rho} d\rho, \quad (45)$$

where

$$B = \left[\frac{\partial^2 F}{\partial \rho^2} + \frac{1}{\rho} \frac{\partial F}{\partial \rho} + (k^2 - \tau^2) \right] J_0(\tau\rho) - 2\tau \frac{\partial F}{\partial \rho} J_1(\tau\rho) = \left(\frac{\partial^2}{\partial \rho^2} + \frac{1}{\rho} \frac{\partial}{\partial \rho} + k^2 \right) (F J_0). \quad (46)$$

These are the elements of the effective surface impedance matrix, and it is seen that they depend on the direction of the incident field as specified by the factors k_x , k_y and $k_z = \sqrt{k^2 - \tau^2}$.

§ 7. *A study of equation (41).* The properties of the boundary condition (41) are best described in terms of the impedance condition which obtains at the (smooth) surface of material of large but finite refractive index. This condition is usually attributed to Leontovich, and can be written as

$$\mathbf{E} - (\hat{\mathbf{n}} \cdot \mathbf{E})\hat{\mathbf{n}} = \eta Z \hat{\mathbf{n}} \times \mathbf{H}, \quad (47)$$

where (\mathbf{E}, \mathbf{H}) is the field in the region outside the material (which region is regarded as free space), and $\hat{\mathbf{n}}$ is a unit vector normal in the outward direction. The parameter η is proportional to the reciprocal of the complex refractive index and is defined by the equation

$$\eta = \left[\frac{\mu_0}{\mu} \left(\frac{\varepsilon}{\varepsilon_0} + i \frac{\sigma}{\omega \varepsilon_0} \right) \right]^{-\frac{1}{2}}, \quad (48)$$

where ε , μ and σ are respectively the permittivity, permeability and conductivity of the material; the suffix 'o' denotes the same quantities for free space. Eq. (47) is valid for surfaces of varying curvature as well as materials whose refractive index differs from point to point providing the tangential variation of the field is relatively slow, and with this restriction the boundary condition is accurate to the first order in η . A full discussion is given in ¹⁾.

In recent years this type of boundary condition has been increasingly used in the analysis of propagation and scattering problems. Because of the restriction to small values of η , it is natural to regard it as a means for obtaining a perturbation about the solution for perfect conductivity, but in addition solutions which are mathematically exact and subject only to the (physical) approximation implied by (47) have been obtained for certain simple shapes of body. Examples are the sphere, the circular cylinder, the half plane and the wedge of arbitrary angle.

For the particular case in which the imperfectly conducting material occupies the half space $z < 0$, so that the interface is an infinite plane, (47) reduces to

$$\begin{pmatrix} E_x & E_y \end{pmatrix} = \begin{pmatrix} \eta & 0 \\ 0 & \eta \end{pmatrix} \begin{pmatrix} -ZH_y \\ ZH_x \end{pmatrix}, \quad (49)$$

and this is the most elementary form of the impedance boundary condition. If (41) and (49) are now compared, it is seen that the boundary condition for the rough surface is only equivalent to a

Leontovich condition if $A_{11} = A_{22}$ and $A_{12} = A_{21} = 0$, and although this is true for selected angles of incidence, it is not true in general.

The fact that the elements A_{ij} are functions of the angle of incidence is a direct consequence of the nature of the surface and represents a fundamental difference between imperfectly conducting and rough surfaces. This is in spite of the roughness being small and isotropic. As long as the mean scattering surface is a plane, the dependence is not a severe handicap, but it does mean that the tensor surface impedance is a variable function of position on the surface unless the incident field is a plane wave. For this reason the boundary condition will seldom permit an exact solution of the boundary value problem, and the usefulness of the condition then rests on the degree to which it facilitates a perturbation solution.

For certain angles of incidence the boundary condition (41) takes on a simpler form, and to demonstrate this fact we shall consider the example of a plane wave incident in a direction specified by the angles α and β defined in § 6. If the incidence is normal to the mean surface ($\beta = 0$), then $k_x = k_y = \tau = 0$ and (43) through (45) give

$$A_{11}, A_{22} = -\frac{ik\zeta_0^2}{2} \int_0^\infty \left(\frac{\partial^2 F}{\partial \rho^2} + \frac{1}{\rho} \frac{\partial F}{\partial \rho} + 2k^2 F \right) e^{ik\rho} d\rho,$$

$$A_{12}, A_{21} = 0.$$

In this case (41) becomes

$$(E_x, E_y) = \begin{pmatrix} \eta_\perp & 0 \\ 0 & \eta_\perp \end{pmatrix} \begin{pmatrix} -ZH_y \\ ZH_x \end{pmatrix}, \quad (50)$$

where

$$\eta_\perp = -\frac{ik\zeta_0^2}{2} \int_0^\infty \left(\frac{\partial^2 F}{\partial \rho^2} + \frac{1}{\rho} \frac{\partial F}{\partial \rho} + 2k^2 F \right) e^{ik\rho} d\rho, \quad (51)$$

and this is now the boundary condition for the surface $z = 0$. The condition is of the standard Leontovich type and is accurate to the first order in the (small) parameter η_\perp , where η_\perp is the effective surface impedance.

If the incidence is not normal, the true situation becomes ap-

parent on writing the expressions for the A_{ij} as

$$A_{11} = ik\zeta_0^2 \left\{ \frac{1}{2} \frac{k_x^2 - k_y^2}{k^2} Q - \int_0^\infty \left[\left(1 - \frac{1}{2} \frac{\tau^2}{k^2} \right) B - \frac{1}{2} \left(\frac{\partial^2 F}{\partial \rho^2} + \frac{1}{\rho} \frac{\partial F}{\partial \rho} \right) J_0(\tau \rho) \right] e^{ik\rho} d\rho \right\}, \quad (52)$$

$$A_{12}, A_{21} = ik\zeta_0^2 \frac{k_x k_y}{k^2} Q, \quad (53)$$

$$A_{22} = ik\zeta_0^2 \left\{ -\frac{1}{2} \frac{k_x^2 - k_y^2}{k^2} Q - \int_0^\infty \left[\left(1 - \frac{1}{2} \frac{\tau^2}{k^2} \right) B - \frac{1}{2} \left(\frac{\partial^2 F}{\partial \rho^2} + \frac{1}{\rho} \frac{\partial F}{\partial \rho} \right) J_0(\tau \rho) \right] e^{ik\rho} d\rho \right\}, \quad (54)$$

where

$$Q = \int_0^\infty \left[B - \left(\frac{k}{\tau} \right)^2 \left(\frac{\partial^2 F}{\partial \rho^2} - \frac{1}{\rho} \frac{\partial F}{\partial \rho} \right) J_2(\tau \rho) \right] e^{ik\rho} d\rho, \quad (55)$$

and from these it is seen that the Leontovich form of impedance condition is only obtained if $k_x k_y$ and $k_x^2 - k_y^2$ are both zero (as in the case of normal incidence) or $Q = 0$. It is a trivial matter to show that Q is not identically zero nor, in general, is it small compared with the other terms common to A_{11} and A_{22} .

Nevertheless, there is another situation in which the boundary condition simplifies. In many problems involving rough surfaces it is sufficient if the approximate magnitude of the roughness effect can be determined, and for the purposes of such analyses it is only necessary that the boundary condition employed reveal the main roughness effect. Under these circumstances it seems probable that the dependence on the angle of incidence will not be of prime importance, and can be suppressed without destroying the efficacy of the boundary condition. One way in which the suppression can be achieved is to average the condition over all angles of incidence.

To this end we recall that in the right hand side of (41) the field components H_x and H_y can be replaced by the corresponding components for a perfectly conducting surface at $z = 0$, and accordingly

$$H_x = 2H_x^i, \quad H_y = 2H_y^i,$$

where the affix ' i ' denotes the incident field. If $\beta \neq \frac{1}{2}\pi$, H_x^i and H_y^i

can be assigned values on $z = 0$ which are independent of one another, and which are independent of α and β providing the strength and polarization of the equivalent source are suitably adjusted. If (41) is now averaged over all α and β with H_x and H_y kept constant, then since $0 \leq \alpha \leq 2\pi$ and $0 \leq \beta \leq \frac{1}{2}\pi$,

$$\text{av. } k_x, k_y, k_x k_y = 0,$$

$$\text{av. } k_x^2, k_y^2 = \frac{1}{4}k^2,$$

$$\text{av. } \tau^2 = \frac{1}{2}k^2.$$

This process has the effect of making zero *) the coefficients of the unwanted terms in (52) through (54) and produces a boundary condition at $z = 0$ of the type shown in (49). The surface impedance is

$$\eta' = -\frac{ik\zeta_0^2}{4} \int_0^\infty \left\{ \left(\frac{\partial^2}{\partial \rho^2} + \frac{1}{\rho} \frac{\partial}{\partial \rho} + 2k^2 \right) \left[FJ_0 \left(\frac{k\rho}{\sqrt{2}} \right) \right] - \frac{k}{\sqrt{2}} \frac{\partial F}{\partial \rho} J_1 \left(\frac{k\rho}{\sqrt{2}} \right) \right\} e^{ik\rho} d\rho \quad (56)$$

and can be regarded as the average for a field incident at any angle. The evaluation of the integral is described in § 8.

Before leaving this discussion of (41), a few words should be said about the exceptional case of grazing incidence, $\beta = \frac{1}{2}\pi$. This is the case treated by Feinberg ²⁾³⁾ and its relevance to the present work is that it leads to a "bastard" form of the Leontovich condition if the coordinate system is suitably chosen. When $\beta = \frac{1}{2}\pi$, H_x^i and H_y^i cannot be assigned values on the surface independently of one another and, indeed,

$$k_x H_x^i = -k_y H_y^i \quad (57)$$

which introduces an apparent ambiguity into (41) as long as H_x and H_y are given the values of the incident field components.

The difficulty, however, can be overcome by considering separately fields which propagate in the x and y directions. If the propagation is in the x direction, $k_y = 0$ and (57) shows that H_x^i is then zero.

*) Note that (52) through (54) only involve even powers of τ .

Since $k_x = \tau = k$,

$$A_{11} = -\frac{ik\zeta_0^2}{2} \int_0^\infty \left[\left(\frac{\partial^2 F}{\partial \rho^2} + \frac{1}{\rho} \frac{\partial F}{\partial \rho} \right) J_0(k\rho) - \left(\frac{\partial^2 F}{\partial \rho^2} - \frac{1}{\rho} \frac{\partial F}{\partial \rho} \right) J_2(k\rho) \right] e^{ik\rho} d\rho,$$

$$A_{21} = 0,$$

and (41) gives

$$E_x = -\eta_{\parallel} Z H_y, \quad (58)$$

$$E_y = 0,$$

with

$$\eta_{\parallel} = \frac{ik\zeta_0^2}{2} \int_0^\infty \left[\left(\frac{\partial^2 F}{\partial \rho^2} + \frac{1}{\rho} \frac{\partial F}{\partial \rho} \right) J_0(k\rho) - \left(\frac{\partial^2 F}{\partial \rho^2} - \frac{1}{\rho} \frac{\partial F}{\partial \rho} \right) J_2(k\rho) \right] e^{ik\rho} d\rho. \quad (60)$$

Equations (58) and (59) are consistent with a Leontovich boundary condition for a field having $H_x = 0$. Similarly, if $k_x = 0$

$$E_x = 0, \quad (61)$$

$$E_y = \eta_{\parallel} Z H_x \quad (62)$$

on $z = 0$, where η_{\parallel} is again *) given by (60), and this value for the surface impedance is equivalent to the one obtained by Feinberg who likewise assumed propagation in the direction of a coordinate axis. But if neither k_x nor k_y is zero, the impedance reverts to a tensor form and no reduction of (41) is then possible.

§ 8. *Values for the surface impedance.* We shall now examine in rather more detail the integral expressions for η_{\perp} , η' and (briefly) η_{\parallel} . Although the precise form of $F(\rho)$ is left unspecified to begin with, it should be noted that $F(0) = 1$ and $(\partial F / \partial \rho)_{\rho=0} = 0$ by virtue of the type of rough surface under consideration.

If integration by parts is applied to (51), it is found that

$$\eta_{\perp} = -\frac{ik\zeta_0^2}{2} \left[ik + \int_0^\infty \left(\frac{1}{\rho} \frac{\partial F}{\partial \rho} + k^2 F \right) e^{ik\rho} d\rho \right]$$

*) The fact that the impedances are the same in both cases is a consequence of the isotropy of the surface.

and similarly

$$\eta' = -\frac{ik\zeta_0^2}{4} \left\{ ik + \int_0^\infty \left[\left(\frac{1}{\rho} \frac{\partial}{\partial \rho} + k^2 \right) \left\{ F J_0 \left(\frac{k\rho}{\sqrt{2}} \right) - \right\} \right. \right. \\ \left. \left. - \frac{k}{\sqrt{2}} \frac{\partial F}{\partial \rho} J_1 \left(\frac{k\rho}{\sqrt{2}} \right) \right] e^{ik\rho} d\rho \right\}. \quad (63)$$

For roughnesses whose scale is such that $kl \ll 1$, these equations further reduce to

$$\eta_\perp = -\frac{ik\zeta_0^2}{2} \int_0^\infty \frac{1}{\rho} \frac{\partial F}{\partial \rho} e^{ik\rho} d\rho, \\ \eta' = -\frac{ik\zeta_0^2}{4} \int_0^\infty \frac{1}{\rho} \frac{\partial F}{\partial \rho} e^{ik\rho} d\rho, \quad (64)$$

which may be compared with the value

$$\eta_\parallel = \frac{ik\zeta_0^2}{2} \int_0^\infty \frac{1}{\rho} \frac{\partial F}{\partial \rho} e^{ik\rho} d\rho,$$

deduced from (60) under the same restriction. Hence, for small kl ,

$$\eta_\perp = 2\eta' = -\eta_\parallel. \quad (65)$$

To proceed further with the evaluation of these integrals it is necessary to insert an expression for the function $F(\rho)$. In practice, this expression should be determined by a study of the actual surface, but for small scale roughness at least it is unlikely that the impedance will depend critically on the choice of F . One of the simplest cases to consider is a Gaussian function, and for convenience this is assumed throughout the subsequent analysis. It is believed that the results obtained are typical.

If $F(\rho)$ is defined as

$$F(\rho) = e^{-4\rho^2/l^2} \quad (66)$$

where l is interpreted as the scale of roughness, then

$$\frac{\partial F}{\partial \rho} = -\frac{8\rho}{l^2} F$$

and (64) now gives

$$\eta' \sim i \frac{\sqrt{\pi}}{2} \frac{k\zeta_0^2}{l}. \quad (67)$$

The corresponding value for $\eta_{||}$ (see (65)) is in agreement with Feinberg's result for small scale roughness.

If desired, the surface impedance can be associated with an equivalent conductivity by using (48) and attributing the non-zero value of η to a conductivity σ rather than to a permittivity ϵ . Providing the conductivity term is dominant,

$$\sigma = -iYk/\eta^2 \text{ mhos/m}$$

where, for simplicity, μ has been put equal to μ_0 , and by inserting the above expression for η' we arrive at the equivalent conductivity

$$\sigma' = i \frac{4}{\pi} Y \frac{l^2}{k^2 \epsilon_0^4} \text{ mhos/m.} \quad (68)$$

Taking, for example, $kl = 1/5$ and $k\zeta_0 = 1/100$,

$$|\sigma'| \sim (10^5/\lambda) \text{ mhos/m}$$

and at X band frequencies this is similar to the conductivity of ordinary metals.

For larger values of kl (but still not large compared with unity), the approximations made in going from (63) to (64) are no longer valid, and it becomes necessary to employ the full expression for η' given in (63) and similarly for $\eta_{||}$ and η_{\perp} . As long as kl is less than (about) 2.5, however, an analytic evaluation is still possible, and has been used to compute the formula for η' . For this purpose, (63) is written as

$$\eta' = (\tfrac{1}{2}k\zeta_0)^2(L + iM), \quad (69)$$

where L and M are real and functions only of the parameter $u = (\tfrac{1}{2}kl)^2$. The expressions for L and M are

$$L = 1 - \frac{\sqrt{2}}{u} \int_0^\infty [(1 - \tfrac{3}{4}u)J_0(x) + \tfrac{1}{4}uJ_2(x) - 2xJ_1(x)] e^{-2x^2/u} \sin(x\sqrt{2}) dx,$$

$$M = \frac{\sqrt{2}}{u} \int_0^\infty [(1 - \tfrac{3}{4}u)J_0(x) + \tfrac{1}{4}uJ_2(x) - 2xJ_1(x)] e^{-2x^2/u} \cos(x\sqrt{2}) dx$$

and if the series expansions for the Bessel functions are inserted, each integral can be reduced to a sum of Fresnel integrals. These in turn can be replaced by their expansions for small argument, leading to the expression of L and M as series in ascending powers

of u , which series are convergent for u less than (about) 1.5. Based on these formulae, numerical values of L and M have been computed for roughness scales up to 0.39λ , and are plotted in fig. 1. It is seen that the imaginary part of η' does not depart significantly from the value indicated by (67) until kl exceeds 0.8, by which time the real part of η is also becoming important. The real and imaginary parts are equal for $kl = 2.06$ (approx).

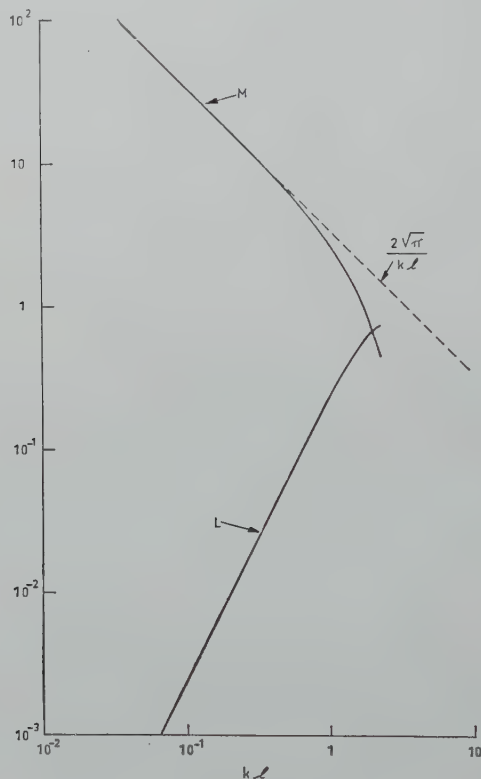


Fig. 1. Real part L and imaginary part M of the normalized surface impedance as a function of the scale of roughness kl .

§ 9. *General discussion.* In the preceding sections it has been shown that for a perfectly conducting plane which is perturbed, or roughened, in a random sort of manner, the boundary condition can be expressed as a form of impedance condition at a neighbouring mean surface. This is valid for a wide variety of small and statis-

tically uniform perturbations, and if the higher order effects are ignored, the boundary condition is as shown in (41). The result will be regarded as exact for the purposes of the following remarks.

If the boundary condition were only applicable to a flat mean surface it would be of little practical value, and we shall now consider how it can be generalized to a mean surface which is curved. By means of a local analysis it is not difficult to see that under certain circumstances the boundary condition can be taken over as it stands. Although a rigorous proof of this fact is difficult, the extension can be justified in part by the semi-intuitive argument which appears in ¹⁾, and this indicates that a sufficient restriction on the type of surface is for the radii of curvature (and, if the surface is closed, dimensions of the body) to be large in comparison with the wavelength. The requirement is therefore taken to be

$$R \gg \lambda,$$

where R is the smallest length parameter associated with the mean surface, and if this is satisfied the curvature enters into the boundary condition only in the higher order terms. We observe in passing that for the roughness scales considered here the restriction also ensures that $R \gg l$.

In (41) the elements of the impedance matrix (A_{ij}) are functions of the direction of the incident field relative to the surface, and although this is not a serious drawback to the use of this condition for analysing the scattering of a plane wave by an infinite perturbed plane, it does mean that when the same condition is applied to a mean surface which is curved, or to a flat surface under point source illumination, the effective surface impedance becomes a function of position on the surface. This complication is additional to the one posed by the tensor nature of the impedance. Few (if any) mathematical techniques are available for treating problems with boundary conditions of this type, and consequently there is little hope of using the condition (41) to obtain exact solutions for scattering by rough bodies.

On the other hand, the boundary condition (41) is well suited to the method of successive approximations. Knowing the field of the smooth body at all points in space and, in particular, on the mean surface itself, the boundary values of the tangential magnetic field can be inserted into the right hand side of (41), thereby specifying

the components of the tangential electric field at the mean surface. These in turn can be fed into the radiation integral to give the field of the rough body at all points.

In the above method the values of k_x and k_y are obtained from the direction of the incident field, and consequently k_x and k_y will, in general, vary over the surface. A difficulty arises, however, if a portion of the body is in shadow, since it is then unlikely that the phase behaviour of the field over the dark portion of the body will be determined to a sufficient degree of approximation by the incident field alone. In this case it may be necessary to also calculate k_x and k_y from the smooth body solution and, in effect, regard (28), and the corresponding equation for E_y , as the fundamental equations representing the boundary condition.

In many instances, however, the accuracy provided by these boundary conditions may not be fully required, and a simpler form of condition may then prove sufficient. If, for example, the body and all its radii of curvature are *very* large in comparison with the wavelength, the field in the shadow region is unlikely to exert a profound effect on the return at angles less than (say) 60° from back scattering, which suggests that a precise statement of the phase dependence of the smooth body field on the unilluminated side may be unnecessary. The parameters k_x and k_y can then be found from the incident field alone.

A further, and more striking, simplification is possible if the bulk of the return is provided by either a surface at constant inclination to the incident field, or by a relatively small portion of the whole surface. The latter case is one in which the smooth body has a specular point, and here it may be sufficient to use (41) with the incident field direction appropriate to this point. The same condition would then be applied regardless of position on the body, and this is particularly valuable in back scattering since the surface impedance reduces to a scalar at normal incidence.

With all these simplifications, however, approximations are introduced additional to those inherent in the boundary condition itself, and each body must therefore be considered on its merits to see which approximations (if any) are warranted.

From the above remarks it will be appreciated that a rigorous discussion of scattering by even the simplest rough body remains a problem of considerable complexity in spite of the assistance

provided by the boundary condition (41). On the other hand, if the aim of the analysis is only to determine the approximate magnitude of the roughness effect, it may be sufficient to average (41) over all directions of the incident field, and this produces a tremendous simplification. The boundary condition is now the one shown in (49), and is seen to be of the standard Leontovich type with a surface impedance η' given by (63). This condition has been used with some success to calculate the effects of minor surface roughnesses on the back scattering cross-section of a large sphere. The results obtained are in reasonable agreement with experiment and are described in 5).

A normalized form of the surface impedance η' is plotted as a function of kl in fig. 1, and changes from being purely reactive for small kl to part resistive and part reactive for values of kl near to unity. Since this impedance can be interpreted in terms of the physical properties associated with the equivalent scattering surface, it may be of interest to examine in more detail the variation with kl . In the first place, a pure imaginary η' corresponds to a displacement of the surface parallel to itself, the displacement being in the outwards direction when the imaginary part is positive. The fact that the imaginary part is always positive in the present case is a direct consequence of the random nature of the irregularities and the chosen location of the mean surface, the ensemble averaging having removed the first order displacement (which may be either positive or negative) leaving a positive second order effect. In general, such a displacement can be expected to increase the scattered field, and this is clearly seen in the case of scattering by a large sphere. As distinct from this a portion of both the real and imaginary parts of η' can be attributed to a true surface resistivity, and if the conduction current is large compared with the displacement current the corresponding impedance has argument $-\pi/4$. This portion of η' is associated with a dissipation (or storage) of energy by the surface, and may be expected to decrease the scattered field in the direction of observation.

From fig. 1 it is now seen that for roughnesses of very small scale the dominant effect is a straightforward displacement of the surface which will usually lead to an increase in the scattering, but as the scale increases the resistivity increases and introduces an opposing trend. With any given value of kl , the question as to whether the

scattering cross-section is increased or decreased depends upon the associated amplitude of the roughness, and this is apparent from the formula for the back scattering cross-section of a rough sphere (see ⁵). For this body at least the resistivity will often outweigh the effect of surface displacement as the roughness increases in scale, and the back scattered field will then be less than that of a smooth sphere of radius equal to the radius of the mean surface.

§ 10. *Conclusions.* The method by which the features of surface roughness are incorporated in the boundary conditions would appear to have advantages not only where precise solutions are required for particular types of body, but also in those cases where the desire is merely to estimate the approximate magnitude of the surface roughness effects.

Acknowledgement. This research was sponsored by the U. S. Air Force under Contracts AF 30(602)-1808, AF 30(602)-2099 and AF 19(604)-5470.

Received 26th July, 1960.

REFERENCES

- 1) Senior, T. B. A., Appl. Sci. Res. B **9** (1961) 418.
- 2) Feinberg, E. L., Izv. Akad. Nauk SSSR, Ser. Fiz. **8** (1944) 109.
- 3) Feinberg, E. L., J. Phys. USSR **8** (1944) 317.
- 4) Stratton, J. A., Electromagnetic Theory, McGraw-Hill, New York, 1941.
- 5) Hiatt, R. E., T. B. A. Senior, and V. H. Weston, to be published in Proc. Instn Radio Engrs. (1960).

USE OF STOKES' STREAM FUNCTION FOR DISCONTINUITIES OF POTENTIAL AT A SPHERICAL BOUNDARY

by G. POWER

The University, Nottingham, England

and H. L. W. JACKSON

College of Technology, Derby, England

Summary

A use of Stokes' stream function is here presented which allows for discontinuities of potential at a spherical surface of separation. It is of special importance in heat problems where the 'radiation' boundary condition applies. Results obtained previously depending upon the continuity of potential across the surface can also be deduced. The fact that 'flow-sheets' can be determined directly from the given formulae is often advantageous.

§ 1. *Introduction.* Butler ¹⁾ discussed the Stokes' stream function for the internal and external cases of axisymmetrical motion of homogeneous incompressible inviscid fluid in the presence of a rigid sphere. Power ²⁾ extended these results to include problems in magnetism and electricity which depend on the continuity of potential distribution across the spherical boundary surface. It is possible that the use of Stokes' stream function may be advantageous when surface discontinuities in potential arise, for example in heat problems involving the 'radiation' boundary condition, thus enabling "flow-sheets" to be determined directly. It is therefore of interest to derive the Stokes' stream functions corresponding to the potential functions given by Power and Jackson ³⁾ in their general sphere theorem. All flows, of course, are assumed to be axisymmetrical.

§ 2. *Theorem.* Let $\psi_0(r) \equiv \psi_0(r, \theta)$ be the Stokes' stream function for a distribution lying entirely outside the sphere $r = a$, and

$\psi_1(r) \equiv \psi_1(r, \theta)$ be Stokes' stream function for a distribution lying entirely within this sphere. The function $\psi(r) \equiv \psi(r, \theta)$ given by

$$\left. \begin{aligned} \psi(r) = \psi_e(r) = \psi_0(r) - \frac{r}{a} \psi_0\left(\frac{a^2}{r}\right) - \frac{r}{a} \int_0^1 F(s) \psi_0\left(\frac{sa^2}{r}\right) ds + \\ + \int_1^\infty G(s) \psi_1(sr) ds \quad \text{for } r \geq a, \\ \psi(r) = \psi_i(r) = \psi_1(r) - \frac{r}{a} \psi_1\left(\frac{a^2}{r}\right) - \frac{r}{a} \int_1^\infty g(s) \psi_1\left(\frac{sa^2}{r}\right) ds + \\ + \int_0^1 f(s) \psi_0(sr) ds \quad \text{for } r \leq a, \end{aligned} \right\} \quad (1)$$

with

$$\left. \begin{aligned} F(s) = P_1 s^{\alpha_1-1} + P_2 s^{\alpha_2-1}, \quad f(s) = Q_1 s^{\alpha_1-1} + Q_2 s^{\alpha_2-1}, \\ G(s) = R_1 s^{\gamma_1-1} + R_2 s^{\gamma_2-1}, \quad g(s) = S_1 s^{\gamma_1-1} + S_2 s^{\gamma_2-1}, \\ v_1 P_1 = -v_2 Q_1 = \frac{v_3(1+2\alpha_1)}{(\alpha_2 - \alpha_1)}, \quad v_1 P_2 = -v_2 Q_2 = \frac{v_3(1+2\alpha_2)}{(\alpha_1 - \alpha_2)}, \\ -v_1 R_1 = v_2 S_1 = \frac{v_4(1+2\gamma_1)}{(\gamma_2 - \gamma_1)}, \quad -v_1 R_2 = v_2 S_2 = \frac{v_4(1+2\gamma_2)}{(\gamma_1 - \gamma_2)}, \end{aligned} \right\} \quad (2)$$

where α_1, α_2 are the roots of the equation $\alpha^2 + \alpha(1+k) - v_3/v_1 = 0$ γ_1, γ_2 are the roots of $\gamma^2 + \gamma(1-k) + v_4/v_2 = 0$, where $k = -(v_4/v_2 + v_3/v_1)$, and all the integrals are uniformly convergent, has the following properties:

$$\left. \begin{aligned} \nabla^2(\phi - \phi_0) &= 0 \quad \text{for } r \geq a, \\ \nabla^2(\phi - \phi_1) &= 0 \quad \text{for } r \leq a, \\ v_1 a \frac{\partial \phi_e}{\partial r} &= v_2 a \frac{\partial \phi_i}{\partial r} = v_3 \phi_e - v_4 \phi_i \quad \text{on } r = a, \end{aligned} \right\} \quad (3)$$

v_1, v_2, v_3, v_4 being constants. The ϕ 's are the harmonic potentials corresponding to the ψ 's.

The above results can be obtained directly or by transformation of the results given by Power and Jackson ³) remembering that

Stokes' stream function $\psi(r, \theta)$ satisfies the equation

$$\left[r^2 \frac{\partial^2}{\partial r^2} + \sin \theta \frac{\partial}{\partial \theta} \left(\frac{1}{\sin \theta} \frac{\partial}{\partial \theta} \right) \right] \psi(r, \theta) = 0$$

and is related to the potential ϕ by

$$\frac{\partial \psi}{\partial \mu} = -r^2 \frac{\partial \phi}{\partial r}, \quad \frac{\partial \psi}{\partial r} = (1 - \mu^2) \frac{\partial \phi}{\partial \mu}, \quad \text{where } \mu = \cos \theta.$$

Thus to the solutions $r^n P_n(\mu)$ and $r^{-(n+1)} P_n(\mu)$ of Laplace's equation correspond respectively

$$\frac{(1 - \mu^2)}{(n + 1)} r^{n+1} \frac{\partial P_n(\mu)}{\partial \mu} \quad \text{and} \quad - \frac{(1 - \mu^2)}{n} \frac{1}{r^n} \frac{\partial P_n(\mu)}{\partial \mu},$$

with the usual notation.

The normal uniqueness theorems hold.

§ 3. *Applications.* The most obvious use of this theorem is in the case of steady heat flow when there is a spherical surface of separation of two media of different conductivities. In most cases, heat transfer between the two media takes place with the rate of transfer between the two surfaces in contact being proportional to their temperature difference. Thus the properties (3) are immediately relevant to this type of problem where $v_3 = v_4$ is the surface conductance.

Other results for which one boundary condition is $\phi_e = \phi_i$ on $r = a$ can also be deduced. For example, consider the electrical problem in which there is a homogeneous sphere of dielectric constant k_i set in a homogeneous medium of dielectric constant k_0 . Set $v_3 = v_4$, $v_1/v_2 = k_0/k_i$ and then let $v_1 \rightarrow 0$. There are finite roots $\alpha_1 = -k_i/(k_0 + k_i)$, $\gamma_1 = -k_0/(k_0 + k_i)$ and roots α_2, γ_2 which become infinite in the limit. By proceeding as in §3, we obtain

$$\left. \begin{aligned} \psi_e(r) = \psi_0(r) + \frac{(k_i - k_0)}{(k_i + k_0)} \frac{r}{a} \psi_0 \left(\frac{a^2}{r} \right) + \frac{k_i(k_i - k_0)}{(k_i + k_0)^2} \frac{r}{a} \\ \cdot \int_0^1 t^{-(2k_i - k_0)/(k_i + k_0)} \psi_0 \left(\frac{a^2 s}{r} \right) ds \\ + \frac{2k_i}{(k_1 + k_0)} \psi_1(r) + \frac{k_i(k_i - k_0)}{(k_0 + k_i)^2} \int_1^\infty t^{-(2k_0 + k_i)/(k_i + k_0)} \psi_1(rs) ds, \end{aligned} \right\} \quad (4)$$

$$\psi_i(r) = \psi_1(r) + \frac{(k_0 - k_i)}{(k_0 + k_i)} \frac{r}{a} \psi_1\left(\frac{a^2}{r}\right) + \frac{k_0(k_i - k_0)}{(k_0 + k_i)^2} \frac{r}{a} \cdot \left[\int_0^\infty t^{-(2k_0+k_i)/(k_0+k_i)} \psi_1\left(\frac{a^2 s}{r}\right) ds \right. \\ \left. + \frac{2k_0}{(k_i+k_0)} \psi_0(r) + \frac{k_0(k_i-k_0)}{(k_i+k_0)^2} \int_0^1 t^{-(2k_i+k_0)/(k_i+k_0)} \psi_0(rs) ds \right] \quad (4)$$

The formulae (4) have been given by Power ²⁾, and Butler's ¹⁾ results are special cases of these.

Further, to obtain the exterior heat solution corresponding to the results given by Yeh, Martinek and Ludford ⁴⁾ we simply set $v_4 = 0$, $v_3 = v_1 ah$ with $\psi_1 = 0$ in ψ_e . The corresponding interior solution is found by setting $v_3 = 0$, $v_4 = v_2 ah$ with $\psi_0 = 0$ in ψ_i . Similarly, solutions corresponding to all the special cases mentioned in ⁴⁾ can be deduced.

Received 20th June, 1960.

REFERENCES

- 1) Butler, S. F. J., Proc. Camb. Phil. Soc. **49** Pt 1(1953) 169.
- 2) Power, G., Pac. J. Math. **4** (1954) 79.
- 3) Power, G. and H. L. W. Jackson, Appl. Sci. Res. B **8** (1960) 254.
- 4) Yeh, G. C. K., J. Martinek and G. S. S. Ludford, Z. angew. Math. Mech. **36** (1956) 111.

RAYLEIGH'S PROBLEM IN MAGNETOHYDRODYNAMICS FOR A NON-PERFECT CONDUCTOR

by D. G. DRAKE

Department of Applied Mathematics, University of Liverpool, Liverpool, England.

Summary

The extension of Rayleigh's problem to magnetohydrodynamics is considered for a non-perfect conductor in the presence of a transversely applied magnetic field. The governing equations for the fluid velocity and the electromagnetic quantities are obtained, and the Laplace transform of their solution found. Results obtained for the particular cases of a perfect conductor and an insulator are compared. The viscous boundary layer solution and the shearing stress are found, and their dependence on the conductivity of the conductor is discussed.

§ 1. *Introduction.* In recent papers Ludford ¹⁾ and Chang and Yen ²⁾ have considered the impulsive motion of a perfectly conducting infinite plate through a conducting fluid in the presence of a transversely applied uniform magnetic field. The plate was taken to move with constant velocity in its own plane and the fluid as viscous and incompressible. This is an extension to magnetohydrodynamics of the well known problem of Rayleigh ³⁾ for a non-conducting fluid, and in the present paper the corresponding problem for a non-perfect conductor is considered. The treatment includes that for a perfect conductor and an insulator as particular cases, given by letting the conductivity of the solid tend to infinity and zero respectively.

Taking a fixed in space rectangular Cartesian coordinate system, the conducting solid is assumed to occupy the region $y < 0$ and the conducting fluid the region $y > 0$. Starting at time $t = 0$, the solid moves with uniform velocity u_0 in the positive x -direction. The solution of the governing equations for the fluid velocity and the induced magnetic and electric fields is found by means of the

Laplace transform. However, the inversion of the resulting expressions in transformed space is found to be possible in terms of known functions only in certain special cases. In particular, consideration of the insulator case when the viscosity is equal to the magnetic diffusivity shows that the electromagnetic body force may be a decelerating force, whereas for a perfect conductor it is always an accelerating force. Further, under certain conditions the results are shown to be applicable to an infinite plate of finite thickness.

The boundary layer solution for small viscosity and a calculation of the inviscid flow outside the boundary layer gives a flow pattern in the insulator case which differs greatly from that for a solid with non-zero conductivity.

Also, it is seen that the shearing stress for a non-perfect conductor can take a value which is less than that for a non-conducting fluid, unlike the shearing stress for a perfect conductor which is always greater. For a fluid with infinite conductivity the shearing stress is independent of the conductivity of the solid.

§ 2. *Formulation.* In the fluid, i.e. for $y > 0$, noting that all quantities must be functions of y and t only, it may be shown ¹⁾ that the governing equations are ^{*)}

$$\frac{\partial E}{\partial y} = -\mu_0 \frac{\partial H}{\partial t}, \quad (1)$$

$$-\frac{\partial H}{\partial y} = \sigma(E + uH_0\mu_0) \quad (2)$$

and

$$\rho \frac{\partial u}{\partial t} = \nu \rho \frac{\partial^2 u}{\partial t^2} + H_0\mu_0 \frac{\partial H}{\partial y}, \quad (3)$$

where the velocity \mathbf{v} , electric field \mathbf{E} and magnetic field \mathbf{H} are given by $(u, 0, 0)$, $(0, 0, E)$ and $(H, H_0, 0)$ respectively. Here, the usual assumption of magnetohydrodynamics, i.e. that the displacement current may be neglected, has been made, and H_0 is the applied

^{*)} Here ρ is the density, ν the viscosity and σ the conductivity of the fluid; σ' is the conductivity and K' the dielectric constant of the solid; K_0 is the dielectric constant of vacuum; and the permeability of the fluid and the solid have been taken equal to the permeability of vacuum μ_0 .

constant magnetic field. The current $\mathbf{J} \equiv (0, 0, J)$ is given by

$$J = -\frac{\partial H}{\partial y}. \quad (4)$$

In the solid, i.e. for $y < 0$, retaining the displacement current, the Maxwell equations give

$$\frac{\partial E'}{\partial y} = -\mu_0 \frac{\partial H'}{\partial t} \quad (5)$$

and

$$-\frac{\partial H'}{\partial y} - \frac{\partial D'}{\partial t} = J', \quad (6)$$

where the electric field \mathbf{E}' , the magnetic field \mathbf{H}' , the displacement current \mathbf{D}' and the current \mathbf{J}' are given by $(0, 0, E')$, $(H', H_y, 0)$, $(0, 0, D')$ and $(0, 0, J')$ respectively. Further, from continuity of normal induction and $\text{div } \mathbf{B}' = 0$, the magnetic induction \mathbf{B}' is seen to be $(B', \mu_0 H_0, 0)$.

In addition the electromagnetic quantities in the solid, which is moving with constant velocity u_0 in the positive x -direction relative to the fixed in space coordinate system, satisfy the supplementary conditions ⁴⁾

$$B' = \mu_0 H', \quad (7)$$

$$D' = K'E' + (K'\mu_0 - K_0\mu_0) u_0 H_y, \quad (8)$$

$$\mu_0 H_0 = \mu_0 H_y + (K'\mu_0 - K_0\mu_0) u_0 E' \quad (9)$$

and

$$J' = \sigma'(E' + u_0 \mu_0 H_0) \quad (10)$$

on neglecting terms $O(u_0^2 c^2)$ where c is the speed of light. With these relations the magnetic induction \mathbf{B}' becomes $(\mu_0 H', \mu_0 H_0, 0)$, and (6) may be written as

$$-\mu_0 \frac{\partial H'}{\partial y} - \alpha \frac{\partial E'}{\partial t} = \sigma' \mu_0 (E' + u_0 \mu_0 H_0), \quad (11)$$

where

$$\alpha = \mu_0 K' - (K'\mu_0 - K_0\mu_0)^2 u_0^2. \quad (12)$$

To find the fluid velocity and the electromagnetic quantities at any instant (1)–(3) for u , E and H and (5) and (11) for E' and H'

are to be solved subject to the initial and boundary conditions. The initial conditions are

$$t = 0: \quad u, E, E', H, H' = 0 \quad \text{for all } y, \quad (13)$$

whilst along $y = 0$ the fluid velocity is equal to the velocity of the solid and the tangential components of the electric and magnetic fields are continuous, i.e.

$$u = u_0, \quad E = E', \quad H = H' \quad \text{when } y = 0. \quad (14)$$

§ 3. *Solution.* To obtain the solution of the above system it is expedient to introduce a Laplace transform with respect to the time variable. Letting p be the transform variable and denoting the transform of a quantity by a bar, (1)–(3) and (13) give that \bar{H} and \bar{u} satisfy

$$\left(\eta \frac{d^2}{dy^2} - p \right) \bar{H} + H_0 \frac{d\bar{u}}{dy} = 0 \quad (15)$$

and

$$H_0 \left(\nu \frac{d^2}{dy^2} - p \right) \bar{u} + A_0^2 \frac{d\bar{H}}{dy} = 0, \quad (16)$$

where $A_0 = (\mu_0 H^2 / \rho)^{\frac{1}{2}}$ is the Alfvén velocity and $\eta = 1/\sigma\mu_0$ is the magnetic diffusivity. Using Ludford's notation¹⁾ the solution of (15) and (16) which vanishes for large positive values of y is

$$\bar{H} = A e^{-my} + B e^{-ny}, \quad (17)$$

$$\bar{u} = \left(\frac{\eta m^2 - p}{m H_0} \right) A e^{-my} + \left(\frac{\eta n^2 - p}{n H_0} \right) B e^{-ny}, \quad (18)$$

where A and B are arbitrary constants, and

$$m = (a + b p)^{\frac{1}{2}} + (a + c p)^{\frac{1}{2}}, \quad n = (a + b p)^{\frac{1}{2}} - (a + c p)^{\frac{1}{2}}$$

with

$$a = A_0^2 / 4\eta\nu, \quad b = (\eta^{\frac{1}{2}} + \nu^{\frac{1}{2}})^2 / 4\eta\nu, \quad c = (\eta^{\frac{1}{2}} - \nu^{\frac{1}{2}})^2 / 4\eta\nu. \quad (19)$$

From (2), \bar{E} is then given by

$$\bar{E} = \frac{\mu_0 A p}{m} e^{-my} + \frac{\mu_0 B p}{n} e^{-ny}. \quad (20)$$

Similarly, (5), (11) and (12) lead to

$$\frac{d^2 \bar{H}'}{dy^2} - (1/\eta' + \alpha p) p \bar{H}' = 0 \quad (21)$$

where $\eta' = 1/\sigma'\mu_0$, the solution which vanishes for large negative y being

$$\bar{H}' = C e^{sy} \quad (22)$$

where C is an arbitrary constant and $s = (p, \eta' + \alpha p^2)^{\frac{1}{2}}$. Then, from (11) it is seen that

$$\bar{E}' = -\frac{\mu_0 p}{s} C e^{sy} - \frac{\mu_0 u_0 H_0}{\eta' s^2}. \quad (23)$$

The arbitrary constants A , B and C are determined by the boundary conditions (14) along $y = 0$. Thus, after some lengthy algebra, it is found that in the fluid

$$\begin{aligned} \bar{H} &= H_0 \beta (m\gamma e^{-my} - n\delta e^{-ny}), \\ \bar{E} &= H_0 \mu_0 p \beta (\gamma e^{-my} - \delta e^{-ny}), \\ \bar{u} &= \beta [(\eta m^2 - p) \gamma e^{-my} - (\eta n^2 - p) \delta e^{-ny}] \end{aligned} \quad (24)$$

and in the solid

$$\begin{aligned} \bar{H}' &= H_0 \beta (m\gamma - n\delta) e^{sy}, \\ \bar{E}' &= -\frac{\mu_0 u_0 H_0}{\eta' s^2} - \frac{H_0 \mu_0 p \beta}{s} (m\gamma - n\delta) e^{sy}. \end{aligned} \quad (25)$$

Here, β , γ and δ are functions of p given by

$$\begin{aligned} \beta &= \frac{u_0}{\eta'(m-n)sp[\eta nm + p + s\eta(n+m)]}, \\ \gamma &= (\eta n^2 - p) + \eta'(ns + s^2) \end{aligned}$$

and

$$\delta = (\eta m^2 - p) + \eta'(ms + s^2).$$

The results for a perfect conducting solid can be found by letting the conductivity σ' tend to infinity in the above and are in agreement with those found by Ludford¹). Also, putting the conductivity equal to zero gives the results for an insulator.

The above for an arbitrary value of the conductivity σ' are complicated functions of the transform variable p and cannot be

inverted in terms of known functions. Ludford has shown for a perfect conductor that the inversion can be carried out for the special case when $\eta = \nu$, and this can also be done for an insulator, although the resulting expressions are complicated. For example, for the insulator ($\sigma' = 0$) in this case

$$\begin{aligned} \bar{H}_{\sigma'=0} = & -\frac{u_0 H_0}{p A_0} \sinh\left(\frac{A_0 y}{2\eta}\right) \exp\left[-\left(p + \frac{A_0^2}{4\eta}\right) \frac{y}{\eta^{\frac{1}{2}}}\right] + \\ & + \frac{u_0 H_0 \alpha^{\frac{1}{2}}}{2p[1 + \alpha^{\frac{1}{2}} \eta^{\frac{1}{2}}(p + A_0^2/4\eta)^{\frac{1}{2}}]} \cosh\left(\frac{A_0 y}{2\eta}\right) \exp\left[-\left(p + \frac{A_0^2}{4\eta}\right) \frac{y}{\eta^{\frac{1}{2}}}\right] \end{aligned} \quad (26)$$

and

$$\bar{H}'_{\sigma'=0} = \frac{u_0 H_0 \alpha^{\frac{1}{2}} e^{\alpha^{1/2} p y}}{2p[1 + \alpha^{\frac{1}{2}} \eta^{\frac{1}{2}}(p + A_0^2/4\eta)^{\frac{1}{2}}]}.$$

Thus, with the help of a set of tables⁵⁾ it is found that

$$\begin{aligned} H_{\sigma'=0} = & -\frac{u_0 H_0}{2A_0} \left\{ \left[\sinh\left(\frac{A_0 y}{2\eta}\right) + \cosh\left(\frac{A_0 y}{2\eta}\right) \frac{A_0 \alpha^{\frac{1}{2}}}{A_0 \alpha^{\frac{1}{2}} - 2} \right] e^{-A_0 y/2\eta} \cdot \right. \\ & \cdot \operatorname{erfc}\left(\frac{y + A_0 t}{2\eta^{\frac{1}{2}} t^{\frac{1}{2}}}\right) + \left[\sinh\left(\frac{A_0 y}{2\eta}\right) - \cosh\left(\frac{A_0 y}{2\eta}\right) \frac{A_0 \alpha^{\frac{1}{2}}}{A_0 \alpha^{\frac{1}{2}} - 2} \right] e^{-A_0 y/2\eta} \cdot \\ & \cdot \operatorname{erfc}\left(\frac{y - A_0 t}{2\eta^{\frac{1}{2}} t^{\frac{1}{2}}}\right) - \frac{4A_0 \alpha^{\frac{1}{2}}}{A_0^2 \alpha - 4} \cosh\left(\frac{A_0 y}{2\eta}\right) \exp\left(\frac{t}{\eta \alpha} + \frac{y}{\eta \alpha^{\frac{1}{2}}} - \frac{A_0^2 t}{4\eta}\right) \cdot \\ & \left. \cdot \operatorname{erfc}\left(\frac{y}{2\eta^{\frac{1}{2}} t^{\frac{1}{2}}} + \frac{t^{\frac{1}{2}}}{\eta^{\frac{1}{2}} \alpha^{\frac{1}{2}}}\right) \right\} \end{aligned} \quad (28)$$

and

$$\begin{aligned} H'_{\sigma'=0} = & 0, \quad t < -\alpha^{\frac{1}{2}} y \\ = & \frac{2u_0 H_0 \alpha^{\frac{1}{2}}}{A_0^2 \alpha - 4} \left\{ 1 - \frac{A_0 \alpha^{\frac{1}{2}}}{2} + \frac{A_0 \alpha^{\frac{1}{2}}}{2} \operatorname{erfc}\left[\frac{A_0}{2\eta^{\frac{1}{2}}}(t + \alpha^{\frac{1}{2}} y)^{\frac{1}{2}}\right] - \right. \\ & \left. - \exp\left[\left(\frac{4 - A_0^2 \alpha}{4\alpha \eta}\right)(t + \alpha^{\frac{1}{2}} y)\right] \cdot \operatorname{erfc}\left[\frac{1}{\alpha^{\frac{1}{2}} \eta^{\frac{1}{2}}}(t + \alpha^{\frac{1}{2}} y)^{\frac{1}{2}}\right] \right\}, \quad t > -\alpha^{\frac{1}{2}} y. \end{aligned} \quad (29)$$

For a perfect conductor ($\sigma' = \infty$) when $\eta = \nu$

$$H_{\sigma'=\infty} = -\frac{H_0 u_0}{2A_0} \left[\operatorname{erf}\left(\frac{y + A_0 t}{2\eta^{\frac{1}{2}} t^{\frac{1}{2}}}\right) - \operatorname{erf}\left(\frac{y - A_0 t}{2\eta^{\frac{1}{2}} t^{\frac{1}{2}}}\right) \right] \quad (30)$$

and

$$H'_{\sigma'=\infty} = 0. \quad (31)$$

In fig. 1 the above are plotted against y for a particular value of the time t and various values of α , which depends essentially on the dielectric constant and velocity of the solid.

Whereas there is no induced magnetic field within the solid in the case of a perfect conductor, it is seen from (29) and fig. 1 that for an insulator a magnetic field is induced in the x -direction to a depth $t/\alpha^{\frac{1}{2}}$ from the surface at any instant. Further, from (9) and

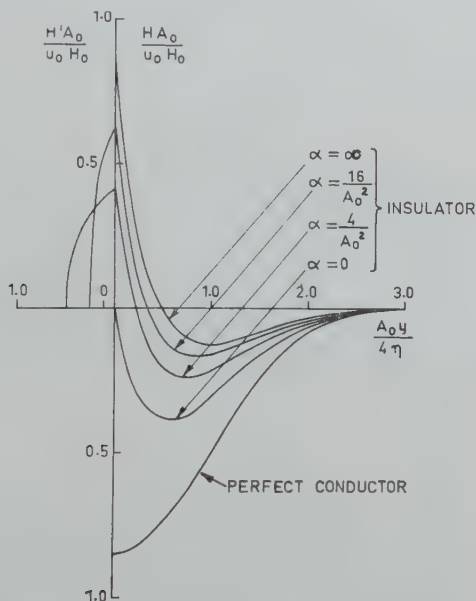


Fig. 1. $HA_0/\dot{u}_0 H_0$ and $H'A_0/u_0 H_0$ against $A_0 y/4\eta$ when $\eta = \nu$.

(25) it follows that the induced magnetic field in the y -direction and the induced electric field are confined to within this layer of thickness $t \propto^{\frac{1}{2}}$ at the surface. Thus, the above results for an insulator hold for an infinite plate (insulator) for values of the time t such that $2t/\alpha^{\frac{1}{2}}$ is less than the thickness of the plate. This conclusion is not restricted to the particular case when $\eta = \nu$ as is clear by the presence of the factor $\exp(p\alpha^{\frac{1}{2}}y)$ in (25) for \bar{H}' and \bar{E}' .

The electromagnetic body force, from (2), is proportional to $\partial H/\partial y$, and for a perfect conductor this is always positive²⁾ so that the electromagnetic body force is always an accelerating force. On the other hand fig. 1 shows that for an insulator $\partial H/\partial y$ can be negative and the electromagnetic body force a decelerating force.

§ 4. *Viscous boundary layer solution.* The boundary layer solution will give a picture of the flow when ν is small and is obtained by letting $\nu \rightarrow 0$ with $y/\nu^{\frac{1}{2}}$ fixed. Then, for any $\eta \neq 0$, it is found that

$$\bar{H} = - \frac{u_0 H_0}{p(1 + \eta' \alpha p)^{\frac{1}{2}} [p^{\frac{1}{2}} \eta'^{\frac{1}{2}} + (1 + \eta' \alpha p)^{\frac{1}{2}} (A_0^2 + \eta p)^{\frac{1}{2}}]},$$

$$\bar{E} = - \frac{u_0 H_0 (A_0^2 + \eta p)^{\frac{1}{2}}}{p(1 + \eta' \alpha p)^{\frac{1}{2}} [p^{\frac{1}{2}} \eta'^{\frac{1}{2}} + (1 + \eta' \alpha p)^{\frac{1}{2}} (A_0^2 + \eta p)^{\frac{1}{2}}]}$$

and

$$\begin{aligned} \bar{u} = & \frac{u_0}{p} \exp \left[- (p + A_0^2/\eta)^{\frac{1}{2}} \frac{y}{\nu^{\frac{1}{2}}} \right] + \\ & + \frac{u_0 A_0^2}{p(1 + \eta' \alpha p)^{\frac{1}{2}} (A_0^2 + \eta p)^{\frac{1}{2}} [p^{\frac{1}{2}} \eta'^{\frac{1}{2}} + (1 + \eta' \alpha p)^{\frac{1}{2}} (A_0^2 + \eta p)^{\frac{1}{2}}]} \\ & \cdot \left\{ 1 - \exp \left[- (p + A_0^2/\eta)^{\frac{1}{2}} \frac{y}{\nu^{\frac{1}{2}}} \right] \right\}. \end{aligned} \quad (32)$$

Again, these cannot in general be inverted in terms of known functions, although for an insulator

$$\begin{aligned} H_{\sigma'=0} &= 0, \\ E_{\sigma'=0} &= 0, \\ u_{\sigma'=0} &= \frac{u_0}{2} \left[\exp \left(\frac{A_0 y}{\nu^{\frac{1}{2}} \eta^{\frac{1}{2}}} \right) \operatorname{erfc} \left(\frac{y}{2\nu^{\frac{1}{2}} t^{\frac{1}{2}}} + \frac{A_0 t^{\frac{1}{2}}}{\eta^{\frac{1}{2}}} \right) + \right. \\ & \quad \left. + \exp \left(- \frac{A_0 y}{\nu^{\frac{1}{2}} \eta^{\frac{1}{2}}} \right) \operatorname{erfc} \left(\frac{y}{2\nu^{\frac{1}{2}} t^{\frac{1}{2}}} - \frac{A_0 t^{\frac{1}{2}}}{\eta^{\frac{1}{2}}} \right) \right] \end{aligned} \quad (33)$$

and for a perfect conductor

$$\begin{aligned} H_{\sigma'=\infty} &= - \frac{u_0 H_0}{A_0} \operatorname{erf} \left(\frac{A_0 t^{\frac{1}{2}}}{\eta^{\frac{1}{2}}} \right), \\ E_{\sigma'=\infty} &= - u_0 H_0 \end{aligned}$$

and

$$u_{\sigma'=\infty} = u_0 [1 - e^{-A_0^2 t/\eta} \operatorname{erf}(y/2\nu^{\frac{1}{2}} t^{\frac{1}{2}})]. \quad (34)$$

For arbitrary values of the conductivity σ' of the solid the character of the flow can be determined for small and large values of the time t). For example, when t is small ($y \neq 0$).

$$u \sim \frac{2u_0 \nu^{\frac{1}{2}} t^{\frac{1}{2}}}{\pi^{\frac{1}{2}} y} \exp(-y^2/4\nu t), \quad (35)$$

and when t is large

$$\begin{aligned} u &\sim u_0 \exp(-yA_0/\nu^{\frac{1}{2}}\eta^{\frac{1}{2}}), \quad \sigma' = 0 \\ &\sim u_0, \quad \sigma' \neq 0. \end{aligned} \quad (36)$$

Thus, within the boundary layer, for small values of the time the flow pattern is independent of the conductivity σ' , the fluid velocity decreasing from u_0 on the boundary of the solid to zero at the edge of the layer. For large values of t the fluid velocity is u_0 at all points for all values of σ' , except in the particular case of an insulator when the velocity decreases to zero at the edge of the layer.

The inviscid flow outside the boundary layer, obtained by solving the problem with $\nu = 0$, is given by

$$\bar{u} = \frac{u_0 A_0^2 \exp[-p y / (A_0^2 + \eta p)^{\frac{1}{2}}]}{p(1 + \eta' \alpha p)^{\frac{1}{2}} (A_0^2 + \eta p)^{\frac{1}{2}} [p^{\frac{1}{2}} \eta'^{\frac{1}{2}} + (1 + \eta' \alpha p)^{\frac{1}{2}} (A_0^2 + \eta p)^{\frac{1}{2}}]}. \quad (37)$$

For an insulator the fluid velocity is zero outside the boundary layer for all time, whereas for $\sigma' \neq 0$ it increases from 0 to u_0 with time.

§ 5. *Shearing stress.* The shearing stress τ is given by (3) as

$$\tau = \rho \nu \frac{\partial u}{\partial y} + \mu_0 H_0 H, \quad (38)$$

and, from (24), its transform $\bar{\tau}$ on $y = 0$ is seen to be

$$\begin{aligned} \bar{\tau} = & - \frac{\rho}{p(1 + \eta' \alpha p)^{\frac{1}{2}}} [p^{\frac{1}{2}} \eta'^{\frac{1}{2}} + \eta^{\frac{1}{2}} (1 + \eta' \alpha p)^{\frac{1}{2}} (p + a/b)^{\frac{1}{2}}]^{-1} \\ & \cdot \left\{ \frac{A_0^2 u_0 \eta^{\frac{1}{2}}}{\eta^{\frac{1}{2}} + \nu^{\frac{1}{2}}} + u_0 \nu^{\frac{1}{2}} [p \eta^{\frac{1}{2}} (1 + \eta' \alpha p) + p^{\frac{1}{2}} \eta'^{\frac{1}{2}} (1 + \eta' \alpha p)^{\frac{1}{2}} (p + a/b)^{\frac{1}{2}}] \right\}. \end{aligned} \quad (39)$$

In the particular case when the fluid has infinite conductivity, $\eta = 0$ and (39) becomes

$$\bar{\tau} = -u_0 \rho \nu^{\frac{1}{2}} (p + A_0^2/\nu)^{\frac{1}{2}} p^{-1}, \quad (40)$$

which may be inverted to give

$$\frac{\tau}{\rho} = -u_0 A_0 \operatorname{erf}(A_0 t^{\frac{1}{2}}/\nu^{\frac{1}{2}}) - \frac{u_0 \nu^{\frac{1}{2}}}{\pi^{\frac{1}{2}} t^{\frac{1}{2}}} \exp(-A_0^2 t/\nu), \quad (41)$$

which is independent of the conductivity of the solid.

For non-infinite values of the conductivity of the fluid the shearing stress can be found for small and large values of the time. For small t ,

$$\begin{aligned} \frac{\tau}{\rho} &\sim -\frac{u_0 v^{\frac{1}{2}}}{\pi^{\frac{1}{2}} t^{\frac{1}{2}}} - \frac{t^{\frac{1}{2}}}{\pi^{\frac{1}{2}}} \frac{u_0 A_0^2}{(\eta^{\frac{1}{2}} + v^{\frac{1}{2}})^2} (v^{\frac{1}{2}} + 2\eta^{\frac{1}{2}}) + O(t), \quad \sigma' = \infty \\ &\sim -\frac{u_0 v^{\frac{1}{2}}}{\pi^{\frac{1}{2}} t^{\frac{1}{2}}} + \frac{u_0 v^{\frac{1}{2}} A_0^2}{(\eta^{\frac{1}{2}} + v^{\frac{1}{2}})^2} \cdot \frac{t^{\frac{1}{2}}}{\pi^{\frac{1}{2}}} + O(t), \quad \sigma' \neq \infty \end{aligned} \quad (42)$$

and for large t

$$\begin{aligned} \frac{\tau}{\rho} &\sim -A_0 u_0 + O(t^{-\frac{1}{2}}), \quad \sigma' \neq 0 \\ &\sim -\frac{u_0 v^{\frac{1}{2}} A_0}{\eta^{\frac{1}{2}} + v^{\frac{1}{2}} + \eta^{\frac{1}{2}} \alpha^{\frac{1}{2}} A_0} + O(t^{-\frac{1}{2}}), \quad \sigma' = 0. \end{aligned} \quad (43)$$

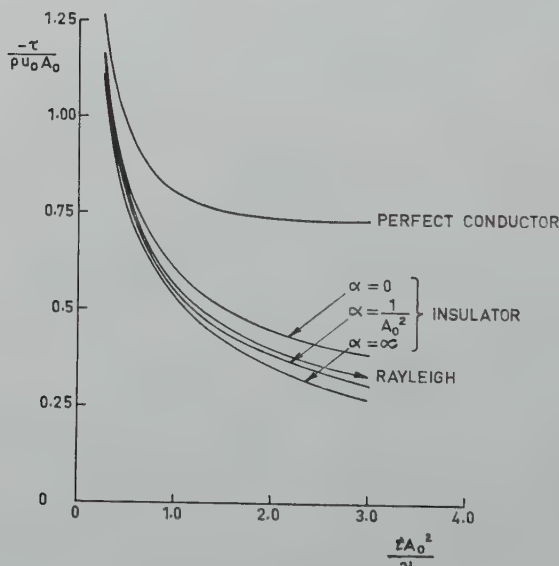


Fig. 2. $-\tau/\rho u_0 A_0$ against $t A_0^2/v$ for $\eta = 9v$.

In the particular cases of a perfect conductor and an insulator (39) may be inverted to give

$$\frac{\tau_{\sigma'=\infty}}{\rho} = -u_0 A_0 \operatorname{erf}\left(\frac{A_0 t^{\frac{1}{2}}}{\eta^{\frac{1}{2}} + v^{\frac{1}{2}}}\right) - \frac{u_0 v^{\frac{1}{2}}}{\pi^{\frac{1}{2}} t^{\frac{1}{2}}} \exp\left[-\frac{A_0^2 t}{(\eta^{\frac{1}{2}} + v^{\frac{1}{2}})^2}\right] \quad (44)$$

for a perfect conductor, and

$$\frac{\tau_{\sigma', 0}}{\rho} = -\frac{u_0 v^{\frac{1}{2}} \eta^{\frac{1}{2}} \alpha^{\frac{1}{2}} A_0^2}{(\eta^{\frac{1}{2}} + v^{\frac{1}{2}})^2 - \eta \alpha A_0^2} \left[\exp\left(\frac{t}{\eta \alpha} - \frac{A_0^2 t}{(\eta^{\frac{1}{2}} + v^{\frac{1}{2}})^2}\right) \operatorname{erfc}\left(\frac{t^{\frac{1}{2}}}{\eta^{\frac{1}{2}} \alpha^{\frac{1}{2}}}\right) + \right. \\ \left. + \frac{(\eta^{\frac{1}{2}} + v^{\frac{1}{2}})}{A_0 \eta^{\frac{1}{2}} \alpha^{\frac{1}{2}}} \operatorname{erf}\left(\frac{A_0 t^{\frac{1}{2}}}{\eta^{\frac{1}{2}} + v^{\frac{1}{2}}}\right) - 1 \right] - \frac{u_0 v^{\frac{1}{2}}}{\pi^{\frac{1}{2}} t^{\frac{1}{2}}} e^{-A_0^2 t / (\eta^{1/2} + v^{1/2})^2} \quad (45)$$

for an insulator. The expressions (44) and (45) are plotted in fig. 2 against the time t for the particular case when $\eta = 9\nu$ and for various values of α . Fig. 2 and (42) show that the shearing can take values less than in the non-conducting fluid case, unlike the perfect conductor when the shearing stress is always greater than that for a non-conducting fluid. However, from (43) it is seen that for large values of the time the shearing stress is always least for the non-conducting fluid.

The author is indebted to Dr. W. E. Williams for suggesting the problem and for his continued interest.

Received 20th June, 1960.

REFERENCES

- 1) Ludford, G. S. S., Arch. Rat. Mech. Anal. **3** (1959) 14.
- 2) Chang, C. C. and J. T. Yen, Phys. Fluids **2** (1959) 393.
- 3) Rayleigh, Lord, Phil. Mag., Ser. VI, **21** (1911) 697.
- 4) Sommerfeld, A., Electrodynamics, Academic Press, New York 1952.
- 5) Erdélyi, A., Tables of Integral Transforms, Vol. I., McGraw-Hill, 1954.
- 6) McLachlan, N. W., Complex Variable and Operational Calculus, Cambridge 1939.

ANALYTIC SUBJECT INDEX

Appl. Sci. Res. B 8

	Page		Page
Acoustic forces , Acoustic forces and torques on a system of strips - K. Saermark . . .	13	- , The electromagnetic fields of a dipole in the presence of a thin plasma sheet - J. R. Wait . .	397
Antenne theory , Transient phenomena associated with Sommerfeld's horizontal dipole problem - H. J. Frankena . .	357	- , see scattering, transmission, diffraction, impedance boundary conditions	
- , Radiation of pulses generated by a vertical electric dipole above a plane, non-conducting earth - A. T. de Hoop and H. J. Frankena	369	Electromagnets , A criterion for the efficiency of iron core electromagnets - D. de Klerk and C. J. Gorter	265
Charged particles , motion of, On the motion of a charged particle in an almost homogeneous magnetic field - L. J. F. Broer and L. van Wijngaarden	159	Electrostatic field , The surface charge of a semi-infinite cylinder due to an axial point charge - H. A. Lauwerier . . .	277
Counters , Characteristic parameters of gas-tube proportional counters I - R. W. Kiser . . .	183	Ferrites , On the specific heat of Mn-Zn and Ni-Zn ferrite between 20°C and 350°C - J. L. Verhaeghe, G. G. Robbrecht and W. M. Bruynooghe . . .	128
- , Characteristic parameters of Geiger-Muller counter gases I - C. D. Storrs and R. W. Kiser .	387	- , see scattering	
Diffraction , Diffraction by an imperfectly conducting half-plane at oblique incidence - T. B. A. Senior	35	Hall effect , A mechanical Hall effect - Letter to the Editor - L. J. F. Broer, L. A. Peletier and L. van Wijngaarden . . .	259
- , The diffraction of a plane wave through two or more slits in a plane screen - E. B. Hansen . .	73	Hydrogen , permeability of, see vacuum technique. . .	
Electromagnetic field , Propagation of electromagnetic pulses in a homogeneous conducting earth - J. R. Wait . .	213	Infrared measurements , Infrared spectra of ion-producing species in hydrocarbons - A. Gemant	149
		Impedance boundary conditions , Impedance boundary conditions for imperfectly con-	

- | | Page | | Page |
|--|------|---|------|
| ducting surfaces - T. B. A. Senior | 418 | Neutrons, diffusion of, A corner effect in plane diffusion theory - H. Levine. | 105 |
| -, Impedance boundary conditions for statistically rough surfaces - T. B. A. Senior | 437 | Plasmas, Heating of an ionized gas sheath by microwaves - M. S. Sodha | 208 |
| Magnetohydrodynamics, Rayleigh's problem in magnetohydrodynamics for a non-perfect conductor - D. G. Drake | 467 | -, Plasma dynamics in an arc formed by low-voltage sparkover of a liquid dielectric - P. K. Eckman and E. M. Williams | 299 |
| Mathematical methods, The method of images and the solution of certain partial differential equations - G. Rowlands | 62 | -, see electromagnetic field | |
| -, Extremum methods for certain electrical problems involving homogeneous anisotropic material - G. Power | 84 | Scattering, Comments on far field scattering from bodies of revolution - K. M. Siegel, R. F. Goodrich and V. H. Weston | 8 |
| -, On the solution of an eigenvalue equation of the Wiener-Hopf type in finite and infinite ranges - R. Mittra | 201 | -, A reciprocity theorem for the electromagnetic field scattered by an obstacle - A. T. de Hoop | 135 |
| -, Sphere and circle theorems involving surface discontinuities of potential - G. Power and H. L. W. Jackson | 254 | -, Scattering of electromagnetic waves by coaxial ferrite cylinders of different tensor permeabilities - Yutze Chow | 290 |
| -, Use of Stokes' stream function for discontinuities of potential at a spherical boundary - G. Power and H. L. W. Jackson | 463 | Seismology, A modification of Cagniard's method for solving seismic pulse problems - A. T. de Hoop | 349 |
| Microwaves, A power stabilizer for frequency modulated microwave oscillators - H. A. Dijkerman, C. Huiszoon and A. Dymanus | 1 | Semiconductors, On the influence of shape and variations in conductivity of the sample on four-point measurements - E. B. Hansen | 93 |
| -, Wave propagation in an inhomogeneous transversely magnetized rectangular waveguide - Chen To Tai | 141 | Susceptibility, Susceptibility measurements of Nb between room temperature and liquid helium temperatures - A. van Itterbeek, W. Peelaers and F. Steffens | 177 |
| -, A harmonic generator and detector for the short millimeter wave region - H. W. de Wijn | 261 | -, The magnetic susceptibility of Ag-Mn and Cu-Mn solid solutions between 1.2°K and 368°K - A. van Itterbeek, W. Peelaers and W. Steffens | 337 |
| -, Characteristics of ridge waveguides - F. Young and J. Hermann | 321 | | |
| -, see plasmas | | | |

	Page		Page
Transmission, Transmission coefficient for a system of parallel slits in a thin, plane screen - K. Saermark	29	ments on the permeability of hydrogen from H_2 and H_2O through steel, stainless steel and aluminium - F. Boeschoten, W. van Egmond and H. M. J. Kinderdijk	378
Vacuum technique, Measure-			

